



SAPIENZA, UNIVERSITY OF ROME

FACULTY OF MATHEMATICAL, NATURAL AND PHYSICAL SCIENCES

PHYSICS DEPARTMENT

DOCTORAL THESIS

**RELICS FROM THE EARLY UNIVERSE:
PRIMORDIAL GRAVITATIONAL WAVES, AXIONS AND NEUTRINOS**

AUTHOR:
WILLIAM GIARÈ

SUPERVISOR:
Prof. ALESSANDRO MELCHIORRI

A THESIS SUBMITTED IN FULFILLMENT OF THE REQUIREMENTS
FOR THE DEGREE OF DOCTOR OF PHILOSOPHY

IN

ASTRONOMY AND ASTROPHYSICS

ACADEMIC YEAR 2020/2021

"Stories are relics, part of an undiscovered pre-existing world"

- STEPHEN KING

RELICS FROM THE EARLY UNIVERSE: PRIMORDIAL GRAVITATIONAL WAVES, AXIONS AND NEUTRINOS

WILLIAM GIARÈ,

Physics Department and INFN, Università di Roma “La Sapienza”,
Piazzale Aldo Moro 2, 00185, Rome, Italy

✉ william.giare@uniroma1.it

🆔 0000-0002-4012-9285

(Submitted 1 November 2021; revised 9 December 2021; defended 23 December 2021)

ABSTRACT

Over the last decades our knowledge of the Universe has reached an unprecedented level of accuracy. The observations of the Cosmic Microwave Background and the large scale structure of the Universe opened the so-called epoch of precise cosmology, enabling us to test with increasing precision several aspects of fundamental physics, from the first principles of the cosmological model to global theoretical scenarios beyond *General Relativity* and the *Standard Model* of elementary particles. The research subject of this PhD thesis goes exactly in this direction: working at the interface of cosmology, gravitation and (astro)particle physics, I analyze cosmological and astrophysical observations to identify, characterize and constrain possible hints for new physics in light of their implications for the Early Universe.

SCIENTIFIC PRODUCTION

This thesis is based on the following papers (ordered by date) that I authored or co-authored during my PhD.

- REF. [1]: **William Giarè**, Eleonora Di Valentino, and Alessandro Melchiorri "*Testing the inflationary slow-roll condition with tensor modes*", *Phys. Rev. D* **99**, 123522
- REF. [2]: **William Giarè** and Alessandro Melchiorri "*Probing the inflationary background of gravitational waves from large to small scales*", *Phys. Lett. B* **815** (2021) 136137 , [arXiv:2003.04783]
- REF. [3]: **William Giarè** and Fabrizio Renzi, "*Propagating speed of Primordial Gravitational Waves*", *Phys. Rev. D* **102**, 083530 , [arXiv:2007.04256]
- REF. [4]: **William Giarè**, Fabrizio Renzi and Alessandro Melchiorri, "*Higher-Curvature corrections and Tensor Modes*", *Phys.Rev D* **103**, 043515 , [arXiv:2012.00527]
- REF. [5]: **William Giarè**, Eleonora Di Valentino, Alessandro Melchiorri, and Olga Mena, "*New cosmological bounds on hot relics: Axions & Neutrinos* ", *MNRAS* **505** (2021) 2 , [arXiv:2011.14704]
- REF. [6]: Matteo Forconi, **William Giarè**, Eleonora Di Valentino and Alessandro Melchiorri "*Cosmological constraints on slow roll inflation: an update*" , *Phys.Rev D* **104**, 103528 , [arXiv:2110.01695]
- REF. [7]: **William Giarè**, Fabrizio Renzi, Alessandro Melchiorri, Olga Mena and Eleonora Di Valentino "*Cosmological forecasts on thermal axions, relic neutrinos and light elements* ", [arXiv:2110.00340]
-

I discuss how they fit the storyline in the subsequent **overview** while I briefly summarize all the major results in the **conclusion**. Other forthcoming works have been omitted from the discussion because they don't fit the overall topic.

OVERVIEW

In this thesis I discuss how non-standard physics, either in the gravitational sector or in the Standard Model of particle physics can be hidden in different kinds of relics from the Early Universe and how we can use current and future cosmological and astrophysical large and small scale observations to unveil it. Here I briefly summarize the structure of the work to guide the interested reader. What follows is *not* a summary of the results, that instead can be found in the [conclusion](#).

This thesis is made of three chapters.

- [1] In [chapter I](#) I provide an exhaustive review of the field of cosmology, paying special attention to the physics of the Early Universe. This chapter is thought to contextualize the original results discussed in the subsequent two chapters. All the different topics reviewed should be largely known to the expert reader. Nevertheless, I tried to organize the discussion in the most possible original way, trying always to follow what I considered the best approach to derive the different results. The chapter is organized as follows.
- In [section I.I](#) I review the so-called Hot Big Bang Cosmology: a predictive theory of the Universe based on Einstein's theory of General Relativity and the Standard Model of particle physics. This section is organized as follows.
 - * In [subsection I.I.I](#) I review the geometrical large-scale structure of the cosmological space-time following an approach based on symmetries.
 - * In [subsection I.I.II](#) I solve the Einstein equations for the FRW metric deriving the equations of motion that relate the dynamics of the Universe to its matter and energy content.
 - * In [subsection I.I.III](#) I collect the basic equations that describe the thermodynamics in an expanding Universe and then I review the most important steps of the thermal history.
 - In [section I.II](#) I study the small scale structure of the Universe, introducing the cosmological perturbation theory and following this path
 - * In [subsection I.II.I](#) I classify the different perturbations into three categories: scalar, vector and tensor. Then I prove the so-called Scalar-Vector-Tensor decomposition theorem, showing that they evolve independently.
 - * In [subsection I.II.II](#) I derive the linearized Einstein Equations for scalar and tensor perturbations around a FRW spacetime.
 - * In [subsection I.II.III](#) I study the dynamics of scalar perturbations along the different cosmological epochs using the linearized Theory developed in the previous subsection.
 - * In [subsection I.II.IV](#) I describe the dynamical evolution of tensor perturbations in an expanding Universe.
 - In [section I.III](#) I introduce perhaps the most important cosmological observable: the Cosmic Microwave Background. I describe the physics of temperature anisotropies and polarization, connecting the small irregularities observed in the CMB with the physics of the Early Universe. In particular
 - * In [subsection I.III.I](#) I review the theory of CMB temperature anisotropies, discussing different physical mechanisms able to produce primary and secondary anisotropies and the respective signatures left in the angular power spectrum.
 - * In [subsection I.III.II](#) I review the theory of CMB polarization, discussing in details different physical mechanisms able to produce them and highlighting the effects of relic gravitational waves from the Early Universe.

- In [section I.IV](#) I introduce the theory of cosmological inflation, showing how an early epoch of fast accelerated expansion can solve many fine-tuning problems with the initial conditions. Then I extend the discussion following the subsequent path.
 - * In [subsection I.IV.I](#) I characterize the simplest dynamical models of inflation that involve a scalar field and a sufficiently flat potential to allow a phase of slow-roll evolution.
 - * In [subsection I.IV.II](#) I show that inflation provides an elegant mechanism able to generate the primordial scalar and tensor perturbations. I perform a detailed and complete calculation in quantum field theory, deriving the expressions for the spectra of scalar and tensor perturbations in an almost de-Sitter spacetime.
 - * In [subsection I.IV.III](#) I study how inflation can emerge as a theory of broken time diffeomorphisms and I point out the most relevant strengths of the Effective Theory of inflation.
 - In [section I.V](#) I finally introduce the standard Λ CDM cosmological model, pointing out all the theoretical assumptions beyond the main unknown ingredients of this standard scenario:
 - * In [subsection I.V.I](#) using the most recent cosmological and astrophysical datasets to date, I detailed review the most recent observational constraints on this standard scenarios, highlighting the implications for the physics of the Early Universe.
 - * In [subsection I.V.II](#) I discuss why one should consider the possibility to explore extensions of the Λ CDM cosmological model, and I explain why among the different extension maybe the most interesting ones are those connected with extensions to fundamental physics. Finally I outline the research project that I develop in the subsequent two chapters.
- [2] In [chapter II](#) I present the results obtained during my PhD in the field of inflation and Primordial Gravitational Waves. This chapter is entirely based on original results discussed in different papers published along the years. In particular
- In [section II.I](#) I provide an updated review of the observational constraints on the standard slow roll paradigm of inflation based on the techniques and the results obtained in the following works that I authored and co-authored
 - [1] **William Giarè**, Eleonora Di Valentino, and Alessandro Melchiorri "*Testing the inflationary slow-roll condition with tensor modes*", [Phys. Rev. D 99, 123522](#)
 - [6] Matteo Forconi, **William Giarè**, Eleonora Di Valentino and Alessandro Melchiorri "*Cosmological constraints on slow roll inflation: an update*" , [Phys.Rev D 104, 103528](#) , [[arXiv:2110.01695](#)]
 - In [section II.II](#) I discuss the implications of direct gravitational wave observations for models of inflation beyond the standard slow-roll paradigm with Einstein gravity, reviewing the results published in
 - [2] **William Giarè** and Alessandro Melchiorri "*Probing the inflationary background of gravitational waves from large to small scales*", [Phys. Lett. B 815 \(2021\) 136137](#) , [[arXiv:2003.04783](#)]
 - In [section II.III](#) I discuss the implications for the cosmological observables of a non trivial propagation of gravity during the inflationary epoch, retracing the results published in
 - [3] **William Giarè** and Fabrizio Renzi, "*Propagating speed of Primordial Gravitational Waves*", [Phys. Rev. D 102, 083530](#) , [[arXiv:2007.04256](#)]
 - In [section II.IV](#) I investigate the effects of higher-curvature gravity in models of inflation with a minimal breaking of conformal symmetry, following the results published in
 - [4] **William Giarè**, Fabrizio Renzi and Alessandro Melchiorri, "*Higher-Curvature corrections and Tensor Modes*", [Phys.Rev D 103, 043515](#) , [[arXiv:2012.00527](#)]
- [3] In [chapter III](#) I use cosmological and astrophysical observations to probe and constrain well motivated extensions of the standard model of particle physics that involve spineless axions as a solution of the

strong CP problem in Quantum Chromodynamics. In particular I focused on QCD Axions produced in the Early Universe via interactions with other particles in realistic mixed hot dark matter scenarios that consider also massive neutrinos as additional thermal relics. The chapter is organized as follows.

- In [section III.I](#) I provide a brief review of the axion theory. In particular:
 - * In [subsection III.I.I](#) I discuss some aspects of the quantum theory of strong interactions;
 - * In [subsection III.I.II](#) I discuss the nature of the strong CP problem in the Standard Model of elementary particles;
 - * In [subsection III.I.III](#) I show how axions can arise from the Peccei Quinn solution of the strong CP problem and I characterize their underlying physical properties.
- In [section III.II](#) I discuss the implications of cosmological observations for axions produced thermally in the Early Universe, and, in light of the most recent cosmological and astrophysical measurements, I derive new cosmological constraints on hot thermal relics following the results published in [\[5\] William Giarè, Eleonora Di Valentino, Alessandro Melchiorri, and Olga Mena, "New cosmological bounds on hot relics: Axions & Neutrinos", MNRAS 505 \(2021\) 2, 2703–2711, \[arXiv:2011.14704\]](#)
- In [section III.III](#) I study the improvement in the constraining power on hot relics expected by the next-gen CMB and BAO observations. I investigate and discuss the implications for axions (thermalized before the QCD transition), neutrinos and BBN elements, following the results presented in [\[7\] William Giarè, Fabrizio Renzi, Alessandro Melchiorri, Olga Mena and Eleonora Di Valentino "Cosmological forecasts on thermal axions relic neutrinos and primordial elements", \[arXiv:2012.00527\]](#)

Along with these three main chapters, the work is enriched by two other different appendices:

[A] In the [Supplementary Material \(Appendix A\)](#) I provide different secondary results that were always derived and discussed in the works this thesis is based on, Refs [\[1–7\]](#). While they are not essential to the comprehension of the main discussion, this information is very useful because it enriches the overall presentation through a multitude of different practical examples and detailed calculations. Furthermore, sometimes I generalize the major results to scenarios beyond the theoretical assumptions under which they were originally derived. The [Supplementary Material](#) is organized as follows.

- In [section A.1](#) I review the standard slow roll relations among the higher-order (scalar and tensor) inflationary parameters proving that a set of consistency relation exists at any order in the power-law expansion. These results were derived first in Ref. [\[1\]](#).
- In [section A.2](#) I study inflation in relation with the spatial curved of the cosmological spacetime, discussing the implication of curvature for the slow-roll dynamics. This section is based on Ref. [\[6\]](#).
- In [section A.3](#) I show different examples of negligible and non-negligible scale dependence in the tensor two-point function originally discussed in Ref. [\[2\]](#).
- In [section A.4](#) I provide a detailed computation of the primordial tensor spectrum using an effective field theory approach and allowing a non-standard propagation of gravity. This section follows the discussion in Ref. [\[3\]](#).
- In [section A.5](#) I generalize the results discussed in [section II.III](#) for non linear propagation of gravity as done in Ref. [\[3\]](#).
- In [section A.6](#) I discuss the effects of a superluminal propagation of gravity during inflation following Ref. [\[3\]](#).
- In [section A.7](#) I discuss how to relate our constraints on the propagation of gravity at early epochs with those one can obtain by direct GW measurements, showing they perfectly agree. This section is based on Ref. [\[3\]](#).

– In [section A.8](#) I generalize the results discussed in [section II.IV](#) for generic inflaton-Weyl couplings following Ref. [\[4\]](#).

[B] In the [Appendix B](#) for completeness I provide a review of axions produced non-thermally that are natural candidates for the cold dark matter component of the Universe.

CONVENTIONS

A few remarks on the conventions adopted in this thesis. They are useful to avoid misunderstanding with the reader.

UNITS, CONVERSIONS AND CONSTANTS

Even though sometimes I will keep the fundamental constants explicit in the equations, in this work I will largely adopt the so-called natural units: $c = \hbar = k_b = 1$. In this way there is only one fundamental dimension:

$$[\text{Energy}] = [\text{Mass}] = [\text{Temperature}] = \frac{1}{[\text{Length}]} = \frac{1}{[\text{Time}]}.$$

Some useful conversion factors for these units are listed below:

$$1\text{g} = 5.61 \times 10^{23}\text{GeV}$$

$$1\text{s} = 1.5 \times 10^{24} \frac{1}{\text{GeV}}$$

$$1\text{ Kelvin} = 8.6 \times 10^{-14}\text{GeV}$$

$$1\text{cm} = 5.1 \times 10^{13} \frac{1}{\text{GeV}}$$

$$1\text{ Mpc} = 3.08 \times 10^{22}\text{ m} = 1.56 \times 10^{38} \frac{1}{\text{GeV}}$$

Some useful fundamental constants are listed below:

$$\text{Planck Mass} \doteq M_{pl} \doteq \sqrt{\frac{\hbar c}{G}} = 1.22 \times 10^{19}\text{ GeV}$$

$$\text{Reduced Planck Mass} \doteq \bar{M}_p \doteq \sqrt{\frac{\hbar c}{8\pi G}} = 2.43 \times 10^{18}\text{ GeV} = 2.2 \times 10^{-5}\text{ g}$$

$$\text{Planck time} \doteq t_p \doteq \frac{1}{M_{pl}} = 5.4 \times 10^{-44}\text{ s}$$

$$\text{Planck length} \doteq l_p \doteq \frac{1}{M_{pl}} = 1.6 \times 10^{-33}\text{ cm}$$

$$\text{Planck temperature} \doteq T_p \doteq M_{pl} = 1.42 \times 10^{32}\text{ Kelvin}$$

$$\text{Hubble constant} \doteq H_0 = 100 h \text{ Km/s/Mpc} = 2.1 h \times 10^{-42}\text{ GeV}$$

$$\text{Critical Density} \doteq \rho_c = 1.87 h^2 \times 10^{-29}\text{ g cm}^{-3} = 8.1 h^2 \times 10^{-47}\text{ GeV}^4$$

METRIC AND SPACETIME

In this work, I adopt the signature $(-,+,+,+)$ for the metric tensor. I recall that the signature of a metric tensor is defined as the number (counted with multiplicity) of positive, negative and zero eigenvalues of the real symmetric matrix associated to the metric tensor with respect to a basis. Here, the "-" is associated to the time dimension, and the "(+, +, +)" to the space and physical dimension. With this choice, the line element

of a flat maximally symmetric Minkowsky spacetime reads

$$ds^2 = -c dt^2 + dx^2 + dy^2 + dz^2$$

and the three-dimensional Euclidean sub-space admits a positive scalar product. The interval between timelike separated events (*i.e.* the interval between a given event and the set of points that are inside its past and future light cone) is negative ($\Delta s^2 < 0$), while the interval between spacelike events (*i.e.* the interval between a given event and the set of points that are outside its past and future light cone) is positive ($\Delta s^2 > 0$). Finally, light-like events ($\Delta s^2 = 0$) define the limit between the two cases.

PERTURBED FRW LINE ELEMENT

In [chapter I I](#) define the most general perturbed line element for a FRW spacetime with a signature $(-,+,+,+)$ as

$$ds^2 = -(1 + 2\Phi) dt^2 + 2 a(t) B_i dx^i dt + a^2(t) [(1 - 2\Psi) \delta_{ij} + 2E_{ij}] dx^i dx^j,$$

deriving the linearized Einstein Equations accordingly. In literature this line element is often defined with the opposite sign for Ψ , *i.e.*,

$$ds^2 = -(1 + 2\Phi) dt^2 + 2 a(t) B_i dx^i dt + a^2(t) [(1 + 2\Psi) \delta_{ij} + 2E_{ij}] dx^i dx^j.$$

Notice that some authors often change Ψ with Φ in the line elements and other common definitions are

$$ds^2 = -(1 + 2\Psi) dt^2 + 2 a(t) B_i dx^i dt + a^2(t) [(1 - 2\Phi) \delta_{ij} + 2E_{ij}] dx^i dx^j,$$

and

$$ds^2 = -(1 + 2\Psi) dt^2 + 2 a(t) B_i dx^i dt + a^2(t) [(1 + 2\Phi) \delta_{ij} + 2E_{ij}] dx^i dx^j,$$

Finally in literature the metric signature is sometimes chosen to be $(+,-,-,-)$. To correctly derive the linearized Einstein Equations we should remain consistent with the convention we chose, but clearly the final results do not rely on it.

DIMENSIONLESS PRIMORDIAL SPECTRA

For a generic Gaussian random field ψ_k , the spectrum is defined in terms of its two-point correlation function as

$$\langle \psi_k \psi_{k'} \rangle \doteq (2\pi)^3 \delta_{k+k'}^3 P_\psi(k)$$

and that the other higher-order correlation functions are expected to vanish. It is worth noting that in this thesis I work in terms of the *dimensionless* primordial spectra defined as

$$\mathcal{P}_\psi(k) \doteq (k^3 / 2\pi^2) P_\psi(k)$$

We should be ready to start!

CONTENTS

ABSTRACT	iii
SCIENTIFIC PRODUCTION	iv
OVERVIEW	v
CONVENTIONS	ix
I THE EARLY UNIVERSE	1
I.I HOT BIG BANG THEORY	2
I.I.I GEOMETRY	2
I.I.II DYNAMICS	4
I.I.III THERMODYNAMICS	7
I.II COSMOLOGICAL PERTURBATION THEORY	18
I.II.I SCALAR, VECTOR AND TENSOR PERTURBATIONS	19
I.II.II LINEARIZED EINSTEIN EQUATIONS	20
I.II.III DYNAMICS OF SCALAR PERTURBATIONS	24
I.II.IV DYNAMICS OF TENSOR PERTURBATIONS	30
I.III COSMIC MICROWAVE BACKGROUND RADIATION	32
I.III.I ANISOTROPIES	32
I.III.II POLARIZATION	38
I.IV INFLATION THEORY	44
I.IV.I SINGLE FIELD SLOW-ROLL INFLATION	45
I.IV.II QUANTUM INFLATIONARY FLUCTUATIONS	48
I.IV.III EFFECTIVE FIELD THEORY OF INFLATION	53
I.V THE STANDARD MODEL OF COSMOLOGY	59
I.V.I DATA STORYTELLING	60
I.V.II BEYOND THE STANDARD COSMOLOGICAL MODEL	66
II PRIMORDIAL GRAVITATIONAL WAVES	68
II.I COSMOLOGICAL CONSTRAINTS ON SLOW ROLL INFLATION	69
II.I.I METHODOLOGY	70
II.I.II COSMOLOGICAL CONSTRAINTS	73
II.II INFLATIONARY GRAVITY WAVES FROM LARGE TO SMALL SCALES	84
II.II.I BREAKING THE POWER LAW EXPANSION	85
II.III PROPAGATING SPEED OF PRIMORDIAL GRAVITATIONAL WAVES	87
II.III.I THEORY	87
II.III.II CONSTRAINTS	92
II.IV HIGHER CURVATURE CORRECTIONS AND TENSOR MODES	101
II.IV.I THEORY	102
II.IV.II CONSTRAINTS	104

III HOT RELICS: AXIONS & NEUTRINOS	108
III.I THE STRONG CP PROBLEM AND AXIONS	109
III.I.I ASPECTS OF QUANTUM CHROMODYNAMICS	109
III.I.II THE STRONG CP PROBLEM	114
III.I.III THE PECCEI QUINN SOLUTION	115
III.II NEW COSMOLOGICAL BOUNDS ON AXIONS AND NEUTRINOS	117
III.II.I THERMAL AXIONS	118
III.II.II NUMERICAL ANALYSES	120
III.II.III COSMOLOGICAL BOUNDS	121
III.III COSMOLOGICAL FORECASTS ON AXIONS NEUTRINOS AND LIGHT ELEMENTS	127
III.III.I FORECAST METHODS	127
III.III.II FORECASTED RESULTS	130
CONCLUSION	136
ACKNOWLEDGEMENTS	140
A SUPPLEMENTARY MATERIAL	141
A.1 HIGHER-ORDER SLOW ROLL CONSISTENCY RELATIONS	141
A.2 INFLATION AND SPATIAL CURVATURE	143
A.3 EXAMPLES OF SCALE-EFFECTS IN THE PGWS PRODUCTION	149
A.4 A DETAILED DERIVATION OF THE TENSOR SPECTRUM	154
A.5 BEYOND THE LINEAR ORDER IN THE PROPAGATING SPEED	156
A.6 SUPERLUMINAL GRAVITY PROPAGATION DURING INFLATION	157
A.7 MATCHING SMALL-SCALES CONSTRAINTS ON THE TENSOR SPEED	159
A.8 INFLATON-WEYL COUPLING FUNCTION	160
B AXION COLD DARK MATTER	162
REFERENCES	173

LIST OF FIGURES

I.1	Degrees of freedom in the Early Universe	10
I.2	Time Evolution of Adiabatic Perturbations	31
I.3	Map of temperature anisotropies in the Cosmic Microwave Background	33
I.4	Map of the polarized Cosmic Microwave Background anisotropies	39
I.5	Angular power spectra of the Cosmic Microwave Background Radiation	40
I.6	Comparison between scalar and tensor contributions in the CMB angular spectra	43
I.7	The typical shape of an Inflationary Potential	48
I.8	Cosmological Constraints for Λ CDM (6 standard Parameters)	63
I.9	Cosmological Constraints for Λ CDM (Derived Parameters)	64
II.1	Cosmological Constraints for the Λ CDM + $\alpha_s + \beta_s$ cosmological model.	75
II.2	Cosmological Constraints for the Λ CDM + $r + \alpha_s$ cosmological model	77
II.3	Implications for slow-roll Inflationary models	83
II.4	Braking the power-law spectrum and the small scale constraints on the tensor tilt	86
II.5	Propagating speed of PGWs: Marginalized posteriors for the inflationary parameters	94
II.6	Propagating speed of PGWs: Marginalized posteriors for the Slow-Roll parameters	95
II.7	Propagating speed of PGWs: Consistency Relations	97
II.8	Propagating speed of PGWs: Constraints from small scales	98
II.9	Propagating speed of PGWs: combined Constraints from large and small scales	101
II.10	Higher-Curvature corrections: Tensor spectrum	104
II.11	Higher-Curvature Corrections: Marginalized posteriors	107
III.1	Axion-Gluon scattering: marginalized 2D and 1D posteriors.	123
III.2	Axion-Pion scattering: Marginalized 2D and 1D posteriors in the plane $(m_a, C_{a\pi})$	124
III.3	Axion limits in the plane $(m_a, g_{a\gamma})$	125
III.4	Fiducial BAO datasets employed in our forecasts	129
III.5	Marginalized 2D and 1D forested posteriors for cosmological parameters and hot relics	132
III.6	Forecasted 2D posteriors in the plane (m_a, Y_p^{BBN}) when the BBN predictions are assumed	134
III.7	Forecasted 2D posteriors in the plane (m_a, Y_p^{BBN}) when the BBN predictions are relaxed	135
A.1	Cosmological Constraints for the Λ CDM + $r + \Omega_k$ cosmological model	144
A.2	Cosmological Constraints the Λ CDM + $r + \alpha_s + \Omega_k$ cosmological model	145
A.3	The implications of a curved spacetime on Inflation.	148
A.4	$\Omega_{\text{GW}}(k)$ in the Starobinsky model	150
A.5	Particle Production during Inflation: Parameters	152
A.6	$\Omega_{\text{GW}}(k)$ in the particle production model	154
A.7	Superluminal Propagation	158
A.8	Extrapolating small scales constraints on the Tensor Speed	160
A.9	Tensor running for a generic Inflaton-Weyl coupling	161

LIST OF TABLES

I.1	Results for the Standard Model of Cosmology.	62
II.1	Parameter Priors for the analysis of Slow Roll Inflation	72
II.2	Results for the Λ CDM + $\alpha_s + \beta_s$ cosmological model	74
II.3	Results for the Λ CDM + $r + \alpha_s$ cosmological model	76
II.4	Propagating speed of PGWs: list of the parameter priors	93
II.5	Propagating speed of PGWs: cosmological constraints	93
II.6	Higher-Curvature Corrections: list of the parameter priors and cosmological constraints . . .	105
III.1	Parameter priors for the Thermal Axion Analyses	121
III.2	Cosmological Bounds on the Axion-Gluon thermalization channel.	122
III.3	Cosmological Bounds on the Axion-Pion thermalization channel.	122
III.4	Forecasted results for the Λ CDM + $m_a + \sum m_\nu$ cosmological model	131
III.5	Forecasted results for the Λ CDM + $m_a + \sum m_\nu + Y_p^{\text{BBN}}$ cosmological model	133
A.1	Results for the Λ CDM + $r + \Omega_k$ cosmological model	146
A.2	Results for the Λ CDM + $r + \alpha_s + \Omega_k$ cosmological model	147

CHAPTER I

THE EARLY UNIVERSE

In this chapter I review some of the major aspects of Physical Cosmology paying special attention to the physics of the Early Universe. I start pointing out the large-scale structure of the cosmological spacetime, discussing the dynamics and thermodynamics of the cosmic expansion and revisiting the main steps of the thermal evolution. Then I study the small-scale dynamics of primordial perturbations, highlighting their connections with the Cosmic Microwave Background Radiation and the implications for the theory of Cosmic inflation. Finally, I introduce the Standard Λ CDM Cosmological Model, reviewing the theoretical assumptions and the most recent observational constraints.

I.I HOT BIG BANG THEORY

Modern Cosmology is based on Einstein's Theory of General Relativity [8–10] (GR) which relates the space-time geometry and its dynamics to the matter-energy content and distribution. In this section we introduce and review the major aspects of the so-called Hot Big Bang Theory, *i.e.*, the predictive theory which, starting from first principles, is able to describe the large scale dynamics and the thermal evolution of our Universe.

I.I.I GEOMETRY

Despite the fact that our observable Universe is full of highly inhomogeneous structures such as stars, galaxies and galaxy clusters, the central premise of modern cosmology is that, *on large scales*, the Universe can be regarded as *homogeneous* and *isotropic*. Homogeneity and isotropy are physical requirements that imply symmetries. In modern physics symmetries are acquiring an increasing importance and in this chapter, as well as in the rest of this thesis, we will often follow approaches based on symmetries to derive our results.

Here we start discussing the spacetime geometry of maximally symmetric spaces. A D -dimensional space is said to be maximally symmetric if it has $1/2 D(D + 1)$ independent isometries¹. A first obvious consequence of isometries on the manifold is that the curvature is the same in every point in space and the Ricci scalar R is constant. Moreover, because of invariance under rotations and translations, the geometry must look the same in every direction constraining the Riemann tensor to be invariant under Lorentz transformations. Since by definition the Minkowski metric tensor is invariant under Lorentz transformations itself, we can write the Riemann curvature tensor in a local inertial frame as a combination of Lorentz invariant quantities. The only possible combination which preserves all the symmetries reads [10]:

$$R_{\alpha\beta\mu\nu} = \frac{R}{D(D-1)} (g_{\alpha\mu}g_{\beta\nu} - g_{\alpha\nu}g_{\beta\mu}), \quad R_{\beta\nu} = \left(\frac{R}{D}\right) g_{\beta\nu}. \quad (\text{I.1})$$

If we focus on $D = 4$ dimensions we see that the Einstein equations in the vacuum

$$R_{\mu\nu} - \frac{1}{2} g_{\mu\nu} R + \Lambda g_{\mu\nu} = 0, \quad (\text{I.2})$$

imply $R = \Lambda/4$ and, depending on R , we can classify three different maximally symmetric solutions [10, 11]:

- the **Minkowski spacetime** with vanishing curvature $R = 0$ (or $\Lambda = 0$),
- the **de Sitter spacetime** with positive curvature $R > 0$ (or $\Lambda > 0$),
- the **anti-de Sitter spacetime** with negative curvature $R < 0$ (or $\Lambda < 0$).

We will appreciate their importance in Modern Cosmology. Anyway, it is clear that, if we want to describe a realistic Universe, our cosmological spacetime cannot be maximally symmetric as this would imply invariance under time translation and the Universe would appear the same at each time. We are forced to reduce the degrees of symmetries requiring homogeneity and isotropy only on space. This request is often called *cosmological principle*.

It is well known that a spatially homogeneous and isotropic spacetime which evolves in time can be foliated into space-like slices [10, 11]. Therefore we can consider our spacetime to be described by a Manifold $\mathcal{M} = \mathbb{R} \times \Sigma$ where \mathbb{R} represents the time direction and where Σ is a 3-dimensional homogeneous and isotropic surface (*i.e.* a surface of a maximally symmetric 3-dimensional manifold). In our spacetime foliation we can choose the threading to be orthogonal to the slices which gives for the metric $g_{0i} = 0$.

¹We can think to \mathbb{R}^D : it is invariant under translations and rotations and so we have D isometries related to invariance under translation and $1/2 D(D - 1)$ isometries related to invariance under rotations giving a total number of $D + 1/2 D(D - 1) = 1/2 D(D + 1)$ isometries

Furthermore, thanks to homogeneity, time intervals among slices do not depend on the position and so we can choose a universal time coordinate t in such a way that $g_{00} = -1$. These coordinates are called *comoving coordinates*. Note that only a comoving observer (*i.e.*, an observer at rest in these coordinates) will see an isotropic Universe, while a non-comoving observer will see anisotropies due to the Doppler effect because a non-vanishing velocity in his frame breaks symmetry under rotations and introduces a preferred direction.

Introducing a function of time $R(t)$ (with the dimension of a length), in comoving coordinates, the metric reads:

$$ds^2 = -dt^2 + R^2(t) d\sigma^2, \quad (\text{I.3})$$

where $d\sigma^2$ is the metric of the 3-dimensional maximally symmetric slices Σ that we can write in full generality as

$$d\sigma^2 = -dt^2 + R^2(t) \left[\frac{dr^2}{1 - Kr^2} + r^2 d\Omega^2 \right]. \quad (\text{I.4})$$

where $d\Omega^2 = d\theta^2 + \sin^2\theta d\phi^2$ and $K \doteq R^{(3D)}/6$ with $R^{(3D)}$ the 3D-Ricci scalar on Σ . From equation (I.4) we see that one can absorb the physical size of the manifold into the factor $R(t)$ normalizing K in such a way that $K = \{+1, 0, -1\}$. Moreover using the fact that the metric is invariant under the following simultaneous set of transformations:

$$\begin{cases} R \rightarrow \lambda^{-1} R, \\ r \rightarrow \lambda r, \\ K \rightarrow \lambda^{-2} K. \end{cases} \quad (\text{I.5})$$

one can write

$$ds^2 = -dt^2 + a^2(t) \left[\frac{dr^2}{1 - \kappa r^2} + r^2 d\Omega^2 \right]. \quad (\text{I.6})$$

This is called Friedmann Robertson Walker (FRW) metric. The dimensionless time dependent function $a(t)$ is called *scale factor* and, with this normalization, the radial coordinate r has the dimension of a length. The quantity κ is related to the spatial curvature and now can take any value. We can distinguish three different cases:

- $\kappa > 0$ corresponding to a positive curved space (closed Universe);
- $\kappa = 0$ corresponding to a flat space (flat Universe);
- $\kappa < 0$ corresponding to a negative curved space (open Universe).

For our future discussion it is worth pointing out the causal structure of FRW spacetime. We recall that causality is defined by null geodesics $ds^2 = 0$ and, in an isotropic Universe, by the radial propagation of photons. It is easy to show that the FRW metric is conformally equivalent to the Minkowski metric. We recall that Conformal Transformations are a local metric re-scaling [11]:

$$\tilde{g}_{\mu\nu} = \Omega^2(x^\alpha) g_{\mu\nu}, \quad (\text{I.7})$$

with $\Omega(x^\alpha)$ a regular non-vanishing function defined on the whole Manifold. Clearly conformal transformations do not alter the causal structure as $d^2s = 0$ implies $d\tilde{s} = 0$. Using an important quantity called *Conformal time* defined as

$$\eta \doteq \int \frac{dt}{a(t)}. \quad (\text{I.8})$$

the conformal equivalence between (flat) FRW and Minkowski is trivially proved

$$ds^2 = a^2(\eta) \left[-d\eta^2 + \frac{dr^2}{1 - \kappa r^2} + r^2 d\Omega^2 \right]. \quad (\text{I.9})$$

I.I.II DYNAMICS

So far we used symmetries to find out an appropriate cosmological spacetime geometry. Here we discuss its large-scale dynamics. Modern cosmology is based on general relativity, and the Einstein's equations relate the FRW metric to the matter/energy content of the Universe. We recall the Einstein equations

$$R_{\mu\nu} - \frac{1}{2} g_{\mu\nu} R + \Lambda g_{\mu\nu} = 8\pi G T_{\mu\nu} \quad (\text{I.10})$$

where the stress-energy tensor $T_{\mu\nu}$ satisfies the local covariant conservation law

$$\nabla_\nu T^{\mu\nu} = 0. \quad (\text{I.11})$$

Notice also that in what follows we will consider the cosmological constant term $\Lambda g_{\mu\nu}$ in the Einstein equations as a component of the stress energy tensor. In cosmology matter and energy are commonly modeled as a perfect fluid where both viscosity and heat flow are assumed negligible. Within these assumptions the stress-Energy tensor takes the following form:

$$T_\nu^\mu = (\rho + P) u^\mu u_\nu + P \delta_\nu^\mu \quad (\text{I.12})$$

where ρ is the energy density, P is the pressure and u^μ is the fluid 4-velocity. Moreover, as we deal with extremely rarefied fluid, we can use a linear equation of state $P = \omega\rho$, with the dimensionless parameter ω such that $\omega = 0$ for matter, $\omega = \frac{1}{3}$ for radiation and $\omega = -1$ for the cosmological constant (we will prove this in what follows).

Finally, to solve the Einstein Equations, we need the Ricci tensor and the Ricci scalar for the FRW metric. After some calculations one can obtain what follows [9, 10].

- **Non zero Christoffel symbols for FRW metric**

$$\Gamma_{11}^0 = \frac{a \dot{a}}{1 - \kappa r^2} \quad (\text{I.13a})$$

$$\Gamma_{22}^0 = a \dot{a} r^2 \quad (\text{I.13b})$$

$$\Gamma_{33}^0 = \dot{a} a r^2 \sin^2 \theta \quad (\text{I.13c})$$

$$\Gamma_{01}^1 = \Gamma_{02}^2 \quad (\text{I.13d})$$

$$\Gamma_{22}^1 = -r(1 - \kappa r^2) \quad (\text{I.13e})$$

$$\Gamma_{11}^1 = \frac{\kappa r}{1 - \kappa r^2} \quad (\text{I.13f})$$

$$\Gamma_{33}^1 = -r(1 - \kappa r^2) \sin^2 \theta \quad (\text{I.13g})$$

$$\Gamma_{12}^2 = \Gamma_{13}^3 = \frac{1}{r} \quad (\text{I.13h})$$

$$\Gamma_{33}^2 = -\sin \theta \cos \theta \quad (\text{I.13i})$$

$$\Gamma_{03}^3 = \frac{\dot{a}}{a} \quad (\text{I.13j})$$

$$\Gamma_{23}^3 = \cot \theta \quad (\text{I.13k})$$

- **Non zero Ricci tensor's components for the FRW metric**

$$R_{00} = -3\frac{\ddot{a}}{a} \quad (\text{I.14a})$$

$$R_{11} = \frac{\ddot{a}a + 2\dot{a}^2 + 2\kappa}{1 - \kappa r^2} \quad (\text{I.14b})$$

$$R_{22} = r^2 (\ddot{a}a + 2\dot{a}^2 + 2\kappa) \quad (\text{I.14c})$$

$$R_{33} = r^2 (\ddot{a}a + 2\dot{a}^2 + 2\kappa) \sin^2 \theta \quad (\text{I.14d})$$

- **Ricci scalar for the FRW metric**

$$R = 6 \left[\frac{\ddot{a}}{a} + \left(\frac{\dot{a}}{a} \right)^2 + \frac{\kappa}{a^2} \right] \quad (\text{I.15})$$

We can now find out the equations of motions. A first important relation can be easily obtained using Eq. (I.11):

$$\dot{\rho} + 3\frac{\dot{a}}{a}(\rho + P) = 0. \quad (\text{I.16})$$

This is called *Continuity equation* and it holds for each component of the cosmic fluid which is uncoupled from the others. Sometimes it is said to be the analog of energy conservation for the spacetime motion, even though this is perhaps misleading since actually energy is not conserved during the cosmic expansion (we will prove this in what follows).

Because of symmetries, we can derive only two other independent relations that correspond to the components $(\mu, \nu) = (0, 0)$ and $(\mu, \nu) = (i, j)$ of the Einstein Equations. After a few simplifications, we obtain:

$$\left(\frac{\dot{a}}{a} \right)^2 = \frac{8\pi G}{3} \rho - \frac{\kappa}{a^2}, \quad (\text{I.17})$$

$$\frac{\ddot{a}}{a} = -\frac{4\pi G}{3}(\rho + 3p). \quad (\text{I.18})$$

Together they are known as *Friedmann equations*, but sometimes we will refer to Eq. (I.18) as "acceleration equation". At this point it is convenient to introduce the following quantities:

- **the Hubble parameter:**

$$H(t) \doteq \frac{\dot{a}}{a} \quad (\text{I.19})$$

- **the critical density:**

$$\rho_c(t) \doteq \frac{3H^2}{8\pi G} \quad (\text{I.20})$$

- **the density parameter:**

$$\Omega(t) \doteq \frac{\rho(t)}{\rho_c(t)} \quad (\text{I.21})$$

- **the curvature parameter:**

$$\Omega_\kappa(t) = 1 - \Omega(t). \quad (\text{I.22})$$

Notice that Eq. (I.17) can be easily written in terms of $H(t)$ and the curvature parameter as

$$\Omega_\kappa(t) = -\frac{\kappa}{(aH)^2} \quad (\text{I.23})$$

from which it follows that $\Omega_\kappa = 0$ corresponds to a spatially flat Universe while $\Omega_\kappa < 0$ and $\Omega_\kappa > 0$ correspond to a spatially closed and open Universe, respectively.

In what follows we will appreciate that different kinds of components such as baryons, photons, neutrinos, dark matter and dark energy can contribute to the energy density and the pressure in the cosmic fluid. Therefore ρ and P should be considered as the sum of all these different components

$$\rho(t) = \sum_i \rho_i(t), \quad P(t) = \sum_i P_i(t). \quad (\text{I.24})$$

Consequently, it is convenient to define a density parameter $\Omega_i(t) \doteq \rho_i(t)/\rho_c(t)$ for each component i , related to the density parameter $\Omega(t)$ and the curvature parameter $\Omega_\kappa(t)$ by

$$\Omega(t) = \sum_i \Omega_i(t), \quad \Omega(t) + \Omega_\kappa(t) = 1. \quad (\text{I.25})$$

To simplify the notation, from now on, when we refer to the density parameters evaluated *at the present time*, $t = t_0$, we drop the time-dependence in such a way that $\Omega_{i,\kappa}(t_0) \equiv \Omega_{i,\kappa}$. We also adopt the commonly used normalization $a(t = t_0) \doteq a_0 = 1$ and the notation $H_0 \doteq H(t = t_0) = \frac{\dot{a}_0}{a_0} = \dot{a}_0$ for the present day Hubble parameter. By noting that from the continuity equation we get $\rho \propto a^{-3(\omega+1)}$, the Friedmann equation (I.17) can be easily written in terms of present density parameters:

$$\left(\frac{H}{H_0}\right)^2 = \sum_i \Omega_i a^{-3(1+\omega_i)} + \Omega_\kappa a^{-2}. \quad (\text{I.26})$$

Notice that we could also describe curvature as another component of cosmic fluid with equation of state $\omega = -\frac{1}{3}$ writing down the more compact expression

$$\left(\frac{H}{H_0}\right)^2 = \sum_i \Omega_i a^{-3(1+\omega_i)} \quad (\text{I.27})$$

with

$$\omega_i = \begin{cases} 0; & \text{for Non relativistic Matter,} \\ \frac{1}{3}; & \text{for Radiation,} \\ -\frac{1}{3}; & \text{for Curvature,} \\ -1; & \text{for Cosmological constant.} \end{cases} \quad (\text{I.28})$$

It is also worth evaluating the behavior of the scale factor when the Universe is dominated by different component of the cosmic fluid. In the most relevant case of flat Universe (*i.e.*, $\kappa = 0$) an easy computation gives:

$$a(t) \propto \begin{cases} t^{\frac{2}{3(\omega+1)}} & \text{if } \omega \neq -1, \\ e^{Ht} & \text{if } \omega = -1. \end{cases} \quad (\text{I.29})$$

Therefore a (flat) Universe dominated by matter, radiation or cosmological constant expands with time. We may ask if such an expansion is accelerated or decelerated. This information can be derived by equation (I.18) from which we see that only components with $\omega < -\frac{1}{3}$ give positive acceleration. It follows that both matter and radiation give deceleration while the cosmological constant gives acceleration.

Cosmological Horizon

We conclude this subsection spending a few words on some causal Horizons for the FRW spacetime as they play a primary role in our subsequent discussions. Consider an observer which measures particles velocity in his frame at a given time. In an expanding Universe, the particle velocity can be obtained as

$$v = \frac{dx}{dt} = \frac{d}{dt} [a(t)r] = \dot{a}(t)r = H(t)a(t)r, \quad (\text{I.30})$$

where r is a comoving coordinate. We can define the Hubble Horizon as the boundary among particles that are moving slower and faster than light $v = c = 1$. We immediately see that this defines the so-called (Comoving) Hubble Radius

$$\text{Comoving Hubble Radius} \doteq (aH)^{-1}, \quad (\text{I.31a})$$

$$\text{Hubble Radius} \doteq H^{-1}. \quad (\text{I.31b})$$

If particles at the time t are separated by distances greater than the (comoving) Hubble radius they are not in causal contact at that time and they cannot talk to each other. In a Universe dominated by a fluid with equation of state ω , we have

$$(aH)^{-1} = H_0^{-1} a^{\frac{1}{2}(3\omega+1)} \quad (\text{I.32})$$

which means that the Hubble radius grows for each fluid with equation of state $\omega > -\frac{1}{3}$. Therefore, given a physical length λ corresponding to a wavenumber $k = 2\pi a/\lambda$ we see that λ is well outside or inside the Hubble radius if $k/(aH) \ll 1$ or $k/(aH) \gg 1$, respectively.

Since the age of the Universe and the light velocity have finite values, there is another horizon which represents the longest distance we can receive information from the past and defines the past observable Universe. Since light signals satisfy the geodesic equation $ds^2 = 0$, because of the homogeneity and isotropy, without loss of generality, we can focus on radial propagation to find that the maximum comoving distance that light can run between an initial time $t_i = 0$ and some later time t is given by the so called (comoving) Particle Horizon:

$$\text{Comoving Particle Horizon} \doteq \int_0^t \frac{dt'}{a(t')} \quad (\text{I.33a})$$

$$\text{Particle Horizon} \doteq a(t) \int_0^t \frac{dt'}{a(t')}. \quad (\text{I.33b})$$

If the (comoving) particle horizon is finite, it would naturally set the boundary between the visible Universe and that part of the Universe from which light has not reached us, yet. It is important to point out that we can write the (comoving) particle horizon in terms of the comoving Hubble radius $(aH)^{-1}$ as

$$\text{Comoving Particle Horizon} = \int_0^a d \ln(a) (aH)^{-1}, \quad (\text{I.34a})$$

$$\text{Particle Horizon} = a(t) \int_0^a d \ln(a') (aH)^{-1}. \quad (\text{I.34b})$$

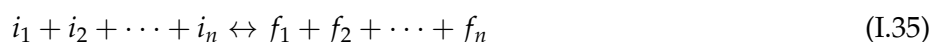
We see that also the comoving particle horizon grows for each fluid with equation of state $\omega > -\frac{1}{3}$.

I.I.III THERMODYNAMICS

We now collect the basic equations that describe the (equilibrium) thermodynamics in an expanding Universe. Then we review the most important steps of the thermal history, too.

Equilibrium Thermodynamics in the Expanding Universe

We start noting that the rate of interactions among particles in the Universe is often much higher than the expansion rate $H(t)$. Therefore the cosmic medium is in thermal equilibrium almost at any time of the cosmological history. For this reason it is useful to describe the equilibrium thermodynamics of a system with different particle species in terms of the chemical potential μ . Consider the reaction



where $\{i_j\}$ are the initial particles and $\{f_j\}$ are the final ones. In thermal equilibrium, we have:

$$\mu_{i_1} + \mu_{i_2} + \cdots + \mu_{i_n} = \mu_{f_1} + \mu_{f_2} + \cdots + \mu_{f_n}. \quad (\text{I.36})$$

Applying this relation to the process $e^-e^- \rightarrow e^-e^-\gamma$ we immediately see that the chemical potential of a photon is zero: $\mu_\gamma = 0$. Instead if we apply the relation (I.36) to the process $e^+ + e^- \leftrightarrow 2\gamma$, we see that $\mu_{e^+} = -\mu_{e^-}$. Generalizing, we can conclude that the chemical potential of a given particle is equal to the chemical potential of its antiparticle, but with the opposite sign. For much of the thermal history, we can ignore interaction energies among particles in such a way that the particle energy is simply given by

$$E = \sqrt{p^2 + m^2} \quad (\text{I.37})$$

where $p \equiv |\vec{p}|$ is the magnitude of the momentum. Furthermore, interactions among particles in cosmic plasma are often fairly weak and the equilibrium distributions of Bosons and Fermions spatial momenta p are well described by the Bose-Einstein and Fermi-Dirac distributions, respectively:

$$f(\mathbf{p}) = \frac{1}{(2\pi)^3} \frac{1}{e^{\frac{(E(\mathbf{p})-\mu)}{T}} \pm 1}. \quad (\text{I.38})$$

We recall that the sign $+$ corresponds the Fermi-Dirac distribution which describes the behavior of *fermions* while the sign $-$ corresponds to the Bose-Einstein distribution for *bosons*. Finally, neglecting the term ± 1 in the denominator, one obtains the classical Boltzmann distribution

$$f(\mathbf{p}) = \frac{1}{(2\pi)^3} e^{-\frac{(E(\mathbf{p})-\mu)}{T}} \quad (\text{I.39})$$

which can be adopted to describe a low density gas made of non-relativistic particles. From now on, in this subsection we refer to T as to the mean temperature of the Universe that can be approximated with the photon temperature $T \equiv T_\gamma$ since photons are the dominant specie. The number density n , the energy density ρ and the pressure P of a dilute gas of weakly interacting particles with g internal degrees of freedom can be written in terms of its phase-space distribution function $f(\mathbf{p})$ as [12–16]:

$$n = \frac{g}{(2\pi)^3} \int d^3p f(\mathbf{p}) \quad (\text{I.40a})$$

$$\rho = \frac{g}{(2\pi)^3} \int d^3p E(\mathbf{p}) f(\mathbf{p}) \quad (\text{I.40b})$$

$$P = \frac{g}{(2\pi)^3} \int d^3p \frac{|\mathbf{p}|^2}{3E(\mathbf{p})} f(\mathbf{p}) \quad (\text{I.40c})$$

Using that $E dE = |\mathbf{p}| d|\mathbf{p}|$ and neglecting the chemical potential at the thermal equilibrium we have

$$n = \frac{g}{2\pi^2} \int_m^\infty dE E \frac{(E^2 - m^2)^{1/2}}{\exp(E/T) \pm 1} \quad (\text{I.41a})$$

$$\rho = \frac{g}{2\pi^2} \int_m^\infty dE E^2 \frac{(E^2 - m^2)^{1/2}}{\exp(E/T) \pm 1} \quad (\text{I.41b})$$

$$P = \frac{g}{6\pi^2} \int_m^\infty dE \frac{(E^2 - m^2)^{3/2}}{\exp(E/T) \pm 1} \quad (\text{I.41c})$$

These relations can be studied distinguishing two interesting physical limits and discriminating whether particles are relativistic or not.

- In the *non-relativist limit*, the distribution function of a dilute gas of non-relativistic particles is described by the Boltzmann distribution (I.39). As a result, then number density is

$$n = g \left(\frac{mT}{2\pi} \right)^{3/2} e^{-\frac{\mu-m}{T}}, \tag{I.42}$$

while the energy density and pressure read

$$\rho = m n + \frac{3}{2} n T, \quad P = T n \ll \rho. \tag{I.43}$$

Therefore, up to corrections of order $\mathcal{O}(T/m)$, the equation of state of non relativistic matter is $P = 0 + \mathcal{O}(T/m)$ and we recover the result $\omega = 0$ anticipated before.

- In the *relativistic limit* $T \gg m$ the number density, the energy-density and the pressure instead reads:

$$n = \begin{cases} g \frac{\zeta(3)}{\pi^2} T^3 - \text{Bose} \\ \frac{3}{4} g \frac{\zeta(3)}{\pi^2} T^3 - \text{Fermi} \end{cases} \tag{I.44a}$$

$$\rho = \begin{cases} g \frac{\pi^2}{30} T^4 - \text{Bose} \\ \frac{7}{8} g \frac{\pi^2}{30} T^4 - \text{Fermi} \end{cases} \tag{I.44b}$$

$$P = \frac{\rho}{3} \tag{I.44c}$$

where $\zeta(3) \approx 1.2$. We see that for relativistic matter $\omega = 1/3$ as anticipated. Notice also that in the non-relativist case the energy density is exponentially smaller than in the relativist case. So the contribution of non-relativistic particle to total energy-density of a plasma made of both relativistic and non-relativist particles is essentially negligible.

In the case on many relativistic particles one can write

$$\rho_{\text{tot}} = 3P_{\text{tot}} = g_* \frac{\pi^2}{30} T^4 \tag{I.45}$$

where

$$g_*(T) = \sum_{\text{bosons}} g_i \left(\frac{T_i}{T} \right)^4 + \frac{7}{8} \sum_{\text{fermions}} g_i \left(\frac{T_i}{T} \right)^4 \tag{I.46}$$

counts the effective total number of relativistic degrees of freedom in the cosmic plasma as a function of temperature. Assuming the particle content expected in the standard model of elementary particles, we have that [12–18]

- for $T \gtrsim 100$ GeV all the standard model degrees of freedom (dof) are relativistic and we have $g_*^{\text{Boson}} = 28$ (2 dof for photons, 9 for W^\pm and Z_0 , 16 for gluons, 1 for Higgs) and $g_*^{\text{Fermion}} = 90$ (72 dof for quarks, 12 for charged leptons and 6 for neutrinos) so that $g_* = g_*^{\text{Boson}} + 7/8 g_*^{\text{Fermion}} = 106.75$;
- for $T \sim 30$ GeV the heaviest particles of the Standard Model, the top quarks which have 12 fermionic dof, are annihilated and we have $g_* = 106.75 - 7/8 \times 12 = 96.25$;
- for $T \sim 10$ GeV the Higgs boson (1 bosonic dof) and the gauge bosons W^\pm and Z_0 (9 bosonic dof) are annihilated and we have $g_* = 96.25 - 10 = 86.25$;

- for $10 \text{ GeV} \lesssim T \lesssim 160 \text{ MeV}$ we first have the bottom quarks annihilation (12 fermionic dof) which gives $g_* = 86.25 - 7/8 \times 12 = 75.75$, then we have the charm quarks (12 fermionic dof) and the tau leptons (4 fermionic dof) annihilation giving $g_* = 75.75 - 7/8 \times (12 + 4) = 61.75$.
- for $T \lesssim 160 \text{ MeV}$ we have the QCD phase transition and quarks combine with gluons into baryons (protons, neutrons, etc) and mesons (pions, etc). So, after the QCD phase transition there are many different species of baryons and mesons, but all except the pions are non-relativistic below the temperature of the QCD phase transition. Thus, the only relativistic species are pions (3 bosonic dof), electrons (4 fermionic dof), muons (4 fermionic dof), neutrinos (6 fermionic dof), and photons (2 bosonic dof) giving $g_* = 5 + 7/8 \times 14 = 17.25$
- for $T \sim 10 \text{ MeV}$ muons and pions annihilate giving $g_* = 17.25 - 3 - 7/8 \times 4 = 10.75$
- for $T \lesssim 0.5 \text{ MeV}$ finally electrons and positrons annihilate and the residual relativistic degrees of freedom today is made of photons (2 bosonic dof) and Neutrinos. Anyway the calculation of the residual relativistic degrees of freedom can be estimated only by entropy conservation since shortly after the neutrino decoupling, the electron positron heats photons and the neutrino decoupling is not instantaneous. A precise computation gives $g_* = 2 + 7/8 \times 2N_{\text{eff}} (4/11)^{4/3} = 3.36$ where $N_{\text{eff}} = 3.046$ is the *effective* number of relativistic species in the standard model (3 neutrino species and a further contribution of 0.046 which comes from the non-instantaneous neutrino decoupling).

We show the relativistic degrees of freedom in the Early Universe in [Figure I.1](#).

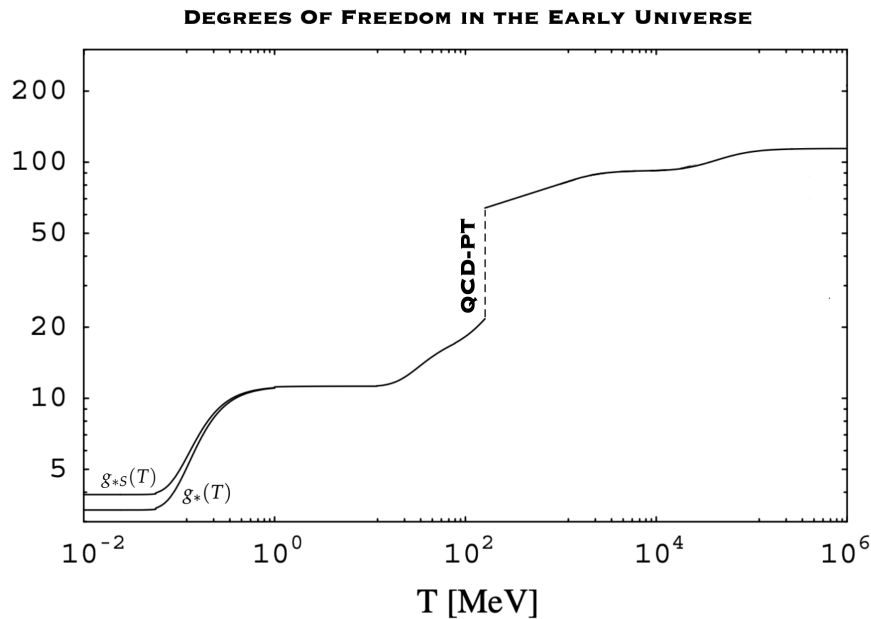


FIGURE I.1: Relativistic (entropic) degrees of freedom in the Early Universe as predicted by the Standard Model of elementary particles. Figure based on Ref. [17].

Geodesic motion in the Expanding Universe

Now we want to investigate in some details the physical consequences of the cosmic expansion for light propagation. Let us consider the geodesic equation

$$\frac{d^2 x^\alpha}{d\tau^2} + \Gamma_{\mu\nu}^\alpha \frac{dx^\mu}{d\tau} \frac{dx^\nu}{d\tau} = 0, \tag{I.47}$$

where by definition $dx^\alpha/d\tau = (E, \vec{p})$. Let us focus on the $\alpha = 0$ component of this equation, since, $\Gamma_{00}^0 = 0$, we have:

$$\frac{d^2x^0}{d\tau^2} + \Gamma_{ij}^0 \frac{dx^i}{d\tau} \frac{dx^j}{d\tau} = \frac{d^2x^0}{d\tau^2} + \Gamma_{ij}^0 p^i p^j = 0, \quad (\text{I.48})$$

In a flat Universe we have $\Gamma_{ij}^0 = \delta_{ij} \dot{a}a$ and so:

$$\frac{d^2x^0}{d\tau^2} + \dot{a}a \delta_{ij} p^i p^j = 0, \quad (\text{I.49})$$

Performing the following manipulation

$$\frac{d}{d\tau} = \frac{dx^0}{d\tau} \frac{d}{dx^0} = E \frac{d}{dt}, \quad (\text{I.50a})$$

$$\frac{d^2x^0}{d\tau^2} = \left(\frac{d}{d\tau} \right) \left(\frac{d}{d\tau} x^0 \right) = \left(E \frac{d}{dt} \right) \left(E \frac{dt}{dt} \right) = E \frac{dE}{dt} \quad (\text{I.50b})$$

equation (I.49) reads

$$E \frac{dE}{dt} + \dot{a}a \delta_{ij} p^i p^j = 0. \quad (\text{I.51})$$

The term $\dot{a}a \delta_{ij} p^i p^j$ can be estimated as follows. We remember that we are interested in photons and by definition we have $g_{\mu\nu} p^\mu p^\nu = 0$ and using a flat FRW metric we get $E^2 - a^2 \delta_{ij} p^i p^j = 0$ It follows that

$$a \delta_{ij} p^i p^j = \frac{E^2}{a}. \quad (\text{I.52})$$

Using Eq. (I.51) we finally obtain the equation for the Energy of a photon in an expanding (flat) Universe:

$$\frac{dE}{dt} + \left(\frac{\dot{a}}{a} \right) E = 0 \quad (\text{I.53})$$

It is easy to convince yourself by direct substitution that

$$E \propto 1/a \quad (\text{I.54})$$

is the solution of the equation (I.53). We have found a very important result: the energy of a photon decays as the Universe expands. That's why we claimed in the previous section that energy is not conserved during the cosmic expansion. Remembering that $E = \frac{hc}{\lambda}$, we find that $\lambda \propto a$ and so that the relation between the wave length $\lambda(t_e) \equiv \lambda_e$ of the emitted photon and the wave length $\lambda(t_o) \equiv \lambda_o$ of the observed photon is

$$\frac{\lambda_e}{\lambda_o} = \frac{a(t_e)}{a(t_o)} \quad (\text{I.55})$$

If we define the *redshift* as

$$z = \frac{\lambda_o - \lambda_e}{\lambda_e} \quad (\text{I.56})$$

we have:

$$z + 1 = \frac{a(t_o)}{a(t_e)}. \quad (\text{I.57})$$

This relation is usually written considering $t_o = \text{today}$ so that $a(t_o) = a_0 = 1$, so that relabeling $t_e \rightarrow t$ we find the relation between the redshift and the scale factor $a(t)$:

$$a(t) = \frac{1}{z+1} \quad (\text{I.58})$$

Entropy in the Expanding Universe

Entropy is an important thermodynamic characteristic of a system. In the general case of variable number of particles, the first law of thermodynamics reads

$$dE = TdS - PdV + \sum_i \mu_i dN_i \quad (\text{I.59})$$

where the subscript i labels the particle specie. In terms of the entropy density $s = S/V$, the number density $n = N/V$ and the energy density $\rho = E/V$, we can write

$$(Ts - P - \rho + \mu n)dV + (Tds - d\rho + \mu dn)V = 0. \quad (\text{I.60})$$

This relation is valid both for the entire system and for any of its parts. Focusing on a region of constant volume we obtain $Tds = d\rho - \mu dn$ that put in (I.60) gives for the whole volume:

$$s = \frac{P + \rho - \mu n}{T} \quad (\text{I.61})$$

Neglecting the chemical potential as usual, *in the relativistic case* we obtain:

$$s = \frac{P + \rho}{T} = \frac{4}{3} \frac{\rho}{T} = \begin{cases} g_S \frac{2\pi^2}{45} T^3 - \text{Bose} \\ \frac{7}{8} g_S \frac{2\pi^2}{45} T^3 - \text{Fermi} \end{cases} \quad (\text{I.62})$$

where g_S counts the entropic degree of freedom. In the case of many different relativistic species, the total entropy density is straightforward generalized to

$$s = \frac{2\pi^2}{45} g_{*S} T^3 \quad (\text{I.63})$$

where g_{*S} now counts the *total entropic degrees of freedom*:

$$g_{*S}(T) = \sum_{\text{bosons}} g_i \left(\frac{T_i}{T} \right)^3 + \frac{7}{8} \sum_{\text{fermions}} g_i \left(\frac{T_i}{T} \right)^3. \quad (\text{I.64})$$

For most of the story of the Universe all particles had the same temperature and before the neutrino freeze-out $g_{*S} = g_*$ while after the neutrino freeze-out, the present residual entropic degrees of freedom can be computed as $g_{*S} = 2 + 7/8 \times 2N_{\text{eff}} (4/11) \simeq 3.91$ [17], see also [Figure I.1](#).

Finally, notice that for any closed system we expect the entropy in a comoving volume to be conserved

$$\frac{dS}{dt} = \frac{d(a^3 s)}{dt} = 0 \quad (\text{I.65})$$

Using the relation (I.63), entropy conservation gives $(a^3 g_{*S} T^3) = \text{const}$ and so we find out that, in general during the expansion

$$T \propto g_{*S}^{-\frac{1}{3}} a^{-1} \quad (\text{I.66})$$

As long as $g_{*S} = \text{const}$, the usual inverse relation between the temperature and the scale factor $T \propto \frac{1}{a}$ is restored, as well. This means that as the Universe expands temperature decreases and so energy does.

As a matter of fact, the Early Universe was denser and warmer: going much back in time, we come to some epochs that cannot be directly probed by observations with current particle colliders. Instead we can use cosmology as a literally *unique* laboratory to test and constrain fundamental physics which is an important achievement of the subsequent discussion. Anyway, in what follows we give a brief overview of the different steps of the thermal evolution.

Phase Transitions

At high temperatures there are many epochs of interest, at least from a theoretical point of view, such as phase transitions [19–23]. Some theoretical hints suggest that at temperatures $T \gtrsim 10^{16}$ GeV, the fundamental forces (excluding gravity) can be described as unique *Grand force* with no distinction between strong, weak and electromagnetic interactions [24–27]. Anyway we don't know if these temperatures actually existed in the Universe, but, if so, we expect a first phase transition on GUT scales. Furthermore, we expect another phase transition at $T \gtrsim 100$ GeV from weak interactions. Indeed, before the electroweak phase transition, the Higgs condensate is absent, and the W^- and Z^- bosons have zero masses while at $T \sim 100$ GeV the electroweak symmetry is spontaneously broken and they acquire mass due to the Higgs mechanism [28–30]. Lastly, we expect another phase transition by strong interactions. The QCD phase transition is the transition from quark-gluon plasma to the hadronic matter. Its temperature is determined by the energy scale of strong interactions, about $T_{\text{QCD}} \lesssim 200$ MeV. For $T > T_{\text{QCD}}$, quarks and gluons behave as individual particles, while for $T \lesssim T_{\text{QCD}}$ they are confined in colorless bound states, hadrons [31–35]. The QCD phase transition will be a hot-topic in the last chapter of this work.

Neutrino Decoupling

Another important steps in the cosmic evolution is represented by the neutrinos decoupling. Neutrinos today contribute only to the radiation component of the total energy density of the Universe which is negligible small in the total balance. Anyway going back in time, the neutrino density becomes a crucial parameter for the Early Universe Cosmology. For example the neutrino number density plays a crucial role during the Big Bang Nucleosynthesis [36] as neutrinos affect the expansion rate and hence the cooling rate of the primordial plasma [37–41]. Here we want to give a roughly estimation of the temperature at which the interactions between neutrinos and the cosmic plasma switch off and estimate their relic number density today.

Neutrinos participate only to weak interactions since they have no charge. At energies of interest, the interactions cross sections are proportional to G_{F}^2 , where $G_{\text{F}} \simeq 1.17 \times 10^{-5}$ GeV⁻² is the Fermi constant. The relevant processes in the picture are (i) neutrino scattering off electrons or positrons; (ii) neutrino-antineutrino annihilation into electrons and (iii) positrons or neutrino-antineutrino annihilation into neutrino and antineutrino pairs of different types. At the temperature of interest all the particles involved are relativistic and all the cross section σ_v are $\sigma_v \sim G_{\text{F}}^2 E^2 \sim G_{\text{F}}^2 T^2$ where the energy E is a typical collision energy, $E \sim T$. The mean free time τ_v is given by $1/\tau_v = \langle n v \sigma_v \rangle$ where v is the relative velocity of neutrino and the colliding particle, n is the number density of the latter particles. Being all the particles involved relativist, we have $v \sim c \sim 1$ and $n \sim T^3$. This means

$$1/\tau_v \sim G_{\text{F}}^2 T^5. \quad (\text{I.67})$$

Using the Freedman relation (I.17) and the relativistic relation between temperature and energy-density, Eq. (I.45), one can relate the temperature to the Hubble parameter in a radiation dominated Universe as

$$H = \sqrt{\frac{4\pi^3}{45} g_*(T)} \left(\frac{T^2}{M_{\text{pl}}} \right), \quad (\text{I.68})$$

with $M_{\text{pl}} = 1/\sqrt{G}$ the Planck mass in natural units. As the Universe cools down, τ_v increases faster than $1/H$ and so, being the free time shorter than the Hubble time, neutrinos are in thermal equilibrium with

matter. One can estimate the number of neutrinos collisions since the time t as [15, 16]

$$N(t) \sim \int_t^\infty \frac{dt'}{\tau_\nu(t')} = \int_t^\infty \frac{dt'}{t'} \frac{t'}{\tau_\nu(t')} \sim \frac{t}{\tau_\nu(t)} \sim \frac{1}{H(t)\tau_\nu(t)} \quad (\text{I.69})$$

where we made use of the fact that in a radiation dominated era the Hubble parameter is $H(t) = 1/(2t)$. Therefore if $N(t) \gg 1$ neutrinos are in thermal equilibrium while when $N(t) \lesssim 1$ interactions switch off. We can therefore estimate the neutrinos decoupling temperature $T_{\nu,d}$ as the temperature when

$$\frac{1}{\tau_\nu(T_{\nu,d})} \sim H(T_{\nu,d}) \quad (\text{I.70})$$

obtaining that Neutrinos decouple at temperature $T_{\nu,d} \sim 2 - 3$ MeV and propagate freely through the Universe. Today relic neutrinos temperature can be estimated as

$$T_{\nu,d} = T_{\nu,0} \left(\frac{a(t_0)}{a(t_{\nu,d})} \right) = (1 + z_{\nu,d}) T_{\nu,0} \quad (\text{I.71})$$

where $t_{\nu,d}$ and $z_{\nu,d}$ are the time and the redshift at neutrino decoupling, respectively. The easiest way to compute the temperature of relic neutrinos is to associate it to the photon temperature. At the time of freeze-out, neutrino temperature equals that of photons but after neutrino decoupling their temperature starts decreasing with the expansion of the Universe. Instead photons are still in thermal equilibrium since they decouple later. When the temperature drops, because of the electron-positron annihilation $e^+ + e^- \rightarrow \gamma$, photons acquire energy and their temperature becomes higher than the effective neutrino temperature. This effect can be quantified using entropy conservation (in comoving volume): $g_*(T)a^3T^3 = \text{const}$. After the neutrinos decoupling, the plasma is basically made of relativistic electrons, positrons and photons. The total number of relativistic degrees of freedom therefore is given by $g_*(T_{\nu,d}) = 2 + 7/8 \times (2 + 2) = 11/2$. When all free electrons and positrons annihilate away because of electron-positron annihilation, the effective number of relativistic degrees of freedom will be all due to photons and therefore we have $g_*(T_0) = 2$. Applying entropy conservation it follows that

$$g_*(T_{\nu,d}) a(t_{\nu,d})^3 T_{\nu,d}^3 = g_*(T_0) a(t_0)^3 T_{\gamma,0}^3. \quad (\text{I.72})$$

Using Eq. (I.71) we can write $g_*(T_{\nu,d}) T_{\nu,0}^3 = g_*(T_0) T_{\gamma,0}^3$ from which it follows

$$\frac{T_{\nu,0}}{T_{\gamma,0}} = \left(\frac{g_*(T_0)}{g_*(T_{\nu,d})} \right)^{\frac{1}{3}} = \left(\frac{4}{11} \right)^{\frac{1}{3}} \quad (\text{I.73})$$

As we will see, the temperature of relic photons today is measured with great precision to be $T_{\gamma,0} \simeq 2.75$ K [42], implying for the relic neutrinos $T_{\nu,0} \simeq 1.95$ K and by Eq. (I.44a)

$$n_{\nu,0} = 2 \cdot \frac{3}{4} \frac{\zeta(3)}{\pi^2} T_{\nu,0}^3 \simeq 112 \text{ cm}^{-3} \quad (\text{I.74})$$

of the same order of the temperature and number density of photons, but, unfortunately, direct detection of relic neutrinos is very difficult from an experimental point of view.

Big Bang Nucleosynthesis

One of the most important step in the cosmological evolution is the Big Bang Nucleosynthesis (BBN) [36, 43–45]. The BBN is the period in the Early Universe during which the primordial light elements are formed. It starts at temperatures $T \lesssim 0.1$ MeV and finishes at temperature $T \sim 50$ KeV, corresponding to an epoch lasted from about 1 to 300 seconds after the Big Bang singularity. Most of the light nuclei formed in this

phase are helium-4 (the most tightly bound light nucleus) but there are also small amounts of deuterium, helium-3 and lithium-7. Notice that the binding energy of the elements are [15, 16]:

- D: binding energy $\simeq 2.2$ MeV
- ^3H : binding energy $\simeq 8.4$ MeV
- ^3He : binding energy $\simeq 7.7$ MeV
- ^4He : binding energy $\simeq 28.3$ MeV

A first question naturally arises: why does BBN start so late if the binding energies of primordial elements are so high? The answer is that, at higher temperatures, the elements that were forming are suddenly destroyed by scatterings with the CMB photons. Indeed, due to the huge number of photons per baryon (we recall that we have about 10^9 photons for each baryon) in the energy distribution tails there were still too many energetic free CMB photons that could hit and break the primordial elements as they were forming. However as the Universe cooled down, at $T \sim 0.1$ MeV, also light nuclei could form without being destroyed by photons. The computation of the abundance of the primordial nuclei, that makes use of General Relativity and the nuclear physics, predicts a given amount for each primordial specie and these predictions can be tested by observation even if with some efforts. Anyway, we can say that there is a good agreement between theory and observations and that BBN is one of the cornerstones of the Hot Big Bang Cosmology. Here we only briefly review this process.

We start considering the number density of protons and neutrons. Since BBN occurs at temperatures $T \sim 0.1$ MeV while the masses of protons and neutrons are $m_p \simeq 938.28\text{MeV}$ and $m_n \simeq 939.57\text{MeV}$ respectively, we can use the expression non relativistic limit (I.42) to obtain

$$n_n = g \left(\frac{m_B T}{2\pi} \right)^{3/2} \exp \left(\frac{\mu_n - m_n}{T} \right) \quad (\text{I.75})$$

$$n_p = g \left(\frac{m_B T}{2\pi} \right)^{3/2} \exp \left(\frac{\mu_p - m_p}{T} \right) \quad (\text{I.76})$$

where since $m_n \simeq m_p$ we have considered the difference in the neutron and proton masses only in the exponential but not in the overall factor where we have denoted $m_B \simeq m_p \simeq m_n$. Let now suppose that the particles 1 and 2 annihilate in order to form the particles 3 and 4. The generic particle has to satisfy the Boltzmann equation (that in what follows we write for the particle 1)

$$\begin{aligned} a^{-3} \frac{d(n_1 a^3)}{dt} = & \int \frac{d^3 p_1}{(2\pi)^3 2 E_1} \frac{d^3 p_2}{(2\pi)^3 2 E_2} \frac{d^3 p_3}{(2\pi)^3 2 E_3} \frac{d^3 p_4}{(2\pi)^3 2 E_4} \cdot \\ & \cdot (2\pi)^4 \delta^3(p_1 + p_2 - p_3 - p_4) \delta(E_1 + E_2 - E_3 - E_4) \cdot \\ & \cdot |\mathcal{M}|^2 \{f_3 f_4 [1 \pm f_1] [1 \pm f_2] - f_1 f_2 [1 \pm f_3] [1 \pm f_4]\} \end{aligned} \quad (\text{I.77})$$

where:

- $a^{-3} \frac{d(n_1 a^3)}{dt}$ is essentially the time variation of the specie n_1 (and would be 0 without interactions)
- the factors $1/2E_i$ come from the fact that we are integrating over all the momenta that satisfy the relation $E^2 = m^2 + p^2$
- f_1, f_2, f_3 and f_4 are the distribution functions of the different particles
- in $[1 \pm f_i]$, the sign depends on the species (+ for bosons and - for fermions)
- $\delta^3(p_1 + p_2 - p_3 - p_4)$ ensures the total momentum conservation
- $\delta(E_1 + E_2 - E_3 - E_4)$ ensures the total energy conservation

- \mathcal{M} is the scattering matrix that carries information about the physics of nuclear interaction

In the non relativistic limit we have that

$$f(E) \simeq e^{\frac{\mu-E}{T}} \quad (\text{I.78})$$

from which

$$\{f_3 f_4 [1 \pm f_1] [1 \pm f_2] - f_1 f_2 [1 \pm f_3] [1 \pm f_4]\} \simeq e^{-\frac{E_1+E_2}{T}} \left[e^{\frac{\mu_3+\mu_4}{T}} - e^{\frac{\mu_1+\mu_2}{T}} \right] \quad (\text{I.79})$$

Defining the number density in the non-relativistic limit evaluated at $\mu = 0$ as

$$n_{i,0} \doteq g_i \left(\frac{m_i T}{2\pi} \right)^{3/2} e^{-\frac{m_i}{T}} \quad (\text{I.80})$$

and the time averaged cross section as

$$\langle \sigma v \rangle \doteq \frac{(2\pi)^4}{n_{1,0} n_{2,0}} \int \frac{d^3 p_1}{(2\pi)^3 2 E_1} \frac{d^3 p_2}{(2\pi)^3 2 E_2} \frac{d^3 p_3}{(2\pi)^3 2 E_3} \frac{d^3 p_4}{(2\pi)^3 2 E_4} e^{-\frac{E_1+E_2}{T}} \cdot \delta^3(p_1 + p_2 - p_3 - p_4) \delta(E_1 + E_2 - E_3 - E_4) \cdot |\mathcal{M}|^2 \quad (\text{I.81})$$

with v the particle velocity, the Boltzmann equation (I.77) becomes:

$$a^{-3} \frac{d(n_1 a^3)}{dt} = n_{1,0} n_{2,0} \langle \sigma v \rangle \left[\frac{n_3 n_4}{n_{3,0} n_{4,0}} - \frac{n_1 n_2}{n_{1,0} n_{2,0}} \right] \quad (\text{I.82})$$

It is useful to study this equation in the limit of strong couplings. If we define the usual interaction rate $\Gamma \doteq n \langle \sigma v \rangle$ we know that particles are strongly coupled when $\Gamma(t) \gg H(t)$ and so they are essentially in thermal equilibrium. Expanding the derivative in the left side term

$$a^{-3} \frac{d(n_1 a^3)}{dt} = n_1 a^{-3} \frac{d a^3}{dt} = 3 n_1 \frac{\dot{a}}{a} \sim \mathcal{O}(H) \quad (\text{I.83})$$

and noting that $n_{1,0} n_{2,0} \langle \sigma v \rangle \sim \Gamma \gg H$, we see that Eq. (I.82) naturally implies

$$\left[\frac{n_3 n_4}{n_{3,0} n_{4,0}} - \frac{n_1 n_2}{n_{1,0} n_{2,0}} \right] \simeq 0 \quad (\text{I.84})$$

which is translated into

$$\mu_1 + \mu_2 \simeq \mu_3 + \mu_4. \quad (\text{I.85})$$

We recovered nothing but the result discussed at the beginning of this section: the chemical potential is conserved in thermal equilibrium. Let us suppose that nuclei of atomic mass A made of Z protons and $A - Z$ neutrons are formed by a reaction in the thermal equilibrium limit. Because of Eq. (I.85) (sometimes called Saha equation) we have

$$\mu_A = Z \mu_p + (A - Z) \mu_n. \quad (\text{I.86})$$

Defining the Binding energy as

$$B_A \doteq Z m_p + (A - Z) m_n - m_Z \quad (\text{I.87})$$

with m_Z the mass of the formed element, and reversing the Eqs. (I.75) and (I.76) we can write the number density n_A for the nuclei A as:

$$n_A = g_A 2^{-A} A^{\frac{3}{2}} \left(\frac{2\pi}{m_B T} \right)^{\frac{3(A-1)}{2}} n_p^Z n_n^{A-Z} e^{\frac{B_A}{T}}. \quad (\text{I.88})$$

We now introduce the so called mass function defined as $X_A \doteq A (n_A/n_B)$ where n_B is the Baryon number density and the baryon to photon ratio $\hat{\eta} = n_B/n_\gamma \simeq 10^{-9}$. We can easily write all the number density in

terms of these quantities as:

$$n_A = \hat{\eta} n_\gamma \frac{X_A}{A} \quad (\text{I.89a})$$

$$n_p = n_p X_p = \hat{\eta} n_\gamma X_p \quad (\text{I.89b})$$

$$n_n = n_n X_n = \hat{\eta} n_\gamma X_n \quad (\text{I.89c})$$

Using $n_\gamma = (2\zeta(3)/\pi^2) \times T^3$ we eventually find

$$X_A = f(A) \left(\frac{T}{m_B} \right)^{\frac{3(A-1)}{2}} \hat{\eta}^{A-1} X_p^Z X_n^{A-Z} e^{\frac{B_A}{T}} \quad (\text{I.90})$$

with

$$f(A) = g_A A^{\frac{5}{2}} \left[2^{\frac{3A-5}{2}} \pi^{\frac{1-A}{2}} \zeta(3)^{A-1} \right]. \quad (\text{I.91})$$

Notice that in the expression of X_A there is a term $\hat{\eta}^{A-1} \ll 1$ and to have an X_A of order one the exponential $e^{\frac{B_A}{T}}$ must be sufficiently large. This means that the temperature T must be sufficiently smaller than the binding energy B_A . This explains why the BBN starts at temperatures smaller than the binding energy of the primordial elements. For example, from Eq. (I.90) we can roughly estimate the temperature at which the mass function X_A becomes of order one to obtain

$$T = \begin{cases} 0.07 \text{ MeV} & \text{for D,} \\ 0.10 \text{ MeV} & \text{for } ^3\text{H,} \\ 0.11 \text{ MeV} & \text{for } ^3\text{He,} \\ 0.28 \text{ MeV} & \text{for } ^4\text{He.} \end{cases} \quad (\text{I.92})$$

We conclude this discussion, deriving an estimation of the abundance of primordial Helium. The agreement between the observation and the estimation is one of the most important success of cosmology. In our toy-model we assume thermal equilibrium and that all the neutrons produce only ^4He . This is clearly a strong approximation and extremely precise calculations can be done. Nevertheless, consider the following processes $\nu + n \longleftrightarrow p + e^-$ and $e^+ + n \longleftrightarrow p + \bar{\nu}$, where e^+ is the positron and $\bar{\nu}$ is some anti-neutrino. Because of the conservation of chemical potential (I.36) we have $\mu_n + \mu_\nu = \mu_p + \mu_e$ and $\mu_n - \mu_e = \mu_p - \mu_\nu$, where we have used that $\mu_{e^+} = -\mu_{e^-}$ and $\mu_{\bar{\nu}} = -\mu_\nu$. Combining the previous equations above: $\mu_n - \mu_p = \mu_e - \mu_\nu$. Using that $\mu_e \simeq \mu_\nu \simeq 0$ we find $\mu_p \simeq \mu_n$ which means:

$$\frac{n_n}{n_p} \simeq \frac{X_n}{X_p} = e^{-\frac{\Delta m}{T}} \quad (\text{I.93})$$

where $\Delta m = m_n - m_p \simeq 1.3 \text{ MeV}$. When $T \simeq 0.7 \text{ MeV}$ the ratio between neutron and proton freezes out at the value $n_n/n_p \simeq 1/6$. Nevertheless at temperature of the order of $T \sim 0.1 \text{ MeV}$, because of the β -decay the above mentioned ratio acquires a correction and it is estimated to be $1/7$. Assuming that all the neutrons form ^4He , we can estimate the abundance of the primordial helium to be

$$Y_p = \frac{4 \cdot n_n/2}{n_n + n_p} = \frac{2 \left(\frac{n_n}{n_p} \right)}{1 + \left(\frac{n_n}{n_p} \right)} \simeq 0.25 \quad (\text{I.94})$$

Therefore our approximate computation suggests a primordial abundance of Helium-4 of about 25%. This abundance, as well as the abundance of all the other primordial elements, today is computed with high

precision integrating the Boltzmann equations, as we show in the next sections and chapters². Moreover observations are in good agreement with the theoretical estimations (even if there are some tensions with ${}^7\text{Li}$) and the BBN represents one milestone in modern cosmology. We don't provide other details on the physics of the BBN, but we want only to discuss the following interesting aspect. Thanks to the observational constraints on the abundance of primordial elements, we are able to constrain with precision the total amount of Baryonic matter in our Universe to be $\Omega_b \simeq 0.05$. We also measure the total amount of matter in the Universe to be $\Omega_m \simeq 0.3$. This implies that most of the matter in the Universe is *not* made of Baryon and it is one of the major indirect evidences for Dark Matter.

Recombination

In the Early Universe there is full ionization as long as the temperature remains high compared to the hydrogen ionization energy [12, 13]. Matter is ionized and photons, strongly coupled to electrons through Compton scattering, are in thermal equilibrium with a black-body distribution of momenta. On the other hand, at lower temperatures the formation of neutral atoms is favored and the Compton scattering is no more an efficient process. Photons decouple from electrons giving a fossil radiation: the so called Cosmic Microwave Background (CMB). In order to visualize this fact, we define the optical depth

$$\tau(t) \doteq \sigma_T \int_t^{t_0} n_e(t) dt \quad (\text{I.95})$$

where σ_T is the Thomson scattering cross-section and $n_e(t)$ is the number density of free electrons at the cosmic time t . Notice that $n_e\sigma_T$ is the probability per unit time for a photon to scatter, so we can express the probability P that a CMB photon traveled freely since the time t in terms of the optical depth as

$$\frac{dP}{dt} = n_e(t) \sigma_T P = -\frac{d\tau}{dt} P, \quad (\text{I.96})$$

from which it follows $P(t) = e^{-\tau(t)}$. On the other hand, the probability that a photon scattered in the interval time between t and $t + dt$ travelling free since then is

$$g(t) \equiv \frac{dP}{dt} = -\frac{d\tau}{dt} e^{-\tau(t)} = n_e(t) \sigma_T e^{-\tau(t)}. \quad (\text{I.97})$$

The function $g(t)$, known as visibility function, can be thought also as a function of the redshift and so as the probability for a photon to be scattered between z and $z + dz$. From the recombination era on, $\tau \rightarrow 0$ because there are no free electrons, $n_e \rightarrow 0$. Therefore we expect the visibility function to be highly peaked. Its maximum can be estimated to be around $z \sim 1100$ and it defines the epoch when the CMB photons last scattered on electrons. After recombination, the Universe becomes transparent and photons can propagate in all directions freely. Given its importance for this work and in general for cosmology, we will dedicate the whole [section I.III](#) to the Cosmic Microwave Background Radiation.

I.II COSMOLOGICAL PERTURBATION THEORY

So far we studied the large-scale behavior of the Universe assuming Homogeneity and Isotropy. However on small scales the Universe is not so regular but highly inhomogeneous structures such as stars, galaxies, and galaxy clusters are formed by the gravitational collapse of primordial inhomogeneities. Indeed, the Early Universe was not perfectly homogeneous, but small irregularities $\delta T/T \sim 10^{-5}$ are observed in the temperature distribution of the Cosmic Microwave Background relic photons. Such irregularities are extremely small and therefore they can be analyzed in linear perturbation theory around a homogeneous

²For example, within the standard model of cosmology, a precise evaluation of primordial Helium abundance is $Y_p = 0.246721 \pm 0.000057$ at 68% CL (from BBN and Planck TT TE EE and lensing data), see also [Table I.1](#)

and isotropic background in such a way that the Einstein equations eventually reduce to a set of ordinary differential equations. In this section, our aim is to review the dynamics of primordial perturbations.

I.II.I SCALAR, VECTOR AND TENSOR PERTURBATIONS

Given a generic quantity $Q(t, \mathbf{x})$ we can split it into a homogeneous part and a spatially dependent perturbation: $Q(t, \mathbf{x}) = \tilde{Q}(t) + \delta Q(t, \mathbf{x})$. Since we are interested into perturbations around a FRW spacetime, we can use the background symmetries to classify perturbations into three different categories: *Scalar*, *Vector* and *Tensor*. We work in the Fourier space, defining the Fourier transform and anti-transform of a generic quantity as

$$\delta Q(t, \mathbf{k}) = \int d^3x \delta Q(t, \mathbf{x}) e^{-ik_i x^i}, \quad (\text{I.98a})$$

$$\delta Q(t, \mathbf{x}) = \int \frac{d^3k}{(2\pi)^3} \delta Q(t, \mathbf{k}) e^{ik_i x^i}. \quad (\text{I.98b})$$

We can classify perturbations using their *helicity*. Consider a rotation of the coordinate system around the wave-vector \mathbf{k} by an angle θ ; a perturbation is said to have helicity m if its amplitude is multiplied by $e^{im\theta}$ under rotation: $\delta Q(t, \mathbf{k}) \rightarrow e^{im\theta} \delta Q(t, \mathbf{k})$. So we define:

- **Scalar perturbations** those with helicity $m = 0$;
- **Vector perturbations** those with helicity $m = \pm 1$;
- **Tensor perturbations** those with helicity $m = \pm 2$.

We now show that these three kinds of perturbations evolve independently. Consider the linear time evolution of N perturbations δQ_n , with $n = \{1, \dots, N\}$ from a time t_1 to a time t_2 . Without loss of generalities we can write:

$$\delta Q_n(t_2, \mathbf{k}) = \sum_{\ell=1}^N \int d^3\tilde{\mathbf{k}} O_{n\ell}(t_1, t_2, \mathbf{k}, \tilde{\mathbf{k}}) \delta Q_\ell(t_1, \tilde{\mathbf{k}}), \quad (\text{I.99})$$

where $O_{n\ell}(t_1, t_2, \mathbf{k}, \tilde{\mathbf{k}})$ is an operator which gives the evolution and that in general can mix different \mathbf{k} -modes. Notice that it could be computed using the Einstein equations but here we do not need its exact expression. Indeed, symmetries are enough to find out how modes with different k and helicity evolve. In particular, we can use invariance under translations and rotations. We start considering the translation $x'^i = x^i + \alpha^i$. By equation (I.98a) we see that the relation between $\delta Q_n(t, \mathbf{k})$ and $\delta Q'_n(t, \mathbf{k})$ is

$$\delta Q'_n(t, \mathbf{k}) = \int d^3x \delta Q(t, \mathbf{x}) e^{-ik_i(x^i + \alpha^i)} = \delta Q_n(t, \mathbf{k}) e^{-ik_i \alpha^i} \quad (\text{I.100})$$

and using Eq. (I.99) we obtain

$$\delta Q'_n(t, \mathbf{k}) e^{ik_i \alpha^i} = \sum_{\ell=1}^N \int d^3\tilde{\mathbf{k}} O_{n\ell}(t_1, t_2, \mathbf{k}, \tilde{\mathbf{k}}) \delta Q'_\ell(t_1, \tilde{\mathbf{k}}) e^{i\tilde{\mathbf{k}}_i \alpha^i}. \quad (\text{I.101})$$

Thus the evolution equation (I.99) in the primed coordinate system reads

$$\delta Q'_n(t, \mathbf{k}) = \sum_{\ell=1}^N \int d^3\tilde{\mathbf{k}} O_{n\ell}(t_1, t_2, \mathbf{k}, \tilde{\mathbf{k}}) e^{i(\tilde{\mathbf{k}}_i - k_i) \alpha^i} \delta Q'_\ell(t_1, \tilde{\mathbf{k}}) \quad (\text{I.102})$$

$$\equiv \sum_{\ell=1}^N \int d^3\tilde{\mathbf{k}} O'_{n\ell}(t_1, t_2, \mathbf{k}, \tilde{\mathbf{k}}) \delta Q'_\ell(t_1, \tilde{\mathbf{k}}). \quad (\text{I.103})$$

Notice that because of invariance under translations the equation of motion must be the same in both the coordinate systems, $O_{n\ell} = O'_{n\ell}$ which implies

$$O_{n\ell}(t_1, t_2, \mathbf{k}, \tilde{\mathbf{k}}) e^{i(\tilde{k}_i - k_i)\alpha^i} = O_{n\ell}(t_1, t_2, \mathbf{k}, \tilde{\mathbf{k}}). \quad (\text{I.104})$$

This must hold for any α^i giving $\tilde{k}_i = k_i$. We found out that, because of translation invariance, Fourier modes with different wave-vector \mathbf{k} evolve independently.

We now consider a rotation around the wave-vector k by an angle θ . Perturbations transform as:

$$\delta Q'_n(t, \mathbf{k}) = e^{im\theta} \delta Q_n(t, \mathbf{k}), \quad (\text{I.105})$$

putting into (I.99) and remembering that Fourier modes with different wave-vector k evolve independently we get

$$\delta Q'_n(t, \mathbf{k}) e^{-im_n\theta} = \sum_{\ell=1}^N \int d^3k O_{n\ell}(t_1, t_2, \mathbf{k}) \delta Q'_\ell(t_1, \mathbf{k}) e^{-im_\ell\theta}, \quad (\text{I.106})$$

therefore

$$\delta Q'_n(t, \mathbf{k}) = \sum_{\ell=1}^N \int d^3k O_{n\ell}(t_1, t_2, \mathbf{k}) e^{-i(m_\ell - m_n)\theta} \delta Q'_\ell(t_1, \mathbf{k}) \quad (\text{I.107})$$

$$\equiv \sum_{\ell=1}^N \int d^3k O'_{n\ell}(t_1, t_2, \mathbf{k}) \delta Q'_\ell(t_1, \mathbf{k}). \quad (\text{I.108})$$

Again, because of invariance under rotations, the equation of motion must be the same in both the coordinate systems, $O_{n\ell} = O'_{n\ell}$ implying

$$O_{n\ell}(t_1, t_2, \mathbf{k}) = O_{n\ell}(t_1, t_2, \mathbf{k}) e^{-i(m_\ell - m_n)\theta}. \quad (\text{I.109})$$

This holds for any θ and the only way is that $m_n = m_\ell$. So, because of invariance under rotation, perturbations with different helicity m evolve independently: we can consider scalar tensor and vector perturbations as independent. With these results in mind, we can now write down the perturbed metric and Stress-energy tensor.

I.II.II LINEARIZED EINSTEIN EQUATIONS

We consider small perturbations to the background metric. The most general line element is [46–54]

$$ds^2 = -(1 + 2\Phi) dt^2 + 2a(t)B_i dx^i dt + a^2(t) [(1 - 2\Psi) \delta_{ij} + 2E_{ij}] dx^i dx^j, \quad (\text{I.110})$$

where

- Φ is a 3-scalar called *Lapse*;
- Ψ is a 3-scalar called *spatial curvature perturbation*;
- B_i is a 3-vector called *shift*;
- E_{ij} is a spatial symmetric and traceless 3-tensor called *shear*.

Due to the SVT decomposition we can write

$$B_i = \underbrace{\partial_i B}_{\text{Scalar}} - \underbrace{S_i}_{\text{Vector}}, \quad \text{and} \quad E_{ij} = \underbrace{2\partial_{ij} E}_{\text{Scalar}} + \underbrace{2\partial_{(i} F_{j)}}_{\text{Vector}} + \underbrace{h_{ij}}_{\text{Tensor}}, \quad (\text{I.111})$$

where we used the notation $t_{(\mu\nu)} \equiv \frac{1}{2}(t_{\mu\nu} + t_{\nu\mu})$. Notice that the vector perturbations must satisfy the transverse conditions $\partial^i S_i = 0 = \partial^i F_i$ while tensor perturbations are transverse and trace-less: $h_i^i = \partial^i h_{ij} = 0$.

As concerns the stress-energy tensor, while for a perfect fluid it can be described in terms of the energy density ρ , the pressure P and the 4-velocity u^μ , when we consider perturbations we may also need an *anisotropic stress tensor* $\Sigma^{\mu\nu}$. Energy density and pressure perturbations can be defined as [54]

$$\delta\rho(t, \mathbf{x}) = \rho(t, \mathbf{x}) - \tilde{\rho}(t), \quad \delta P(t, \mathbf{x}) = P(t, \mathbf{x}) - \tilde{P}(t). \quad (\text{I.112})$$

while for the perturbed metric (I.110), the perturbed 4-velocity reads

$$u_\mu = (-1 - \Phi, a(t)v_i), \quad (\text{I.113})$$

with v_i the velocity of the perturbations. The anisotropic stress is a first-order perturbation because it vanishes in the unperturbed case. It is defined to be orthogonal to the 4-velocity $u_\nu \Sigma^{\mu\nu} = 0$. This implies that only its spatial components are non-zero and that its trace is zero; *i.e.*, it is a symmetric traceless 3-tensor. The perturbed components of the Stress-Energy tensor are [54]

$$T_0^0 = -(\tilde{\rho} + \delta\rho), \quad (\text{I.114a})$$

$$T_i^0 = (\tilde{\rho} + \tilde{P}) a(t) v_i \doteq a \delta q_i, \quad (\text{I.114b})$$

$$T_0^i = -(\tilde{\rho} + \tilde{P}) \frac{v^i - B^i}{a(t)}, \quad (\text{I.114c})$$

$$T_j^i = (\tilde{P} + \delta P) \delta_j^i + \Sigma_j^i \quad (\text{I.114d})$$

where in equation (I.114b) we have defined the 3-momentum density $\delta q_i \doteq (\tilde{\rho} + \tilde{P}) v_i$. In a multi-component fluid the total stress-energy tensor is instead given by the sum of the different components: $T_{\mu\nu} = \sum_s T_{\mu\nu}^{(s)}$.

Gauge Freedom

Before going further, we need to stress an important aspect. Comoving coordinates define a privileged coordinate system in which the Universe appears to be homogeneous and isotropic. In any other coordinate system the Universe would not appear so regular. For example, in an unperturbed homogeneous and isotropic Universe, where the energy density is only a function of time $\rho = \rho(t)$, fictitious perturbations could appear as a consequence of a time coordinate transformation of type $\tilde{t} = t + \delta t(t, \mathbf{x})$. Indeed this transformation defines new slices of constant time \tilde{t} and in general the hypersurfaces of constant time \tilde{t} would have an inhomogeneous energy density $\tilde{\rho}(\tilde{t}(t, \mathbf{x}))$. Of course, we can reverse the process and say that, in an unperturbed Universe, requiring not to have fake irregularities defines a privileged coordinate choice (the comoving coordinates). Anyway, if we want to describe a perturbed Universe we must be careful because the split into homogeneous background and perturbations is not unique, but it depends on the coordinates and, because of irregularities, there is not a privileged coordinate system, anymore. We have the so-called *Gauge freedom*: when we chose a Gauge to define the slicing and threading of the spacetime we implicitly also define perturbations and fake perturbations could appear or real perturbations could disappear because of our Gauge choice. To say the truth, tensor perturbations are intrinsically *gauge-invariant*, but both scalar perturbations and vector perturbations are not. Even though Vector perturbations are not of interest for our purpose (they decay with the expansion of the Universe and above all are not naturally generated during inflation), the issue of gauge freedom is crucial for scalar perturbations and deserves to be clarified carefully.

To solve ambiguities between real and fake perturbations, it is useful to derive some Gauge independent combinations of perturbations. We start considering the gauge transformation given by $t \rightarrow t + \alpha$, and $x^i \rightarrow x^i + (\partial_j \beta) \delta^{ij}$; it is possible to show that scalar perturbations in the metric transform as [15, 16, 54]

$$\Phi \rightarrow \Phi - \dot{\alpha}, \quad (\text{I.115a})$$

$$\Psi \rightarrow \Psi + H \alpha, \quad (\text{I.115b})$$

$$B \rightarrow B + \frac{\alpha}{a(t)} - a(t) \dot{\beta}, \quad (\text{I.115c})$$

$$E \rightarrow E - \beta. \quad (\text{I.115d})$$

while perturbations in Stress-Energy perturbations transform as [15, 16, 54]

$$\delta\rho \rightarrow \delta\rho - \dot{\tilde{\rho}} \alpha, \quad (\text{I.116a})$$

$$\delta P \rightarrow \delta P - \dot{\tilde{P}} \alpha, \quad (\text{I.116b})$$

$$\delta q \rightarrow \delta q + (\tilde{\rho} + \tilde{P}) \alpha. \quad (\text{I.116c})$$

We decompose the pressure perturbation δP into an adiabatic part and an entropic part as [15, 16, 54]:

$$\delta P = \delta P_{\text{ad}} + \delta P_{\text{en}}, \quad (\text{I.117})$$

where:

$$\delta P_{\text{ad}} = \frac{\dot{\tilde{P}}}{\tilde{\rho}} \delta\rho, \quad (\text{I.118a})$$

$$\delta P_{\text{en}} = \delta P - \frac{\dot{\tilde{P}}}{\tilde{\rho}} \delta\rho. \quad (\text{I.118b})$$

Using equations (I.116a) and (I.116b) it is easy to show that the entropic part (I.118b) is Gauge independent. Two other important Gauge independent quantities are the *Bardeen potentials*:

$$\Phi_{\text{B}} \equiv \Phi - \frac{d}{dt} \left[a^2(t) \left(\dot{E} - \frac{B}{a(t)} \right) \right], \quad (\text{I.119})$$

$$\Psi_{\text{B}} \equiv \Psi + a^2(t) H \left(\dot{E} - \frac{B}{a(t)} \right). \quad (\text{I.120})$$

Moreover, combining the Stress-Energy perturbations with the metric perturbations we can find the following other important gauge invariant variables

- **The primordial curvature perturbation ζ :**

$$-\zeta \equiv \Psi + \frac{H}{\tilde{\rho}} \delta\rho. \quad (\text{I.121})$$

- **The comoving curvature perturbation \mathcal{R} :**

$$\mathcal{R} \equiv \Psi - \frac{H}{\tilde{\rho} + \tilde{P}} \delta q, \quad (\text{I.122})$$

Geometrically, ζ measures the spatial curvature of constant-density hypersurfaces (*i.e.*, the hypersurfaces on which $\rho = \text{const}$), while \mathcal{R} measures the curvature on comoving hypersurfaces. Using equations (I.115a)

- (I.116c) it is easy to check that both ζ and \mathcal{R} are Gauge independent. Furthermore the Einstein equations give a link between ζ and \mathcal{R} . Indeed it can be shown that

$$-\zeta = \mathcal{R} + \frac{k^2}{(aH)^2} \frac{2\tilde{\rho}}{3(\tilde{\rho} + \tilde{P})} \Psi_B. \quad (\text{I.123})$$

From which we see that on superhorizon scale ($k \ll aH$) we get

$$\zeta = -\mathcal{R}. \quad (\text{I.124})$$

Einstein equations for Scalar Perturbations

Einstein equations relate the Stress-Energy perturbations and the metric perturbations. Because of the SVT-Decomposition we can deal with Scalar, Vector and Tensor perturbations separately. Here, we are interested only in scalar and tensor modes. We start with scalar modes. The perturbed Einstein equations $\delta G_{\mu\nu} = 8\pi G \delta T_{\mu\nu}$ in the scalar case give the following equations (in the Fourier space):

$$3H(\dot{\Psi} + H\Phi) + \frac{k^2}{a^2} [\Psi + H(a^2(t)\dot{E} - a(t)B)] = -4\pi G \delta\rho, \quad (\text{I.125})$$

$$\dot{\Psi} + H\Phi = -4\pi G \delta q, \quad (\text{I.126})$$

$$\ddot{\Psi} + 3H\dot{\Psi} + H\dot{\Phi} + (3H^2 + 2\dot{H})\Phi = 4\pi G \left(\delta p - \frac{2}{3}k^2\delta\Sigma \right), \quad (\text{I.127})$$

$$\Psi_B - \Phi_B = 8\pi G a^2(t) \delta\Sigma. \quad (\text{I.128})$$

The Stress-Energy conservation law $\nabla_\nu T^{\mu\nu} = 0$ gives other two equations:

$$\delta\rho + 3H(\delta\rho + \delta P) = \frac{k^2}{a^2(t)}\delta q + (\tilde{\rho} + \tilde{P}) \left[3\dot{\Psi} + k^2 \left(\dot{E} + \frac{B}{a(t)} \right) \right], \quad (\text{I.129})$$

$$\delta q + 3H\delta q = -\delta P + \frac{2}{3}k^2\delta\Sigma - (\tilde{\rho} + \tilde{P})\Phi. \quad (\text{I.130})$$

A very interesting relation for our purpose is the Eq. (I.129). It can be written in terms of Gauge independent variables as

$$\dot{\zeta} = -H \frac{\delta P_{en}}{\tilde{\rho} + \tilde{P}} + \frac{H}{3} \frac{k^2}{(aH)^2} \left[\zeta - \Psi_B \left(1 - \frac{2\tilde{\rho}}{9(\tilde{\rho} + \tilde{P})} \frac{k^2}{(aH)^2} \right) \right] \quad (\text{I.131})$$

Einstein equations for Tensor Perturbations

As concerns tensor perturbations, they are intrinsically gauge-invariant at linear order. It is useful to introduce the eigenmodes of the spatial Laplacian $\nabla^2 e_{ij} = -k^2 e_{ij}$ so that we can decompose the tensor perturbations h_{ij} as $h_{ij}^{+, \times} = h(t) e_{ij}^{+, \times}$ where $+$ and \times denote the two possible polarization states of the gravitational waves. The evolution of gravitational waves in an expanding Universe can be described by Einstein equations that in the case of tensor perturbations reduce to only one equation. Assuming the anisotropic stress negligible this equation reads [12, 14, 15, 54]:

$$\ddot{h} + 3H\dot{h} + \frac{k^2}{a^2}h = 0. \quad (\text{I.132})$$

We will see that Gravitational waves can be sourced during inflation, but unfortunately they decay with the expansion of the Universe. Anyway their amplitude at the time of recombination might be large enough to leave a signature in the Cosmic Microwave Background B-modes spectrum on large angular scales and their detection can be regarded as one of the main goal on modern cosmology.

I.II.III DYNAMICS OF SCALAR PERTURBATIONS

Here we study the dynamics of cosmological perturbations using the linearized Theory developed in the previous subsection. More precisely, here we analyze the evolution of scalar perturbations before recombination while we discuss the dynamics of tensor perturbations in the next subsection. Notice that this is the period when CMB photons decouple from baryonic matter and perturbations at that epoch are directly related to CMB observations [12–16, 55]. Moreover, perturbations of dark matter and baryons at recombination provide the initial conditions for the subsequent evolution that leads to structure formation [15, 47, 49].

Single Ideal Fluid Approximation

Studying primordial perturbations is rather complicated from an analytic point of view, and so it is useful to start with the simplest case of single-component fluid approximation. This is of great interest because it can be used to describe perturbations in the component which dominates the background dynamics at a given cosmological epoch. Anyway then we also generalize our result for the multi-component case. In both cases we work in the framework of negligible anisotropic stress tensor ($\delta\Sigma \simeq 0$), assuming the cosmic fluid to be ideal. Notice that the cosmic medium is not always ideal and this assumption becomes particularly important for baryon-electron-photon plasma and neutrino components [12, 15]. However for our aim an ideal-fluid approximation is accurate enough.

Before recombination, the independent components in the cosmic fluid are baryon-electron-photon plasma, dark matter and neutrinos (while photons and baryons become two separate components only after recombination). We can write down the linearized Einstein equation (in the momentum representation) for a single ideal fluid by choosing a gauge. In what follows we work in the *Conformal Newtonian Gauge* defined by $E = B = 0$ and³

$$ds^2 = a^2(t) \left[-(1 + 2\Phi) d\eta^2 + (1 - 2\Psi) dx^i dx_i \right]. \quad (\text{I.133})$$

In this gauge Φ has the meaning of Newtonian gravitational potential while Ψ is the space curvature. Notice however that assuming an ideal fluid ($\delta\Sigma = 0$) for Eq.(I.128), it follows that $\Phi = \Psi$. In this case only two of Eqs. (I.125) - (I.130) are independent and, working in conformal time ($d\eta = a dt$), we can write [12, 56]

$$k^2\Phi + 3\frac{a'}{a}\Phi' + 3\frac{a'^2}{a^2}\Phi = -4\pi Ga^2\delta\rho \quad (\text{I.134a})$$

$$\Phi'' + 3\frac{a'}{a}\Phi' + \left(2\frac{a''}{a} - \frac{a'^2}{a^2}\right)\Phi = 4\pi Ga^2\delta P \quad (\text{I.134b})$$

where the prime represents a derivative with respect to the conformal time. Assuming an equation of state $\delta P = u_s^2 \delta\rho$ we can combine the two equations into a single master differential equation for the gravitational potential which reads

$$\Phi'' + 3\frac{a'}{a}(1 + u_s^2)\Phi' + \left[2\frac{a''}{a} - \frac{a'^2}{a^2}(1 - 3u_s^2)\right]\Phi + u_s^2 k^2\Phi = 0 \quad (\text{I.135})$$

³It is worth noting that quite often in literature the spatial curvature perturbation Ψ is defined with a different sign with respect to that adopted here in Eqs.(I.110) and (I.133). In that case the all the relations differ by an additional minus sign in front of Ψ (and its derivatives) and the relation between Ψ and Φ becomes $\Phi = -\Psi$, see also the [conventions](#).

Notice that using the second Freedman equation, the element in square brackets can be put in the form

$$2\frac{a''}{a} - \frac{a'^2}{a^2} (1 - 3u_s^2) = -8\pi G a^2 (P - u_s^2 \rho) = 0 \quad (\text{I.136})$$

where in the last line we assumed to consider the specie which dominates the cosmological expansion in such a way that $\omega = u_s^2$ (i.e., $P = u_s^2 \rho$). We can therefore simplify the master equation to

$$\Phi'' + 3\frac{a'}{a} (1 + u_s^2) \Phi' + u_s^2 k^2 \Phi = 0 \quad (\text{I.137})$$

To study the behavior of this equation, it is helpful to introduce the so-called *sound acoustic Horizon* as⁴

$$\text{sound acoustic Horizon} \doteq u_s H^{-1}. \quad (\text{I.138})$$

and the density contrast as

$$\delta \doteq \frac{\delta \rho}{\rho}. \quad (\text{I.139})$$

For perturbations with wavelengths well outside the *acoustic horizon*, $\lambda \gg u_s H^{-1}$, we see that the last term in Eq.(I.137) becomes negligibly small and we get the trivial solution $\Phi = \Phi_i = \text{Const}$. Therefore, on super-horizon scales ($k \ll a'/a$) we have

$$\delta = \delta_{(i)} = -2\Phi_{(i)} \quad (\text{I.140})$$

On the other hand, for sub-sound horizon modes, the solution of Eq.(I.137) depends strongly on the equation of state.

- For **Relativistic Matter** ($a \propto \eta$ and $\omega = u_s^2 = 1/3$) we have

$$\Phi(\eta) = -3\Phi_{(i)} \cdot \frac{1}{(u_s k \eta)^2} \left[\cos(u_s k \eta) - \frac{\sin(u_s k \eta)}{u_s k \eta} \right] \quad (\text{I.141})$$

and well inside the sound horizon ($u_s k \eta \gg 1$) it describes a wave with decaying amplitude and definite phase:

$$\Phi(\eta) = -3\Phi_{(i)} \frac{1}{(u_s k \eta)^2} \cos(u_s k \eta). \quad (\text{I.142})$$

The behavior of the energy-density perturbations $\delta \rho_{\text{rad}}$ can be obtained by using Eq.(I.134a), from which it follows that

$$\delta \rho_{\text{rad}}(\eta) = -\frac{1}{4\pi G} \frac{k^2}{a^2} \Phi(\eta) \quad (\text{I.143})$$

while using also the Freedman equations, we get

$$\delta_{\text{rad}}(\eta) = 6\Phi_{(i)} \cos(u_s k \eta) = -3\delta_{\text{rad},(i)} \cos(u_s k \eta) \quad (\text{I.144})$$

from which we easily see that energy density perturbations undergo acoustic oscillations and their amplitude nor decreases neither grows at radiation domination epoch.

- For **Non-Relativistic Matter** ($a \propto \eta^2$ and $\omega = u_s^2 = 0$) we get $\Phi(\eta) = \text{const}$ and the density perturbation reads

$$\delta \rho = -\frac{1}{4\pi G a^2} \left(k^2 + \frac{12}{\eta^2} \right) \Phi \quad (\text{I.145})$$

⁴Notice that the sound-horizon must not be confused with the causal cosmological horizon $(aH)^{-1}$. In what follows when we say "super/sub-horizon" modes, we always refer to modes outside/inside the *causal horizon*, while we always specify "sound" when we refer to the sound horizon.

On super-horizon scales ($k\eta \ll 1$) the second term in the round brackets dominates and we have $\delta\rho \propto a^{-3}$ which gives $\delta \doteq \delta\rho/\rho = -2\Phi$. Instead on sub-horizon scales ($k\eta \gg 1$) it is the first term which dominates resulting into $\delta \propto a(\eta)$. This means that matter perturbations start growing with the scale factor.

- For **Matter perturbations at late times** (*i.e.*, after the matter to cosmological constant transition) Eq.(I.136) is no longer valid and it is convenient to use Eq.(I.134b) which for a Λ dominated Universe with $\delta\rho_\Lambda = \delta P_\Lambda = 0$ and $a \propto e^{Ht}$ gives

$$\Phi'' - \frac{3}{\eta}\Phi' + \frac{3}{\eta^2}\Phi = 0. \quad (\text{I.146})$$

On sub-horizon scales, the solutions are $\Phi \propto \eta \propto 1/a$ and $\delta = \text{const.}$ It follows that matter perturbations stop growing when the cosmological constant dominates. Structure formation is over; forever.

Multi Component Ideal Fluid Approximation

In the real Universe, the cosmological fluid is composed of several components such as baryons, photons, neutrinos, dark matter and dark energy [12, 16, 56]. At late times, there is no interaction between the different species, except for the gravitational one. Anyway, it should be noted that gravitational interaction between the components affects perturbations in each of them and so in principle all the different species should be considered together. In this case the full set of linearized Einstein Equations is [14, 37, 56]

$$k^2\Phi + 3\frac{a'}{a}\Phi' + 3\frac{a'^2}{a^2}\Phi = -4\pi Ga^2 \sum_\lambda \delta\rho_\lambda \quad (\text{I.147a})$$

$$\Phi' + \frac{a'}{a}\Phi = -4\pi Ga^2 \sum_\lambda (\rho_\lambda + P_\lambda)v_\lambda \quad (\text{I.147b})$$

$$\Phi'' + 3\frac{a'}{a}\Phi' + \left(2\frac{a''}{a} - \frac{a'^2}{a^2}\right)\Phi = 4\pi Ga^2 \sum_\lambda \delta P_\lambda \quad (\text{I.147c})$$

while the covariant conservation law gives the following two relations

$$\delta\rho'_\lambda + 3\frac{a'}{a}(\delta\rho_\lambda + \delta P_\lambda) - (\rho_\lambda + P_\lambda)(k^2v_\lambda + 3\Phi') = 0 \quad (\text{I.148a})$$

$$[(\rho_\lambda + P_\lambda)v_\lambda]' + 4\frac{a'}{a}(\rho_\lambda + P_\lambda)v_\lambda + \delta P_\lambda + (\rho_\lambda + P_\lambda)\Phi = 0 \quad (\text{I.148b})$$

Here λ runs over the different species in the cosmic fluid. Notice that for an ideal fluid with n component the system above reduces to $2n + 3$ equations for $2n + 1$ unknowns ($P_\lambda = u_{s,\lambda}^2 \rho_\lambda$; v_λ and Φ) and so not all the equations are independent. As in the previous subsection it is helpful to use the density contrast $\delta_\lambda = \delta\rho_\lambda/\rho_\lambda$. Recalling that

$$\delta\rho_\lambda = \rho_\lambda\delta_\lambda, \quad \delta P_\lambda = u_{s,\lambda}^2\delta\rho_\lambda = u_{s,\lambda}^2\rho_\lambda\delta_\lambda, \quad P_\lambda = w_\lambda\rho_\lambda \quad (\text{I.149})$$

and noting that in this case $w_\lambda \neq u_{s,\lambda}^2$ and that in principle they can both depend on time, the covariant conservation laws Eqs.(I.148a) and (I.148b) read

$$\delta'_\lambda + 3\frac{a'}{a}(u_{s,\lambda}^2 - w_\lambda)\delta_\lambda - (1 + w_\lambda)k^2v_\lambda = 3(1 + w_\lambda)\Phi' \quad (\text{I.150a})$$

$$[(1 + w_\lambda)v_\lambda]' + \frac{a'}{a}(1 - 3w_\lambda)(1 + w_\lambda)v_\lambda + u_{s,\lambda}^2\delta_\lambda = -(1 + w_\lambda)\Phi. \quad (\text{I.150b})$$

Before going further we need to specify the initial conditions for perturbations. The initial conditions are typically specified well inside the radiation dominated epoch and, in linear perturbation theory, solutions will be linear in the initial conditions. Primordial perturbations can be decomposed into two different modes: *adiabatic* modes and *isocurvature* modes that behave in a fairly different way. While adiabatic perturbations are measured in the Cosmic Microwave Background, no evidences are currently found about the existence of isocurvature modes [57, 58] and so, in what follows, we define the differences between these two classes but then we focus exclusively on adiabatic modes.

There are many ways to define Adiabatic and Isocurvature perturbations. A common practice in literature [12, 13, 15, 50, 59] is to define *Adiabatic modes* those corresponding to the situation where, well inside the radiation dominated epoch, the relativistic matter has non-vanishing energy density perturbations (*i.e.*, space-dependent temperature fluctuations) and the composition of the cosmic fluid is assumed to be spatially homogeneous. Notice that, in the formal limit $\eta \rightarrow 0$ (which corresponds to consider the super-horizon regime) the adiabatic modes must therefore satisfy the following relation for the (conserved) number (density) of baryon and Cold Dark Matter per unit of entropy (density) [12, 15]:

$$\delta \left(\frac{n_b}{s} \right) = \delta \left(\frac{n_{CDM}}{s} \right) = 0 \quad (\text{I.151})$$

Conversely, *Isocurvature modes* are defined as those corresponding to the situation where, well inside the radiation dominated epoch, the relativistic matter has vanishing energy-density perturbations (*i.e.*, vanishing temperature fluctuations) but the composition of the cosmic fluid is spatially inhomogeneous. While these definitions capture the physical meaning of these two kinds of perturbations, it should be noted that they are not gauge invariant. Indeed, through a gauge transformation, we can *always* choose hypersurfaces of constant time where temperature is spatially homogeneous at each moment of time. The latter gauge anyway will be different from Newtonian gauge.

A more formal and gauge independent definition of adiabatic (and isotropic) perturbations can be obtained as follows. Let us consider the primordial curvature perturbation ζ which, by definition, is a gauge invariant quantity. In the super-horizon limit $k/(aH) \ll 1$, the equation of motion of ζ , Eq.(I.131), reduces to [50, 54, 55]

$$\dot{\zeta} \simeq -H \frac{\delta P_{en}}{\bar{\rho} + \bar{P}} \quad (\text{I.152})$$

where we recall that δP_{en} is the entropic part of perturbations. We define adiabatic perturbations those with $\delta P_{en} = 0$ and isocurvature perturbations those with $\delta P_{en} \neq 0$. Notice that this definition does not differ much from the previous one since we have already pointed out that when the cosmic fluid is assumed to be spatially homogeneous perturbations of entropy per baryon and entropy per dark matter are expected to vanish while when temperature perturbations are absent, but the cosmic fluid is inhomogeneous, we expect non-vanishing perturbations of entropy per baryon and entropy per dark matter particle, respectively. Since isocurvature modes are not of interest for this thesis, from now on we omit them from the discussion, focusing exclusively on adiabatic modes.

With the previous definition in mind, the initial condition for adiabatic perturbations can be derived straightforward. Indeed, we immediately see that for adiabatic modes on super-horizon scales ζ freezes out [12, 54, 55]:

$$\dot{\zeta} \rightarrow 0 \Rightarrow \zeta = \text{const.} \quad (\text{I.153})$$

Since in the Newtonian gauge (within the ideal fluid approximation) ζ reads

$$\zeta = -\Phi + \frac{\delta \rho_{\text{tot}}}{3(\rho_{\text{tot}} + P_{\text{tot}})} \quad (\text{I.154})$$

well inside the radiation dominated epoch, when the relativistic matter is widely the most important specie ($\rho_{\text{tot}} \simeq \rho_{\text{rad}} = 3P_{\text{rad}} \simeq 3P_{\text{tot}}$), we have

$$\zeta = -\Phi + \frac{1}{4} \frac{\delta\rho_{\text{rad}}}{\rho_{\text{rad}}} = -\Phi + \frac{1}{4} \delta_{\text{rad}} = -\frac{3}{2} \Phi \quad (\text{I.155})$$

where in the last line we used that, in the RD epoch and on super horizon scales the single fluid approximation holds giving $\delta_{\text{rad}} = -2\Phi$, see Eq. (I.140). Notice also that, if the cosmic fluid is spatially homogeneous, by definition the density contrast of all the relativistic species will be the same: $\delta_\gamma = \delta_\nu = \delta_{\text{rad}} = -2\Phi$. As concerns the density contrast of non-relativistic matter, it can be easily obtained by noting that $\rho_M \propto a^{-3}$ and $\rho_{\text{rad}} \propto a^{-4}$ from which it follows that $\delta_M \doteq \delta\rho_M/\rho_M = 3/4 \delta\rho_{\text{rad}}/\rho_{\text{rad}} \doteq 3/4 \delta_{\text{rad}}$. Given that for adiabatic perturbations the density contrast of all the non-relativistic species is the same as well ($\delta_b = \delta_{\text{CDM}} = \delta_M$), in the Radiation dominated epoch we finally get

$$\delta_{\text{CDM}} = \delta_b = \frac{3}{4} \delta_\gamma = \frac{3}{4} \delta_\nu = -\frac{3}{2} \Phi. \quad (\text{I.156})$$

This is exactly the equation that fixes the initial conditions for *each* component of the cosmic fluid. Notice that, this equation can be also expressed in term of the primordial curvature perturbation for each single specie, ζ_λ , defined as

$$\zeta_\lambda = -\Phi + \frac{\delta\rho_\lambda}{3(\rho_\lambda + P_\lambda)} = -\Phi + \frac{\delta_\lambda}{3(1 + \omega_\lambda)}. \quad (\text{I.157})$$

It easily follows that Eq. (I.156) is equivalent to set $\zeta_{\text{CDM}} = \zeta_b = \zeta_\gamma = \zeta_\nu = \zeta$. These relations provide an elegant formal definition of adiabatic perturbations. Now that the initial conditions for adiabatic perturbations have been pointed out, in principle we could solve the system of differential Equations to find out the small-scale dynamics of perturbations. Anyway, the evolution itself is fairly complex, and a general solution cannot be derived analytically. A complete precise analysis is therefore possible only adopting numerical methods. Notice also that a description of the effects beyond the ideal fluid approximation can be obtained by a system of Boltzmann equations that can be solved only numerically, as well. A full numerical treatment of the dynamics of primordial perturbations is beyond the aim of this section. In what follows we study only some interesting limits where an analytic description is possible.

The evolution of primordial perturbations depends on their wavelength. Adiabatic modes with large wavelength enter the *causal* horizon at matter domination (MD), while perturbations with small wavelength enter the *sound* horizon at radiation domination (RD). These two limits can be studied analytically within the ideal fluid approximation.

- **Large Wavelength Limit.** Modes with large wavelengths enter the causal horizon at the matter domination epoch. Therefore, during the radiation domination epoch, these modes are super-horizon. The super-horizon evolution of adiabatic modes is rather simple because, due to Eq. (I.131), they remain constant until they enter the causal horizon. After the horizon entry, during the MD epoch, relativistic matter gives very small contribution to the energy density of the Universe which we can assume to be negligible. Therefore the evolution of modes proceeds in analogy to the single component fluid approximation with the matter contrast δ_M growing linearly with the scale factor. On the other hand, we can study how the gravitational potential Φ changes between the RD and the MD epoch. Since super-horizon modes are frozen, at the matter domination, when perturbations in the non-relativistic matter already dominate, by Eq. (I.140) we have $\delta_M = -2\Phi_{\text{MD}}$ and by Eq.(I.154), (with $P_M = 0$) we can easily find out that $\zeta = -\Phi + 1/3\delta_M$ from which it follows that

$$\Phi_{\text{MD}} = -\frac{3}{5} \zeta \quad (\text{I.158})$$

Since ζ does not evolve on super-horizon scales it will be equal to its initial value, that, because of Eq.(I.155), is $\zeta = -3/2 \Phi_{\text{RD}}$. So we finally get

$$\Phi_{\text{MD}} = \left(\frac{9}{10}\right) \Phi_{\text{RD}}. \quad (\text{I.159})$$

For these modes the gravitational potential decreases by a factor of 9/10 at radiation-matter equality. Notice also that, because of Eq. (I.156), in the MD epoch we have

$$\delta_\gamma = \frac{4}{3}\delta_M = -\frac{8}{3}\Phi_{\text{MD}} = -\frac{12}{5}\Phi_{\text{RD}} \quad (\text{I.160})$$

- **Small Wavelength Limit.** We now study what happens when perturbations with small wavelengths enter the sound horizon during radiation domination. It is useful to distinguish perturbations in the *relativistic* component, perturbations in the *Dark Matter* component and perturbations in the *baryon-photon plasma*.

- Perturbations in the *Relativistic Component* dominate during the RD epoch and their evolution is well described by the single fluid approximation. They will therefore evolve according to Eq.(I.141) with the adiabatic initial condition $\Phi_{(i)} = -2/3 \zeta$.
- Perturbations in *Dark Matter* are subdominant during the RD epoch. Nevertheless here we highlight that they logarithmically grow during this period. This effect is crucial for structure formation since, without it, the growth of dark matter perturbations during the MD epoch would not be enough to produce $\delta_M \sim 1$. To find out the dynamics of CDM perturbations we can write down Eqs. (I.150a) and (I.150b) for the matter component in RD ($\omega_{\text{CDM}} = u_s^2 = 0$ and $a \propto \eta$), obtaining

$$\delta'_{\text{CDM}} - k^2 v_{\text{CDM}} = 3\Phi', \quad (\text{I.161a})$$

$$v'_{\text{CDM}} + \frac{1}{\eta} v_{\text{CDM}} = -\Phi, \quad (\text{I.161b})$$

We also recall that the evolution of gravitational potential Φ during the RD epoch is given by Eq.(I.141) and that it rapidly decays well inside the sound horizon, when $u_s k \eta \gg 1$. Therefore we can consider the homogeneous equations

$$\delta'_{\text{CDM}} - k^2 v_{\text{CDM}} = 0, \quad (\text{I.162a})$$

$$v'_{\text{CDM}} + \frac{1}{\eta} v_{\text{CDM}} = 0. \quad (\text{I.162b})$$

From Eq.(I.162b) we get $v_{\text{CDM}} = c_1 / (k^2 \eta)$ and inserting in Eq.(I.162a) it gives

$$\delta_{\text{CDM}} = c_1 \log k \eta + c_2 \quad (\text{I.163})$$

where c_1 and c_2 are integration constants that can be derived [15]. Anyway for our task it is enough to note that Dark Matter perturbation actually grows during the RD epoch. After the RD epoch, when matter becomes the dominant component in the Universe, its evolution is well described within the single fluid approximation and we have already pointed out that they linearly grow with the scale factor.

- Perturbations in the *Baryon-Photon plasma* are subdominant at the period from radiation-matter equality to recombination. Nonetheless they are extremely important from the point of view of Cosmic Microwave Background as they produce the so-called acoustic oscillations. First, notice that, due to intense photon-electron scatterings and Coulomb interaction between electrons and

baryons, the baryon-photon plasma can be regarded as a single ideal fluid. This is sometimes called tight-coupling limit. We can therefore assume that baryons and photons share then same velocities $v_\gamma = v_b \doteq v_{b\gamma}$. Furthermore the adiabatic initial conditions imply $\delta_\gamma = \delta_b$. In what follows we write Eq.(I.150a) for Baryon and photons separately obtaining

$$\delta'_b - k^2 v_{b\gamma} = 3\Phi' \quad \text{and} \quad \delta'_\gamma - \frac{4}{3}k^2 v_{b\gamma} = 4\Phi' \quad (\text{I.164})$$

respectively. On the other hand, it is useful to write Eq.(I.150a) in terms of δ_γ and a new variable

$$R_b(\eta) \doteq 3\rho_b/4\rho_\gamma \quad (\text{I.165})$$

getting

$$v'_{B\gamma} + \frac{a'}{a} \frac{R_B}{1+R_B} v_{B\gamma} + \frac{3}{4} u_s^2 \delta_\gamma + \Phi = 0, \quad (\text{I.166})$$

with the sound speed of the baryon-photon plasma $u_s^2(\eta)$ given by

$$u_s^2(\eta) = \frac{\delta P}{\delta \rho} = \frac{1}{3} \frac{\delta \rho_\gamma}{\delta \rho_\gamma + \delta \rho_b} = \frac{1}{3(1+R_b)}. \quad (\text{I.167})$$

We also define the *sound horizon* for a time-dependent sound speed as

$$\text{Sound Horizon} \doteq r_s(\eta) \doteq \int_0^\eta d\tilde{\eta} u_s(\eta) \quad (\text{I.168})$$

which is clearly a generalization of Eq.(I.138). By noting that for the sub-horizon modes (at matter domination) $\Phi' \ll k\Phi$ we can neglect derivatives in Φ and, combining Eqs.(I.164) into a single relation for δ_γ , we obtain

$$\delta''_\gamma + \frac{a'}{a} \left(\frac{R_b}{1+R_b} \right) \delta'_\gamma + k^2 u_s^2 \delta_\gamma = -\frac{4}{3} k^2 \Phi \quad (\text{I.169})$$

As we will see, this equation captures many features of the angular spectrum of CMB photons anisotropies [12, 15, 60]. Here, without the intention to be mathematically accurate, we only note that it describes acoustic oscillation in the baryon-photon component: its solution basically contains oscillating terms with a definite phase that are nothing but the generalization of the oscillations discussed in the single fluid approximation for the relativistic species. We will come back to this equation in the next section when we discuss the CMB anisotropies, providing a more quantitative discussion and highlighting they are of primary importance for the CMB angular spectrum.

We conclude this section with Figure I.2 which summarizes the evolution of Cosmological perturbations (and the gravitational potential Φ) both before and after recombination. Notice that here we just focused on their evolution before recombination as we are mainly interested in their signature in CMB. Anyway, after recombination, perturbations in the Baryon component, δ_b are importantly enhanced, $\delta_b = \delta_{CDM} \propto \eta^2$, and this is of primary relevance for the process of structure formation in the Universe [15, 47, 49].

III.IV DYNAMICS OF TENSOR PERTURBATIONS

Tensor Modes are of primary interest in this work: along with scalar perturbations, they can be sourced during inflation and their detection represents maybe one of the main goals of modern cosmology. In this subsection we describe the dynamical evolution of tensor perturbations.

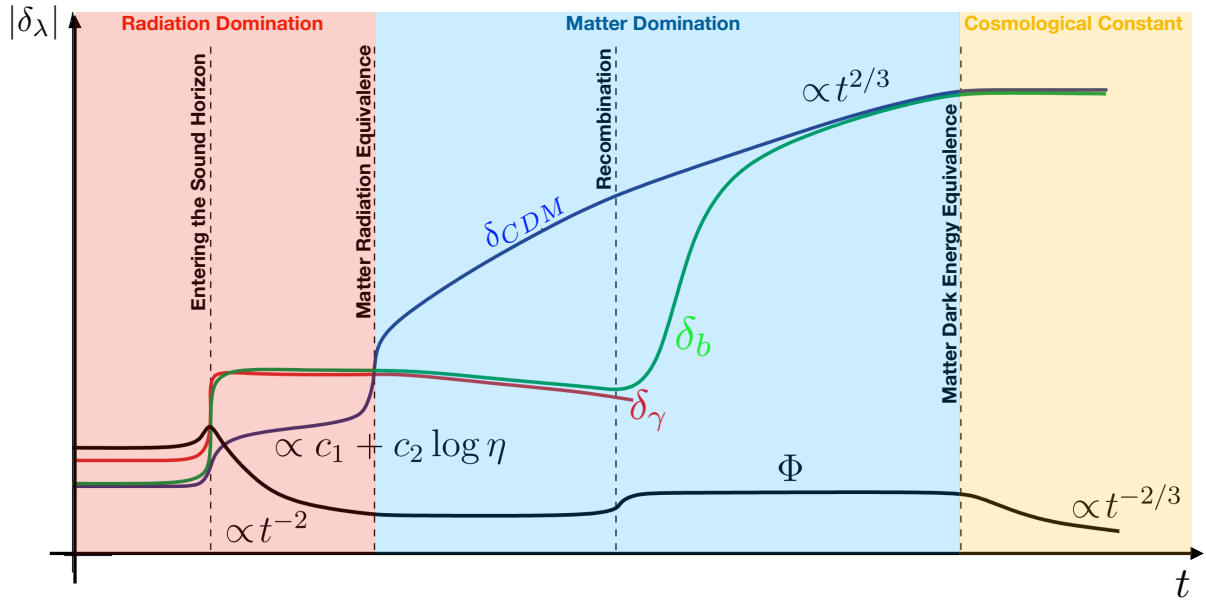


FIGURE I.2: Time evolution of adiabatic modes towards different cosmological epochs. Normalization is arbitrary. Figure based on Ref. [15].

We start recalling that the equation of motion of tensor modes is given by Eq.(I.132) which we can write in term of conformal time as

$$h'' + 2\frac{a'}{a}h' + k^2h = 0 \tag{I.170}$$

where for sake of simplicity we are dropping the two polarization states + and ×. As usual, we can identify two different cases: depending whether perturbations are super-horizon $k \ll a'/a$ or sub-horizon $k \gg a'/a$.

Super-Horizon Tensor Modes

When tensor modes are on super-horizon scales $k \ll a'/a$ or equivalently $k\eta \ll 1$, the equation of motion simply reduces to

$$h'' + 2\frac{a'}{a}h' = 0 \tag{I.171}$$

with the trivial solution $h = \text{const}$. Therefore on super-horizon scales tensor modes do not evolve at all.

Sub-Horizon Tensor Modes

To study the sub-horizon evolution, it is useful to write the equation of motion in term of the field $u(\eta) = a(\eta)h(\eta)$ getting

$$u'' + \left[k^2 - \frac{a''}{a} \right] u = 0 \tag{I.172}$$

this is often called *Mukhanov Equation* and we will study it extensively when we discuss the Quantum inflationary Fluctuations. Here we just note that the $a''/a \propto 1/\eta^2$ and on sub-horizon scales $k \gg a'/a$ or equivalently $k\eta \gg 1$ the equation is simplified to $u'' + k^2u = 0$ and we come to the oscillator equation. The general solution for $h(\eta)$ is

$$h(\eta) = \frac{A}{a(\eta)} \cos(k\eta + \alpha) \tag{I.173}$$

where A and α are the (conformal) time-independent amplitude and phase, respectively that can be obtained by fixing the initial conditions [15]. After the horizon crossing, tensor perturbations describe gravity waves whose amplitude decays with the cosmic expansion as $\propto 1/a(\eta)$.

I.III COSMIC MICROWAVE BACKGROUND RADIATION

The Cosmic Microwave Background represents maybe the most important observable in Cosmology. After recombination the Universe becomes transparent to photons and today the Universe is embedded into this fossil electromagnetic radiation that dates back to 380.000 years after the Big Bang singularity. This fossil radiation carries *unique* information about Primordial Universe and was first accidentally measured by Penzias and Wilson, awarded with Nobel Prize in Physics in 1978. They found a black-body thermal energy coming from all parts of the sky. We recall that the specific intensity of a gas of photons with a black-body spectrum is

$$I_\nu = \frac{4\pi\hbar\nu^3}{c^2} \left[e^{\frac{2\pi\hbar\nu}{k_b T}} - 1 \right]^{-1}. \quad (\text{I.174})$$

Today we measure the CMB black-body spectrum with unbelievable precision and the theoretical curve fixes the present day CMB photon temperature to $T = 2.7260 \pm 0.0013\text{K}$ [57, 61]. We also recall that as the Universe expands the temperature decreases as $T \propto 1/a$ and this is why today CMB photons are in the microwave frequency band.

Despite Cosmic Microwave Background radiation appears to be very homogeneous and isotropic; we observe small intrinsic temperature *anisotropies* and *polarization* that are crucial in our understanding of the underlying physics of the Early Universe. In what follows we point out their primary role in modern cosmology with particular attention to the link with the primordial perturbations.

I.III.I ANISOTROPIES

The physics of CMB anisotropies [60, 62–67] is well understood and described in terms of linear perturbation theory [14, 55]. The angular variations in temperature that we observe today, see Figure I.4, are a snapshot of the *local* properties of relic photons at redshift $z \sim 1100$ that must be related to primordial perturbations [12, 14, 55]. Therefore anisotropies encode information on the primordial perturbation itself. Here we first introduce the formalism used to describe CMB anisotropies and then we review the main physical processes that sourced them.

Multipoles Expansion and Angular Spectra

It is useful to define the so-called *brightness function*

$$\Theta(\eta, x, \hat{n}) \equiv \frac{\delta T(\eta, x, \hat{n})}{T(\eta)}, \quad (\text{I.175})$$

where $\hat{n} = \mathbf{p}/p$ is the unitary vector which defines the direction of the photon momentum; x is a given point of the space and η is the conformal time. It is somehow useful to define also the direction in which the photon is seen $\hat{e} = -\hat{n}$. Indeed the brightness function depends equivalently on \hat{n} or \hat{e} . Since the photons we observe today were emitted on a 3-sphere given by the intersection between the last scattering surface and our past light cone, it is natural to expand the bright function into spherical harmonics. The multipoles expansion reads [12, 55]

$$\Theta(\eta, x, \hat{n}) = \sum_{\ell \geq 1} \sum_m (-1)^\ell \Theta_{\ell m}(\eta, x) Y_{\ell m}(\hat{n}). \quad (\text{I.176})$$

where

$$Y_{\ell m} = \left[\frac{2\ell + 1}{4\pi} \frac{(\ell - m)!}{(\ell + m)!} \right]^{\frac{1}{2}} P_\ell^m(\cos \theta) e^{im\phi}. \quad (\text{I.177})$$

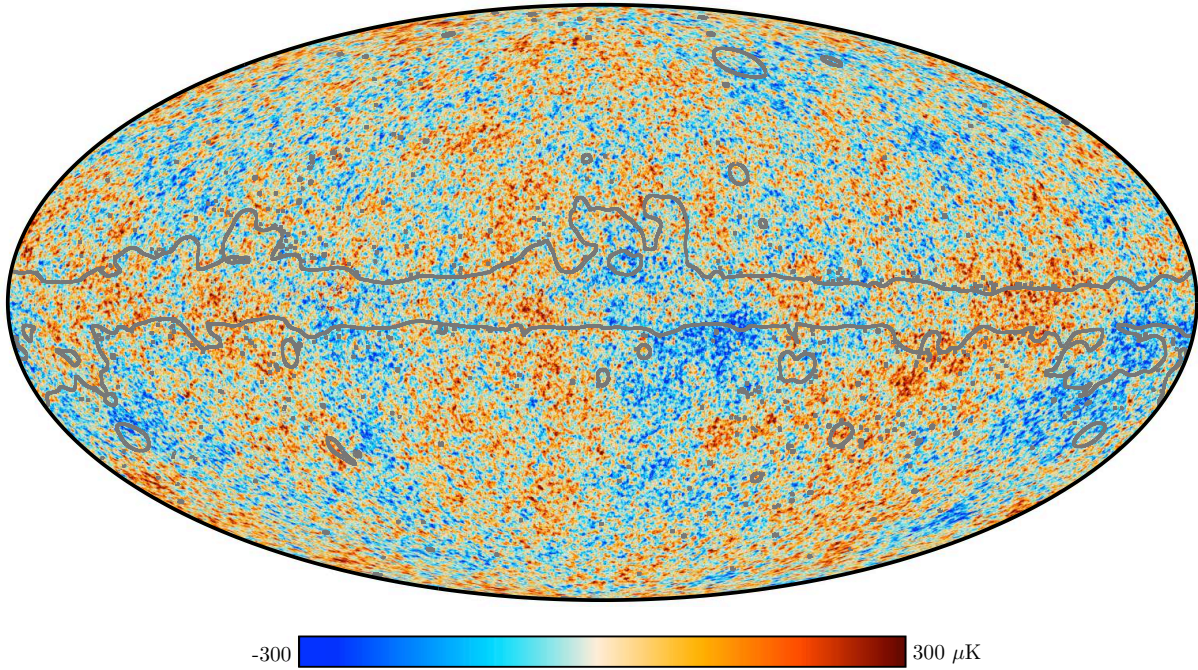


FIGURE I.3: The map of temperature anisotropies in the Cosmic Microwave Background as measured by the Planck Collaboration. Figure adopted from the Planck legacy archive [42].

are the spherical harmonics while θ and ϕ represent the usual spherical coordinates that identify the direction \hat{n} . $P_\ell^m(\cos \theta)$ are the associated Legendre functions

$$P_\ell^m(x) = (-1)^m \frac{(1-x^2)^{\frac{m}{2}}}{2^\ell \ell!} \frac{d^{\ell+m}}{dx^{\ell+m}} (1-x^2)^\ell. \quad (\text{I.178})$$

It is well known that the Spherical harmonics are a complete orthonormal set of functions which means that

$$\int Y_{\ell m} Y_{\ell' m'}^* d\Omega = \delta_{\ell\ell'} \delta_{mm'}. \quad (\text{I.179})$$

Notice also that in the equation (I.176) we can absorb the factor $(-1)^m$ into spherical harmonics using \hat{e} instead of \hat{n} :

$$\Theta(\eta, x, \hat{n}) = \sum_{\ell \geq 1} \sum_m \Theta_{\ell m}(\eta, x) Y_{\ell m}(\hat{e}). \quad (\text{I.180})$$

In the sum we do not consider the monopole contribution $\ell = 0$. The reason is that such term carries information about the energy of relic photons at different positions but we cannot measure CMB photons at positions different than ours and so we cannot measure this effect which is proportional to the photons energy fluctuations [55]. For this reason we start the spherical harmonics expansion considering the dipole contribution $\ell = 1$.

The dipole term, $\ell = 1$, in the sum is due to the doppler shift caused by the relative motion between the observer and the photons fluid. We stress that we are *not* comoving observers because we move by the Earth's motion. Therefore in our frame a dipole effect is expected and indeed observed. We can evaluate the Doppler shift to the first order in the relative photon velocity v_γ :

$$\sum_m \Theta_{1m}(\eta, x) Y_{1m}(\hat{e}) = -v_\gamma \cdot \hat{e}. \quad (\text{I.181})$$

While the CMB dipole is the dominant effect, it does not give any appreciable information about the intrinsic primordial temperature fluctuations and consequently should be removed from the map of CMB

anisotropies.

Multipoles with $\ell \geq 2$. In this case the effect of Earth motion on multipoles is proportional to $(v_\gamma)^\ell$ and so it becomes small as $v_\gamma \ll 1$. Multipoles with $\ell \geq 2$ show a small magnitude of order 10^{-5} , that cannot be brought back to the Earth motion effect since this is expected to be at least of order 10^{-6} for $\ell = 2$. Therefore multipoles with $\ell \geq 2$, while small, are a snapshot of the intrinsic anisotropies in the CMB radiation that are related to its underlying physical production and evolution. From now on, we call such terms $a_{\ell m}$:

$$a_{\ell m} \doteq \Theta_{\ell m}(\eta_0, x_0 = 0), \quad \text{for } \ell \geq 2. \quad (\text{I.182})$$

Here x_0 is our position chosen to be the origin of coordinates. We are interested in the stochastic properties of the CMB multipoles $a_{\ell m}$. We first note that invariance under rotations implies that $\langle a_{\ell m} \rangle = 0$ and that the two-point correlator therefore reads

$$\langle a_{\ell m} a_{\ell' m'}^* \rangle = C_\ell^{\text{TT}} \delta_{\ell \ell'} \delta_{m m'}, \quad (\text{I.183})$$

where $C_\ell^{\text{TT}} \doteq \langle |a_{\ell m}|^2 \rangle$ is the *angular power spectrum* of the CMB anisotropies. Given a model of the Early Universe, the angular power spectrum can be computed. It is an important tool in the statistical analysis of the CMB anisotropies as it describes the physical information contained in the million pixels of the CMB anisotropies in a very compact way. The angle brackets in the equation (I.183) denote the average over an ensemble of random fluctuations. For the moment we assume such fluctuations to be Gaussian. We will appreciate next how the simplest models of inflation predict Gaussianity at early times. We see that multipoles $a_{\ell m}$ are uncorrelated for different ℓ and m . If we assume gaussianity, they become also independent and the power spectrum provides a complete statistical description of the temperature anisotropies. For this reason measuring the anisotropies power spectrum has been one of the main goals of observational cosmology.

If we measured the temperature fluctuations over the full sky in an ideal situation of noise-free, the CMB power spectrum could be simply estimated as:

$$\hat{C}_\ell = \frac{1}{2\ell + 1} \sum_m |a_{\ell m}|^2. \quad (\text{I.184})$$

This gives for sure an estimator of the “true” angular power spectrum, but it must be noted that there is an irremovable cosmic variance, due to the finite $(2\ell + 1)$ modes that we can observe. In other words, assuming the temperature anisotropies to be Gaussian distributed, the estimator has a χ^2 distribution with $2\ell + 1$ degrees of freedom and a variance given by [12, 55]:

$$\text{var} [\hat{C}_\ell] \equiv \langle \hat{C}_\ell \hat{C}_\ell \rangle - \langle \hat{C}_\ell \rangle^2 = \frac{2}{(2\ell + 1)} C_\ell^2. \quad (\text{I.185})$$

The cosmic variance is negligible at higher ℓ while it becomes an important limitation at low multipoles. Furthermore, in practice estimating the power spectrum is complicated by a number of real-world complexities such as partial sky coverage and instrumental noise. Describing the experimental methods used to estimate the temperature power spectrum is beyond our aim and we remand to the vast literature dedicated. Here instead we would like to stress that, given a model of the Early Universe, the angular power spectrum can be computed using cosmological perturbation theory. One can write a system of coupled Einstein-Boltzmann equations that can be integrated numerically and predictions can be compared with observations. In Figure I.5 we show the angular spectra for temperature anisotropies (and polarization) as measured by the Planck Collaboration together with the best fit obtained with the standard Λ CDM model of cosmology. We see a remarkable agreement between theory and observations which provides one of the greatest successes of modern cosmology.

Primary Anisotropies

Temperature fluctuations in the CMB photons, as well as their measured power spectrum shown in Fig.(I.5), carry information about the Early Universe and can be sourced by interactions of the photons with other fields, such as gravity and density perturbations [12, 13, 15, 16, 38, 40, 46, 55, 60, 67]. Here we study anisotropies originated on the last scattering surface, before (or at least at) the time of recombination. Sometimes these are called *primary anisotropies* and are strongly linked with the primordial perturbations discussed in the previous section. In what follows we briefly review the main processes that generated them and their signature in the power spectrum.

There are basically three processes which contributed to primary anisotropies: (i) the Sachs-Wolfe effect due to the gravitational potential fluctuations on the last scattering surface [68], (ii) the intrinsic adiabatic fluctuations of the baryon-photon plasma [69] and lastly (iii) the Doppler effect due to the peculiar velocity of the different regions on the last scattering surface [70], for which photons emerging from regions that move in opposite (same) direction to the observer are red-shifted (blue-shifted). The total temperature fluctuations are simply given by the sum of the three contributions and so the measured mean squared temperature fluctuations are given by

$$\left\langle \left(\frac{\Delta T}{T} \right)^2 \right\rangle = (\Phi + \Theta)^2 + (\hat{n} \cdot \vec{v}_b)^2 \quad (\text{I.186})$$

Looking at Figure I.5, we can identify three different regions in the angular power spectrum:

- **The Sachs-Wolfe Plateau** on scales greater than the horizon at decoupling $2 \lesssim \ell \lesssim 100$. On such large scales the main contribution is due to fluctuations in the gravitational potential at recombination. In particular, depending on whether the fluctuations in the gravitational potential generate a potential well or a potential peak, photons are red-shifted and blue-shifted, respectively. The fluctuations in the photons temperature are simply given by

$$\left[\frac{\delta T}{T} \right]_{SW} = \frac{\delta \Phi}{\Phi} \quad (\text{I.187})$$

Also, due to the intrinsic adiabatic fluctuations in the baryon-photon plasma, photons diffused from over-dense regions ($\delta_b > 0$) will be hotter, while those coming from sub-dense regions ($\delta_b < 0$) will be colder. This is another primary isotropy which affects the same multipole range than the Sachs-Wolfe effect and in this case the fluctuations in the CMB Photons temperature are given by

$$\left[\frac{\delta T}{T} \right]_{\delta_b} = \frac{1}{3} \frac{\delta \rho_b}{\rho_b} = -\frac{2}{3} \frac{\delta \Phi}{\Phi} \quad (\text{I.188})$$

where we have used $\rho_b \propto 1/a^3 \propto T^3$ and in the last line we used the adiabatic conditions that relate fluctuations in the cosmic fluid to the gravitational potential. So, notice that this effect is opposed to the SW effect and the sum of the two effects is in favor of gravity.

- **Acoustic Peaks** at intermediate scales $100 \lesssim \ell \lesssim 1000$. In the previous section we saw that, during the matter dominated epoch, perturbations in baryon-photon plasma, falling in the gravitational potential, generate relativistic sound waves that propagate until recombination. These waves lead to the dramatic acoustic oscillations in the angular spectrum of CMB temperature anisotropies on scales between 0.1 and 2 angular degrees. As anticipated, these features are captured by Eq.(I.169) that, by noting that $\rho_\gamma \propto 1/a^4 \propto T^4$, we can easily write in term of $\Theta = \delta T/T$ as

$$\Theta'' + \frac{a'}{a} \left(\frac{R_b}{1 + R_b} \right) \Theta' + k^2 u_s^2 \Theta = -\frac{1}{3} k^2 \Phi. \quad (\text{I.189})$$

We recall that u_s is given by Eq.(I.167) and that we are ignoring the time variations of the potential (which is a good approximation since recombination happens during matter dominance when the potential is approximately constant, see also Figure I.2). To point out much of the physics underlying this equation, we can consider a simple toy model, getting rid of Θ' and writing

$$\Theta'' + k^2 u_s^2 \Theta = -\frac{1}{3} k^2 \Phi \quad (\text{I.190})$$

This is the equation of a simple harmonic oscillator with a constant gravitational forcing term. For adiabatic initial conditions $\Theta(0) = -2/3\Phi$ and $\Theta'(0) = 0$, the general solution is

$$\Theta(\eta, k) = \frac{1}{3} (1 + 3R_b) \Phi(k) \cos(kr_s) - (1 + R_b) \Phi(k) \quad (\text{I.191})$$

with r_s the sound horizon of the baryon-photon plasma, Eq.(I.168). We can use this simple solution to study some interesting limits. First, when photons dominate the cosmic fluid we can take the limit $R_b \rightarrow 0$ from which we see that (I.191) becomes the equation of motion of a harmonic oscillator with a zero-point displaced by gravity. This means that photons oscillate in and out the potential well and because of these oscillations after decoupling different modes will arrive in different phases of their evolution. Therefore there will be a set of discrete wave-numbers $\{k_n\} = n\pi/r_s(\eta_r)$ which will correspond to the oscillation peaks at recombination time ($\eta = \eta_r$). In other words a single scale k , which has done half-oscillation at recombination, is in the maximum compression in the potential wells and in the maximum rarefaction on the peaks. This scale would produce the highest $\delta T/T$, *i.e.*, the first peak of the CMB power spectrum. On the other hand, the scale corresponding to the half of the previous scale, has done a complete oscillation at recombination, and is in the maximum compression on the potential peaks, and in the maximum rarefaction in the wells. This latter scale corresponds to the second acoustic peak of the CMB power spectrum. Therefore, in practice, the odd acoustic peaks, of the CMB power spectrum, correspond to the maximum compression in the potential wells while the even acoustic peaks correspond to the maximum compression on the potential peaks. These are nothing but the peaks that we observe in the CMB angular spectrum. Anyway it should be noted that, without Baryons ($R_b = 0$), we would not have acoustic waves at all since the two contributions of density and velocity of the fluid would cancel each other. Therefore one has to consider also R_b and, from the general solution (I.191), we see that the displacement is further enhanced by Baryons. In other words, Baryons allow a greater compression of the fluid in the potential well and this is translated into an enhancements of all the peaks due to compression over those from rarefaction.

- **Dumping tail** on small scales $\ell \gtrsim 1000$. Due to photons diffusion, the temperature fluctuations are washed out. Indeed on those scales the ideal fluid approximation used to derive the dynamics of primordial perturbation breaks down and it can be shown that [12]

$$\Theta \propto e^{-k^2/k_D^2} \cos(kr_s). \quad (\text{I.192})$$

where k_D is also known as Silk damping scale [12, 13, 15]. It can be shown that a detailed calculation of the damping scale involving the quadruple moment in the Einstein-Boltzmann equations gives [12, 15]

$$k_D^{-2}(k) \doteq \int_0^\eta \frac{d\tilde{\eta}}{6(1+R_b)n_e\sigma_T a(\tilde{\eta})} \left[\frac{R_b^2}{1+R_b} + \frac{8}{9} \right] \quad (\text{I.193})$$

where n_e is the number of free electrons and σ_T the Thompson cross section.

Secondary Anisotropies

We refer to the anisotropies generated after recombination, when photons freely traveled from the last scattering surface to us, as *secondary anisotropies*. In what follows we review the main formation processes

- **(early and late) Integrated Sachs-Wolf Effect:** after decoupling, if the CMB photons cross a time-dependent gravitational potential, they will be red-shifted or blue-shifted depending on the variation in the potential. This is exactly what happened also before recombination with the SW effect, but with the difference that, instead of occurring on the last scattering surface, in this case the shift is integrated along the photon's path. Notice that if the Universe is matter dominated, at linear order in perturbation theory, the gravitational potential is constant and therefore the Integrated Sachs-Wolf (ISW) effect is zero. Anyway, in a realistic cosmological model the matter domination is not instantaneous and, for a short period after decoupling, the gravitational potential still slightly changes in (conformal) time. Furthermore, at late time, after the matter-dark energy equality, the gravitational potential starts changing again, see [Figure I.2](#). So, we can actually distinguish the *Early ISW*, that occurs shortly after decoupling, when matter does not completely dominate, and the *Late ISW*, that instead occurs quite recently, when dark energy starts dominating. The ISW leaves signatures in the CMB angular spectrum on multipoles $\ell \lesssim 200$.
- **Gravitational Weak Lensing:** on large scales the Universe is full of structures, such as galaxies, that can both produce secondary anisotropies and distort primary anisotropies through the so called gravitational lensing. Consider a pair of photons that move towards the observer forming at the beginning an angle θ between their directions of propagation. Due to the lensing effect the observer will see instead an angle $\theta + \delta\theta$. The distortion of light is typically of a few arcmins and the result is the smearing of the oscillations of the CMB angular power spectrum at small scales [[12](#), [15](#), [71](#)].
- **Sunyaev-Zel'dovich Effect:** this effect is due to the inverse Compton scattering between low energy CMB photons and high energy free electrons in the hot ionized gas in a cluster of galaxies. This effect produces two distinct signatures: first, photons, crossing the cluster, are scattered by the random motion of free electrons, deforming the black body spectrum and leading to a reduction (increment) in temperature at the low (high) frequencies. Second, because of the peculiar velocity of the hot ionized gas in galaxies, CMB photons will be red-shifted or blue-shifted for the Doppler effect [[12](#), [15](#), [70](#), [72](#)].
- **Reionization:** at late times, the Universe reionized again and CMB photons scattered off free electrons, reaching the observer from a different direction with respect to the initial one. While the physical nature of reionization is still discussed, its signature on the CMB angular spectrum can be observed, giving a decrease of the power in the spectra on multipoles $\ell \gtrsim 10$ that are reduced by a factor $e^{-2\tau}$ where τ is the optical depth defined as [[12](#), [16](#)]

$$\tau \doteq \int_{\eta_{\text{reion}}}^{\eta_0} d\tilde{\eta} n_e \sigma_T a \quad (\text{I.194})$$

While reionization suppresses the peaks amplitude in the temperature anisotropies spectrum, these effects are completely degenerate with other cosmological parameters. On the other hand, the reionization signal dominates the position and the height of the peaks in the polarization spectra at multipoles $\ell \lesssim 10$. Therefore it is worth noting that the constraints on τ come basically from polarization and not from anisotropies.

- **Relic Gravity Waves:** tensor perturbations that enter the horizon after recombination in general contribute to the C_ℓ^{TT} and so produce temperature anisotropies. Here we briefly show that the contribution of primordial gravity waves to CMB anisotropies is extremely small. It is useful to relate the mode with wave-vector k at the time η to the primordial amplitude defining the so-called transfer function $\mathfrak{h}(k, \eta)$ as

$$h(\eta, k) = \mathfrak{h}(k, \eta) \cdot h_i(k) \quad (\text{I.195})$$

where $h_i(k)$ is the primordial amplitude. We have shown that after the horizon re-entry, tensor perturbations behave as gravitational waves which decay with the expansion of the Universe. It can be shown that their contribution to the C_ℓ is given by [15]

$${}^{\text{GW}}C_\ell^{\text{TT}} = \frac{9\pi}{2} \frac{(l+2)!}{(l-2)!} \int_0^\infty \frac{dk}{k} \mathcal{P}_T(k) \cdot \left(\int_{\eta_r}^{\eta_0} d\eta \frac{\partial h(k, \eta)}{\partial \eta} \frac{j_l[(\eta_0 - \eta)k]}{(\eta_0 - \eta)^2 k^2} \right)^2 \quad (\text{I.196})$$

where $\mathcal{P}_T(k)$ is the primordial spectrum of tensor perturbations predicted by inflation (that we will introduce in the next section and will be the central topic of the next chapter) and j_l are the spherical Bessel function. This integral depends basically on (the parametrization of) the primordial spectrum and (derivative of) the transfer function. We will see that the simplest inflationary scenarios predict a basically flat tensor spectrum, while the term inside the round brackets gives non-negligible contributions only on scales $k(\eta_0 - \eta) \sim \ell$ and $k\eta \sim 1$. In this regime the spherical Bessel functions behave as $j_l[(\eta_0 - \eta)k] \sim \ell^{-1}$ and so the integrals behave as $\sim (\ell^{-3})^2 \sim \ell^{-6}$. Since the overall factor grows as ℓ^4 and we finally get

$${}^{\text{GW}}C_\ell^{\text{TT}} \propto \ell^{-2}. \quad (\text{I.197})$$

Gravity waves contribution decays very rapidly on multipoles $\ell \gtrsim 100$ because in that case tensor modes enter the horizon before recombination. On multipoles $2 \lesssim \ell \lesssim 50$ they instead behave similar to the SW effect, but in any case, also on such large angular scales, their contribution is always subdominant because the primordial amplitude of tensor modes is at least 100 times smaller than the amplitude of scalar modes, see also Figure I.6 where we compare the scalar and tensor contribution in the different angular spectra. Fortunately a more promising approach for the detection of primordial tensor modes can be obtained by searching their signatures in the B-modes polarization. We would like to conclude with a final remark: the parametrization of the primordial spectrum, plays an important role in deriving this result. As a matter of fact, if during inflation the power spectrum is sufficiently "blue" (*i.e.*, the gravity wave production is amplified at large k) the contribution of short waves is enhanced, and hence ${}^{\text{GW}}C_\ell^{\text{TT}}$ may not be so small at large ℓ . We will discuss some of these models in the next chapter.

I.III.II POLARIZATION

The temperature anisotropies originated from primordial fluctuations, are polarized by the Thomson scattering [71, 73–75]. Recombination was not an instantaneous process: while protons and electrons were combining into neutral hydrogen, the photons developed a quadrupole anisotropy that was converted into CMB polarization by the Thomson scattering. A combined analysis of polarization and anisotropies allows us to evaluate the consistency of the standard cosmological model: measuring the CMB polarization increases the accuracy the cosmological parameters are measured with. Moreover, the search for B-modes in the CMB polarization is one of the target of observational cosmology as they are related to the inflationary production of gravitational waves on super-horizon scale which is a unique prediction of inflation theory. Therefore it is worth recalling the classic theory of polarized electromagnetic radiation.

Consider a plane wave coming from the positive direction of the z axis:

$$E(t) = \frac{1}{2} \left[\mathbf{E} e^{i\omega t} + \mathbf{E}^* e^{-i\omega t} \right], \quad (\text{I.198})$$

the amplitude \mathbf{E} can be decomposed into its (x, y) components as $E_\phi = E_x \cos \phi + E_y \sin \phi$. Defining the unpolarized intensity I

$$I \equiv \overline{|E_x|^2} + \overline{|E_y|^2}, \quad (\text{I.199})$$

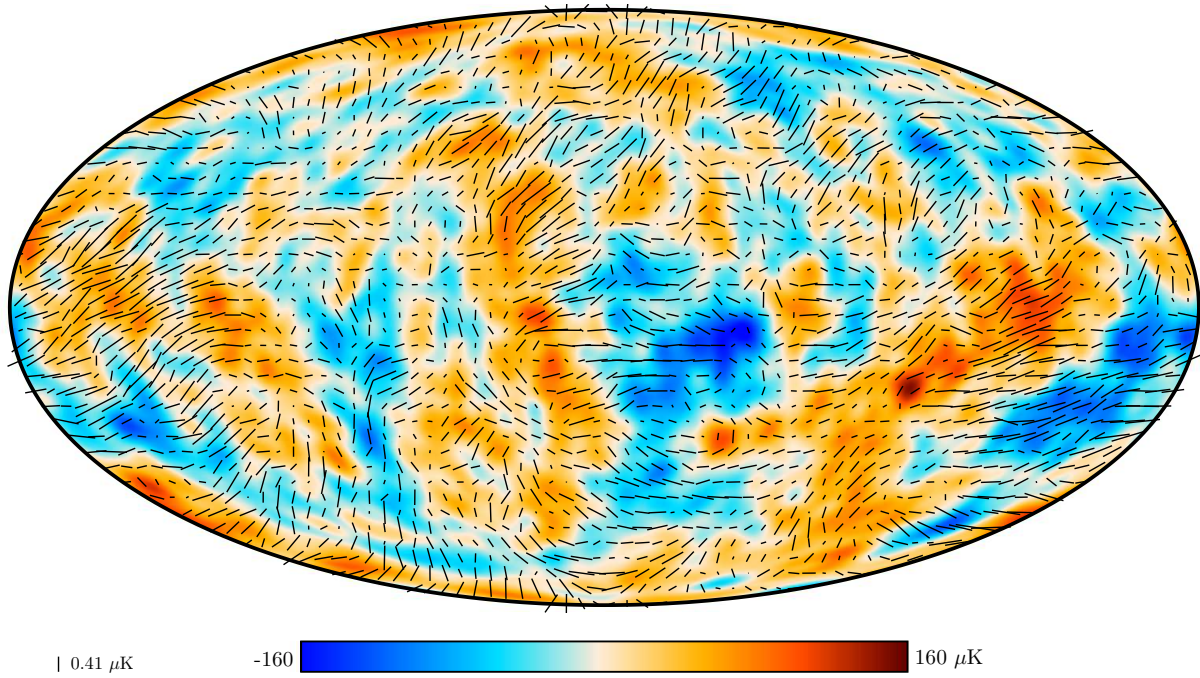


FIGURE I.4: The map of polarized Cosmic Microwave Background anisotropies as measured by the Planck Collaboration. Figure adopted from the Planck legacy archive [42].

and the **Stokes parameters** $\{Q, U, V\}$

$$Q \equiv \overline{|E_x|^2} - \overline{|E_y|^2}, \tag{I.200a}$$

$$U \equiv 2 \operatorname{Re} [\overline{E_x^* E_y}], \tag{I.200b}$$

$$V \equiv 2 \operatorname{Im} [\overline{E_x^* E_y}] \tag{I.200c}$$

one obtains

$$\overline{|E_\phi^2|} = I + Q \cos 2\phi + U \sin 2\phi. \tag{I.201}$$

We recall that Q and U are two Stokes parameters that specify the polarization plane, while V is a third Stokes parameter that measures the intensity of circular polarization. If we perform a rotation around the axis z of an angle φ so that $\phi \rightarrow \phi + \varphi$ clearly $\overline{|E_\phi^2|}$ must not change. This implies that under rotation the Stokes parameters (Q, U) change as [55]

$$\begin{pmatrix} Q \\ U \end{pmatrix} \rightarrow \begin{pmatrix} \cos 2\varphi & -\sin 2\varphi \\ \sin 2\varphi & \cos 2\varphi \end{pmatrix} \begin{pmatrix} Q \\ U \end{pmatrix}. \tag{I.202}$$

Using the combination $Q_\pm \equiv Q \pm iU$ we find a more compact expression:

$$Q_\pm \rightarrow e^{\pm 2i\varphi} Q_\pm \tag{I.203}$$

which implies the existence of a preferred direction, *i.e.*, the direction in which the Stokes parameter U vanishes. Therefore, because of the assumption of spatial isotropy, in an unperturbed Universe the Stokes parameters must be all null. Anyway in our Universe small deviations from homogeneity and isotropy are observed as well as a map of polarized CMB anisotropies, see **Figure I.4**. To understand why, we can consider a toy model where a photon travels in the direction of an incident single free electron. In a frame in which the electron is located at the origin, the electron itself will oscillate with a displacement $r(t)$ and with an acceleration $\ddot{r} = -\frac{e}{m_e} E(t)$. This will induce a dipole momentum $d(t) = -er(t)$ and a corresponding

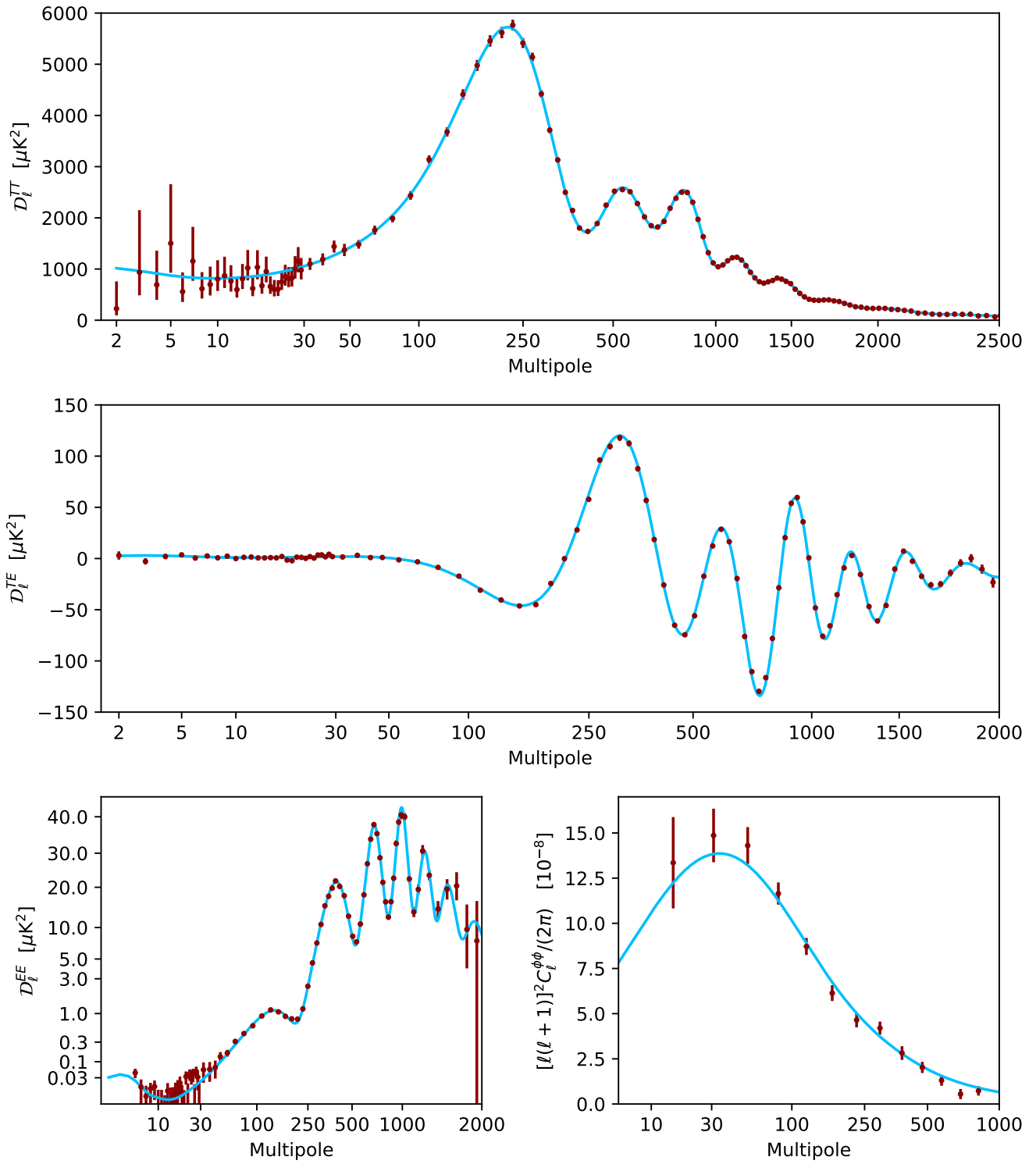


FIGURE I.5: The TT, TE, EE and Lensing (bottom right) angular power spectra of Cosmic Microwave Background Radiation as measured by the Planck Collaboration with $D_{\ell}^{X,Y} \equiv T_0^2 \frac{\ell(\ell+1)}{2\pi} C_{\ell}^{X,Y}$. The blue solid line represents the best fit obtained within the standard Λ CDM cosmological model. Figure adopted from the Planck legacy archive [42].

outgoing scattered spherical wave $E = \frac{1}{4\pi r} (\ddot{d}(t-r) \times \hat{n}') \times \hat{n}'$ whose components (E'_x, E'_y) are related to the original radiation components (E_x, E_y) as follows:

$$E'_x = \frac{e^2}{4\pi m_e r} E_x \cos \theta, \quad E'_y = \frac{e^2}{4\pi m_e r} E_y \quad (\text{I.204})$$

In terms of the outgoing and ingoing Stokes parameters this reads:

$$I' = \frac{3\sigma_T}{8\pi r^2} [2(\cos^2 \theta + 1) I + (\cos^2 \theta - 1) Q_+ + (\cos^2 \theta - 1) Q_-] \quad (\text{I.205})$$

$$Q'_\pm = \frac{3\sigma_T}{8\pi r^2} [2(\cos^2 \theta - 1) I + (\cos \theta \pm 1)^2 Q_+ + (\cos \theta \mp 1)^2 Q_-] \quad (\text{I.206})$$

The second of these relations clearly shows that the outgoing Stokes parameters are non zero also for unpolarized radiation. This description can be applied also to CMB radiation. However since for a black-body radiation $I \propto T^4$ and since we work with $\Theta = \frac{\delta T}{T} = \frac{\delta I}{4I}$, it is useful to redefine the Stokes parameters in a cosmological context with the following normalization

$$Q_\pm \rightarrow \frac{Q_\pm}{4I} \quad (\text{I.207})$$

According to the Q_\pm transformation propriety under rotations (I.203), we clearly see that it is a spin-2 field that can be expanded in terms of spin-weighted spherical harmonics. The *spin-weighted spherical harmonics* can be defined in terms of rotations matrices a:

$${}_s Y_{\ell m}(\theta, \phi) = \sqrt{\left(\frac{2\ell+1}{4\pi}\right)} \mathcal{D}_{-s, m}^\ell(\phi, \theta, 0). \quad (\text{I.208})$$

They reduce to ordinary spherical harmonics when $s = 0$. In this case $s = 2$ and defining ${}_2 Y_{\ell m} \equiv Y_{\ell m}^\pm$, one can expand Q_\pm as:

$$Q_\pm(\hat{e}) = \sum_{\ell=2}^{\infty} \sum_{m=-\ell}^{\ell} Q_{\ell m}^\pm Y_{\ell m}^\pm(\hat{e}). \quad (\text{I.209})$$

At this point we can introduce the Polarization multipoles $E_{\ell m}$ and $B_{\ell m}$ defined as:

$$Q_{\ell m}^\pm \equiv E_{\ell m} \pm i B_{\ell m} \quad (\text{I.210})$$

One can show that under parity transformation $\hat{e} \rightarrow -\hat{e}$ the E modes $E_{\ell m} \rightarrow (-1)^\ell E_{\ell m}$ while the B modes $B_{\ell m} \rightarrow (-1)^{\ell+1} B_{\ell m}$. Therefore the E-modes are *parity-even* while the B-modes are *parity-odd*. Roughly speaking, we can think of the E-modes as the gradient of a scalar and the B-modes as the curl of a vector. The stochastic properties under rotations and parity transformations allow us to define the following correlators among $a_{\ell m}$, $E_{\ell m}$ and $B_{\ell m}$

$$\langle a_{\ell m} a_{\ell' m'}^* \rangle = C_\ell^{TT} \delta_{\ell \ell'} \delta_{m m'} \quad (\text{I.211a})$$

$$\langle a_{\ell m}^* E_{\ell' m'} \rangle \equiv C_\ell^{TE} \delta_{\ell \ell'} \delta_{m m'} \quad (\text{I.211b})$$

$$\langle E_{\ell m}^* E_{\ell' m'} \rangle \equiv C_\ell^{EE} \delta_{\ell \ell'} \delta_{m m'} \quad (\text{I.211c})$$

$$\langle B_{\ell m}^* B_{\ell' m'} \rangle \equiv C_\ell^{BB} \delta_{\ell \ell'} \delta_{m m'}, \quad (\text{I.211d})$$

where for sake of completeness we wrote also the correlator (I.183). Notice that since B is parity-odd, while T and E are parity-even, in a parity-conserving theory we expect $C_\ell^{TB} = C_\ell^{EB} = 0$ and for each ℓ we can

define the so called *covariance matrix*

$$\hat{C}_\ell \doteq \begin{pmatrix} C_\ell^{TT} & C_\ell^{TE} & 0 \\ C_\ell^{ET} & C_\ell^{EE} & 0 \\ 0 & 0 & C_\ell^{BB} \end{pmatrix}. \quad (\text{I.212})$$

Today, the spectrum of E modes polarization (as well as the cross-correlator TE spectrum) is measured with good precision by the Planck Collaboration, see also [Figure I.5](#). Again a remarkable agreement with the prediction of standard cosmological model is found. Measurements of C_ℓ^{TE} and C_ℓ^{EE} give additional information on the cosmological parameters, often braking the degeneracy between them. In particular

- The spectrum C_ℓ^{TT} of temperature anisotropies is mostly sensitive to scalar perturbations and the gravitational potential.
- The spectrum C_ℓ^{EE} on large multipoles $100 \lesssim \ell \lesssim 1000$ is mostly determined by the velocity of the baryon-photon plasma at the recombination epoch while on low multipoles it strongly depends on the optical depth at reionization: $C_\ell^{EE} \propto \tau^2$. We clearly show this dependence in [Figure I.6](#) where the effect of τ on the low multipoles of the EE angular spectrum has been emphasized adopting an unrealistic large value $\tau = 0.2$.
- The spectrum C_ℓ^{TE} on low multipoles strongly depends on the optical depth at reionization: $C_\ell^{TE} \propto \tau$. Once again, in [Figure I.6](#) we show the effect of τ in the TE spectrum for an unrealistic large value of $\tau = 0.2$. The (combined) measurement of C_ℓ^{TE} and C_ℓ^{EE} allows us to constrain τ which would be difficult within only the spectrum of temperature anisotropies C_ℓ^{TT} as in that case it turns out to be extremely degenerate with the other parameters. Notice also that since both C_ℓ^{EE} and C_ℓ^{TE} are dominated by reionization on low multipoles, the cosmic variance sets a natural limit on the maximum precision τ can be measured with. We are already close to such limit.
- The spectrum C_ℓ^{BB} is *not* measured. Anyway scalar perturbations can produce only E-modes while tensor perturbations can produce both E-modes and B-modes. Hence a detection of B-modes can be a hint for the existence of tensor modes. However the B-mode spectrum can have two different contributions: together with tensor perturbations, also gravitational lensing can mixes E modes and the B modes, converting the first into the second. Therefore a careful characterization of the B-mode spectrum is required to distinguish the two sources. In what follows we give some details.

E-modes from relic gravity waves

Tensor modes produce both temperature anisotropies and E and B modes polarization in the CMB radiation. Therefore they not only contribute to the angular spectrum of temperature anisotropies via [Eq.\(I.196\)](#) but they contribute also to the TE EE and BB angular spectra. In particular the EE and TE contributions can be estimated to be [\[15\]](#)

$$\begin{aligned} \text{GW } C_\ell^{EE} \propto \int_0^\infty \frac{dk}{k} \mathcal{P}_T(k) \left(\frac{\partial \mathfrak{h}}{\partial \eta} \right)^2 & \left\{ \frac{(l+2)(l+1)}{(2l-1)(2l+1)} j_{l-2} [(\eta_0 - \eta_r) k] \right. \\ & \left. - \frac{6(l+2)(l-1)}{(2l-1)(2l+3)} j_l [(\eta_0 - \eta_r) k] + \frac{l(l-1)}{(2l+1)(2l+3)} j_{l+2} [(\eta_0 - \eta_r) k] \right\}^2 \end{aligned} \quad (\text{I.213})$$

and

$$\begin{aligned}
 {}^{\text{GW}}C_{\ell}^{\text{TE}} \propto & \sqrt{\frac{(l+2)!}{(l-2)!}} \int_0^{\infty} \frac{dk}{k} \mathcal{P}_T(k) \left(\frac{\partial \mathfrak{h}}{\partial \eta}\right) \int_{\eta_r}^{\eta_0} d\eta \left(\frac{\partial \mathfrak{h}}{\partial \eta}\right) \frac{j_l[(\eta_0 - \eta)k]}{(\eta_0 - \eta)^2 k^2} \\
 & \times \left\{ \frac{(l+2)(l+1)}{(2l-1)(2l+1)} j_{l-2}[(\eta_0 - \eta_r)k] - \frac{6(l+2)(l-1)}{(2l-1)(2l+3)} j_l[(\eta_0 - \eta_r)k] \right. \\
 & \left. + \frac{l(l-1)}{(2l+1)(2l+3)} j_{l+2}[(\eta_0 - \eta_r)k] \right\}
 \end{aligned} \tag{I.214}$$

respectively. The effect of gravitational waves in the angular spectra of CMB polarization is shown in **Figure I.6**. As one can see, also for unrealistic large values of the tensor amplitude, the tensor contribution is always sub-dominant with respect to the scalar counterpart both in the EE and EE spectra. This is one of the reason why a detection of tensor perturbations is extremely challenging from an experimental point of view. Fortunately, while scalar modes do not produce B-mode polarization, tensor modes contribute also in the BB spectrum and so searching for B-modes polarization is a more promising way for detecting Primordial Gravitational Waves.

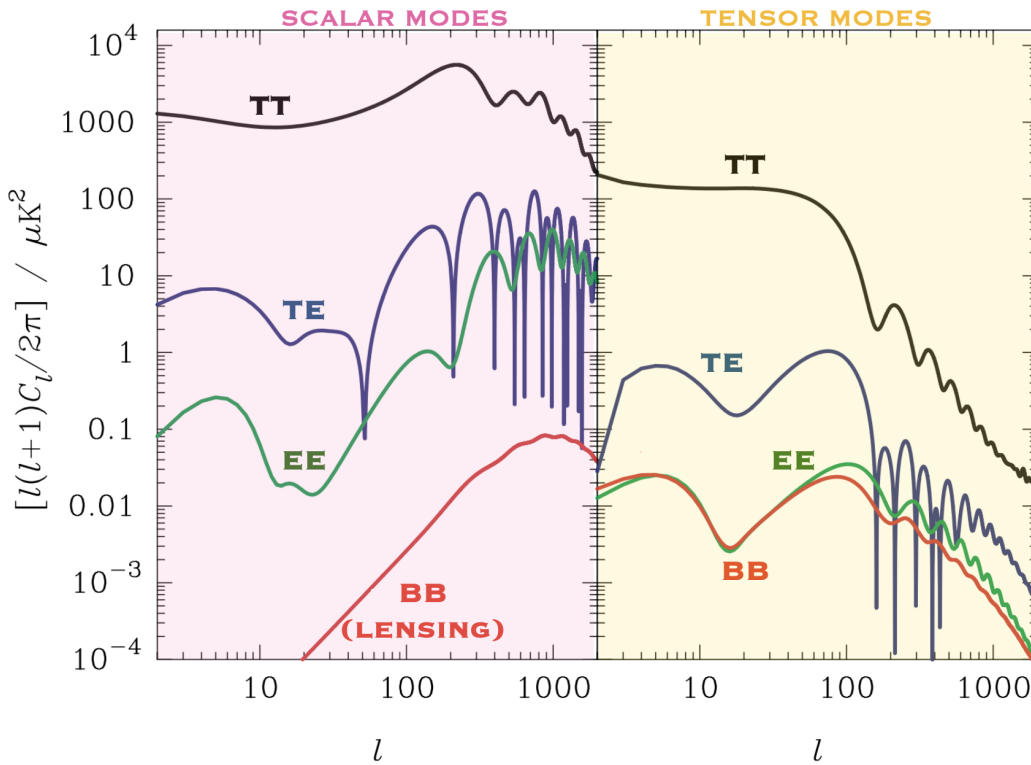


FIGURE I.6: A comparison between scalar and tensor contributions in the CMB temperature anisotropy and polarization angular spectra. On the left the contributions from adiabatic scalar perturbations (and lensing) in the TT TE EE (and BB) spectra. On the right the contributions from tensor perturbations in the same spectra. To better emphasize the effects of tensor modes and reionization, the tensor amplitude and the optical depth are fixed to the unrealistically large values of $r = 0.4$ and $\tau = 0.2$, respectively. Figure based on Ref. [15].

B-modes from relic gravity waves

The detection of B-mode polarization can be considered a major task of observational cosmology as it can be produced by inflationary gravity waves. Here we briefly review the signatures that relic gravitational

radiations may have left in the B-spectrum. A detailed computation of the relic gravity waves contributions to C_ℓ^{BB} would be rather expensive, involving the polarization tensor and some maths. Here we avoid to get lost in mathematical details and we just point out that this contribution can be computed to be [15]

$${}^{\text{GW}}C_\ell^{BB} \propto \int_0^\infty \frac{dk}{k} \mathcal{P}_T(k) \left(\frac{\partial \mathfrak{h}}{\partial \eta} \right)^2 \times \left[\frac{\ell+2}{2\ell+1} j_{\ell-1}(k\eta_0) - \frac{\ell-1}{2\ell+1} j_{\ell+1}(k\eta_0) \right]^2 \quad (\text{I.215})$$

where the constant of proportionality is rather small. In any case, one can see that

- Tensor perturbations that are super-horizon at recombination give small contributions in the integral as in that case the modes are frozen and the derivative with respect to the conformal time is extremely small.
- The largest contribution in Eq.(I.215) is given by tensor modes that enter the horizon exactly at the time of recombination ($k\eta_r \sim 1$) which corresponds to multipoles $\ell \lesssim \eta_0/\eta_r \sim 50$ or to angles smaller than about 3 degrees. Indeed in that region $\partial \mathfrak{h}/\partial \eta \propto 1/\eta_r$ while the spherical Bessel functions result to be $j_\ell(k\eta_0) \sim 1/(k\eta_0)$. Therefore C_ℓ^{BB} is constant in ℓ in that range of multipoles and its magnitude will depend on the amplitude of tensor modes as sourced by inflation: if during inflation a satiable background of primordial gravitational waves is generated this contribution can be dominant on these scales.
- On smaller scales, $50 \lesssim \ell \lesssim 1000$ the behavior of the integral is very different as it saturates for $k \sim \ell/\eta_0$. Indeed on small scales $\partial \mathfrak{h}/\partial \eta \propto 1/\eta_r^2 \propto 1/\ell$ as well as $j_\ell(k\eta_0) \propto 1/\ell$. Therefore we get that $C_\ell^{BB} \propto 1/\ell^4$ which decays very rapidly with ℓ . Furthermore on small scales the B-mode spectrum is dominated by the signal due to gravitational lensing which, converting E modes into B modes, contains information related to the different cosmological parameters, such as dark matter, dark energy or spatial curvature.

We conclude that CMB polarization is particularly important also from the viewpoint of the search for tensor perturbations. Indeed the analysis of temperature anisotropies C_ℓ^{TT} alone has a limited sensitivity on tensor perturbations both because the cosmic variance affects signals at low multipoles and above all because of degeneracy with the other cosmological parameters. While the measurement of E-mode polarization improves the sensitivity to tensor modes, the analysis of B-mode offers us a *unique* opportunity. In particular, of primary interest is the study of B-mode at intermediate angular scales, where the cosmic variance is not very significant and gravitational lensing is not dominant, yet. While currently there is no evidence for B-mode polarization, future cosmological experiments are designed specifically for probing the range of multipoles of interest for tensor perturbations, possibly leading to a first detection of relic gravity waves and opening to the possibility to test and constrain fundamental physics on the inflationary energy scales, literally at the dawn of time. In the next chapter we will discuss exactly how non-standard physics on the inflationary energy scales can be encoded in the inflationary parameters and how we can test and probe it using primordial gravitational waves.

I.IV INFLATION THEORY

As often happens in Science, observations challenge theories. Many evidences are extremely difficult to explain in contest of the Hot Big Bang Theory. For example the previous discussion of the Cosmic Microwave background teaches us that the Early Universe was very homogeneous and all the CMB photons share the same temperature within small fluctuations of order $\delta T/T \approx 10^{-5}$. This is very hard to explain in the theoretical framework we described so far because CMB photons are separated by a distance greater than the particle horizon and they have never communicated [54, 76, 77]. So, according to Hot Big Bang Theory, the last scattering surface should consist of many causally disconnected regions and there is any dynamical reason why such regions (that never "talked") could share similar physical conditions. We are forced to suppose a fine-tuning of thousands initial conditions to explain homogeneity in the Early Universe.

Another observational evidence is that the Universe is spatially flat [78]. We pointed out that the Hubble radius $1/(aH)$ grows with time for each component of the cosmic fluid with equation of state $\omega > -\frac{1}{3}$. Therefore when the Universe is dominated by radiation or matter we have $\Omega - 1 \propto a^2$ and $\Omega - 1 \propto a$, respectively. In both cases $\Omega - 1$ decreases and so going backwards with time $|1 - \Omega|$ should diverge. Flatness is not a tracking solution of the FRW dynamics and in the Hot Big Bang cosmology, a flat geometry today would require an extreme fine-tuned Ω at early times. We can roughly deduce its value at the Planck time (*i.e.*, the time when the temperature of the Universe is the Planck epoch):

$$\frac{|\Omega - 1|_{T=T_{\text{Planck}}}}{|\Omega - 1|_{T=T_0}} \approx \left(\frac{a_{\text{Pl}}^2}{a_0^2} \right) \approx \left(\frac{T_0^2}{T_{\text{Pl}}^2} \right) \approx \mathcal{O}(10^{-64}) \quad (\text{I.216})$$

where we have assumed a Radiation dominated Universe, we have used that $T \propto \frac{1}{a}$ and we remember that the present epoch temperature of the Universe is $T_0 \approx 10^{-13}$ GeV. Is it something meaningful to require a precision in the initial conditions within 1 part over 10^{60} ?

Although all these "problems" are not inconsistencies able to falsify the Big Bang picture, it is clear that one would prefer a physical mechanism able to fix all the required initial conditions without controversial assumptions. Inflation [79], an early epoch of "fast" accelerated expansion with repulsive gravity, is largely believed to be exactly the physical mechanism able to set the correct initial conditions [54, 55, 76, 77, 80–83].

To figure out how a phase of repulsive gravity can drive the Universe towards homogeneity and flatness, we recall that an accelerated expansion requires $\omega < -\frac{1}{3}$ and that in this case also the Hubble radius $(aH)^{-1}$ decreases over the time. This automatically solves also the flatness problem:

$$\underbrace{|1 - \Omega(a)|}_{\text{Driven to flatness}} = \underbrace{|-\kappa(aH)^{-2}|}_{\leftarrow \text{decrease}}. \quad (\text{I.217})$$

In particular it should be noted that in the de Sitter limit, $\omega = -1$, the spacetime expansion becomes exponentially accelerated as well as the Hubble sphere exponentially shrinks: $(aH)^{-1} \propto e^{-Ht}$. In terms of the particle horizon, $\eta = -(1/H)e^{-Ht}$, we see that the initial singularity is pushed back to $\eta_i \rightarrow -\infty$ with the hypersurface $\eta = 0$ corresponding to the end of inflation. So, not only the curvature is exponentially driven to flatness but now there is an "infinite" amount of conformal time to let the past light-cones of CMB photons intersect in such a way that the homogeneity observed in the CMB radiation is simply explained in terms of thermal equilibrium.

Anyway it is also evident that in an exact de Sitter background the end of inflation is reached at the cosmological time $t = \infty$ which means that inflation would go on forever. This is clearly due to the isometries of the de Sitter background which, being a maximally symmetric solution, preserve invariance under time translations. Therefore to ensure the end of inflation, the de Sitter limit, although valid at early times, must be broken near the end of inflation. Therefore we need a dynamical process able to transit from an inflating phase to a radiation dominated era.

I.IV.I SINGLE FIELD SLOW-ROLL INFLATION

The simplest dynamical model of Inflation involves a scalar field ϕ , which from now on we call the inflaton, minimally coupled to gravity. The action of the field reads [54, 55, 76, 77, 80–83]

$$S = S_{\text{EH}} + S_\phi = \int d^4x \sqrt{-g} \left[\frac{\bar{M}_p^2}{2} R + \frac{1}{2} g^{\mu\nu} \partial_\mu \phi \partial_\nu \phi - V(\phi) \right], \quad (\text{I.218})$$

with $\bar{M}_p = 1/\sqrt{8\pi G}$ the *reduced* Planck Mass in the natural units $c = \hbar = 1$ (see also the **conventions**). This theory is said to be "minimal coupled to gravity" because there is not a direct coupling between the inflaton field and the metric tensor in the action. The equation of motion can be obtained minimizing the

action with respect to the field $\delta S_\phi / \delta \phi = 0$. A trivial computation gives:

$$\frac{1}{\sqrt{-g}} \partial_\mu (\sqrt{-g} \partial^\mu \phi) + \frac{\delta V(\phi)}{\delta \phi} = 0. \quad (\text{I.219})$$

In principle, to solve this equation in full generality we should use the FRW metric with a non-vanishing curvature since it is the inflation itself that drives the spacetime to be flat. Anyway the observational consequences of the inflation come out from its ending phase when the spacetime is already nearly flat. So a consistent theory of initial conditions is not required for investigating the inflationary predictions and we can simply use a flat FRW metric. In this way from Eq. (I.219) we obtain

$$\ddot{\phi} + 3H\dot{\phi} - a^{-2}(t) \nabla^2 \phi + \frac{\delta V(\phi)}{\delta \phi} = 0. \quad (\text{I.220})$$

If we restrict our attention on homogeneous scalar fields, the gradient term vanishes $\nabla^2 \phi = 0$ and the functional derivative $\delta V(\phi) / \delta \phi$ reduces to the ordinary one $dV(\phi) / d\phi \equiv V'(\phi)$. The equation of motion eventually becomes

$$\ddot{\phi} + 3H\dot{\phi} + V'(\phi) = 0. \quad (\text{I.221})$$

Minimizing the action with respect to the metric $\delta S / \delta g^{\mu\nu} = 0$ we can find the relation for Stress-Energy tensor

$$T_{\mu\nu}^\phi = g_{\mu\nu} \mathcal{L}_\phi - 2 \frac{\delta \mathcal{L}_\phi}{\delta g^{\mu\nu}} = -\partial_\mu \phi \partial_\nu \phi + g_{\mu\nu} \left(\frac{1}{2} \partial_\alpha \phi \partial^\alpha \phi - V(\phi) \right) \quad (\text{I.222})$$

and get the relation for the energy-density and pressure in a inflaton-dominated Universe, namely:

$$\rho_\phi = \frac{1}{2} \dot{\phi}^2 + V(\phi), \quad (\text{I.223})$$

$$p_\phi = \frac{1}{2} \dot{\phi}^2 - V(\phi). \quad (\text{I.224})$$

The equation of state ω is now a function of the scalar field

$$\omega_\phi \equiv \frac{p_\phi}{\rho_\phi} = \frac{\frac{1}{2} \dot{\phi}^2 - V(\phi)}{\frac{1}{2} \dot{\phi}^2 + V(\phi)}. \quad (\text{I.225})$$

and we clearly see that if $V \gg \dot{\phi}^2$ a phase of repulsive gravity $\omega_\phi \approx -1 < -1/3$ is obtained and the Universe starts inflating. This scenario is commonly called slow roll inflation. The price to pay for this paradigm of inflation is that we need to put some restrictions on the scalar field ϕ and above all on the shape of its potential $V(\phi)$ in order to obtain a de sitter expansion. First of all it is useful to write down the Friedman equations (I.17) and (I.18) for a Universe dominated by the homogeneous scalar field ϕ :

$$3\bar{M}_p^2 H^2 = \rho_\phi = \left(\frac{1}{2} \dot{\phi}^2 + V(\phi) \right), \quad (\text{I.226})$$

$$\bar{M}_p^2 \left(\frac{\ddot{a}}{a} \right) = -\frac{1}{6} (\rho_\phi + 3p_\phi) = -\frac{1}{3} (\dot{\phi}^2 - V(\phi)). \quad (\text{I.227})$$

Taking the derivative of the equation (I.226) and using the equation of motion (I.221) we have:

$$2\bar{M}_p^2 \dot{H} = -\dot{\phi}^2 \quad (\text{I.228})$$

During the slow roll phase we want an almost exponentially expansion and so we have to require $\omega_\phi \approx -1$ that implies $\dot{\phi}^2 \ll V(\phi)$. So from equation (I.226)

$$V(\phi) \approx 3 \bar{M}_p^2 H^2, \quad (\text{I.229})$$

and the slow roll condition is equivalent to require that

$$\frac{|\dot{H}|}{H^2} \ll 1. \quad (\text{I.230})$$

On the other hand, taking the derivative of Eq.(I.229) and using the slow roll condition we get also

$$V'(\phi) \approx -3 H \dot{\phi}, \quad (\text{I.231})$$

that implies $|\ddot{\phi}| \ll 3 H |\dot{\phi}|$. Therefore it is useful to introduce the following potential slow-roll parameters

$$\epsilon_V \doteq \bar{M}_p^2 \frac{1}{2} \left(\frac{V_\phi^2}{V^2} \right), \quad (\text{I.232a})$$

$$\eta_V \doteq \bar{M}_p^2 \left(\frac{V_{\phi\phi}}{V} \right), \quad (\text{I.232b})$$

$$\zeta_V^2 \doteq \bar{M}_p^4 \left(\frac{V_\phi V_{\phi\phi\phi}}{V^2} \right), \quad (\text{I.232c})$$

$$\omega_V^3 \doteq \bar{M}_p^6 \left(\frac{V_\phi^2 V_{\phi\phi\phi\phi}}{V^3} \right) \quad (\text{I.232d})$$

where $V_{\phi\dots\phi} \doteq V^{'\dots'}$ indicates the derivatives of the potential with respect to the field. Notice that the potential parameters will be largely used in the subsequent discussion together with the parameters $\{\epsilon_i\}$ defined as

$$\epsilon_1 \doteq -\frac{\dot{H}}{H^2} \simeq \epsilon_V, \quad \epsilon_{i>1} \doteq \frac{d \log \epsilon_{i-1}}{d \log k}. \quad (\text{I.233})$$

that are instead clearly related to the background dynamics. During the slow-roll phase all these parameters are expected to be small with the limit $1 \gg |\epsilon_V| \simeq |\epsilon_1| \rightarrow 0$ corresponding to an exactly de Sitter expansion.

Inflation can be easily achieved when the potential looks like that shown in [Figure I.7](#). Along the flat plateau the kinetic energy of the scalar field $\dot{\phi}$ becomes negligible with respect to the potential energy $V(\phi)$ which is instead approximately constant. In this way, $\omega_\phi \approx -1$ and we have an almost de Sitter phase. On the other hand, when this condition breaks down, inflation ends and the scalar field typically falls into a potential well starting oscillating. This phase of oscillation around the vacuum state is called reheating [84–93] and is required to restore particles in the Universe. Indeed during the slow period, the Universe is exponentially driven towards flatness and homogeneity but all its pre-inflationary contents are exponentially diluted as well. This means that at the end of inflation the Universe appears nearly empty and dominated by a scalar field in a state of coherent oscillation about the vacuum state. This looks far away from the Hot Big Bang picture: there is no radiation or particles but only an enormous amount of energy. Indeed, as by definition the energy-density during the inflationary expansion remains constant, the total energy $E_i = \rho V_i$ exponentially expands with the volume of the Universe. Such an exponential amount of energy can easily decay into radiation and particles when the field starts oscillating during the reheating phase. The details of reheating clearly depend on the specific shape of the potential, nevertheless this is typically a very rapid process. When the field is oscillating around the minimum, we can approximate the

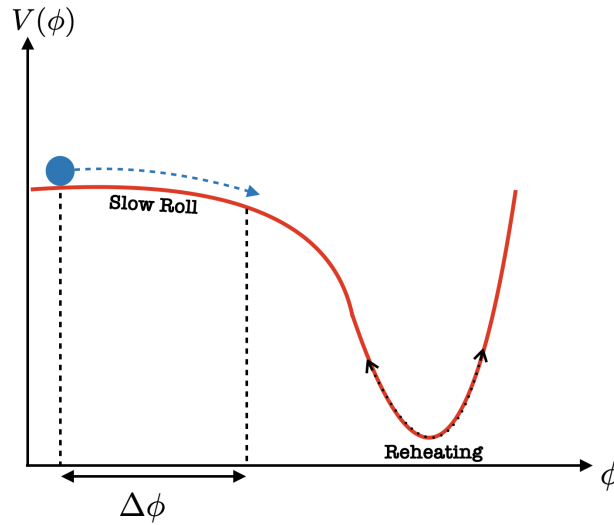


FIGURE I.7: The typical shape of a good Inflationary Potential.

potential as $V(\phi) \approx \frac{\lambda^2}{2} \phi^2$ so that:

$$\rho_\phi = \frac{1}{2} (\dot{\phi}^2 + \lambda^2 \phi^2), \tag{I.234}$$

taking the time derivative, $\dot{\rho}_\phi = \dot{\phi} \ddot{\phi} + \lambda^2 \phi \dot{\phi}$, and using Eq. (I.221) we get:

$$\dot{\rho}_\phi + 3H\rho_\phi = \frac{3H}{2} \underbrace{(\lambda^2 \phi^2 - \dot{\phi}^2)}_{\text{oscillates}}. \tag{I.235}$$

The oscillating factor on the right hand side averages out to zero over one oscillation period and the long-time behavior of the energy density eventually reads:

$$\dot{\bar{\rho}}_\phi + 3H\bar{\rho}_\phi = 0. \tag{I.236}$$

Note that the inflaton field is doing small oscillations around the potential minimum and the energy density can decay into particles. If the decay is slow the inflaton energy density follows the equation:

$$\dot{\bar{\rho}}_\phi + (3H + \Gamma)\bar{\rho}_\phi = 0, \tag{I.237}$$

where Γ represents the inflation decay rate and so $-\Gamma\rho_\phi$ is the energy transferred to other particles. Whether the inflaton decays into bosons, the process may be very rapid and violent and it is known as pre-heating. Anyway the particles produced in this stage will eventually interact, creating other particles unless the thermal equilibrium will be restored at some temperature so that the standard Hot Big Bang evolution can start.

I.IV.II QUANTUM INFLATIONARY FLUCTUATIONS

In the previous section we described the dynamics of scalar and tensor perturbation and their imprinting in the cosmic microwave background, but we said nothing about their origin: which is the physical nature of primordial perturbations? One could say that they simply exist, but a remarkable aspect of the CMB is that the primordial perturbations are correlated on scale well outside the horizon at the time of decoupling. This can be considered as another aspect of the horizon problem: how can perturbations that have never interacted be correlated? Here we want to answer all these questions showing that inflation provides a fascinating mechanism able to unveil the nature of primordial density perturbations. This is maybe one

of the most relevant aspects of inflation theory: one can calculate the power spectrum both of scalar and tensor perturbations and since this spectra are related to the CMB anisotropies, this calculation provides an important prediction directly connected with observations.

The basic idea underlying the origin of the primordial perturbations is that, during inflation, the inflaton field ϕ evolving on the potential $V(\phi)$ will not have a completely classical dynamics, but it will also have some small quantum fluctuations around its classical trajectory. Quantum fluctuations of the inflaton field are so blown up on superhorizon scales by inflation itself becoming classical perturbations: the source of the primordial power spectra of scalar and tensor fluctuations. Therefore inflation, combined with quantum mechanics, provides an elegant mechanism for generating the initial seeds of all structures in the Universe [13, 55, 77, 94, 95].

To describe a rigorous picture of quantum fluctuations, in general, we should consider perturbations in the metric, too. Nevertheless the Einstein equations relate perturbations in the metric to perturbations in the fields and so there is essentially only one physical degree of freedom [83, 96]. If we choose to work in the so called spatially flat Gauge, namely the Gauge in which the curvature of space-like hypersurfaces is zero and the spatial part of the metric is unperturbed, we can quantify this degree of freedom as the field fluctuations $\delta\phi$, leaving the metric unperturbed [53, 82, 83, 96]. At the same level of accuracy, we can also drop the contribution that arises from the inflationary potential $V(\phi)$, considering the field to be free. In this way, we can just focus on $\delta\phi$, and, according to the perturbation theory, we split field and the fluctuations $\phi \rightarrow \phi + \delta\phi$. The perturbations in general will not be homogeneous, $\delta\phi = \delta\phi(t, x)$, so in their equation of motion we must consider also the spatial dependence and, in light of Eq. (I.220), we write

$$\ddot{\delta\phi} + 3H\dot{\delta\phi} - a^{-2}(t) \nabla^2 \delta\phi = 0. \quad (\text{I.238})$$

It is useful to use the conformal coordinates $\partial_t = (1/a)\partial_\eta$ in such a way that

$$\delta\phi'' + 2\left(\frac{a'}{a}\right)\delta\phi' - \nabla^2 \delta\phi = 0 \quad (\text{I.239})$$

where we used the notation $(\dots)' \equiv \partial_\eta(\dots)$. We have to quantize the field in a FRW spacetime. We proceed analogously to the canonical quantization process, expanding the field $\delta\phi$ into its Fourier components

$$\delta\phi(\eta, \mathbf{x}) = \int \frac{d^3k}{(2\pi)^3} \left[\delta\phi_{\mathbf{k}}(\eta) b_{\mathbf{k}} e^{i\mathbf{k}\cdot\mathbf{x}} + \delta\phi_{\mathbf{k}}^*(\eta) b_{\mathbf{k}}^* e^{-i\mathbf{k}\cdot\mathbf{x}} \right] \quad (\text{I.240})$$

and promoting the field $\delta\phi$ to be an operator $\delta\phi \rightarrow \hat{\delta\phi}$ and $(b_{\mathbf{k}}, b_{\mathbf{k}}^*) \rightarrow (\hat{b}_{\mathbf{k}}, \hat{b}_{\mathbf{k}}^\dagger)$. We interpret $(\hat{b}_{\mathbf{k}}, \hat{b}_{\mathbf{k}}^\dagger)$ as the common creation and annihilation operators. We also impose the canonical quantization conditions:

$$\left[\hat{b}_{\mathbf{k}}, \hat{b}_{\mathbf{k}'}^\dagger \right] = \delta^3(\mathbf{k} - \mathbf{k}'), \quad (\text{I.241})$$

$$\left[\hat{b}_{\mathbf{k}}, \hat{b}_{\mathbf{k}'} \right] = \left[\hat{b}_{\mathbf{k}}^\dagger, \hat{b}_{\mathbf{k}'}^\dagger \right] = 0. \quad (\text{I.242})$$

Using the equation of motion (I.239), we easily find the equation for the Fourier components [13, 14, 55]

$$\delta\phi_k'' + 2\left(\frac{a'}{a}\right)\delta\phi_k' + k^2\delta\phi_k = 0 \quad (\text{I.243})$$

where with k^2 we are intending the spatial Euclidean amplitude $k^2 = |\mathbf{k}|^2$. At this point it is useful to introduce the following field redefinition:

$$u_k \equiv a(\eta) \delta\phi_k(\eta), \quad (\text{I.244})$$

The equation for the Fourier modes (I.243) in terms of the new field u_k reads

$$u_k'' + \left[k^2 - \frac{a''}{a} \right] u_k = 0. \quad (\text{I.245})$$

This is nothing but the *Mukhanov equation* we have already discussed in section I.II and can be considered the generalization of the Klein-Gordon equation in an expanding Universe. In the so called *Ultraviolet limit* $k \gg \frac{a''}{a}$, Eq. (I.245) simplifies to

$$u_k'' + k^2 u_k = 0. \quad (\text{I.246})$$

whose solution is given by

$$u_k(\eta) = \frac{1}{\sqrt{2k}} \left(A_k e^{-ik\eta} + B_k e^{ik\eta} \right) \quad (\text{I.247})$$

with A_k and B_k to be fixed by choosing an appropriate vacuum state (we will do this soon). On the other hand, in the so called *Infrared limit* $k \ll \frac{a''}{a}$ the equation (I.245) reads

$$a u_k'' - a'' u_k = 0, \quad (\text{I.248})$$

with the easy solution

$$u_k \propto a(\eta) \Rightarrow \delta\phi_k = \text{const.} \quad (\text{I.249})$$

proving a very interesting feature: the Fourier mode $\delta\phi_k$ does not evolve on the super-horizon scales (i.e. $k \ll a(t)H$). This phenomenon is called *mode freezing*.

We now come back to the issue of the vacuum state. The mode amplitude depends on the constant A_k and B_k and all of their physics boils down the boundary condition for the field perturbations in the ultraviolet limit. This problem is strictly related to the vacuum selection in the canonical quantization process. Indeed with some efforts, one can show that the canonical quantization condition for the operators $(\hat{b}_k, \hat{b}_k^\dagger)$ translates into a boundary condition for the u_k and u_k^* modes that is nothing else but the *Wronskian condition*

$$W(u_k, u_k^*) \equiv u_k (u_k^*)' - (u_k)' u_k^* = i. \quad (\text{I.250})$$

Using the solution (I.247) it is easy to see that this implies $|A_k|^2 - |B_k|^2 = 1$, the same condition that one would obtain in a Minkowski spacetime. Anyway, it is not enough to complete the solution and, in fact, a second relation arises from the vacuum selection in our FRW spacetime. We define the vacuum state for the FRW spacetime as the state where all the comoving observers see no particles which is to require that in the ultraviolet limit the FRW spacetime is asymptotically Minkowskian, i.e., $A_k = 1$ and $B_k = 0$. This is known as the *Bunch-Davies vacuum*. It is not the only discussed choice in literature (see e.g., Refs [97–102]), but it is of course the most reasonable and we will adopt it. With this choice the solution in the ultraviolet limit eventually becomes

$$u_k(\eta) = \frac{1}{\sqrt{2k}} e^{-ik\eta}, \quad (\text{I.251})$$

Notice that equation (I.245) depends on the spacetime background by a term $\frac{a''}{a}$ and so it is quite difficult to find a generic solution for this equation. However, here, we are interested in the quantum inflationary fluctuations and, since during inflation our spacetime is approximately de Sitter, it is worth finding an exact solution in this limit. By noting that in a de Sitter spacetime $\eta = -1/(aH)$, and $a''/a = 2/\eta^2$, the Mukhanov equation becomes:

$$u_k'' + \left(k^2 - \frac{2}{\eta^2} \right) u_k = 0. \quad (\text{I.252})$$

By a direct substitution one can check that an exact solution is:

$$u_k = A_k \frac{e^{-ik\eta}}{\sqrt{2k}} \left(1 - \frac{i}{k\eta} \right) + B_k \frac{e^{ik\eta}}{\sqrt{2k}} \left(1 + \frac{i}{k\eta} \right). \quad (\text{I.253})$$

which fixing the Bunch-Davies vacuum ($A_k = 1$ and $B_k = 0$) eventually becomes

$$u_k = \frac{e^{-ik\eta}}{\sqrt{2k}} \left(1 - \frac{i}{k\eta} \right). \quad (\text{I.254})$$

So we have the complete expression of the field operator $\hat{\delta\phi}$ in the de Sitter spacetime

$$\hat{\delta\phi}(\eta, \mathbf{x}) = \int \frac{d^3k}{(2\pi)^3} \left[\left(\frac{u_{\mathbf{k}}}{a} \right) \hat{b}_{\mathbf{k}} e^{i\mathbf{k}\cdot\mathbf{x}} + \left(\frac{u_{\mathbf{k}}^*}{a} \right) \hat{b}_{\mathbf{k}}^\dagger e^{-i\mathbf{k}\cdot\mathbf{x}} \right]. \quad (\text{I.255})$$

One can now compute the power spectrum of the fluctuations around the vacuum state in the de Sitter limit

$$\langle 0 | \hat{\delta\phi}(\eta, \mathbf{x}) \hat{\delta\phi}(\eta, \mathbf{x}') | 0 \rangle = \int \frac{d^3k d^3k'}{(2\pi)^6} \left(\frac{u_{\mathbf{k}} u_{\mathbf{k}'}^*}{a^2} \right) \langle 0 | b_{\mathbf{k}} b_{\mathbf{k}'}^\dagger | 0 \rangle e^{i\mathbf{k}\cdot\mathbf{x}} e^{-i\mathbf{k}'\cdot\mathbf{x}'} + \dots \quad (\text{I.256})$$

where all the other terms omitted from the integral vanish. The only non vanishing matrix element

$$\langle 0 | b_{\mathbf{k}} b_{\mathbf{k}'}^\dagger | 0 \rangle = \langle 0 | b_{\mathbf{k}} b_{\mathbf{k}'}^\dagger - \underbrace{b_{\mathbf{k}'}^\dagger b_{\mathbf{k}}}_{=0} | 0 \rangle = \langle 0 | [b_{\mathbf{k}}, b_{\mathbf{k}'}^\dagger] | 0 \rangle = \delta^3(\mathbf{k} - \mathbf{k}'). \quad (\text{I.257})$$

gives

$$\langle 0 | \hat{\delta\phi}(\eta, \mathbf{x}) \hat{\delta\phi}(\eta, \mathbf{x}') | 0 \rangle = \int \frac{d^3k d^3k'}{(2\pi)^6} \left(\frac{u_{\mathbf{k}} u_{\mathbf{k}'}^*}{a^2} \right) e^{i\mathbf{k}\cdot\mathbf{x}} e^{-i\mathbf{k}'\cdot\mathbf{x}'} \delta^3(\mathbf{k} - \mathbf{k}') \quad (\text{I.258})$$

$$= \int \frac{d^3k}{(2\pi)^3} \left(\frac{|u_{\mathbf{k}}|^2}{a^2} \right) e^{i\mathbf{k}\cdot(\mathbf{x}+\mathbf{x}')} \quad (\text{I.259})$$

$$\doteq \int \frac{d^3k}{(2\pi)^3} P_{\delta\phi}(k) e^{i\mathbf{k}\cdot(\mathbf{x}+\mathbf{x}')}, \quad (\text{I.260})$$

where in the last line we have defined the power spectrum

$$P_{\delta\phi}(k) \doteq \frac{|u_{\mathbf{k}}|^2}{a^2}, \quad (\text{I.261})$$

and so the dimensionless power spectrum (see also the **conventions**)

$$\mathcal{P}_{\delta\phi} \doteq \frac{k^3}{2\pi^2} P_{\delta\phi}(k) = \frac{k^3}{2\pi^2} \frac{|u_{\mathbf{k}}|^2}{a^2}. \quad (\text{I.262})$$

Using equation (I.251) we obtain for $|u_{\mathbf{k}}|^2$

$$|u_{\mathbf{k}}|^2 = \frac{1}{2k} \left(1 + \frac{1}{k^2\eta^2} \right), \quad (\text{I.263})$$

which gives

$$\mathcal{P}_{\delta\phi} = \left(\frac{H}{2\pi} \right)^2 \left[1 + \left(\frac{k}{aH} \right)^2 \right]. \quad (\text{I.264})$$

This is the expression for the dimensionless power spectrum of the inflaton fluctuations in an exact de Sitter spacetime. Note that well outside the Hubble horizon (*i.e.*, $k \ll (aH)$) it approaches to be a constant:

$$\mathcal{P}_{\delta\phi} = \left(\frac{H}{2\pi} \right)^2. \quad (\text{I.265})$$

This result is consistent with the phenomenon of modes freezing that we discussed above.

Scalar Modes

Thanks to these efforts, computing the power spectrum for the primordial scalar and tensor perturbations is almost trivial. We must use some Gauge-invariant measures for the fluctuations induced in the space-time geometry and for the scalar spectrum we use the primordial curvature perturbation ζ . The inflaton quantum fluctuations can be easily related to the primordial curvature perturbations ζ in the zero spatial curvature Gauge where the spatial component of the metric is unperturbed ($\Psi = 0$) and the spacelike hypersurfaces at constant time are flat. According to equation (I.121), in the spatially flat Gauge, ζ for an inflaton-dominated Universe reads

$$\zeta \approx - \left(\frac{H}{\dot{\phi}} \right) \delta\phi. \quad (\text{I.266})$$

Therefore the calculation of the scalar power spectrum is straightforward:

$$\mathcal{P}_s = \left(\frac{H}{\dot{\phi}} \right)^2 \mathcal{P}_{\delta\phi} \quad (\text{I.267})$$

This is the dimensionless power spectrum for scalar perturbations predicted by inflation at the time of horizon crossing. Note that since ζ is a gauge independent quantity (or more rigorously speaking a gauge fixed quantity), this result is gauge independent as well.

Notice that in the single-field slow roll paradigm the physics at the end of inflation is the same everywhere and the perturbations are adiabatic: since there is only one scalar degree of freedom that measures the slightly density differences where there is an over-density in dark matter there is also a corresponding over-density in the photons, baryons and neutrinos. Notice also that in an exact de Sitter spacetime the spectrum of inflaton fluctuations is exactly scale independent. Therefore in an almost de Sitter epoch, we expect the scale dependence to be very small. This is why the primordial scalar spectrum is commonly parametrized with a power

$$\mathcal{P}_s(k) = A_s \left(\frac{k}{k_*} \right)^{n_s-1} \quad (\text{I.268})$$

which includes only an amplitude $A_s = \mathcal{P}(k_*)$ (evaluated at the pivot scale k_*) and a scalar spectral index (or scalar tilt) $n_s - 1 \doteq d \log \mathcal{P}_s / d \log k$.

We conclude recalling that the inflationary fluctuations are directly related to the small irregularities observed in the Cosmic Microwave Background. A simply way to link them to the statistical properties of the CMB anisotropies and polarizations (i.e. the different $C_{\ell s}$) is to define the so called scalar transfer functions

$$C_{\ell}^{XY, \text{scalar}} = \int_0^{\infty} d \ln k T_{\ell X}^s(k) T_{\ell Y}^s(k) \mathcal{P}_s(k), \quad (\text{I.269})$$

where for scalar perturbations X and Y run over $X, Y = \{T, E\}$. The transfer functions depend only on known physics: a set of coupled Einstein-Boltzmann equations at linear order. Roughly speaking, the form of the linear transformations encoded in the transfer functions probe the (late) time evolution while the primordial power spectrum is determined by inflation.

Tensor Modes

Along with scalar modes, the quantum fluctuations of the inflaton field can source also Tensor modes, a stochastic background of metric fluctuations known as Primordial Gravitational Waves. The underlying reason is easy to understand: during the inflationary epoch the energy density of the Universe is dominated by the energy of the inflaton field. Therefore fluctuations in the field $\phi \rightarrow \phi + \delta\phi$ source fluctuations in the stress energy tensor $T_{\mu\nu}[\phi + \delta\phi] \rightarrow T_{\mu\nu} + \delta T_{\mu\nu}$. The Einstein Equations relate fluctuations in the stress energy tensor to fluctuations in the metric, i.e., Primordial Gravitational Waves. We have already pointed

out that the equation of motion of primordial gravitational waves is

$$\ddot{h}_{\times,+} + 3H\dot{h}_{\times,+} + k^2 h_{\times,+} = 0, \quad (\text{I.270})$$

with the two polarization states \times and $+$. With the efforts of the previous sections the computation of the tensor spectrum is trivial. The only point to be carefully considered is the normalization of the field $h_{\times,+}$. In order to use the formalism developed from a scalar field, we have to be sure that $h_{\times,+}$ and ϕ have the same physical unit. Since in natural units $[\phi] = \text{energy}$ while h is dimensionless, it is useful to introduce the normalized fields

$$\psi_{\times,+} \equiv \sqrt{2} \bar{M}_p h_{\times,+}, \quad (\text{I.271})$$

where the factor $\sqrt{2}$ simply counts the two polarization states. The equation of motion for the normalized fields read

$$\ddot{\psi}_{\times,+} + 3H\dot{\psi}_{\times,+} + k^2 \psi_{\times,+} = 0, \quad (\text{I.272})$$

Using conformal time $dt = a d\eta$ and defining a new field $u_{\times,+} = a(\eta) \psi_{\times,+}$ we get

$$u''_{\times,+} + \left[k^2 - \frac{a''}{a} \right] u_{\times,+} = 0. \quad (\text{I.273})$$

For each polarization (\times and $+$) this is nothing else but the Mukhanov equation (I.245). Therefore we can use the results already derived to obtain the dimensionless tensor power spectrum that, taking into account all the factors corresponding to the two different polarization states, reads:

$$\mathcal{P}_T = \frac{8}{\bar{M}_p^2} \left(\frac{H}{2\pi} \right)^2 \Big|_{k=aH}. \quad (\text{I.274})$$

Once again the symmetries of the almost de Sitter background constrain the scale dependence to be very small and also in this case the tensor spectrum is commonly parametrized with a power

$$\mathcal{P}_T(k) = A_T \left(\frac{k}{k_*} \right)^{n_T} \quad (\text{I.275})$$

which includes only an amplitude $A_T = \mathcal{P}(k_*)$ (evaluated at the pivot scale k_*) and a tensor spectral index (or tensor tilt) $n_T \doteq d \log \mathcal{P}_T / d \log k$.

In the next chapter we will discuss in great details Primordial Gravitational Waves. We conclude this section underlying that, as for scalar modes, also tensor perturbations are directly related to the CMB by Eqs.(I.196), (I.213), (I.214) and (I.215) for the temperature anisotropies, E-mode and B-modes polarization, respectively.

I.IV.III EFFECTIVE FIELD THEORY OF INFLATION

So far we assumed the existence of a fundamental scalar field minimally coupled to gravity, the inflaton. Here we review inflation under a completely different approach based on (broken) symmetries. We formulate inflation as an example of a spontaneous symmetry breaking theory and we describe its underlying Goldstone dynamics [59, 76, 103–106].

Broken time diffeomorphisms

What we really know about inflation is that it is a transient phase of accelerated expansion and the space-time is approximately, but not exactly, de Sitter. A de Sitter spacetime is a maximally symmetric solution of the Einstein equations with a positive cosmological constant. It is well known that the de Sitter spacetime,

being maximally symmetric, has 10 different Killing vectors (*i.e.* the maximum possible number for a 4-dimensional spacetime) that roughly correspond to 10 different isometries, namely: 3 spatial translations, 3 spatial rotations, 1 dilatation and 3 special conformal transformations⁵. However in almost any physical model of inflation the de Sitter symmetries are broken to ensure the end of inflation as if the spacetime is exactly de Sitter it would be invariant under time translations and we could not identify any preferred time slicing. In other words we need a ‘clock’ (*i.e.* an order parameter such as, for example, the Hubble rate H) that measures how long inflationary expansion lasts. Consider a generic clock-field $\psi(t)$ (that can be a matter field or the inflaton field itself) driving inflation. We can point out a privileged time-slicing where the field is taken as uniform. Anyway, if we want to use the formalism of the spontaneous symmetry breaking in the inflationary cosmology, we have to consider the metric tensor $g_{\mu\nu}$ as our fundamental gauge field. It is well known that General Relativity is invariant under spacetime diffeomorphisms of the type:

$$x^\mu \rightarrow x'^\mu(x^\nu). \quad (\text{I.276})$$

In inflationary cosmology we are clearly interested in the time component

$$x^0 \equiv t \rightarrow t'(x^\nu) \equiv x'^0(x^\nu) \quad (\text{I.277})$$

that must be broken since the spacetime dependent transformation $t \rightarrow t + \pi(t, \mathbf{x})$ does not leave the action invariant unless π is constant. An immediate consequence of a broken symmetry is the existence of a Goldstone boson excitation in the direction of the broken generator corresponding to the transformation $U(x) = t + \pi(t, \mathbf{x})$. The formalism of the Goldstone boson is very useful in the cosmological perturbation theory. Indeed a generic adiabatic fluctuation of the clock-field $\psi(t)$ can be easily related to the Goldstone boson:

$$\delta\psi(t) \equiv \psi(t + \pi(t, \mathbf{x})) - \psi(t) \approx \dot{\psi} \pi(t, \mathbf{x}), \quad (\text{I.278})$$

In other words, at linear order, adiabatic fluctuations are proportional to the Goldstone mode [76]. If we decide to work in the so called spatially flat gauge (*i.e.*, the gauge in which the spatial part of the metric is flat) we get [59, 76]

$$g_{ij} = a^2(t) \delta_{ij}, \quad (\text{I.279})$$

and all the metric perturbations are related to the Goldstone mode by the Einstein equations.

The Action in the Unitary Gauge

We can always perform a time shifting $t \rightarrow t - \pi(t, \mathbf{x})$ such that the fluctuations of the clock field vanish: $\delta\psi(t) = 0$. In this way we have no more the Goldstone boson ($\pi = 0$) and its effect is eaten by the metric $g_{\mu\nu}$ since we induce a perturbation to the spatial part of the metric given by [59, 76]:

$$\delta g_{ij} = a^2(t) e^{-2H\pi(t, \mathbf{x})} \delta_{ij}. \quad (\text{I.280})$$

This gauge is called *Unitary Gauge*. In what follows, we derive the most general action in the Unitary gauge compatible with all the symmetries of our problem. In particular, after Gauge fixing, our theory must be invariant only under time-dependent spatial diffeomorphisms $x^i \rightarrow x^i + \zeta^i(t, x^j)$ but it does not have to respect the full diffeomorphism invariance. Therefore, besides the usual curvature invariants like R and $R_{\mu\nu\rho\sigma}R^{\mu\nu\rho\sigma}$ that are invariant under all diffeomorphism by definition, the reduced degrees of symmetry allow other terms in the action. We can think to these terms as those that describe the additional degrees of freedom coming from the Goldstone boson that, in our Gauge, are eaten by the metric. For example it is easy to show that the g^{00} is invariant under the time-dependent spatial diffeomorphism

$$\tilde{g}^{00} = \frac{\partial \tilde{t}}{\partial x^\mu} \frac{\partial \tilde{t}}{\partial x^\nu} g^{\mu\nu} = \delta_\mu^0 \delta_\nu^0 g^{\mu\nu} = g^{00} \quad (\text{I.281})$$

⁵At late times, special conformal transformations act like conformal transformations on the space-like boundary

and so its polynomials can appear freely in the Unitary Gauge action. Instead, to describe the metric fluctuations we follow a geometrical approach: we first define the unit four-vector n_μ on the constant time hypersurfaces Σ_t that in the unitary gauge reads

$$n_\mu = -\frac{\delta_\mu^0}{\sqrt{-g^{00}}}. \tag{I.282}$$

By contracting covariant tensors with n_μ , we can produce objects with un-contracted upper 0 indices, such as g^{00} and R^{00} that we argued to be scalars under spatial diffeomorphisms and so allowed in the action. Generalizing, any four-dimensional covariant tensors with free upper 0 indices (but with all spatial indices contracted) are allowed operators. Furthermore we can have three-dimensional quantities describing the geometry of the hypersurfaces Σ_t . In order to describe the geometry of these hypersurfaces, we can define the so called induced metric $h_{\mu\nu} = g_{\mu\nu} + n_\mu n_\nu$, the extrinsic curvature tensor $K_{\mu\nu} = h_\mu^\rho \nabla_\rho n_\nu$, and the Riemann tensor of the induced metric $\hat{R}_{\alpha\beta\gamma\delta} = h_\alpha^\mu h_\beta^\nu h_\gamma^\rho h_\delta^\sigma R_{\mu\nu\rho\sigma} - K_{\alpha\gamma} K_{\beta\delta} + K_{\alpha\delta} K_{\beta\gamma}$. The most general action will eventually read [54, 59, 76]

$$S = \int d^4x \sqrt{-g} \mathcal{L} [R_{\mu\nu\rho\sigma}, g^{00}, K_{\mu\nu}, \hat{R}_{\mu\nu}, t], \tag{I.283}$$

with the prescription that the only free indices can be upper 0s. Expanding this action around a flat FRW spacetime:

$$g^{00} = -1, \quad R = 12H^2 + 6\dot{H}, \quad K = 3H, \tag{I.284}$$

with some efforts one can show that the action can be put in the following form [59, 76, 80]

$$S = \int d^4x \sqrt{-g} \left[\frac{\bar{M}_p^2}{2} R - f_1(t) - f_2(t)g^{00} \right] + \Delta S \tag{I.285}$$

where $f_1(t)$ and $f_2(t)$ are time dependent functions and ΔS is the part of the action containing quadratic order and higher-terms. We will deal with this part of the action later; now let us focus on the linear order terms. Varying this part of the action respect to $g^{\mu\nu}$ we obtain the following relations:

$$H^2 = \frac{1}{3\bar{M}_p^2} [f_1(t) + f_2(t)], \tag{I.286}$$

$$\dot{H} + H^2 = -\frac{1}{3\bar{M}_p^2} [2f_2(t) - f_1(t)]. \tag{I.287}$$

The equations (I.286) and (I.287) are nothing else but the Freedmen equations that solved give

$$f_1(t) = \bar{M}_p^2 (3H^2 + \dot{H}), \tag{I.288}$$

$$f_2(t) = -\bar{M}_p^2 \dot{H}. \tag{I.289}$$

Therefore the two unknown functions are completely fixed by imposing the FRW background (*i.e.*, specifying $H(t)$). The action becomes:

$$S = \int d^4x \sqrt{-g} \left[\frac{\bar{M}_p^2}{2} R - \bar{M}_p^2 (3H^2 + \dot{H}) + \bar{M}_p^2 \dot{H} g^{00} \right] + \Delta S \tag{I.290}$$

It is worth proving that if the slow roll condition $-\dot{H} \ll H^2$ holds, so the linear part of this action is nothing else than the minimal coupled action (I.218). In the unitary gauge, where $\phi = \phi(t)$, the action (I.218) reads:

$$S = \int d^4x \sqrt{-g} \left[\frac{\bar{M}_p^2}{2} R + \frac{1}{2} g^{\mu\nu} \partial_\mu \phi \partial_\nu \phi - V(\phi) \right] \quad (\text{I.291})$$

$$= \int d^4x \sqrt{-g} \left[\frac{\bar{M}_p^2}{2} R + \frac{1}{2} g^{00} \dot{\phi}^2 - V(\phi) \right] \quad (\text{I.292})$$

$$= \int d^4x \sqrt{-g} \left[\frac{\bar{M}_p^2}{2} R - \bar{M}_p^2 (3H^2 + \dot{H}) + \bar{M}_p^2 \dot{H} g^{00} \right], \quad (\text{I.293})$$

where in the last line we have used the slow roll relations (I.228) and (I.229). Note that it matches the linear part of (I.290).

If we want to consider also the higher order terms ΔS , we have to take into account higher expansions in powers of fluctuations such as [59, 76, 80]:

$$\Delta S = \int d^4x \sqrt{-g} \left[\sum_{n=2}^{\infty} \frac{M_n^4(t)}{n!} (\delta g^{00})^n - \frac{g_1^2(t)}{2} (\delta g^{00} \delta K) - \frac{g_2^2(t)}{2} (\delta g^{00} \hat{R}) - \frac{g_3^2(t)}{2} (\delta K)^2 + \dots \right], \quad (\text{I.294})$$

where we remember that around a flat FRW spacetime $\delta g^{00} = 1 + g^{00}$.

The Goldstone Dynamics

We now introduce the Goldstone boson π again. Sometimes the procedure of reintroducing the Goldstone boson is called Stuckelberg trick. As we are going to see, once that π is reintroduced, also the gauge invariance of the theory is restored. In order to reintroduce the Goldstone boson, we perform a spacetime dependent time reparametrization of the form:

$$t \rightarrow t' = t + \pi(t, x^i) \quad (\text{I.295a})$$

$$x_i \rightarrow x'_i = x_i \quad (\text{I.295b})$$

Let us see how the elements of the action (I.290) transform under such a parametrization. First of all we recall that the volume element $\sqrt{-g} d^4x$ is invariant under general four-dimensional diffeomorphism as well as the Ricci scalar. As concerns the time dependent coefficients, instead they transform as

$$f(t) \rightarrow f(t + \pi) = f(t) + \dot{f}(t) \pi + \frac{1}{2} \ddot{f}(t) \pi^2 + \dots \quad (\text{I.296})$$

while the contravariant components of any tensor transform as

$$t^{\mu\nu} \rightarrow \frac{\partial x'^\mu}{\partial x^\alpha} \frac{\partial x'^\nu}{\partial x^\beta} t^{\alpha\beta} = (\delta_{\mu\alpha} + \delta_{\mu 0} \partial_\alpha \pi) (\delta_{\nu\beta} + \delta_{\nu 0} \partial_\beta \pi) t^{\alpha\beta}. \quad (\text{I.297})$$

As concerns the covariant components, instead we get

$$t_{\mu\nu} \rightarrow \frac{\partial x^\alpha}{\partial x'^\mu} \frac{\partial x^\beta}{\partial x'^\nu} t_{\alpha\beta} = (\delta_{\mu\alpha} + \delta_{\alpha 0} \partial_\mu \pi)^{-1} (\delta_{\nu\beta} + \delta_{\beta 0} \partial_\nu \pi)^{-1} t_{\alpha\beta}. \quad (\text{I.298})$$

We eventually get the following transformation rules for the metric tensor

$$g^{00} \rightarrow g^{00} + 2\partial_\mu \pi g^{0\mu} + \partial_\mu \pi \partial_\nu \pi g^{\mu\nu}, \quad (\text{I.299})$$

$$g^{0i} \rightarrow g^{0i} + \partial_\mu \pi g^{\mu i}, \quad (\text{I.300})$$

$$g^{ij} \rightarrow g^{ij}. \quad (\text{I.301})$$

Considering only powers of δg^{00} in ΔS (without considering the quantities related to the extrinsic curvature), the action for the goldstone boson finally reads [76, 80]:

$$S = \int d^4x \sqrt{-g} \left[\frac{\bar{M}_p^2}{2} R - \bar{M}_p^2 (3H^2 (t + \pi) + \dot{H} (t + \pi)) + \bar{M}_p^2 \dot{H} (g^{00} + 2\partial_\mu \pi g^{0\mu} + \partial_\mu \pi \partial_\nu \pi g^{\mu\nu}) \right] + \underbrace{\int d^4x \sqrt{-g} \sum_{n=2}^{\infty} \frac{M_n^4 (t + \pi)}{n!} (1 + g^{00} + 2\partial_\mu \pi g^{0\mu} + \partial_\mu \pi \partial_\nu \pi g^{\mu\nu})^n}_{\Delta S} \quad (\text{I.302})$$

This appears to be very complicated. Even ignoring ΔS , we see that the goldstone boson π mixes with the metric perturbations and so its dynamics is highly non linear. However a simplification may occur at sufficiently short distances when we expect that, because of the equivalence principle, the Goldstone dynamics can be studied without taking into account the metric fluctuations. In other words, the quadratic terms that mix π and $g_{\mu\nu}$ contain fewer derivatives than the kinetic terms of π . Therefore at sufficiently high energy scales they can be ignored. It is worth studying what happens when we consider the so called decoupling limit defined as

$$\bar{M}_p \rightarrow \infty, \quad \dot{H} \rightarrow 0 \quad \text{for} \quad \bar{M}_p^2 \dot{H} = \text{const} \quad (\text{I.303})$$

This limit suggests that the Goldstone boson decouples from the metric perturbation for frequencies higher than $\omega_{\text{mix}}^2 \approx |\dot{H}|$, where we can consider the metric unperturbed so that the action (I.302) up to terms of order $\omega_{\text{mix}}^2/\omega^2$ reads:

$$S = \int d^4x \sqrt{-g} \left[\frac{\bar{M}_p^2}{2} R - \bar{M}_p^2 (3H^2 (t + \pi) + \dot{H} (t + \pi)) + \bar{M}_p^2 \dot{H} (-1 - 2\dot{\pi} + (\partial_\mu \pi)^2) \right] + \underbrace{\int d^4x \sqrt{-g} \sum_{n=2}^{\infty} \frac{M_n^4 (t + \pi)}{n!} (-2\dot{\pi} + (\partial_\mu \pi)^2)^n}_{\Delta S} \quad (\text{I.304})$$

This works for any arbitrary FRW background. If we are interested in a quasi de Sitter background we have to consider that $-\dot{H} \ll H^2$. In other words the fractional change in H per Hubble time is small. We will assume that this propriety holds also for any other time dependent function and so that all the time dependent parameters vary slowly. Assuming this implies that the action in the quasi de Sitter spacetime will be approximately invariant under time translation. This approximate invariance of the action must not be confused with the broken time diffeomorphism of the Background that is what we have used in order to write the action. In other words this is another approximate global symmetry of the fluctuation and not of the background. Taking into account this consideration, let us see when in a quasi de Sitter spacetime the mixing terms are negligible. Let us consider the Lagrangian for the Goldstone π given by the first part of (I.302) (i.e. we are not considering the higher terms in ΔS) [59, 76, 80]:

$$\mathcal{L}_\pi = -\bar{M}_p^2 (3H^2 (t + \pi) + \dot{H} (t + \pi)) + \bar{M}_p^2 \dot{H} (g^{00} + 2\partial_\mu \pi g^{0\mu} + \partial_\mu \pi \partial_\nu \pi g^{\mu\nu}), \quad (\text{I.305})$$

We have to compare the mixing term $2\bar{M}_p^2 \dot{H} \dot{\pi} \delta g^{00}$ (that comes from the term $2\bar{M}_p^2 \dot{H} \partial_\mu \pi g^{0\mu}$ in (I.305)) with the kinetic term $-\bar{M}_p^2 \dot{H} \dot{\pi}^2$ (that comes from $\bar{M}_p^2 \dot{H} (\partial_\mu \pi \partial_\nu \pi)$ for $\nu = \mu = 0$ always in (I.305).) One can show that the Einstein equations give $\delta g^{00} = 2\epsilon_H H \pi$. Therefore the mixing term becomes $4\bar{M}_p^2 \dot{H} (\epsilon_H H \dot{\pi} \pi)$. Since $\dot{\pi} \pi$ is a total derivative of π this term can be integrated by part in the action (I.302) in order to obtain

a mixing term $-6\bar{M}_p^2\dot{H}(\epsilon_H H^2 \pi^2)$. However a similar term comes from the expansion $-3\bar{M}_p^2 H^2(t + \pi) \approx 3\bar{M}_p^2\dot{H}(\epsilon_H H^2 \pi^2) + \dots$. Combining all these terms the ratio between the mixing term and the kinetic term is:

$$\frac{\text{mixing term}}{\text{kinetic term}} = \frac{-6\bar{M}_p^2\dot{H}(\epsilon_H H^2 \pi^2) + 3\bar{M}_p^2\dot{H}(\epsilon_H H^2 \pi^2)}{-\bar{M}_p^2\dot{H}\dot{\pi}^2} = \frac{3\epsilon_H H^2 \pi^2}{\dot{\pi}^2}. \quad (\text{I.306})$$

We see that the decoupling is reached when:

$$\omega \gg \omega_{\text{mix}} \equiv \sqrt{\epsilon_H} H. \quad (\text{I.307})$$

Therefore in a quasi de Sitter spacetime $\epsilon_H \ll 1$ the decoupling takes place at very low frequencies. For example it is interesting to observe that at the horizon crossing $\omega \approx H$ we are in this limit. If in this regime we evaluate the Lagrangian (I.305) using an unperturbed metric, after a few efforts due to the quite long calculation, one finds that the Lagrangian at the second order in π is very simple and reads:

$$\mathcal{L}_\pi = \bar{M}_p^2 |\dot{H}| \left(\dot{\pi}^2 - \frac{(\partial_i \pi)^2}{a^2} \right) \quad (\text{I.308})$$

The equation (I.308) is the second order (in π) Lagrangian of the inflation. It is a different but equivalent description of the dynamics given by action (I.290) in the unitary gauge that, as we have shown, includes also the slow roll inflation. We have therefore formulated inflation as a theory of broken time diffeomorphism writing its dynamics in terms of the corresponding Goldstone boson. This means that we can also read off the spontaneous symmetry breaking energy scale from the Noether current associated with the Lagrangian (I.308). The Noether current is:

$$J^\mu = -\sqrt{(2\bar{M}_p^2|\dot{H}|)} \partial^\mu \left[\sqrt{(2\bar{M}_p^2|\dot{H}|)} \pi \right] = -\sqrt{(2\bar{M}_p^2|\dot{H}|)} \partial^\mu \pi_c \quad (\text{I.309})$$

The normalization of the current f_π^4 tells us that the energy scale of the symmetry breaking is [76, 80]

$$f_\pi^4 \equiv 2\bar{M}_p^2 |\dot{H}| = \phi^2. \quad (\text{I.310})$$

This result formalizes the intuitive fact that, in the single field inflation, the inflaton itself is responsible of the symmetry breaking because of its time evolution.

It is now useful to briefly provide a different strategy for computing the primordial spectra using the Goldstone Dynamics. We use a different Gauge in which $\delta\phi = 0$ to obtain [76]

$$g_{ij} = a^2(t) \left[\underbrace{(1 - 2\mathcal{R}) \delta_{ij}}_{\text{scalar perturbations}} + \underbrace{h_{ij}}_{\text{tensor perturbations}} \right]. \quad (\text{I.311})$$

where \mathcal{R} is the comoving curvature perturbation defined in (I.122). In this way the inflaton scalar field ϕ is unperturbed and the scalar degree of freedom is described by the metric fluctuations from which both scalar and tensor perturbations arise. In this gauge there is a relation between the comoving curvature perturbation \mathcal{R} and the Goldstone boson π is given by:

$$\mathcal{R} = -H \pi \quad (\text{I.312})$$

Since scalar and tensor perturbations evolve independently at linear order we split the computation. As concerns scalar perturbations, we can write down the Lagrangian (I.308) in term of \mathcal{R} that in the slow-roll approximation reads [76]:

$$S_{\mathcal{R}} = \frac{1}{2} \int d^4x a^3 \frac{\dot{\phi}^2}{H^2} \left[\dot{\mathcal{R}}^2 - \frac{1}{a^2} (\partial_i \mathcal{R})^2 \right]. \quad (\text{I.313})$$

Using the conformal time η and defining the following variables

$$z^2 \equiv a^2 \frac{\dot{\phi}^2}{H^2}, \quad u \equiv z\mathcal{R}, \quad (\text{I.314})$$

one obtains:

$$S_{\mathcal{R}} = \frac{1}{2} \int d\eta d^3x \left[(u')^2 + (\partial_i u)^2 + \frac{z''}{z} u^2 \right]. \quad (\text{I.315})$$

Expanding the field u in its Fourier components, they must satisfy the Mukhanov equation

$$u_k'' + \left(k^2 - \frac{z''}{z} \right) u_k = 0. \quad (\text{I.316})$$

and considering that in the de Sitter limit $z''/z \rightarrow a''a$, the quantization process gives the same results discussed before.

Similarly, for the tensor perturbations the second order action in h_{ij} is [76]:

$$S_h = \frac{\bar{M}_p^2}{8} \int d\eta d^3x a^2 \left[(h'_{ij})^2 - (\partial_i h_{ij})^2 \right]. \quad (\text{I.317})$$

Defining the Fourier expansion

$$h_{ij} = \int \frac{d^3\mathbf{k}}{(2\pi)^3} \sum_{p=(\times,+)} \epsilon_{ij}^{(p)} h_{\mathbf{k}}^{(p)} e^{i\mathbf{k}\cdot\mathbf{x}}, \quad (\text{I.318})$$

with

$$k^i \epsilon_{ij}^{(p)} = 0 \quad \epsilon_{ij}^{(p)} \epsilon_{ij}^{(p')} = 2\delta_{pp'}, \quad (\text{I.319})$$

and normalizing the field

$$u_{\mathbf{k}}^{(p)} \equiv \frac{a}{2} M_p h_{\mathbf{k}}^{(p)}, \quad (\text{I.320})$$

the action eventually becomes:

$$S_h = \sum_{p=(\times,+)} \frac{1}{2} \int d\eta d^3x \left[(u_{\mathbf{k}}^{(p)'})^2 - \left(k^2 - \frac{a''}{a} \right) (v_{\mathbf{k}}^{(p)})^2 \right] \quad (\text{I.321})$$

and we can recognize the Mukhanov equation and so also in the tensor case the quantization process gives the same results.

I.V THE STANDARD MODEL OF COSMOLOGY

We conclude this chapter with a brief overview of the current status of the standard model of cosmology, the so called Λ CDM cosmological model.

Our previous discussions pointed out that to have a good agreement between the Hot Big Bang theoretical picture and the wide surveys of cosmological observations from large to small scales, we essentially need three major unexpected ingredients: an early stage of accelerated expansion, an unknown matter component able to facilitate structure formation and finally an unknown energy component able to explain the current accelerated expansion. Within the standard Λ CDM cosmological models these three ingredients are introduced as follows:

- **Single-Field Slow Roll Inflation:** the early stage of accelerated expansion is regarded to be driven by a single slow-rolling scalar field minimally coupled to gravity. The quantum fluctuations of the scalar field are expected to produce only adiabatic scalar modes while within the standard model of

cosmology isocurvature modes are not expected and Primordial Tensor Modes are usually assumed to be negligibly small. Moreover inflation is supposed to be long enough to drive the spatial geometry towards flatness in such a way that the curvature parameter is set to $\Omega_\kappa = 0$.

- **Cold Dark Matter:** the missing matter component able to facilitate structure formation is parametrized by a pressure-less fluid made of collision-less particles with low momenta known as Cold Dark Matter (here the meaning of CDM in Λ CDM). Since possible interactions/decays are ignored and the energy density of relativistic species decreases very rapidly with the scale factor, other Hot Dark Matter species in the Universe are considered absent or negligible.
- **Cosmological Constant Dark Energy:** the late-time epoch of accelerated expansion is supposed to be due to the cosmological constant term Λ in the Einstein Equations (here the meaning of Λ in Λ CDM). Therefore the late time equation of state is assumed to be $\omega_{\text{DE}} = -1$ (*i.e.*, $P = -\rho$) and there is no dynamical evolution in the dark energy component: $\Omega_{\text{DE}}(t) \equiv \Omega_\Lambda = \text{Const.}$

It should be noted that from a theoretical side, these choices are mostly motivated by simplicity. The theoretical predictions (as well as the computational efforts) become less expensive if we include fewer free parameters in the theory. As a matter of fact the Λ CDM model is made of only six free parameters that we can fix by observations, namely:

- the baryon energy density, $\Omega_b h^2$;
- the cold dark matter energy density, $\Omega_c h^2$;
- the angular size of the horizon at the last scattering surface, θ_{MC} ;
- the optical depth at reionization, τ ;
- the amplitude of the primordial spectrum of scalar inflationary perturbation, A_S ;
- the spectral index of of the primordial spectrum of scalar inflationary perturbation, n_S .

Equivalently we may consider the Hubble constant H_0 ($= 100 h$ [Km/s/Mpc]) instead of θ_{MC} . In what follows we review the current constraints on these parameters.

I.VI DATA STORYTELLING

So far we have outlined a phenomenological model of the Universe with only six degrees of freedom. We can therefore use cosmological observations to constrain such free parameters.

It should be clear from our previous discussion of the Cosmic Microwave Background Radiations that the study of the angular spectrum of CMB polarization and isotropies play a crucial role in observational cosmology since the combined analysis of the TT TE and EE correlators breaks the degeneracy among the different parameters allowing us to obtain precise values for all of them. Furthermore, along with the Cosmic Microwave Background, other cosmological observations can be used to improve these results.

Methodology

Here we use the final release of Planck 2018 temperature and polarization data [42], combined with other cosmological observations, to derive updated bounds on the Λ CDM model. In particular we perform Monte Carlo Markov Chain (MCMC) analyses using the publicly available package CosmoMC [107, 108] and computing the theoretical model with the latest version of the Boltzmann code CAMB [109, 110]. We consider the canonical Λ CDM model described by the usual six-parameters.

The posteriors of our parameter space have been explored using the MCMC sampler developed for CosmoMC and tailored for parameter spaces with a speed hierarchy which also implements the "fast dragging" procedure described in Ref. [111]. The convergence of the chains obtained with this procedure

is tested using the Gelman-Rubin criterion [112] and we choose as a threshold for chain convergence $R - 1 \lesssim 0.02$.

Our baseline data-set consists of:

- Planck 2018 temperature and polarization (TT TE EE) likelihood, which also includes low multipole data ($\ell < 30$) [42, 113, 114]. We refer to this combination as "Planck".
- Planck 2018 lensing likelihood [115], constructed from measurements of the power spectrum of the lensing potential. We refer to this dataset as "lensing".
- Baryon Acoustic Oscillations (BAO) measurements extracted from data from the 6dFGS [116], SDSS MGS [117] and BOSS DR12 [118] surveys. We refer to this dataset as "BAO".
- Type Ia Supernovae (SNeIa) distance moduli measurements from the Pantheon sample [119]. We refer to this dataset as "Pantheon".

In particular we stress that for the Planck data we consider both the high-multipole likelihood (which includes multipoles $30 \lesssim \ell \lesssim 2500$ for the TT spectrum and $30 \lesssim \ell \lesssim 2000$ for TE and EE spectra) and the "low-E" polarization likelihood (which covers the multipole range $2 \leq \ell \leq 30$ for the EE spectrum). In this way, analyzing the Planck anisotropies and polarization measurements, we can derive constraints on all the cosmological parameters of the model. Furthermore, we combine the Planck TT TE EE spectra with the Planck lensing measurement. Indeed the CMB photons that we measure today traversed almost the entire observable Universe and, along their paths, are deflected by gradients in the gravitational potentials associated with inhomogeneities in the Universe. This can cause a smoothing of the acoustic peaks and a conversion of E-mode polarization into B-mode polarization. Therefore the Planck lensing reconstruction, being the most significant detection of CMB lensing to date, is useful to improve the constraints on cosmological parameters, providing sensitivity above all on parameters that affect the late-time expansion and the background geometry. However, while the Planck lensing measurements partially break the geometric degeneracy, it is well known that the inclusion of the baryon acoustic oscillation (BAO) measurements from galaxy surveys is a much more powerful way to break degeneracy in the geometrical sector. BAOs are the counterpart to the CMB acoustic peaks in the baryon distribution which remain imprinted also into the present-day matter distribution. Using the transverse BAOs information one can constrain the ratio between the comoving angular diameter distance (D_M) and the sound horizon (r_d) at the epoch when the baryon evolution becomes unaffected by coupling to photons. On the other hand, from the line-of-sight information we can constrain the quantity $H(z) r_d$. These two information can be combined together to constrain the acoustic-scale distance ratio $D_V/r_d \doteq [cz D_M^2(z) H^{-1}(z)]^{1/3} / r_d$. The acoustic scale measured by BAOs (at around 147 Mpc), being much larger than the scale of virialized structures, makes the BAO measurements relatively simple geometric measurements insensitive to nonlinear physics, providing a robust geometrical test of cosmology. Here, in combination with the Planck data, we use the measurements of D_V/r_d from the 6dF survey at an effective redshift $z_{\text{eff}} = 0.106$ [120], the SDSS Main Galaxy Sample at $z_{\text{eff}} = 0.15$ [117] and the final BOSS DR12 data with separate constraints on $H(z) r_d$ and D_M/r_d in three correlated redshift bins at $z_{\text{eff}} = [0.38, 0.51, 0.61]$ [118].

The results for cosmological parameters are given in Table I.1 for different combinations of the datasets listed above. On the other hand in Figure I.8 we show the 1D and 2D posterior distributions of the six free parameters of the standard Λ CDM cosmological model. It is worth pointing out that, once these parameters are fixed by observations, the whole cosmological evolution is determined as all the other cosmological parameters can be derived starting from the knowledge of these six ones. In Figure I.9 we show the marginalized 2D distributions of different derived cosmological parameters, most of them introduced in the previous discussions. In what follows we briefly review the major results.

Inflation and Adiabatic Scalar Modes

Two of the six parameters of the standard cosmological model are related to inflation. Indeed both the spectral amplitude of adiabatic scalar modes A_s and the spectral index n_s are free parameters in the Λ CDM

Parameter	Planck (TT TE EE)	+ lensing	+ lensing + phanteon	+ lensing + BAO	+ lensing + BAO + Pantheon
$\Omega_b h^2$	0.02236 ± 0.00015	0.02237 ± 0.00015	0.02239 ± 0.00014	0.02242 ± 0.00014	0.02243 ± 0.00013
$\Omega_c h^2$	0.1202 ± 0.0014	0.1200 ± 0.0012	0.1197 ± 0.0011	0.11933 ± 0.00091	0.11921 ± 0.00089
$100 \theta_{MC}$	1.04090 ± 0.00031	1.04092 ± 0.00031	1.04095 ± 0.00031	1.04101 ± 0.00029	1.04102 ± 0.00029
τ	0.0544 ± 0.0079	0.0544 ± 0.0073	0.0551 ± 0.0073	0.0561 ± 0.0071	0.0564 ± 0.007
$\log(10^{10} A_s)$	3.045 ± 0.016	3.044 ± 0.014	3.045 ± 0.014	3.047 ± 0.014	3.047 ± 0.014
n_s	0.9649 ± 0.0044	0.9649 ± 0.0042	0.9655 ± 0.0041	0.9665 ± 0.0038	0.9668 ± 0.0037
H_0 [km/s/Mpc]	67.27 ± 0.60	67.36 ± 0.54	67.48 ± 0.50	67.66 ± 0.42	67.72 ± 0.40
Ω_m	0.3166 ± 0.0084	0.3153 ± 0.0073	0.3136 ± 0.0068	0.3111 ± 0.0056	0.3103 ± 0.0054
Ω_Λ	0.6889 ± 0.0056	0.6847 ± 0.0073	0.6864 ± 0.0068	0.6889 ± 0.0056	0.6897 ± 0.0054
σ_8	0.8120 ± 0.0073	0.8111 ± 0.0060	0.8108 ± 0.0060	0.8102 ± 0.0060	0.8100 ± 0.0060
$S_8 \doteq \sigma_8 (\Omega_m/0.3)^{1/2}$	0.834 ± 0.016	0.832 ± 0.013	0.829 ± 0.012	0.825 ± 0.011	0.824 ± 0.010
$100 \theta_*$	1.04109 ± 0.00030	1.04110 ± 0.00031	1.04113 ± 0.00030	1.04119 ± 0.00029	1.04120 ± 0.00029
$r_{s,*}$ [Mpc]	144.39 ± 0.30	144.43 ± 0.26	144.49 ± 0.25	144.57 ± 0.22	144.59 ± 0.21
k_D [Mpc $^{-1}$]	0.14078 ± 0.00028	0.14087 ± 0.00030	0.14083 ± 0.00029	0.14078 ± 0.00028	0.14076 ± 0.00028
z_{re}	7.68 ± 0.79	7.67 ± 0.73	7.73 ± 0.73	7.82 ± 0.71	7.85 ± 0.7
Y_p^{BBN}	0.246716 ± 0.000059	0.246721 ± 0.000057	0.246729 ± 0.000055	0.246740 ± 0.000052	0.246744 ± 0.000051
Age [Gyr]	13.800 ± 0.024	13.797 ± 0.023	13.793 ± 0.022	13.787 ± 0.020	13.785 ± 0.020

TABLE I.1: Results for the Λ CDM cosmological model obtained for different combinations of datasets. The bounds on parameters are 1σ errors (68% CL).

model and we can fix them only by observation since inflation does not predict their magnitude. From data we obtain at 68% CL

$$\log(10^{10} A_s) = 3.044 \pm 0.014 \quad \text{Planck (TT TE EE + lensing)}, \quad (\text{I.322})$$

$$n_s = 0.9649 \pm 0.0042 \quad \text{Planck (TT TE EE + lensing)}. \quad (\text{I.323})$$

Therefore the spectrum of scalar (adiabatic) perturbations is measured with great precision and it should be noted that the result for the scalar spectral index is one of the major successes of inflation theory. Indeed, in the simplest single field slow roll inflation paradigm, due to the breaking of the de-Sitter isometries by a dynamical scalar field (the inflaton), we expect a slightly red tilted spectrum $n_s = 1 - 2\eta_V - 6\epsilon_V \lesssim 1$ that is exactly what we measure. At the beginning of the next chapter, we will study extensively the observational constraints on the standard paradigm of inflation, so we postpone a more precise discussion of the implications on the physics of inflation to the next chapter.

Acoustic oscillations, sound horizon and dumping tail

The acoustic oscillations in the TT correlator discussed in the previous section on the CMB radiation, correspond to a sharply-defined acoustic angular scale on the sky, given by

$$\theta_* = \frac{r_{s,*}}{D_M} \quad (\text{I.324})$$

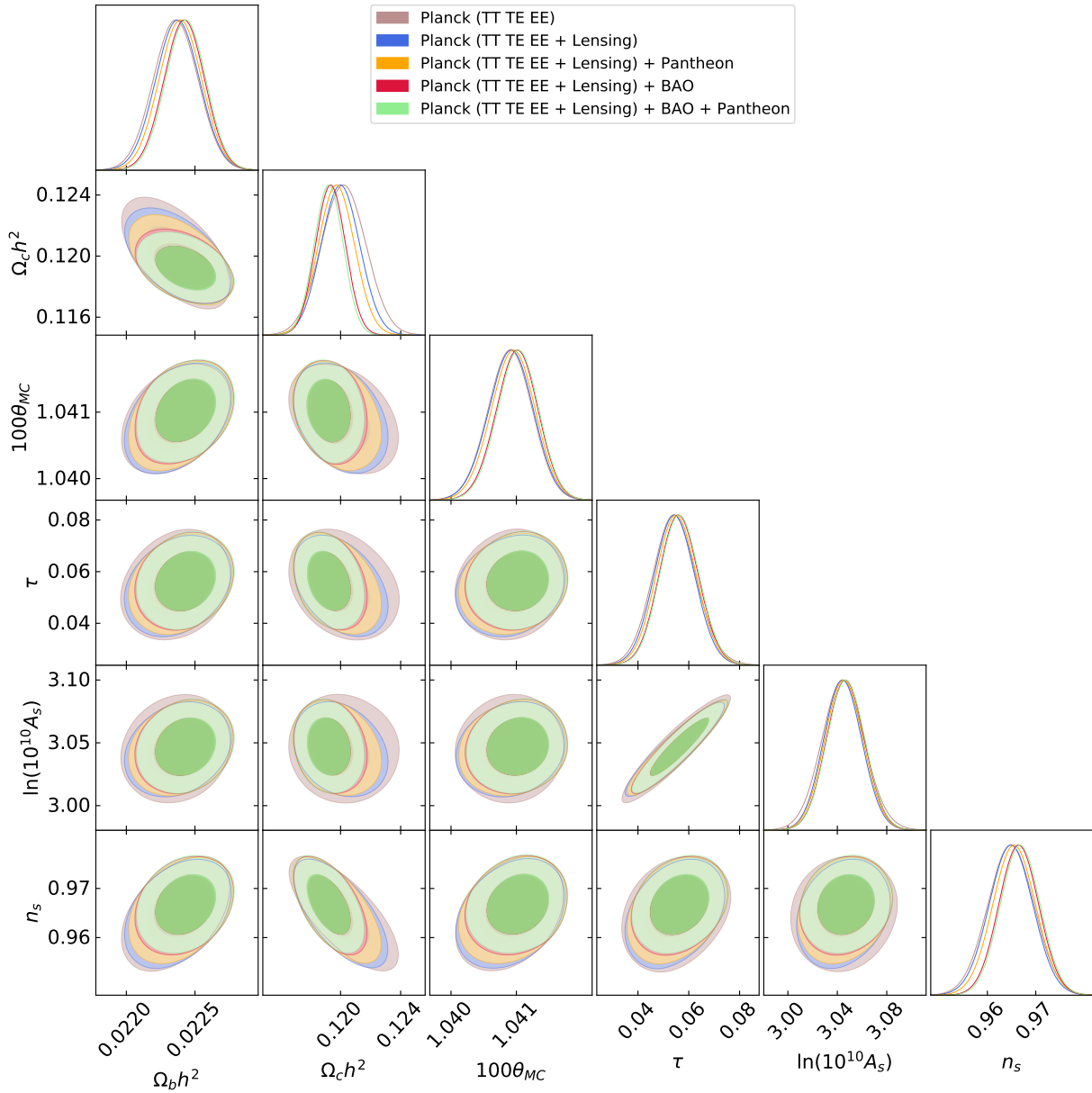


FIGURE I.8: Marginalized 2D and 1D posteriors of the six free parameters of standard Λ CDM Cosmological Model obtained exploiting different combinations of cosmological data-sets listed above.

with $r_{s,*}$ the (comoving) sound horizon at recombination and $D_M = (1 + z) D_A$ the comoving angular distance. In practice θ_* is nothing but the angular distance corresponding to the sound horizon at recombination. The CMB data by the Planck Collaborations measure at 68% CL

$$100 \theta_* = 1.04110 \pm 0.000311 \quad \text{Planck (TT TE EE + lensing)} \quad (\text{I.325})$$

with a precision of about 0.03%. Notice that since θ_* has a simple geometrical interpretation, these results are very robust and almost independent both on the datasets and also on of the cosmological model.

Similarly we can extract information also on the physical size of the Sound Horizon $r_{s,*}$ at recombination, obtaining at 68% CL

$$r_{s,*} = 144.43 \pm 0.26 \text{ Mpc} \quad \text{Planck (TT TE EE + lensing)} \quad (\text{I.326})$$

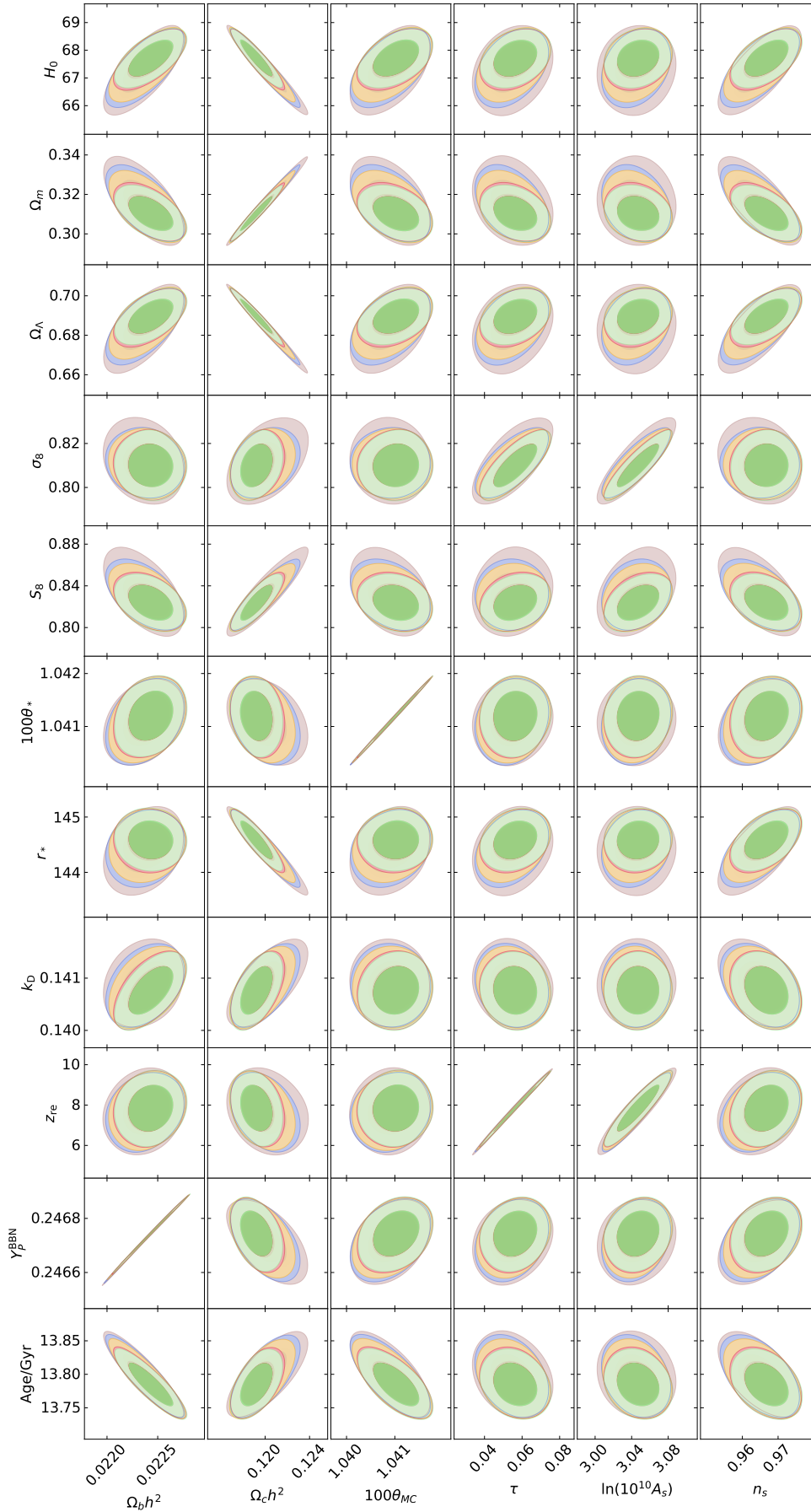


FIGURE I.9: Marginalized 2D contours for different (derived vs primary) parameters and datasets.

and on the dumping scale k_D given by Eq.(I.193) obtaining always at 68% CL

$$k_D = 0.14087 \pm 0.00030 \text{ Mpc}^{-1} \quad \text{Planck (TT TE EE + lensing)} \quad (\text{I.327})$$

Reionization

As we have already pointed out, the sub-horizon CMB anisotropies are scattered by free electrons that are present after reionization, and their observed amplitude decays as $A_s e^{-2\tau}$, where τ is the reionization optical depth, measured with good precision

$$\tau = 0.0544 \pm 0.0073 \quad \text{Planck (TT TE EE + lensing)} \quad (\text{I.328})$$

at 68% CL. Combining the anisotropies and polarization (cross) correlators, see Tab(I.1), one can extract information on the redshift when reionization takes place. Assuming a parametrization for the ionization fraction

$$x_e \doteq \frac{n_e}{n_H} = \frac{1 + n_{\text{He}}/n_H}{2} \left[1 + \tanh \left(\frac{y(z_{\text{re}}) - y(z)}{\Delta y} \right) \right] \quad (\text{I.329})$$

with $y(z) = (1+z)^{3/2}$, $\Delta y \simeq \frac{3}{4}(1+z_{\text{re}})^{1/2}$, this implies a mid-point redshift of reionization measured to be at 68% CL

$$z_{\text{re}} = 7.67 \pm 0.73 \quad \text{Planck (TT TE EE + lensing)} \quad (\text{I.330})$$

which tells us that reionization is a quite recent event in the Universe whose physical nature is still debated.

Dark Matter and Dark Energy

As one can see in Table I.1, the Baryon and Cold Dark Matter content in the Universe, $\Omega_b h^2$ and $\Omega_c h^2$ respectively, are measured with a great precision by current cosmological observations:

$$\Omega_b h^2 = 0.02237 \pm 0.00015 \quad \text{Planck (TT TE EE + lensing)} \quad (\text{I.331})$$

$$\Omega_c h^2 = 0.1200 \pm 0.0012 \text{ Planck (TT TE EE + lensing)} \quad (\text{I.332})$$

both at 68% CL. This means that the matter and energy content of the Universe is well understood. In particular, the matter density can be measured from the CMB spectra using the scale-dependence of the amplitude, as, for fixed θ_* , a larger matter density would reduce the small-scale CMB power. Furthermore, the matter density also affects the amount of lensing in the CMB spectra and the amplitude of the CMB-lensing reconstruction spectrum. Therefore we can obtain at 68% CL the tight constrain

$$\Omega_m = 0.3153 \pm 0.0073 \quad \text{Planck (TT TE EE + lensing)} \quad (\text{I.333})$$

from which it follows that about the 31% of the energy content of the Universe is due to matter. In particular Baryonic matter is only a small fraction (about 4%) while the largest contribution is due to Cold Dark Matter. Indeed baryonic matter can be constrained at sub-percent level, see Table I.1 since changes in the baryon density would affect the CMB angular spectrum in characteristic ways, modifying the relative heights of the even and odd acoustic peaks, see also the discussion on CMB anisotropies. Notice also that, a very important quantity in the matter (power spectrum) measurements is the parameter σ_8 defined to be the root mean squared of the fluctuations over a volume of radius $8 h^{-1}$ Mpc. Indeed this is constrained by the detection of the Baryon Acoustic Oscillations that, due to the effect of the oscillations of baryons (that are tightly coupled to photons before decoupling and then oscillate with them) are imprinted at small scales in the matter power spectrum. From the CMB data, we get at 68% CL for σ_8

$$\sigma_8 = 0.8111 \pm 0.0060 \quad \text{Planck (TT TE EE + lensing)}. \quad (\text{I.334})$$

Alternatively one can use the combination $S_8 \doteq \sigma_8 (\Omega_m/0.3)^{1/2}$ obtaining at 68% CL

$$S_8 = 0.832 \pm 0.013 \quad \text{Planck (TT TE EE + lensing)}. \quad (\text{I.335})$$

Finally, since the Universe is regarded to be spatially flat ($\Omega_k = 0$) and the radiation energy density is expected to be negligibly small ($\Omega_r \ll \Omega_m$), because of Eq.(I.25), this means that the missing fraction of energy density, about $\sim 69\%$, must be accounted by Dark Energy. We recall that within the standard Λ CDM model, Dark Energy is assumed to be the cosmological constant term in the Einstein equations so that $\Omega_\Lambda = 1 - \Omega_m$. From the CMB measurements it follows that at 68% CL

$$\Omega_\Lambda = 0.6847 \pm 0.0073 \quad \text{Planck (TT TE EE + lensing)}. \quad (\text{I.336})$$

that corresponds to a value $\Lambda \simeq 4.2 \times 10^{-66} \text{ eV}^2$ for the cosmological constant. This value is much smaller than those expected for example in Quantum Field Theory where Λ can be interpreted as the vacuum energy and so its physical meaning is not clear yet.

The Expansion Rate and the Age of the Universe

The Hubble constant is one of the most important cosmological parameters since it quantifies the expansion rate of the Universe. The CMB measurements fix H_0 at 68% CL to

$$H_0 = 67.36 \pm 0.54 \text{ [Km/s/Mpc]} \quad \text{Planck (TT TE EE + lensing)} \quad (\text{I.337})$$

Notice that the CMB radiation carries information about the Early Universe while H_0 quantifies the expansion rate today. This means that this value is extrapolated by data within the Λ CDM cosmological model. In the last years several convincing evidences for a statistically significant tension between the value of H_0 derived by measurements of the Early Universe (CMB) and those derived by late time measurements (Supernovae) suggest either systematic in (one of) these experiments or possible modifications to the standard Λ CDM paradigm. We remand to Ref. [121] for an extensive review of the problem and its possible solutions.

Once that the energy-density content and the expansion rate of the Universe are specified, the age of the Universe can be easily computed integrating the cosmological evolution from early to late time. The CMB measurements give at 68% CL

$$\text{Age} = (13.797 \pm 0.023) \times 10^9 \text{ [year]} \quad \text{Planck (TT TE EE + lensing)}. \quad (\text{I.338})$$

which is not very different from a rough estimation that we can obtain simply by $\sim 1/H_0$.

I.V.II BEYOND THE STANDARD COSMOLOGICAL MODEL

The Λ CDM model described so far has been hugely successful in describing most of the cosmological observations of the last century. However it is also true that simplicity is not always a prerogative of nature and this phenomenological model can be regarded as an approximation to a more accurate scenario that still needs to be fully explored (or even understood) both theoretically and experimentally. Therefore it is not guaranteed at all that the same model will fit more precise observations from widely different cosmic epochs and scales from current and future cosmic observers.

As a matter of fact, in the last years several convincing evidences for a statistically significant tension between early and late Universe [121–124] are undermining the stability of the scenario developed in the past century. While these tensions could be explained in terms of systematic errors in the CMB and/or astrophysical experiments currently unaccounted for, they can also suggest possible modifications to the standard Λ CDM paradigm [121, 124]. In addition, the recent debate on the spatial curvature of the Universe [125] opens several other points of discussion.

What is sure is that current and future improvements in the experimental measurements may open up a unique observational window for testing extensions of this standard scenario with increasing precision.

Among all the possible extensions that may be considered, probably the most relevant are those connected with fundamental interactions. In the following chapters of this work we consider different extensions of the standard cosmological model that will allow us to constrain very different branches of fundamental physics, testing global theoretical scenarios beyond General Relativity and the Standard Model of particle physics.

In particular in **chapter II** we focus on relic gravity waves from inflation that, being produced at extremely high energy scales, may carry *unique* information about the theory of gravity nearly the dawn of time, soon after the Big Bang singularity. We study - both from a theoretical, phenomenological and data analysis perspective - the way non standard physics beyond the slow roll paradigm with Einstein gravity can be encapsulated into different cosmological observables.

Conversely, in **chapter III** we explore the possibility to constrain well motivated extensions of the Standard Model of particle physics with current and future cosmological data. In particular we focused on QCD Axions produced in the Early Universe via thermal channels in realistic mixed hot dark matter scenarios that consider also massive neutrinos as extra thermal species.

CHAPTER II

PRIMORDIAL GRAVITATIONAL WAVES

The search for tensor modes, a stochastic background of gravitational waves sourced by a super-adiabatic amplification of zero-point quantum fluctuations during inflation, is one of the major goals of modern cosmology as they may both provide substantial evidence for Primordial Inflation and shed light on its physical nature. In this chapter, after presenting an extensive updated review of the cosmological constraints on slow roll Inflation, I study the way non-standard high-energy physics may be encoded in the tensor two-point function, inferring how the usual power-law parametrization can be broken by large surveys of mechanisms and discussing the implications for large and small scale observations.

II.I COSMOLOGICAL CONSTRAINTS ON SLOW ROLL INFLATION

In the previous chapter we reviewed how in the very Early Universe a phase of almost de Sitter expansion known as Cosmological inflation is supposed to set the initial condition for Hot Big Bang Theory evolution, driving the Universe towards homogeneity and flatness [79].

According to the standard paradigm of inflation, a dynamical scalar field ϕ , the inflaton, can easily induce such an epoch of expansion provided that the inflationary potential $V(\phi)$ is sufficiently flat to allow a phase of slow roll evolution [54, 77, 126, 127]. Furthermore, the quantum fluctuations of the field around its classical trajectory, becoming classical on large scales, can induce energy-density fluctuations, sourcing both rotational invariant scalar modes and, if the energy scale of inflation is sufficiently high, a satiable background of Primordial Gravitational Waves (PGWs) [13, 14, 55, 126–132]. As we anticipated in the first chapter, the search for primordial gravitational waves is one of the main goals of modern cosmology as they can both provide a substantial evidence for primordial inflation and shed light on its physical nature [12–14, 55, 79, 126–129, 133–142]. Being scalar and tensor perturbations decoupled at the linearized level, they can be treated separately. After the end of inflation, scalar perturbations re-enter the observable Universe, setting the seeds for the structure formation and providing a quite natural explanation for the observed anisotropies in the Cosmic Microwave Background (CMB). On the other hand, PGWs may imprints the CMB photon polarization, leading to a very distinctive signature in the B-modes spectrum on large angular scales [12–14, 54, 79, 126–129, 143].

In the framework of single-field inflation with Einstein gravity, primordial scalar and tensor perturbations are expected to be (nearly) Gaussian and hence they can be described in terms of their two-point correlation functions and their primordial spectra. It is well known that the spectrum of the quantum fluctuations of a (massless) scalar field in a de Sitter background is flat. Therefore, since both scalar and tensor perturbations are sourced by the fluctuations of the inflaton field in an almost de Sitter background, we expect nearly but not exactly flat primordial spectra. From Eqs (I.267) and (I.274) it follows that, in terms of the inflationary parameters (I.232a) - (I.232d), the primordial spectra are [12–14, 55, 56, 144–159]

$$\mathcal{P}_s = \left(\frac{1}{8\pi^2 M_{\text{pl}}^2} \right) \left(\frac{H^2}{\epsilon_V} \right) = \left(\frac{1}{12\pi^2 \bar{M}_p^6} \right) \left(\frac{V^3}{V_\phi^2} \right), \quad (\text{II.1})$$

$$\mathcal{P}_T = \left(\frac{2}{\pi^2 \bar{M}_p^2} \right) H^2 = \left(\frac{2}{3\pi^2 \bar{M}_p^4} \right) V. \quad (\text{II.2})$$

Notice that, by definition, the expansion rate is almost but not exactly constant during the slow-roll evolution ($H^2 \gg |\dot{H}|$). Since both the Hubble parameter and the Inflationary potential, slightly evolve with time during Inflation, we evaluate the spectra at the time when the wave-number k exits the causal horizon, namely at $k = aH$. As pointed out in subsection I.IV.II, after the horizon-exit, scalar and tensor modes freeze-out and the spectra approach to a constant value. For this reason, the perturbations produced by generic single-field models are typically well approximated by the following power-law form of the adiabatic scalar and tensor components

$$\log \mathcal{P}_s(k) = \log A_s + (n_s - 1) \log(k/k_*) + \dots \quad (\text{II.3})$$

$$\log \mathcal{P}_T(k) = \log(r A_s) + (n_T) \log(k/k_*) + \dots \quad (\text{II.4})$$

where k_* denotes an arbitrary scale known as *pivot scale*, $A_s \doteq \mathcal{P}_s(k_*)$ and $A_T \doteq \mathcal{P}_T(k_*)$ are the scalar and tensor amplitudes computed at the pivot scale and $r \doteq A_T/A_s$ is the so called tensor-to-scalar ratio. We have also defined the scalar and tensor spectral index (or tilt) respectively as

$$n_s - 1 \doteq \left[\frac{d \log \mathcal{P}_s(k)}{d \log k} \right]_{k=k_*}, \quad (\text{II.5})$$

$$n_T \doteq \left[\frac{d \log \mathcal{P}_T(k)}{d \log k} \right]_{k=k_*}. \quad (\text{II.6})$$

The scalar and tensor tilts quantify the departure from the scale-invariant case and in this simplest scenario we expect slightly tilted spectra because of the field evolution which breaks the de Sitter isometries, providing also a well define clock to measure the time to the end of inflation. Notice anyway that inflation does not predict neither the precise values of the amplitudes nor those of the tilts, but they depend on the details of the inflationary dynamics which is clearly related to the precise shape of the potential. Indeed, using Eqs.(II.1) - (II.2), one can write the scalar and tensor tilt in terms of the slow-roll parameters as

$$n_s - 1 = 2\eta_V - 6\epsilon_V = -2\epsilon_1 - \epsilon_2, \quad (\text{II.7})$$

$$n_T = -2\epsilon_V = -r/8 \quad (\text{II.8})$$

from which we see that constraints on the spectral parameters can be translated into constraints on the inflationary potential and the background dynamics (or vice-versa). Within the power-law parametrization, both n_s and n_T can be assumed to be scale-independent and the higher order terms in Eqs. (II.3) and (II.4) negligible. However this is an approximation and further parametrizations that include also higher-order corrections may be considered [2, 160, 161]. Furthermore, it is worth noting that today only the scalar amplitude and tilt are measured with good precision [78] while a detection of primordial tensor modes is still missing. Indeed, a combined analysis of the Planck measurements of the CMB polarization and anisotropies [78] and the BICEP2/Keck array likelihood for B-modes polarization [162] constrains the amplitude of primordial gravitational waves on scales comparable to the current Hubble length ($a_0 H_0 = 2.248 \times 10^{-4} \text{Mpc}^{-1}$), placing only an upper bound on the tensor to scalar ratio at a pivot scale $k_* = 0.002 \text{Mpc}^{-1}$ of $r_{0.002} < 0.056$ at 95% Confidence Level (CL hereafter).

Therefore, even though current observations show a general agreement with the standard slow-roll predictions and many inflationary models proposed in literature can be ruled out, the missing evidence for tensor modes and, in general, the present day accuracy in data places only generic constraints on inflation that in many cases are obtained within specific assumptions (*e.g.* an exactly flat background geometry, a vanishing scale dependence of the scalar - and tensor - tilt or even a negligible tensor amplitude).

In this section we provide an updated review of the cosmological constraints on slow roll inflation, analyzing different extensions of the standard Λ CDM model. Because of the inflationary perspective of this chapter, we are basically interested in exploring modifications in the primordial sector. By using the slow-roll approximation we derive a set of consistency relations between higher-order scalar and tensor parameters, generalizing the power-law expansion for the primordial spectra up to the third order and constraining the additional parameters in light of the most recent cosmological observations. We also relate the primordial perturbations to the dynamics of the Hubble parameter during inflation and the derivatives of the inflationary potential, constraining these quantities and interpreting the results in terms of the physics of the inflationary epoch.

II.I.1 METHODOLOGY

In this subsection we outline the methodology used in our analysis. We highlight the modifications to the primordial sector and discuss the additional parameters that we introduce in the cosmological model. Then, we review our data-analysis techniques and the datasets used to derive our results.

Cosmological Model

We analyze the slow-roll paradigm of inflation considering different extensions of the standard Λ CDM model. We consider the standard six-parameters of Λ CDM *i.e.*, the baryon $\omega_b \doteq \Omega_b h^2$ and cold dark matter $\omega_c \doteq \Omega_c h^2$ energy densities, the angular size of the horizon at the last scattering surface θ_{MC} , the

optical depth τ , the amplitude of primordial scalar perturbation $\log(10^{10} A_s)$ and the scalar spectral index n_s . Along with them, we consider also other different combinations of additional parameters that involve modifications in the primordial sector. In particular we generalize Eqs.(II.3) to the following expansion

$$\log \mathcal{P}_s(k) = \ln A_s + (n_s - 1) \log(k/k_*) + \frac{\alpha_s}{2} \log^2(k/k_*) + \frac{\beta_s}{6} \log^3(k/k_*) \quad (\text{II.9})$$

introducing a weak scale-dependence in the primordial spectrum modeled by the running of the scalar tilt α_s or also its running of running β_s defined respectively as

$$\alpha_s \doteq \left[\frac{dn_s}{d \log k} \right]_{k=k_*} \quad \beta_s \doteq \left[\frac{d\alpha_s}{d \log k} \right]_{k=k_*} \quad (\text{II.10})$$

where the running α_s quantifies the rate of change of n_s per Hubble time (we recall that $d/d \log k = 1/H d/dt$) while the running of running β_s quantifies the rate of change of α_s per Hubble time. These quantities are related to the shape of the inflationary potential (or equivalently to the dynamics of the background evolution) and consequently to the underlying physics of inflation. Under the slow-roll assumption, α_s and β_s can be both expressed in terms of the potential slow-roll parameters $\{\epsilon_V, \eta_V, \zeta_V^2, \omega_V^3\}$ as

$$\alpha_s = +16\epsilon_V \eta_V - 24\epsilon_V^2 - 2\zeta_V^2 \quad (\text{II.11})$$

$$\beta_s = -192\epsilon_V^3 + 192\epsilon_V^2 \eta_V - 32\epsilon_V \eta_V^2 - 24\epsilon_V \zeta_V^2 + 2\eta_V \zeta_V^2 + 2\omega_V^3$$

or, equivalently, in terms of the parameters $\{\epsilon_i\}$ as

$$\alpha_s = -2\epsilon_1 \epsilon_2 - \epsilon_2 \epsilon_3 \quad (\text{II.12})$$

$$\beta_s = -2\epsilon_1 \epsilon_2^2 - 2\epsilon_1 \epsilon_2 \epsilon_3 - \epsilon_2 \epsilon_3^2 - \epsilon_2 \epsilon_3 \epsilon_4 \quad (\text{II.13})$$

with $\epsilon_V \simeq \epsilon_1 \simeq r/16$ which is clearly related to the amplitude of the tensor spectrum.

Similarly, for the tensor spectrum we adopt the parameterization

$$\log \mathcal{P}_T(k) = \log(r A_s) + (n_T) \log(k/k_*) + \frac{\alpha_T}{2} \log^2(k/k_*) + \frac{\beta_T}{6} \log^3(k/k_*). \quad (\text{II.14})$$

Along this section we adopt the same pivot scale of $k_* = 0.05 \text{ Mpc}^{-1}$ both for scalar and tensor perturbations and we consider the tensor-to-scalar ratio $r \doteq A_T/A_s$ a free parameter while we use the slow-roll consistency relation $n_T = -r/8$ for the tensor tilt. We also relate the higher order tensor runnings

$$\alpha_T \doteq \left[\frac{dn_T}{d \log k} \right]_{k=k_*} \quad \beta_T \doteq \left[\frac{d\alpha_T}{d \log k} \right]_{k=k_*} \quad (\text{II.15})$$

to the scalar ones by a set of slow-roll consistency relations. Indeed, under the assumption of slow-roll inflation, a set of consistency relations among scalar and tensor parameters can be derived at any order¹ [1, 127]. In particular, the slow-roll consistency relations for the tensor running and running of running are [1]

$$\alpha_T = \frac{r}{8}(n_s - 1) + \frac{r^2}{64}, \quad (\text{II.16})$$

$$\beta_T = \frac{r}{8} \left[\alpha_s - (n_s - 1)^2 \right] - \frac{3r^2}{64} (n_s - 1) - \frac{r^3}{256}. \quad (\text{II.17})$$

¹It should be noted that these relations can be violated in many non standard inflationary models, *e.g.* in presence of other spectator (rolling) fields [2, 163–166] or in modified gravity theories [3, 4, 94, 167–171].

Parameter	Prior
$\Omega_b h^2$	[0.005, 0.1]
$\Omega_c h^2$	[0.001, 0.99]
$100 \theta_{MC}$	[0.5, 10]
τ	[0.01, 0.8]
$\log(10^{10} A_S)$	[1.61, 3.91]
n_s	[0.8, 1.2]
α_s	[-1, 1]
β_s	[-1, 1]
r	[0, 3]
Ω_k	[-0.3, 0.3]

TABLE II.1: List of the parameter priors.

Therefore given constraints on the scalar spectral index n_s , its running α_s and on the tensor-to-scalar ratio r , constraints can be derived on the tensor spectral index n_t , its running α_t , its running of running β_t .

Numerical Analyses and Datasets

We perform Monte Carlo Markov Chain (MCMC) analyses using the publicly available package CosmoMC [107, 108] and computing the theoretical model described in the previous subsection with the latest version of the Boltzmann code CAMB [109, 110]. For all the different cosmological parameters we choose flat prior-distributions (unless otherwise stated), varying them uniformly in the conservative ranges listed in Table II.1. We explore the posteriors of our parameter space using the MCMC sampler developed for CosmoMC and tailored for parameter spaces with a speed hierarchy which also implements the "fast dragging" procedure described in Ref. [111]. The convergence of the chains obtained with this procedure is tested using the Gelman-Rubin criterion [112] and we choose as a threshold for chain convergence $R - 1 \lesssim 0.02$.

Our baseline data-set consists of:

- Planck 2018 temperature and polarization (TT TE EE) likelihood, which also includes low multipole data ($\ell < 30$) [42, 113, 114]. We refer to this combination as "Planck".
- Planck 2018 lensing likelihood [115], constructed from measurements of the power spectrum of the lensing potential. We refer to this dataset as "lensing".
- Baryon Acoustic Oscillations (BAO) measurements extracted from data from the 6dFGS [120], SDSS MGS [117] and BOSS DR12 [118] surveys. We refer to this dataset combination as "BAO".
- CMB B-modes power spectrum likelihood cleaned from the foreground contamination as released by Bicep2/Keck Array X Collaboration [162]. We refer to this dataset as "BK15".
- Atacama Cosmology Telescope DR4 likelihood, combined with WMAP 9-years observations data [172] and a Gaussian prior on $\tau = 0.065 \pm 0.015$, as done in [173]. We refer to this dataset combination as "ACTPol+WMAP".

- South Pole Telescope polarization measurements SPT-3G [174] combined with WMAP 9-years observations data [172] and a Gaussian prior on $\tau = 0.065 \pm 0.015$. We refer to this dataset combination as "SPT3G+WMAP".

As concerns the Planck (CMB and Lensing) data and the BAO measurements, we used the same datasets described in subsection I.V.I. Instead, to improve also the constraints in the primordial tensor sector, we exploit the CMB B-modes power spectrum likelihood (cleaned from the foreground contamination) as released by Bicep2/Keck Array X Collaboration [162]. As discussed in the previous chapter, a satiable background of inflationary gravitational waves can produce B-modes polarization on large/intermediate angular scales where the cosmic variance is not very significant and gravitational lensing is not yet dominant. Notice however that the B-modes likelihood basically improves only the constraints on tensor modes. Therefore we include this dataset only when we analyze the tensor spectrum because interested in models with a satiable production of gravitational waves.

Along with these combinations of datasets involving the Planck CMB measurements, we analyze also two other Planck-independent datasets. In particular we use the Atacama Cosmology Telescope DR4 likelihood and the South Pole Telescope polarization measurements. We combine both of them with WMAP 9-years observations data [172]. The reason is that the Atacama Cosmology Telescope has a minimum sensitivity in multipole of 600 in TT, and 350 in TE and EE, and so it lacks data around the first two acoustic peaks in the TT spectrum and the first full peak in TE and EE. Similarly, the South Pole Telescope measures only the TE and EE spectra over a range of multipoles $300 \leq \ell \leq 1400$ for EE and $300 \leq \ell \leq 1700$ for TE. Therefore, the only way to obtain competitive Planck-independent measurements for all the cosmological parameters is to combine these two datasets with the public WMAP 9-year observations at intermediate scales ($2 < \ell < 1200$ for TT and $\ell < 800$ for TE), as also done in [173, 174]. Notice also that we use a Gaussian prior on $\tau = 0.065 \pm 0.015$ both for ACT+WMAP and for SPT3G+WMAP. Indeed, while our primary goal is to obtain a measurement of the cosmological (inflationary) parameters that is Planck-independent, neither ACT nor SPT-3G can constrain the optical depth at reionization τ . Furthermore there is evidence that WMAP large-scale polarization data ($2 < \ell < 23$ in TE spectrum) can be contaminated by dust, possibly affecting the WMAP bounds on τ . For this reason in our analysis we exclude this multipoles range, using instead the conservative Gaussian prior on τ which is based on Planck measurements. This prior on τ is not expected to affect the constraints on the other cosmological parameters [173, 174].

II.I.II COSMOLOGICAL CONSTRAINTS

In this section we present and discuss the updated observational constraints obtained by our MCMC analysis of the inflationary slow-roll paradigm in extended parameter spaces beyond the standard Λ CDM cosmological model.

Scalar Spectrum: running the Running

We start analyzing an extended cosmological model which includes both the running of the scalar spectral index α_s and its running of running β_s as additional free parameters. We refer to this model as Λ CDM + $\alpha_s + \beta_s$. Notice that here we focus exclusively on the adiabatic scalar modes, parametrizing the scalar spectrum by Eq.(II.9) and assuming a negligible gravitational waves production during the slow roll phase. Assuming a negligible tensor amplitude $r = 16\epsilon_V \simeq 16\epsilon_1 \sim 0$ in terms of the slow-roll parameter means to consider $\epsilon_V \simeq \epsilon_1 \sim 0$; *i.e.*, negligibly small in the relations for the scalar tilt and its runnings. We summarize the results obtained within this assumption in Table II.2, while in Figure II.1 we show the 68% and 95% CL contour plots for different combinations of parameters.

Analyzing the Planck data we derive constraints on the scalar tilt $n_s = 0.9612 \pm 0.0054$, its running $\alpha_s = 0.001 \pm 0.010$, and on its running of running $\beta_s = 0.012 \pm 0.013$, all at 68% CL². The inclusion of the lensing spectrum and the BAO data does not change significantly these results and all these bounds

²Unless otherwise stated, we always provide 68% CL values for bounded parameters and 95% CL for upper/lower bounds.

Parameter	Planck18	Planck18 + lensing	Planck18 + BAO	ACTPol + WMAP	SPT3G+WMAP
$\Omega_b h^2$	0.02235 ± 0.00017	0.02237 ± 0.00016	0.02243 ± 0.00015	0.02195 ± 0.00025	0.02251 ± 0.00025
$\Omega_c h^2$	0.1207 ± 0.0015	0.1202 ± 0.0012	0.1195 ± 0.0010	0.1190 ± 0.0029	0.1139 ± 0.0032
$100 \theta_{MC}$	1.04085 ± 0.00031	1.04089 ± 0.00030	1.04100 ± 0.00028	1.04174 ± 0.00066	1.03970 ± 0.00066
τ	0.0575 ± 0.0086	0.0564 ± 0.0080	0.0590 ± 0.0087	0.061 ± 0.013	0.063 ± 0.013
$\log(10^{10} A_S)$	3.053 ± 0.018	3.049 ± 0.015	3.053 ± 0.018	3.051 ± 0.026	3.037 ± 0.026
n_s	0.9612 ± 0.0054	0.9625 ± 0.0048	0.9645 ± 0.0045	0.9680 ± 0.0082	0.978 ± 0.011
α_s	0.001 ± 0.010	0.002 ± 0.010	0.000 ± 0.010	0.035 ± 0.012	0.028 ± 0.017
β_s	0.012 ± 0.013	0.010 ± 0.013	0.009 ± 0.013	0.035 ± 0.013	0.023 ± 0.016
η_V	$-0.0194^{+0.0027}_{-0.0026}$	$-0.0187^{+0.0025}_{-0.0023}$	$-0.0177^{+0.0021}_{-0.0022}$	-0.0160 ± 0.0041	-0.0111 ± 0.0053
ζ_V^2	-0.0005 ± 0.0050	$-0.0008^{+0.0050}_{-0.0049}$	-0.0001 ± 0.0049	-0.0174 ± 0.0058	-0.0141 ± 0.0085
ω_V^3	$0.0058^{+0.0063}_{-0.0061}$	$0.0051^{+0.0062}_{-0.0061}$	$0.0046^{+0.0062}_{-0.0061}$	0.0172 ± 0.0064	0.0115 ± 0.0078
ϵ_2	$0.0388^{+0.0053}_{-0.0054}$	$0.0375^{+0.0047}_{-0.0049}$	$0.0355^{+0.0044}_{-0.0043}$	0.0320 ± 0.0082	0.022 ± 0.011
ϵ_3	-0.02 ± 0.26	$-0.04^{+0.27}_{-0.26}$	0.00 ± 0.28	< -0.02	—

TABLE II.2: Results for Λ CDM + $\alpha_s + \beta_s$. The constraints on parameters are at 68% CL, while upper bounds are at 95% CL. The internal horizontal line divides the primary parameters of the cosmological model (those we directly sample in our MCMC analysis) from the derived parameters (those we obtain from the others by the relations described in the text).

are consistent with the case of vanishing runnings within one standard deviation, see also [Figure II.1](#). We then compare the Planck bounds with other independent measurements derived using the different datasets listed in [subsection III.I.1](#). Considering the SPT-3G data combined with WMAP 9-years observation data, we get $\alpha_s = 0.028 \pm 0.017$ and $\beta_s = 0.023 \pm 0.016$, both and consistent with zero within 1.6 and 1.4 standard deviations with Planck. On the other hand, considering the ACTPol+WMAP data, we obtain a preference for non-vanishing running $\alpha_s = 0.035 \pm 0.012$ and for a non-vanishing running of running $\beta_s = 0.035 \pm 0.013$ at the level of 2.9σ and 2.7σ , respectively. Interestingly, in both the cases positive values for the runnings are preferred with a statistical significance which ranges between about 1.7σ (SPT-3G+WMAP) and 2.9σ (ACTPol+WMAP). While both the ground based telescope measurements are in good agreement one with each other, it should be noted that they are instead in disagreement at more than 2σ with Planck regarding the value of the running α_s , and in tension for the running of running β_s (see also [Figure II.1](#)). This tension indicates a difference from the high multipoles region that can be either an indication of small systematic errors unaccounted for, or an hint for physics beyond the standard model. In other words, the extended inflationary models considered in this section recast the global tension between the datasets already present for a Λ CDM model analysis [[175](#)]

Under the assumption of a negligible tensor amplitude, we derive constraints also on the slow-roll parameters $\{\eta_V, \zeta_V^2, \omega_V^3\}$ and $\{\epsilon_{i=2,3,4}\}$. Due to the Planck data evidence for a tilted scalar spectrum, we obtain non-zero slow-roll parameters $\eta_V = -0.0194^{+0.0027}_{-0.0026}$ or equivalently $\epsilon_2 = 0.0388^{+0.0053}_{-0.0054}$. On the other hand, the missing evidence for scalar runnings only limits the parameter space allowed for higher-order slow-roll parameters to $\zeta_V^2 = -0.0005 \pm 0.0050$ and $\omega_V^3 = 0.0058^{+0.0063}_{-0.0061}$ both consistent with zero within one standard deviation. Similarly, $\epsilon_3 = -0.02 \pm 0.26$ while ϵ_4 turns out to be unbounded for all the datasets considered in this section. Considering also lensing or BAO in combination with Planck, these constraints do not change significantly, see also [Table II.2](#). Conversely, considering the Atacama Cosmology Telescope DR4 likelihood combined with WMAP 9-years, while the bounds on $\eta_V = -0.0160 \pm 0.0041$ and $\epsilon_2 = 0.0320 \pm 0.0082$ remain basically unchanged with respect to the other datasets, the preference for non vanishing runnings is translated into the constraints on higher-order inflationary parameters $\zeta_V^2 = -0.0174 \pm 0.0058$ and $\omega_V^3 = 0.0172 \pm 0.0064$ (or equivalently $\epsilon_3 < -0.02$ at 95% CL) that are all different

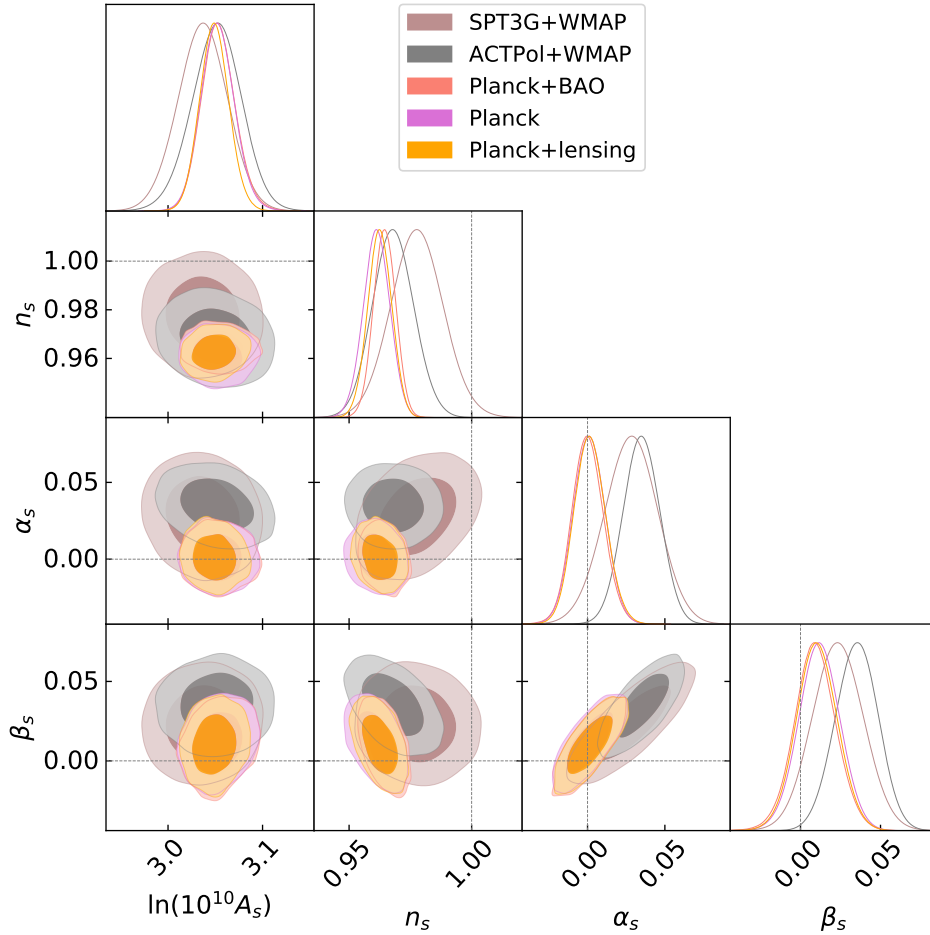


FIGURE II.1: Marginalized 2D and 1D posteriors distributions for the $\Lambda\text{CDM} + \alpha_s + \beta_s$ cosmological model obtained for the different combinations of the datasets listed in [subsection II.I.I](#). The dashed lines represent the case of vanishing inflationary parameters.

from zero at more than 95% CL. Finally, regarding the SPT3G+WMAP case, we find more than 1σ shift towards lower values of both $\eta_V = -0.0111 \pm 0.0053$ and $\epsilon_2 = 0.022 \pm 0.011$, while we find 1σ preference for non-vanishing higher-order parameters $\zeta_V^2 = -0.0141 \pm 0.0085$ and $\omega_V^3 = 0.0115 \pm 0.0078$.

Tensor Spectrum and slow-roll consistency relations

We now include as additional parameters the running of the scalar tilt α_s and the tensor amplitude r , fixing instead the scalar running of running to zero. We refer to this model as $\Lambda\text{CDM} + \alpha_s + r$. We summarize the results obtained for this model in [Table II.3](#) while in [Figure II.2](#) we show the 68% and 95% CL contour plots for different inflationary parameters.

As one can see, for the scalar parameters the constraints on n_s and α_s are slightly changed when we replace the running of running with the tensor-to-scalar ratio. This is due to the fact that also the terms $\propto \epsilon_V$ contribute in the slow roll relations [\(II.7\)](#) and [\(II.12\)](#), modifying the correlation among the inflationary parameters. Furthermore, since α_s and β_s are strongly correlated for all the datasets, see [Figure II.1](#), fixing $\beta_s = 0$ results into a shift of α_s towards lower values. In particular, for the Planck data this shift is translated into a preference for negative values of α_s at the level of slightly more than 1σ even though the constraints on the running are always consistent with zero within two standard deviations. When the lensing and BAO measurements are considered together with Planck these results remain unchanged. Furthermore, ACTPol+WMAP and SPT3G+WMAP shift α_s towards lower values too. This produces a reduction of $\alpha_s = 0.0090 \pm 0.0087$ for ACTPol+WMAP, positive and larger than zero at slightly more than one standard

Parameter	Planck18	Planck18 + lensing	Planck18 + BAO	Planck18 + BK15	ACTPol + WMAP	SPT3G+WMAP
$\Omega_b h^2$	0.02241 ± 0.00016	0.02242 ± 0.00015	0.02247 ± 0.00014	0.02239 ± 0.00015	0.02234 ± 0.00022	0.02273 ± 0.00024
$\Omega_c h^2$	0.1202 ± 0.0014	0.1199 ± 0.0012	0.1193 ± 0.0010	0.1206 ± 0.0014	0.1179 ± 0.0030	0.1138 ± 0.0031
$100 \theta_{\text{MC}}$	1.04091 ± 0.00032	1.04093 ± 0.00030	1.04101 ± 0.00030	1.04087 ± 0.00031	1.04186 ± 0.00065	1.03978 ± 0.00067
τ	0.0562 ± 0.0081	0.0560 ± 0.0076	0.0573 ± 0.0080	0.0570 ± 0.0083	0.058 ± 0.012	0.060 ± 0.013
$\log(10^{10} A_s)$	3.050 ± 0.017	3.049 ± 0.015	3.051 ± 0.017	3.053 ± 0.017	3.049 ± 0.025	3.037 ± 0.026
n_s	0.9642 ± 0.0047	0.9647 ± 0.0044	0.9665 ± 0.0041	0.9629 ± 0.0046	0.9796 ± 0.0074	0.980 ± 0.010
α_s	-0.0094 ± 0.0074	-0.0084 ± 0.0073	-0.0091 ± 0.0075	-0.0080 ± 0.0069	0.0090 ± 0.0087	0.001 ± 0.012
r	< 0.165	< 0.159	< 0.172	< 0.0658	< 0.176	< 0.260
n_T	> -0.0206	> -0.0198	> -0.0215	> -0.0082	> -0.022	> -0.032
α_T	$\left(-18^{+12}_{-10}\right) \cdot 10^{-5}$	$\left(-17 \pm 10\right) \cdot 10^{-5}$	$\left(-16.6^{+11}_{-9.5}\right) \cdot 10^{-5}$	$\left(-11.7^{+7.9}_{-5.9}\right) \cdot 10^{-5}$	$\left(-4.2^{+6.9}_{-10}\right) \cdot 10^{-5}$	$\left(3^{+13}_{-27}\right) \cdot 10^{-5}$
β_T	$\left(11.4^{+6.9}_{-15}\right) \cdot 10^{-5}$	$\left(9.96^{+6.1}_{-14}\right) \cdot 10^{-5}$	$\left(11.8^{+7.2}_{-16}\right) \cdot 10^{-5}$	$\left(3.9^{+2.5}_{-4.8}\right) \cdot 10^{-5}$	$\left(-4.4^{+8.1}_{-6.9}\right) \cdot 10^{-5}$	$\left(5^{+12}_{-21}\right) \cdot 10^{-5}$
$\epsilon_V \simeq \epsilon_1$	< 0.0103	< 0.0099	< 0.0108	< 0.0041	< 0.0110	< 0.0163
η_V	$-0.0058^{+0.0069}_{-0.012}$	$-0.0061^{+0.0066}_{-0.011}$	$-0.0039^{+0.0072}_{-0.012}$	$-0.0130^{+0.0038}_{-0.0050}$	$0.0015^{+0.0074}_{-0.013}$	$0.010^{+0.012}_{-0.019}$
ζ_V^2	0.0044 ± 0.0037	0.0040 ± 0.0036	0.0043 ± 0.0038	0.0038 ± 0.0034	-0.0045 ± 0.0044	$-0.0001^{+0.0056}_{-0.0064}$
ϵ_2	$0.0277^{+0.0095}_{-0.0067}$	$0.0276^{+0.0091}_{-0.0062}$	$0.0250^{+0.0095}_{-0.0064}$	0.0334 ± 0.0054	$0.0126^{+0.012}_{-0.0090}$	$0.006^{+0.016}_{-0.013}$
ϵ_3	—	$0.37^{+0.26}_{-0.34}$	$0.62^{+0.16}_{-0.56}$	0.24 ± 0.21	—	—
$V_{\text{inf}}^{1/4}$	$< 2.04 \times 10^{16} \text{ GeV}$	$< 2.01 \times 10^{16} \text{ GeV}$	$< 2.06 \times 10^{16} \text{ GeV}$	$< 1.62 \times 10^{16} \text{ GeV}$	$< 2.10 \times 10^{16} \text{ GeV}$	$< 2.31 \times 10^{16} \text{ GeV}$

TABLE II.3: Results for $\Lambda\text{CDM} + r + \alpha_s$. The constraints on parameters are at 68% CL, while upper bounds are at 95% CL. The internal horizontal line divides the primary parameters of the cosmological model (those we directly sample in our MCMC analysis) from the derived parameters (those we obtain from the others by the relations described in the text).

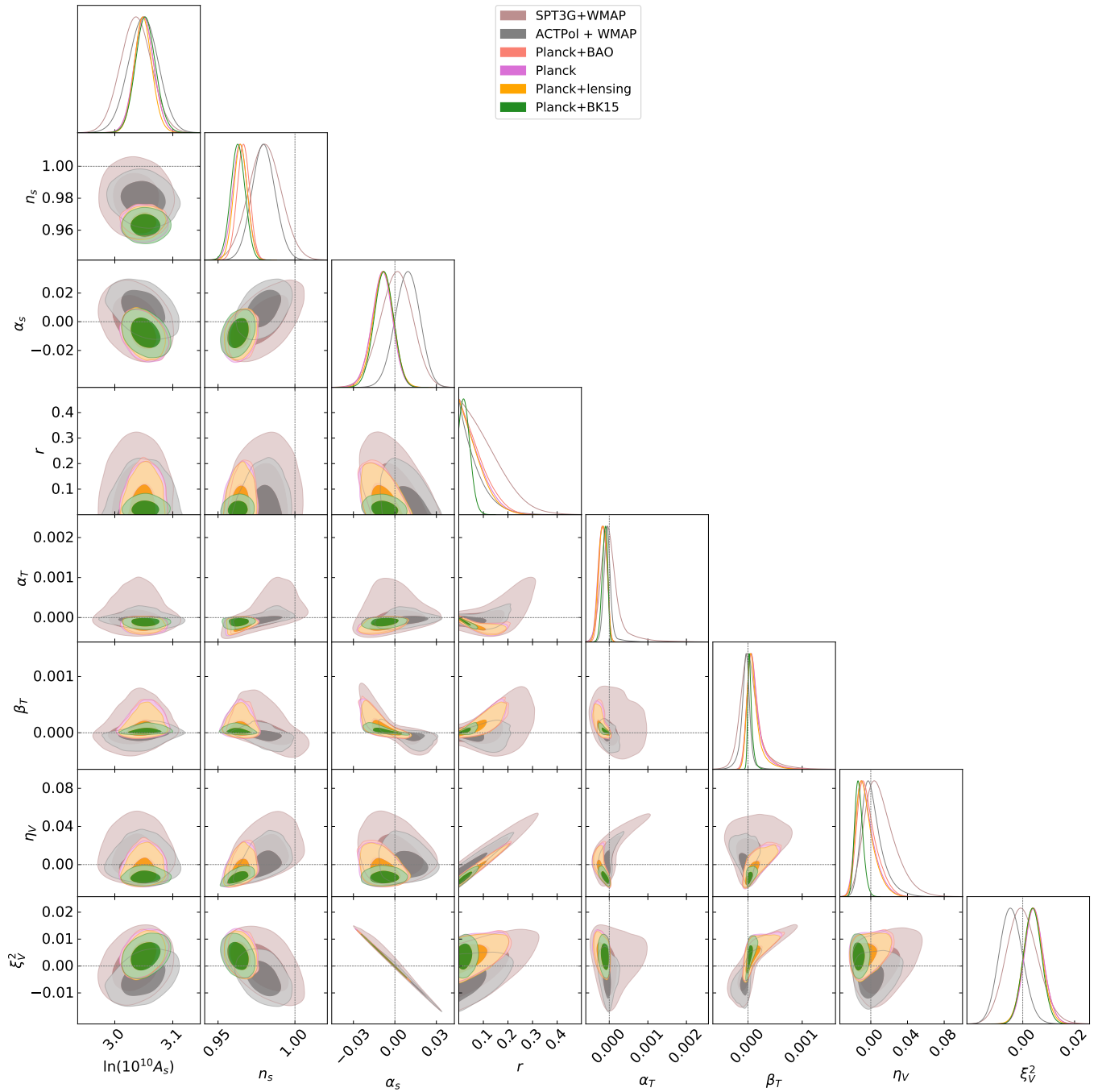


FIGURE II.2: Marginalized 2D and 1D posteriors distributions for the Λ CDM + r + α_s cosmological model obtained for different combinations of datasets listed in subsection III.I.I. The dashed lines represent the case of vanishing inflationary parameters.

deviation, and $\alpha_s = 0.001 \pm 0.012$ for SPT3G+WMAP which is completely in agreement with the case of a vanishing scalar running. It should be noticed anyway that while SPT3G+WMAP is in agreement with Planck for the value of the running α_s , ACTPol+WMAP is instead in disagreement at about 2σ and this tension is still coming from the high multipole region.

As concerns the tensor spectrum, its amplitude is constrained to be $r < 0.165$ (at 95% CL) by the Planck data while ACTPol+WMAP and SPT3G+WMAP give $r < 0.176$ and $r < 0.260$, respectively. A strong improvement in this upper bound is obtained including also the BK15 likelihood that, combined with Planck, gives $r < 0.0658$. Using the slow-roll relation between the tensor amplitude and the tensor tilt, $n_T = -r/8$, these upper bounds on the amplitude can be translated into a lower bounds on the (negative) tensor tilt, see also [Table II.3](#). Furthermore, in the slow-roll framework, any constraint to the tensor amplitude places also a constraint to the energy scale of inflation:

$$V_{\text{inf}}^{1/4} = \bar{M}_{\text{p}} \left(\frac{3}{2} \pi^2 A_s r \right)^{1/4} \text{ GeV.} \quad (\text{II.18})$$

In [Table II.3](#) we show the upper bounds on the energy scale of inflation for the different datasets.

Reversing the slow-roll relations for the scalar and tensor parameters, we derive constraints on the slow-roll parameters $\{\epsilon_V, \eta_V, \zeta_V^2\}$ that are related to the shape of the inflationary potential. In particular from Planck, we get $\epsilon_V < 0.0103$ while the improvement in the constraining power on the tensor amplitude due to the BK15 data is translated into the more stringent upper bound $\epsilon_V < 0.0041$. On the other hand, for η_V and ζ_V^2 the Planck + BK15 data we get $\eta_V = -0.0130^{+0.0038}_{-0.0050}$ and $\zeta_V^2 = 0.0038 \pm 0.0034$, respectively, ruling out the null value at more than one standard deviation. On the contrary, ACTPol+WMAP finds $\eta_V = 0.0015^{+0.0074}_{-0.013}$ and $\zeta_V^2 = -0.0045 \pm 0.0044$, always showing 1σ indication different from zero, but with an opposite sign with respect to Planck. In addition, SPT3G+WMAP prefer both the parameters η_V and ζ_V^2 in agreement with the null value within the 68% CL. Equivalently, we can derive constraints on the parameters $\{\epsilon_2, \epsilon_3\}$. For Planck + BK15 we obtain $\epsilon_2 = 0.0334 \pm 0.0054$ and $\epsilon_3 = 0.24 \pm 0.21$. Instead, the Atacama Cosmology Telescope and the South Pole Telescope data, even if they have larger experimental errors and lead to less constraining bounds, prefer ϵ_2 much lower than Planck, reducing the significance for a value different from zero.

Under the assumption of slow-roll inflation, we see that the parameter space allowed for the (higher-order) tensor parameters in the slow-roll paradigm is strongly reduced since constraints on r and the scalar spectrum are translated into constraints on tensor spectrum, see also [Figure II.2](#). In particular using the Planck+BK15 data we see that the results for the scalar parameters and the upper bound on the tensor amplitude, are translated into constraints for the tensor running and its running of running that are consistent with zero within less than two standard deviations and that, in any case, they are expected to be extremely small and therefore negligible in the slow-roll hierarchy. Similar results can be obtained also exploiting the Planck-independent measurements by ACTPol+WMAP and SPT3G+WMAP, see [Table II.3](#). In particular, for these datasets the bounds on α_T and β_T are less constraining with respect Planck(+BK15) because ACTPol and SPT3G in combination with WMAP have a smaller sensitivity both on the tensor amplitude and on scalar modes. However, given also the large error bars, these bounds are all consistent with each other within 2 standard deviations, leading to predict a scale invariant tensor tilt, unless corrections of order $|dn_T/d \log k| \lesssim 10^{-5}$ for all the different datasets.

Implications for slow-roll inflationary models

Now, we shall focus on the constraints for a few selected models of slow-roll inflation. In particular, we compute the slow-roll parameters and consequently we predict the values of n_s , α_s and r at leading order in the slow-roll approximation. We include an uncertainty in the number of e-folds (before the end of inflation) of $50 < N < 60$ [78]. In [Figure II.3](#) we compare the theoretical predictions with the observational constraints obtained within the $\Lambda\text{CDM} + r + \text{ff}_s$ cosmological model for the different datasets listed in [subsection II.I.I](#).

First, by noting that in a Universe dominated by the energy-density of the inflaton field during the slow-roll regime we have $\dot{H} = -4\pi G\dot{\phi}^2 = d^2N/dt^2$, we can relate the field excursion to the tensor amplitude by $\Delta\phi/M_{\text{pl}} = \sqrt{r/8}N$ and using $N = 50$ we set a lower bound

$$\frac{\Delta\phi}{M_{\text{p}}} = 1.01 \left(\frac{r}{3.26 \times 10^{-3}} \right)^{\frac{1}{2}} \quad (\text{II.19})$$

that is shown in [Figure II.3](#). Notice that both large and small field models are compatible with every dataset. On the other hand, using Eq. (II.18), we get an approximate limit for potentials that work on GUT scales finding that they are ruled out at 95% CL by the combination Planck+BK15 even though they are still compatible with the other datasets, including ACTPol+WMAP and SPT3G+WMAP. This is again an indication of a tension between the Planck satellite results and the ground based telescopes measurements, that prefer a larger value for the scalar spectral index n_s more consistent with a scale invariant spectrum $n_s = 1$. We would like to stress that this is not (only) a volume effect due to the different constraining power of the experiments, but it is an actual shift of the n_s coming from damping tails of the power spectra whose nature needs to be further investigate. Finally, we demand whether the data are in agreement with a convex or a concave potential, being $r = -8/3(n_s - 1)$ the relation which defines the limit between the two different cases. Due to the fact that B-modes polarization measurements are able to give more stringent constraints on tensor modes, in particular on r that appears in the relation aforementioned, the BK15 data indicates that the potential should be concave, excluding a convex shape, whereas the other datasets are unable to give such a restriction.

We give below a concise review of some inflationary models studied in this work and the main results obtained by our analysis.

- **(Generalized) Natural Inflation:** we start from the general natural inflation [176], which consider an axion model where a global $U(1)$ symmetry is spontaneously broken at scale f , with a soft explicit symmetry breaking at a lower scale Λ . The inflaton field corresponds to the pseudo-Nambu-Goldstone boson associated to the symmetry breaking [154] and the potential reads

$$V = 2^{1-m}\Lambda^4 \left[1 + \cos \frac{\phi}{f} \right]^m. \quad (\text{II.20})$$

Fixing $m = 1$ and recovering the natural inflation [177], the parameters are

$$n_s = 1 - \frac{1}{y} \left[\frac{1 + 2y^2(1 + e^{-x})}{1 + 2y^2(1 - e^{-x})} \right], \quad (\text{II.21})$$

$$\alpha_s = -\frac{4(2y^2 + 1)e^x}{y^2(-2y^2 + (2y^2 + 1)e^x)^2}, \quad (\text{II.22})$$

$$r = \frac{16e^{-x}}{1 + 2y^2(1 - e^{-x})}, \quad (\text{II.23})$$

where $x = N/y$ and $y = f/M_{\text{pl}}$. Plotting the above quantities as functions of f/M_{pl} (blue curves in [Figure II.3](#)) we can see that this model is only compatible within one standard deviation for Planck and within two standard deviation with Planck+BK15. Anyway, relaxing the assumption $m = 1$ and leaving m a free parameter, the compatibility with Planck+BK15 increases as long as $m < 1$. Given the tension present in the parameter space between the different experiments (as we can see from [Figure II.2](#)), the model compatibility changes between the datasets. In fact, the South Pole Telescope data show only an agreement at 95% CL for every N in the chosen interval, *i.e.*, both blue lines are in the lighter region of the dataset. Moreover, the shift towards high values of n_s preferred by the Atacama Cosmology Telescope data basically excludes the (generalized) natural inflation from the 95% CL contours. It should be stressed that the ground experiments (ACTPol and SPT-3G) are the ones responsible for the shift of the measurements and consequently changes the compatibility with the model, not WMAP 9-years [61,

178]. Actually, the shift of the n_s bounds is due to the high multipole region accurately constrained by the damping tail of the power spectra.

- **(Non minimally coupled) Power-law inflation:** by taking the limit $f \rightarrow \infty$ in Eq.(II.20), we recover the quadratic potential, a particular case of the general power-law inflation, represented as two yellow straight lines in Figure II.3, and described by the dominant term $\lambda_n \phi^n$. Values of the index $n = 2/3, 1, 2$ have been obtained in string theory [179–182]. The spectral index, the scalar running and r are simply

$$n_s = 1 - \frac{2n + 4}{n + 4N}, \quad (\text{II.24})$$

$$\alpha_s = -\frac{8(n + 2)}{(n + 4N)^2}, \quad (\text{II.25})$$

$$r = \frac{16n}{n + 4N} \quad (\text{II.26})$$

and we can see that there is no agreement when the B-modes BK15 observations are included, whereas we still have a consistency at 95% CL with Planck alone, or up to within 1σ for ACTPol+WMAP and SPT3G+WMAP. Nevertheless, provided a non-minimal coupling with gravity, the simple power-law potential acquires a compatibility up to 68% CL for some values of n as shown by the red lines in Figure II.3. The coupling constant ζ is chosen according to Ref. [183] where the authors have made an analysis imposing this inflationary model at the beginning and using ζ as a free parameter. For sake of completeness the values are listed below

- $\mathbf{n = 4}$, with $\zeta \simeq 0.0016$,

$$n_s = 1 - \frac{1}{N}(3 - 8\zeta N), \quad (\text{II.27})$$

$$\alpha_s = \frac{1}{N^2}(-3 + 96\zeta N - 64\zeta^2 N^2), \quad (\text{II.28})$$

$$r = \frac{16}{N}(1 - 8\zeta N). \quad (\text{II.29})$$

- $\mathbf{n = 2}$, with $\zeta \simeq 0.0015$,

$$n_s = 1 - \frac{2}{N}\left(1 + \frac{4}{3}\zeta^2 N^2\right), \quad (\text{II.30})$$

$$\alpha_s = \frac{2}{N^2}(-1 + 4\zeta\alpha_s N - 96\zeta^2 N^2), \quad (\text{II.31})$$

$$r = \frac{8}{N}(1 - 8\zeta N). \quad (\text{II.32})$$

- $\mathbf{n = \frac{4}{3}}$, with $\zeta \simeq 0.0011$,

$$n_s = 1 - \frac{1}{3N}(5 + 8\zeta N), \quad (\text{II.33})$$

$$\alpha_s = \frac{5}{81N^2}(-27 + 48\zeta N - 704\zeta^2 N^2), \quad (\text{II.34})$$

$$r = \frac{16}{9N}(3 - 32\zeta N). \quad (\text{II.35})$$

- $n = 2/3$, with $\xi \simeq 0.0007$,

$$n_s = 1 - \frac{4}{3N}(1 + 4\xi N), \quad (\text{II.36})$$

$$\alpha_s = \frac{4}{81N^2}(-27 + 84\xi N + 464\xi^2 N^2), \quad (\text{II.37})$$

$$r = \frac{8}{9N}(3 - 40\xi N). \quad (\text{II.38})$$

This model is consistent also with the ATCPol+WMAP and SPT3G+WMAP contours with the preference for higher values of the tensor tilt translated into slightly preferences for lower values of $n < 2$, *e.g.*, the one with $n = 2/3$ acquires a compatibility of 68% CL.

- **Quintessential inflation:** in this scenario the early inflationary period and the late-time acceleration are combined. The potential in this case should be shallow at early times, *i.e.*, satisfying the slow-roll conditions, and steep after. As the usual exponential model does not satisfy the observational constraints [184] a new parameter n is added (II.39) which also influences the steepness of $V(\phi)$, whose form is

$$V = \Lambda e^{-\lambda \frac{\phi^n}{M_{\text{pl}}^n}}, \quad (\text{II.39})$$

with $n > 1$. Imposing $\lambda \ll 1$ we end up with the large field inflation, called quintessential inflation [185]. In this model, the parameters are

$$n_s = 1 - \frac{2(n-1)}{(n-2)N} - \frac{[n(n-2)\lambda N]^{-\frac{2}{n-1}}}{(n-2)^2 N^2}, \quad (\text{II.40})$$

$$\alpha_s = -\frac{2(n-1)}{(n-2)N^2} + \frac{6(n-1)[n(n-2)\lambda N]^{-\frac{2}{n-2}}}{(n-2)^3 N^3}, \quad (\text{II.41})$$

$$r = \frac{8[n(n-2)\lambda N]^{-\frac{2}{n-2}}}{(n-2)^2 N^2}. \quad (\text{II.42})$$

Fixing $\lambda = 10^{-10}$ and varying n , the purple curves in Figure II.3 are drawn, showing, for example as reference, that $n = 7$ is compatible with 95% CL of Planck+BK15 with $N = 60$ whereas it is not for $N = 50$. Lower values of λ move the curves to the right, increasing the inclination, whereas a higher value makes n_s independent of it, as shown in (II.40). Concerning the other datasets, this model is in disagreement with ACTPol+WMAP data unless for significantly lower values of λ , and in tension with SPT3G+WMAP. Also in this case the different agreement of the models with the data is affected by the inconsistency between the datasets explored here.

- **Starobinsky-like inflation:** lastly, we analyze the R^2 inflation [129, 186–189] which is characterized by adding higher curvature corrections to the Einstein-Hilbert action of gravity (I.218). The potential is

$$V = \frac{M_{\text{pl}}^2}{8} \lambda (1 - e^{-\sqrt{\frac{2}{3}} \frac{\phi}{M_{\text{pl}}}})^2 \quad (\text{II.43})$$

and the inflationary parameters are

$$n_s = 1 - \frac{32N + 24}{(4N - 3)^2} \simeq 1 - \frac{2}{N}, \quad (\text{II.44})$$

$$\alpha_s = -\frac{64N(8N - 13)}{(4N - 3)^4} \simeq -\frac{2}{N^2}, \quad (\text{II.45})$$

$$r = \frac{192}{(4N - 3)^2} \simeq \frac{12}{N^2}. \quad (\text{II.46})$$

In this model the hierarchy of the parameters is $\xi \sim \epsilon \ll \eta \ll 1$ instead of the more common $\xi \ll \eta \ll \epsilon \ll 1$. Thus the value of r is expected to be extremely small. In fact, we can see from the cyan line in [Figure II.3](#) that its smallness results in a compatibility within one standard deviation for all the datasets. Small deviation from this model, *i.e.* considering the term R^p with $p \approx 2$ [190], worsen the agreement with Planck+BK15 as shown by the dotted lines which represent terms with $2 + \Delta p$ where $\Delta p = 0.01$. Considering also ACTPol+WMAP, we see that the model is excluded when p is decreased, whereas for SPT3G+WMAP it is still consistent within the 95% CL contours. On the other hand, a bigger value of p is completely in agreement with both datasets at 68% CL.

We would like to conclude this subsection pointing out that the constraints on the slow-roll inflationary models remain basically stable when $dn_s/d \log k$ can freely vary in the sampling, see also the analogous discussion in [78] and also [184, 191–194]. Anyway, the tension [175] among the different cosmological datasets analyzed in this work (*i.e.*, Planck, ACTPol+WMAP and SPT3G+WMAP) produces different constraints on the inflationary parameter and often different results regarding the model compatibility, see also [Figure II.3](#).

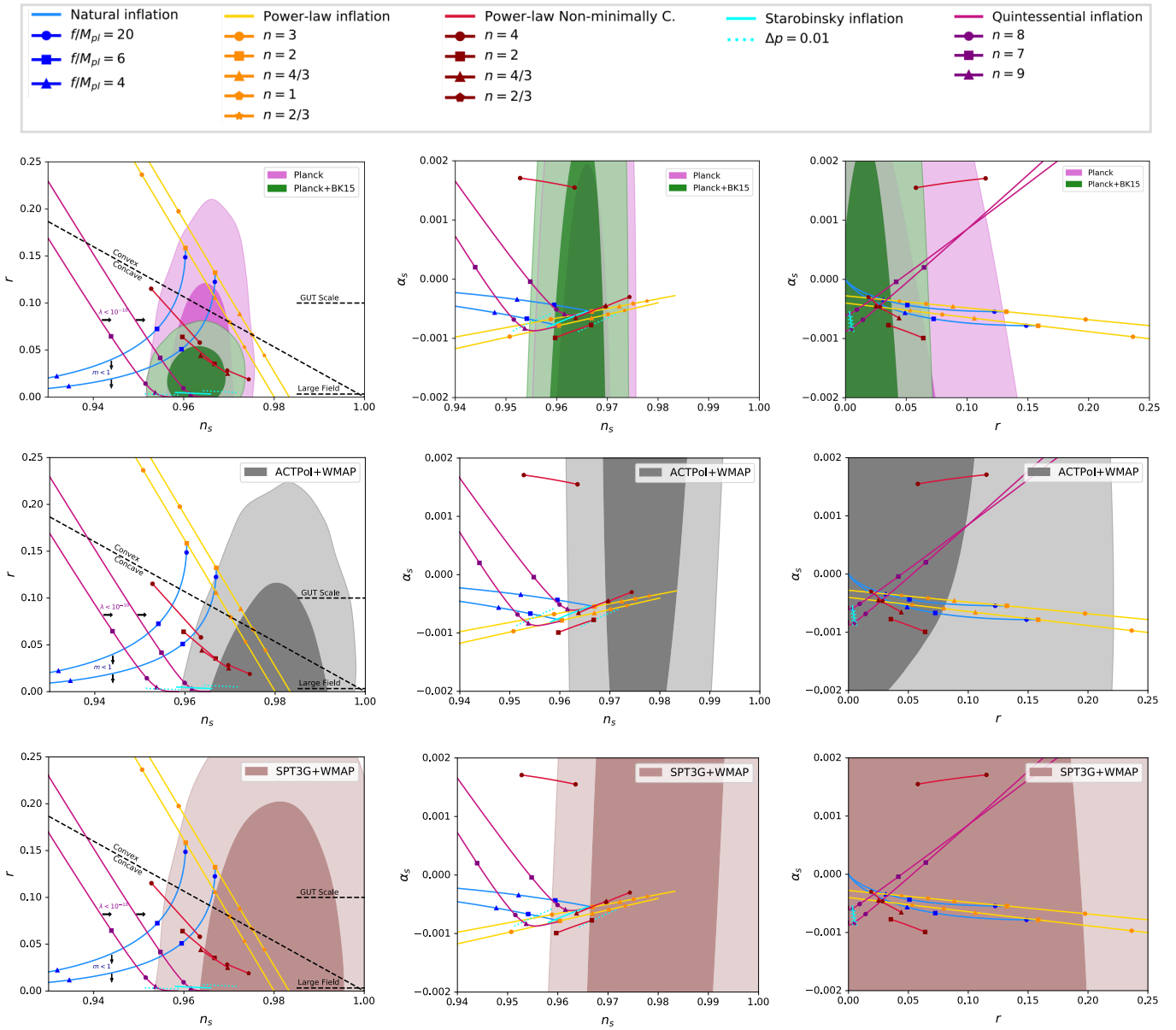


FIGURE II.3: Marginalized joint 68% and 95% CL regions for (n_s, r) , (n_s, α_s) and (r, α_s) from Planck(+BK15) (top panels), ACTPol+WMAP (middle panels) and SPT3G+WMAP (bottom panels) data. The marginalized contours can be compared to the theoretical predictions of some selected inflationary models opportunely described in the text.

II.II INFLATIONARY GRAVITY WAVES FROM LARGE TO SMALL SCALES

In the previous section we discussed how the missing evidence of the B-modes in the Cosmic Microwave Background (CMB) polarization originated from the inflationary tensor modes and, in general, a combined analysis of the Planck and BICEP2/Keck array (BK15) data [162], allow us to set only an upper bound on the amplitude³ of PGWs on the CMB scales $r \lesssim 0.07$ at 95% C.L. at the pivot scale $k_* = 0.05 \text{ Mpc}^{-1}$ [78]. As common practice in literature, in deriving such bounds we have assumed the slow roll consistency relation $n_T = -r/8$ to hold together with other higher-order slow-roll consistency relations among scalar and tensor parameters, Eqs. (II.16) and (II.17). In this way we basically obtained slightly red tilted primordial tensor spectrum $\mathcal{P}_t(k)$ and a scale invariant tensor tilt, unless corrections of order $|dn_T/d \log k| \lesssim 10^{-5}$ for all the different datasets analyzed.

However, the slow roll consistency relations can be violated in many non standard models of inflation, *e.g.* in presence of other spectator (rolling) fields [163–166] or in modified gravity theories [94, 167–171, 201–203]. When they are relaxed, the Planck data only weakly constrain the tensor tilt to $-0.55 < n_T < 2.54$ at 95% C.L. [78]. Always in Ref [78], it was shown that a significant improvement in the upper bound on the tensor tilt can be obtained combining the CMB measurements with the LIGO/VIRGO data on the stochastic background of gravitational waves Ω_{GW} . Indeed, along with B-modes polarization, primordial tensor fluctuations may have imprinted also the stochastic background of gravitational waves, the analogous of CMB for gravitational waves [131]. While a direct detection of the stochastic background has not been provided yet⁴, in the frequency range $f \in (20 - 85.8) \text{ Hz}$, which corresponds to the wave-number range $k \in (1.3 - 5.5) \times 10^{16} \text{ Mpc}^{-1}$, the first and second observing runs of the LIGO/VIRGO collaboration set an upper bound on the stochastic background

$$\Omega_{\text{GW}}(k_{\text{LV}}) \leq 1.7 \times 10^{-7} \quad (\text{II.47})$$

at 95 % C.L. [78, 209]. The Planck Collaboration, including the LIGO/VIRGO limit (II.47) as a half-gaussian prior on the tensor tilt, under the assumption of scale independence (*i.e.*, $dn_T/d \log k = 0$), derived the improved upper bound $n_T < 0.53$ at 95% C.L. [78]. Notice that this constraint is obtained marginalizing over the probability distribution of r , that is typically sampled assuming a flat prior $r \in [r_{\text{min}}, r_{\text{max}}]$ with $r_{\text{min}} \lesssim 10^{-3} \simeq 0$. This makes the constraint on the tensor tilt subject to misunderstanding as if there is no detection of r no reliable constraint can be derived. Moreover, another important assumption beyond this analysis, is to consider the tensor tilt as scale independent extending the well known power law relation (II.4) from the CMB scales ($k \sim 0.05 \text{ Mpc}^{-1}$) all the way up to the small scales probed by the gravitational interferometers ($k \sim 10^{16} \text{ Mpc}^{-1}$). This is clearly an important approximation as Eq. (II.4) is just a leading order expansion and, depending on the model of inflation, n_T can acquire a (slight) scale dependence. Therefore non-linearities may easily break the power-law relation on small scales. It is therefore timely to investigate which is the impact of higher-order corrections on small scales and the implications for the constraints that one can derive on inflation combining GW and CMB observations.

In this section for the first we show time that, due to the huge difference in the scales probed by CMB and GW experiments, higher-order terms in the spectrum, parametrized through the so-called tensor runnings [1, 160], albeit negligibly small on the CMB scales, may give non-negligible contributions on the ultrahigh k probed by direct gravitational observations, drastically changing the final predictions. We point out the implications for the status of current observational constraints on PGWs and for future detection prospects. In the subsequent sections we instead discuss how these model-dependent small-scale

³It is worth noting that in the upcoming decade, a new generation of CMB experiments such as BICEP3 [195], CLASS [196], SPT-3G [197], Advanced ACTPol [198], LBIIRD [199] and CMB-S4 [200] are expected to bring the sensitivity to the tensor amplitude down to $r \sim 0.01 - 0.001$ possibly leading to its first detection.

⁴Notice that the North American Nanohertz Observatory for Gravitational Waves (NANOGrav) found strong evidences for a stochastic common-spectrum process [204]. Even if this will be confirmed as a first genuine detection of a stochastic background of GWs, its inflationary interpretation will be in tension with BBN bounds [205, 206] unless we assume a very low reheating temperature [207, 208].

effects can be relevant to probe and constrain several non-standard realization of inflation, including the rich phenomenology associated to modified theories for gravitational interactions.

II.II.I BREAKING THE POWER LAW EXPANSION

The energy density of the universe due to PGWs at the present time and at a given scale $k = 2\pi f$ is given by [78, 132, 210–212]

$$\Omega_{\text{GW}}(k) \doteq \frac{1}{\rho_c} \frac{d\rho_{\text{GW}}}{d \log k} \simeq \frac{\mathcal{P}_{\text{T}}(k)}{24z_{\text{eq}}} \quad (\text{II.48})$$

where $z_{\text{eq}} \simeq 3400$ is the redshift at the matter-radiation equivalence [78]. Using Eq. (II.4), it is easy to see that, under the assumption of scale-independent tilt, a constraint on the amplitude of the stochastic background $\Omega_{\text{GW}}(k)$ can be translated into an upper bound on the tensor tilt

$$n_{\text{T}} < \frac{\ln\left(\frac{24z_{\text{eq}}\Omega_{\text{GW}}(k)}{rA_{\text{S}}}\right)}{\ln\left(\frac{k}{k_*}\right)} \lesssim 0.39 + 0.025 \times \log(1/r), \quad (\text{II.49})$$

where in the last inequality we considered the LIGO/VIRGO limit (II.47). Note that the constraint (II.49) is derived without any assumption on the tensor amplitude⁵: if future measurements reveal evidence for $r \neq 0$, its detection will immediately place a well defined upper bound on the tensor tilt that however, because of its logarithmic dependence, will not be drastically sensitive to the precise value of the tensor amplitude, see also Figure II.4. The physical reason beyond this weak dependence on the tensor amplitude is that a large positive tilt strongly amplifies the GWs production on the ultrahigh k probed by gravitational detectors, easily compensating a small (but of course not vanishing) tensor amplitude on the CMB scales. On the other hand, it is also true that constraints on n_{T} cannot be derived for a vanishing tensor amplitude, and in fact we may see that taking the limit $r \rightarrow 0$, the right side of Eq. (II.49) logarithmically diverges, as expected.

The constraint (II.49) as well as the upper bound $n_{\text{T}} < 0.53$ at 95% C.L. derived in [78] assume a constant tilt over a range of about eighteen order of magnitude, namely $k \in [0.05, 1.3 \times 10^{16}] \text{Mpc}^{-1}$. In order to parametrize a possible scale dependence, we generalize the power law parametrization to the following expansions:

$$\log \mathcal{P}_{\text{T}}(k) = \log(rA_{\text{S}}) + n_{\text{T}} \log(k/k_*) + \sum_{n=1}^{\infty} \frac{1}{(n+1)!} \left[\frac{d^n n_{\text{T}}}{d \log^n k} \right]_{k=k_*} \log^{n+1}(k/k_*). \quad (\text{II.50})$$

and we define the n -order running of the tensor tilt⁶ as

$$\alpha_n^{\text{T}}(k_*) \doteq \left[\frac{d^n n_{\text{T}}}{d \log^n k} \right]_{k=k_*} \quad (\text{II.51})$$

Including the runnings, the upper bound (II.49) is modified to

$$n_{\text{T}} \lesssim \frac{\ln\left(\frac{24z_{\text{eq}}\Omega_{\text{GW}}(k)}{rA_{\text{S}}}\right)}{\log\left(\frac{k}{k_*}\right)} - \sum_{n=1}^{\infty} \frac{\alpha_n^{\text{T}}(k_*)}{(n+1)!} \left[\log\left(\frac{k}{k_*}\right) \right]^n. \quad (\text{II.52})$$

⁵This is a different approach with respect to those performed in [78] where the upper bound $n_{\text{T}} < 0.53$ at 95% C.L. was derived marginalizing over the distribution of r . Anyway we see that for $r \sim 10^{-2} - 10^{-3}$ we basically recover the same result, see also Figure II.4.

⁶In what follows we will usually avoid to specify that the spectral tilt and the runnings are computed on the pivot scale k_* and, to simplify the notation, we will only write n_{T} and α_n^{T} .

Clearly, in order to exactly compute the sum expansion and to check its convergence we need to estimate all the derivatives $\{a_n^t\}$ and this is possible only fixing a specific model of inflation. Nevertheless we can appreciate how the generic n -order running must at least satisfy the condition $|a_n^t/n_T| \ll (n+1)!/\log^n(k/k_*)$ to give a negligible contribution at the generic scale k . This requirement should become highly non-trivial, above all on the ultra-high k as those directly probed by GW ground-based interferometers.

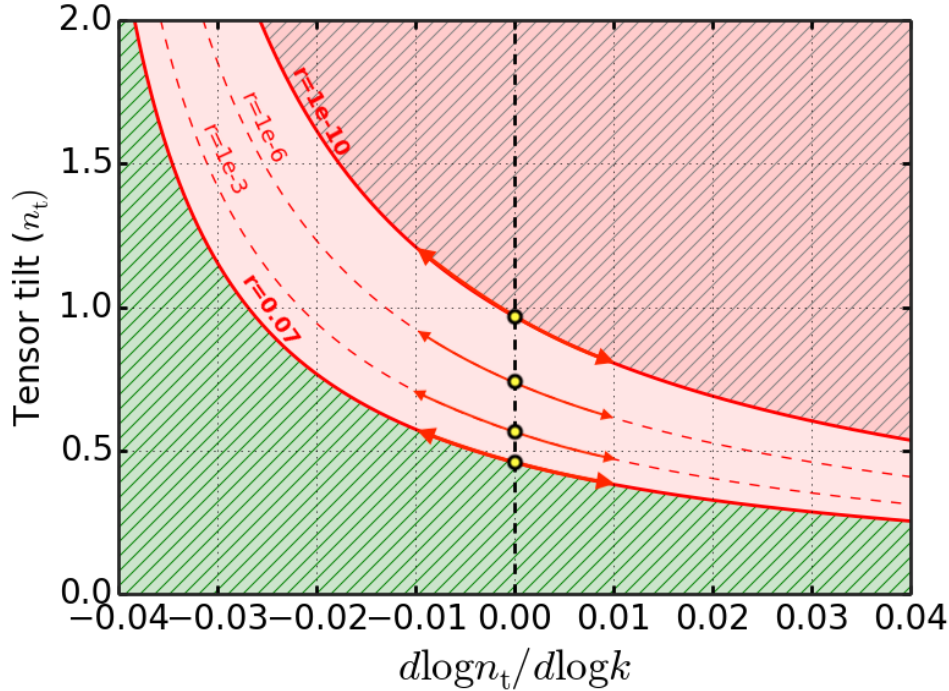


FIGURE II.4: Constraints on the tensor tilt from the LIGO/VIRGO limit on the stochastic background (II.47). The yellow dots represent the upper bounds on n_T for different values of r when scale-dependence is ignored. When a scale dependence $d \log n_T / d \log k \neq 0$ is considered the yellow dots move on the red lines at constant r .

To study how constraints on n_T derived under the assumption of scale independence are modified in presence of a (slight) scale dependence, we derive the upper bound on the tensor tilt by the LIGO/VIRGO limit (II.47) for different values of the tensor to scalar ratio, varying the rate of change of the tensor tilt with respect to the scale, $d \log n_T / d \log k$, in a range $d \log n_T / d \log k \in [-0.04, 0.04]$. We find out that, due to the huge distance between the scales probed by CMB and GW data, a small departure from scale independence ($\lesssim 4\%$) can significantly change the final results, see also Figure II.4. In particular, a small negative (positive) running⁷, suppressing (amplifying) the amplitude of PGWs on small scales, can remarkably worsen (improve) the upper bound derived under the assumption $d \log n_T / d \log k = 0$ (yellow dots in Figure II.4). This is clearly translated also into a strong degeneracy between scale-dependence and the tensor amplitude (see Figure II.4) that can be broken only by an independent measurement of r from future CMB experiments. Furthermore, it should be noted that Primordial tensor modes with wavelengths corresponding to the high frequencies of direct GW detection, will exit the horizon very close to the end of inflation which is precisely when the slow-roll approximation breaks down, see also Ref. [213]. Therefore, it is not sure at all that a power-law expansion holds even approximately on ultra-high k . As a matter of fact, near the end of inflation, the shape of the tensor spectrum will be strongly related to the shape of the inflationary potential and large departures from the power-law parametrization are typically expected. In the [supplementary material, section A.3](#), we show different examples of negligible and non-negligible gravitational wave production. We conclude that the small-scale constraints on n_T may be very sensitive to the assumption of scale independence. Non-negligible model-dependent contributions can arise from

⁷We recall that $d \log n_T / d \log k \doteq a_1^t / n_T$.

non-linear corrections and cannot be always ignored when constraints on the inflationary parameters are derived combining CMB and GW data.

II.III PROPAGATING SPEED OF PRIMORDIAL GRAVITATIONAL WAVES

In the previous section we have seen that a simple power-law parametrization may be not enough to capture the behavior of primordial tensor modes with wavelengths corresponding to the high frequencies of direct GW detection. The higher-order terms in the spectrum, parametrized through the so-called tensor runnings, albeit negligibly small on the CMB frequencies, may give non-negligible contributions on scales of direct GW observations. It should be noted that such terms carry information about the specific model of inflation, possibly changing the small-scale behavior of tensor anisotropies in a model-dependent manner. In this and the following section, we focus on the way non standard physics in the gravitational sector may be encoded in the primordial tensor two-point function. The increased precision in the constraints on the primordial tensor modes from the current (and above all future) small and large scale experiments opens up the possibility of probing the physics of inflation with primordial gravitational waves, testing deviations from the standard slow roll predictions as a hint for new physics. It is therefore timely to investigate which constraints one can obtain from current CMB and GW data on inflationary models that can lead to deviations from the standard inflationary consistency relations. We will show how the aforementioned model-dependent small-scale effects can play a crucial role in testing, constraining and possibly discriminating a vast phenomenology, including modified theories for gravitational interactions. In particular, in this section we study the implications of a modified propagation of gravity for the tensor spectrum and the inflationary observables while in the next section we focus on higher curvature gravity and on its implications for the inflationary observables.

We start by noting that direct measurements of gravitational waves show good agreements with the GR predictions on gravity propagation [214–217]. For example, the only multi-messenger event ever measured so far, GW170817 [214, 218], sets very constraining bounds $|c_T - 1| \lesssim 10^{-15}$. Anyway, it should be noted also that these results refer to a precise range of frequencies (or equivalently to a precise range of the wave-number k), namely the small scales probed by direct gravitational observations. Without specific model-dependent assumptions, these limits should not be trivially extended to different frequencies. Indeed, in many modified gravity theories beyond GR, such as the Horndeski theory of gravity [219–235], the Gauss-Bonnet gravity [236–252] and also the low-energy effective string theory with higher-order corrections [4, 94, 253–268] gravity can propagate differently from GR and both deviations from the speed of light and frequency-dependencies often arise. For this reason, testing the condition $c_T = 1$ (at different frequencies) means to test the theory of gravity (at different energies) and so an independent test of the gravity propagation on large scales would clearly provide an independent test of GR.

Here we shall focus on the propagation of relic inflationary gravitons [167–170, 266, 269–293]. Under the assumption of slow-roll inflation, we derive for the first time a set of generalized consistency relations for the spectral index and its higher-order runnings in presence of a non-trivial gravity propagation during inflation. In this way we connect the CMB scales to the LIGO/Virgo band ($f \sim 100$ Hz), showing that a running in frequency of the propagating speed of gravity can induce a scale-dependence of the tensor two-point function, amplifying the PGWs production on small scales. We exploit these effects for constraining both the speed of gravity and above all its frequency variation.

II.III.I THEORY

In what follows, we derive a set of equations that relate the propagating speed to the inflationary parameters and that generalize the usual slow roll consistency relations that are, in fact, recovered when the GR prescription $c_T = 1$ is restored. We start by generalizing the theory of the primordial tensor perturbations during inflation [59, 76, 83, 144, 146, 149, 150, 155] allowing for non-trivial gravity propagation. The action

for the single field inflation in the unitary gauge is [59, 76, 103, 294]:

$$S = \frac{\bar{M}_p^2}{2} \int d^4x \sqrt{-g} \left[R - c_1(t) - c_2(t)g^{00} - \left(1 - \frac{1}{c_T^2(t)}\right) (\delta K_{\mu\nu} \delta K^{\mu\nu} - \delta K^2) \right] \quad (\text{II.53})$$

where $c_1(t) = 2(\dot{H} + 3H^2)$, $c_2(t) = -2\dot{H}$ and $K_{\mu\nu}$ is the extrinsic curvature of the spatial slices. Here a dot denotes the derivative with respect to the cosmic time $\dot{x} \equiv dx/dt$. Note that in the standard slow roll case ($c_T = 1$) the part of the action involving the extrinsic curvature vanishes and one recovers the standard GR action in the unitary gauge. It should be noted also that a non-trivial propagating speed does not affect the spectrum of the scalar perturbation and so we can consider only the tensor perturbations whose quadratic action is

$$S_\gamma^{(2)} = \frac{\bar{M}_p^2}{8} \int d\tau d^3x \frac{a^2}{c_T^2(t)} \left[\left(\frac{d\gamma_{ij}}{d\tau} \right)^2 - c_T^2(t) (\vec{\nabla} \gamma_{ij})^2 \right] \quad (\text{II.54})$$

where $a(t)$ is the scale factor, $d\tau = dt/a(t)$ is the conformal time and γ_{ij} is transverse and traceless: $\gamma_{ii} = 0$ and $\partial_i \gamma_{ij} = 0$. We expand γ_{ij} in the Fourier series:

$$\gamma_{ij}(\tau, \mathbf{x}) = \int \frac{d^3k}{(2\pi)^3} e^{-i\mathbf{k}\cdot\mathbf{x}} \sum_{p=+, \times} \gamma_p(\tau, k) a_{(p)}(\mathbf{k}) \lambda_{ij}^{(p)}(\mathbf{k}) + \text{h.c.} \quad (\text{II.55})$$

where the sum should be considered over the polarization states $p = (+, \times)$ while the polarization tensor $\lambda_{ij}^{(p)}(\mathbf{k})$ satisfies the usual conditions

$$k_j \lambda_{ij}^{(p)}(\mathbf{k}) = 0, \quad (\text{II.56})$$

$$\lambda_{ii}^{(p)}(\mathbf{k}) = 0 \quad (\text{II.57})$$

$$\lambda_{ij}^{(p)}(\mathbf{k}) \lambda_{ij}^{*(p')}(\mathbf{k}) = \delta_{pp'} \quad (\text{II.58})$$

$$\lambda_{ij}^{*(p)}(\mathbf{k}) = \lambda_{ij}^{*(p)}(-\mathbf{k}), \quad (\text{II.59})$$

and the creation and annihilation operators satisfy

$$\left[a_{(p)}(\mathbf{k}), a_{(p')}^\dagger(\mathbf{k}') \right] = \delta_{pp'} \delta^3(\mathbf{k} - \mathbf{k}'). \quad (\text{II.60})$$

It is trivial to check that, defining the fields

$$u(\tau, k) \doteq \gamma_{(p)}(\tau, k) z_T, \quad z_T \doteq \frac{M_p}{2} \left(\frac{a}{c_T(t)} \right) \quad (\text{II.61})$$

the equation of motion is

$$\frac{d^2 u}{d\tau^2} + \left(c_T^2 k^2 - \frac{1}{z_T} \frac{d^2 z_T}{d\tau^2} \right) u = 0. \quad (\text{II.62})$$

In what follows we work under the following conditions:

- we fix a background slow roll dynamics requiring that $|\dot{H}| \ll H^2$,
- we assume the slow roll parameter $0 < \epsilon_1 \ll 1$ in such a way that the Null Energy Condition (NEC) is preserved as well as we consider $|\epsilon_{i>1}| \ll 1$,
- we also assume the variation of the propagating speed per Hubble time to be small and we define similar parameters

$$\epsilon_1^T \doteq \frac{\dot{c}_T(t)}{H c_T(t)}, \quad (\text{II.63a})$$

$$\epsilon_{i>1}^T \doteq \frac{d \log \epsilon_{i-1}^T}{d \log k} \simeq \frac{\dot{\epsilon}_{i-1}^T}{H \epsilon_{i-1}^T}, \quad (\text{II.63b})$$

with $|\epsilon_1^T| \ll 1$ and $|\epsilon_{i>1}^T| \ll 1$.

In this way one can show that

$$\frac{1}{z_T} \frac{d^2 z_T}{d\tau^2} \simeq \frac{1}{a} \frac{d^2 a}{d\tau^2} \simeq \frac{2}{\tau^2} \quad (\text{II.64})$$

at least of corrections of order ϵ , see the [supplementary material, section A.4](#), for further details. It is also easy to check that one can define a new wave vector $\tilde{k} \doteq c_T(t)k$ that can be regarded as constant in the conformal time since its derivative is of order ϵ_1^T . At the end of the game, unless corrections of order ϵ , we can write our equation as

$$\frac{d^2 u}{d\tau^2} + \left(\tilde{k}^2 - \frac{2}{\tau^2} \right) u = 0 \quad (\text{II.65})$$

with the solution (obtained fixing the Bunch-Davies vacuum)

$$u(\tau, \tilde{k}) = \frac{e^{-i\tilde{k}\tau}}{\sqrt{2\tilde{k}}} \left(1 - \frac{i}{\tilde{k}\tau} \right). \quad (\text{II.66})$$

A more detailed derivation of this solution is given in the [supplementary material, section A.4](#). Interestingly, this is exactly the standard solution with $k \rightarrow \tilde{k} \doteq c_T(t)k$ therefore, in the presence of a non-trivial propagating speed c_T , the primordial tensor and scalar spectra at a given scale k are written as [\[76, 83, 276\]](#)

$$\mathcal{P}_T(k) = \frac{2}{M_p^2 \pi^2} \frac{H^2}{c_T} \left(\frac{c_T k}{aH} \right)^{-2\epsilon_1 - \epsilon_1^T} \quad (\text{II.67})$$

$$\mathcal{P}_S(k) = \frac{1}{8\pi^2 M_p^2} \frac{H^2}{\epsilon_1} \left(\frac{k}{aH} \right)^{-2\epsilon_1 - \epsilon_2} \quad (\text{II.68})$$

Generalized Consistency Relations

Here we are going to generalize the inflationary consistency relations among the spectral parameters in presence of a generic propagating speed c_T . The effects of a non-trivial propagating speed during inflation are encoded in the inflationary parameters and translated into different consistency relations with respect to the standard case [\[1\]](#). Future detection of the tensor spectrum and a consequent test of these consistency relations can therefore be used to constrain the propagating speed c_T testing possible deviations from GR on the inflationary energy scales.

Because of the propagating speed c_T , the scalar and tensor perturbations now exit the horizon at different scales. In fact the tensor perturbation will cross the horizon at $c_T k = aH$ while the scalar perturbation will cross the horizon⁸ at $k = aH$. Deriving the primordial spectra, we can compute the scalar and tensor tilts:

$$n_S - 1 \doteq \left. \frac{d \log \mathcal{P}_S}{d \log k} \right|_{k=k_*} = -2\epsilon_1 - \epsilon_2 + \mathcal{O}(\epsilon^2) \quad (\text{II.69})$$

$$n_T \doteq \left. \frac{d \log \mathcal{P}_T}{d \log k} \right|_{k=k_*} = -2\epsilon_1 - \epsilon_1^T + \mathcal{O}(\epsilon^2) \quad (\text{II.70})$$

where k_* is the pivot scale and the expressions above hold both for $k_* = aH$ and for $k_* = \frac{aH}{c_T}$ at least of corrections of order $\mathcal{O}(\epsilon^2)$ and therefore negligible. As concerns the scalar and tensor amplitudes, also in

⁸We are considering the case of a scalar speed $c_S = 1$

this case they do not depend drastically on the pivot scale

$$\mathcal{P}_T \Big|_{k_* = \frac{aH}{c_T}} = \frac{2}{M_p^2 \pi^2} \frac{H^2}{c_T} \simeq \frac{2 H^2}{M_p^2 \pi^2} (c_T)^{n_T-1} = \mathcal{P}_T \Big|_{k_* = aH} \quad (\text{II.71})$$

$$\mathcal{P}_S \Big|_{k_* = \frac{aH}{c_T}} = \frac{(c_T)^{1-n_S} H^2}{8\pi^2 M_p^2 \epsilon_1} \simeq \frac{1}{8\pi^2 M_p^2} \frac{H^2}{\epsilon_1} = \mathcal{P}_S \Big|_{k_* = aH} \quad (\text{II.72})$$

and so does the tensor-to-scalar ratio

$$r \Big|_{k_* = \frac{aH}{c_T}} = 16\epsilon_1 (c_T)^{n_S-2} \simeq \frac{16\epsilon_1}{c_T} \simeq 16\epsilon_1 (c_T)^{n_T-1} = r \Big|_{k_* = aH} \quad (\text{II.73})$$

In the equations above we have used the fact that we measure $n_S \simeq 0.96$ [78] and we expect $|n_T| \ll 1$. Note also that we are not interested in a large deviation from the standard GR prescription $c_T/c = 1$ and that the same results should be obtained computing the scalar and tensor spectra at their respective (different) exit scales. Since we proved that the choice of the pivot scale is not crucial, in what follows we adopt the conventional pivot scale $k_* = aH = 0.05 \text{ Mpc}^{-1}$.

A first obvious consequence of a non-trivial propagating speed is that the amplitude of the tensor spectrum does not fix anymore the energy scale of inflation directly. Indeed in the standard case $\mathcal{P}_T \propto H^2 \propto \rho_{\text{inf}}$ while from Eq. (II.71) we see that $\mathcal{P}_T \propto \frac{H^2}{c_T}$.

A more interesting effect of a slightly time dependent propagating speed is that the expression for the tensor tilt n_T acquires a new term ϵ_1^T with respect to the standard case. Therefore the sign of n_T now depends on the parameter ϵ_1^T that quantifies the variation of c_T in a Hubble time. If we consider Eq.(II.70) we see that⁹ if during the inflation the propagating speed increases or remains constant in time ($\epsilon_1^T \geq 0$) the tensor tilt is necessarily red ($n_T < 0$). Instead if the propagating speed reduces in time ($\epsilon_1^T < 0$), the sign of n_T depends on the magnitude of ϵ_1^T . For $-2\epsilon_1 < \epsilon_1^T < 0$ the dismissing is small enough to ensure a negative tensor tilt while for $\epsilon_1^T < -2\epsilon_1$ the dismissing is translated into a blue tensor tilt $n_T > 0$. As discussed so far, a positive tensor tilt would amplify the PGWs production on small scales and this is why we can use small scale experiments (such as LIGO and VIRGO) to constrain the propagating speed.

Moreover, as one can see from (II.70) and (II.73), also the usual consistency relation $r = -8n_T$ is violated in the presence of a non-trivial propagating speed. In practice, however, there are many ways to violate the consistency relation between r and n_T that do not imply a deviation from GR, see also the [supplementary material, section A.3](#). This means that, if a violation of the consistency relation $r = -8n_T$ is observed, we need a way to recognize if such a violation is due to a non-trivial tensor propagating speed during inflation or not.

As we are going to show we can derive a set of consistency relations among the inflationary parameters and the propagating speed $c_T(t)$. For simplicity we suppose that, during inflation, c_T increases or decreases linearly with time, so that

$$\ddot{c}_T(t) \simeq 0. \quad (\text{II.74})$$

In other words, we take into account only the linear term in the Taylor expansion of $c_T(t)$. This (reasonable) approximation is not crucial for our results, but simplifies the relations we are going to derive. Anyway we discuss scenarios beyond the assumption of linear time evolution for the tensor propagating speed in the [supplementary material, section A.5](#). To relate the propagating speed c_T to the inflationary parameters we make use of the scalar and tensor runnings

$$\alpha_S \doteq \frac{dn_S}{d \log k} \Big|_{k=k_*} = -2\epsilon_1 \epsilon_2 - \epsilon_2 \epsilon_3 \quad (\text{II.75})$$

⁹Remember that $\epsilon_1 > 0$ to ensure the Null Energy Condition.

$$\alpha_T \doteq \left. \frac{d n_T}{d \log k} \right|_{k=k_*} = -2\epsilon_1 \epsilon_2 - \epsilon_1^T \epsilon_2^T \quad (\text{II.76})$$

because of (II.74), ϵ_2^T can be calculated from its definition (II.63b)

$$\epsilon_2^T \doteq \frac{\dot{\epsilon}_1^T}{H \epsilon_1^T} = \frac{1}{H \epsilon_1^T} \frac{d}{dt} \frac{\dot{c}_T}{H c_T} = \frac{1}{H \epsilon_1^T} \left[\epsilon_1 \frac{\dot{c}_T}{c_T} - \frac{\dot{c}_T^2}{H c_T^2} \right] = \epsilon_1 - \epsilon_1^T \quad (\text{II.77})$$

that gives for α_T

$$\alpha_T = -2\epsilon_1 \epsilon_2 - \epsilon_1^T (\epsilon_1 - \epsilon_1^T) \quad (\text{II.78})$$

Equations (II.69) (II.70) (II.73) (II.75) and (II.78) can be reversed together to obtain

$$\epsilon_1 = \frac{1}{16} (r c_T) \quad (\text{II.79})$$

$$\epsilon_1^T = -n_T - \frac{1}{8} (r c_T) \quad (\text{II.80})$$

$$\epsilon_2 = 1 - n_S - \frac{1}{8} (r c_T) \quad (\text{II.81})$$

$$\epsilon_3 = \frac{\alpha_S}{n_S - 1 + 1/8 (r c_T)} - \frac{1}{8} (r c_T) \quad (\text{II.82})$$

Using the above equations in α_T one gets

$$\alpha_T = n_T^2 + \frac{5}{128} (r c_T)^2 + \frac{1}{8} (r c_T) \left[(n_S - 1) + \frac{5}{2} n_T \right]. \quad (\text{II.83})$$

Equation (II.83) is a consistency relation between n_S , n_T , α_T and c_T that generalizes the usual slow roll relation. Note that we can obtain as many relations as we want; for example, considering also the running of running β_T

$$\beta_T \doteq \left. \frac{d \alpha_T}{d \log k} \right|_{k=k_*} = -2\epsilon_1 \epsilon_2^2 - 2\epsilon_1 \epsilon_2 \epsilon_3 - \epsilon_1^T \left[(\epsilon_1 - \epsilon_1^T)^2 + \epsilon_1 \epsilon_2 - \epsilon_1^T (\epsilon_1 - \epsilon_1^T) \right] \quad (\text{II.84})$$

it is easy to see that, using (II.79), (II.80), (II.81), (II.82) and solving Eq.(II.83) for c_T one obtains a new consistency relation $\beta_T = \beta_T(n_S, \alpha_S, r, n_T, \alpha_T)$. This can be trivially generalized to all orders following the procedure described in [1] for the standard case. It is, however, more interesting to study some limits of Eq.(II.83). The limit $\epsilon_1^T = 0$ describes a constant propagating speed not necessarily equal to the speed of light. Because of (II.80) we have

$$c_T = \frac{-8 n_T}{r} \quad (\text{II.85})$$

Using Eq. (II.85) in the consistency relations (II.83) we obtain

$$\alpha_T = n_T^2 - n_T (n_S - 1) \quad (\text{II.86})$$

That is the same consistency relation among n_T , α_T and n_S than in the standard slow roll case [1]. Similarly the equation for β_T

$$\beta_T = n_T (\alpha_T - \alpha_S) + \frac{\alpha_T^2}{n_T} \quad (\text{II.87})$$

is the same than the standard slow roll. This means that if during inflation $c_T = \text{const} \neq 1$, the consistency relation between r and n_T will be violated but all the other consistency relations will be preserved. If together with $\epsilon_1^T = 0$ we fix also $c_T = 1$ (recovering the standard GR prescriptions) the relation $r = -8 n_T$

as well as all the other standard slow roll results will be restored.

For completeness we briefly discuss another interesting case in which at the horizon crossing the propagating speed reaches the value $c_T \simeq 1$ even with a non vanishing $\epsilon_1^T \neq 0$ ¹⁰. In this case we have to simply put $c_T = 1$ in the Eq. (II.83) obtaining

$$\alpha_T = n_T^2 + \frac{5}{128} r^2 + \frac{r}{8} \left[(n_S - 1) + \frac{5}{2} n_T \right] \quad (\text{II.88})$$

that is different from the standard slow roll relation (II.86). Indeed being $\epsilon_1^T \neq 0$ because of Eq. (II.80) also $n_T \neq \frac{-r}{8}$. This means that a time variation of c_T can leave a trace even if at the horizon exit the usual GR condition $c_T = c = 1$ is restored. We conclude that, together with the propagating speed c_T , another interesting parameter to analyze is ϵ_1^T .

II.III.II CONSTRAINTS

So far we derived a set of consistency relations that generalize the standard slow roll relations introducing the effects of a non-trivial propagation of gravity during inflation. We have shown that the propagating speed can be related to the inflationary parameters which means that they can be used to constrain the propagating speed itself and to test possible deviations from GR at the high energy scales of inflation.

Here, we discuss the constraints coming from present cosmological data and imposing the generalized consistency relations that we have derived so far. The theoretical model is calculated using the latest version of the Boltzmann code CAMB [109, 110] and we use the python sampler Cobaya [295] to extract cosmological constraints. The posteriors of our parameter space have been explored using the Monte Carlo Markov-Chain (MCMC) sampler developed for CosmoMC [107, 108] and tailored for parameter spaces with a speed hierarchy which also implements the "fast dragging" procedure described in [111]. The convergence of the chains obtained with this procedure is tested using the Gelman-Rubin criterium [112] and we choose as a threshold for chain convergence $R - 1 \lesssim 0.01$. To compare current data with our theoretical model, we employ the Planck's 2018 temperature and polarization likelihood which also includes low multipole data ($\ell < 30$) [113] combined with the lensing likelihood of Planck's 2018 data release based on temperature and polarization lensing reconstruction [115] and the CMB power spectrum likelihood of Bicep2/Keck Array X (BK15) [162]. Then we focus on the constraints from the LIGO/VIRGO upper limit on the stochastic gravitational waves background, that we denote with LV. Indeed, for a blue tilted spectrum, the stochastic background of primordial gravitational waves Ω_{GW} can be strongly amplified on small scales and we can use the small scales experiment data on the stochastic background to constrain the propagating speed and its time variation. Anyway, in light of the results discussed in the previous section, it is clear that to derive constraints on the inflationary parameters by direct GW observations we need to consider also the small-scale effects caused by higher-order corrections in the tensor spectrum. We do this relating the CMB and GW scales trough several generalized higher-order consistency relations discussed so far and assuming that the effects of a non trivial propagating speed dominate the behavior of the tensor spectrum on small scales. Finally, we combine the CMB data and the LIGO/VIRGO bound on the stochastic background to improve the final results on the inflationary parameters.

Constraints from CMB

In this subsection we present the results of our MCMC analysis. Let us start by noting that the Boltzmann integrator CAMB [109, 110] employs the standard power law parametrization of the primordial scalar and

¹⁰This is possible if for example the initial propagating speed was smallest than the speed of light and, at some point, it starts constantly increasing ($\epsilon_1^T > 0$) to reach the value $c_T \simeq 1$ at the horizon exit.

Parameter	Prior
$\Omega_b h^2$	[0.005, 0.1]
$\Omega_c h^2$	[0.001, 0.99]
$100 \theta_{MC}$	[0.5, 10]
τ	[0.01, 0.8]
$\log(10^{10} A_S)$	[1.61, 3.91]
n_S	[0.8, 1.2]
c_T	[0.01, 1]
$16 \epsilon_1$	[0, 1]
ϵ_1^T	[-0.5, 0.5]
ϵ_3	[-0.5, 1]

TABLE II.4: List of the parameters used in the MCMC sampling and their external flat priors assumed in [section II.III.II](#). In [section II.III.II](#) we sampled the same parameters with the same external priors except for ϵ_1^T on which we also impose a Half-Gaussian prior to include LIGO/VIRGO data on the stochastic background [[296, 297](#)]

	P18+BK15	P18+BK15+LV
$\Omega_b h^2$	0.02242 ± 0.00015	0.02241 ± 0.00015
$\Omega_c h^2$	0.1200 ± 0.0012	0.1200 ± 0.0012
τ	0.0566 ± 0.0076	0.0564 ± 0.0079
$\ln(10^{10} A_S)$	3.051 ± 0.015	3.050 ± 0.016
r	< 0.0961	< 0.0599
n_S	0.9645 ± 0.0044	0.9646 ± 0.0044
α_S	-0.0067 ± 0.0067	-0.0069 ± 0.0069
n_T	$0.20^{+0.27}_{-0.13}$	$-0.084^{+0.10}_{-0.047}$
α_T	$0.087^{+0.049}_{-0.098}$	$0.0141^{+0.0035}_{-0.021}$
c_T	> 0.178	> 0.219
ϵ_1^T	< 0.203	$0.082^{+0.047}_{-0.11}$
χ^2	3530	3530

TABLE II.5: Constraints on parameters are at 1σ level (68% C.L.) while upper bounds are at 2σ (95% C.L.) for the full Planck 2018 likelihood [[113, 115](#)] and Biceps/Keck 2015 B-mode [[162](#)] likelihood with and without the inclusion of the prior on ϵ_1^T coming from LIGO/VIRGO data [[209](#)]

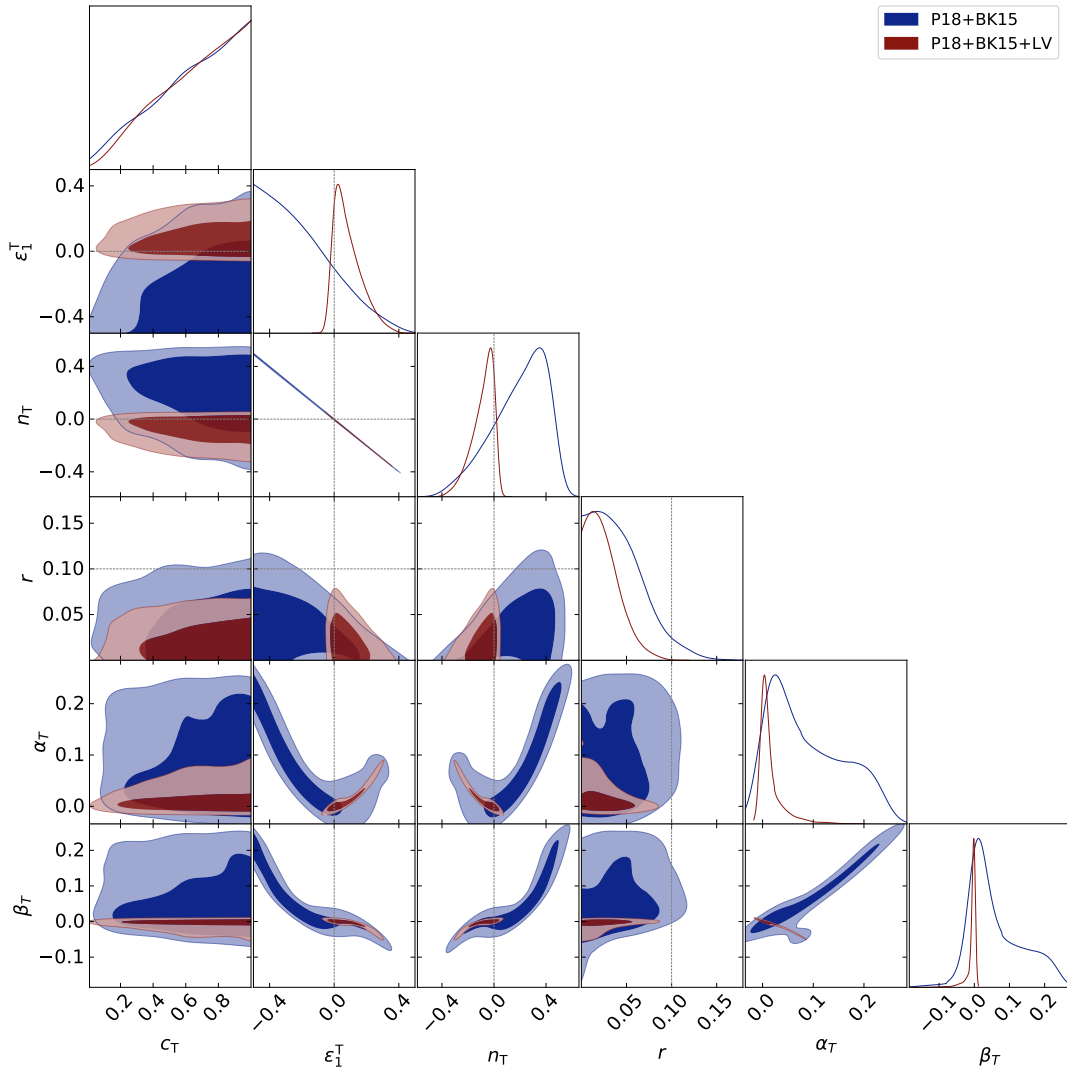


FIGURE II.5: Marginalized 2D and 1D posteriors for the combination of Planck 2018 [113, 115] and Biceps/Keck 2015 [162] data for the parameters of the tensor spectrum and their combination with the LIGO/VIRGO upper limit on the stochastic background amplitude [296, 297] (P18+BK15+LV).

tensor power spectra *i.e.* :

$$\mathcal{P}_S^{\text{CAMB}}(k) = A_S^{\text{CAMB}} \left(\frac{k}{k_{*,S}} \right)^{n_S - 1 + \frac{1}{2} \alpha_S \log(k/k_{*,S})} \quad (\text{II.89})$$

$$\mathcal{P}_T^{\text{CAMB}}(k) = A_T^{\text{CAMB}} \left(\frac{k}{k_{*,T}} \right)^{n_T + \frac{1}{2} \alpha_T \log(k/k_{*,T})} \quad (\text{II.90})$$

where $k_{*,T}$ and $k_{*,S}$ are the tensor and scalar pivot scale and the tensor-to-scalar ratio is defined as $r^{\text{CAMB}} = \mathcal{P}_T^{\text{CAMB}}(k_{*,T}) / \mathcal{P}_S^{\text{CAMB}}(k_{*,S})$. While the inclusion of a non-trivial tensor propagating speed leaves unchanged the scalar spectrum, it impacts the tensor spectrum by rescaling its amplitude of a factor $c_T^{n_T - 1}$. We therefore modify CAMB in order to include this correction by rescaling r^{CAMB} accordingly (*i.e.* $r = r_{0.05} = r^{\text{CAMB}} c_T^{n_T - 1}$) and calculating the amplitude of the spectra at the same pivot scale $k_{*,T} = k_{*,S} = aH = 0.05 \text{ Mpc}^{-1}$. This choice ensures that r is calculated to a well-defined scale and allows our constraints to

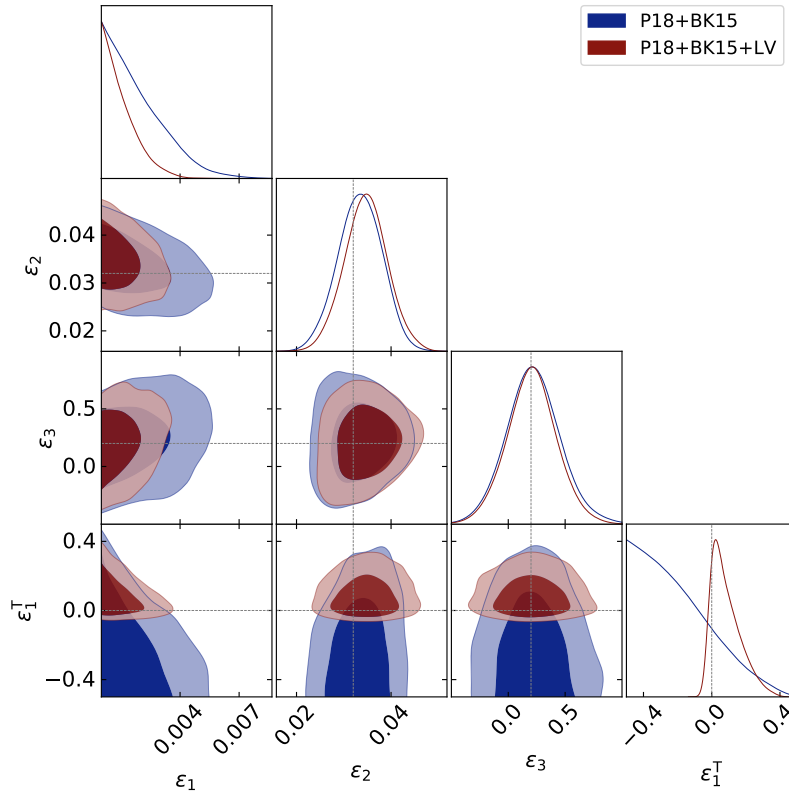


FIGURE II.6: Marginalized 2D and 1D posterior for the combination of Planck 2018 [113, 115] and Biceps/Keck 2015 [162] data (P18+BK15) for the first and second order slow parameters and their combination with the LIGO/VIRGO upper limit on the stochastic background amplitude [296, 297] (P18+BK15+LV).

be directly compared with the results reported by the Planck Collaboration [78, 114]. In our MCMC analysis we consider the six parameters of the standard Λ CDM model *i.e.*, the baryon $\omega_b \doteq \Omega_b h^2$ and cold dark matter $\omega_c \doteq \Omega_c h^2$ energy densities, the angular size of the horizon at the last scattering surface θ_{MC} , the optical depth τ , the amplitude of primordial scalar perturbation $\log(10^{10} A_S)$ and the scalar spectral index n_S . As discussed before, the inclusion of (the tensor and scalar) runnings is mandatory to relate the shape of the spectrum at different scales and so, along with the six standard Λ CDM parameters, we also include in our analysis the scalar running α_S , the tensor-to-scalar ratio r , the tensor spectral index n_T , the tensor running α_T , the propagating speed c_T and the parameter ϵ_1^T that quantifies its time variation per Hubble time. Instead of directly sampling these parameters (as it is commonly done, see e.g [78, 114]) we choose to do the MCMC sampling using, along with the standard Λ CDM parameters, the following four $\{c_T, 16\epsilon_1, \epsilon_1^T, \epsilon_3\}$ and to derive the value of the tensor and scalar runnings from the generalized consistency relations introduced in section II.III.I. The flat priors¹¹ on our parameter space are reported in Table II.4.

In Table II.5 we show the constraints on the parameters from the combination of Planck and Biceps/Keck data while in Figure II.11 we report their 68% and 95% contour plots. A first aspect we would like to stress is that our results confirm that a non-trivial time-dependent propagating speed does not alter the constraints on the scalar parameters from the Planck data (which assume $c_T = 1$) as expected from our theoretical discussion.

As concerns the inflationary tensor parameters, the tensor propagating speed c_T is only weakly constrained with the 95% C.L. contours showing a preference for $c_T \gtrsim 0.18$. This is expected since the CMB data only constrain the amplitude of tensor perturbations $A_T = r A_S = 16\epsilon_1 A_S c_T^{n_T-1}$. Then Planck data

¹¹Note that in our MCMC sampling we are considering only the parameter space of subluminal velocities. We discuss superluminal velocities in the [supplementary material, section A.6](#)

are only able to bound the product ϵ_1/c_T and since they prefer a tensor amplitude consistent with zero this leads to a weakly constrained propagating speed of tensor perturbations; only an upper bound can be placed on the tensor-to-scalar ratio $r < 0.096$ at 95% C.L. Nevertheless we can derive the upper bound $\epsilon_1^T < 0.203$ at 95% C.L. on the parameter that quantifies the time dependence of c_T . The fact that the region $\epsilon_1^T < 0$ is essentially unconstrained from the Planck data is translated into the fact that the tensor tilt can assume large positive values as well as the tensor running α_T .

We note that the bound we derive on the tensor-to-scalar ratio is $\sim 60\%$ worse with respect to the results obtained from a combination of Planck and Biceps data without considering the runnings of the tensor spectrum. Conversely, the bound on the tensor spectral index n_T is significantly improved. In particular, $-0.23 \leq n_T \leq 0.54$ at 95% C.L. showing an improvement of a factor of 2 in the negative tail and a factor of 5 improvement in the positive tail in place of the Planck results of $-0.55 \leq n_T \leq 2.54$. This situation is again a direct consequence of considering a non-vanishing tensor running and imposing the generalized consistency relation (II.83). When α_T is non-zero the tensor spectrum acquires a term $\sim \alpha_T \log^2 k$ leading to a growth on small scales (high k). The freedom in n_T is so partially transferred to α_T that it results to be almost the same order of magnitude as n_T . Moreover, from Eq. (II.84) one can also derive a constraint on the second-order tensor running β_T that we found to be $\beta_T = 0.060_{-0.093}^{+0.046}$ at 68% C.L. (i.e. again of almost the same order than n_T and α_T)¹² This shows that also the results can be sensitive to the higher-order terms in the primordial spectra, enforcing the importance of a proper parametrization to correctly connect and describe the large and small scale behavior of the tensor spectrum.

For completeness we also report the bound on the standard slow roll parameters that can be derived accordingly to the consistency relation derived in section II.III.I. We obtain the following constraints from the combination P18+BK15:

$$\epsilon_1 < 0.0046 \quad (95\% \text{ C.L.}) \quad (\text{II.91})$$

$$\epsilon_2 = 0.0334 \pm 0.0046 \quad (68\% \text{ C.L.}) \quad (\text{II.92})$$

$$\epsilon_3 = 0.22 \pm 0.23 \quad (68\% \text{ C.L.}) \quad (\text{II.93})$$

in very good agreement with the results derived in section II.I within GR. We show the 2D marginalized contour plots and 1D marginalized posterior distributions of these parameters in Figure II.6.

Constraints from small scale experiments on Gravitational Waves

If during inflation the propagating speed of gravitational waves decreases enough (i.e. if ϵ_1^T is negative enough), the tensor tilt can become blue amplifying the Primordial Gravitational Waves production on small scales. Small scale experiments on gravitational waves such as LIGO/VIRGO and, in the future, LISA and Einstein Telescope (ET), are sensitive to the stochastic background, Ω_{GW} and can be used to improve the constraints on the inflationary parameters. In particular Eq. (II.49) provides a rough estimation of the upper bounds we can set on the blue tensor tilt from small scale experiments. However ground based interferometers probe scales that are separated from the CMB by a factor of 10^{18} in k . We have already said that on such small scales the higher-order corrections parametrized by the tensor runnings can be non-negligible and that should be included in the analysis [2]. Therefore, as also done in the previous section, we generalize the parametrization to Eq. (II.50)

In order to estimate the higher order contributions given by the sum (II.50), we work under the following important assumption: we consider the tensor parameters dominated by the time variation of the propagation speed through the parameter ϵ_1^T in such a way that:

$$n_T = -2\epsilon_1 - \epsilon_1^T \simeq -\epsilon_1^T \quad (\text{II.94})$$

¹²These results are consistent with the relation $\beta_T \simeq 2n_T^3 \simeq 2\alpha_T^{3/2}$, discussed below.

and consequently because of Eq. (II.77)

$$\alpha_n^T \doteq \left(\frac{d}{d \log k} \right)^n n_T \simeq n! \left(-\epsilon_1^T \right)^{n+1} \simeq n! (n_T)^{n+1} \quad (\text{II.95})$$

This approximation is in great accordance with the results derived in the previous section as it is possible to see from Figure II.7. In the left panel we plot the constraints in the plane (n_T, ϵ_1^T) while in the middle and right panels of the same figure we plot the constraints on the first two runnings (i.e. $\alpha_1^T \equiv \alpha_T$ and $\alpha_2^T \equiv \beta_T$) in the planes (n_T, α_T) and (n_T, β_T) , respectively. As one can see from the left panel the linear relation (II.94) between n_T and ϵ_1^T is confirmed and the impact of the parameter ϵ_1 is indeed negligible. The middle and right panels, instead validate the relation (II.95) between the runnings and the tensor tilt (or equivalently between the runnings and ϵ_1^T). As one can see $\alpha_T \simeq (n_T)^2 \simeq (\epsilon_1^T)^2$ while $\beta_T \simeq 2 (n_T)^3 \simeq 2 (-\epsilon_1^T)^3$: this is exactly what we expect from Eq. (II.95). Therefore when ϵ_1^T is negative, not only the tensor tilt is blue but also the runnings are positive. This amplifies the PGWs production on small scales allowing us to improve the constraints on the inflationary parameters. At the end of this section we will come back to further

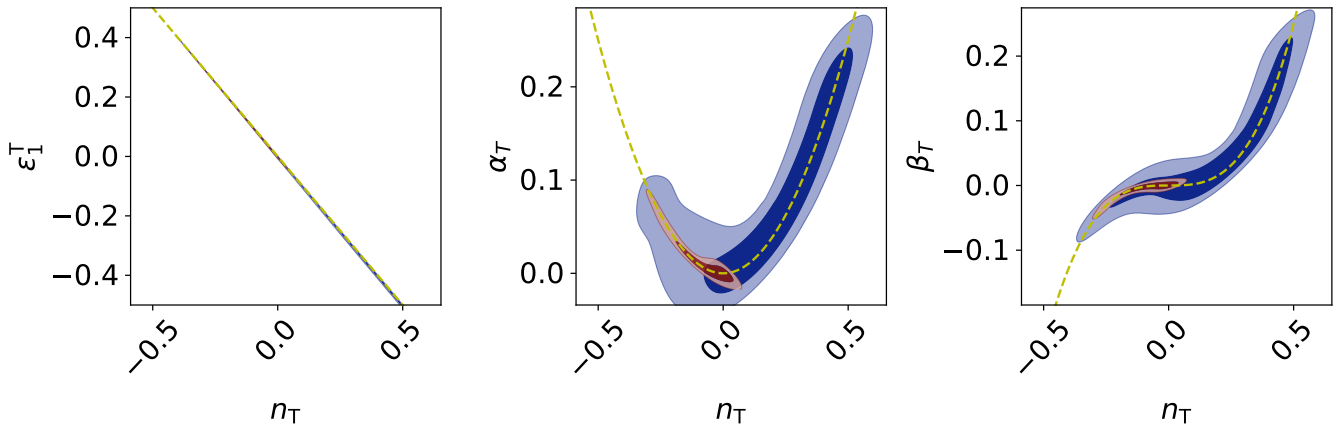


FIGURE II.7: Marginalized 2D posterior in the planes (n_T, r) and (α_T, r) . The blue contours are derived from the combination of Planck 2018 [113, 115] and Biceps/Keck 2015 [162] data (see section II.III.II) while the red contours include also the LIGO/VIRGO data on the stochastic background [296, 297] (see section II.III.II). The yellow dashed lines represent the relations (II.94) and (II.95) we used to derive the small scale constraints in section II.III.II.

discuss the validity of our approximation.

Since we are going to constrain the region of the parameter space $\epsilon_1^T < 0$ it is convenient to use $-\epsilon_1^T = |\epsilon_1^T|$. Putting (II.94) and (II.95) into (II.50), we can estimate the sum

$$\Omega_{\text{GW}}(k) = \frac{r A_S}{24z_{\text{eq}}} \left(\frac{k}{k_*} \right)^{-\frac{\log(1-|\epsilon_1^T| \log(\frac{k}{k_*}))}{\log(\frac{k}{k_*})}}. \quad (\text{II.96})$$

As one can see from Eq. (II.96), on the generic ultra-high $\tilde{k} \gg k_*$ the spectrum is well defined if $|\epsilon_1^T| \lesssim 1/\log(\tilde{k}/k_*)$. More precisely: if $|\epsilon_1^T| \ll 1/\log(\tilde{k}/k_*)$ the spectrum is essentially flat $\Omega_{\text{GW}} \simeq r A_S/24z_{\text{eq}}$ while if $|\epsilon_1^T| \simeq 1/\log(\tilde{k}/k_*)$ the spectrum is still flat for $k < \tilde{k}$, but it exponentially grows at $k \sim \tilde{k}$.

Here we derive a cutoff on ϵ_1^T simply demanding the spectrum to be well defined *at least* from the CMB scales all the way up to the ultra-high k probed by gravitational detectors and matching the LIGO/VIRGO constraints. We recall that in the frequency range $f \in (20 - 85.8)$ Hz, which corresponds to the wave-number range $k_{\text{LV}} \in (1.3 - 5.5) \times 10^{16} \text{ Mpc}^{-1}$, the LIGO and VIRGO data set an upper bound on the

stochastic background given by Eq.(II.47). Interestingly, reversing Eq. (II.96)

$$|\epsilon_1^T| = \frac{1 - \frac{r A_S}{24z_{\text{eq}}\Omega_{\text{GW}}(k)}}{\log\left(\frac{k}{k_*}\right)}. \tag{II.97}$$

the LIGO/VIRGO limit on the stochastic background can be translated into a lower bound on ϵ_1^T

$$\epsilon_1^T \geq -\frac{1 - \frac{r A_S}{24z_{\text{eq}}\Omega_{\text{GW}}(k_{\text{LV}})}}{\log\left(\frac{k_{\text{LV}}}{k_*}\right)} \simeq -0.0249 + (3.5 \times 10^{-9}) r \tag{II.98}$$

that is almost insensitive to the value of the tensor-to-scalar ratio r . Equivalently Eq. (II.98) puts a stringent upper limit on the blue tensor tilt

$$n_T \lesssim 0.025 \tag{II.99}$$

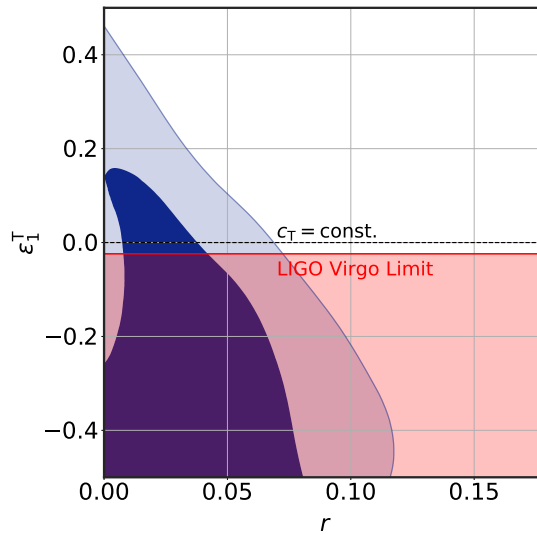


FIGURE II.8: Marginalized 2D posterior for the combination of Planck 2018 [113, 115] and Biceps/Keck 2015 [162] data in the plane (r, ϵ_1^T) . The red region is excluded by the LIGO/VIRGO data on the stochastic background of GWs (see section II.III.II).

We plotted the LIGO/VIRGO limit on ϵ_1^T in Figure II.8. As one can see comparing the upper bound (II.99) with that plotted in Figure II.10, once that higher order corrections (i.e. the tensor runnings) are included in the analysis we can improve the final constraints of more than 1 order of magnitude.

Note also that the constraints on ϵ_1^T can be translated into constraints on c_T since ϵ_1^T quantifies how the propagating speed changes with respect to the scale. To see this, since here we are focusing only on the linear terms assuming that $\dot{c}_T \simeq 0$, we can consider a simple toy model where the propagating speed constantly decreases for almost all the e-fold of inflation in such a way that the equation of motion reads

$$c_T(t) - c_T(t_i) \doteq \int_{t_i}^t \dot{c}_T dt = \dot{c}_T (t - t_i) = \epsilon_1^T c_T(t) \Delta N \tag{II.100}$$

where $\Delta N = H\Delta t$ is the total number of e-fold between the initial time t_i (when c_T starts to decrease) and the time t . In this case c_T is given by

$$c_T = \frac{c_T(t_i)}{1 - \epsilon_1^T \Delta N}. \tag{II.101}$$

Assuming $c_T(t_i) = 1$ and $\Delta N \simeq 60$, the LIGO/VIRGO constraint on ϵ_1^T implies¹³

$$c_T \gtrsim 0.4 \quad (\text{II.102})$$

that is consistent with the 2D marginalized posteriors shown in [Figure II.11](#) where values of c_T smaller than 0.4 times the speed of light seem to be disfavored, at least within the 68% C.L. contours.

As concerns the next generation of gravitational waves experiments, LISA and ET are expected to have a sensitivity to the stochastic background $\Omega_{\text{GW}}(k_{\text{LISA}}) \simeq 1 \times 10^{-12}$ on scales $k_{\text{LISA}} \approx 1 \times 10^{13} \text{ Mpc}^{-1}$ [210] and $\Omega_{\text{GW}}(k_{\text{ET}}) \simeq 3 \times 10^{-13}$ on scales $k_{\text{ET}} \approx 5 \times 10^{15} \text{ Mpc}^{-1}$ [298], respectively. Considering the higher-order corrections in $\mathcal{P}_T(k)$, we see that the improvement in sensitivity expected from LISA and ET is not translated into constraining power on ϵ_1^T and consequently on the tensor tilt at the CMB scales¹⁴. This result seems to contradict the common intuition but the key aspect here is scale-dependence. Assuming the generalized tensor spectrum of Eq. (II.50), we can define a *scale-dependent* tensor tilt $n_T(k)$

$$n_T(k) \doteq n_T(k_*) + \underbrace{\sum_{n=1}^{\infty} \frac{a_n^T}{(n+1)!} [\log(k/k_*)]^n}_{\doteq S(k)} \quad (\text{II.103})$$

in such a way that we can always derive constraints by Ω_{GW} , trivially generalizing Eq. (II.49) for the scale-dependent case as

$$n_T(k) < \frac{\ln\left(\frac{24 z_{\text{eq}} \Omega_{\text{GW}}(k)}{r \mathcal{P}_S(k_*)}\right)}{\ln\left(\frac{k}{k_*}\right)} \quad (\text{II.104})$$

with $n_T(k)$ given by (II.103). Notice that the improvement in the sensitivity expected by LISA and ET is *again* translated into an improvement in the constraints on $n_T(k)$, but now these constraints must be referred to the tensor tilt evaluated at different scales. Therefore the improvement in the constraints expected from LISA and ET is not trivially translated into an improvement in the constraints on the tensor tilt on the CMB scales. In fact, the constraints on a given scale k are related to the constraints on the CMB scales k_* through the sum $S(k)$ that carries information about the specific model¹⁵. In the inflationary model considered here, the constraints on $n_T(k_*)$ remain almost the same for the three experiments. Indeed while $n_T(k_{\text{ET}}) \lesssim n_T(k_{\text{LISA}}) < n_T(k_{\text{LV}})$ it is also true that $S(k_{\text{LV}}) > S(k_{\text{ET}}) > S(k_{\text{LISA}})$ and the two terms in Eq. (II.103) compensate each other leaving almost the same freedom on the CMB scales for $n_T(k_*)$. This is again an effect due to the result discussed in [section II.II](#); *i.e.*, on small scales the PGW production is strongly model dependent and inflationary models that behave at the same way on the CMB scales (where all the physics is well captured by a power-law parametrization) may instead behave differently on small scales.

Before concluding this subsection, we want to briefly come back on the approximations (II.94) and (II.95) on which our results are based. Even if we have already shown that the analysis performed in the previous section confirms their validity, it is worthwhile to additionally prove their robustness. The shape of the tensor tilt plotted in [Figure II.7](#) and, in general, the validity of our approximation can be further understood as follows: using Eq. (II.73), we see that the value of ϵ_1 is fixed by the value of c_T and r :

$$\epsilon_1 = \frac{r}{16} c_T \lesssim \frac{r}{16} \quad (\text{II.105})$$

¹³We want to stress that this example is used to show that constraints on ϵ_1^T can be translated into constraints on c_T assuming that we know how the tensor speed evolves during inflation. However to derive our final results (shown in [Table II.5](#)) we did not assume any specific evolution. Notice also that in the [supplementary material, section A.7](#), we discuss the consistency between our final results and the current small scale measurement of c_T .

¹⁴In this model, the constraints on $n_T(k_*)$ expected by future experiments are $n_T(k_*) \lesssim 0.032$ for LISA and $n_T(k_*) \lesssim 0.025$ for ET.

¹⁵The scale-dependence is encoded in the runnings $\{a_n^T\}$ that define the shape of $n_T(k)$ relating its value on the CMB scales with its value on the generic scale k by Eq. (II.103).

where in the last inequality we have used that $c_T \lesssim 1$. From the CMB data we know that r is constrained to be very small, if for example we fix the tensor-to-scalar ratio to $r \sim 10^{-2}$, we immediately see that $\epsilon_1 \sim 10^{-4}$ and¹⁶ $\epsilon_2 \sim 10^{-2}$. So for $|\epsilon_1^T| \sim 10^{-2}$ (i.e. the order of the limit we derived from the LIGO and VIRGO data), comparing the terms involved in the generic n order running,

$$|\epsilon_1^T| (\epsilon_1)^n \sim \epsilon_2 (\epsilon_1)^n \sim 10^{-2(2n+1)} \quad (\text{II.106})$$

$$\epsilon_1 (\epsilon_2)^n \sim \epsilon_1 (|\epsilon_1^T|)^n \sim 10^{-2(n+2)} \quad (\text{II.107})$$

$$(|\epsilon_1^T|)^{n+1} \sim 10^{-2(n+1)} \quad (\text{II.108})$$

we find that $\alpha_n^T \simeq n! (-\epsilon_1^T)^{n+1}$ unless corrections at least 2 order of magnitude smaller. The approximation is even better for smaller r while it is trivial to see that it is still valid for the whole range of r explored in our MCMC analysis as [Figure II.7](#) confirms.

Combined constraints from CMB and Small scale experiments

The LIGO/VIRGO limit on the stochastic background amplitude reduces significantly the allowed parameter space for ϵ_1^T (see also [Figure II.8](#)). Therefore, it is worth combining this small scale bound ([II.98](#)) with CMB data. We include the LIGO/VIRGO upper bound as a half-Gaussian prior on ϵ_1^T and we sample the same parameter space using the same method and the same priors as those considered in [section II.III.II](#). In [Table II.5](#) we give the constraints on the parameters from a combination of Planck and Biceps/Keck with the LIGO/VIRGO constraints, while in [Figure II.11](#) we report their 68% and 95% C.L. contour plots. As one can see neither the inclusion of the small scale data is enough to derive precise constraints on the primordial tensor speed that we found to be $c_T > 0.22$ at 95% C.L.. Nevertheless, a proper parametrization of the small scale behavior of the tensor spectrum allows us to set tight constraints on its time dependence parameter $\epsilon_1^T = 0.082_{-0.11}^{+0.047}$ at 68% C.L. and consequently on the other inflationary parameters. In particular, we constrain the tensor-to-scalar ratio $r < 0.0599$ at 95% C.L., which is in perfect agreement with the constraints derived by the Planck Collaboration [78]. We also constrain the tensor tilt to be $n_T = -0.084_{-0.047}^{+0.10}$ at 68% C.L. and its running $\alpha_T = 0.0141_{-0.022}^{+0.0035}$ always at 68% C.L. These constraints show an improvement of more than an order of magnitude with respect to those derived in [section II.III.II](#) only from the Planck and Biceps/Keck data. Moreover using ([II.84](#)) we can obtain derived constraints on the second-order running β_T , namely $\beta_T = -0.0061_{-0.0027}^{+0.011}$ at 68% C.L., again one order of magnitude better than our estimation provided in [section II.III.II](#). For completeness we report also the constraints on the other slow roll parameters that can be derived according to the consistency relation discussed in [section II.III.I](#). We obtain the following constraints from the combination P18+BK15+LV:

$$\epsilon_1 < 0.00276 \quad (95\% \text{ C.L.}) \quad (\text{II.109})$$

$$\epsilon_2 = 0.0347 \pm 0.0046 \quad (68\% \text{ C.L.}) \quad (\text{II.110})$$

$$\epsilon_3 = 0.21 \pm 0.22 \quad (68\% \text{ C.L.}) \quad (\text{II.111})$$

Our almost constraints on the inflationary parameters reduce significantly the parameter space allowed for models of inflation with non-trivial tensor speed. Indeed the positive (negative) values of n_T (α_T) are now very tightly constrained (see also [Figure II.9](#)). This means that a future detection of a large positive (negative) tensor tilt (running), allowed by the present bounds once the generalized consistency relations are relaxed, cannot be brought back to a time variation of the primordial tensor speed, as our results proved. Besides, thanks to the great improvement in the constraints derived combining the CMB and small scales data, one can better test gravity on the inflationary energy scale. We would like to stress that the generalized consistency relations obtained in [section II.III.I](#) and assumed in our MCMC analysis, generalize the standard slow roll relations that we prove to be recovered when the GR prescriptions $c_T = 1$ and $\epsilon_1^T = 0$

¹⁶Using Eq. ([II.69](#)) and the fact that $n_s \simeq 0.96$ [78]

are restored. Since any departure from these prescriptions would imply physics beyond GR on the inflationary energy scales, it is important to check the consistency between the constraints and the standard slow roll predictions in the GR framework. Let us start noting that the condition $\epsilon_1^T = 0$ that ensures a constant propagating speed c_T is consistent with our constraints within one standard deviation. Moreover in Figure II.9 we plot the 2D marginalized contours at 68% and 95% C.L. in the planes (n_T, r) and (α_T, r) . The standard consistency relations, yellow dashed lines in the figure, are consistent with our constraints and, above all when the small scale limit (II.47) is included, no significant deviations are observed.

We can, therefore, conclude that our results, even not strong enough to definitively exclude departures from GR on the inflationary energy scales, set interesting constraints on the inflationary models with non-trivial tensor speed, significantly reducing the allowed parameter space for such models. Moreover, they show remarkable accordance between the current data and the standard predictions expected in a GR slow roll scenario. In particular only deviations from GR of the order of $\sim \times 10^{-1}$ are allowed to combine large and small scale data for models with non-trivial tensor speed, see Figure II.9.

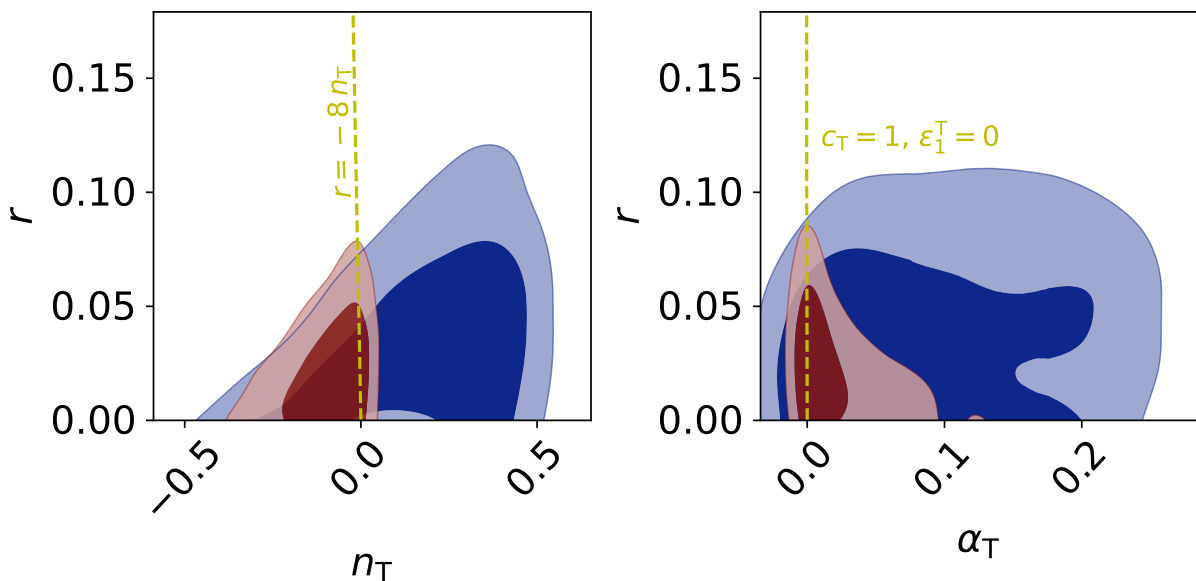


FIGURE II.9: Marginalized 2D posterior in the planes (n_T, r) and (α_T, r) . The blue contours are derived from the combination of Planck 2018 [113, 115] and Biceps/Keck 2015 [162] data (see section II.III.II) while the red contours take into account the LIGO/VIRGO data on the stochastic background [296, 297] (see section II.III.II). The yellow dashed lines represent the standard slow roll relations in the GR limit *i.e.* $c_T = 1$ and $d \log c_T / d \log k = 0$.

II.IV HIGHER CURVATURE CORRECTIONS AND TENSOR MODES

In the previous section we studied the effects of a non trivial gravity propagation during inflation without assuming any underlying model of modified gravity, but introducing the propagating speed in the framework of the effective field theory of inflation. In this section we instead focus on corrections from higher-curvature tensors.

Several high-energy theoretical models, such as String Theory [299–302], predict higher-curvature corrections to the gravitational effective action [76, 273, 303–305] and if the inflationary energy scale is sufficiently high, such corrections can lead to testable features in the primordial perturbations [94, 95, 227, 240–242, 253–255, 273, 304–327]. Here we further investigate the effects of a coupling of the inflaton field to higher-curvature tensors in models with a minimal breaking of conformal symmetry. In Ref. [94], it was clearly shown that, at leading order in the breaking of conformal symmetry, a coupling to the squared Weyl tensor can reproduce the most general higher-curvature corrections to the tensor spectrum. As we pointed

out in the previous sections, introducing non-standard (gravitational) physics during inflation we basically break the consistency relation between r and n_T and the higher order parameters, possibly leading to blue tensors. However these relations are violated in many other non standard models of inflation and even if a deviation from standard inflation will be observed by future experiments, one may ask how we could convince ourselves that it comes from the higher-curvature effects.

In this section we show for the first time that an observable violation of the tensor consistency relation(s) from higher-curvature tensors implies also a relatively large running of the tensor tilt, enhanced even by some order of magnitude with respect to the standard slow roll hierarchy [1, 127, 161]. This may affect the small scale behavior of tensor perturbations [2, 160, 328–330] and leave signatures in the tensor two-point function that we could test to recognize higher-curvature effects, above all if they are translated into a blue tilted spectrum visible by future Gravitational Wave experiments. Exploiting current cosmic microwave background and gravitational wave data we finally infer that large higher-curvature corrections seem to be disfavored.

II.IV.I THEORY

The action that reproduces the most general high-curvature corrections to the tensor two-point function at leading order in the breaking of conformal symmetry is [94, 331]¹⁷

$$S = S_{\text{EH}} + S_\phi + \frac{\bar{M}_p^2}{2} \int d^4x \sqrt{-g} f(\phi) \frac{W^2}{M^2} \quad (\text{II.112})$$

where S_{EH} and S_ϕ are the Einstein-Hilbert action and the action for the inflaton field ϕ , respectively. W is the Weyl tensor

$$\begin{aligned} W_{\mu\nu\rho\sigma} &\doteq R_{\mu\nu\rho\sigma} \\ &- \frac{1}{2} (g_{\mu\rho} R_{\nu\sigma} - g_{\mu\sigma} R_{\nu\rho} - g_{\nu\rho} R_{\mu\sigma} + g_{\nu\sigma} R_{\mu\rho}) \\ &+ \frac{R}{6} (g_{\mu\rho} g_{\nu\sigma} - g_{\nu\rho} g_{\mu\sigma}). \end{aligned} \quad (\text{II.113})$$

involved in the inflaton-Weyl coupling $f(\phi)W^2/M^2$ with

$$W^2 \equiv W^{\mu\nu\rho\sigma} W_{\mu\nu\rho\sigma} = R^{\mu\nu\rho\sigma} R_{\mu\nu\rho\sigma} - 2 R^{\mu\nu} R_{\mu\nu} + \frac{1}{3} R^2 \quad (\text{II.114})$$

and M is the scale suppressing higher-curvature corrections. Starting from Eq. (II.112), the primordial spectra can be computed to obtain the same results (II.67) and (II.68) derived in the previous section, with the exception that in this case we can get a precise relation for tensor propagating speed [3, 167, 217, 271–279] which reads

$$c_T \simeq 1 - 4 \left(\frac{H^2}{M^2} \right) f(\phi). \quad (\text{II.115})$$

Furthermore in principle here also the speed of scalar perturbations is not exactly unitary but the corrections are suppressed in slow-roll expansion and we can ignore them: $c_S \simeq 1 + (\epsilon_1/3)(c_T - 1) \simeq 1$. Notice also that we are considering the inflaton-Weyl coupling as a perturbative correction to the gravitational action¹⁸ and so c_T cannot deviate much from unity putting constraints on the function $f(\phi)$ and consequently on its scale dependence. In what follows we consider a simple coupling $df(\phi)/d\phi \sim \pm 1/\Lambda$ with $\Lambda < M_p$ and we assume negligible the higher-order derivatives: $d^n f(\phi)/d\phi^n \simeq 0$. We postpone the discussion of a

¹⁷Note that a further term $\sim h(\phi)W\tilde{W}/M^2$ can be considered basically violating parity of primordial tensor modes [94, 331–335]. In our work we ignore such coupling.

¹⁸Note that in this way the theory is safe from ghost instabilities [59, 94].

generic coupling-function $f(\phi)$ to the [supplementary material, section A.8](#). Finally, we do not specify the sign of the coupling. Indeed, while the sign could be constrained by requiring tensor to propagate subliminally, as shown in Refs. [336, 337] (see also Ref. [338]) this is not always a safe assumption and, depending on the model, it can be possible to perform a change of frame so that in the new frame the tensor speed is c , but the speed of the other massless particles is greater than c leaving us with a situation where we have actually constrained the speed of normal species to be superluminal, in tension with causality.

As we discussed on the previous section, the presence of a non trivial tensor speed breaks the inflationary slow roll consistency relation between $r \simeq 16\epsilon_1/c_T \simeq 16\epsilon_1$ and the tensor tilt $n_t \simeq -r/8 - \epsilon_T$ with $\epsilon_T \doteq d \log c_T / d \log k$ [3, 94]. From Eq. (II.115) it follows that [94]

$$n_T = -\frac{r}{8} + \lambda r^{1/2} \quad (\text{II.116})$$

where we have ignored negligible terms $\propto (c_S - 1)$ that are further suppressed by a factor ϵ_1 and we have defined the dimensionless parameter

$$\lambda \doteq \sqrt{2} \bar{M}_p \left(\frac{H^2}{M^2} \right) \frac{df(\phi)}{d\phi} \sim \pm \sqrt{2} \left(\frac{\bar{M}_p}{\Lambda} \right) \left(\frac{H^2}{M^2} \right) \quad (\text{II.117})$$

that weights the size of high-curvature corrections to the inflationary parameters. As discussed in Ref. [94], if the inflationary energy scale H^2 is close to M^2 , these corrections can be the dominant effect as the parameter λ is also amplified by the factor M_p/Λ that can be large. Note also that for enough large positive λ , higher-curvature corrections can end-up in a blue tensor spectrum, amplifying the PGWs production on the small scales probed by gravitational detectors, as we discussed so far.

Along with the tensor tilt, also the other inflationary parameters can acquire non negligible corrections from higher-curvature terms. In particular, by noting that¹⁹

$$\frac{d\lambda}{d \log k} = -2\lambda \epsilon_1 = -\frac{r}{8} \lambda \quad (\text{II.118})$$

we derive the expression of the tensor running $\alpha_T \doteq dn_T / d \log k$, namely

$$\alpha_T = \alpha_T^{\text{SR}} + \lambda \left[-\frac{3}{16} r^{3/2} - \frac{1}{2} r^{1/2} (n_S - 1) \right]. \quad (\text{II.119})$$

where α_T^{SR} represents the standard slow roll relation (II.16) and the terms in the square brackets are the correction introduced by higher-curvature tensors. While in the standard slow roll scenario this relation is $\mathcal{O}(\epsilon^2)$, implying an extremely small running $\alpha_T^{\text{SR}} \simeq -5 \times 10^{-n-3}$ for $r \simeq 10^{-n}$, higher-curvature corrections may instead give a relatively large running $\alpha_T/\lambda \simeq 2 \times 10^{-n/2-2}$, see also [Figure II.10](#). A large tensor running can leave non trivial features in the shape of the tensor two-point function, affecting the small scale behavior of tensor anisotropies and, if higher-curvature corrections are translated into blue tensors, further enhancing the gravitational wave production on small scales as those probed by gravitational detectors. Therefore if a violation of the consistency relation $r = -8n_T$ is observed by future CMB and/or small scales measurements, a combined analysis of the tilt and the running should in principle shed light on its higher-curvature nature.

As concerns the other inflationary parameters, a computation for the running of running $\beta_T \doteq d\alpha_T / d \log k$ gives:

$$\beta_T = \beta_T^{\text{SR}} + \lambda \left[\frac{15}{256} r^{5/2} + \frac{3}{8} r^{3/2} (n_S - 1) + \frac{1}{4} r^{1/2} (n_S - 1)^2 - \frac{1}{2} r^{1/2} \alpha_S \right] \quad (\text{II.120})$$

¹⁹We recall the useful relation $d/d \log k = \sqrt{2} M_p \epsilon_1^{1/2} d/d\phi$.

where $\beta_T^{\text{SR}} \sim \mathcal{O}(\epsilon^3) \lesssim 10^{-6}$ [1] represents the standard slow roll term given by Eq.(II.17). We see that higher-curvature corrections still provide a dominant effect $\beta_T/\lambda \simeq 10^{-n/2-4}$, which is however extremely small.

By taking higher order derivatives it is also easy to see that $\alpha_j^T \doteq (d/d \log k)^j n_T \lesssim 2^j \lambda \times 10^{-\frac{n}{2}-2j}$ from which it follows that the running of order $j + 1$ is expected to be a factor $\sim 10^{-2}$ smaller than the running of order j . Despite the fact that higher order runnings can be strongly amplified on ultrahigh k , it is easy to see that in this case such terms still remain negligible even on the scales probed by GW interferometers²⁰. So, along with the tensor tilt, any relevant correction to the spectrum is captured only by the running α_T and eventually the running of running β_T .

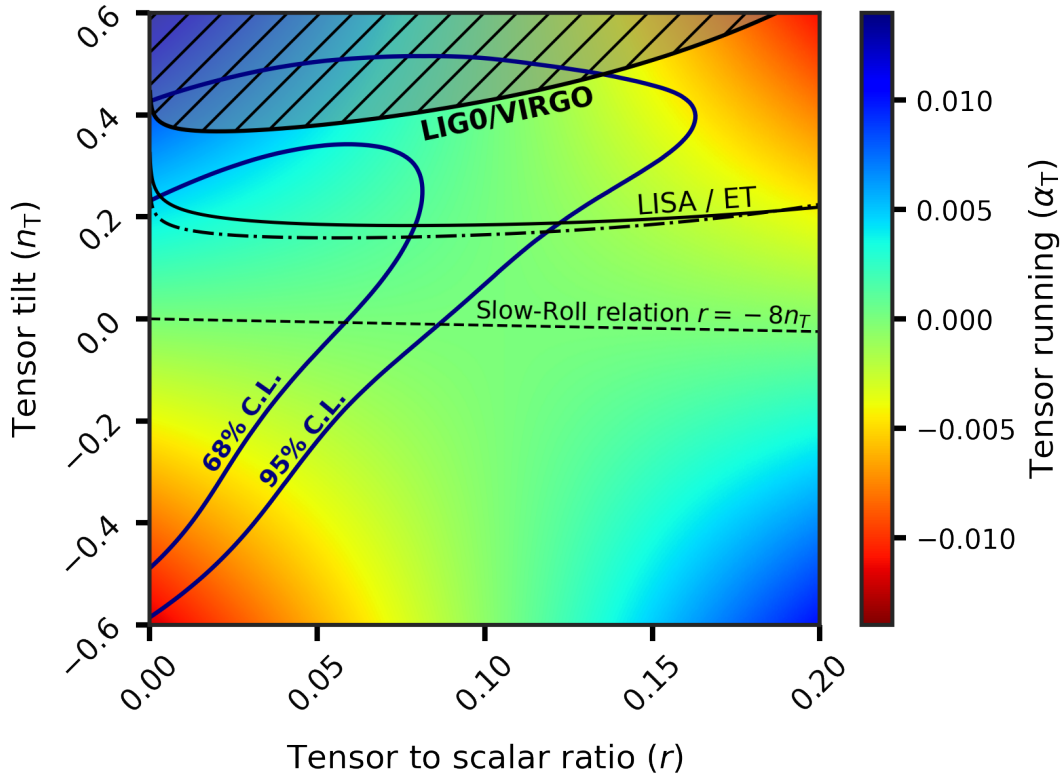


FIGURE II.10: Tensor spectrum expected by higher-curvature corrections. For each point in the plane (r, n_T) the tensor running α_T is fixed by the equations (II.116) and (II.119). The dashed region is excluded by the LIGO/VIRGO limit on the stochastic background (II.47); the black solid (dashed) line represents the sensitivity expected by LISA (Einstein Telescope). The blue contours are the 68% and 95% C.L. bounds for a combination of Planck 2018 [113, 115], BICEP2/Keck 2015 [162] and the LIGO/VIRGO [296, 297] (P18+BK15+LV) data.

II.IV.II CONSTRAINTS

We first derive constraints on higher-curvature corrections using the small scale data on the stochastic background of GWs and then we combine such information with the current CMB data performing a Monte Carlo Markov Chain (MCMC) analysis. We use the same methods, techniques and datasets discussed previously in the [subsection II.III.II](#)

²⁰We recall that the generic running of order j gives a correction to the tensor tilt that is weighted by a factor $\log^j(k/k_*)/(j+1)!$ on the generic scale k .

Parameter	Prior/Derived	Constraints (P18+BK15+LV)
$\Omega_b h^2$	[0.005, 0.1]	0.02240 ± 0.00015
$\Omega_c h^2$	[0.001, 0.99]	0.1200 ± 0.0012
$100 \theta_{MC}$	[0.5, 10]	1.04091 ± 0.00031
τ	[0.01, 0.8]	0.0564 ± 0.0078
$\log(10^{10} A_S)$	[1.61, 3.91]	3.050 ± 0.015
n_S	[0.8, 1.2]	0.9653 ± 0.0044
ϵ_3	[-0.5, 1]	0.12 ± 0.23
r	[0, 1]	< 0.123
ϵ_T	[-0.5, 0.5]	-
α_S	Derived	$-0.0041^{+0.0077}_{-0.0059}$
n_T	Derived	$0.08^{+0.28}_{-0.19}$
α_T	Derived	$-0.0004^{+0.0031}_{-0.0020}$
β_T	Derived	$-0.00022^{+0.00084}_{-0.00042}$
λ	Derived	$0.1^{+2.0}_{-1.2}$

TABLE II.6: The external priors used in our MCMC sampling and the results obtained combining the full Planck 2018 likelihood [113, 115], the BICEP2/Keck 2015 B-mode [162] likelihood and the LIGO/VIRGO data on the stochastic background [209]. The constraints on parameters are at 1σ level (68% C.L.) while upper bounds are at 2σ (95% C.L.). We indicate as Derived those parameters obtained by the others using the consistency relations.

Constraints from Gravitational Waves

In this case we parametrize the primordial tensor spectrum by Eq.(II.14) and we impose the relations (II.116) and (II.119) for the inflationary parameters relating the LIGO/VIRGO limit (II.47) to higher-curvature corrections. In Figure II.10 we plot the constraints in the plane (r, n_T) showing that values $n_T \gtrsim 0.4$ are excluded by the LIGO/VIRGO limit (II.47). Note also that these constraints can be easily translated into constraints on the dimensionless parameter λ , *i.e.* on the size of the higher-curvature corrections. A large positive tensor tilt implies a large positive running α_T that is completely fixed by the values of n_T and r by equations (II.116) and (II.119). If a violation of the slow roll consistency relation is observed, a test of (II.119) could in principle shed light on its higher-curvature nature. Testing this relation with current and future CMB measurements could be extremely challenging as the tensor running, even enhanced by some order of magnitude by higher-curvature corrections, clearly gives higher-order corrections to the tensor spectrum on the CMB scales. Nevertheless, if higher-curvature corrections are translated into a sufficiently large blue tilted spectrum, leading to an Ω_{GW} visible by future GW experiments, combining the CMB and GW data we might strongly improve the constraining power as proved in the previous section. Indeed always in Figure II.10 we show the sensitivity curves of future gravitational wave experiments such as LISA [339] and Einstein Telescope [340]. They are expected to bring the LIGO/VIRGO upper limits down by a factor ~ 2 leading to either a detection or to tighter constraints. Because of (II.116) and (II.119), a detection of Ω_{GW} at a given scale k will immediately fix the parameter λ to

$$\lambda = \frac{\frac{\ln\left(\frac{24 z_{eq} \Omega_{GW}(k)}{r \mathcal{P}_S(k_*)}\right)}{\ln(k/k_*)} + \frac{r}{8} - \frac{\alpha_T^{SR}}{2} \ln(k/k_*)}{r^{1/2} - \left[\frac{3}{16} r^{3/2} + \frac{1}{2} r^{1/2} (n_S - 1)\right] \ln(k/k_*)}. \quad (\text{II.121})$$

Supposing that future CMB experiments lead to a first detection of the tensor amplitude r , we can use measurements of $\Omega_{\text{GW}}(k)$ at different scales (*e.g.* the scales probed by LISA and ET) as a consistency check for λ and so as a test of equations (II.116) and (II.119).

We conclude this subsection with a final remark: it is well known that the multi-messenger event GW170817 [214, 218] sets strong bounds on modified gravity theories, constraining $c_T - 1 \lesssim 10^{-15}$. Therefore one could consider the possibility of using this bound to derive constraints on this model. While it is easy to see that adopting the GW170817 limit higher-curvature corrections will be severely suppressed²¹, it is also worth noting that the event GW170817 only constrains the propagating speed of gravity in a precise range of frequencies that is far away from the CMB scales. Because of the running in frequency $\epsilon_T = d \log c_T / d \log k$, we may not simply use the GW170817 bound as it refers different scales, but we can use constraints on λ to relate values of c_T at different frequencies.

Constraints from Cosmic Microwave Background and Gravitational Waves

For our MCMC analysis, we consider the six parameters of the standard Λ CDM model, *i.e.* the baryon $\omega_b \doteq \Omega_b h^2$ and cold dark matter $\omega_c \doteq \Omega_c h^2$ energy densities, the angular size of the horizon at the last scattering surface θ_{MC} , the optical depth τ , the amplitude of primordial scalar perturbation $\log(10^{10} A_S)$ and the scalar spectral index n_S . Along with the six standard Λ CDM parameters, we also considered the scalar running α_S , the tensor-to-scalar ratio r , the tensor spectral index n_T , the tensor running α_T , and the running of running β_T . However, instead of directly sampling all these parameters (as it is commonly done, see *e.g.* [78, 114]), along with the standard Λ CDM parameters, we sample only $\{r, \epsilon_3, \epsilon_T\}$ and we use the relations derived in subsection II.IV.I to compute the others. More precisely we derive the tensor tilt n_T by Eq. (II.116), its running α_T by Eq. (II.119) and its running of running β_T by Eq. (II.120) with $\alpha_S = \alpha_T^{\text{SR}} + (1 - n_S - r/8) \epsilon_3$. In this way we are also able to derive constraints on the dimensionless parameters λ defined by Eq.(II.117), as we discuss below.

In Table II.6 we show both the priors used for the sampled parameters, denoting as "Derived" those obtained by consistency relations, and the constraints from the combination of Planck (P18), BICEP2/Keck (BK15) and LIGO/VIRGO (LV) limit on the stochastic background, Eq.(II.47). We include the LIGO/VIRGO limit as an half-Gaussian prior on the amplitude of tensor spectrum at the smallest scale probed by those gravitational wave interferometers. In Figure II.11 we instead report the 68% and 95% contour plots for the tensor parameters.

Although our results do not exclude the possibility that observable departures from the slow roll consistency relation can arise from higher-curvature tensors, see also Figure II.10, they strongly reduce the parameter space allowed for such deviations. In particular our analysis shows a preference for a small running of the tensor tilt $\alpha_T = -0.0004_{-0.0020}^{+0.0031}$ at 68% C.L., consistent with zero as expected in the standard slow-roll hierarchy. The constraints on the tensor running can be translated into a constraint on the dimensionless parameter λ that weighs the higher-curvature corrections to the inflationary parameters, namely $\lambda = 0.1_{-1.2}^{+2}$ at 68% C.L., see also Table II.6 and the discussion in section II.IV.II. Also in this case a remarkable preference for values of λ consistent with zero is found, disfavoring large corrections from higher curvature tensors, see also the posterior distribution of λ in Figure II.11. Notice also that future experiments on GW such as LISA and ET, once combined with current and future CMB data, can further constrain the parameter space allowed for this model. In Figure II.10, we can appreciate that the sensitivity curves of future gravitational wave experiments intersect the current CMB constraints, which means that a large range of the parameter space currently allowed can be probed by future measurements, leading to either a detection or to tighter bounds on higher-curvature corrections.

²¹ Assuming a coupling function $f(\phi) \sim \phi/\Lambda$ with $\phi \lesssim 10^{15} \text{GeV}$ the GW170817 limit would imply $|\lambda| \simeq 10^{-11} \ll 1$.

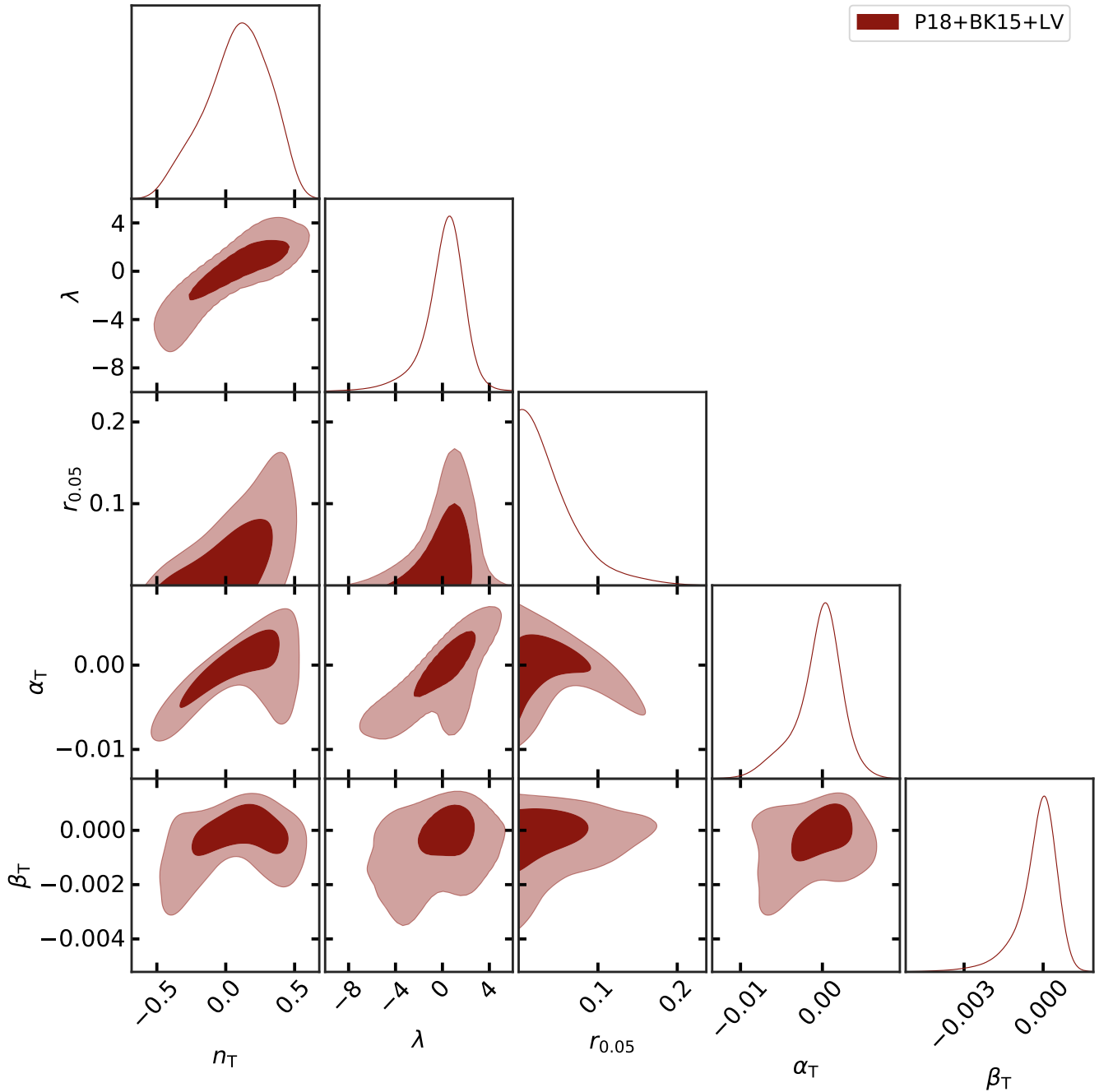


FIGURE II.11: Marginalized 2D and 1D posteriors for the combination of Planck 2018 [113, 115], BICEP2/Keck 2015 [162] and the LIGO/VIRGO upper limit on amplitude of the stochastic background [296, 297] (P18+BK15+LV).

CHAPTER III

HOT RELICS: AXIONS & NEUTRINOS

In this chapter I discuss well motivated extensions of the Standard Model of elementary particles that involve axions thermalized in the early Universe by scatterings with other particles as a solution of the strong CP problem in quantum chromodynamics. After providing a brief review of the axion theory, I analyze realistic mixed hot-dark-matter scenarios that include both axions and massive neutrinos. In light of the most recent cosmological and astrophysical observations, I present new robust bounds on hot relics able to constrain a significant range of the parameter space, with important implications for direct axion and neutrino searches. Finally, I extend the discussion to future cosmological observations.

III.I THE STRONG CP PROBLEM AND AXIONS

The most elegant and promising solution of the strong CP problem in quantum chromodynamics was provided by Peccei and Quinn in 1977 [341, 342]. They postulated that the full Lagrangian of the standard model was invariant under an additional global $U(1)_{PQ}$ symmetry spontaneously broken at some energy scale. The result is a new spineless particle named axion. In this section, we give a brief overview both of the strong CP problem and the Peccei Quinn solution, pointing out the most important properties of axion theory.

III.I.I ASPECTS OF QUANTUM CHROMODYNAMICS

We start our discussion from another problem known as $U_A(1)$ problem. It seems peculiar, but we will see that the strong CP problem actually arises from the solution of the $U_A(1)$ problem. To understand the nature of the $U_A(1)$ problem we need to briefly review the basic aspects of QCD and the chiral structure of the Dirac spinor fields [343, 344]. As nuclei are formed from protons and neutrons, in the same way Hadrons (*i.e.* particles that undergo strong interactions) are made of bound states of charged quarks. Quarks can have three different colors (*red, blue, green*) and different flavors (*i.e. up, down, strange, charm, bottom, top*). At the beginning, when quarks were first introduced, they were considered a convenient way to motivate the appearance of particular representations of the approximate symmetry group $SU(3)$ and for this reason dynamical problems such as the absence of free quarks were neglected. Instead quarks can be described as interacting particles by a fundamental quantum field theory. QCD (*i.e.* the quantum theory of strong interactions) is a non abelian gauge field theory based on the gauge group $SU(3)$. The particles linked to the gauge field are said gluons, and their role is to bind Hadrons together. A non-abelian gauge theory in some sense is similar to an abelian one and indeed quarks in QCD appear in a very similar way that electrons in QED, while gluons are analogous to photons. Anyway there are some important differences such as the fact that unlike electrons and photons, quarks and gluons never appear as physical particles. The fact that quarks and gluons are never observed as free particles is solved by the so called confinement requirement which asserts that the dynamics of QCD are such that only $SU(3)$ singlet states are present in the space of finite energy physical states. Furthermore in QCD there are no mass-less states (as photons in QED) except the Pions and associated pseudo-scalar particles in the limit of vanishing quark masses. Note that a crucial consequence of the confinement requirement is that QCD cannot be described in the conventional perturbation theory since free particle states are the starting point of any perturbation theory. Anyway one can show that for non abelian gauge theories, uniquely in four spacetime dimensions, perturbation theory has the correct property of asymptotic freedom and this justifies the application of the perturbation theory in order to calculate quantitatively measurable predictions.

The Lagrangian of a non abelian $SU(3)$ gauge theory has 8 gauge fields A_μ^a ($a = 1\dots 8$) corresponding to 8 different gluons. The strength tensor reads

$$G_{\mu\nu}^a = \partial_\mu A_\nu^a - \partial_\nu A_\mu^a + g f_{abc} A_\mu^b A_\nu^c \quad (\text{III.1})$$

where g is the coupling constant and the f_{abc} are the totally antisymmetric structure constants of the $SU(3)$ group. In terms of the 3×3 Gell-Mann matrices λ_a we have

$$\left[\frac{1}{2} \lambda_a, \frac{1}{2} \lambda_b \right] = i f_{abc} \frac{1}{2} \lambda_c \quad (\text{III.2})$$

The quark fields belong to the complex 3-dimensional representation of $SU(3)$ defined by matrices λ_a . The QCD Lagrangian therefore is

$$\mathcal{L}_{\text{QCD}} = -\frac{1}{4} G_a^{\mu\nu} G_{\mu\nu}^a + \sum_f \bar{q}_f (i\gamma^\mu D_\mu - m_f) q_f \quad (\text{III.3})$$

where the sum is over the spinor indices (suppressed for brevity), the different quark color indices (suppressed for brevity, as well) and over the different flavor indices f . Note that each flavor quark has a given mass m_f . D_μ is the covariant derivative defined in such a way that:

$$D_\mu q_f = \partial_\mu q_f - ig A_\mu^a \frac{1}{2} \lambda_a q_f \quad (\text{III.4})$$

Local infinitesimal SU(3) gauge transformation reads:

$$\begin{cases} \delta A_{\mu a} = \frac{1}{g} (\partial_\mu \zeta_a + g f_{abc} A_{\mu b} \zeta_c) \\ \delta q_f = i \zeta_a \frac{1}{2} \lambda_a q_f \end{cases} \quad (\text{III.5})$$

and it easy to show that the QCD Lagrangian (III.3) is invariant under (III.5). We do not want to investigate further general details of the QCD Theory since this goes beyond our goals and we remand the interested reader to the literature dedicated.

As a preliminary to describe the $U_A(1)$ problem we examine the chiral structure of the Dirac fields. Such fields (that could be the electron or the quark field) satisfy the Dirac equation:

$$(i\gamma^\mu \partial_\mu - m) \psi(x) = 0, \quad (\text{III.6})$$

that is obtained from the Lagrangian

$$\mathcal{L}(x) = \bar{\psi}(x) (i\gamma^\mu \partial_\mu - m) \psi(x). \quad (\text{III.7})$$

where $\bar{\psi} = \psi^\dagger \gamma^0$ and the γ^μ matrices are defined by $\{\gamma^\mu, \gamma^\nu\} = 2g^{\mu\nu} I$ and we introduce also the further matrix $\gamma_5 \equiv \gamma^0 \gamma^1 \gamma^2 \gamma^3$ which by definition trivially satisfies $(\gamma_5)^2 = 1$ and $\gamma_5 \gamma^\mu = -\gamma^\mu \gamma_5$. At this point we introduce the Left handed and Right handed Dirac fields respectively as

$$\psi_L = \frac{1}{2} (1 - \gamma_5) \psi, \quad \bar{\psi}_L = \frac{1}{2} (1 + \gamma_5) \bar{\psi} \quad (\text{III.8})$$

$$\psi_R = \frac{1}{2} (1 + \gamma_5) \psi, \quad \bar{\psi}_R = \frac{1}{2} (1 - \gamma_5) \bar{\psi} \quad (\text{III.9})$$

in such a way that $\psi = \psi_L + \psi_R$ and $\bar{\psi} = \bar{\psi}_L + \bar{\psi}_R$. In term of ψ_L and ψ_R , the Lagrangian reads

$$\mathcal{L}(x) = \bar{\psi}_R i\gamma^\mu \partial_\mu \psi_R + \bar{\psi}_L i\gamma^\mu \partial_\mu \psi_L - m [\bar{\psi}_R \psi_L + \bar{\psi}_L \psi_R] \quad (\text{III.10})$$

and we see that the kinetic part is a sum of two terms involving the right and left chiral components separately, while the mass term couples right to left and left to right. From this point of view the fermion mass comes from an interaction that transforms left handed (or negative helicity) particles into right handed (or positive helicity) ones; and vice versa. For example an (approximately) massless neutrino has no interaction inducing such a L-R flip so that it remains purely left-handed. Another interesting fact is that for massless particles, since $\gamma_5 \gamma^\mu = -\gamma^\mu \gamma_5$, we have that $\gamma_5 (i\gamma^\mu \partial_\mu \psi) = 0 = -(i\gamma^\mu \gamma_5 \psi)$ and so both ψ_L and ψ_R respect the Dirac equation: $i\gamma^\mu \partial_\mu \psi_R = i\gamma^\mu \partial_\mu \psi_L = 0$.

With this result in mind, we now come back to the QCD Lagrangian (III.3) and focusing on the quark Dirac field term $\sum_f \bar{q}_f (i\gamma^\mu D_\mu - m_f) q_f$ we see that in the limit $m_f \rightarrow 0, \forall f$, both the Right and the Left handed Dirac fields respect the Dirac Equation and so for f flavors of quarks, we have a large global symmetry

$$U_R(f) \times U_L(f) \quad (\text{III.11})$$

which corresponds to the freedom of arbitrary chiral rotations of the f flavor of quarks into each other. We can use the chiral rotation invariance in order to define the Vectorial component (V=R+L) and the Axial

component (A=R-L) so that, in the quark vanishing masses, the exact symmetry of the theory is

$$U_V(\mathbf{f}) \times U_A(\mathbf{f}) \quad (\text{III.12})$$

If we call Λ_{QCD} the dynamical energy scale of the QCD, since the masses of the up and down quarks are $m_u, m_d \ll \Lambda_{\text{QCD}}$ we have that

$$U_V(2) \times U_A(2) \quad (\text{III.13})$$

is a very good approximate symmetry of the theory that can be further decomposed as:

$$\boxed{\underbrace{SU_V(2) \times U_V(1)}_{U_V(2)} \times \underbrace{SU_A(2) \times U_A(1)}_{U_A(2)}} \quad (\text{III.14})$$

Let us focus on the vectorial part and on the axial part separately.

The $SU_V(2)$ part is the symmetry group associated with the quark field transformations:

$$q_i \rightarrow \left[e^{i \frac{\vec{\alpha} \vec{\tau}}{2}} \right]_{ij} q_j \quad (\text{III.15})$$

and the Noether current:

$$\vec{J}_V^\mu = \bar{q} \gamma^\mu \frac{\vec{\tau}}{2} q \quad (\text{III.16})$$

This symmetry is exact if $m_u = m_d$. However since $m_u, m_d \ll \Lambda_{\text{QCD}}$ so $SU_V(2)$ must be a good approximated symmetry. The conservation quantity associated with this symmetry is the *Isospin*. On the other hand it is easy to show that $U_V(1)$ is always an exact symmetry of the theory (*i.e.*, independently from the value of the quark masses) corresponding to the quark field transformations:

$$q_i \rightarrow e^{i\alpha} q_i \quad (\text{III.17})$$

and the Noether current

$$J_V^\mu = \bar{q} \gamma^\mu q. \quad (\text{III.18})$$

The conservation of the Noether current is nothing else but the *Barion Number*.

The situation is very different if we consider the Axial $SU_A(2) \times U_A(1)$ symmetry. The reason is that in QCD the dynamical formation of quark and anti-quark condensation $\langle \bar{q}q \rangle$ breaks both the global $SU_A(2)$ and $U_A(1)$ symmetries.

The $SU_A(2)$ symmetry is associated with the quark field transformations

$$q_i \rightarrow \left[e^{i \frac{\vec{\alpha} \vec{\tau} \gamma_5}{2}} \right]_{ij} q_j \quad (\text{III.19})$$

and the Noether Axial current

$$\vec{J}_A^\mu = \bar{q} \gamma^\mu \gamma_5 \frac{\vec{\tau}}{2} q. \quad (\text{III.20})$$

As to the broken symmetries correspond Goldstone bosons, the break of the $SU_A(2)$ symmetry is associated with the π -triplet with masses $m_\pi \approx 0$.

On the other hand the $U_A(1)$ symmetry corresponds to the quark field transformations

$$q_i \rightarrow e^{i\alpha \gamma_5 / 2} q_i \quad (\text{III.21})$$

and it is associated with the Noether axial current

$$J_5^\mu = \frac{1}{2} \bar{q} \gamma^\mu \gamma_5 q. \quad (\text{III.22})$$

The very interesting fact is that the broken $U_A(1)$ symmetry (in the limit of finite but small quark masses) would imply a Goldstone boson essentially degenerate with the pions triplet that instead is not observed in hadron spectrum. Why? This is what is known as the $U_A(1)$ problem. In order to solve this problem we have to briefly review the structure of the vacuum state of the Gauge Theories and in particular the structure of the QCD vacuum.

Chiral Anomaly

One can think that a possible solution of the $U_A(1)$ problem may be represented by the chiral anomaly of the $U_A(1)$ Axial current J_5^μ . In other words the divergence of J_5^μ gets quantum correction

$$\partial_\mu J_5^\mu = n_f \frac{g_s^2}{32\pi^2} G_a^{\mu\nu} \tilde{G}_{\mu\nu}^a \quad (\text{III.23})$$

where n_f is the number of different flavors f and $\tilde{G}_{\mu\nu}^a$ is the dual strength energy tensor

$$\tilde{G}_{\mu\nu}^a \equiv \frac{1}{2} \epsilon_{\mu\nu\alpha\beta} G_a^{\alpha\beta}. \quad (\text{III.24})$$

In this way, even if the QCD is formally invariant under the $U_A(1)$ transformations, the chiral anomaly will change the action introducing a term

$$\delta S \propto \int d^4x \partial_\mu j_5^\mu \propto \int d^4x G_a^{\mu\nu} \tilde{G}_{\mu\nu}^a \quad (\text{III.25})$$

so it seems that the $U_A(1)$ is no more a symmetry at the quantum level. Unfortunately the quantity $G_a^{\mu\nu} \tilde{G}_{\mu\nu}^a$ can be expressed as a total divergence

$$G_a^{\mu\nu} \tilde{G}_{\mu\nu}^a = \partial_\mu K^\mu \quad (\text{III.26})$$

where

$$K^\mu = \epsilon^{\mu\alpha\beta\gamma} A_{a\alpha} \left[G_{a\beta\gamma} - \frac{g_s}{3} f_{abc} A_{b\beta} A_{c\gamma} \right]. \quad (\text{III.27})$$

Therefore choosing the usual condition $A_a^\mu = 0$ at the spatial infinity the chiral term (III.25) vanishes

$$\delta S \propto \int d^4x G_a^{\mu\nu} \tilde{G}_{\mu\nu}^a \propto \int d^4x \partial_\mu K^\mu \propto \int d\Sigma_\mu K^\mu = 0 \quad (\text{III.28})$$

and the $U_A(1)$ is a good symmetry of the theory again. The problem is not solved.

The structure of the QCD vacuum

The real solution of the $U_A(1)$ problem comes from the understanding of the structure of the QCD vacuum state that implies different boundary conditions for the gauge field A_a^μ that must be a pure gauge field at the spatial infinity. As a matter of fact, the vacuum state of non abelian gauge field theories (like QCD) is more complex and structured than one may expect: in a gauge theory we have some freedom that we use to require that the gauge fields (i.e. the gluon fields) A_a^μ respect the condition $A_a^0 = 0$. This is known as *Temporal Gauge*. In this gauge the fields are time independent and, under a gauge transformation $\Omega(\vec{r})$, transform as

$$\frac{\tau_a}{2} A_a^i(\vec{r}) \equiv A^i(\vec{r}) \rightarrow \Omega(\vec{r}) A^i(\vec{r}) \Omega(\vec{r})^{-1} + \frac{i}{g} \Omega(\vec{r}) \nabla^i \cdot \Omega^{-1}(\vec{r}) \quad (\text{III.29})$$

The vacuum state is of course defined to be the state where the vector potential is either zero or in a gauge equivalent configuration to zero. From Eq. (III.29), one can see that in this case the vacuum gauge equivalent configurations correspond to the term $\frac{i}{g}\Omega(\vec{r})\nabla^i\Omega^{-1}(\vec{r})$. If we require that at the spatial infinity $\Omega(\vec{r} \rightarrow \infty) \rightarrow 1$, we can classify all these gauge equivalent vacuum states by how $\Omega(\vec{r})$ goes to unity at spatial infinity. In other words

$$\lim_{\vec{r} \rightarrow \infty} \Omega(\vec{r}) \rightarrow e^{i2n\pi} \quad (\text{III.30})$$

where the integer number n is called *winding number* (or sometimes *topological charge* or even *instanton number*) and it is related to the Jacobian of a $S_3 \rightarrow S_3$ transformation that maps the physical space onto the group space. It can be shown that [345]

$$n = \frac{ig_s^3}{24\pi^2} \int d^3r \text{Tr} \epsilon_{ijk} A_n^i(\vec{r}) A_n^j(\vec{r}) A_n^k(\vec{r}) \quad (\text{III.31})$$

where A_n is the transformed gauge field under the transformation Ω_n . We can so use the winding number n in order to classify the different vacuum states $|n\rangle$ corresponding to the different ways of how $\Omega(\vec{r}) \rightarrow 1$ at the spatial infinity. Moreover we can note that, because of eq. (III.30), we can obtain the gauge transformation Ω_n using n -times Ω_1 and so that the vacuum states are not really gauge invariant since for example the action of the gauge transformation Ω_1 on n -vacuum state gives a different $(n+1)$ -vacuum state

$$\Omega_1|n\rangle = |n+1\rangle. \quad (\text{III.32})$$

However it is possible to show that superimposing n different vacuum states, one can obtain a gauge invariant vacuum, the so called θ -vacuum [346]

$$|\theta\rangle \equiv \sum_n e^{-in\theta} |n\rangle. \quad (\text{III.33})$$

This is of course a gauge invariant vacuum state, but the very interesting fact of the θ -vacuum is that the vacuum to vacuum transition is non zero:

$${}_+\langle\theta|\theta\rangle_- = \sum_{m,n} e^{im\theta} e^{-in\theta} + \langle m|n\rangle_- = \sum_\nu e^{i\nu\theta} \left[\sum_n + \langle n+\nu|n\rangle_- \right] \quad (\text{III.34})$$

where $\nu = m - n$ is the difference in the winding number. One can show that ν is given by:

$$\nu = \frac{g_s^2}{32\pi^2} \int d^4x G_{a\mu\nu} \tilde{G}_a^{\mu\nu} = \frac{g_s^2}{32\pi^2} \int d\Sigma_\mu K^\mu \neq 0 \quad (\text{III.35})$$

Thus the complex structure of the QCD θ -vacuum provides a very interesting fact: the term that comes from the chiral anomaly $\int d^4x G_{a\mu\nu} \tilde{G}_a^{\mu\nu}$ is not zero but it is equal to the difference in winding numbers ν . Using the path integral formalism in order to describe the vacuum to vacuum transition, one finds:

$${}_+\langle\theta|\theta\rangle_- = \sum_\nu \int \delta A^\mu e^{iS_{\text{eff}}[A]} \delta \left[\nu - \frac{g_s^2}{32\pi^2} \int d^4x G_a^{\mu\nu} \tilde{G}_{a\mu\nu} \right] \quad (\text{III.36})$$

where the effective action S_{eff} is given by:

$$S_{\text{eff}} = S_{\text{QCD}}[A] + \theta \frac{g_s^2}{32\pi^2} \int d^4x G_a^{\mu\nu} \tilde{G}_{a\mu\nu} \quad (\text{III.37})$$

Therefore the θ -term that arises from the non trivial vacuum structure of the gauge theories can be interpreted as a further term in the action of the theory. This additional term violates both P and CP symmetries (while of course it preserves the CPT symmetry). Recovering our analogy to the electromagnetic theory,

we may say that this term roughly corresponds to the $\vec{E}_a \cdot \vec{B}_a$ interactions.

The solution to the $U_A(1)$ problem, should be clear now. We have to consider that the boundary condition to impose on the gauge transformation (*i.e.*, their behavior at the spatial infinity) and the consequent non trivial structure of the vacuum state connect the chiral anomaly with the sectors of vacuum to vacuum transition with $\nu \neq 0$. In other words we have to consider that there are sectors of the theory where $\nu \neq 0$. Since the QCD perturbation theory is connected to the $\nu = 0$ sector where the $G\tilde{G}$ term vanishes, the effects of the $\nu \neq 0$ sectors are necessarily non-perturbative but of course they must be considered. In these sectors the chiral anomaly plays a crucial role since the charge Q_5 associated with the Noether current J_5^μ , eq.(III.22), becomes

$$\Delta Q_5 = \int d^4x \partial_\mu J_5^\mu = n_f \frac{g_s^2}{32\pi^2} \int d^4x G_a^{\mu\nu} \tilde{G}_{a\mu\nu} = n_f \nu \quad (\text{III.38})$$

and so it is never conserved if $\nu \neq 0$. Thus, if we include the $\nu \neq 0$ sectors in the QCD theory (as we have to do), $U_A(1)$ is *never* a symmetry.

III.I.II THE STRONG CP PROBLEM

It is interesting and maybe singular that the solution of the $U_A(1)$ problem generates the so called strong CP problem. Indeed if together with the QCD we consider also the weak interactions another term similar to that obtained from the $U_A(1)$ problem solution appears. The origin of this additional term is due to the mass matrix of quarks which emerges from the spontaneous breakdown of the electroweak gauge symmetry. The mass matrix of quarks is neither Hermitian nor diagonal and in general it is complex so that the respective terms in the Lagrangian are

$$\mathcal{L}_{\text{mass}} = -\bar{q}_{R_i} M_{ij} q_{L_j} - \bar{q}_{L_i} \left(M^\dagger \right)_{ij} q_{R_j} \quad (\text{III.39})$$

If one wants to go to a physical basis then the matrix must be diagonalized by separate unitary transformations of the chiral quark fields that encompass also the $U_A(1)$ chiral rotations

$$\begin{cases} q_R \rightarrow e^{i\frac{\alpha}{2}} q_R \\ q_L \rightarrow e^{-i\frac{\alpha}{2}} q_L \end{cases} \quad (\text{III.40})$$

where $\alpha = 1/n_f \text{Arg det } M$. With analogous considerations to those discussed in the previous section one can show that such chiral rotation alters the vacuum angle in such a way that, if we define

$$\tilde{Q}_5 \equiv \int d^3x \tilde{J}_5^0 \quad (\text{III.41})$$

the effect of a chiral rotation on the vacuum state is

$$e^{i\alpha \tilde{Q}_5} |\theta\rangle = |\theta + n_f \alpha\rangle \quad (\text{III.42})$$

Therefore, using again the path integral formalism to describe the vacuum to vacuum transition as in the previous section, but considering also this effect coming from the electroweak interactions, one finds that the full additional term to include in the Lagrangian (or equivalently in the action) is

$$\mathcal{L}_{\text{CP}} = (\theta + \text{Arg det } M) \frac{g_s^2}{32\pi^2} G_{a\mu\nu} \tilde{G}_a^{\mu\nu}. \quad (\text{III.43})$$

It is so useful to define the parameter $\bar{\theta} \equiv \theta + \text{Arg det } M$ so that we eventually have

$$\mathcal{L}_{\text{CP}} = \bar{\theta} \frac{g_s^2}{32\pi^2} G_{a\mu\nu} \tilde{G}_a^{\mu\nu}. \quad (\text{III.44})$$

The Lagrangian (III.44) contains all the terms coming from QCD and EW interactions that violate the CP symmetry. The parameter $\bar{\theta}$, that is a combination of QCD and electroweak parameters, gives us a measure of the CP violation. This is a free parameter of the theory and so it can assume all the values with the same probability. The parameter $\bar{\theta}$ is strongly constrained from the electric dipole momentum of the neutron d_n that reads [347–349]

$$d_n \approx \bar{\theta} \left(\frac{e m_q}{m_N^2} \right) < 3^{-26} [e \text{ cm}] \quad (\text{III.45})$$

That implies $\bar{\theta} < 10^{-9}$. Why is it so small? How is it possible that completely different contributes of order $\mathcal{O}(1)$, coming from completely different physics (QCD and EW) compensate each other within a precision of one part over 10^9 ? Even if all the values of $\bar{\theta}$ have the same probability we would like to find a dynamical mechanism able to explain a value of $\bar{\theta}$ so small. This is known as *Strong CP problem*. An easy solution to the strong CP problem would be requiring a new additional chiral symmetry in such a way that we could always rotate $\bar{\theta}$ to be zero. This could always be done whether the mass of one quark, say m_u , is zero. In this way, with a chiral rotation, one may choose $\theta = 0$ and $\bar{\theta} \propto \det M \propto m_u = 0$. Anyway, in general, both from the theoretical and experimental side, quarks are regarded to be massive and this is not a good way to solve the problem.

III.I.III THE PECCEI QUINN SOLUTION

To solve the strong CP problem, in 1977, Roberto Peccei and Helen Quinn postulate the *full Lagrangian* of the standard model was invariant under an additional global chiral $U(1)$ symmetry, known as $U_{PQ}(1)$ (Peccei-Quinn) symmetry [341, 342]. If the $U_{PQ}(1)$ symmetry exists and is exact, so the strong CP problem would be trivially solved by performing a chiral rotation and setting $\bar{\theta} = 0$. However, such a symmetry cannot be exact but it must be spontaneously broken at some energy scale f_A . Indeed if $U_{PQ}(1)$ is spontaneously broken, $\bar{\theta}$ is dynamically driven to zero. In this case there will be an associated pseudo Goldstone boson in the theory, that is named *axion* [341, 342, 346, 350–362]. Axions are not mass-less since the chiral $U_{PQ}(1)$ symmetry is anomalous and they get a mass of order $\sim \Lambda_{\text{QCD}}^2 / f_A$.

Let us try to understand in more details which are the implications coming from the Peccei Quinn $U_{PQ}(1)$ symmetry. First of all we notice that since the axion field ϕ_A is the field of the Goldstone boson associated with the spontaneously broken symmetry $U_{PQ}(1)$, this field translates under the $U_{PQ}(1)$ transformations

$$\phi_A(x) \xrightarrow{U_{PQ}(1)} \phi_A(x) + \alpha f_A \quad (\text{III.46})$$

where α is the phase parameter of the transformation $e^{i\frac{\alpha}{f_A}}$ and f_A is again the breakdown symmetry scale. Then if we want the Lagrangian that describes the full theory to be invariant under the $U_{PQ}(1)$ symmetry we need to insert the axion field only derivatively coupled so that when ϕ_A transforms according to Eq. (III.46) the term αf_A vanishes being constant. Moreover we have to consider also the chiral anomaly that forces us to introduce also a direct coupling between the axion field and the Gluon field. All these considerations completely fix the form of the additional terms in the effective Lagrangian \mathcal{L}_{eff} which reads

$$\mathcal{L}_{\text{eff}} = \mathcal{L}_{\text{SM}} + \underbrace{\bar{\theta} \frac{g_s^2}{32\pi^2} G_a^{\mu\nu} \tilde{G}_{\mu\nu}^a}_{\text{CP violating}} - \underbrace{\frac{1}{2} \partial_\mu \phi_A \partial^\mu \phi_A + \frac{\phi_A}{f_A} \zeta \frac{g_s^2}{32\pi^2} G_a^{\mu\nu} \tilde{G}_{\mu\nu}^a}_{\text{Free Axion Lagrangian } \mathcal{L}_A} + \underbrace{\mathcal{L}_{\text{int.}} \left[\frac{\partial^\mu \phi_A}{f_A}; \{\psi\} \right]}_{\text{interaction Lagrangian}} \quad (\text{III.47})$$

where $\{\psi\}$ are all the other fields in the theory and ζ is a model dependent parameter defined by the chiral anomaly of the $U_{PQ}(1)$ current J_{PQ}^μ as

$$\partial_\mu J_{PQ}^\mu = \zeta \frac{g_s^2}{32\pi^2} G_a^{\mu\nu} \tilde{G}_{\mu\nu}^a \quad (\text{III.48})$$

Let us focus on the free axion Lagrangian \mathcal{L}_A in (III.47):

$$\mathcal{L}_A = -\frac{1}{2}\partial_\mu\phi_A\partial^\mu\phi_A + \frac{\phi_A}{f_A}\xi\frac{g_s^2}{32\pi^2}G_a^{\mu\nu}\tilde{G}_{\mu\nu}^a \quad (\text{III.49})$$

we can recognize the axion potential

$$V_A = -\frac{\phi_A}{f_A}\xi\frac{g_s^2}{32\pi^2}G_a^{\mu\nu}\tilde{G}_{\mu\nu}^a \quad (\text{III.50})$$

If we do not take into account the QCD effects, minimizing the vacuum expectation value (VEV) of the potential $\langle V_A \rangle = -\frac{\xi}{f_A}\frac{g_s^2}{32\pi^2}\langle G_a^{\mu\nu}\tilde{G}_{\mu\nu}^a \rangle$, one can see that all the values $0 \leq \langle \phi_A \rangle \leq 2\pi f_A/\xi$ are allowed. On the contrary, taking into account the CP violating term (III.47) (i.e., considering the QCD anomalies), because of the periodicity of $\langle G_a^{\mu\nu}\tilde{G}_{\mu\nu}^a \rangle$, we have an effective potential V_A^{eff} in the effective $\bar{\theta} + \langle \phi_A \rangle \frac{\xi}{f_A}$ vacuum angle

$$V_A^{\text{eff}} \sim \cos\left(\bar{\theta} + \frac{f_A}{\xi}\langle \phi_A \rangle\right) \quad (\text{III.51})$$

that can be minimized to obtain the axion VEV:

$$\langle \phi_A \rangle = -\frac{f_A}{\xi}\bar{\theta} \quad (\text{III.52})$$

so that

$$\left\langle \frac{\partial V_A}{\partial \phi_A} \right\rangle = -\frac{\xi}{f_A}\frac{g_s^2}{32\pi^2}\left\langle G_a^{\mu\nu}\tilde{G}_{\mu\nu}^a \right\rangle\Big|_{\langle \phi_A \rangle = -\frac{f_A}{\xi}\bar{\theta}} = 0. \quad (\text{III.53})$$

Note also that expanding the potential around the minimum, axions acquire a mass given by:

$$m_{\phi_A} = \left\langle \frac{\partial^2 V_A}{\partial \phi_A^2} \right\rangle = -\frac{\xi}{f_A}\frac{g_s^2}{32\pi^2}\frac{\partial}{\partial \phi_A}\left\langle G_a^{\mu\nu}\tilde{G}_{\mu\nu}^a \right\rangle\Big|_{\langle \phi_A \rangle = -\frac{f_A}{\xi}\bar{\theta}} \quad (\text{III.54})$$

So, being the axion field massive, the mass term must be introduced in the Lagrangian. We want to show that, with all these efforts, the strong CP problem is automatically solved. Indeed if we define the physical axion field ϕ_A^{phys}

$$\phi_A^{\text{phys}} \doteq \phi_A - \langle \phi_A \rangle = \phi_A + \frac{f_A}{\xi}\bar{\theta} \quad (\text{III.55})$$

the Lagrangian (III.47) in terms of ϕ_A^{phys} (and the above mentioned mass term) eventually reads:

$$\mathcal{L}_{\text{eff}} = \mathcal{L}_{\text{SM}} - \frac{1}{2}\partial_\mu\phi_A^{\text{phys}}\partial^\mu\phi_A^{\text{phys}} - \frac{1}{2}m_{\phi_A}^2(\phi_A^{\text{phys}})^2 + \frac{\xi}{f_A}\phi_A^{\text{phys}}\frac{g_s^2}{32\pi^2}G_a^{\mu\nu}\tilde{G}_{\mu\nu}^a + \mathcal{L}_{\text{int.}}\left[\frac{\partial^\mu\phi_A}{f_A};\{\psi\}\right] \quad (\text{III.56})$$

We see that the CP violating term with $\bar{\theta}$ is cancelled. The effect of the Peccei-Quinn $U_{\text{PQ}}(1)$ symmetry must be clear now: the static free parameter $\bar{\theta}$ of the theory is replaced by dynamical scalar field, the axion field, that is dynamically driven to zero. The strong CP problem is solved.

The original model of the axion was proposed by Weinberg and Wilczek, based on the idea of Peccei and Quinn. This is called the Peccei-Quinn-Weinberg-Wilczek (PQWW) model, or the *visible axion model*. In this model, the axion field is identified as a phase direction of the standard model Higgs field. It is necessary to introduce two (or more) Higgs doublets, since the axion degree of freedom does not exist in the theory with single Higgs doublet. Let us denote two Higgs doublets as ϕ_1 and ϕ_2 . The PQWW axion is visible, in the sense that it predicts observable signatures in the laboratory experiments. However, the theoretical predictions of the PQWW axion contradict with experimental limits. The problem of the original visible axion model can be avoided if the PQ symmetry is broken at some energy scale higher than the electroweak scale since the couplings of axions with other particles are suppressed as $\propto \frac{1}{f_A}$. This fact

motivates the “invisible” axion model. In this model, the axion is not the phase direction of the standard model Higgs doublet. We must introduce a complex singlet scalar field, whose phase would be identified as the axion. Such models are called *invisible axion models*.

The role of non perturbative physics is crucial for axions and it becomes important at some temperature $T_{\text{NP}} \ll f$ providing a periodic potential for the axions. If we define Λ_A the scale of non perturbative physics the potential can therefore be put in the form

$$V_A = \Lambda_A^4 U(x) \quad (\text{III.57})$$

where $U(x)$ has at least one minimum and one maximum on the interval $x \in [-\pi, \pi]$. Indeed, even if for a more detailed discussion on the structure of the QCD vacuum and its energy we remand to [363], we have already explained that we expect a periodic contribute coming from the CP violating term. A particularly simple choice for the potential is therefore

$$V_A(\phi_A) = \Lambda_A^4 \left[1 - \cos \left(\frac{N_{\text{DW}} \phi_A}{f_A} \right) \right] \quad (\text{III.58})$$

where N_{DW} is an integer number called *Domain Wall number* that, unless otherwise stated, here we set to $N_{\text{DM}} = 1$ ¹. It is important to remark that the potential (III.58) is not unique since we cannot predict it exactly without a full knowledge of the non perturbative physics. For example in the potential one can include the so called higher order instanton corrections that will add the terms $\sim \cos^n \left(\frac{\phi_A}{f_A} \right)$ to the potential (III.58). Anyway if $\phi_A \ll f_A$ the potential can be expanded as

$$V_A(\phi_A) \approx \frac{1}{2} m_A^2 \phi^2 \quad (\text{III.59})$$

with $m_A \equiv \Lambda_A^4 / f_A^2$. Since the symmetry breaking scale f_A is typically rather high, while the non perturbative scale λ_A is typically lower, the axion mass is expected to be small.

III.II NEW COSMOLOGICAL BOUNDS ON AXIONS AND NEUTRINOS

As we discussed so far, the most elegant solution at present to the strong CP problem in Quantum Chromodynamics (QCD) would require the Lagrangian of the Standard Model of elementary particles to be invariant under an additional global $U(1)_{\text{PQ}}$ (Peccei-Quinn) symmetry, spontaneously broken at some energy scale f_a [341, 342, 346, 350–360], with an associated Pseudo Nambu Goldstone Boson (PNGB), the so-called axion [355–359, 361, 364–368]. A strong experimental effort has been devoted in different fields to search for axions [369–377]. If these elusive particles exist, they can be copiously produced via both thermal and non-thermal processes in the early universe. Axions produced via non-thermal processes, *e.g.* by the vacuum realignment mechanism [378–384] and/or by topological defects decay [385–392], are natural cold dark matter candidates². Conversely, thermal axions, *i.e.* the population of axions created and annihilated during interactions among particles in the primordial universe, contribute to the hot dark matter component instead.

Here we shall focus on the thermal axion scenario [393–402]. While still relativistic, thermal axions, as other hot relics, behave as extra dark radiation, contributing to the effective number of relativistic degrees of freedom N_{eff} , defined by the relation

$$\rho_{\text{rad}} = \left[1 + \frac{7}{8} \left(\frac{4}{11} \right)^{4/3} N_{\text{eff}} \right] \rho_\gamma, \quad (\text{III.60})$$

¹See also [Appendix B](#) for a discussion on Domain Walls

²See also the brief review on axion Cold Dark Matter provided in the [Appendix B](#)

with ρ_γ the present Cosmic Microwave Background (CMB) energy-density. The reference value is $N_{\text{eff}} = 3.045$ [403–407], and a departure from this standard scenario may leave different signatures in the cosmological observables, modifying the damping tail of the CMB temperature angular power spectrum and changing two important scales at recombination: the sound horizon and the Silk damping scales. In addition, the primordial abundances of light elements predicted by the Big Bang Nucleosynthesis (BBN) are also sensitive to extra light species, *i.e.* to a larger value of N_{eff} . Indeed the expansion rate of the universe during the BBN epoch strongly depends on the effective number of relativistic degrees of freedom and extra light species, which will increase the expansion rate and lead to a higher freeze-out temperature for weak interactions, implying a higher fraction of primordial helium.

When thermal axions become non-relativistic particles they leave identical signatures in the different cosmological observables as massive neutrinos, increasing the amount of the (hot) dark matter mass-energy density in our universe, suppressing structure formation at scales smaller than their free-streaming scale and leaving an imprint on the CMB temperature anisotropies, via the early integrated Sachs-Wolfe effect. This is why a large degeneracy between the axion and the total neutrino masses is expected [398, 400].

III.II.I THERMAL AXIONS

The thermal axion scenario can be described by two parameters: the axion coupling constant f_a and the axion mass m_a , related as

$$m_a = \frac{f_\pi m_\pi}{f_a} \frac{\sqrt{R}}{1+R} \simeq 0.6 \text{ eV} \times \frac{10^7 \text{ GeV}}{f_a}, \quad (\text{III.61})$$

where $R \doteq m_u/m_d \simeq 0.553 \pm 0.043$ is the up-to-down quark mass ratio and $f_\pi \simeq 93 \text{ MeV}$ is the pion decay constant [408]. The axion contribution to the effective number of relativistic degrees of freedom

$$\Delta N_{\text{eff}} \simeq \frac{4}{7} \left[\frac{43}{4 g_{*S}(T_d)} \right]^{4/3}, \quad (\text{III.62})$$

depends on the temperature T_d at which axions decouple from the thermal bath via the number of entropic degrees of freedom $g_{*S}(T)$. Axions decouple from the thermal bath when the reaction rate Γ_a falls below the Hubble expansion rate

$$H(T) = \sqrt{\frac{4\pi^3}{45} g_*(T)} \left(\frac{T^2}{M_{pl}} \right). \quad (\text{III.63})$$

with $M_{pl} \simeq 1.22 \times 10^{19} \text{ GeV}$ the Planck Mass. Considering only the two-body processes with cross sections $\sigma_i = \sigma(p_i a \leftrightarrow p_j p_k)$ and with all the particles in thermal equilibrium, we can define the decay rate as [367, 393]

$$\Gamma_a \propto \sum_i n_i \langle v \sigma_i \rangle \quad (\text{III.64})$$

where n_i is the number density of p_i , $v \simeq 1$ the relativistic velocity and the brackets denote a thermal average. Solving the usual freeze-out condition

$$\Gamma_a(T_d) = H(T_d), \quad (\text{III.65})$$

one can estimate the decoupling temperature of a thermal axion population with mass m_a , while the axion contribution to the relativistic degrees of freedom is simply given by $g_*(T_d) = g_*^{\text{SM}}(T_d) + 1$. After decoupling ($T < T_d$) axions maintain a thermal distribution which basically remains unaffected by other phenomena occurring in the plasma. Therefore we can estimate the current axion number density simply as

$$n_a = \frac{g_{*S}(T_0)}{g_{*S}(T_d)} \times \frac{n_\gamma}{2}, \quad (\text{III.66})$$

with $n_\gamma \simeq 411 \text{ cm}^{-3}$ the present photon density and $g_{*S}(T_0) \simeq 3.91$ the current number of entropic degrees of freedom.

In the early Universe, there are several different processes that can produce distinct population of thermal axions. In this work we shall study a thermal axion population from axion-gluon and axion-pion scatterings separately [409–414].

Axion-Gluon coupling

In any QCD axion model, axions couple with free gluons. The relevant processes for axion thermalisation are [415]

- $a + q \leftrightarrow g + q$ and $a + \bar{q} \leftrightarrow g + \bar{q}$;
- $a + g \leftrightarrow q + \bar{q}$;
- $a + g \leftrightarrow g + g$.

Following Di Luzio et al. [367], the decoupling temperature for this population of thermal axions reads as

$$T_d \simeq 12.5 \frac{\sqrt{g_*(T)} f_a^2}{\alpha_s^3 M_{pl}} \text{GeV}. \quad (\text{III.67})$$

It is easy to see that for $T_d \gg T_c$, we expect a contribution $n_a \simeq 7.5 \text{ cm}^{-3}$. It is also worth noting that the decoupling temperature must be smaller than the PQ breaking scale (above which there is no axion) and that if the scale of inflation and the reheating temperature are below T_d , this thermal population gets inflated away. In this section, taking into account these caveats and exploiting current cosmological datasets, we constrain the sub-eV axion mass range allowed for this process in realistic scenarios that include also massive neutrinos.

Axion-Pion Coupling

After the QCD phase transition, $T < T_c$, axions can couple with hadrons. In practice, however, nucleons are so rare in the early universe with respect to pions that the only relevant process is the axion-pion interaction $\pi + \pi \leftrightarrow \pi + a$.

The leading order Lagrangian for axion-pion interaction reads

$$\mathcal{L}_{a\pi} = C_{a\pi} \frac{\partial_\mu a}{f_a f_\pi} (\pi^0 \pi^+ \partial_\mu \pi^- + \pi^0 \pi^- \partial_\mu \pi^+ - 2\pi^+ \pi^- \partial_\mu \pi^0), \quad (\text{III.68})$$

where the axion-pion coupling

$$C_{a\pi} = \frac{1}{3} \left(\frac{m_d - m_u}{m_u + m_d} + c_d^0 - c_u^0 \right), \quad (\text{III.69})$$

is a model-dependent quantity sensitive to the nature of axion-fermion interactions via the axion-quark couplings c_d^0 and c_u^0 . Starting from Eq.(III.68), the leading order axion-pion interaction rate can be computed to obtain [367, 415]

$$\Gamma_{a\pi}^{\text{LO}} \simeq 0.215 C_{a\pi}^2 \frac{T^5}{f_a^2 f_\pi^2} h_{\text{LO}} \left(\frac{m_\pi}{T} \right), \quad (\text{III.70})$$

with $h(x)$ a rapidly decreasing function of its arguments normalized to $h(0) = 1$. As usual, solving the freeze out condition (III.65) we can estimate the decoupling temperature for an axion population with mass m_a , while by Eq. (III.66) we can derive its current number density.

However it should be noted that the thermal production of axions via pion scattering is strongly model-dependent since the relation between the axion mass and the (decoupling) temperature changes accordingly to the axion-pion interaction strength. Consequently, the thermal production of axions from pion

scattering could range between relatively large thermal abundances to negligible ones, depending on the precise value of $C_{a\pi}$. For example, in the KSVZ axion model [355, 356, 367] the coupling between axions and fermions vanishes at tree level: $c_d^0 = c_u^0 = 0$ and $C_{a\pi} = (1 - R)/(3 + 3R) \simeq 0.12$ leading to a sizable amount of relic axions. On the other hand, in the DFSZ scenario [357, 367, 416] because of the presence of extra Higgs doublets, QCD axions couple to SM fermions at tree level - $c_u^0 = \frac{1}{3} \cos^2(\beta)$, $c_d^0 = \frac{1}{3} \sin^2(\beta)$ with $\tan \beta \in [0.25, 170]$ because of the unitarity of tree-level fermion scatterings [367] - and the axion production can be either enhanced or suppressed: $C_{a\pi} = (1 - R)/(3 + 3R) - 1/9 \cos(2\beta)$, see the recent discussion by Ferreira, Notari, and Rompineve [414].

Furthermore, the authors of Ref. [415] have recently shown that for temperatures $T_\chi \gtrsim 62$ MeV the next-to-leading order term in the axion-pion interaction rate

$$\Gamma_{a\pi}^{\text{NLO}} \simeq -0.62 C_{a\pi}^2 \frac{T^7}{f_a^2 f_\pi^4} h_{\text{NLO}} \left(\frac{m_\pi}{T} \right), \quad (\text{III.71})$$

becomes comparable with the leading order part, $\Gamma_{a\pi}^{\text{NLO}}(T_\chi) \simeq 0.5 \Gamma_{a\pi}^{\text{LO}}(T_\chi)$, and the chiral perturbation theory breaks down. Interestingly, for the KSVZ model these controversial values for the temperatures precisely correspond to the sub-eV axion mass range of interest for current and future CMB experiments. Therefore, it is mandatory to adopt a model-independent approach to be able to compute reliable thermal axion mass limits from cosmology until a robust lattice QCD method provides the precise answer for a given model in these temperature ranges.

In order to study the thermalisation from axion-pion scatterings in the most broad and reliable scenario, we restrict ourselves to explore exclusively to the parameter space where the next-to-leading order term $\Gamma_{a\pi}^{\text{NLO}}(T)$ remains small with respect to leading order part $\Gamma_{a\pi}^{\text{LO}}(T)$, which basically means to consider decoupling temperatures $T_d \lesssim T_\chi \simeq 62$ MeV. In addition, we shall not assume in the following any specific underlying theoretical model for the axion-pion interactions, leaving the axion-pion coupling $C_{a\pi}$ as a free parameter. In this way, we are not only able to explore different axion models beyond the usual KSVZ and DFSZ scenarios³, but also to derive well-defined constraints on the sub-eV axion mass range in realistic scenarios which include also massive neutrinos.

III.II.II NUMERICAL ANALYSES

The final release of Planck 2018 temperature and polarization data [42], offers a unique opportunity to derive updated bounds on the thermal axion mass, accounting also for the fact that neutrinos are massive particles, as robustly indicated by oscillation experiments [418, 419]. Cosmology provides the most powerful mean to constrain their masses [419–426].

We therefore analyze an extension of the Λ CDM model which includes both axions and neutrinos as hot thermal massive relics. We perform Monte Carlo Markov Chain (MCMC) analyses using a modified version of the publicly available package CosmoMC [107, 108] and computing the theoretical model with the latest version of the Boltzmann code CAMB [109, 110]. We consider the canonical Λ CDM model described by the usual six-parameters, *i.e.*, the baryon $\omega_b \equiv \Omega_b h^2$ and cold dark matter $\omega_c \equiv \Omega_c h^2$ energy densities, the angular size of the horizon at the last scattering surface θ_{MC} , the optical depth τ , the amplitude of primordial scalar perturbation $\log(10^{10} A_S)$ and the scalar spectral index n_s . Together with the standard Λ CDM parameters, we add the thermal axion mass m_a and the sum of three active neutrino masses $\sum m_\nu$ (both in eV). For the axion-pion thermalization channel we consider also the coupling $C_{a\pi}$ and we restrict our scan only to decoupling temperatures $T_d \lesssim 62$ MeV where $\Gamma_{a\pi}^{\text{NLO}}(T)$ remains small with respect to $\Gamma_{a\pi}^{\text{LO}}(T)$. In this case, for each sampled point $(T_d, C_{a\pi})$ we compute the axion mass $m_a(T_d, C_{a\pi})$ by solving Eq.(III.65). We vary these parameters in a range of external and conservative priors listed in Table III.1.

³While the KSVZ and DFSZ are widely considered as benchmark scenarios, there are other models in which both the new heavy quarks and the Higgs doublets carry $U(1)_{\text{PQ}}$ charges, see *e.g.* Kim and Carosi [417] and Di Luzio et al. [367].

Parameter	Prior for axion-gluon	Prior for axion-pion
$\Omega_b h^2$	[0.005, 0.1]	[0.005, 0.1]
$\Omega_c h^2$	[0.005, 0.1]	[0.005, 0.1]
$100 \theta_{\text{MC}}$	[0.5, 10]	[0.5, 10]
τ	[0.01, 0.8]	[0.01, 0.8]
$\log(10^{10} A_S)$	[1.61, 3.91]	[1.61, 3.91]
n_S	[0.8, 1.2]	[0.8, 1.2]
$\sum m_\nu$ [eV]	[0.06, 5]	[0.06, 5]
m_a [eV]	[0.1, 10]	-
T_d [MeV]	-	< 62
$C_{a\pi}$	-	[0, 0.5]

TABLE III.1: List of the parameter priors.

The posteriors of our parameter space have been explored using the MCMC sampler developed for CosmoMC and tailored for parameter spaces with a speed hierarchy which also implements the "fast dragging" procedure described in Ref. [111]. The convergence of the chains obtained with this procedure is tested using the Gelman-Rubin criterion [112] and we choose as a threshold for chain convergence $R - 1 \lesssim 0.02$. Our baseline data-set consists of:

- Planck 2018 temperature and polarization (TT TE EE) likelihood, which also includes low multipole data ($\ell < 30$) [42, 113, 114]. We refer to this combination as "Planck".
- Planck 2018 lensing likelihood [115], constructed from measurements of the power spectrum of the lensing potential. We refer to this dataset as "lensing".
- Baryon Acoustic Oscillations (BAO) measurements extracted from data from the 6dFGS [116], SDSS MGS [117] and BOSS DR12 [118] surveys. We refer to this dataset as "BAO".
- Type Ia Supernovae (SNIa) distance moduli measurements from the Pantheon sample [119]. We refer to this dataset as "Pantheon".
- Galaxy clustering and cosmic shear measurements, as well as their cross-correlations, from the Dark Energy Survey [427–429]. We refer to this dataset as "DES".
- The Hubble constant measurement from the SH0ES collaboration analysing type-Ia supernovae data from the Hubble Space Telescope [430]. We refer to this dataset as "R20".

III.II.III COSMOLOGICAL BOUNDS

In this section we present the results obtained by our MCMC analysis of the mixed hot dark matter scenario which includes axions and neutrinos as hot thermal massive relics. We consider both the axion-gluon and the axion-pion thermalization channels.

Axion-Gluon scatterings

Table III.2 summarizes the results for the axion-gluon thermalization channel obtained from our MCMC analyses of the $\Lambda\text{CDM} + \sum m_\nu + m_a$ model. Figure III.1 shows the 68% and 95% CL contour plots for different cosmological parameters.

DATASET	AXION-GLUON COUPLING							
	$\Omega_b h^2$	$\Omega_c h^2$	$100 \theta_{MC}$	τ	$\log(10^{10} A_S)$	n_s	m_a [eV]	Σm_ν [eV]
Planck	0.02236 ± 0.00016	$0.1188^{+0.0033}_{-0.0014}$	1.0476 ± 0.00032	$0.0546^{+0.0072}_{-0.0082}$	$3.047^{+0.015}_{-0.017}$	0.9631 ± 0.0046	< 8.35	< 0.324
Planck +lensing	0.02236 ± 0.00015	$0.1191^{+0.0030}_{-0.0012}$	1.04076 ± 0.00031	0.0553 ± 0.0075	3.049 ± 0.015	0.9626 ± 0.0044	< 8.03	< 0.272
Planck +BAO	0.02248 ± 0.00014	$0.1176^{+0.0029}_{-0.00083}$	1.04099 ± 0.00029	$0.0568^{+0.0072}_{-0.0083}$	$3.048^{+0.015}_{-0.017}$	0.9672 ± 0.0040	< 8.14	< 0.158
Planck +Pantheon	0.02242 ± 0.00014	$0.1181^{+0.0034}_{-0.0011}$	1.04086 ± 0.00031	$0.0554^{+0.0073}_{-0.0085}$	$3.046^{+0.015}_{-0.017}$	0.9648 ± 0.0044	< 8.62	< 0.209
Planck +DES	0.02248 ± 0.00015	$0.1160^{+0.0028}_{-0.0016}$	1.04093 ± 0.00032	0.0549 ± 0.0079	3.043 ± 0.016	0.9661 ± 0.0044	< 8.40	< 0.346
Planck +R20	0.02258 ± 0.00015	$0.1168^{+0.0028}_{-0.00097}$	1.04113 ± 0.00030	$0.0579^{+0.0073}_{-0.0082}$	3.048 ± 0.017	0.9697 ± 0.0043	< 7.92	< 0.129
Planck +lensing +BAO +DES +Pantheon	0.02255 ± 0.00013	$0.1159^{+0.0029}_{-0.0012}$	1.04105 ± 0.00029	$0.0594^{+0.0068}_{-0.0079}$	$3.052^{+0.013}_{-0.016}$	0.9677 ± 0.0038	< 8.13	< 0.136
Planck +lensing +BAO +DES +Pantheon +R20	0.02265 ± 0.00013	$0.1156^{+0.0026}_{-0.0010}$	1.04118 ± 0.00030	$0.0624^{+0.0073}_{-0.0087}$	$3.057^{+0.015}_{-0.017}$	0.9701 ± 0.0038	< 7.46	< 0.114

TABLE III.2: Results for the Axion-Gluon thermalization channel obtained for different combination of the datasets listed in [subsection III.II.II](#). The bounds on parameters are 1σ errors (68% CL), while the upper bounds are 2σ (95% CL) constraints.

DATASET	AXION-PION COUPLING, $T_d < 62$ MeV							
	$\Omega_b h^2$	$\Omega_c h^2$	$100 \theta_{MC}$	τ	$\log(10^{10} A_S)$	n_s	m_a [eV]	Σm_ν [eV]
Planck	0.02261 ± 0.00015	$0.1252^{+0.0022}_{-0.0016}$	1.04012 ± 0.00032	$0.0567^{+0.0072}_{-0.0083}$	$3.064^{+0.015}_{-0.017}$	0.9703 ± 0.0058	< 2.41	< 0.269
Planck +lensing	0.02257 ± 0.00015	$0.1266^{+0.0016}_{-0.0014}$	1.04004 ± 0.00032	$0.0592^{+0.0072}_{-0.0087}$	$3.071^{+0.014}_{-0.017}$	$0.9706^{+0.0056}_{-0.0049}$	< 1.96	< 0.221
Planck +BAO	0.02279 ± 0.00014	0.1238 ± 0.0012	1.04043 ± 0.00029	$0.0609^{+0.0075}_{-0.0091}$	$3.066^{+0.015}_{-0.018}$	0.9819 ± 0.0040	< 1.04	< 0.134
Planck +Pantheon	0.02268 ± 0.00015	$0.1250^{+0.0017}_{-0.0015}$	1.04023 ± 0.00031	$0.0582^{+0.0072}_{-0.0086}$	$3.064^{+0.015}_{-0.017}$	$0.9758^{+0.0052}_{-0.0046}$	< 1.78	< 0.169
Planck +DES	0.02270 ± 0.00014	0.1239 ± 0.0013	1.04024 ± 0.00031	$0.0568^{+0.0076}_{-0.0085}$	$3.061^{+0.015}_{-0.017}$	0.9727 ± 0.0056	< 2.16	< 0.257
Planck +R20	0.02281 ± 0.00014	0.1240 ± 0.0013	1.04041 ± 0.00030	$0.0608^{+0.0077}_{-0.0092}$	$3.067^{+0.016}_{-0.018}$	0.9811 ± 0.0043	< 1.17	< 0.124
Planck +lensing +BAO +DES +Pantheon	0.02286 ± 0.00013	$0.1233^{+0.0010}_{-0.00090}$	1.04047 ± 0.00029	$0.0683^{+0.0081}_{-0.0095}$	$3.082^{+0.016}_{-0.018}$	0.9828 ± 0.0037	< 1.04	< 0.115
Planck +lensing +BAO +DES +Pantheon +R20	0.02292 ± 0.00013	0.12271 ± 0.00091	1.04059 ± 0.00028	$0.0706^{+0.0084}_{-0.010}$	$3.085^{+0.016}_{-0.019}$	0.9848 ± 0.0036	< 0.91	< 0.105

TABLE III.3: Results for the Axion-Pion thermalization channel obtained for different combination of the datasets listed in [subsection III.II.II](#). The bounds on parameters are 1σ errors (68% CL), while the upper bounds are 2σ (95% CL) constraints.

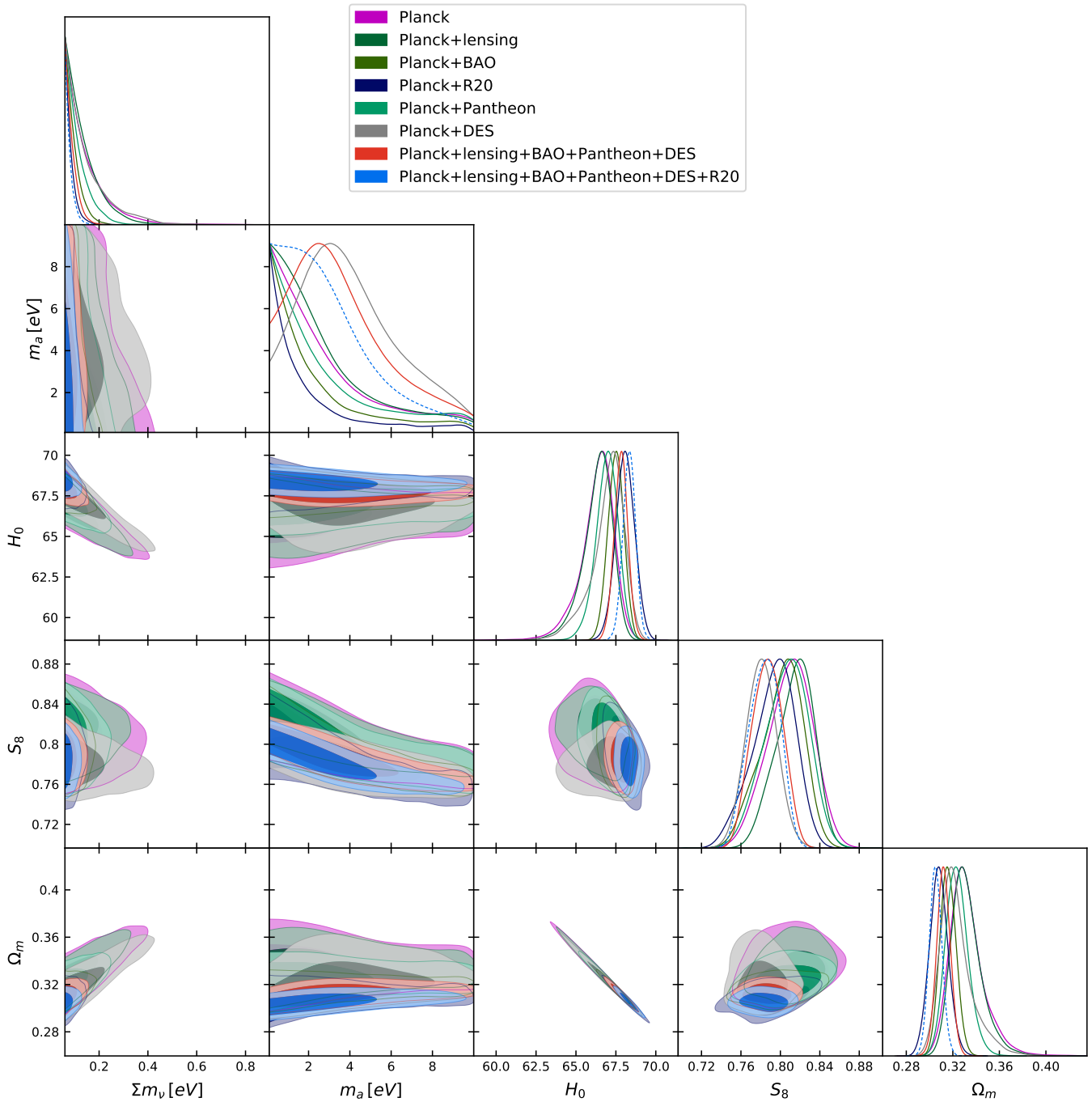


FIGURE III.1: Axion-Gluon thermalization channel. Marginalized 2D and 1D posteriors for different combinations of the datasets listed in [subsection III.II.II](#).

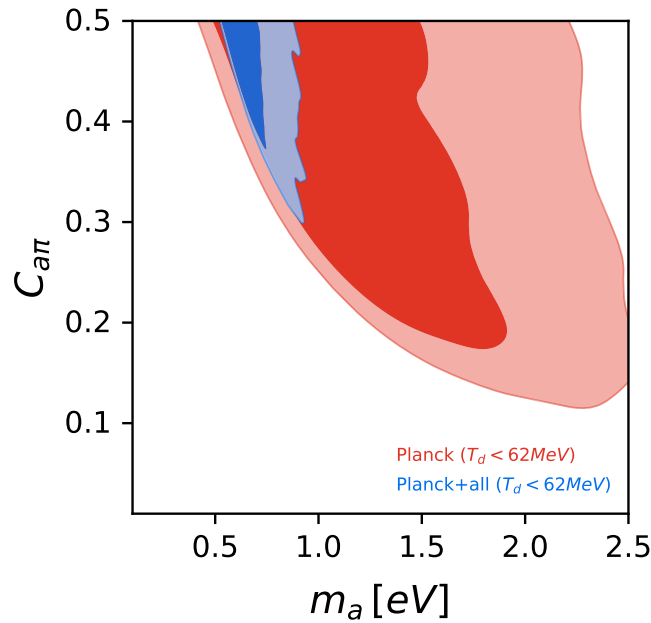


FIGURE III.2: Axion-Pion thermalization channel. Marginalized 2D and 1D posteriors in the plane $(m_a, C_{a\pi})$ with the prior $T_d < 62 \text{ MeV}$.

As discussed in the introduction, a large degeneracy is expected between the axion and neutrino masses, see also Figure III.1, where a strong anticorrelation is clearly noticed from the allowed contours in the $(\sum m_\nu, m_a)$ plane. Furthermore, these two parameters show similar degeneracies with other cosmological parameters and quantities such as H_0 , S_8 and Ω_m .

Exploiting the last release of Planck's temperature and polarization (TT,TE,EE+lowP) data, we derive the 95% CL upper bounds $\sum m_\nu < 0.324 \text{ eV}$ and $m_a < 8.35 \text{ eV}$. Notice that due to the lower contribution in $\Omega_a h^2$ and ΔN_{eff} expected by the axion-pion thermalization channel, the bounds on the axion mass are much less tight than those presented for the axion-pion case in Ref. [400]. Indeed for the axion-gluon thermalization channel, eV axion masses correspond to high decoupling temperatures $T_d \gg T_c$ and for $T_d \gtrsim 150 \text{ GeV}$ all particles of the Standard Model are relativistic so that $g_* \simeq 107.75$. From Eq. (III.66) one can notice that this will lead to a number density of relic axion $n_a \simeq 7.5 \text{ cm}^{-3}$ (that does not depend on the decoupling temperature), giving a very small contribution $\Delta N_{\text{eff}} \simeq 0.027$ to the effective number of relativistic degrees of freedom, which is well beyond the constraining power of Planck data.

As concerns the other datasets involved in our analyses, we notice that the axion mass bounds only weakly change with the dataset. For example, the inclusion of CMB lensing measurements from the Planck satellite only slightly improves the neutrino mass bound to $\sum m_\nu < 0.272 \text{ eV}$ at 95% CL, leaving the constraints on the axion mass almost unchanged ($m_a < 8.03 \text{ eV}$ at 95% CL). Instead, the combination of Planck and DES data slightly worsens both the bounds on the axion mass ($m_a < 8.40 \text{ eV}$ at 95% CL), and the bounds on neutrinos ($\sum m_\nu < 0.346 \text{ eV}$ at 95% CL). This is due to the lower value of the clustering parameter σ_8 preferred by DES measurements, which is translated into higher hot thermal relic masses. Conversely, due to the smaller error in Ω_m , the inclusion of Pantheon data leads to a significant improvement in the constraints on the sum of neutrino masses ($\sum m_\nu < 0.209 \text{ eV}$ at 95%CL), but not in those on the axion mass ($m_a < 8.62 \text{ eV}$, at 95% CL).

As expected, the largest impact on Planck bounds arises from the inclusion of the large-scale structure information from BAO measurements. As also discussed by Di Valentino et al. [400], hot thermal particles as axions and neutrinos suppress structure formation at small scales and therefore galaxy clustering information becomes crucial to set bounds on the amount of dark matter in the form of these relics. Indeed, combining Planck and BAO data we derive the upper bounds $m_a < 8.14 \text{ eV}$ and $\sum m_\nu < 0.158 \text{ eV}$, both at 95% CL. Combining together all the datasets, we obtain the robust 95% CL upper limits of $m_a < 8.13 \text{ eV}$

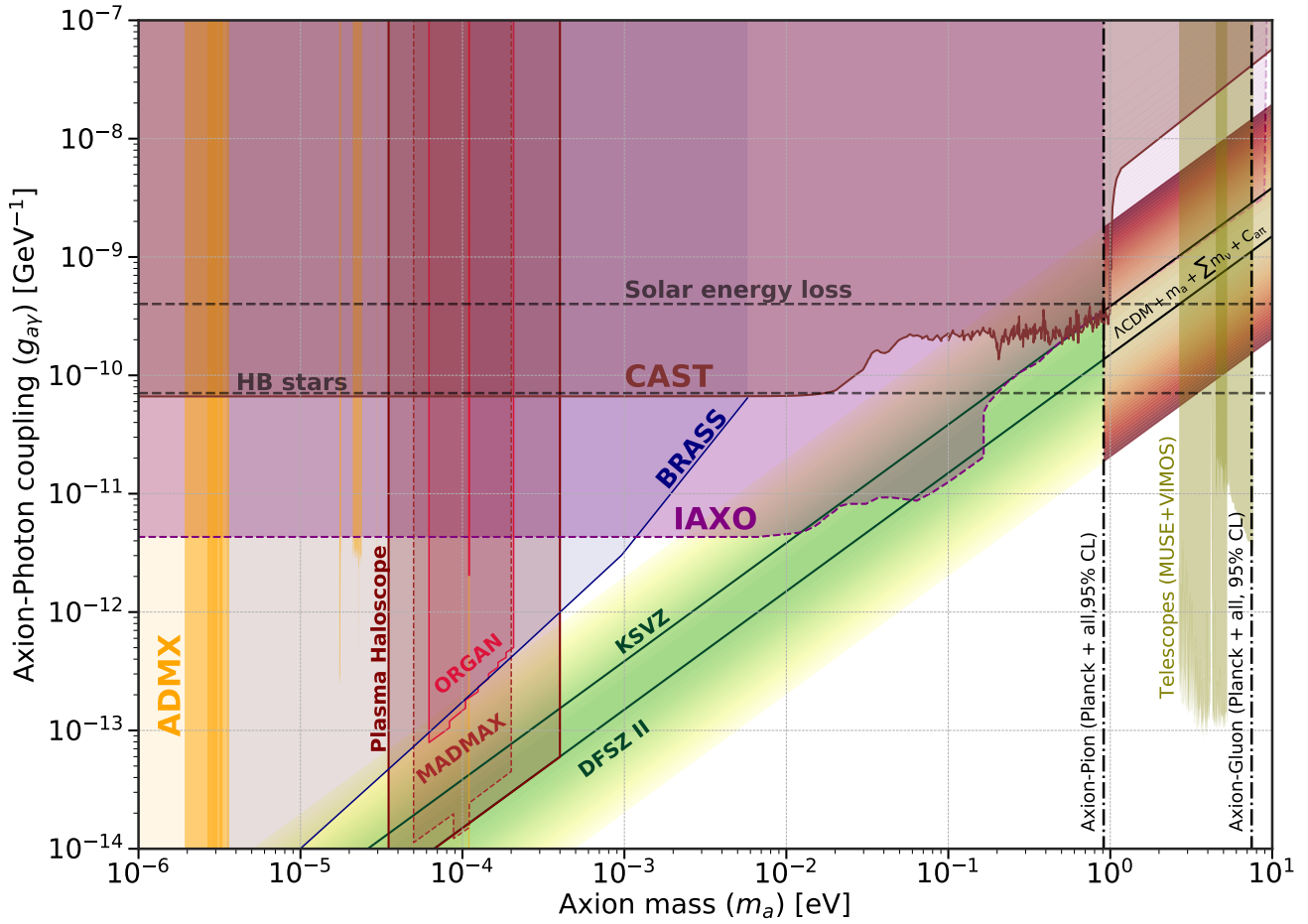


FIGURE III.3: Axion limits in the plane $(m_a, g_{a\gamma})$. We quote our most constraining cosmological bounds (both at 95% CL) for the axion-pion and the axion-gluon thermalization channels. We also show current limits and future detection sensitivity forecasts for different experiments: CAST [370], IAXO [371, 372], ORGAN [373], MADMAX [374], Plasma Haloscope [375], ADMX [376, 377], Telescopes [431, 432] and BRASS. The horizontal dashed lines represent the limits from the Sun and horizontal branch (HB) stars energy loss [433].

and $\sum m_\nu < 0.136 \text{ eV}$.

Despite the fact that there is a very large tension among CMB estimates and low redshift measurements of the Hubble constant - with a statistical significance above 4σ [121, 122, 434] -, this tension is considerably reduced in the presence of additional relativistic degrees of freedom. Sub-eV thermal axions are relativistic at decoupling and therefore will ease the well-known Hubble constant tension. Consequently, the addition of the prior on H_0 as measured by the Hubble Space Telescope in our cosmological analyses is perfectly justified and leads to a further strong improvement in the constraints on $\sum m_\nu$. The reason beyond this improvement can be easily understood in terms of the large degeneracy between the neutrino masses and the Hubble constant. It is well known that an increase on $\sum m_\nu$ induces a shift in the distance to last scattering that can be easily compensated by lowering H_0 , leading to a strong degeneracy between these two parameters. Such a degeneracy can be broken by an independent measurement of H_0 as that provided by the SH0ES Collaboration. Combining R20 and Planck data leads to upper bounds on the thermal relic masses of $\sum m_\nu < 0.129 \text{ eV}$ and $m_a < 7.92 \text{ eV}$, both at 95% CL. Including also Planck lensing measurements, BAO, Pantheon and DES data, the upper bound on the neutrino mass becomes $\sum m_\nu < 0.114 \text{ eV}$ at 95% CL, while the bound on the axion mass is slightly improved to $m_a < 7.46 \text{ eV}$ at 95% CL. Notice that the former upper limit on the total neutrino mass is very close to the inverted neutrino mass ordering prediction, implying that a future measurement of the nature's mass ordering could be translated into a limit on the thermal axion parameter space.

Axion-Pion scatterings

We shall now focus on the axion-pion thermalization channel. In this case the chiral perturbation theory adopted to compute the abundance of relic axions produced via pion scattering becomes unsafe for values of the decoupling temperatures above $T_\chi \simeq 62 \text{ MeV}$ [415]. For any axion model, this limit defines the smallest mass which can be safely explored within a perturbative approach:

$$m_a \gtrsim m_a(T_\chi, C_{a\pi}) \simeq 1.2 \times \left(\frac{0.12}{C_{a\pi}} \right) \text{ eV}. \quad (\text{III.72})$$

Notice that when $m_a \lesssim 1.2 \times (0.12/C_{a\pi}) \text{ eV}$ any bound derived using effective field theory is not completely reliable. Until robust lattice QCD methods provide a definitive answer, we have basically two choices: either we assume that when temperatures exceed 62 MeV perturbation theory still provides a reasonable approximation of a more accurate non-perturbative result, or, more conservatively, we limit our scan only to temperatures below 62 MeV . Here, we present and discuss the results obtained following the latter more conservative approach. Table III.3 summarizes the constraints for the model $\Lambda\text{CDM} + \sum m_\nu + m_a + C_{a\pi}$ for the different datasets listed in subsection III.II.II. Figure III.2 clearly illustrates the fact that requiring $T_d < 62 \text{ MeV}$ implies less constraining bounds on the axion mass. We estimate the upper bound on the axion mass as the value which corresponds to the 95% of its integrated posterior distribution function. Therefore, we derive strong conservative bounds without extending the theory in a region beyond its validity. Exploiting the last release of Planck temperature and polarization (TT,TE,EE+lowP) data, we derive the upper bound $m_a < 2.41 \text{ eV}$ at 95% CL on the axion mass and $\sum m_\nu < 0.269 \text{ eV}$ at 95% CL on neutrinos. As concerns the other datasets considered in our analyses, in this case their impact on the axion-mass bounds is relevant. Indeed, we may appreciate that the inclusion of CMB lensing measurements from the Planck satellite improve both the neutrino mass bound ($\sum m_\nu < 0.221 \text{ eV}$ at 95% CL) and the constraints on the axion mass ($m_a < 1.96 \text{ eV}$ at 95% CL). Due to the lower value of the clustering parameter σ_8 preferred by DES measurements, in this case the combination of Planck and DES data gives $m_a < 2.16 \text{ eV}$ and $\sum m_\nu < 0.257 \text{ eV}$, both at 95% CL. On the other hand, the smaller error in Ω_m of Pantheon data leads to an improvement both in the constraints on the sum of neutrino masses ($\sum m_\nu < 0.169 \text{ eV}$ at 95%CL), and in the constraints on the axion mass ($m_a < 1.78 \text{ eV}$, at 95% CL). Once again, the largest impact on Planck bounds arises from the inclusion of large-scale structure information from BAO measurements. Indeed, combining Planck and BAO data we derive the upper bounds $m_a < 1.04 \text{ eV}$ and $\sum m_\nu < 0.134 \text{ eV}$, both

at 95% CL. Combining together all the aforementioned datasets, we obtain the very tight and robust 95% CL upper limits of $m_a < 1.04$ eV and $\sum m_\nu < 0.115$ eV. Considering also the prior on H_0 as measured by the Hubble Space Telescope and combining together the R20 and Planck data, we obtain the upper bounds on the thermal relic masses $\sum m_\nu < 0.124$ eV and $m_a < 1.17$ eV, both at 95% CL. Including also Planck lensing measurements, BAO, Pantheon and DES data the upper bound on the neutrino mass is improved to $\sum m_\nu < 0.105$ eV at 95% CL, while the bound on the axion mass is improved to $m_a < 1.04$ eV at 95% CL. In this axion-pion thermalization case, the most constraining upper limit on the total neutrino mass lies extremely close to the inverted neutrino mass ordering prediction, enforcing our main message, that is, a multi-messenger search of axion and neutrino properties and for a joint analysis of their expected sensitivities. [Figure III.3](#) illustrates our cosmological constraints in the axion mass - axion-photon coupling plane $(m_a, g_{a\gamma})$. We focus exclusively on the parameter space of interest for thermal axions⁴, covering a mass range $m_a \in [10^{-6}, 10]$ eV and quoting our most constraining 95% CL bounds for the two thermalization channels together with current experimental limits and future detection sensitivity forecasts. From the limits depicted in [Figure III.3](#) one can notice that a significant range of the parameter space can be probed by cosmological data. Furthermore, a future cosmology-independent limit on the axion mass may provide an important test of the cosmological constraint, and also can be translated into a limit on the hot dark matter component in the form of massive neutrinos, strongly supporting multi-messenger searches of axions and neutrino properties.

III.III COSMOLOGICAL FORECASTS ON AXIONS NEUTRINOS AND LIGHT ELEMENTS

While the bounds discussed in the previous section are able to probe a significant range of the parameter space allowed by direct axion searches, see also [Figure III.3](#), the current constraining power on the total variation of the effective number of relativistic species due to extra dark radiation ($\Delta N_{\text{eff}} \lesssim 0.4$ at 95% CL) represents an important limitation as it is not accurate enough to reveal the presence of thermal axions produced before the QCD transition. These axions would lead to $\Delta N_{\text{eff}} \lesssim 0.1$, which lies well below the present sensitivity to ΔN_{eff} . In this regard, the next generation of CMB experiments is expected to significantly increase the constraints on N_{eff} . Indeed one of the targets of future Cosmic Microwave Background and Baryon Acoustic Oscillation measurements is to improve the current accuracy in the neutrino sector and reach a much better sensitivity on extra dark radiation in the Early Universe. We conclude this thesis studying how these improvements can be translated into constraining power for well motivated extensions of the Standard Model of elementary particles that involve axions thermalized before the QCD phase transition by scatterings with gluons. Assuming a fiducial Λ CDM cosmological model, here we simulate future data for CMB-S4-like and DESI-like surveys following the methodology discussed in [Equation III.III.I](#) and analyze a mixed scenario of axion and neutrino hot dark matter. We further account also for the effects of these QCD axions on the light element abundances predicted by Big Bang Nucleosynthesis.

III.III.I FORECAST METHODS

In this subsection we describe the method followed for our forecasted analyses, focusing on future CMB and BAO observations. In particular, we simulate future data for a CMB-S4-like [\[200\]](#) observatory and for a DESI-like [\[440, 441\]](#) BAO survey. These probes are expected to provide scientific results in the next few years and have been carefully designed to improve the constraints on the neutrino sector and other forms of dark radiation in a significant way [\[200, 440, 442, 443\]](#). Finally, we also address the effect of additional thermal species on the observational prediction of BBN on light element abundances up to Beryllium-7.

All our forecasted datasets make use of the COBAYA software [\[295\]](#). The code allows to build synthetic realization of cosmological data for both CMB and BAO observations and test them again a given

⁴For a review of the limits on axion-like particles covering larger ranges see O'Hare [\[435\]](#) and also O'Hare and Vitagliano [\[436\]](#), O'Hare et al. [\[437\]](#), Dafni et al. [\[438\]](#), and Knirck et al. [\[439\]](#) for interesting discussions.

cosmological model. The parameter posteriors have been sampled using the MCMC algorithm developed for CosmoMC [107, 108]. The predictions of the theoretical observational probes are calculated using the latest version of the cosmological Boltzmann integrator code CAMB [109, 110]. To include the effect of the axion-gluon coupling as an additional form of dark radiation we have modified the CAMB package accordingly to the detailed description in the previous section. The strength of the coupling and its effect on the neutrino sector are functions only of the axion mass that we include as an additional cosmological parameter in our analyses.

To complete this picture one needs to choose a fiducial cosmological model to build the forecasted data. We perform our forecasts using values of the parameters that are in agreement with the latest Planck 2018 constraints for a Λ CDM scenario [114]. In particular we choose the following values for the standard six cosmological parameters : $n_s = 0.965$, $\omega_b = 0.0224$, $\omega_c = 0.12$, $H_0 = 67.4$, $\tau = 0.055$, $A_s = 2.1 \times 10^{-9}$, $N_{\text{eff}} = 3.046$, $\sum m_\nu = 0.06$ eV and $m_a = 0$ eV. The above values are those commonly used in the forecasts available in the literature, and, therefore, for the sake of comparison, are the most convenient and useful ones, despite the fact that none of these previous works have considered m_a as a parameter to be constrained.

CMB-S4 forecasts

We build our forecast for future CMB observations using a well-established and robust method that is now a common practice in cosmological analyses. Using the fiducial model introduced above, we compute the angular power spectra of temperature C_ℓ^{TT} , E and B polarization $C_\ell^{EE, BB}$ and cross temperature-polarization C_ℓ^{TE} anisotropies. Then, we consider an experimental noise for the temperature angular spectra of the form [444]:

$$N_\ell = w^{-1} \exp(\ell(\ell+1)\theta^2/8 \ln 2), \quad (\text{III.73})$$

where θ is the FWHM angular resolution and w^{-1} is the experimental sensitivity in units of $\mu\text{K arcmin}$. The polarization noise is derived assuming $w_p^{-1} = 2w^{-1}$ (one detector measures two polarization states). The simulated spectra are compared with theoretical ones using the following likelihood \mathcal{L} [132, 444]:

$$-2 \ln \mathcal{L}_{\text{CMB}} = \sum_\ell (2\ell+1) f_{\text{sky}} \left(\frac{D_\ell}{|C_\ell|} + \ln \frac{|C_\ell|}{|\hat{C}_\ell|} - 3 \right), \quad (\text{III.74})$$

where \hat{C} and C are the theoretical and simulated spectra (plus noise), respectively and are defined by :

$$|C_\ell| = C_\ell^{TT} C_\ell^{EE} C_\ell^{BB} - (C_\ell^{TE})^2 C_\ell^{BB}; \quad (\text{III.75})$$

$$|\hat{C}_\ell| = \hat{C}_\ell^{TT} \hat{C}_\ell^{EE} \hat{C}_\ell^{BB} - (\hat{C}_\ell^{TE})^2 \hat{C}_\ell^{BB}, \quad (\text{III.76})$$

while D is :

$$D_\ell = \hat{C}_\ell^{TT} C_\ell^{EE} C_\ell^{BB} + C_\ell^{TT} \hat{C}_\ell^{EE} C_\ell^{BB} + C_\ell^{TT} C_\ell^{EE} \hat{C}_\ell^{BB} - C_\ell^{TE} \left(C_\ell^{TE} \hat{C}_\ell^{BB} + 2C_\ell^{TE} C_\ell^{BB} \right). \quad (\text{III.77})$$

In this study we construct synthetic realizations of CMB data for only one experimental configuration, namely CMB-S4 (see e.g. [445]), using $\theta = 3'$ and $w = 1 \text{ K arcmin}$. The range of multipoles is $5 \leq \ell \leq 3000$ and the sky coverage of the 40% ($f_{\text{sky}} = 0.4$). We do not include CMB lensing derived from trispectrum data.

DESI (BAO) forecasts

For the future BAO dataset we consider the DESI experiment [441]. As a tracer for BAO observations we employ the volume average distance defined as:

$$D_V(z) \equiv \left(\frac{(1+z)^2 D_A(z)^2 c z}{H(z)} \right)^{\frac{1}{3}}, \quad (\text{III.78})$$

where D_A is the angular diameter distance and $H(z)$ the Hubble parameter. Assuming the fiducial model described previously, we compute the theoretical values of the ratio D_V/r_s for several redshifts in the range $z = [0.15 - 1.85]$, where r_s is sound horizon at the photon-baryon decoupling epoch. The uncertainties on D_V/r_s are calculated propagating those for D_A/r_s and $H(z)$ reported in [440]. The simulated BAO data are compared to the theoretical D_V/r_s values through a multivariate Gaussian likelihood :

$$-2 \ln \mathcal{L}_{\text{BAO}} = \sum (\mu - \hat{\mu}) C^{-1} (\mu - \hat{\mu})^T, \quad (\text{III.79})$$

where μ and $\hat{\mu}$ are the vectors containing the simulated and theoretical values of D_V/r_s at each redshift and C their simulated covariance matrix.

It would also be possible to forecast BAO data considering D_A/r_s and $H(z)$ as independent measurements, allowing for stronger constraints. However some small tension (~ 1 sigma) has been identified between the current constraints from D_A/r_s and $H(z)$ [446]. Given the difficulty of properly accounting for this small tension between D_A/r_s and $H(z)$, we decided to follow the approach of [447] and employ the volume average distance for our BAO forecasts. The resulting dataset is the same obtained in Ref. [448] (see also their Table 2) while a plot representing the forecasted dataset is presented in Figure III.4.

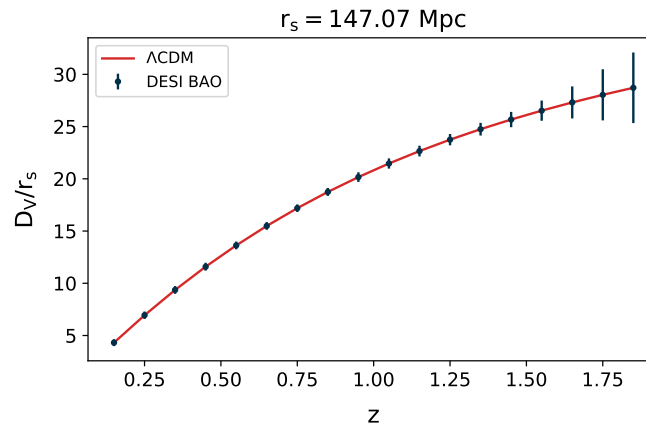


FIGURE III.4: The fiducial BAO datasets employed in our forecasts. Error bars refer to 3σ CL uncertainties.

BBN primordial light element abundances

Big Bang Nucleosynthesis (BBN) is a cornerstone of the Hot Big Bang cosmology which explains the formation of the first light nuclei (from H up to ${}^7\text{Li}$) by a solid understanding of the nuclear interactions involved in the production of elements.

The set of differential equations that regulate those interactions in the primordial plasma can be solved numerically [449–452] after neutrino decoupling ($T \gtrsim 1$ MeV) up the end of BBN ($T \sim 10$ keV), yielding the total abundance of primordial elements in terms of their ratio with respect to the hydrogen abundance. BBN provides a natural laboratory to probe new physical scenarios of the early Universe and its predictions can be compared to the primordial abundances of light elements inferred by astrophysical and cosmological observations. Given current uncertainties, BBN predictions and primordial light element measurements

show a good agreement [453–455]⁵. Notice also that since the BBN epoch ends before recombination, its outcome does not have any impact on the recombination epoch or else on the CMB power spectra. In other words, recombination and BBN are two independent and complementary probes that can be combined to check the consistency of particles interactions in the early universe. What is relevant for CMB is the BBN prediction for the Helium abundance, that can be used to estimate the baryon density through a simple formula:

$$\Omega_b h^2 = \frac{1 - 0.007125 Y_p^{\text{BBN}}}{273.279} \left(\frac{T_{\text{CMB}}}{2.7255 \text{ K}} \right)^3 \eta_{10}, \quad (\text{III.80})$$

where $\eta_{10} \doteq 10^{10} n_b / n_\gamma$ is the photon-baryon ratio today, T_{CMB} is the CMB temperature at the present time and $Y_p^{\text{BBN}} \doteq 4n_{\text{He}} / n_b$ is the helium nucleon fraction defined as the ratio of the 4-Helium to the baryon density one. Furthermore, BBN depends on the expansion rate $H(z)$, which sets the value of the temperature of the Universe during the radiation epoch via a function of the radiation density:

$$H(z) \simeq \frac{8\pi G}{3} \rho_{\text{rad}} \simeq \frac{7\pi G}{3} N_{\text{eff}} \left(\frac{4}{11} \right)^{4/3} \rho_\gamma, \quad (\text{III.81})$$

making BBN a very powerful tool to constrain the total number of relativistic species via $H(z)$.

In this section, we made use of the code PARTHENOPE [452]. Using the values of N_{eff} , τ_n (the neutron lifetime⁶) and η_{10} (or equivalently $\Omega_b h^2$), the code computes the value of Y_p^{BBN} and other light element abundances. To include the BBN code predictions in our MCMC analysis, we follow the same procedure used by the Planck collaboration [114]. Namely, we fix the neutron life time and create an interpolation grid varying $\Omega_b h^2$ and $\Delta N_{\text{eff}} = N_{\text{eff}} - 3.045$ within a given range. We choose these ranges to be $\Delta N_{\text{eff}} \in [-3; 3]$ and $\Omega_b h^2 \in [0.0073; 0.033]$. The neutron lifetime is fixed to $\tau_n = 879.4 \text{ s}$, corresponding to the latest measurement reported by the Particle Data Group ($\tau_n = 879.4 \pm 0.6 \text{ s}$) [31]⁷.

III.III.II FORECASTED RESULTS

We present the results obtained with the forecasting method discussed in the previous subsection. As a baseline model, we employ an extension of the standard cosmological model that includes both neutrinos and axions as thermal massive relics. We refer to it with $\Lambda\text{CDM} + \sum m_\nu + m_a$. Within this model, we study the improvement on the bounds of QCD axions achievable by future CMB and BAO experiments. As aforementioned, thermal axions also contribute as additional relativistic species prior to recombination, increasing the value of N_{eff} thus leading to modifications of the standard BBN predictions. Therefore we also take into account the effect of additional thermal species on the observational predictions of BBN light element abundances. Finally, we shall also compare the constraints on the hot relics and on the Helium nucleon fraction Y_p^{BBN} achievable with our simulated datasets without employing the BBN code, testing the dependence of our results on the assumptions adopted for the BBN sector and proving their robustness.

Parameter	Fiducial value	CMB-S4	CMB-S4 + DESI
$\Omega_b h^2$	0.0224	0.022420 ± 0.000034	0.022422 ± 0.000034
$\Omega_c h^2$	0.12	0.12066 ± 0.00062	0.12019 ± 0.00032
H_0 [Km/s/Mpc]	67.4	$66.94^{+0.63}_{-0.57}$	67.39 ± 0.24
τ	0.05	0.0508 ± 0.0026	0.0508 ± 0.0025
$\log(10^{10} A_S)$	3.044	3.0491 ± 0.0049	3.0478 ± 0.0047
n_s	0.965	0.9647 ± 0.0021	0.9659 ± 0.0017
Σm_ν [eV]	0.06	< 0.183	< 0.122
m_a [eV]	0.0	< 1.60	< 0.924
Y_p^{BBN}	0.247	$0.247268^{+0.000052}_{-0.000085}$	$0.247244^{+0.000030}_{-0.000042}$
10^5 D/H	2.514	2.5211 ± 0.0065	2.5200 ± 0.0063
10^7 T/H	0.808	0.8104 ± 0.0022	0.8101 ± 0.0021
10^5 He3/H	1.032	1.03374 ± 0.00095	1.03358 ± 0.00094
10^{10} Li7/H	4.67	4.670 ± 0.015	4.671 ± 0.015
10^{10} Be7/H	4.40	4.396 ± 0.031	4.398 ± 0.015

TABLE III.4: Results for the $\Lambda\text{CDM} + m_a + \Sigma m_\nu$ cosmological model and on the primordial light element abundances. The constraints on the parameters are at 68% CL, while upper bounds are quoted at 95% CL. We make use of the PARTHENOPE package to compute the BBN predictions.

Mixed Hot Dark Matter: Axions and Neutrinos

Table III.4 summarizes the results obtained from our forecasting methods for future CMB and BAO experiments while Figure III.5 shows the 68% and 95% CL contour plots for different cosmological parameters.

Using our forecasting data for future CMB-S4 observations, we derive the 95% CL upper bounds on thermal relics of $\Sigma m_\nu < 0.183$ eV and $m_a < 1.60$ eV. These values should be compared with those derived in [5] for the same cosmological model, exploiting the last CMB data release provided by the Planck Collaboration. In particular, one can appreciate that future CMB-S4 measurements are expected to improve the current bounds on the axion-gluon interaction scenario by a factor of ~ 5 , while we estimate the improvement in the constraining power on the neutrino sector to be ~ 2 . This enhancement in the constraining

⁵Nevertheless, there are some discrepancies in the observed abundance of ^7Li (which is a factor of ~ 2 smaller than those measured from low-metallicity stars [456, 457]) and in that of the primordial deuterium (which exhibit a 1.8σ discrepancy with the CMB+BAO value [453]).

⁶It is worth noting that, the interaction rates used in BBN codes assume a prior knowledge of τ_n , which sets the efficiency of nuclear reactions. Therefore, BBN abundances are significantly affected even by a small change in the precise value of this parameter.

⁷This estimate of the neutron life time is derived averaging over a large number of measurements. However, beam-only and bottle-only experiments show a 4σ discrepancy in measuring the neutron lifetime, leading respectively to $\tau_n = 888.0 \pm 2.0$ s and $\tau_n = 879.2 \pm 0.6$ s (see also the discussion in Ref. [458]). Interestingly, independent constraints can be derived by CMB data only, but these limits are not accurate enough to disentangle between the two results ($\tau_n = 851 \pm 60$ s). Nevertheless, the neutron lifetime discrepancy is beyond the scope of this work and we therefore fix its value to that of Ref. [31], even if this could produce a systematic error in N_{eff} [459].

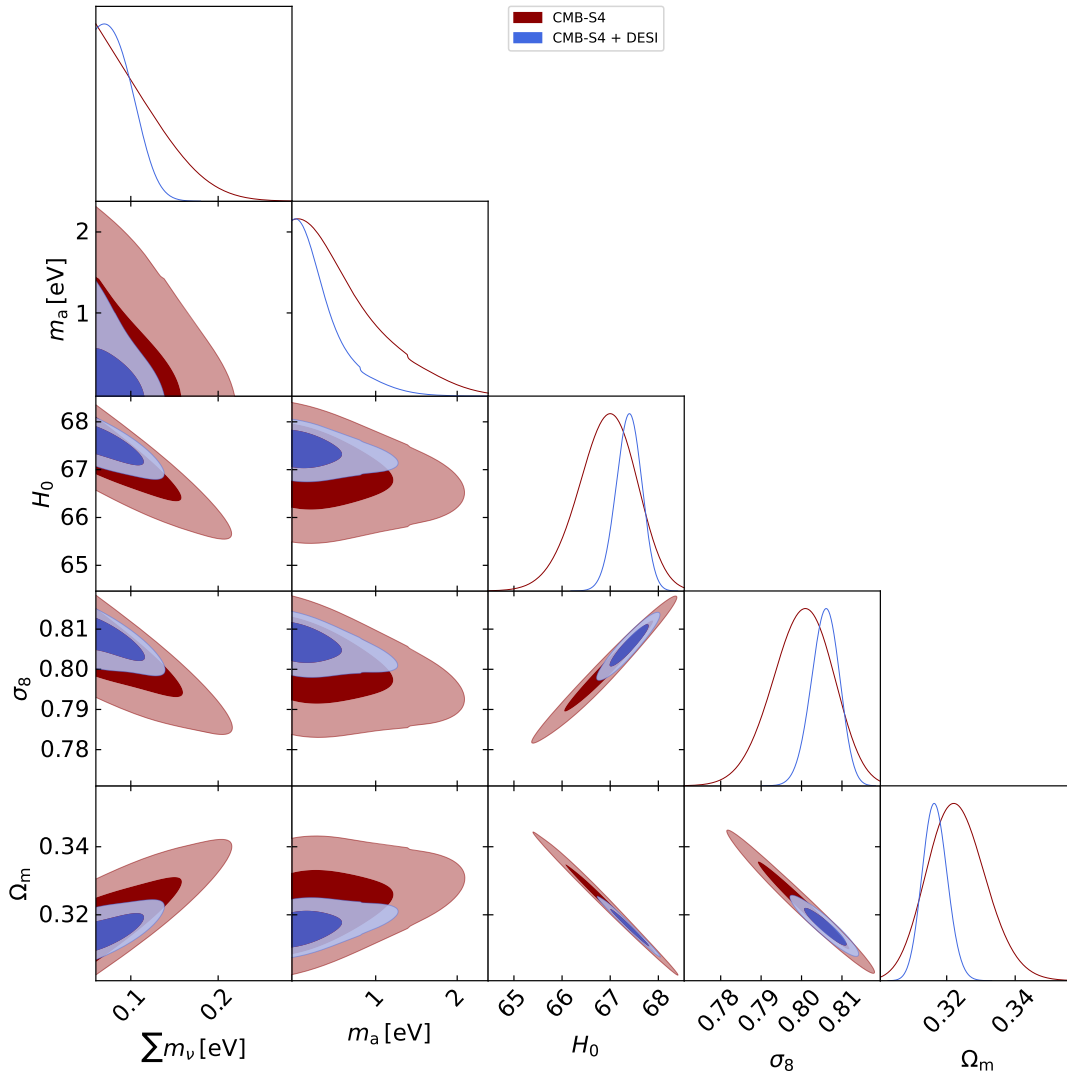


FIGURE III.5: Marginalized 2D and 1D posteriors for different cosmological parameters obtained from the forecasting data and methods.

power on thermal relic masses is mostly due to the much higher sensitivity to the effective number or relativistic degrees of freedom N_{eff} expected from future CMB measurements⁸.

Notice that, due to the degeneracy between the axion and the neutrino masses discussed in the introductory section, the contours in the $(\sum m_\nu, m_a)$ show a clear anti-correlation. Furthermore, these two parameters show very similar degeneracies with other cosmological parameters such as H_0 , σ_8 and Ω_m . It is well-known that hot thermal particles suppress structure formation at small scales and therefore galaxy clustering information becomes crucial to set bounds on the amount of dark matter in the form of these relics. As discussed in [5] the largest impact on CMB bounds on hot relics arises from the inclusion of the large-scale structure information from BAO measurements. For this reason, here, together with the likelihood for future CMB-S4 observations, we consider also a likelihood for future BAO measurements from the DESI-like experiment. Combining our simulated CMB-S4 and DESI forecasts, we obtain a further improvement in the cosmological constraining power for thermal relics, reaching the 95% CL limits $m_a < 0.924 \text{ eV}$ and $\sum m_\nu < 0.122 \text{ eV}$. In this case these bounds can be compared with those obtained for current Planck+BAO real data [5], observing an improvement of a factor ~ 8 and ~ 1.5 in the sensitivity

⁸We recall that, while the current Planck data lead to a 95% CL upper limit of $\Delta N_{\text{eff}} \lesssim 0.4$, future CMB-S4-like experiments are expected to bring this upper limit down by a factor of ~ 10 , resulting in a much more tighter limit on dark radiation, $\Delta N_{\text{eff}} \lesssim 0.06$.

on the axion and neutrino masses, respectively.

Our results clearly state that future cosmological observations can substantially improve the current constraints on m_a , exploring a much larger range of the parameter space currently allowed for QCD thermal axion and reaching the sub-eV mass range. Conversely, when axions are included in the picture as additional thermal species, the possibility to detect the expected minimum neutrino mass of 0.06 eV is no longer possible, and only upper bounds, close to the inverted mass ordering prediction, can be derived.

Parameter	Fiducial value	CMB-S4	CMB-S4 + DESI
$\Omega_b h^2$	0.0224	0.022399 ± 0.000050	0.022406 ± 0.000050
$\Omega_c h^2$	0.12	0.12070 ± 0.00062	0.12020 ± 0.00031
H_0 [Km/s/Mpc]	67.4	$66.90^{+0.65}_{-0.57}$	67.37 ± 0.24
τ	0.05	0.0506 ± 0.0026	0.0507 ± 0.0025
$\log(10^{10} A_S)$	3.044	3.0486 ± 0.0049	3.0474 ± 0.0047
n_s	0.965	0.9635 ± 0.0034	0.9649 ± 0.0030
$\sum m_\nu$ [eV]	0.06	< 0.183	< 0.120
m_a [eV]	0.0	< 1.63	< 0.991
Y_p^{BBN}	0.247	$0.2458^{+0.0057}_{-0.0058}$	$0.2460^{+0.0057}_{-0.0058}$

TABLE III.5: Results for $\Lambda\text{CDM} + m_a + \sum m_\nu + Y_p^{\text{BBN}}$ case (i.e. leaving the Helium nucleon fraction as a free parameter of the model, without assuming the BBN theoretical predictions). The constraints on parameters are at 68% CL, while the quoted upper bounds are at 95% CL.

Primordial abundances of light elements

Thermal axions contribute to the effective number of relativistic degrees of freedom, modifying the expansion rate at the radiation epoch and affecting, indirectly, the canonical BBN predictions. Even though the latest results of the Planck collaboration place tight bounds on both the baryon density ($\Omega_b h^2 = 0.0224 \pm 0.0001$) and N_{eff} (limiting the amount of additional relativistic degrees of freedom to $\Delta N_{\text{eff}} \lesssim 0.4$), the impact of axions on the Helium fraction is extremely small and the Planck uncertainties on $\Omega_b h^2$ are still too large to provide robust theoretical predictions on the Helium abundance in presence of the axion. However, the next generation of CMB and BAO observations will substantially improve the bounds on the baryon energy density by a factor of 2, strongly reducing the theoretical uncertainties on Y_p^{BBN} , and, possibly, allowing to test signatures of the axion in the primordial abundances. Figure III.6 shows a comparison between CMB-S4 and Planck in determining the Helium fraction. In particular, we show the theoretical Helium fraction predictions in the $\Lambda\text{CDM} + m_a + \sum m_\nu$ cosmological model as a function of the axion mass (or, equivalently, as a function of the axion contribution to ΔN_{eff}) together with the 2D marginalized posterior distribution obtained for the CMB-S4 and CMB-S4+DESI simulated data. Notice that the BBN predictions introduce a strong correlation between the axion mass and the Helium fraction (Y_p^{BBN}) that, combined with the substantial improvement in the constraining power expected by CMB-S4 and DESI, suggests that the BBN could be a useful tool to make predictions on hot axions and that astrophysical measurements of the primordial fraction of Helium could be used as an independent test together with the cosmological observations. For this reason we included all the BBN light elements in our analysis. We provide the 68% CL results for the other light elements up to Beryllium-7 in Table III.4. It should be noticed however that these results are derived without considering the experimental error in the measurement of the neutron life-time τ_n . This error could dominate the total error budget, enlarging the theoretical uncertainties on

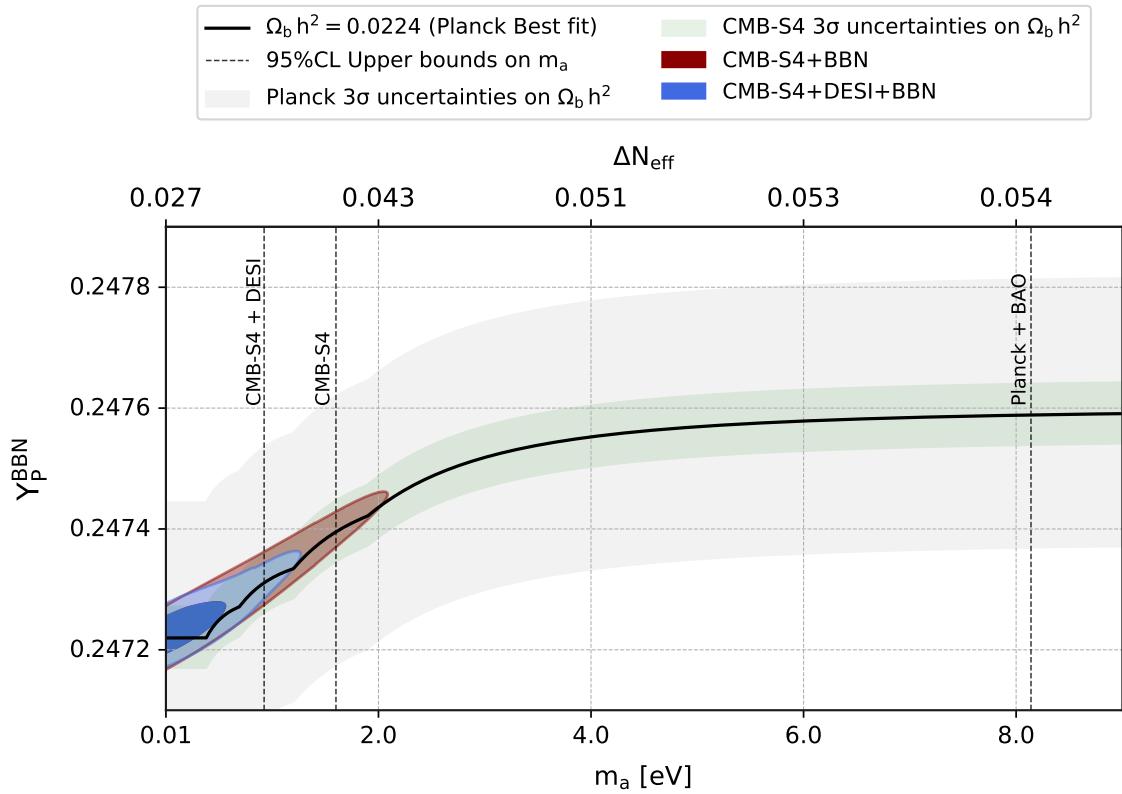


FIGURE III.6: Theoretical Helium fraction predictions in the $\Lambda\text{CDM} + m_a + \sum m_\nu$ cosmological model. The black solid line represents the Helium fraction as a function of the axion mass (with the corresponding ΔN_{eff} on the top axis) obtained fixing $\Omega_b h^2 = 0.0224$. The green (gray) region represents the 3σ uncertainties on Y_p^{BBN} by CMB-S4 (Planck). The vertical lines are the 95% C.L. upper limits on m_a from current cosmological data and from CMB and BAO future experiments, together with the respective 68% and 95% CL contours.

the BBN predictions for Y_p^{BBN} by a factor of ~ 3 ($\Delta Y_p^{\text{BBN}}(\Delta\tau_n) \simeq 0.00012$), producing the same effect as an extra dark radiation component [459]. Consequently a large degeneracy between the axion mass and the neutron life-time is expected and this effect may change the correlations between the primordial Helium fraction and the axion mass. For this reason, to prove the robustness of our results on hot massive relics, it is mandatory to follow also a very conservative approach and study the impact of additional hot relics on the abundances of primordial elements without assuming the BBN theoretical predictions but leaving all the parameters varying in uninformative flat priors. We therefore analyze a cosmological model where, together with axions and massive neutrinos, we also include the abundance of primordial Helium as an additional free parameter. We refer to this model as $\Lambda\text{CDM} + m_a + \sum m_\nu + Y_p^{\text{BBN}}$ and report the results obtained with our CMB and BAO forecasting data in Table III.5. In this case, the 68% and 95% CL marginalized contours in the plane (m_a, Y_p^{BBN}) are shown in Figure III.7.

Removing the BBN predictions the strong positive correlation between the axion mass and the Helium fraction Y_p^{BBN} is relaxed as well. Furthermore the bounds on the Helium fraction are much less constraining, with 68% CL bounds of $Y_p^{\text{BBN}} = 0.2458^{+0.0057}_{-0.0058}$ and $Y_p^{\text{BBN}} = 0.2460^{+0.0057}_{-0.0058}$ for CMB-S4 and CMB-S4+DESI, respectively. On the other hand, the constraints on hot dark matter are basically unchanged. Exploiting our forecasting data for future CMB-S4 observations we can still derive the 95% CL upper bounds $m_a < 1.63$ eV and $\sum m_\nu < 0.183$ eV for axions and neutrinos, respectively. The upper limit on the total neutrino mass is exactly the same as that derived including the BBN code as well as the upper bound on the total axion mass. Similarly, combining future CMB-S4 and BAO data the upper bound on neutrinos masses is unchanged

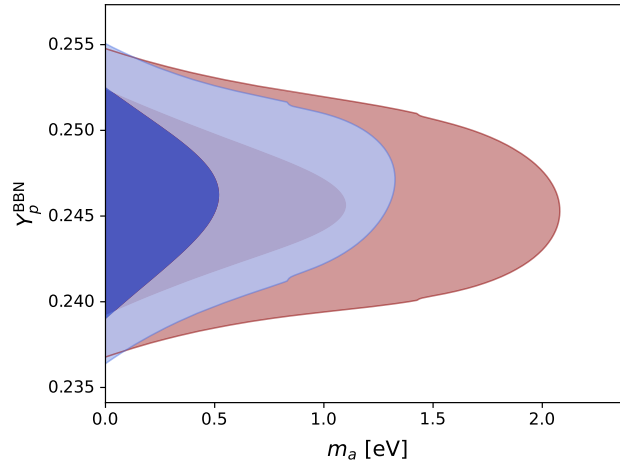


FIGURE III.7: Marginalized 2D posteriors in the plane (m_a, Y_p^{BBN}) when the BBN predictions are relaxed and the Helium fraction is considered as a free parameter.

($\sum m_\nu < 0.120$ eV at 95% CL) while the upper bound on axions is only slightly worsened to $m_a < 0.991$ eV at 95%CL. These results prove that the impact of the BBN uncertainties on axion and neutrino masses is negligible and therefore the extraction of both m_a and m_ν does not rely on the assumptions adopted for the neutron-life time.

We conclude supporting and underlying again the relevance of multi-messengers searches of axions, neutrinos and primordial light element measurements. Indeed, cosmology-independent limits on the axion and neutrino masses, combined with precise astrophysical measurements of light elements, may provide an important cosmological test for checking the BBN predictions. On the other hand, future cosmic observations should also be able to probe scenarios with hot axions with masses $m_a \gtrsim 1$ eV and a missing evidence would constrain the axion mass at the sub-eV level, favoring the normal ordering as the one governing the mass pattern of neutral fermions. In the same multi-messenger spirit, future cosmology-independent probes of neutrino masses (i.e. future terrestrial double beta decay and/or long baseline neutrino experiments) will play, even if indirectly, a crucial role on axion searches.

CONCLUSION

In this thesis, working at the interface of cosmology, gravitation and (astro)particle physics, we studied, characterized and constrained different global theoretical scenarios beyond *General Relativity* and the *Standard Model* of elementary particles in light of their implications for the physics of the Early Universe. In particular, after providing in [chapter I](#) an exhaustive review of the major aspects of physical cosmology, we focus on two different types of relics: gravitational waves from inflation and hot thermal relics from the Early Universe.

GRAVITATIONAL WAVES FROM INFLATION

In [chapter II](#), a particular attention is devoted to the inflationary background of gravitational waves sourced by a super-adiabatic amplification of zero-point quantum fluctuations during inflation. We are entering in an exciting decade for inflationary cosmology as the next generation of Cosmic Microwave Background experiments (*e.g.* BICEP3, CLASS, SPT-3G, LBIRD and CMB-S4) are expected to reach a much better sensitivity on B-modes polarization, possibly leading to a first detection of Primordial Gravitational Waves (PGWs). Moreover, future Gravitational Wave experiments (*e.g.* LISA and Einstein Telescope) are expected to strongly improve the current LIGO/VIRGO sensitivity to the stochastic background of Gravitational Waves, as well. This could open up a *unique* observational window to probe physics at the extremely high energy scales, allowing us to test a rich phenomenology, including modified gravity theories and/or signatures from quantum-gravity models. Anyway a careful characterization of the underlying phenomenology is needed because the standard inflationary predictions may be violated in many non-trivial realizations of inflation as well as several different plausible mechanisms may lead to a stochastic background of gravitational waves testable by future experiments, resulting into a large degeneracy of the theoretical predictions. In this thesis we derive and discuss the following original results.

- In [section II.I](#) we start by providing an extensive updated review of the cosmological constraints on slow roll inflation. We analyze different extended scenarios beyond the Λ CDM cosmological model that involve modifications in the primordial sector. Imposing a set of consistency relations between higher-order scalar and tensor parameters, we generalize the power-law expansion for the primordial scalar and tensor spectra up to the third order and constrain the additional inflationary parameters in light of the most recent cosmological observations.

We show that, under the assumption of slow-roll inflation with Einstein gravity, different combinations of the Planck, lensing, BAO and BK15 data, do not give evidence for higher-order terms in the scalar spectrum such as a running $\alpha_s \doteq dn_s/d\log k$ or a running of running $\beta_s \doteq d\alpha_s/d\log k$. Conversely, analyzing the ACTPol+WMAP data we find a preference for non-zero α_s and β_s at the level of 2.9σ and 2.7σ , respectively. Anyway, such a preference is reduced when the running of running is replaced by tensor amplitude in the model.

We interpret the results in terms of the physics of the inflationary epoch showing that the shift towards higher values of n_s preferred by the ACTPol+WMAP data actually strongly disfavors some inflationary models that are instead compatible with Planck bounds; in some cases leading to completely different conclusions for the model selection. In other words, we prove that the extensions to the primordial sector considered in this section recast the global tension between the datasets already present for a Λ CDM model analysis on a difference among the inflationary parameters.

As concerns the spectrum of inflationary gravitational waves, we provide different updated upper bounds on the tensor amplitude, with $r < 0.0658$ at 95% CL our most constraining bound for Planck+BK15 data at the pivot scale $k_* = 0.05\text{Mpc}^{-1}$. Furthermore, given the constraints on the tensor spectrum and

the upper limits on the tensor amplitude, we show that the usual consistency relations strongly reduce the parameter space allowed for the tensor spectrum, basically leading to predict a scale-independent tensor tilt, unless corrections of order $dn_T/d\log k \lesssim 10^{-5}$, for all the datasets analyzed.

- In [section II.II](#), we instead study what happens relaxing the aforementioned inflationary slow-roll consistency relations that, in fact, can be violated in many non standard inflationary models.

In particular, as shown by the Planck Collaboration in Ref. [78], when the slow-roll consistency relation between the tensor amplitude and the tensor tilt is relaxed ($n_T \neq -r/8$) the observations of the Cosmic Microwave Background are no more able to place stringent constraints on the tensor tilt and the final 95%CL bound $-0.55 < n_T < 2.54$ allows for the possibility of having a strongly blue tilted primordial tensor spectrum ($n_T > 0$). Always in Ref. [78], it was shown that an improvement in the constraining power on blue tilted models can be achieved combining the Planck CMB observations with the LIGO-Virgo data on the stochastic background of gravitational waves. The reason beyond this improvement is that a blue tensor tilt can strongly amplify the power of PGWs on small scales, possibly producing a signal testable by ground-based interferometers. The LIGO-Virgo upper limit on the stochastic gravitational wave background is so translated into an upper bound on the tensor tilt of $n_T < 0.53$ at 95%CL.

However, in performing this analysis, the usual power-law parametrization was adopted for the tensor spectrum, basically extending a leading-order expansion over a range of frequencies of about 18 order of magnitude: from the microwave scales probed by the Planck satellite ($k \sim 0.01 \text{ Mpc}^{-1}$) all the way up to the scales of direct gravitational wave detection probed by LIGO and Virgo ($k \sim 1 \times 10^{16} \text{ Mpc}^{-1}$). In this section, we discuss for the first time the effects of non-linearities induced by higher-order terms beyond the power-law expansion, parametrized through the so-called tensor runnings. We show that such terms, albeit negligibly small on the CMB scales, may give non-negligible contributions on the ultrahigh k probed by gravitational interferometers, possibly breaking the power-law assumption. We point out that direct GW observations do not always constrain the tensor tilt on the CMB scales but, due to the huge distance between the scales probed by CMB and GW data, even a small departure from scale independence ($\lesssim 4\%$) is enough to relax the final constraints, see also [Figure II.4](#). Finally, we discuss the implications for the status of current observational constraints and future detection prospects.

- In [section II.III](#) and [section II.IV](#) we study how non-standard high-energy physics may be encapsulated in the tensor two-point function and in the inflationary observables, inferring that the usual power-law parametrization can be broken by a large survey of different physical mechanisms. We also discuss how the aforementioned non-linear effects can play an important role in discriminating among different models beyond the standard slow roll paradigm with Einstein gravity. Indeed, affecting the small scale behavior of tensor anisotropies in a model-dependent manner, they can break the degeneracy in the large-scale predictions, helping us to shed light both on the physics of inflation and on the underlying theory of gravitation. From a data analysis perspective, we instead outline a methodology to *properly* combine small and large scale cosmological and astrophysical measurements in order to increase the data constraining power on inflation within specific theories/models.

In particular, in [section II.III](#) we study non-standard cosmological models where gravity can propagate differently from GR at early epochs.

In many modified gravity theories, such as Horndeski gravity, Gauss-Bonnet gravity and also low-energy effective string theory, gravitational interactions can propagate differently from GR at high energies. Therefore testing the propagation of gravity at different frequencies means testing General Relativity at different energy scales.

Here, using a slow-roll effective field theory approach, we derive for the first time a set of generalized consistency relations for the spectral index and its higher-order runnings that include the effects of non-trivial gravity propagation on the spectrum of inflationary gravitational waves. We show that a running in frequency of the propagating speed of gravity during inflation can induce a scale-dependence in the tensor two-point function, amplifying or suppressing the PGWs production on small scales. Exploiting

the generalized relations, we connect the CMB scales to the LIGO/Virgo band ($f \sim 100$ Hz), constraining both the speed of gravity and above all its frequency variation to $d \log c_T / d \log k = 0.082_{-0.11}^{+0.047}$ (68% CL) at the pivot scale $k_* = 0.05 \text{Mpc}^{-1}$. This places remarkable constraints on gravity propagation at the CMB frequencies, providing, at the same time, an independent test of General Relativity on the inflationary energy scales, see also [Figure II.9](#).

In [section II.IV](#) we instead focus on higher-curvature tensors in the gravitational action.

It is well known that several high-energy theoretical models predict higher-curvature terms in the gravitational effective action and that, for sufficiently high-scale Inflation, such corrections can leave characteristic signatures in the tensor spectrum, for instance breaking the usual slow-roll consistency relations.

In this section, for the first time, we generalize the slow-roll consistency relations to include the effects of a coupling of the inflaton field to higher-curvature tensors, in models of inflation with a minimal breaking of conformal symmetry. We point out that higher-curvature tensors can induce large non-linear corrections, characterizing the different signatures in the tensor two-point function that we could test to recognize them. For instance, we prove that an observable violation of the tensor consistency relations due to higher-curvature tensors necessarily implies also a relatively large running of the tensor tilt, enhanced even by some order of magnitude with respect to the standard slow roll hierarchy, see also [Figure II.10](#). Opportunely defying by [Eq. \(II.117\)](#) a new parameter λ that weighs the corrections from higher curvature tensors (with $\lambda = 0$ corresponding to GR and $|\lambda| \gtrsim \mathcal{O}(1)$ in higher-curvature gravity) we exploit the most recent cosmological and astrophysical observations to derive constraints on the inflationary parameters. We infer that large higher-curvature corrections appear to be disfavored by current data ($\lambda = 0.1_{-1.2}^{+2.0}$ at 68%CL), remarkably reducing the room allowed for higher-curvature effects, see also [Figure II.11](#).

HOT RELICS: AXIONS AND NEUTRINOS

In [chapter III](#) we focus on the possibility to use current and future cosmological and astrophysical observations to probe and constrain well motivated extensions of the Standard Model of particle physics that involve spineless axions as a solution of the strong CP problem in Quantum Chromodynamics. In particular, we consider QCD Axions produced in the Early Universe via interactions with other particles of the Standard Model in realistic mixed hot dark matter scenarios that include also massive neutrinos as additional thermal species. Notice that cosmology and astrophysics provide powerful and elegant means to test extension of the Standard Model. For instance, additional thermal species in the Early Universe, behaving as extra dark radiation, may leave several signatures in the different cosmological observables, modifying the damping tail of the CMB temperature angular power spectrum, changing the sound horizon and the Silk damping scale at recombination and the abundances of light elements predicted by the Big Bang Nucleosynthesis by increasing the expansion rate of the universe and leading to a higher freeze-out temperature for weak interactions. Furthermore hot thermal particles beyond the SM suppress structure formation at small scales and therefore astrophysical galaxy clustering measurements turn out to be crucial to reveal the possible presence of additional relics in the form of dark matter. Exploiting the most recent cosmological and astrophysical observations, we derive and discuss the following original results.

- In [section III.II](#), in light of the most recent cosmological and astrophysical observations, we analyze a mixed Hot Dark Matter scenario that includes both axions and massive neutrinos as additional thermal relics. We distinguish between axions decoupled before or after the QCD phase transition. In the former case we analyze the axion–gluon scattering constraining the axion and neutrino masses to $m_a < 7.46$ eV and $\sum m_\nu < 0.114$, both at 95% CL. In the latter case we study the axion–pion scattering and, without assuming any specific model for the axion–pion interactions and remaining in the range of validity of the chiral perturbation theory, we improve our bounds to $m_a < 0.91$ eV and $\sum m_\nu < 0.105$ eV (always at 95% CL). In both cases, the total neutrino mass lies very close to the inverted neutrino mass ordering prediction. If future terrestrial double beta decay and/or long baseline neutrino experiments find that

the nature mass ordering is the inverted one, this could rule out a wide region in the currently allowed thermal axion window. Our results are summarized in [Figure III.3](#) where we show that a significant range of the parameter space can be probed by cosmological data. Furthermore, a future cosmology-independent limit on the axion mass may provide an important test of the cosmological constraint, and can also be translated into a limit on the hot dark matter component in the form of massive neutrinos, strongly supporting multi-messenger searches of axions and neutrino properties.

- In [section III.III](#), for the first time, we study how the declared improvements expected by the next generation cosmic microwave background and baryon acoustic oscillation measurements can be translated into constraining power for well motivated extensions of the Standard Model of particle physics that involve axions thermalized before the QCD phase transition by scatterings with gluons. Assuming a fiducial Λ CDM cosmological model, we simulated future data for CMB-S4-like and DESI-like surveys and analyze a mixed scenario of axion and neutrino hot dark matter. We further account for the effects of these QCD axions on the light element abundances predicted by Big Bang Nucleosynthesis. The most constraining forecasted limits on the hot relic masses are $m_a \lesssim 0.92$ eV and $\sum m_\nu \lesssim 0.12$ eV at 95%CL, showing that future cosmic observations can substantially improve the current bounds, supporting multi-messenger analyses of axion and neutrino properties and possibly opening a window for a combined analysis with primordial light element abundances, see also [Figure III.6](#).

FUTURE DEVELOPMENTS

In future all the methods and techniques underlying this thesis can be employed and further developed to study other non standard realizations of inflation and different extensions of the Standard Model to characterize the different scenarios of the Early Universe that we may be able to test with current and future cosmological and astrophysical observations, using cosmology as a laboratory to test and constrain fundamental physics.

ACKNOWLEDGEMENTS

The first person I would like to sincerely thank is my Supervisor, **ALESSANDRO MELCHIORRI**, for the long collaboration started years ago during my Bachelor Degree and continued both during my Master Degree and my PhD. The importance of all his teachings, suggestions and encouragements along these years goes much beyond the realization of this work. Thank you for always giving me enormous independence in pursuing my research interests and ideas.

The role of **ELEONORA DI VALENTINO** has been equally or even more important for my professional and personal growth. I am immensely grateful to her for the passion put into training me as a scientist and for all the precious help, support and advice. Thanks for always being an important point of reference during these years.

I don't have words to express how much I am grateful to **OLGA MENA** for her inestimable work, incredible precision and immense patience and passion. Even though I was not officially her student, she always mentored me any time I needed help or advice and I learned a lot from her.

A special mention deserves **FABRIZIO RENZI**, a great scientist and friend. Our scientific collaboration is quickly turned into a beautiful friendship and working together has been amazing and fruitful, both on the scientific and human side.

I thank **MASSIMO GUIDI** and **MATTEO FORCONI**, two other PhD students and friends whose work, I'm sure, will contribute to our understanding of the Universe. Thanks Massimo for all our talks that accompanied us along this long journey. Thanks Matteo for your consideration, your work and the precious contribution to this thesis.

I would like to thank all the other people I had the privilege to interact with during these years. Among them, special mentions deserve **ANTONIO RIOTTO** for his valuable teachings and precious suggestions; **SUNNY VAGNOZZI** for his interest in my research line and all his important contributions to it and **LUCA VISINELLI** for his crucial help in our works on axions. All of them importantly contributed to this thesis.

Finally, I would like to sincerely thank **FIORENZA DONATO** and **SABINO MATARRESE** for the prompt and detailed review of my PhD thesis. Their feedback, suggestions and advices importantly improved the quality of this work.

DATA AND SOFTWARE AVAILABILITY

In this thesis I made use of the following python packages that are not explicitly mentioned in the text : SciPy [460] for numerical sampling of the statistical distributions involved in our data analysis, GetDist [461] a tool for the analysis of MCMC samples, Matplotlib [462] for the realization of the plots and NumPy [463] for numerical linear algebra.

All the data underlying this article are publicly available. Further information about the calculations, numerical codes and likelihoods underlying this thesis may be shared upon reasonable request.

WILLIAM GIARÈ,
Rome, December 15, 2021

Appendix A

SUPPLEMENTARY MATERIAL

In this Appendix I provide different secondary results that were always derived and discussed in the works this thesis is based on, Refs [1-7]. While they are not essential to the comprehension of the main discussion, this information is very useful because it enriches the overall presentation through a multitude of different practical examples and detailed calculations. Furthermore, sometimes here I generalize the major results to scenarios beyond the theoretical assumptions under which they were originally derived in the manuscript.

A.1 HIGHER-ORDER SLOW ROLL CONSISTENCY RELATIONS

We briefly review the standard slow roll consistency relations among the higher-order (scalar and tensor) inflationary parameters. Using the parameters (I.233), we can prove a quite general result: in the single field slow roll inflation, if we fix the scalar parameters up to the scalar running $\frac{d^{n-1}n_s}{d(\log k)^{n-1}}$, we immediately fix all the tensor spectral parameters up to the tensor running $\frac{d^n n_t}{d(\log k)^n}$ proving that, for the single field slow roll inflation, one can obtain as many relations as he wants. We recall that the scalar and tensor spectral indices in terms of these parameters read

$$n_s - 1 = \frac{d \log \mathcal{P}_s}{d \log k} = \frac{d \log H^2}{d \log k} - \frac{d \log \epsilon_1}{d \log k} = -2\epsilon_1 - \epsilon_2 \quad (\text{A.1})$$

$$n_T = \frac{d \log \mathcal{P}_t}{d \log k} = \frac{d \log H^2}{d \log k} = -2\epsilon_1 \quad (\text{A.2})$$

It is therefore easy to convince yourself that in the scalar case the first n scalar parameters will be (regular) functions of the first $n + 1$ Hubble parameters:

$$\left\{ \begin{array}{l} n_s - 1 = -2\epsilon_1 - \epsilon_2 \equiv f_1(\epsilon_1, \epsilon_2) \\ \frac{dn_s}{d \log k} \equiv \alpha_s = -2\epsilon_1\epsilon_2 - \epsilon_2\epsilon_3 \equiv f_2(\epsilon_1, \epsilon_2, \epsilon_3) \\ \frac{d^2 n_s}{d(\log k)^2} \equiv \beta_s = -2\epsilon_1\epsilon_2^2 - 2\epsilon_1\epsilon_2\epsilon_3 - \epsilon_2\epsilon_3^2 - \epsilon_2\epsilon_3\epsilon_4 \equiv f_3(\epsilon_1, \epsilon_2, \epsilon_3, \epsilon_4) \\ \dots \\ \frac{d^{n-1}n_s}{d(\log k)^{n-1}} = f_n(\epsilon_1, \dots, \epsilon_{n+1}), \end{array} \right. \quad (\text{A.3})$$

In the tensor case, the first $n + 1$ tensor parameters will be (regular) functions of the first $n + 1$ Hubble parameters:

$$\left\{ \begin{array}{l} n_T = -2\epsilon_1 \equiv g_1(\epsilon_1) \\ \frac{dn_T}{d\log k} \equiv \alpha_T = -2\epsilon_1\epsilon_2 \equiv g_2(\epsilon_1, \epsilon_2) \\ \frac{d^2n_T}{d(\log k)^2} \equiv \beta_T = -2\epsilon_1\epsilon_2^2 - 2\epsilon_1\epsilon_2\epsilon_3 \equiv g_3(\epsilon_1, \epsilon_2, \epsilon_3) \\ \frac{d^3n_T}{d(\log k)^3} = \frac{d\beta_T}{d\log k} = -2\epsilon_1\epsilon_2^3 - 6\epsilon_1\epsilon_2^2\epsilon_3 - 2\epsilon_1\epsilon_2\epsilon_3^2 - 2\epsilon_1\epsilon_2\epsilon_3\epsilon_4 \equiv g_4(\epsilon_1, \epsilon_2, \epsilon_3, \epsilon_4) \\ \dots \\ \frac{d^n n_T}{d(\log k)^n} = g_{n+1}(\epsilon_1, \dots, \epsilon_{n+1}). \end{array} \right. \quad (\text{A.4})$$

Note that the two sets of functions $\{f_1, \dots, f_n\}$ and $\{g_1, \dots, g_n\}$ are introduced only to render explicit the dependency of the scalar and tensor parameters in terms of the Hubble parameters.

Because of the structure of the tensor runnings (A.4), it is easy to reverse the equations in such a way that we can express the Hubble parameters $\{\epsilon_1, \dots, \epsilon_{n+1}\}$ as functions $\{\tilde{g}_1, \dots, \tilde{g}_n\}$ of the tensor parameters $\{n_T, \alpha_T, \beta_T, \dots, \frac{d^n n_T}{d(\log k)^n}\}$:

$$\left\{ \begin{array}{l} \epsilon_1 = -\frac{1}{2}n_T \equiv \tilde{g}_1(n_T) \\ \epsilon_2 = \frac{\alpha_T}{n_T} \equiv \tilde{g}_2(n_T, \alpha_T) \\ \epsilon_3 = \frac{\beta_T}{\alpha_T} - \frac{\alpha_T}{n_T} \equiv \tilde{g}_3(n_T, \alpha_T, \beta_T) \\ \epsilon_4 = \left(\frac{n_T}{n_T\beta_T - \alpha_T^2} \right) \left[\frac{d^3n_T}{d(\log k)^3} + \frac{\alpha_T^3}{n_T^3} - \frac{\alpha_T\beta_T}{n_T} - \frac{\beta_T^2}{\alpha_T} \right] \equiv \tilde{g}_4(n_T, \alpha_T, \beta_T, \frac{d^3n_T}{d(\log k)^3}) \\ \dots \\ \epsilon_{n+1} = \tilde{g}_{n+1}(n_T, \alpha_T, \beta_T, \frac{d^3n_T}{d(\log k)^3}, \dots, \frac{d^n n_T}{d(\log k)^n}). \end{array} \right. \quad (\text{A.5})$$

Substituting in the scalar equations (A.3) we obtain the following n relations among scalar and tensor parameters:

$$\left\{ \begin{array}{l} n_s - 1 = n_T - \frac{\alpha_T}{n_T} \\ \frac{dn_s}{d\log k} \equiv \alpha_s = \alpha_T + \left(\frac{\alpha_T}{n_T} \right)^2 - \frac{\beta_T}{n_T} \\ \frac{d^2n_s}{d(\log k)^2} \equiv \beta_s = \beta_T - 2 \left(\frac{\alpha_T^3}{n_T^3} \right) + 3 \left(\frac{\alpha_T\beta_T}{n_T^2} \right) - \frac{1}{n_T} \left(\frac{d^3n_T}{d(\log k)^3} \right) \\ \dots \\ \frac{d^{n-1}n_s}{d(\log k)^{n-1}} = \tilde{f}_n(n_T, \alpha_T, \beta_T, \frac{d^3n_T}{d(\log k)^3}, \dots, \frac{d^n n_T}{d(\log k)^n}). \end{array} \right. \quad (\text{A.6})$$

Note that here the tilded functions are nothing else than the un-tilded functions up to a variables redefinition. However we also know that, for the single field slow roll inflation, $r = -8n_T$ and so the set of all the $n + 1$ relations is:

$$\left\{ \begin{array}{l} r = -8n_T \\ n_s - 1 = n_T - \frac{\alpha_T}{n_T} \\ \frac{dn_s}{d\log k} \equiv \alpha_s = \alpha_T + \left(\frac{\alpha_T}{n_T} \right)^2 - \frac{\beta_T}{n_T} \\ \frac{d^2n_s}{d(\log k)^2} \equiv \beta_s = \beta_T - 2 \left(\frac{\alpha_T^3}{n_T^3} \right) + 3 \left(\frac{\alpha_T\beta_T}{n_T^2} \right) - \frac{1}{n_T} \left(\frac{d^3n_T}{d(\log k)^3} \right) \\ \dots \\ \frac{d^{n-1}n_s}{d(\log k)^{n-1}} = \tilde{f}_n(n_T, \alpha_T, \beta_T, \frac{d^3n_T}{d(\log k)^3}, \dots, \frac{d^n n_T}{d(\log k)^n}). \end{array} \right. \quad (\text{A.7})$$

Note that if all the left side members of (A.7) (i.e. r and all the n scalar parameters) are fixed, all the $n + 1$ right side tensor parameters are fixed as well. Therefore by the system above, one can calculate how many consistency relations he wants. The first three lines of (A.7) are nothing else than the three consistency relations for the spectral index, its running and its running of running used in SecII.I derived in the previous subsection, while the fourth line is another explicit consistency relation that can be put in the form

$$\frac{d\beta_T}{d \log k} \equiv \gamma_T = n_T (\beta_T - \beta_s) - 2 \left(\frac{\alpha_T^3}{n_T^2} \right) + 3 \left(\frac{\alpha_T \beta_T}{n_T} \right). \quad (\text{A.8})$$

Therefore, in practice, if single field slow-roll inflation is valid, a determination of r and of the first n scalar parameters immediately fixes also the first $n + 1$ tensor parameters. An independent measurement of these tensor parameters can be therefore used for testing the slow-roll condition.

A.2 INFLATION AND SPATIAL CURVATURE

Adopting the same framework and following the same methodology discussed in section III.I, we consider the spatial curvature density parameter Ω_k as an additional free parameter of the model, exploring the possibility of a non trivial background geometry as a consistency check of the standard slow-roll paradigm. Indeed the vast majority of inflationary models predict flatness and constraints on the spatial curvature are an important test of this standard scenario. Here we study two different extensions of the standard cosmological model that both include the curvature parameter Ω_k as an additional free parameter. In particular we first analyze the case $\Lambda\text{CDM} + r + \Omega_k$ and then we add also the running of the scalar tilt, $\Lambda\text{CDM} + r + \alpha_s + \Omega_k$. For both the models, we adopt the common power-law parameterization for the primordial spectra, assuming the usual slow-roll consistency relations to hold. Notice that, since the vast majority of inflationary models predict flatness, the constraints on the spatial curvature provide an important consistency check of this standard scenario [78].

In Table A.1 we summarize the constraints derived for the model $\Lambda\text{CDM} + r + \Omega_k$ and in Figure A.1 we show the 68% and 95% CL marginalized contours for different inflationary parameters in the same model. On the other hand, in Table A.2 we present the results for the $\Lambda\text{CDM} + r + \alpha_s + \Omega_k$ model showing in Figure A.2 the 68% and 95% CL contours.

For the inflationary parameters we see that in both the models, slightly higher values for scalar tilt are preferred with respect to the flat case (with $\Omega_k = 0$). In particular the Planck data gives $n_s = 0.9720 \pm 0.0052$ ($n_s = 0.9728 \pm 0.0052$) when the running α_s is included (excluded). We can also appreciate that these constraints are 1σ shifted towards higher values for the different datasets, including ACTPol+WMAP and SPT3G+WMAP. As concerns the scalar running, the bounds on α_s are consistent with those derived without considering Ω_k , see also Table A.2.

For the tensor amplitude, we see that, ignoring the scalar running, Planck data gives $r < 0.170$ at 95% CL while including α_s this bound is less stringent: $r < 0.250$. Interestingly, for ACTPol+WMAP the upper bound $r < 0.210$ becomes more stringent ($r < 0.185$) including α_s . We also confirm that for the dataset ACTPol+WMAP the preference observed for a non-vanishing scalar running is reduced when the tensor amplitude can freely vary. A strong improvement in the constraining power is clearly obtained including also the B-modes BK15 likelihood and, in fact, including (excluding) the running, the combination Planck+BK15 gives $r < 0.0637$ ($r < 0.0613$). Also in this case the results appear to be stable and consistent with the case in which Ω_k is not varied.

Using the slow-roll consistency relations among the inflationary parameters, we can appreciate how also in this case the parameter space allowed for the tensor spectrum is strongly constrained. On the other hand reversing the slow-roll relations for the scalar and tensor parameters, we can derive constraints on the slow-roll parameters $\{\epsilon_V, \eta_V, \zeta_V^2\}$. Exploiting the Planck+BK15 data, for the $\Lambda\text{CDM} + r + \Omega_k$ model we obtain $\epsilon_V < 0.0038$ and $\eta_V = -0.0094^{+0.0038}_{-0.0049}$ such results remain similar even if we let the scalar running α_s free to vary, in this scenario, however, we have also the result for the slow-roll parameter of the third order: $\zeta_V^2 = 0.0013 \pm 0.0034$. Considering the ACTPol+WMAP and SPT3G+WMAP datasets combination,

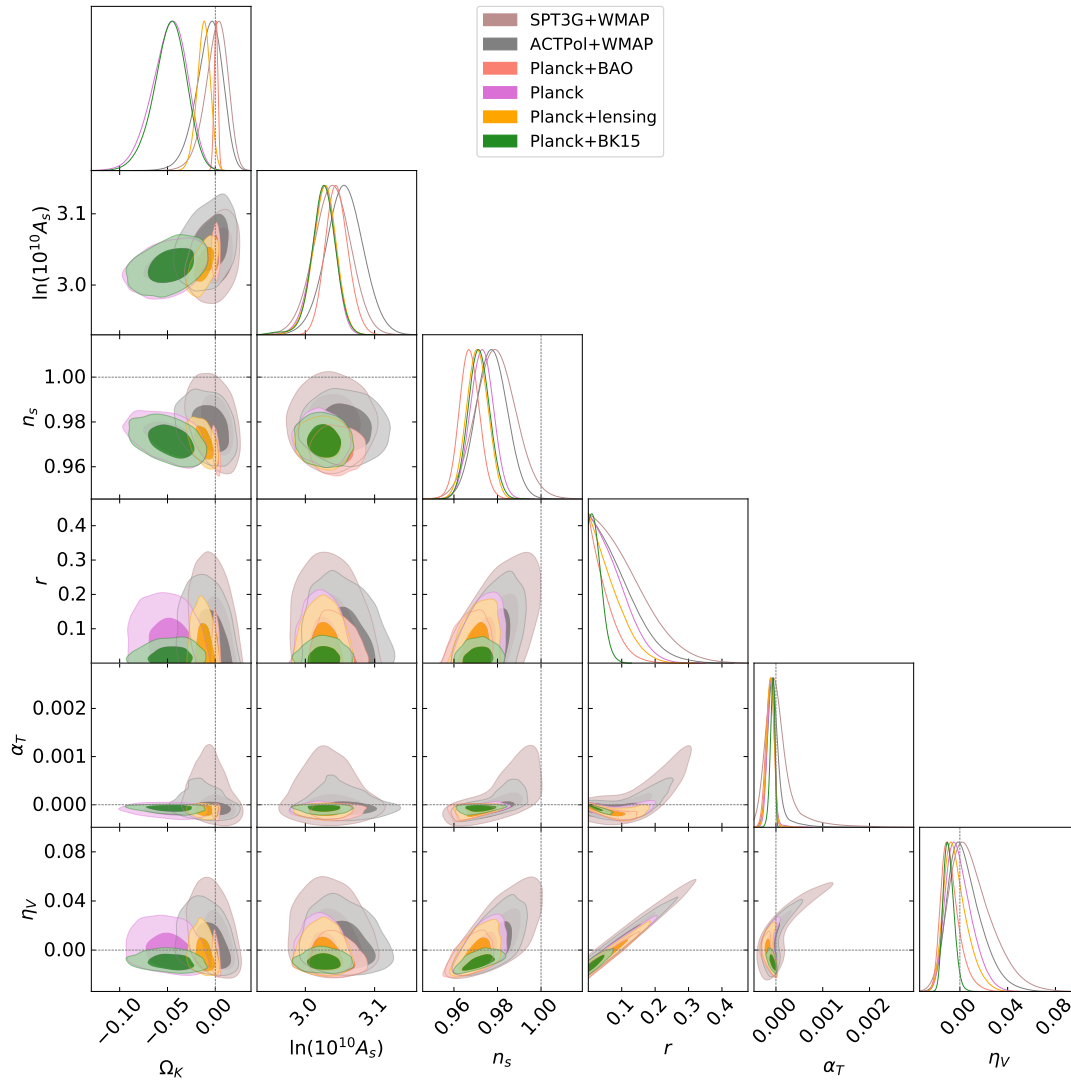


FIGURE A.1: Marginalized 2D and 1D posteriors distributions for the $\Lambda\text{CDM} + r + \Omega_k$ cosmological model obtained for different combinations of the datasets listed in [subsection II.I.I](#). The dashed lines represent the case of vanishing inflationary parameters and flat spacetime geometry.

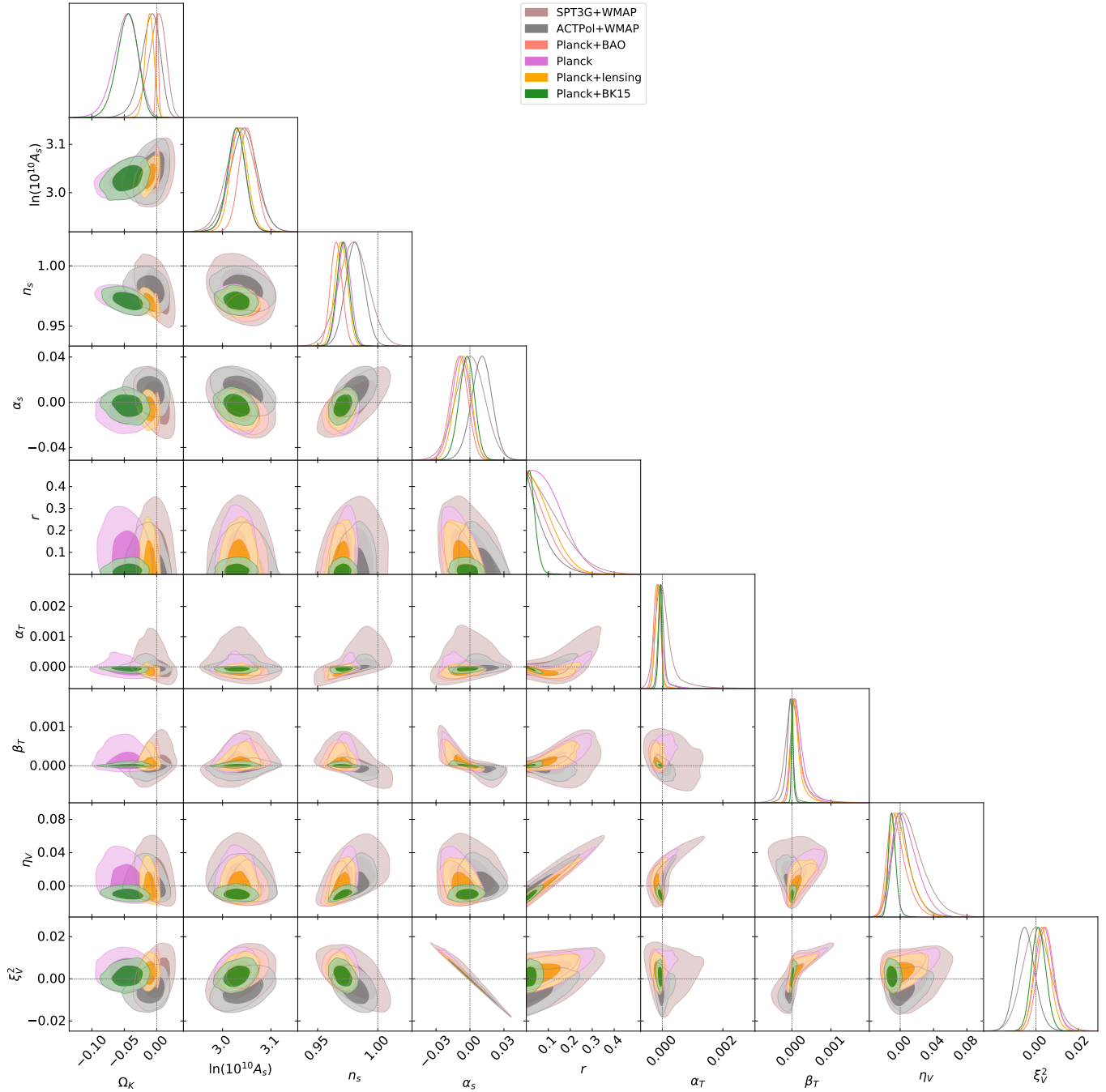


FIGURE A.2: Marginalized 2D and 1D posteriors distributions for the Λ CDM + r + α_s + Ω_k cosmological model obtained for different combinations of the datasets listed in [subsection III.I.I](#). The dashed lines represent the case of vanishing inflationary parameters and flat spacetime geometry.

Parameter	Planck18	Planck18 + lensing	Planck18 + BAO	Planck18 + BK15	ACTPol + WMAP	SPT3G+WMAP
$\Omega_b h^2$	0.02263 ± 0.00018	0.02252 ± 0.00017	0.02241 ± 0.00015	0.02262 ± 0.00017	0.02245 ± 0.00022	0.02273 ± 0.00025
$\Omega_c h^2$	0.1177 ± 0.0016	0.1181 ± 0.0015	0.1196 ± 0.0014	0.1179 ± 0.0015	0.1184 ± 0.0030	0.1141 ± 0.0033
$100 \theta_{MC}$	1.04120 ± 0.00033	1.04110 ± 0.00032	1.04097 ± 0.00031	1.04118 ± 0.00033	1.04181 ± 0.00065	1.03975 ± 0.00070
τ	$0.0480^{+0.0087}_{-0.0072}$	$0.0487^{+0.0085}_{-0.0075}$	0.0554 ± 0.0080	$0.0477^{+0.0086}_{-0.0072}$	0.059 ± 0.013	0.060 ± 0.013
$\log(10^{10} A_s)$	$3.026^{+0.018}_{-0.015}$	$3.027^{+0.018}_{-0.016}$	$3.045^{+0.015}_{-0.017}$	3.026 ± 0.018	3.057 ± 0.027	3.039 ± 0.026
n_s	0.9728 ± 0.0052	0.9707 ± 0.0049	0.9671 ± 0.0046	0.9715 ± 0.0048	0.9773 ± 0.0070	0.9793 ± 0.0091
r	< 0.170	< 0.154	< 0.120	< 0.0613	< 0.210	< 0.259
Ω_k	$-0.048^{+0.020}_{-0.016}$	$-0.0123^{+0.0072}_{-0.0063}$	0.0007 ± 0.0020	$-0.047^{+0.018}_{-0.015}$	$-0.007^{+0.016}_{-0.012}$	$0.0008^{+0.013}_{-0.0097}$
n_T	> -0.0212	> -0.0192	> -0.0150	> -0.0077	> -0.0262	> -0.0324
α_T	$(-10.8 \pm 8.5) \cdot 10^{-5}$	$(-12 \pm 7.8) \cdot 10^{-5}$	$(-12.7^{+9.5}_{-7.3}) \cdot 10^{-5}$	$(-7.5^{+5.6}_{-3.8}) \cdot 10^{-5}$	$(-3.7^{+8}_{-16}) \cdot 10^{-5}$	$(5^{+14}_{-31}) \cdot 10^{-5}$
$\epsilon_V \simeq \epsilon_1$	< 0.0106	< 0.0097	< 0.0075	< 0.0038	< 0.0131	< 0.0162
η_V	$-0.0005^{+0.0081}_{-0.013}$	$-0.0033^{+0.0069}_{-0.012}$	$-0.0079^{+0.0053}_{-0.0091}$	$-0.0094^{+0.0038}_{-0.0049}$	$0.005^{+0.010}_{-0.016}$	$0.0096^{+0.013}_{-0.021}$
ϵ_2	$0.0184^{+0.011}_{-0.0080}$	$0.0217^{+0.0098}_{-0.0070}$	$0.0272^{+0.0081}_{-0.0058}$	0.0252 ± 0.0055	$0.012^{+0.015}_{-0.010}$	$0.007^{+0.019}_{-0.013}$
$V_{inf}^{1/4}$	$< 2.08 \times 10^{16} \text{ GeV}$	$< 2.03 \times 10^{16} \text{ GeV}$	$< 1.90 \times 10^{16} \text{ GeV}$	$< 1.61 \times 10^{16} \text{ GeV}$	$< 2.19 \times 10^{16} \text{ GeV}$	$< 2.31 \times 10^{16} \text{ GeV}$
ΔN_{tot}	$63.55^{+0.30}_{-0.21}$	—	—	$63.31^{+0.31}_{-0.23}$	—	—
$\Delta N(k_{exit})$	$1.55^{+0.30}_{-0.21}$	—	—	$1.31^{+0.31}_{-0.23}$	—	—

TABLE A.1: Results for Λ CDM + r + Ω_k . The constraints on parameters are at 68% CL, while upper bounds are at 95% CL. The internal horizontal line divides the primary parameters of the cosmological model (those we directly sample in our MCMC analysis) from the derived parameters (those we obtain from the others by the relations described in the text).

we find instead both ϵ_V and η_V in agreement with zero within the 68% CL when the scalar running is fixed to zero or free to vary, while it appears 1σ indication for a negative ξ_V^2 for ACTPol+WMAP in the Λ CDM + r + α_s + Ω_k model. Equivalently, we can constrain the parameters $\{\epsilon_i\}$ obtaining $\epsilon_2 = 0.0256 \pm 0.0057$ ($\epsilon_2 = 0.0252 \pm 0.0055$) and $\epsilon_3 = 0.10 \pm 0.29$ when α_s is considered (excluded) for Planck+BK15. This indication for the ϵ_2 parameter different from zero is reduced to more than 1σ for ACTPol+WMAP and disappears for SPT3G+WMAP. We would like to stress that all the results obtained analyzing the Planck 2018 data are in agreement with the ACTPol+WMAP and SPT3G+WMAP data within the 95% CL.

Interestingly, as concerns the spatial curvature, the Planck preference for a closed universe [114, 124, 125, 464] is confirmed in both the scenarios, and slightly enforced when the BK15 data are combined together with Planck Data. Indeed in the extended parameter space of Λ CDM + r + Ω_k we obtain $\Omega_k = -0.048^{+0.020}_{-0.016}$ for Planck and $\Omega_k = -0.047^{+0.018}_{-0.015}$ for Planck+BK15. Considering also the running of the scalar tilt as an additional parameter, the results are essentially unchanged. In any case, Planck and Planck+BK15 data prefer $\Omega_k < 0$ at 2.4σ and 2.6σ , respectively. Anyway, considering the lensing spectrum as measured by the Planck Collaboration the evidence for $\Omega_k \neq 0$ is reduced to less than two standard deviations ($\Omega_k = -0.0123^{+0.0072}_{-0.0063}$ and $\Omega_k = -0.0113 \pm 0.0066$ ignoring and considering α_s , respectively). Finally, we have the indication for a spatially flat universe using also the BAO data ($\Omega_k = 0.0007 \pm 0.0020$, for both the models), but this result should be considered with caution because these measurements are in strong disagreement with Planck when the curvature parameter is free to vary [124, 125, 464], so they cannot in principle be combined together. Similarly, exploiting the data from the Atacama Cosmology Telescope and the South Pole Telescope we do not find any evidence for $\Omega_k \neq 0$, with the constraints reading $\Omega_k = -0.007^{+0.016}_{-0.012}$ ($\Omega_k = -0.010^{+0.017}_{-0.011}$) for ACTPol+WMAP and $\Omega_k = -0.0008^{+0.013}_{-0.0097}$ ($\Omega_k = -0.000^{+0.015}_{-0.011}$) for SPT3G+WMAP when the running is excluded (included). It is important to stress here, that also in these extended scenario including a curvature free to vary the ACTPol+WMAP and SPT3G+WMAP dataset combinations show a tension with respect to the results obtained by Planck, as we can see in Figure A.1 and Figure A.2, always driven by the same effect discussed before. So, albeit the Universe is spatially flat or

Parameter	Planck18	Planck18 + lensing	Planck18 + BAO	Planck18 + BK15	ACTPol + WMAP	SPT3G+WMAP
$\Omega_b h^2$	0.02268 ± 0.00018	0.02255 ± 0.00017	0.02245 ± 0.0016	0.02263 ± 0.00017	0.02236 ± 0.00022	0.02274 ± 0.00024
$\Omega_c h^2$	0.1176 ± 0.0016	0.1182 ± 0.0015	0.1197 ± 0.0015	0.1180 ± 0.0015	0.1171 ± 0.0032	0.1141 ± 0.0038
$100 \theta_{MC}$	1.04121 ± 0.00033	1.04110 ± 0.00032	1.04097 ± 0.00032	1.04118 ± 0.00032	1.04189 ± 0.00067	1.03979 ± 0.00069
τ	0.0491 ± 0.0085	0.0514 ± 0.0083	$0.0573^{+0.0077}_{-0.0086}$	0.0487 ± 0.0086	$0.056^{+0.013}_{-0.012}$	0.060 ± 0.013
$\log(10^{10} A_s)$	3.029 ± 0.018	3.034 ± 0.018	3.052 ± 0.018	3.029 ± 0.018	3.043 ± 0.028	3.038 ± 0.029
n_s	0.9720 ± 0.0052	0.9696 ± 0.0051	0.9655 ± 0.0048	0.9710	0.9810 ± 0.0077	0.980 ± 0.012
α_s	-0.0078 ± 0.0080	$-0.0064^{+0.0078}_{-0.0070}$	-0.0097 ± 0.0076	-0.0029 ± 0.0068	0.0102 ± 0.0090	0.000 ± 0.013
r	< 0.250	< 0.205	< 0.188	< 0.0637	< 0.185	< 0.282
Ω_k	$-0.048^{+0.020}_{-0.016}$	-0.0113 ± 0.0066	0.0007 ± 0.0020	$-0.046^{+0.017}_{-0.014}$	$-0.010^{+0.017}_{-0.011}$	$0.000^{+0.015}_{-0.011}$
n_T	> -0.0312	> -0.0256	> -0.0235	> -0.0080	> -0.0231	> -0.0352
α_T	$(-9.6^{+8.4}_{-15}) \cdot 10^{-5}$	$(-13.6^{+8.8}_{-10}) \cdot 10^{-5}$	$(-17 \pm 11) \cdot 10^{-5}$	$(-7.9^{+6.0}_{-3.9}) \cdot 10^{-5}$	$(-2.5^{+2.7}_{-8.8}) \cdot 10^{-5}$	$(5^{+16}_{-34}) \cdot 10^{-5}$
β_T	$(16^{+11}_{-22}) \cdot 10^{-5}$	$(10.6^{+7.3}_{-16}) \cdot 10^{-5}$	$(13.4^{+8}_{-18}) \cdot 10^{-5}$	$(1.7^{+2.0}_{-3.4}) \cdot 10^{-5}$	$(-5.8^{+9.3}_{-7.3}) \cdot 10^{-5}$	$(6^{+16}_{-25}) \cdot 10^{-5}$
$\epsilon_V \simeq \epsilon_1$	< 0.0156	< 0.0128	< 0.0118	< 0.0040	< 0.0116	< 0.0176
η_V	$0.006^{+0.011}_{-0.018}$	$0.0003^{+0.0089}_{-0.015}$	$-0.0034^{+0.0079}_{-0.014}$	$-0.0095^{+0.0037}_{-0.0049}$	$0.0030^{+0.0079}_{-0.014}$	$0.011^{+0.013}_{-0.021}$
ζ_V^2	$0.0040^{+0.0039}_{-0.0044}$	$0.0031^{+0.0035}_{-0.0040}$	0.0046 ± 0.0038	0.0013 ± 0.0034	-0.0050 ± 0.0046	0.0004 ± 0.0066
ϵ_2	$0.0146^{+0.014}_{-0.0096}$	$0.0201^{+0.012}_{-0.0082}$	$0.0253^{+0.011}_{-0.0074}$	0.0256 ± 0.0057	$0.0107^{+0.013}_{-0.0095}$	$0.006^{+0.019}_{-0.016}$
ϵ_3	—	—	—	0.10 ± 0.29	—	—
$V_{inf}^{1/4}$	$< 2.3 \times 10^{16} \text{ GeV}$	$< 2.2 \times 10^{16} \text{ GeV}$	$< 2.1 \times 10^{16} \text{ GeV}$	$< 1.6 \times 10^{16} \text{ GeV}$	$< 2.12 \times 10^{16} \text{ GeV}$	$< 2.35 \times 10^{16} \text{ GeV}$
ΔN_{tot}	$63.67^{+0.29}_{-0.21}$	—	—	$63.33^{+0.30}_{-0.22}$	—	—
$\Delta N(k_{exit})$	$1.67^{+0.29}_{-0.21}$	—	—	$1.34^{+0.30}_{-0.22}$	—	—

TABLE A.2: Results for $\Lambda\text{CDM} + r + \alpha_s + \Omega_k$. The constraints on parameters are at 68% CL, while upper bounds are at 95% CL. The internal horizontal line divides the primary parameters of the cosmological model (those we directly sample in our MCMC analysis) from the derived parameters (those we obtain from the others by the relations described in the text).

closed is still a very disputed issue, see also [465–470], in what follows we brief discuss about the inflationary dynamics in a curved cosmological spacetime.

inflationary dynamics in a curved Universe

Here we take into account the Planck(+BK15) preference for a closed cosmological spacetime discussed at the end of II.I, investigating the implication of curvature for the slow-roll background dynamics.

Inflation in a curved Universe has been largely discussed in literature, see *e.g.* Refs [471–483]. As a matter of fact, during inflation the spatial curvature is exponentially driven to flatness and so the only way to obtain an inflationary universe with $\Omega_k \neq 0$ is to assume that it inflated only by a finite (small) number of e-folds ΔN_{tot} . Furthermore, in a curved inflationary background, the power-law relations adopted in this work to compute the primordial spectra become disputed at low multipoles $\ell \lesssim 20$ and more reliable parameterizations should be considered [473–476]. Anyway the differences are typically limited to low multipoles and the Planck estimation of cosmological parameters remains robust under the inclusion of positive spatial curvature [474]. In what follows we therefore neglect these corrections and we provide constraints on the e-fold of inflation compatible with Planck(+BK15) preference for a closed Universe. Indeed, in the case of a positive curvature, $\Omega_k < 0$, assuming a slow-roll evolution and a reheating phase

taking place just after the end of inflation ($\rho_{\text{reh}} \simeq V_{\text{inf}}$), the total of e-fold can be estimated as [478, 479]

$$\Delta N_{\text{tot}} \simeq \frac{1}{2} \log \left(\frac{(1 + \delta_0 - \Omega_{\text{rad}}) \mathcal{R} + \Omega_{\text{rad}} \mathcal{R}^2}{\delta_0} \right) \quad (\text{A.9})$$

with $\delta_0 = \Omega_0 - 1$, $\Omega_{\text{rad}} \simeq 4 \times 10^{-5} h^{-2}$ the radiation density parameter today [114] and

$$\log \mathcal{R} \simeq 66 + \log \left(\frac{V_{\text{inf}}^{1/4}}{10^{16} \text{ GeV}} \right). \quad (\text{A.10})$$

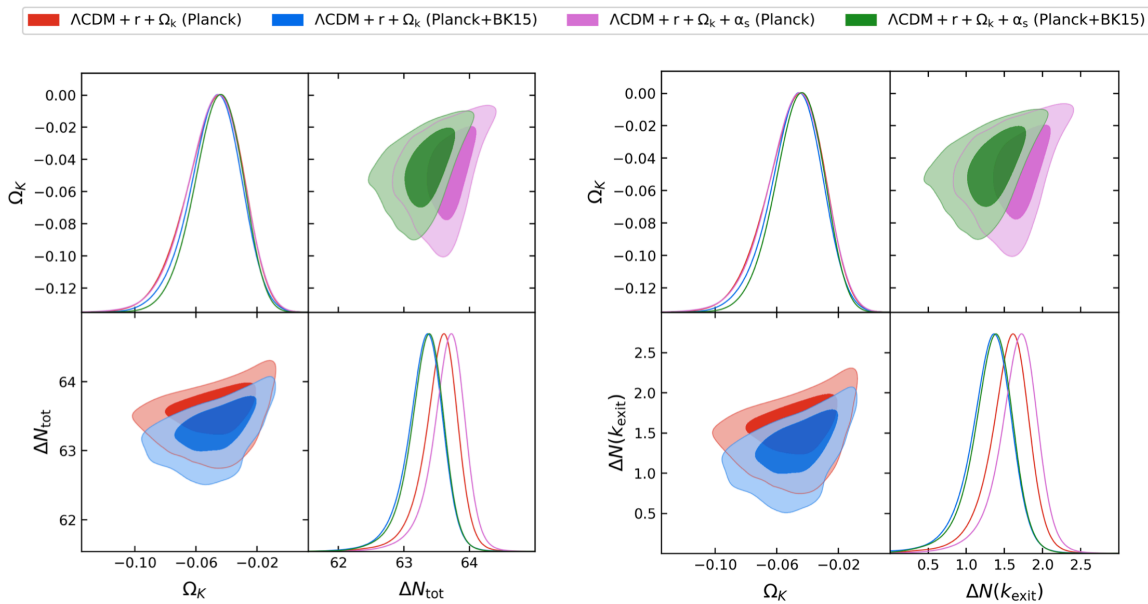


FIGURE A.3: Marginalized 2D and 1D posteriors for the total number of e-fold of inflation ΔN_{tot} in a closed cosmological spacetime (left panel) and for the number of e-fold before the largest observable scale exits the horizon during inflation $\Delta N(k_{\text{exit}})$ (right panel).

In Fig. A.3, we show the 68% and 95% CL marginalized contours for the total number of e-fold of inflation compatible with Planck(+BK15) preference for a closed Universe. Within the $\Lambda\text{CDM} + r + \Omega_k$ model, using only the Planck data, we obtain a maximum number of e-fold $\Delta N_{\text{tot}} = 63.55^{+0.30}_{-0.21}$ at 68% CL while including also the B-modes likelihood, for Planck+BK15 we get $\Delta N_{\text{tot}} = 63.31^{+0.31}_{-0.23}$ at 68% CL. Including the scalar running in the sampling, the results remain almost unchanged, see also Tab A.2 and Fig. A.3. This means that if the Planck(+BK15) evidence for a closed Universe will be confirmed by future measurements, one would need about 63 e-fold of expansion while the total number of e-folds in many physical models of inflation is typically extremely large, *e.g.* in power-law inflation one expects $\Delta N_{\text{tot}} \sim 10^{12}$ [96, 484]. This would strongly constrains the background dynamics before the largest observable scale exit the horizon, with important implications for the observed homogeneity in the Cosmic Microwave Background. Indeed, assuming a standard slow-roll inflation followed by a canonical reheating phase and supposing the Universe to be radiation-dominated from the end of reheating to the matter-radiation equality, the number of e-folds between when the scale k crosses the horizon and the end of inflation can be estimated as [479, 485, 486]

$$N(k) \simeq 128 - \log \mathcal{R} - \log \left(\frac{k}{a_0 H_0} \right) + 2 \log \left(\frac{V_{\text{inf}}^{1/4}}{10^{16} \text{ GeV}} \right) - \log \left(\frac{H_0}{100 \text{ Km/s/Mpc}} \right) + \mathcal{O}(\log(V_k/V_{\text{inf}})) \quad (\text{A.11})$$

where, for a slow-roll dynamics, the effects of assuming $V_k \simeq V_{\text{inf}}$ are expected to be small for the scales of interest. By noting that the CMB roughly probes scales from 10 to 10^4 Mpc, one can estimate the number of e-fold before the largest observable scale in the Universe exits the horizon $\Delta N(k_{\text{exit}}) \simeq \Delta N_{\text{tot}} - N(k_{\text{min}})$. By noting that for the parameter space explored in this work $N(k_{\text{min}}) \simeq 61 - 62$, see also [479], from Planck(+BK15) data it follows that, within the $\Lambda\text{CDM} + r + \Omega_k$ model, $\Delta N(k_{\text{exit}}) = 1.55^{+0.30}_{-0.21}$ ($\Delta N(k_{\text{exit}}) = 1.31^{+0.31}_{-0.23}$), while including also α_s we get $\Delta N(k_{\text{exit}}) = 1.67^{+0.29}_{-0.21}$ ($\Delta N(k_{\text{exit}}) = 1.34^{+0.30}_{-0.22}$), see also Fig. A.3. Although the allowed number of e-fold compatible with the constraints by structure formation (*i.e.*, 50 - 60 e-folds between the horizon exit and the end of inflation [78]) are enough also to solve ‘flatness’ with an accuracy represented by the precision in Ω_k (a fine tuning of about 1% is typically enough [472]), it should be also noted that the main difficulty for a successfully closed inflationary model is represented by homogeneity and isotropy. Indeed, in most of the models proposed in the literature, when the universe does not inflate long enough to become flat, the density perturbations on the horizon scale are typically expected to be much larger than those observed, except for a specific class of models [472].

A.3 EXAMPLES OF SCALE-EFFECTS IN THE PGWS PRODUCTION

To further validate our discussion, in Sec.II.II we study two physical models of inflation. We first analyze the Starobinsky model that, being pure slow roll, by definition predicts an almost scale independent slightly red tilted spectrum. It represents an example of models where higher order corrections are typically negligible also on small scales. However this cannot be true in more elaborated scenarios: as a counterexample we study a model of particle production where non linear corrections lead to a non negligible scale dependence.

Starobinsky Inflation

In this subsection we want to estimate the impact of the scale dependence choosing a specific slow roll model of inflation, namely the Starobinsky model [129] that predicts the following well known relations:

$$n_s - 1 \simeq -\frac{2}{N}, \quad r \simeq \frac{12}{N^2} \quad (\text{A.12})$$

where N is the e-fold number of inflation that we can fix since we measure $n_s \simeq 0.96$ with good precision [78]. The tensor tilt and its runnings read

$$n_T \simeq -\frac{3}{2} \left(\frac{1}{N}\right)^2; \quad \alpha_n^T \simeq -\frac{3}{2}(n+1)! \left(\frac{1}{N}\right)^{n+2} \quad (\text{A.13})$$

The sum expansion that quantifies the scale dependence of the tensor tilt can be easily computed to be

$$\sum_{n=1}^{\infty} \frac{\alpha_n^T(k_*)}{(n+1)!} \left[\log\left(\frac{k}{k_*}\right) \right]^n \simeq n_T \left(\frac{\frac{1}{N} \log\left(\frac{k}{k_*}\right)}{1 - \frac{1}{N} \log\left(\frac{k}{k_*}\right)} \right) \quad (\text{A.14})$$

In Fig. A.4 we plot $\Omega_{\text{GW}}(k)$ from the CMB scales all the way up to the GW scales both including (black solid line) and neglecting (gray dashed line) the runnings. As one can see the runnings lead to negligible corrections also on small scales. This is not surprising since by definitions the slow roll paradigm predicts an almost scale independent slightly red tilt. We actually study this model to provide an example of negligible scale dependence and to show how the situation can be drastically different in more elaborated scenarios as those discussed in the next subsection.

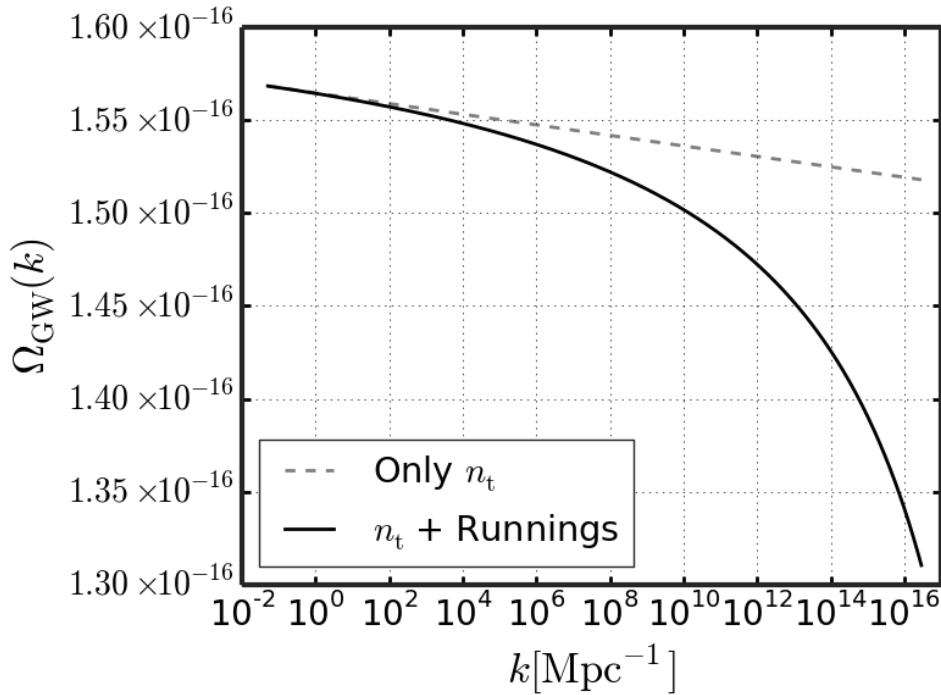


FIGURE A.4: $\Omega_{\text{GW}}(k)$ in the Starobinsky model both including (solid lines) and neglecting (dashed lines) the runnings. The scale dependence is negligible.

Particle Production

In this subsection we want to provide a counterexample studying a different physical model of inflation that employs a pseudo scalar axion naturally coupled to gauge fields. In this model a mechanism of particle production takes place during the rolling inflation and this can be translated into a blue spectrum of gravitational waves. We will show that the tensor tilt can acquire a non trivial scale dependence as well. We start giving a brief description of the model, more details can be found in [163–165, 487–489]. We consider a simple theory of a Pseudo Nambu Goldstone Boson inflation. In this model the inflaton field ϕ and the axion ψ are minimally coupled to gravity and the axion is also coupled with a $U(1)$ gauge field in a way consistent with symmetries¹. The action of the theory is

$$S = \int d^4x \sqrt{-g} \left[\frac{M_p^2}{2} R - \frac{1}{2} (\partial\phi)^2 - V(\phi) - \frac{1}{2} (\partial\psi)^2 - U(\psi) - \frac{1}{4} F^{\mu\nu} F_{\mu\nu} - \frac{\psi}{4f} F_{\mu\nu} \tilde{F}^{\mu\nu} \right] \quad (\text{A.15})$$

$F_{\mu\nu}$ and $\tilde{F}^{\mu\nu} \doteq \frac{1}{2} \epsilon^{\mu\nu\alpha\beta} F_{\alpha\beta}$ are the field-strength tensor of the gauge field and its dual, respectively; f is the axion decay constant while $V(\phi)$ and $U(\psi)$ are the inflation and axion potential. We also assume a flat FRW metric and that both the inflaton and the axion take a homogeneous vacuum expectation value (vev) while the gauge field carries no vev. Under this assumption the equations of motion for the inflaton and the axion are

$$\ddot{\bar{\phi}} + 3H\dot{\bar{\phi}} + V'(\bar{\phi}) = 0 \quad (\text{A.16})$$

$$\ddot{\bar{\psi}} + 3H\dot{\bar{\psi}} + U'(\bar{\psi}) = 0 \quad (\text{A.17})$$

where the prime denotes the derivatives with respect to the argument and the over-dots denote the derivatives with respect to time. We also assume that the contribution of the axion on the background evolution

¹Note that the axion is not the inflaton itself but another distinct field.

is negligible compared to that of the inflaton i.e. $|U| \ll V$ and $\dot{\psi}^2 \ll \dot{\phi}^2$. We introduce the parameter

$$\zeta \equiv \frac{\dot{\psi}}{2Hf} \quad (\text{A.18})$$

that will play a crucial role in our future discussion. We assume ζ to be nearly but not exactly scale independent:

$$\zeta_1 \doteq \frac{d \log \zeta}{d \log k} = \frac{\dot{\zeta}}{\zeta H} \ll 1. \quad (\text{A.19})$$

We instead assume ζ_1 to be constant i.e. $d \log \zeta_1 / d \log k \approx 0$. In our future discussion we restrict our attention to the case $\zeta > 1$ that allows a blue tensor tilt. We are not going to discuss in details the peculiarities of this model such as the gauge quanta production [487] that are reviewed also in [163, 165] and the references within, but for our aim it is sufficient to observe that, in order to avoid a significant back-reaction of the produced gauge quanta to the background dynamics, we have to require that

$$\frac{e^{\pi\zeta}}{\zeta^{5/2}} \ll \frac{13.5}{\sqrt{\epsilon_1 \mathcal{P}_0}} \frac{f}{M_p} \quad (\text{A.20})$$

where $\mathcal{P}_0 = \left(\frac{1}{8\pi^2 M_p^2}\right) \left(\frac{H^2}{\epsilon_1}\right)$ is the primordial scalar spectrum without source (i.e. as predicted by the slow roll inflation). The scalar and tensor spectra for this model are [163, 490, 491]:

$$\mathcal{P}_s \simeq \mathcal{P}_0 \left(1 + c_s \epsilon_1^2 \mathcal{P}_0 \frac{e^{4\pi\zeta}}{\zeta^6}\right) \Big|_{k=k_*} \quad (\text{A.21})$$

$$r \simeq \frac{16 \epsilon_1 \left(1 + c_t \epsilon_1 \mathcal{P}_0 \frac{e^{4\pi\zeta}}{\zeta^6}\right)}{\left(1 + c_s \epsilon_1^2 \mathcal{P}_0 \frac{e^{4\pi\zeta}}{\zeta^6}\right)} \Big|_{k=k_*} \quad (\text{A.22})$$

where $c_s = 2.5 \cdot 10^{-6}$ and $c_t = 3.4 \cdot 10^{-5}$ are constants. We compute the spectral tilts from the relation (A.21) and (A.22) taking the logarithm derivatives:

$$n_s - 1 \doteq \frac{d \log \mathcal{P}_s}{d \log k} \Big|_{k=k_*} = \frac{d \log \mathcal{P}_0}{d \log k} + \frac{c_s}{1 + c_s \epsilon_1^2 \frac{e^{4\pi\zeta}}{\zeta^6}} \frac{d}{d \log k} \left(\epsilon_1^2 \mathcal{P}_0 \frac{e^{4\pi\zeta}}{\zeta^6} \right) \quad (\text{A.23})$$

$$= -2(1 + f_s) \epsilon_1 - (1 - f_s) \epsilon_2 + f_s (4\pi\zeta - 6) \zeta_1 \quad (\text{A.24})$$

$$\simeq -2\epsilon_1 - \epsilon_2 \quad (\text{A.25})$$

and

$$n_T \doteq \frac{d \log \mathcal{P}_t}{d \log k} \Big|_{k=k_*} = \frac{d \log \epsilon_1}{d \log k} + \frac{d \log \mathcal{P}_0}{d \log k} + \frac{c_t}{1 + c_t \epsilon_1 \frac{e^{4\pi\zeta}}{\zeta^6}} \frac{d}{d \log k} \left(\epsilon_1 \mathcal{P}_0 \frac{e^{4\pi\zeta}}{\zeta^6} \right) \quad (\text{A.26})$$

$$= -2(1 + f_t) \epsilon_1 + f_t (4\pi\zeta - 6) \zeta_1 \quad (\text{A.27})$$

where the functions

$$f_s \doteq \frac{c_s \mathcal{P}_0 \epsilon_1^2 \frac{e^{4\pi\zeta}}{\zeta^6}}{1 + c_s \mathcal{P}_0 \epsilon_1^2 \frac{e^{4\pi\zeta}}{\zeta^6}} \ll 1 \quad (\text{A.28})$$

and

$$f_t \doteq \frac{c_t \mathcal{P}_0 \epsilon_1 \frac{e^{4\pi\zeta}}{\zeta^6}}{1 + c_t \mathcal{P}_0 \epsilon_1 \frac{e^{4\pi\zeta}}{\zeta^6}} \quad (\text{A.29})$$

weigh the corrections to the slow roll predictions for the scalar and tensor parameters respectively. In what follows we fix \mathcal{P}_s and n_s to the observed values $\mathcal{P}_s \simeq 2.1 \times 10^{-9}$ and $n_s \simeq 0.96$ [78]. We also fix the tensor to scalar ratio r to reference value $r \simeq 10^{-2}$ and $\zeta_1 \simeq 5 \times 10^{-3} \ll 1$. Note that our results are marginally sensitive to the value of r and ζ_1 and that we are not interested into a parameter analysis for this specific model: our task is simply to show that also in physical models of inflation scale dependence can be non-negligible.

We use the Eqs. (A.21) and (A.22) in order to explicit ϵ_1 and \mathcal{P}_0 as functions of ζ . This means that when ζ changes, $\epsilon_1(\zeta)$ and $\mathcal{P}_0(\zeta)$ change in such a way that \mathcal{P}_s and r remain constant. Moreover because of Eq. (A.27) also n_T is only a function of ζ . Being n_s fixed by observations, we can also use the relation (A.25) in order to find ϵ_2 as a function of ζ so that when ζ changes, $\epsilon_2(\zeta)$ changes leaving n_s fixed to its observed value. So in this model all the inflationary parameters² become known functions of ζ . We plot them in Fig. A.5 letting ζ vary in the range $\zeta \in [1, 7]$.

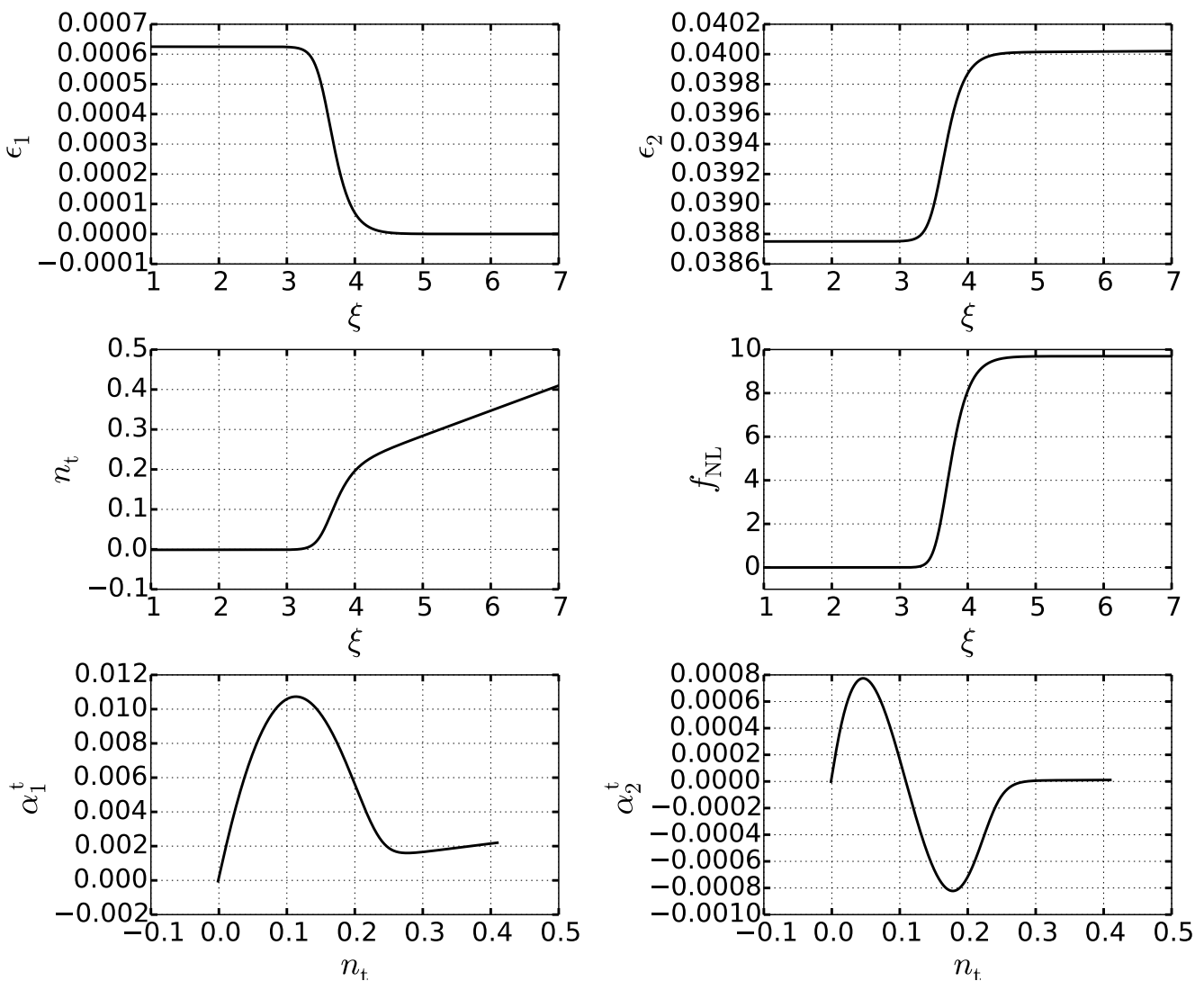


FIGURE A.5: The parameters of the model as functions of ζ .

First of all we want to stress that we have carefully checked that the scalar spectrum (A.21) remains essentially equal to \mathcal{P}_0 (that is what predicted by the single field slow roll inflation). As a matter of fact, if we decompose the scalar spectrum $\mathcal{P}_s = \mathcal{P}_0 + \mathcal{P}_{s,\text{sourced}}$ we find that the sourced term induces corrections

²The inflationary parameters are to be considered evaluated to the pivot scale $k = k_* = 0.05\text{Mpc}^{-1}$ which means that also the parameter ζ in the equations above is computed on the CMB scales $\zeta = \zeta(k = k_*)$.

that are extremely small compared to the vacuum contribution $\mathcal{P}_{s,\text{sourced}} \sim 10^{-4} \mathcal{P}_0$ for all the values of ζ . In other words, the corrections to the scalar spectrum are completely negligible ($f_s \approx 0$), and the scalar parameters are essentially equal to that obtained in the simplest slow roll models. This can be understood by noting that the scalar corrections are suppressed by a factor $\epsilon_1^2 \mathcal{P}_0$ and that ϵ_1 exponentially decreases with ζ in order to keep r fixed, see also Fig. A.5. The fact that the scalar spectrum is essentially indistinguishable from the single field slow roll models is crucial since in this way all the tight constraints on the scalar perturbations (e.g. their high level of gaussianity) are respected as well [490, 492]. On the other hand the corrections to the tensor spectrum can be dominant for an appreciable range of the parameter space, allowing also a blue tensor tilt, see Fig. A.5. The sourced tensor modes could also leave a sizable non-gaussianity of nearly equilateral shape on the CMB anisotropies and polarization. The amount of non-gaussianity is controlled by the parameter f_{NL} estimated as [163, 493]:

$$f_{\text{NL}} \simeq 1.1 \times 10^{-14} \left(\epsilon_1 \frac{e^{2\pi\zeta}}{\zeta^3} \right)^3 \quad (\text{A.30})$$

and its shape given in Fig. A.5, as well. We estimate the scale dependence of the tensor tilt performing a second order computation and deriving the expression for the tensor running $\alpha_1^{\text{T}} \doteq dn_{\text{T}}/d \log k$ and the running of the running $\alpha_2^{\text{T}} \doteq d\alpha_1^{\text{T}}/d \log k$:

$$\alpha_1^{\text{T}} \doteq \left. \frac{dn_{\text{T}}}{d \log k} \right|_{k=k_*} = -2(1+f_t)\epsilon_1\epsilon_2 - 2f_t'\epsilon_1 + f_t'(4\pi\zeta - 6)\zeta_1 + 4\pi f_t\zeta\zeta_1^2 \quad (\text{A.31})$$

$$\alpha_2^{\text{T}} \doteq \left. \frac{d\alpha_1^{\text{T}}}{d \log k} \right|_{k=k_*} = -2(1+f_t)(\epsilon_1\epsilon_2^2 + \epsilon_1\epsilon_2\epsilon_3) - 4f_t'\epsilon_1\epsilon_2 - 2f_t''\epsilon_1 + f_t''(4\pi\zeta - 6)\zeta_1 + 8\pi f_t'\zeta\zeta_1^2 + 4\pi f_t\zeta\zeta_1^3 \quad (\text{A.32})$$

where we have defined:

$$f_t' \doteq \left. \frac{df_t}{d \log k} \right|_{k=k_*} = \left[\frac{-2\epsilon_1 + (4\pi\zeta - 6)\zeta_1}{1 + c_t \mathcal{P}_0 \epsilon_1 \frac{e^{4\pi\zeta}}{\zeta^6}} \right] f_t \quad (\text{A.33})$$

and

$$f_t'' \doteq \left. \frac{df_t'}{d \log k} \right|_{k=k_*} = \left[\frac{-2\epsilon_1 + (4\pi\zeta - 6)\zeta_1}{1 + c_t \mathcal{P}_0 \epsilon_1 \frac{e^{4\pi\zeta}}{\zeta^6}} \right]^2 f_t + \left[\frac{(1 + c_t \mathcal{P}_0 \epsilon_1 \frac{e^{4\pi\zeta}}{\zeta^6})(-2\epsilon_1\epsilon_2 + 4\pi\zeta\zeta_1^2) - c_t \mathcal{P}_0 \epsilon_1 \frac{e^{4\pi\zeta}}{\zeta^6} [-2\epsilon_1 + (4\pi\zeta - 6)\zeta_1]^2}{(1 + c_t \mathcal{P}_0 \epsilon_1 \frac{e^{4\pi\zeta}}{\zeta^6})^2} \right] f_t \quad (\text{A.34})$$

In this model the tensor tilt can acquire a non trivial scale dependence. In fact, depending on the parameters, $d \log n_{\text{T}}/d \log k \simeq 0.1$, see Fig. A.5. As we discussed in Sec. II.II.I, this can lead to non negligible corrections on small scales.

As explained before all these quantities are known functions³ of ζ or equivalently n_{T} . However, since for large values $\zeta \gtrsim 5$ the backreaction becomes typically non negligible as well as the primordial non gaussianity, we decide to restrict our attention to a safer region of the parameter space. We therefore fix $n_{\text{T}} \simeq 0.1$ (or equivalently $\zeta \simeq 3.5$) in such a way that both backreaction and non gaussianity are still under control, see Fig. A.5. In this way the running $\alpha_1^{\text{T}} \simeq 0.01$ and the running of running $\alpha_2^{\text{T}} \simeq 3 \times 10^{-6}$ are fixed as well. We let evolve $\Omega_{\text{GW}}(k)$ from the CMB scales all the way up to the ultra high k probed by the ground based interferometers both including and neglecting α_1^{T} and α_2^{T} , see Fig. A.6. The importance

³Note that we parametrized the slow parameter ϵ_3 appearing in (A.32) as $\epsilon_3 = \gamma \epsilon_2$. Letting γ vary in a range $\gamma \in [-1, 1]$ no significant changes in α_2^{T} are observed. We therefore fixed $\epsilon_3 \simeq 0$.

of scale dependence in this model is evident as Ω_{GW} differs by many orders of magnitude when the non-linear corrections are considered, possibly becoming visible to future gravitational wave experiments such as LISA [339] and Einstein Telescope [340].

While we have shown that the impact of the second order running α_2^{T} is completely negligible, see also Fig.A.6, one may ask if the higher order terms $\alpha_{n>2}^{\text{T}}$ can instead give an appreciable contribution possibly changing the shape of $\Omega_{\text{GW}}(k)$. For our aim it is sufficient to note that being the tensor tilt only a function of ξ , the derivative with respect to the scale can be written as $d/d \log k = (d\xi/d \log k) d/d\xi = (\xi\zeta_1) d/d\xi$ and that the overall factor $\xi\zeta_1 \sim 10^{-2}$ will further suppress the higher order derivatives. We therefore expect such terms to be smaller and smaller at least in this range of the parameters space. We leave the detailed analysis of the sum expansion convergence suitable for future works.

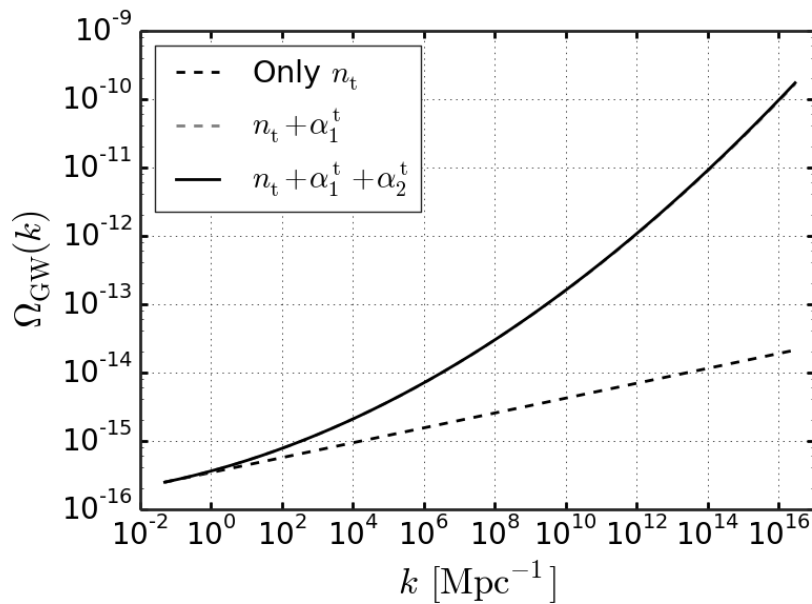


FIGURE A.6: $\Omega_{\text{GW}}(k)$ in the particle production model both including and neglecting the first two runnings. The scale dependence is not negligible.

A.4 A DETAILED DERIVATION OF THE TENSOR SPECTRUM

We review in more details the computation of the primordial tensor spectrum with a non-trivial time dependent tensor speed c_{T} , showing that under the assumptions $|\epsilon_1^{\text{T}}| \ll 1$, the solution of (II.62) is given by Eq. (II.66). First of all, keeping in mind that

$$\frac{d a(t)}{d\tau} \doteq a(t) \frac{da(t)}{dt} = a^2(t) H \quad (\text{A.35})$$

$$\frac{d a^2(t)}{d\tau} = 2 a^3(t) H^2 + \mathcal{O}(\epsilon_1) \quad (\text{A.36})$$

we see that for $z_T(t)$ defined in Eq. (II.61) we have

$$\frac{dz_T(t)}{d\tau} = \frac{M_p}{2} a(t) \frac{d}{dt} \left[a(t) c_T^{-1} \right] \quad (\text{A.37})$$

$$= \frac{M_p}{2} a(t) \left[\dot{a}(t) c_T^{-1} - a(t) \dot{c}_T c_T^{-2} \right] \quad (\text{A.38})$$

$$= \frac{M_p}{2} a(t) \left[a(t) H c_T^{-1} - a(t) H c_T^{-1} \left(\frac{\dot{c}_T}{H c_T} \right) \right] \quad (\text{A.39})$$

$$= \frac{M_p}{2} a(t)^2 H c_T^{-1} \left[1 - \epsilon_1^T \right] \quad (\text{A.40})$$

$$= \frac{M_p}{2} \frac{da(t)}{d\tau} c_T^{-1} \left[1 - \epsilon_1^T \right] \quad (\text{A.41})$$

$$\simeq \frac{M_p}{2} \frac{da(t)}{d\tau} c_T^{-1} \quad (\text{A.42})$$

and

$$\frac{d^2 z_T(t)}{d\tau^2} \simeq \frac{M_p}{2} \left[\frac{d^2 a(t)}{d\tau^2} c_T^{-1} + \frac{da(t)}{d\tau} a(t) \frac{d}{dt} c_T^{-1} \right] \quad (\text{A.43})$$

$$\simeq \frac{M_p}{2} \left[\frac{d^2 a(t)}{d\tau^2} c_T^{-1} - \epsilon_1^T a^3(t) H^2 c_T^{-1} \right] \quad (\text{A.44})$$

$$\simeq \frac{M_p}{2} c_T^{-1} \frac{d^2 a(t)}{d\tau^2} \left[1 - \frac{\epsilon_1^T}{2} \right] \quad (\text{A.45})$$

$$\simeq \frac{M_p}{2} c_T^{-1} \frac{d^2 a(t)}{d\tau^2} \quad (\text{A.46})$$

Therefore the equation of motion (II.62) is equivalent to (II.65) unless corrections of order $|\epsilon_1^T| \ll 1$. Now we want to prove that $u(\tau, \tilde{k})$ given by Eq. (II.66) correctly solves Eq. (II.65). First of all, remembering that $\tilde{k}(t) \doteq c_T(t) k$, it is worth deriving the following relations:

$$\frac{d\tilde{k}}{d\tau} = -\epsilon_1^T \frac{\tilde{k}}{\tau} \quad (\text{A.47})$$

$$\frac{d(\tilde{k}\tau)}{d\tau} = \tilde{k} \left(1 - \epsilon_1^T \right) \simeq \tilde{k} \quad (\text{A.48})$$

$$\frac{d}{d\tau} \left(\frac{e^{-i\tilde{k}\tau}}{\sqrt{2\tilde{k}}} \right) \simeq \frac{e^{-i\tilde{k}\tau}}{\sqrt{2\tilde{k}}} \left[-i\tilde{k} + \frac{1}{4} \frac{\epsilon_1^T}{\tau} \right] \quad (\text{A.49})$$

where in (A.47) we have used that in the de Sitter spacetime $\tau \simeq -(aH)^{-1}$. Now we take the following derivatives:

$$\frac{du}{d\tau} = \frac{e^{-i\tilde{k}\tau}}{\sqrt{2\tilde{k}}} \left[-i\tilde{k} - \frac{1}{\tau} \left(1 - \frac{1}{4} \epsilon_1^T \right) + \frac{i}{\tilde{k}\tau^2} \left(1 - \frac{1}{4} \epsilon_1^T \right) \right] \quad (\text{A.50})$$

$$\simeq \frac{e^{-i\tilde{k}\tau}}{\sqrt{2\tilde{k}}} \left[-i\tilde{k} - \frac{1}{\tau} + \frac{i}{\tilde{k}\tau^2} \right] \quad (\text{A.51})$$

and finally

$$\frac{d^2 u}{d\tau^2} \simeq \frac{e^{-i\tilde{k}\tau}}{\sqrt{2\tilde{k}}} \left[-\tilde{k}^2 + \frac{i\tilde{k}}{\tau} \left(1 + \frac{3}{4}\epsilon_1^T \right) + \frac{2}{\tau^2} \left(1 - \frac{1}{8}\epsilon_1^T \right) - \frac{2i}{\tilde{k}\tau^3} \left(1 - \frac{1}{8}\epsilon_1^T \right) \right] \quad (\text{A.52})$$

$$\simeq \frac{e^{-i\tilde{k}\tau}}{\sqrt{2\tilde{k}}} \left[-\tilde{k}^2 + \frac{i\tilde{k}}{\tau} + \frac{2}{\tau^2} - \frac{2i}{\tilde{k}\tau^3} \right] \quad (\text{A.53})$$

$$\simeq \frac{e^{-i\tilde{k}\tau}}{\sqrt{2\tilde{k}}} \underbrace{\left(1 - \frac{i}{\tilde{k}\tau} \right)}_{u(\tau, \tilde{k})} \left(\frac{2}{\tau^2} - \tilde{k}^2 \right) \quad (\text{A.54})$$

$$\simeq - \left(\tilde{k}^2 - \frac{2}{\tau^2} \right) u(\tau, \tilde{k}) \quad (\text{A.55})$$

that is nothing but Eq. (II.65). Therefore, now that we have proved that (II.66) is the correct solution, the derivation of the primordial spectra is trivial: it is sufficient to follow the standard procedure (see e.g. [76, 83]) with $k \rightarrow \tilde{k}$ that leads us to (II.71).

A.5 BEYOND THE LINEAR ORDER IN THE PROPAGATING SPEED

In Sec II.III we have derived some equations that relate the tensor propagating speed c_T to the inflationary parameters under the assumption that the second-order time derivative $\ddot{c}_T \simeq 0$. In other words, expanding the propagating speed $c_T(t)$ we have taken into account only the linear term. For completeness, we would like to briefly discuss slightly more complicated scenarios in which we consider also the higher-order terms in the Taylor expansion.

Let us see what happens including also the quadratic term \ddot{c}_T : the relation (II.77) is modified as follows

$$\epsilon_2^T \doteq \frac{\dot{\epsilon}_1^T}{H\epsilon_1^T} = \epsilon_1 - \epsilon_1^T + \eta_T \quad (\text{A.56})$$

where we have to introduce the new parameter

$$\eta_T \doteq \frac{\ddot{c}_T}{H\dot{c}_T}. \quad (\text{A.57})$$

Neglecting the third order time derivative $\ddot{\ddot{c}}_T \simeq 0$ we find

$$\frac{d\eta_T}{d\log k} = \frac{1}{H} \frac{d}{dt} \left[\frac{\ddot{c}_T}{H\dot{c}_T} \right] = \eta_T (\epsilon_1 - \eta_T) \quad (\text{A.58})$$

and α_T and β_T now will read

$$\alpha_T = -2\epsilon_1\epsilon_2 - \epsilon_1^T (\epsilon_1 - \epsilon_1^T + \eta_T) \quad (\text{A.59})$$

$$\beta_T = -2\epsilon_1\epsilon_2^2 - 2\epsilon_1\epsilon_2\epsilon_3 - \epsilon_1^T \left[(\epsilon_1 - \epsilon_1^T + \eta_T)^2 + \epsilon_1\epsilon_2 - \epsilon_1^T (\epsilon_1 - \epsilon_1^T + \eta_T) + \eta_T (\epsilon_1 - \eta_T) \right] \quad (\text{A.60})$$

Note that considering the second order derivative of c_T with respect to time provides a correction only to the runnings and not to the spectral tilt that in fact is always given by Eq. (II.70). Moreover even considering the new term η_T a set of consistency relations can always be derived. Indeed reversing (A.59)

$$\eta_T = (\epsilon_1 - \epsilon_1^T) + \frac{\alpha_T + 2\epsilon_1\epsilon_2}{\epsilon_1^T} \quad (\text{A.61})$$

and using the Eqs. (II.79), (II.80), (II.81), (II.82) and (A.61), it is easy to see that Eq. (A.60) still provides a consistency relation for the propagating speed c_T and the inflationary parameters. However in this case the relation will be cubic in the slow roll parameters and will involve also the scalar running α_s and the tensor running of running β_T that are not involved in the respective quadratic relation in the slow roll parameter (II.83) derived under the linear order expansion of c_T .

This procedure can be generalized at any order: if we expand $c_T(t)$ taking all the terms up to the order n and assuming that $\left(\frac{d}{dt}\right)^{n+1} c_T \simeq 0$, we can always find a consistency relation between c_T and the inflationary parameters. This relation will include the scalar runnings up to α_{n-1}^S and the tensor runnings up to α_n^T .

Clearly, to test the time dependence of c_T beyond the linear expansion, we need an accuracy that we do not have at present. We conclude that the choice to adopt the simply linear approximation for $c_T(t)$ is reasonable because it allows us to test its time dependence without complicating the equations or introducing higher-order parameters that will be difficult to constrain with the current cosmological data.

A.6 SUPERLUMINAL GRAVITY PROPAGATION DURING INFLATION

In Sec. II.III, we have restricted our attention to the parameter space $c_T < 1$ excluding the superluminal propagation from the MCMC sampling. One may ask if such an artificial exclusion leads to a biased conclusion and, in general, what happens including superluminal velocities. In this appendix we want to clarify some aspects about superluminal velocities and motivate our decision to impose a prior $c_T < 1$ in our MCMC sampling.

First of all we want to stress that we have carefully checked that our constraints were not biased by our choice of not exploring superluminal velocities. As a matter of fact, the constraints on c_T are almost uncorrelated with the constraints on the other parameters and, even extending our MCMC prior to $c_T > 1$, we will end up with almost the same results, see Fig. A.7.

We also would like to point out that our theoretical framework holds for both subluminal and superluminal velocities indifferently and that we excluded the superluminal propagation only in our MCMC analysis. This is crucial since, from a theoretical point of view, imposing subluminal propagation is not as safe an assumption as one may think. In fact, as shown in [336, 337], depending on the model, it can be possible to perform a change of frame so that in the new frame the tensor speed is c , but the speed of the other massless particles is greater than c ending up with a situation where we have actually constrained the speed of normal species to be superluminal, in tension with causality.

However we decided to exclude superluminal velocities from our MCMC analysis for the following reason: as one can see from Eq. (II.73), superluminal velocities will suppress the amplitude of tensor perturbations leading to a completely different phenomenology with respect to subluminal velocities. In fact when $c_T < 1$ the amplitude of the tensor spectrum grows, eventually becoming greater than the Planck experimental error and allowing us to provide a well defined lower bound on the tensor speed. Conversely when $c_T > 1$ the amplitude of the tensor spectrum decreases and the effect of c_T on the primordial spectrum is buried in the experimental error, preventing us from achieving a well defined upper bound. In other words when the MCMC prior on c_T is extended to superluminal velocities, since the Planck data prefer a vanishing r , the posterior distribution of the propagating speed is pushed to $c_T \gg 1$ and the upper bound on c_T is completely dominated by the *a-priori* imposed prior, see Fig. A.7.

Furthermore when the prior on the tensor speed is extended to $c_T > 1$ most of the area of the posterior distribution is found for values of c_T close to the upper limit of the prior. Specifically enlarging the prior on c_T by a factor of 5 we now get a lower limit $c_T > 0.92c$ (pushed forward by the same amount with respect to the subluminal case).

This is clearly a biased result which stems from the fact that we are unable to place an upper bound on the propagating tensor speed with the theoretical framework presented in the work. The reason behind this is that the MCMC samples accumulate at the higher edge of the imposed range for c_T leading to exclude

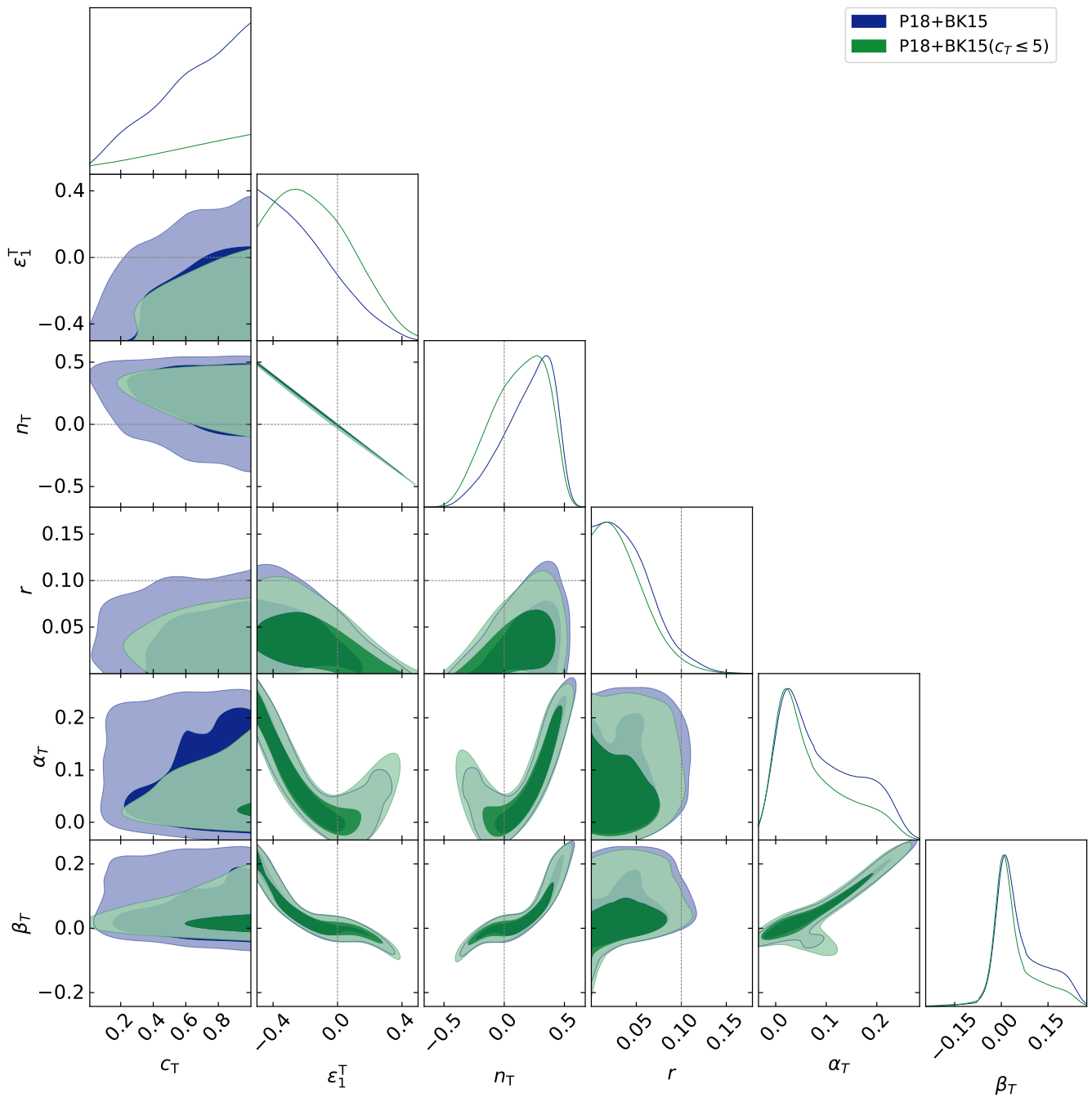


FIGURE A.7: Marginalized 2D and 1D posteriors for the combination of Planck 2018 [113, 115] and Biceps/Keck 2015 [162] data for the parameters of the tensor spectrum. The blue contours are those obtained exploring only subluminal velocities while the green contours are obtained extending the prior to superluminal velocities $c_T < 5$. As one can see the choice of exploring only subluminal velocities does not lead to significant bias on the inflationary parameters. Nevertheless, once the superluminal velocities are considered, since the Planck data prefer a vanishing tensor amplitude, the posterior of c_T is pushed to $c_T \gg 1$ leading to a prior dependent upper (and lower) bound.

values of c_T much smaller than the upper limit at more than two standard deviation resulting in a biased lower bound for the tensor speed. Note that this example is merely to show that even pushing the prior on c_T to $c_T \gg 1$ only the posterior of the tensor speed is affected while all other parameters are almost unaffected.

It is also worth noting that to correctly analyze the region $c_T > 1$, along with the consistency relation we found, one has to consider also the different phenomenology induced by superluminal propagation. For example a tensor speed different from unity will generate non-gaussian features in the primordial perturbations $f_{\text{NL}} \sim 1 - c_T^2$ [272, 278]. Of course this (and other) information can be used to place an upper bound on $c_T > 1$, but constraining the superluminal part of c_T goes outside the aim of this work since here we are mainly interested in constraining the shape and amplitude of the tensor spectrum in non-standard theories of inflation with a scale dependent propagating speed. We plan to tackle down the issue of superluminal velocities in a subsequent work.

A.7 MATCHING SMALL-SCALES CONSTRAINTS ON THE TENSOR SPEED

Even if the main goal of Sec. II.III was to constrain the shape and the amplitude of the tensor two-point function in a non trivial theory of inflation, in Sec. II.III.II we have derived constraints on the propagating speed c_T that clearly refer to its value on the CMB scales, with Eqs. (II.71) and (II.72) evaluated at the horizon crossing. In this appendix, we want to discuss the accordance between our results and the current measurement $c_T \simeq c$ provided by gravitational experiments. Let us stress that the current observed value $c_T \sim c$ refers to the propagating speed of the astrophysical gravitational waves measured by the gravitational detectors on astrophysical scales $k \sim k_{\text{LV}}$ and not to the propagating speed of primordial tensor perturbations that are instead generated during the inflationary epoch at energies that can be extremely larger. We have several observational pieces of evidence that Einstein's theory of general relativity works appropriately on the astrophysical energy scales, but theoretical arguments suggest that it may need to be modified at high energies and some well motivated extended theories predict a non unitary propagating speed [94, 219, 221–225, 236–242, 253–263]. In our work we have used an effective field theory approach (that, by definition, provides an approximate description of an underlying physical theory at a specific energy scale) to show that if the inflationary energy scale is sufficiently high, high-energy deviations from GR could leave signatures during the inflationary epoch and primordial tensor perturbations could provide a unique observational window to probe gravity at those energy scales. However, in a consistent theory of gravity, GR has to emerge in the low energies limit in such a way that all the observational evidences for GR (including the observed value $c_T \sim c$ on the astrophysical scales) can remain consistent through the evolution of the universe. Therefore it is worth showing that, our constraints on $c_T(k_*)$ are not in conflict with those derived by gravitational detectors.

Considering the expansion of $\log c_T(k)$ we can write

$$c_T(k) = c_T(k_*) \left(\frac{k}{k_*} \right)^{\gamma(k)} \quad (\text{A.62})$$

where

$$\gamma(k) = \sum_{n=0}^{\infty} \left[\left(\frac{d}{d \log k} \right)^n \epsilon_1^{\text{T}} \right]_{k=k_*} \frac{\log^n \left(\frac{k}{k_*} \right)}{(n+1)!} \quad (\text{A.63})$$

Because of the discussion provided in sec II.III.II, we can estimate the derivatives of ϵ_1^{T} as

$$\left(\frac{d}{d \log k} \right)^n \epsilon_1^{\text{T}} = (-1)^n n! \left(\epsilon_1^{\text{T}} \right)^{n+1} \quad (\text{A.64})$$

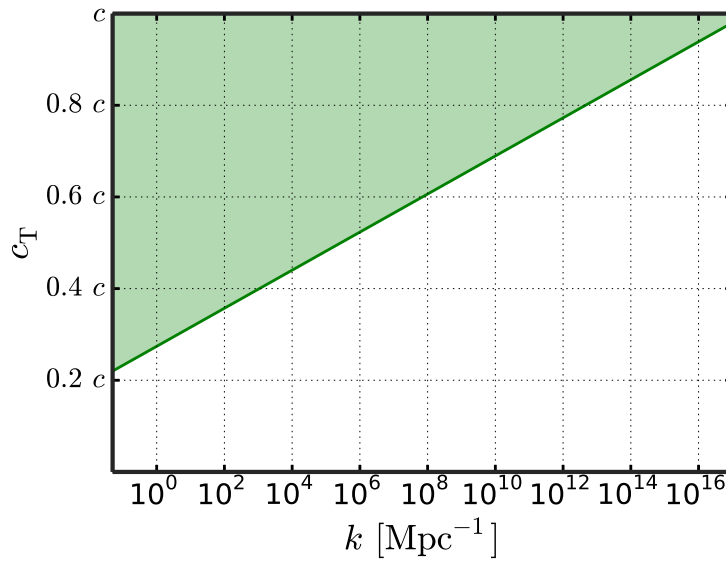


FIGURE A.8: Constraints on the propagating speed c_T at the generic scale k extrapolated from the constraints on the CMB scales fixing $\epsilon_1^T = 0.082$ and $c_T(k_*) > 0.2$. Remarkably on the LIGO/VIRGO scales we can extrapolate the lower limit $c_T(k_{LV}) \gtrsim 0.94$, in perfect agreement with the constraints on the astrophysics GWs.

that gives for γ

$$\gamma = -\epsilon_1^T \frac{\log(1 - f(k))}{f(k)} \tag{A.65}$$

where $f(k) = -\epsilon_1^T \log(k/k_*)$. As one can see, the value of the propagating speed at the generic scale k depends on both $c_T(k_*)$ and ϵ_1^T . Interestingly, using the value derived for $\epsilon_1^T \simeq 0.082$, the lower bound for $c_T \gtrsim 0.22$ on the CMB scale is translated into the constraints plotted in Fig. A.8 at the generic scale k . Even on ultra-high k the power law expansion (II.115) provides reasonable values remarkably close to $c_T = c$. In particular on the LIGO/VIRGO scales we have $c_T(k_{LV}) \gtrsim 0.94c$ that is in very good agreement with the constraints on the propagating speed of gravitational waves derived on astrophysical scales [214–216]. We therefore conclude that our results are not in conflict with those of gravitational experiments.

A.8 INFLATON-WEYL COUPLING FUNCTION

In Sec II.IV, we studied the higher-curvature corrections to the inflationary parameters considering a coupling between the Weyl tensor and the Inflaton of the form $df(\phi)/d\phi \sim \pm 1/\Lambda$, assuming negligible the higher-order derivatives: $d^n f(\phi)/d\phi^n \simeq 0$. In this appendix we want to generalize our computation for a generic function $f(\phi)$. Introducing the dimensionless parameters

$$\lambda_n \doteq (\sqrt{2}M_p)^n \left(\frac{H^2}{M^2}\right) \left(\frac{d}{d\phi}\right)^n f(\phi) \tag{A.66}$$

that generalize Eq. (II.117) with $\lambda_1 \equiv \lambda$, we see that Eq. (II.118) is generalized to

$$\frac{d\lambda_n}{d \log k} = -2\lambda_n \epsilon_1 + \lambda_{n+1} \epsilon_1^{1/2} \tag{A.67}$$

$$= -\frac{1}{8} \lambda_n r + \frac{1}{4} \lambda_{n+1} r^{1/2} \tag{A.68}$$

So for a generic function $f(\phi)$, while the tensor tilt $n_T = -2\epsilon_1 - \epsilon_T$ is always given by Eq. (II.116), the tensor running becomes

$$\alpha_T = \alpha_T^{\text{SR}} + \left[-\frac{3\lambda_1}{16} r^{3/2} - \frac{\lambda_1}{2} r^{1/2}(n_S - 1) + \frac{\lambda_2}{4} r \right]. \quad (\text{A.69})$$

It differs from Eq. (II.119) by a further term $(\lambda_2/4)r$ that can give appreciable contribution only if $|\lambda_2| \simeq |\lambda_1|$. Because of Eq. (A.66), this means a coupling function of the form $f(\phi) \propto e^{\pm\phi/M_p}$. However in this case we have a further enhancement of the running of tensor tilt, see also Fig. A.9. This scenario is even more disfavored by our results that instead show a preference for small running, as we discussed in Sec. II.IV.II.

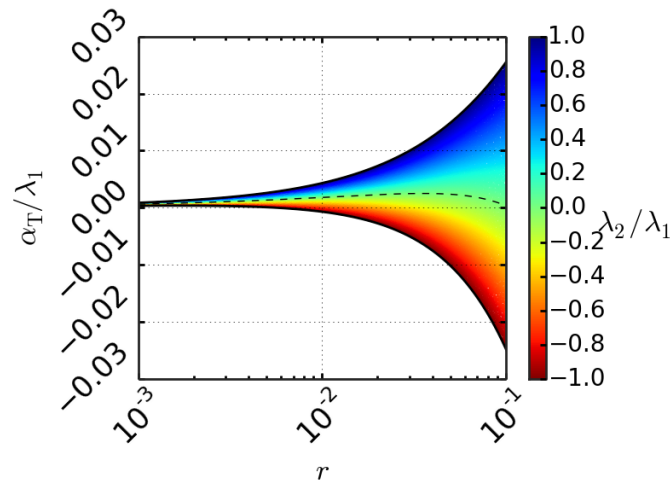


FIGURE A.9: Tensor running for a generic coupling $f(\phi)$. The dashed line represents the model adopted in Sec II.IV.

Appendix B

AXION COLD DARK MATTER

Here we focus on non-thermally produced axions, natural candidates for the cold dark matter component of the Universe. We give an overview of non thermal axion production, studying the evolution of the cosmological Axion field from the moment when the $U(1)_{PQ}$ is spontaneously broken during the PQ phase transition to the moment when axions acquire mass during the QCD phase transition. As we will see, the phenomenology of non thermal axions is maybe larger than that of thermal axions since a lot of non standard scenarios may happen such as the formation of topological defects like cosmic strings or domain walls.

VACUUM REALIGNMENT

The equation of motion of the axion field ϕ_A can be derived assuming in the early universe the usual F.R.W. flat metric

$$ds^2 = -dt^2 + a^2(t)\delta_{ij}dx_i dx_j \quad (B.1)$$

and assuming that the axion field is minimal coupled to gravity. So we write the action:

$$S = \int d^4x \sqrt{-g} \left[\frac{\bar{M}_p^2}{2} R + \frac{1}{2} g^{\mu\nu} \partial_\mu \phi_A \partial_\nu \phi_A - V_A(\phi_A) \right]. \quad (B.2)$$

Minimizing the action with respect to the Axion field ϕ_A we can find the equation of motion that reads:

$$\left[\partial_t^2 + 3H\partial_t - \frac{1}{a^2} \nabla_x^2 \right] \phi_A(x) + V'_A[\phi_A(x)] = 0 \quad (B.3)$$

where prime indicates a derivative with respect to ϕ_A and where V_A is the effective periodic potential for the axion field that, accounting for non-perturbative QCD effects associated with instantons, can be qualitatively written as

$$V_A = f_A^2 m_A^2(t) \left[1 - \cos\left(\frac{\phi_A}{f_A}\right) \right] \quad (B.4)$$

The axion mass is a function of temperature and hence of time: $m_A(t) = m_A[T(t)]$. High temperature effects ($T \approx 1$ GeV) of QCD instantons give [362, 378–380]:

$$m_A(T) \simeq 4 \times 10^{-9} \text{eV} \left(\frac{10^{12} \text{GeV}}{f_A} \right) \left(\frac{\text{GeV}}{T} \right)^4 \quad (B.5)$$

The axion mass is strongly suppressed at temperatures that are large compared to the QCD scale, but it turns on when the temperature approaches Λ_{QCD} . In practice, the axion mass becomes important when

$m_A(t) \propto t$, so it is useful to define a time t_* at which the axion mass turns on¹:

$$m_A(t_*)t_* = 1 \quad (\text{B.6})$$

Putting the potential (B.4) into the equation of motion (B.3) we obtain:

$$\left[\partial_t^2 + 3H\partial_t - \frac{1}{a^2} \nabla_x^2 \right] \phi_A(x) + m_A^2(t) f_A \sin\left(\frac{\phi_A(x)}{f_A}\right) = 0 \quad (\text{B.7})$$

On the other hand, minimizing the action with respect to the metric tensor we can find the well known relations for the axion energy density and pressure that are:

$$\rho_A = \frac{1}{2} \dot{\phi}_A^2 + V_A \quad (\text{B.8})$$

$$p_A = \frac{1}{2} \dot{\phi}_A^2 - V_A \quad (\text{B.9})$$

and so:

$$\omega_A \equiv \frac{p_A}{\rho_A} = \frac{\frac{1}{2} \dot{\phi}_A^2 - V_A}{\frac{1}{2} \dot{\phi}_A^2 + V_A} \quad (\text{B.10})$$

The axion field evolves according to equation (B.7). So once we have solved it and computed $\phi_A(x)$ we can also predict the axion energy density and pressure from the equations (B.8) and (B.10). However we need to specify the axion field initial condition that are completely random. Moreover causal disconnected region of spacetime in general have uncorrelated values of $\phi_A(x)$. Nevertheless it is well known that the size of the causal horizon grows exponentially during inflation and so it can homogenize the axion field over enormous distances. Therefore, before solving equation (B.7), we have to distinguish two different cases. Let us call T_{RH} the temperature of the reheating after the inflation, if:

1. $T_{\text{PQ}} > T_{\text{RH}}$ so the inflation occurs after the PQ symmetry breaking and the axion field is homogenized over enormous distances.
2. $T_{\text{PQ}} < T_{\text{RH}}$ so the inflation occurs before the PQ symmetry breaking and the axion field has non-zero modes and carries topological defects such as strings and domain walls.

The first possibility, inflation occurring after the PQ symmetry breaking, is of course the simplest since in this way we do not have to worry about the topological defects production and the axion field is homogenized over large distances. However in what follows we will study both the situations.

Case 1: $T_{\text{PQ}} > T_{\text{RH}}$

Focus our attention on the first case $T_{\text{PQ}} > T_{\text{RH}}$. Inflation homogenizes the axion field over very large distances and so we can assume that the axion field does not depend on the space coordinate \bar{x} so that the equation of motion (B.7) becomes:

$$\left[\frac{d^2}{dt^2} + \frac{3}{2t} \frac{d}{dt} \right] \phi_A(t) + m_A^2(t) f_A \sin\left(\frac{\phi_A(t)}{f_A}\right) = 0 \quad (\text{B.11})$$

where we have used $H = \frac{1}{2t}$. Because of our previous discussion about the time (or temperature) dependence of the axion mass $m_A(t)$, we are allowed to distinguish two different regimes $t \ll t_*$ when the axion mass can be neglected and $t \gtrsim t_*$ when the axion mass turns on.

¹for $T \approx 1 \text{ GeV}$, $t_* \simeq 2 \times 10^{-7} \text{ s} \left(\frac{f_a}{10^{12} \text{ GeV}} \right)^{1/3}$

In the regime $t \ll t_*$ we can neglect the axion mass $m_A(t \ll t_*) \approx 0$ and the equation to solve becomes:

$$\left[\frac{d^2}{dt^2} + \frac{3}{2t} \frac{d}{dt} \right] \phi_A(t) = 0 \quad (\text{B.12})$$

We immediately see that the most general solution is

$$\phi_A(t) = \phi_0 + \phi_1 t^{-\frac{1}{2}} \quad (\text{B.13})$$

where ϕ_0 and ϕ_1 are constants. Therefore the expansion of the universe (in a Radiation dominated era $a(t) \propto t^{\frac{1}{2}}$) freezes the axion field to a constant value. Therefore the axion field is overdamped and frozen at its initial value by Hubble friction. The equation of state at early times is so $\omega_A = -1$ and the axion behaves as a contribution to the vacuum energy: if axions were able to dominate the energy density of the universe when still overdamped with equation of state $\omega < -\frac{1}{3}$, they could even drive a period of accelerated expansion.

When t approaches t_* , the axion field starts oscillating because of the axion mass contribution. Let us suppose that $\phi_A(t) \ll f_A$ so that we can expand $f_A \sin\left(\frac{\phi_A(t)}{f_A}\right) \approx \phi_A(t)$ in the equation of motion that so becomes:

$$\left[\frac{d^2}{dt^2} + \frac{3}{2t} \frac{d}{dt} \right] \phi_A(t) + m_A^2(t) \phi_A(t) \quad (\text{B.14})$$

It is useful to study this equation performing the following substitution:

$$\chi(t) = t^{\frac{3}{4}} \phi(t) \quad (\text{B.15})$$

So that the equation of motion becomes:

$$\left[\frac{d^2}{dt^2} + \omega^2(t) \right] \chi(t) = 0, \quad (\text{B.16})$$

where

$$\omega^2(t) = m_A^2(t) + \frac{3}{16t^2}. \quad (\text{B.17})$$

In other words for $t \gtrsim t_*$ the axion field is oscillating with frequency $\omega \approx m_A$. The solution of equation (B.16) is therefore given by:

$$\chi(t) \simeq \frac{C}{\sqrt{m_A(t)}} \cos \left[\int_t dt' \omega(t') \right] \quad (\text{B.18})$$

where $C = \text{const}$. For $\phi_A(t)$ this translates into

$$\phi_A(t) = \phi_0(t) \cos \left[\int_t dt' \omega(t') \right] \quad (\text{B.19})$$

with

$$\phi_0(t) = \frac{C t^{-\frac{3}{4}}}{\sqrt{m_A(t)}} \quad (\text{B.20})$$

Putting the solution (B.19) into equation (B.8) one can check that

$$\rho_A \propto m_A(t)^2 \phi_0(t)^2 \propto t^{-\frac{3}{2}} \quad (\text{B.21})$$

remembering that $a(t) \propto t^{-\frac{1}{2}}$, we finally obtain the following very important result:

$$\rho_A \propto a(t)^{-3}. \quad (\text{B.22})$$

This is the same behavior of ordinary matter, and this is why misalignment axions are a valid candidate for the cold dark matter. We can also estimate the late time number density of axions by saying that the axion field has a random initial value $\phi_A(t_*) = f_A \theta_*$ where θ_* is said initial misalignment angle and it evolves according to the equation of motion

$$\ddot{\theta}_* + 3H\dot{\theta}_* + m_A(t)^2\theta_* \quad (\text{B.23})$$

Since the potential is periodic with period $2\pi f_A$, the relevant range of θ_* is $[-\pi, \pi]$. The number density of axion at time t_* is given by [378–380]

$$n_A^{\text{vac}}(t_*) \sim \frac{1}{2} m_A(t_*) \phi_A^2(t_*) = \frac{f_A^2}{2t_*} \theta_*^2 \quad (\text{B.24})$$

The number of axions is an adiabatic invariant after t_* and so, since they behave like matter, their number density at any given time $t > t_*$ is:

$$n_A^{\text{vac}}(t) \sim \frac{f_A^2}{2t_*} \theta_*^2 \left(\frac{a(t_*)}{a(t)} \right)^3 \quad (\text{B.25})$$

and so, today ($t = t_0$):

$$n_A^{\text{vac}}(t_0) \sim \frac{f_A^2}{2t_*} \theta_*^2 \left(\frac{a(t_*)}{a(t_0)} \right)^3 \quad (\text{B.26})$$

Note that from the axion number density we can obtain the axion energy density simply multiplying for their mass:

$$\rho_A^{\text{vac}}(t) \sim \frac{m_A f_A^2}{2t_*} \theta_*^2 \left(\frac{a(t_*)}{a(t)} \right)^3 \quad (\text{B.27})$$

This mechanism of axion production is called *vacuum realignment* or also *misalignment mechanism*.

Case 2: $T_{\text{PQ}} < T_{\text{RH}}$

So far we have studied in details the case when inflation homogenizes the axion field over large distances. Now we want to study the vacuum realignment in the case in which no inflation occurs and the value of the field depends on the spatial coordinates and the equation to solve is the eq. (B.7). As we will see the only difference with the previous case is a contribution coming from the non zero momentum modes.

Let us start considering the regime $t \ll t_*$ when the axion mass is suppressed. In this case it is convenient to expand the axion field in the Fourier space

$$\phi_A(\mathbf{x}, t) = \int d^3\mathbf{k} \tilde{\phi}_A(\mathbf{k}, t) e^{i\mathbf{k}\cdot\mathbf{x}} \quad (\text{B.28})$$

where the Fourier modes $\phi(\mathbf{k}, t)$ satisfy the equation of motion in the Fourier space that reads:

$$\left(\partial_t^2 + \frac{3}{2t} \partial_t + \frac{k^2}{a(t)^2} \right) \tilde{\phi}_A(\mathbf{k}, t) = 0. \quad (\text{B.29})$$

As well known, in an expanding universe, the wavelength $\lambda(t) = 2\pi \frac{a(t)}{k}$ of each mode is stretched by the expansion itself and so two further different regimes arise. The evolution is in fact different depending on the larger or smaller wavelength than the causal horizon.

For the modes outside the horizon, $k/a(t) \ll H(t)$, the third term on the left hand side of Eq. (B.29) is

dropped, and the solution is given by:

$$\tilde{\phi}_A(\mathbf{k}, t) = \phi_0(\mathbf{k}) + \phi_1(\mathbf{k}) t^{-\frac{1}{2}} \quad (\text{B.30})$$

where $\phi_0(\mathbf{k})$ and $\phi_1(\mathbf{k})$ are some k -dependent constants. Therefore, for wavelengths larger than the causal horizon, each mode goes to a constant and the axion field is frozen by causality.

On the other hand, for modes inside the horizon, $k/a(t) \gg H(t)$, we cannot neglect the third term on the left hand side of Eq. (B.29) that, performing the substitution

$$\chi(\mathbf{k}, t) = a(t)^{\frac{3}{2}} \tilde{\phi}_A(\mathbf{k}, t), \quad (\text{B.31})$$

can be rewritten as follows:

$$[\partial_t^2 + \omega^2(t)] \chi(\mathbf{k}, t) = 0 \quad (\text{B.32})$$

where

$$\omega^2(t) = \frac{k^2}{a^2(t)} + \frac{3}{16t^2} \simeq \frac{k^2}{a^2(t)}. \quad (\text{B.33})$$

The most general solution is

$$\tilde{\phi}(\mathbf{k}, t) = \frac{C}{a(t)} \cos \left[\int^t dt' \omega(t') \right] \quad (\text{B.34})$$

where $C = \text{const.}$ This is an oscillating solution with a frequency $\omega \simeq k/a(t)$ and whose amplitude decreases with time as $\frac{1}{a(t)}$.

When $t \gtrsim t_*$ the axion mass term becomes non-negligible. The modes outside the causal Horizon, $k/a(t) \ll H(t)$, start oscillating with frequency $\omega \simeq m_A(t)$. In fact the equation of motion becomes exactly the same than that studied in the previous scenario with $T_{\text{PQ}} > T_{\text{RH}}$: we call these modes zero modes. As concerns the modes inside the Horizon, $k/a(t) \gg H(t)$, they contribute to the higher momentum modes.

The axion number density in this case is therefore given by the sum of the contribution of the zero momentum modes $n_A^{\text{vac},0}(t)$ and the contribution of the higher momentum modes $n_A^{\text{vac},1}(t)$:

$$n_A^{\text{vac}}(t) = n_A^{\text{vac},0}(t) + n_A^{\text{vac},1}(t). \quad (\text{B.35})$$

The zero momentum modes contribution is given by equation (B.25), but since in this case the initial misalignment angle is different from one QCD horizon to another and since the average of θ_*^2 is of order one we have

$$n_A^{\text{vac},0}(t) \sim \frac{f_A^2}{2t_*} \left(\frac{a(t_*)}{a(t)} \right)^3. \quad (\text{B.36})$$

On the other hand, one can show [362, 494] that the higher momentum modes contribution at the time $t = t_*$ is:

$$n_A^{\text{vac},1}(t_*) \sim \frac{N^2 f_A^2}{2t_*} \quad (\text{B.37})$$

where the factor N is defined saying that the typically variation of the Axion field from one horizon to the next is $\sim N f_A$. Since after t_* almost all these axions are non-relativistic they behave like ordinary matter and so:

$$n_A^{\text{vac},1}(t) \sim \frac{N^2 f_A^2}{2t_*} \left(\frac{a(t_*)}{a(t)} \right)^3 \quad (\text{B.38})$$

TOPOLOGICAL DEFECTS

Since the physics of the early universe is described by gauge theories which undergo spontaneous symmetry breaking, the universe is expected to have gone through various phase transitions as it cooled after the big bang. These phase transitions can give rise to topological defects. The Peccei Quinn phase transition is one of the primordial phase transition that can produce such topological defects. If inflation occurs after the PQ phase transition ($T_{\text{PQ}} > T_{\text{RH}}$), then topological defects are exponentially diluted in such a way that today it is extremely improbable to observe them in our universe. Otherwise, if inflation occurs before the PQ phase transition, topological defects are not diluted and so their evolution can have left a trace in our observable universe. So in this section we will focus on this scenario studying the different topological defects and the Axion production from topological defects. We do not pretend to be mathematically precise. For a more formal description the interested reader can see refs [385, 386, 390, 495]. Before studying the Axion production from topological defects, we need to be accurate to classify the different type of defects. The type of topological defects depends on the topology of the gauge theory and in particular on the topology of the vacuum manifold \mathcal{M} . In what follows let us assume that the universe is correctly described by a gauge theory which undergoes spontaneous symmetry breaking of its symmetry group G at some critical temperature. The generic field ϕ (not necessary the axion field ϕ_A) undergoing spontaneous symmetry breaking can be taken to have a minimum at $\phi = 0$ in the high temperature phase while it takes a vacuum expectation value $\langle 0|\phi|0\rangle = \langle\phi\rangle \neq 0$. Let us suppose that $\langle\phi\rangle$ is invariant under sub-group transformations $H \in G$. The vacuum manifold \mathcal{M} therefore is given by $\mathcal{M} = \frac{G}{H}$ the space of degenerate states which breaks the original symmetry. During the phase transition, $\phi(x)$ will take a vacuum expectation value in \mathcal{M} that will be uncorrelated in causal disconnected regions of spaces. To say the truth, for energetic reasons (because in general a spatial derivative term appears in the Hamiltonian) a constant or slowly varying vacuum expectation value is preferred but, depending on the topology of \mathcal{M} , some boundaries may survive among domains where instead $\phi(x) = 0$. These are nothing else that the topological defects: topologically stable configurations of the higher-energy state.

We are basically interested in two different types of topological defects: *Domain Walls* and *Cosmic strings*. Domain walls are two-dimensional topological defects, which are formed when the vacuum manifold \mathcal{M} is disconnected. This happens for example when \mathcal{M} is made up by only two points corresponding to two different values of the vacuum expectation value $\langle\phi\rangle = \pm\eta$. In each causal disconnected region $\langle\phi\rangle$ can be $+\eta$ or $-\eta$ randomly and then causal disconnected neighboring regions will tend to fall randomly into the different states. The common boundary surface between these regions is what we call domain wall. Since one cannot pass from $\langle\phi\rangle = +\eta$ to $\langle\phi\rangle = -\eta$ without passing through a region where $\langle\phi\rangle = 0$, so the domain walls are such that $\langle\phi\rangle = 0$. Regions with $\langle\phi\rangle = 0$ are in a higher energy state and so high energy walls are formed. The cosmological evolution of a domain wall is determined by its surface tension. The structures will grow with time until they are comparable to the Hubble scale, leading to large inhomogeneities in the cosmic background radiation that are not observed [72, 386].

Cosmic strings are one dimensional topological defects which are formed when the vacuum manifold \mathcal{M} is not simply connected. Cosmic strings require a more complicated theory than Domain walls. Consider a complex scalar field ϕ . Its vacuum state will have a $U(1)$ symmetry: $\langle\phi\rangle = \eta e^{i\theta}$: at each point in space the field can assume a phase $\theta \in [0, 2\pi]$. Since $\langle\phi\rangle$ is single valued, the total change of θ around any closed loop must be $\Delta\theta = 2\pi n$. If $n \neq 0$ the loop cannot be shrunk to a point and there will be at least one point inside the loop where θ is undefined. If θ is undefined so it must be $\langle\phi\rangle = 0$. The loop can be deformed in order to find another point of false vacuum. All these false vacuum points connect together to form a tube of false vacuum that is what we call cosmic string.

Let us try to understand how topological defects may arise from the invisible axion model. This requires a brief description of the model itself. Let us call T_{PQ} the temperature at which the PQ symmetry is spontaneously broken, we have that

$$T_{\text{PQ}} \simeq v_A \tag{B.39}$$

where v_A is the vacuum expectation value of a complex field $\sigma(x)$, named Peccei Quinn field, whose Lagrangian is:

$$\mathcal{L}_\sigma = \frac{1}{2} \partial_\mu \sigma^\dagger \partial^\mu \sigma - \frac{\lambda}{4} \left(\sigma^\dagger \sigma - v_A^2 \right)^2 + \mathcal{L}_{\text{int}}[\sigma(x), \psi_i] \quad (\text{B.40})$$

where $\mathcal{L}_{\text{int}}[\sigma(x), \psi_i]$ is the Lagrangian of interactions between $\sigma(x)$ and the other fields in the theory. When $T > T_{\text{PQ}}$ the minimum of energy is at $\sigma(x) = 0$ and the PQ symmetry is unbroken. However as the universe cools down $T < T_{\text{PQ}}$ and the temperature of the universe becomes comparable to the QCD scale $\Lambda_{\text{QCD}} \sim 100\text{MeV}$, so the non perturbative nature of QCD becomes relevant, the axions acquire mass and the effective potential arises².

$$V_A(\phi_A) = m_A^2 f_a^2 \left[1 - \cos\left(\frac{N_{\text{DW}} \phi_A}{f_A}\right) \right]. \quad (\text{B.41})$$

The existence of the QCD potential explicitly breaks the $U(1)_{\text{PQ}}$ symmetry and the vacuum expectation value of the field σ becomes a circle whose radius quickly approaches v_A :

$$\langle 0 | \sigma(x) | 0 \rangle = v_A e^{i \frac{\phi_A(x)}{v_A}} \quad (\text{B.42})$$

where $\phi_A(x)$ is the axion field. As we can see, now we have a non trivial vacuum manifold \mathcal{M} that is non simply connected and we are in the situation described before and so cosmic strings are formed. Let us consider the discrete subgroup $Z_{N_{\text{DW}}}$ of the shift symmetry

$$\phi_A \rightarrow \phi_A + 2k\pi \frac{f_A}{N_{\text{DW}}} \quad (\text{B.43})$$

with $k = \{0, 1, \dots, N_{\text{DW}} - 1\}$ that leaves the potential unchanged. Also this $Z_{N_{\text{DW}}}$ symmetry is spontaneously broken because of the vacuum expectation value (B.42) of the axion field. Therefore the vacuum manifold \mathcal{M} becomes more complicated since we have N_{DW} degeneracy vacuums that are equidistant in the curve of the minima. In other words \mathcal{M} not only is not simply connected but it is also disconnected and so Domain walls can be produced. Cosmic strings occur much earlier than the formation of domain walls: the domain walls are formed when the Hubble parameter becomes comparable to the axion mass: $H \sim m_A$.

AXIONS FROM STRING DECAY

Let us consider the axion cosmic strings. Because they are strongly coupled to the axion field, the strings decay very efficiently into axions. We want to estimate this process. For more details one can read [390, 494, 495].

The energy per unit length of an axion string is

$$\mu = \pi v_A^2 \ln(v_A L) \quad (\text{B.44})$$

where L is an infra-red cutoff approximately equal to the distance of the nearest neighbor string. As we have seen, since without inflation³ the size of the causal horizon is of order t , so $\phi_A(x)$ is completely uncorrelated over distances larger than t . At a given time t , there is at least the order of one string per horizon. At the beginning these strings are in the primordial plasma and they are stretched by the Hubble expansion $a(t) \propto t^{-\frac{1}{2}}$. During this time the density of strings grows and they become much more than one per horizon. However with the spacetime expansion, when the temperature of the universe becomes lower than approximately [496] $T_{\text{free}} \sim 2 \times 10^7 \text{GeV} \left(\frac{f_A}{10^{12} \text{GeV}} \right)^2$, they decouple from the primordial plasma and

²So far we have set $N_{\text{DW}} = 1$, but now let us relax this assumption

³Remember that in this scenario inflation occurs before the PQ symmetry breaking, otherwise it will dilute the abundance of topological defects in such a way that their contribution to the universe energy density will be negligible

they make up a network of axion strings moving freely at relativistic speeds. Axions are expected to be largely and efficiently produced by the string loops collapse. Moreover long strings (that by definition are stretched across horizons) reconnect to form loops that then collapse freely in axions. The number density of axions radiated by strings n_A^{str} is given by [362]

$$\frac{dn_A^{\text{str}}}{dt} = -3Hn_A^{\text{str}} + \frac{1}{\omega(t)} \frac{d\rho_{\text{str} \rightarrow A}}{dt} \quad (\text{B.45})$$

where $\omega(t)$ is the average energy of axions radiated in string-decay processes at a given time⁴

$$\frac{1}{\omega(t)} = \left(\frac{d\rho_{\text{str} \rightarrow A}}{dt} \right)^{-1} \int \frac{dk}{k} \frac{d^2\rho_{\text{str} \rightarrow A}}{dtdk} \quad (\text{B.46})$$

while $\frac{d\rho_{\text{str} \rightarrow A}}{dt}$ is the rate at which energy density is converted from strings to axions

$$\frac{d\rho_{\text{str} \rightarrow A}}{dt} = -\frac{d\rho_{\text{str}}}{dt} - 2H\rho_{\text{str}} \quad (\text{B.47})$$

where ρ_{str} is the long sting energy density [362] $\rho_{\text{str}}(t) = \zeta \frac{\mu}{t^2}$. The parameter ζ determines the density of the string network, $\zeta = 1$ corresponds to a density of one long string per horizon. If we want that global strings can decay efficiently into axions we have to require that $\zeta \approx 1$. Numerical simulation of global string networks in an expanding universe found that effectively $\zeta \simeq 1$ [362, 497].

Combining all these equations, maintaining only the terms of order $\ln(v_A t)$, one obtains

$$n_A^{\text{str}}(t) \simeq \frac{\zeta \pi f_a^2 N^2}{t^{3/2}} \int_{t_{\text{PQ}}}^t dt' \frac{\ln(v_A t')}{t'^{3/2} \omega(t')} \quad (\text{B.48})$$

To go further we need to know $\omega(t)$, the average energy of axions radiated at time t . Many analytic approximations or computational techniques can be used in order to estimate $\omega(t)$, see for example [362] and the reference within. What really interests us is that in the range $t^{-1} \lesssim k \lesssim (t_{\text{PQ}} t)^{-1/2}$ the axions coming from string decay have a spectrum $\propto k^{-2}$ and so, at the time t_* they have a momentum $\propto \frac{1}{t_*}$. This means that when the axions acquire a mass they become non-relativistic soon after. Axions produced by cosmic strings decay contribute to cold dark matter and we have that, after t_*

$$\rho_A^{\text{str}}(t) = m_A n_A^{\text{str}}(t_*) \left(\frac{a(t_*)}{a(t)} \right)^3 \quad (\text{B.49})$$

and so today ($t = t_0$)

$$\rho_A^{\text{str}}(t_0) = m_A n_A^{\text{str}}(t_*) \left(\frac{a(t_*)}{a(t_0)} \right)^3 \quad (\text{B.50})$$

AXION FROM DOMAIN WALLS

When the axion mass turns on, at time t_* , each axion string becomes the edge of N_{DW} domain walls. The domain walls produce a cosmological disaster unless there is inflation after the PQ phase-transition (case 1) or unless $N_{\text{DW}} = 1$. Basically what happens is that, when the axion mass turns on, each axion string becomes the edge of N_{DW} domain walls. Let us consider that $N_{\text{DW}} \geq 2$, since there are two or more exactly degenerate vacuum states so there is at least the order of one domain wall per causal horizon. The energy density in domain walls is then

$$\rho_{\text{DW}}(t) \gtrsim \frac{\sigma}{t} \quad (\text{B.51})$$

⁴Note that $\frac{d^2\rho_{\text{str} \rightarrow A}}{dtdk}$ figuring in the equation (B.46) is nothing else that the spectrum of the axions produced.

where σ is the wall energy per unit surface [362]

$$\sigma \simeq 9f_A^2 m_A \simeq 5.5 \times 10^{10} \text{GeV}^3 \left(\frac{f_A}{10^{12} \text{GeV}} \right) \quad (\text{B.52})$$

Therefore we estimate the domain wall energy density today $t = t_0 \simeq 14$ Gyr obtaining:

$$\rho_{\text{DW}}(t_0) \gtrsim \frac{\sigma}{t_0} \simeq 2 \times 10^{-14} \text{g cm}^{-3} \left(\frac{f_A}{10^{12} \text{GeV}} \right) \quad (\text{B.53})$$

The critical density today (i.e. the energy density required in order to have a flat universe) is

$$\rho_c(t_0) \equiv \frac{3H_0^2}{8\pi G} \simeq 10^{-29} \text{g cm}^{-3}. \quad (\text{B.54})$$

We immediately see that the domain wall contribution to the energy density exceeds alone by many orders the magnitude of the critical energy density for closing the universe. Domain Walls would over-close the universe. There are at least two options to avoid the axion domain-wall problem⁵: the first trivial option is to have inflation with $t_{\text{RH}} < T_{\text{PQ}}$ so that the axion field is then homogenized over large distances, and there are no strings or domain walls. The second option is to postulate $N_{\text{DW}} = 1$. In this way, when the axion mass turns on, each string becomes the boundary of a single domain wall. In this case what typically happens is that each string accelerates to relativistic speeds, in the direction of the wall to which it is attached, in less than a Hubble time unzipping the wall and releasing the stored energy in the form of barely relativistic axions [362]. The part of the domain walls that does not decay in axions can decay in gravitational waves. For example this is the case when one considers small symmetry breaking. Domain walls are gravitationally repulsive, a detailed description of their behavior can be found in [392, 498, 499]. Here we just summarize the following results. Domain walls accelerate away from each other with an acceleration $2\pi G\sigma$ and, after a time of order $(2\pi G\sigma)^{-1}$, they recede at the speed of light. By averaging over volumes containing many cells separated by walls, the equation of state of a wall dominated universe is $p_{\text{DW}} = -\frac{2}{3}\rho_{\text{DW}}$. This implies that the energy density of domain walls scales as

$$\rho_{\text{DW}} \propto \frac{1}{a(t)}. \quad (\text{B.55})$$

This, combined with the Friedmann equations, implies that a domain-wall-dominated universe expands as $a(t) \propto t^2$. A domain-wall-dominated universe has an accelerated expansion and so one could be tempted to say that the present-day accelerated expansion of the universe is due to the domain walls. However a domain wall dominated universe would have some proprieties that are far away from what we observe today [362] and we are forced to reject this option.

TOTAL COLD AXION ENERGY DENSITY

The total amount of the cold axion energy density Ω_A can be computed taking into account the different cold dark matter contribution described before. Ignoring the contribution of domain walls and assuming that the contribution of cosmic strings is

$$\rho_A^{\text{str}}(t) \sim 2 \frac{f_A^2}{t_*} \left(\frac{a(t_*)}{a(t)} \right)^3 m_A \quad (\text{B.56})$$

⁵The domain problem $N_{\text{DW}} > 1$ can also be avoided if one assumes a small symmetry breaking in such a way that the true vacuum takes over before the walls dominate the energy density. On the other hand, it must be small enough so that the PQ mechanism still works and so there is a very small portion in the parameter space in which such option works and some fine tuning problems arise.

for the two different cases described above one obtains

$$\Omega_A \sim \left(\frac{f_A}{10^{12} \text{GeV}} \right)^{7/6} \left(\frac{0.7}{h} \right)^2 \times \begin{cases} 0.15 \theta_*^2 & \text{for } T_{\text{PQ}} > T_{\text{RH}} \\ 0.7 & \text{for } T_{\text{PQ}} < T_{\text{RH}} \end{cases} \quad (\text{B.57})$$

where h is defined by $H_0 = h 100 \text{kms}^{-1} \text{Mpc}^{-1}$ and $\Omega_A = \frac{\rho_A}{\rho_c}$. Note that if we want axions to be (part of) Cold Dark Matter of course the total amount of cold axions cannot exceed the total amount of cold dark matter estimated in the universe $\Omega_{\text{CDM}} \approx 0.22$:

$$\Omega_A \leq \Omega_{\text{CDM}} \approx 0.22. \quad (\text{B.58})$$

If we are in the situation in which inflation occurs before the PQ symmetry breaking (so that the axion energy density does not depend on the initial misalignment angle θ_*) this translates into a direct constraint on the PQ symmetry breaking scale

$$f_A < 0.37 \cdot 10^{12} \text{GeV} \quad \text{for } T_{\text{PQ}} < T_{\text{RH}} \quad (\text{B.59})$$

while if we are in the situation of a broken PQ symmetry during inflation this translates into a relation between the initial misalignment angle and the PQ symmetry breaking scale

$$\left| \frac{\theta_*}{\pi} \right| < 0.4 \left(\frac{10^{12} \text{GeV}}{f_A} \right)^{7/12} \quad \text{for } T_{\text{PQ}} > T_{\text{RH}}. \quad (\text{B.60})$$

An initial misalignment angle of order one corresponds to $f_A \sim 10^{12} \text{GeV}$ while, in order to allow regions with $f_A \gg 10^{12}$ (such as $f_A \sim 10^{13} - 10^{14}$) we need to require a very fine tuned value of $\theta_* \approx 0$. Clearly being θ_* an angle it can assume all the value between $-\pi$ and π with the same probability, but to avoid a fine tuning problem (again), we prefer regions of the parameter space with $f_A \lesssim 10^{12} \text{GeV}$ corresponding to $m_A \gtrsim 10^{-5}$. Another interesting characteristic is that more the axion mass is small more the axion energy density is big. This because axions are bosons and so, if the decoupling is non thermal, their momentum is very slow and they behave as a condensate. This is an important difference between axions and other cold dark matter candidates such as WIMPs. Let us conclude this section saying that the axion mass window $m_A \in [1, 100] \mu\text{eV}$ is the most promising in order to have axion cold dark matter and most of the present experimental efforts on axions are focused on searching axions in this range.

AXION ISOCURVATURE PERTURBATIONS

We now turn to isocurvature perturbations of the axion field produced by quantum fluctuation during the inflation. As pointed out in the previous section, we basically have two possibilities: inflation can occur before or later the Peccei Quinn phase transition. If the reheating temperature after inflation is less than the Peccei Quinn temperature T_{PQ} , the axion field is present during inflation and it is subjected to quantum-mechanical fluctuations, just like the inflaton field. Since in this case the axion field is massless and weakly coupled as well as the the inflaton field, so the two fields have the same spectrum of fluctuation [76]. So the spectrum of the axion field perturbation [362] is given by:

$$P_A(k) = \int \frac{d^3\mathbf{x}}{(2\pi)^3} \langle \delta\phi_A(\mathbf{x}, t) \delta\phi_A(\mathbf{x}', t) \rangle e^{-i\mathbf{k}\cdot(\mathbf{x}-\mathbf{x}')} = \left(\frac{H_I}{2\pi} \right)^2 \frac{2\pi^2}{k^3} \quad (\text{B.61})$$

At the start of the QCD phase-transition, the local value of the axion field $\phi_A(x)$ determines the local number density of cold axions produced by the vacuum realignment mechanism

$$n_A(\mathbf{x}, t_*) = \frac{f_A^2}{2t_*} \theta^2(\mathbf{x}, t_*) \quad (\text{B.62})$$

where $\theta(\mathbf{x}, t_*) \equiv \frac{\phi_A(\mathbf{x}, t_*)}{f_A}$ is the initial misalignment angle. Therefore it is clear that the axion field perturbation generates perturbations in the number density of cold axions, in such a way that:

$$\frac{\delta n_A^{\text{iso}}}{n_A} = \frac{2\delta\phi_A}{\phi_A(\mathbf{x}, t_*)} = \frac{H_I}{\pi f_A \theta_*} \quad (\text{B.63})$$

Where $\phi_A(\mathbf{x}, t_*)$ is the value of the axion field at the start of the QCD phase-transition that, because of inflation, is common to our entire visible universe. Since the vacuum-realignment mechanism converts the quark - gluon plasma energy into axion rest mass energy, the energy density of these perturbations obeys to:

$$\delta\rho_A^{\text{iso}}(t_*) = -\delta\rho_{\text{rad}}^{\text{iso}}(t_*) \quad (\text{B.64})$$

while, as known, the density perturbations produced by the fluctuations of the inflaton field satisfy the adiabatic condition. Therefore the perturbations produced by the axion field fluctuations are not adiabatic (as those produced by the inflaton field fluctuations) but they are *isocurvature perturbations*. However note that in this case the density perturbations in the cold axion fluid have both adiabatic and isocurvature components: the adiabatic component is given by the quantum mechanical fluctuations of the inflaton field during inflation, while the isocurvature perturbations are produced by the quantum mechanical fluctuations of the axion field during that same epoch. The adiabatic and axion isocurvature components are of course uncorrelated. The isocurvature perturbations leave a different trace in the cosmic microwave background with respect to adiabatic perturbations. In order to constrain the kind of perturbation observed in the CMB, in general one uses the primordial isocurvature fraction β_{iso} defined as the ratio between the isocurvature perturbation spectrum over the sum of the isocurvature and adiabatic perturbation spectrum:

$$\beta_{\text{iso}} = \frac{\mathcal{P}_{\text{iso}}}{\mathcal{P}_{\text{iso}} + \mathcal{P}_{\text{ad}}} \lesssim 0.04. \quad (\text{B.65})$$

This limit can be used to exclude regions in the parameter space of the PQ scale and the scale of inflation H_I , since they are related via [500]

$$H_I \simeq 0.96 \times 10^7 \text{GeV} \left(\frac{\beta_{\text{iso}}}{0.04} \right)^{1/2} \left(\frac{\Omega_A}{0.120} \right)^{1/2} \left(\frac{f_A}{10^{11} \text{GeV}} \right)^{0.408} \quad (\text{B.66})$$

If we consider the limit (B.65) and if we assume all the cold dark matter made of axions, we have:

$$H_I \leq 0.87 \times 10^7 \text{GeV} \left(\frac{f_A}{10^{11} \text{GeV}} \right)^{0.408} \quad (\text{B.67})$$

Note that another independent estimator of the energy scale of the inflation is the amplitude of the primordial gravitational waves or, equivalently, the tensor to scalar ratio. It is so clear that a future measurement of the primordial gravitational waves would constrain the PQ scale.

REFERENCES

- [1] **Giarè, William**, Eleonora Di Valentino, and Alessandro Melchiorri. “Testing the inflationary slow-roll condition with tensor modes”. In: *Phys. Rev. D* 99.12 (2019), p. 123522. DOI: [10.1103/PhysRevD.99.123522](https://doi.org/10.1103/PhysRevD.99.123522).
- [2] **Giarè, William** and Alessandro Melchiorri. “Probing the inflationary background of gravitational waves from large to small scales”. In: *Phys. Lett. B* 815 (2021), p. 136137. DOI: [10.1016/j.physletb.2021.136137](https://doi.org/10.1016/j.physletb.2021.136137). arXiv: [2003.04783](https://arxiv.org/abs/2003.04783) [[astro-ph.CO](#)].
- [3] **Giarè, William** and Fabrizio Renzi. “Propagating speed of primordial gravitational waves”. In: *Phys. Rev. D* 102.8 (2020), p. 083530. DOI: [10.1103/PhysRevD.102.083530](https://doi.org/10.1103/PhysRevD.102.083530). arXiv: [2007.04256](https://arxiv.org/abs/2007.04256) [[astro-ph.CO](#)].
- [4] **Giarè, William**, Fabrizio Renzi, and Alessandro Melchiorri. “Higher-Curvature Corrections and Tensor Modes”. In: *Phys. Rev. D* 103.4 (2021), p. 043515. DOI: [10.1103/PhysRevD.103.043515](https://doi.org/10.1103/PhysRevD.103.043515). arXiv: [2012.00527](https://arxiv.org/abs/2012.00527) [[astro-ph.CO](#)].
- [5] **Giarè, William** et al. “New cosmological bounds on hot relics: axions and neutrinos”. In: *Mon. Not. Roy. Astron. Soc.* 505.2 (2021), pp. 2703–2711. DOI: [10.1093/mnras/stab1442](https://doi.org/10.1093/mnras/stab1442). arXiv: [2011.14704](https://arxiv.org/abs/2011.14704) [[astro-ph.CO](#)].
- [6] Matteo Forconi, **Giarè, William**, and et al. “Cosmological constraints on slow roll inflation: An update”. In: *Phys. Rev. D* 104.10 (2021), p. 103528. DOI: [10.1103/PhysRevD.104.103528](https://doi.org/10.1103/PhysRevD.104.103528). arXiv: [2110.01695](https://arxiv.org/abs/2110.01695) [[astro-ph.CO](#)].
- [7] **Giarè, William** et al. “Cosmological forecasts on thermal axions, relic neutrinos and light elements”. In: (Oct. 2021). arXiv: [2110.00340](https://arxiv.org/abs/2110.00340) [[astro-ph.CO](#)].
- [8] Albert Einstein. “The Foundation of the General Theory of Relativity”. In: *Annalen Phys.* 49.7 (1916). Ed. by Jong-Ping Hsu and D. Fine, pp. 769–822. DOI: [10.1002/andp.19163540702](https://doi.org/10.1002/andp.19163540702).
- [9] Charles W. Misner, K. S. Thorne, and J. A. Wheeler. *Gravitation*. San Francisco: W. H. Freeman, 1973.
- [10] Sean M. Carroll. *Spacetime and Geometry*. Cambridge University Press, July 2019.
- [11] S. W. Hawking and G. F. R. Ellis. *The Large Scale Structure of Space-Time*. Cambridge Monographs on Mathematical Physics. Cambridge University Press, Feb. 2011. DOI: [10.1017/CB09780511524646](https://doi.org/10.1017/CB09780511524646).
- [12] Scott Dodelson. *Modern Cosmology*. Amsterdam: Academic Press, 2003. ISBN: 978-0-12-219141-1.
- [13] V. Mukhanov. *Physical Foundations of Cosmology*. Oxford: Cambridge University Press, 2005. ISBN: 978-0-521-56398-7.
- [14] Steven Weinberg. *Cosmology*. 2008. ISBN: 978-0-19-852682-7.
- [15] Dmitry S. Gorbunov and Valery A. Rubakov. *Introduction to the theory of the early universe: Cosmological perturbations and inflationary theory*. DOI: [10.1142/7874](https://doi.org/10.1142/7874).
- [16] Valery A. Rubakov and Dmitry S. Gorbunov. *Introduction to the Theory of the Early Universe: Hot big bang theory*. Singapore: World Scientific, 2017. DOI: [10.1142/10447](https://doi.org/10.1142/10447).
- [17] Dominik J. Schwarz. “The first second of the universe”. In: *Annalen Phys.* 12 (2003), pp. 220–270. DOI: [10.1002/andp.200310010](https://doi.org/10.1002/andp.200310010). arXiv: [astro-ph/0303574](https://arxiv.org/abs/astro-ph/0303574).
- [18] K. A. Olive et al. “Review of Particle Physics”. In: *Chin. Phys. C* 38 (2014), p. 090001. DOI: [10.1088/1674-1137/38/9/090001](https://doi.org/10.1088/1674-1137/38/9/090001).

- [19] S. W. Hawking and I. G. Moss. “Supercooled Phase Transitions in the Very Early Universe”. In: *Phys. Lett. B* 110 (), pp. 35–38. DOI: [10.1016/0370-2693\(82\)90946-7](https://doi.org/10.1016/0370-2693(82)90946-7).
- [20] Alan H. Guth and S. H. H. Tye. “Phase Transitions and Magnetic Monopole Production in the Very Early Universe”. In: *Phys. Rev. Lett.* 44 (1980). [Erratum: *Phys.Rev.Lett.* 44, 963 (1980)], p. 631. DOI: [10.1103/PhysRevLett.44.631](https://doi.org/10.1103/PhysRevLett.44.631).
- [21] D. Boyanovsky, H. J. de Vega, and D. J. Schwarz. “Phase transitions in the early and the present universe”. In: *Ann. Rev. Nucl. Part. Sci.* 56 (2006), pp. 441–500. DOI: [10.1146/annurev.nucl.56.080805.140539](https://doi.org/10.1146/annurev.nucl.56.080805.140539). arXiv: [hep-ph/0602002](https://arxiv.org/abs/hep-ph/0602002).
- [22] T. W. B. Kibble. “Phase Transitions in the Early Universe”. In: *Acta Phys. Polon. B* 13 (1982), p. 723.
- [23] Mark B. Hindmarsh et al. “Phase transitions in the early universe”. In: *SciPost Phys. Lect. Notes* 24 (2021), p. 1. DOI: [10.21468/SciPostPhysLectNotes.24](https://doi.org/10.21468/SciPostPhysLectNotes.24). arXiv: [2008.09136](https://arxiv.org/abs/2008.09136) [[astro-ph](https://arxiv.org/abs/astro-ph).C0].
- [24] Andreas Albrecht and Paul J. Steinhardt. “Cosmology for Grand Unified Theories with Radiatively Induced Symmetry Breaking”. In: *Phys. Rev. Lett.* 48 (1982). Ed. by Li-Zhi Fang and R. Ruffini, pp. 1220–1223. DOI: [10.1103/PhysRevLett.48.1220](https://doi.org/10.1103/PhysRevLett.48.1220).
- [25] William J. Marciano and Goran Senjanovic. “Predictions of Supersymmetric Grand Unified Theories”. In: *Phys. Rev. D* 25 (1982), p. 3092. DOI: [10.1103/PhysRevD.25.3092](https://doi.org/10.1103/PhysRevD.25.3092).
- [26] W. de Boer. “Grand unified theories and supersymmetry in particle physics and cosmology”. In: *Prog. Part. Nucl. Phys.* 33 (1994), pp. 201–302. DOI: [10.1016/0146-6410\(94\)90045-0](https://doi.org/10.1016/0146-6410(94)90045-0). arXiv: [hep-ph/9402266](https://arxiv.org/abs/hep-ph/9402266).
- [27] Howard Georgi. “Towards a Grand Unified Theory of Flavor”. In: *Nucl. Phys. B* 156 (1979), pp. 126–134. DOI: [10.1016/0550-3213\(79\)90497-8](https://doi.org/10.1016/0550-3213(79)90497-8).
- [28] Peter W. Higgs. “Broken Symmetries and the Masses of Gauge Bosons”. In: *Phys. Rev. Lett.* 13 (1964). Ed. by J. C. Taylor, pp. 508–509. DOI: [10.1103/PhysRevLett.13.508](https://doi.org/10.1103/PhysRevLett.13.508).
- [29] Peter W. Higgs. “Broken symmetries, massless particles and gauge fields”. In: *Phys. Lett.* 12 (1964), pp. 132–133. DOI: [10.1016/0031-9163\(64\)91136-9](https://doi.org/10.1016/0031-9163(64)91136-9).
- [30] Peter W. Higgs. “Spontaneous Symmetry Breakdown without Massless Bosons”. In: *Phys. Rev.* 145 (1966), pp. 1156–1163. DOI: [10.1103/PhysRev.145.1156](https://doi.org/10.1103/PhysRev.145.1156).
- [31] P. A. Zyla et al. “Review of Particle Physics”. In: *PTEP* 2020.8 (2020), p. 083C01. DOI: [10.1093/ptep/ptaa104](https://doi.org/10.1093/ptep/ptaa104).
- [32] C. R. Allton et al. “The QCD thermal phase transition in the presence of a small chemical potential”. In: *Phys. Rev. D* 66 (2002), p. 074507. DOI: [10.1103/PhysRevD.66.074507](https://doi.org/10.1103/PhysRevD.66.074507). arXiv: [hep-lat/0204010](https://arxiv.org/abs/hep-lat/0204010).
- [33] F. Karsch, E. Laermann, and A. Peikert. “Quark mass and flavor dependence of the QCD phase transition”. In: *Nucl. Phys. B* 605 (), pp. 579–599. DOI: [10.1016/S0550-3213\(01\)00200-0](https://doi.org/10.1016/S0550-3213(01)00200-0). arXiv: [hep-lat/0012023](https://arxiv.org/abs/hep-lat/0012023).
- [34] Krishna Rajagopal and Frank Wilczek. “Static and dynamic critical phenomena at a second order QCD phase transition”. In: *Nucl. Phys. B* 399 (1993), pp. 395–425. DOI: [10.1016/0550-3213\(93\)90502-G](https://doi.org/10.1016/0550-3213(93)90502-G). arXiv: [hep-ph/9210253](https://arxiv.org/abs/hep-ph/9210253).
- [35] Frank R. Brown et al. “On the existence of a phase transition for QCD with three light quarks”. In: *Phys. Rev. Lett.* 65 (1990), pp. 2491–2494. DOI: [10.1103/PhysRevLett.65.2491](https://doi.org/10.1103/PhysRevLett.65.2491).
- [36] R. A. Alpher, H. Bethe, and G. Gamow. “The Origin of Chemical Elements”. In: *Phys. Rev.* 73 (7 Apr. 1948), pp. 803–804. DOI: [10.1103/PhysRev.73.803](https://doi.org/10.1103/PhysRev.73.803). URL: <https://link.aps.org/doi/10.1103/PhysRev.73.803>.
- [37] Karim A. Malik and David R. Matravers. “A Concise Introduction to Perturbation Theory in Cosmology”. In: *Class. Quant. Grav.* 25 (2008), p. 193001. DOI: [10.1088/0264-9381/25/19/193001](https://doi.org/10.1088/0264-9381/25/19/193001). arXiv: [0804.3276](https://arxiv.org/abs/0804.3276) [[astro-ph](https://arxiv.org/abs/astro-ph)].

- [38] Robert H. Brandenberger. “Introduction to Early Universe Cosmology”. In: *PoS ICFI2010* (2010), p. 001. DOI: [10.22323/1.124.0001](https://doi.org/10.22323/1.124.0001). arXiv: [1103.2271](https://arxiv.org/abs/1103.2271) [[astro-ph.CO](#)].
- [39] Mark Trodden and Sean M. Carroll. “TASI lectures: Introduction to cosmology”. In: *Theoretical Advanced Study Institute in Elementary Particle Physics (TASI 2002): Particle Physics and Cosmology: The Quest for Physics Beyond the Standard Model(s)*. Jan. 2004, pp. 703–793. arXiv: [astro-ph/0401547](https://arxiv.org/abs/astro-ph/0401547).
- [40] Gabriele Veneziano. “A Simple / short introduction to pre - big bang physics / cosmology”. In: *International School of Subnuclear Physics, 35th Course: Highlights: 50 Years Later*. Aug. 1997, pp. 364–380. arXiv: [hep-th/9802057](https://arxiv.org/abs/hep-th/9802057).
- [41] David L. Wiltshire. “An Introduction to quantum cosmology”. In: *8th Physics Summer School on Cosmology: The Physics of the Universe*. Jan. 1995, pp. 473–531. arXiv: [gr-qc/0101003](https://arxiv.org/abs/gr-qc/0101003).
- [42] N. Aghanim et al. “Planck 2018 results. I. Overview and the cosmological legacy of Planck”. In: *Astron. Astrophys.* 641 (2020), A1. DOI: [10.1051/0004-6361/201833880](https://doi.org/10.1051/0004-6361/201833880). arXiv: [1807.06205](https://arxiv.org/abs/1807.06205) [[astro-ph.CO](#)].
- [43] Subir Sarkar. “Big bang nucleosynthesis and physics beyond the standard model”. In: *Rept. Prog. Phys.* 59 (1996), pp. 1493–1610. DOI: [10.1088/0034-4885/59/12/001](https://doi.org/10.1088/0034-4885/59/12/001). arXiv: [hep-ph/9602260](https://arxiv.org/abs/hep-ph/9602260).
- [44] Scott Burles, Kenneth M. Nollett, and Michael S. Turner. “Big bang nucleosynthesis predictions for precision cosmology”. In: *Astrophys. J. Lett.* 552 (2001), pp. L1–L6. DOI: [10.1086/320251](https://doi.org/10.1086/320251). arXiv: [astro-ph/0010171](https://arxiv.org/abs/astro-ph/0010171).
- [45] Ann Merchant Boesgaard and Gary Steigman. “Big Bang Nucleosynthesis: Theories and Observations”. In: *Ann. Rev. Astron. Astrophys.* 23 (1985), pp. 319–378. DOI: [10.1146/annurev.aa.23.090185.001535](https://doi.org/10.1146/annurev.aa.23.090185.001535).
- [46] Hideo Kodama and Misao Sasaki. “Cosmological Perturbation Theory”. In: *Prog. Theor. Phys. Suppl.* 78 (1984), pp. 1–166. DOI: [10.1143/PTPS.78.1](https://doi.org/10.1143/PTPS.78.1).
- [47] F. Bernardeau et al. “Large scale structure of the universe and cosmological perturbation theory”. In: *Phys. Rept.* 367 (2002), pp. 1–248. DOI: [10.1016/S0370-1573\(02\)00135-7](https://doi.org/10.1016/S0370-1573(02)00135-7). arXiv: [astro-ph/0112551](https://arxiv.org/abs/astro-ph/0112551).
- [48] Martin Crocce and Roman Scoccimarro. “Renormalized cosmological perturbation theory”. In: *Phys. Rev. D* 73 (2006), p. 063519. DOI: [10.1103/PhysRevD.73.063519](https://doi.org/10.1103/PhysRevD.73.063519). arXiv: [astro-ph/0509418](https://arxiv.org/abs/astro-ph/0509418).
- [49] Ruth Durrer. “Gauge invariant cosmological perturbation theory: A General study and its application to the texture scenario of structure formation”. In: *Fund. Cosmic Phys.* 15 (1994), pp. 209–339. arXiv: [astro-ph/9311041](https://arxiv.org/abs/astro-ph/9311041).
- [50] Kouji Nakamura. “Second-order gauge invariant cosmological perturbation theory: Einstein equations in terms of gauge invariant variables”. In: *Prog. Theor. Phys.* 117 (2007), pp. 17–74. DOI: [10.1143/PTP.117.17](https://doi.org/10.1143/PTP.117.17). arXiv: [gr-qc/0605108](https://arxiv.org/abs/gr-qc/0605108).
- [51] Massimo Pietroni et al. “Coarse-Grained Cosmological Perturbation Theory”. In: *JCAP* 01 (2012), p. 019. DOI: [10.1088/1475-7516/2012/01/019](https://doi.org/10.1088/1475-7516/2012/01/019). arXiv: [1108.5203](https://arxiv.org/abs/1108.5203) [[astro-ph.CO](#)].
- [52] Ruth Durrer. “Cosmological perturbation theory”. In: *Lect. Notes Phys.* 653 (2004). Ed. by E. Papantonopoulos, pp. 31–70. DOI: [10.1007/978-3-540-31535-3_2](https://doi.org/10.1007/978-3-540-31535-3_2). arXiv: [astro-ph/0402129](https://arxiv.org/abs/astro-ph/0402129).
- [53] B. Losic and W. G. Unruh. “Cosmological Perturbation Theory in Slow-Roll Spacetimes”. In: *Phys. Rev. Lett.* 101 (2008), p. 111101. DOI: [10.1103/PhysRevLett.101.111101](https://doi.org/10.1103/PhysRevLett.101.111101). arXiv: [0804.4296](https://arxiv.org/abs/0804.4296) [[gr-qc](#)].
- [54] Daniel Baumann. “Inflation”. In: *Theoretical Advanced Study Institute in Elementary Particle Physics: Physics of the Large and the Small*. July 2009. DOI: [10.1142/9789814327183_0010](https://doi.org/10.1142/9789814327183_0010). arXiv: [0907.5424](https://arxiv.org/abs/0907.5424) [[hep-th](#)].
- [55] David H. Lyth and Andrew R. Liddle. *The primordial density perturbation: Cosmology, inflation and the origin of structure*. 2009.
- [56] Christopher Gordon et al. “Adiabatic and entropy perturbations from inflation”. In: *Phys. Rev. D* 63 (2000), p. 023506. DOI: [10.1103/PhysRevD.63.023506](https://doi.org/10.1103/PhysRevD.63.023506). arXiv: [astro-ph/0009131](https://arxiv.org/abs/astro-ph/0009131).

- [57] N. Aghanim et al. “Planck 2018 results. V. CMB power spectra and likelihoods”. In: *Astron. Astrophys.* 641 (2020), A5. DOI: [10.1051/0004-6361/201936386](https://doi.org/10.1051/0004-6361/201936386). arXiv: [1907.12875](https://arxiv.org/abs/1907.12875) [astro-ph.CO].
- [58] Y. Akrami et al. “Planck 2018 results. VII. Isotropy and Statistics of the CMB”. In: *Astron. Astrophys.* 641 (2020), A7. DOI: [10.1051/0004-6361/201935201](https://doi.org/10.1051/0004-6361/201935201). arXiv: [1906.02552](https://arxiv.org/abs/1906.02552) [astro-ph.CO].
- [59] Steven Weinberg. “Effective Field Theory for Inflation”. In: *Phys. Rev. D* 77 (2008), p. 123541. DOI: [10.1103/PhysRevD.77.123541](https://doi.org/10.1103/PhysRevD.77.123541). arXiv: [0804.4291](https://arxiv.org/abs/0804.4291) [hep-th].
- [60] Wayne Hu and Scott Dodelson. “Cosmic Microwave Background Anisotropies”. In: *Ann. Rev. Astron. Astrophys.* 40 (2002), pp. 171–216. DOI: [10.1146/annurev.astro.40.060401.093926](https://doi.org/10.1146/annurev.astro.40.060401.093926). arXiv: [astro-ph/0110414](https://arxiv.org/abs/astro-ph/0110414).
- [61] N. Aghanim et al. “Planck 2018 results. I. Overview and the cosmological legacy of Planck”. In: *Astron. Astrophys.* 641 (2020), A1. DOI: [10.1051/0004-6361/201833880](https://doi.org/10.1051/0004-6361/201833880). arXiv: [1807.06205](https://arxiv.org/abs/1807.06205) [astro-ph.CO].
- [62] Albert Stebbins. “The CMBR spectrum: A Theoretical introduction”. In: *NATO Advanced Study Institute: The Cosmic Background Radiation (CBR 96)*. May 1996. arXiv: [astro-ph/9705178](https://arxiv.org/abs/astro-ph/9705178).
- [63] Douglas Scott and George F. Smoot. “Cosmic Microwave Background Mini-review”. In: (May 2010). arXiv: [1005.0555](https://arxiv.org/abs/1005.0555) [astro-ph.CO].
- [64] Dorothea Samtleben, Suzanne Staggs, and Bruce Winstein. “The Cosmic microwave background for pedestrians: A Review for particle and nuclear physicists”. In: *Ann. Rev. Nucl. Part. Sci.* 57 (2007), pp. 245–283. DOI: [10.1146/annurev.nucl.54.070103.181232](https://doi.org/10.1146/annurev.nucl.54.070103.181232). arXiv: [0803.0834](https://arxiv.org/abs/0803.0834) [astro-ph].
- [65] Antony Lewis and Anthony Challinor. “Weak gravitational lensing of the CMB”. In: *Phys. Rept.* 429 (2006), pp. 1–65. DOI: [10.1016/j.physrep.2006.03.002](https://doi.org/10.1016/j.physrep.2006.03.002). arXiv: [astro-ph/0601594](https://arxiv.org/abs/astro-ph/0601594).
- [66] D. J. Fixsen. “The Temperature of the Cosmic Microwave Background”. In: *Astrophys. J.* 707 (2009), pp. 916–920. DOI: [10.1088/0004-637X/707/2/916](https://doi.org/10.1088/0004-637X/707/2/916). arXiv: [0911.1955](https://arxiv.org/abs/0911.1955) [astro-ph.CO].
- [67] Ruth Durrer. “The theory of CMB anisotropies”. In: *J. Phys. Stud.* 5 (2001), pp. 177–215. arXiv: [astro-ph/0109522](https://arxiv.org/abs/astro-ph/0109522).
- [68] R. K. Sachs and A. M. Wolfe. “Perturbations of a cosmological model and angular variations of the microwave background”. In: *Astrophys. J.* 147 (1967), pp. 73–90. DOI: [10.1007/s10714-007-0448-9](https://doi.org/10.1007/s10714-007-0448-9).
- [69] Joseph Silk. “Cosmic black body radiation and galaxy formation”. In: *Astrophys. J.* 151 (1968), pp. 459–471. DOI: [10.1086/149449](https://doi.org/10.1086/149449).
- [70] Ya. B. Zeldovich and R. A. Sunyaev. “The Interaction of Matter and Radiation in a Hot-Model Universe”. In: *Astrophys. Space Sci.* 4 (1969), pp. 301–316. DOI: [10.1007/BF00661821](https://doi.org/10.1007/BF00661821).
- [71] Takemi Okamoto and Wayne Hu. “CMB lensing reconstruction on the full sky”. In: *Phys. Rev. D* 67 (2003), p. 083002. DOI: [10.1103/PhysRevD.67.083002](https://doi.org/10.1103/PhysRevD.67.083002). arXiv: [astro-ph/0301031](https://arxiv.org/abs/astro-ph/0301031).
- [72] Ya. B. Zeldovich, I. Yu. Kobzarev, and L. B. Okun. “Cosmological Consequences of the Spontaneous Breakdown of Discrete Symmetry”. In: *Zh. Eksp. Teor. Fiz.* 67 (1974), pp. 3–11.
- [73] Marc Kamionkowski, Arthur Kosowsky, and Albert Stebbins. “Statistics of cosmic microwave background polarization”. In: *Phys. Rev. D* 55 (1997), pp. 7368–7388. DOI: [10.1103/PhysRevD.55.7368](https://doi.org/10.1103/PhysRevD.55.7368). arXiv: [astro-ph/9611125](https://arxiv.org/abs/astro-ph/9611125).
- [74] Paolo Cabella and Marc Kamionkowski. “Theory of cosmic microwave background polarization”. In: *International School of Gravitation and Cosmology: The Polarization of the Cosmic Microwave Background*. Mar. 2004. arXiv: [astro-ph/0403392](https://arxiv.org/abs/astro-ph/0403392).
- [75] Wayne Hu and Martin J. White. “CMB anisotropies: Total angular momentum method”. In: *Phys. Rev. D* 56 (1997), pp. 596–615. DOI: [10.1103/PhysRevD.56.596](https://doi.org/10.1103/PhysRevD.56.596). arXiv: [astro-ph/9702170](https://arxiv.org/abs/astro-ph/9702170).
- [76] Daniel Baumann and Liam McAllister. *Inflation and String Theory*. Cambridge Monographs on Mathematical Physics. Cambridge University Press, May 2015. ISBN: 978-1-107-08969-3. DOI: [10.1017/CB09781316105733](https://doi.org/10.1017/CB09781316105733). arXiv: [1404.2601](https://arxiv.org/abs/1404.2601) [hep-th].

- [77] William H. Kinney. “TASI Lectures on Inflation”. In: (Feb. 2009). arXiv: [0902.1529 \[astro-ph.CO\]](#).
- [78] Y. Akrami et al. “Planck 2018 results. X. Constraints on inflation”. In: *Astron. Astrophys.* 641 (2020), A10. DOI: [10.1051/0004-6361/201833887](#). arXiv: [1807.06211 \[astro-ph.CO\]](#).
- [79] Alan H. Guth. “The Inflationary Universe: A Possible Solution to the Horizon and Flatness Problems”. In: *Phys. Rev. D* 23 (1981). Ed. by Li-Zhi Fang and R. Ruffini, pp. 347–356. DOI: [10.1103/PhysRevD.23.347](#).
- [80] Leonardo Senatore. “Lectures on Inflation”. In: *Theoretical Advanced Study Institute in Elementary Particle Physics: New Frontiers in Fields and Strings*. 2017, pp. 447–543. DOI: [10.1142/9789813149441_0008](#). arXiv: [1609.00716 \[hep-th\]](#).
- [81] Andrew R. Liddle. “An Introduction to cosmological inflation”. In: *ICTP Summer School in High-Energy Physics and Cosmology*. Jan. 1999, pp. 260–295. arXiv: [astro-ph/9901124](#).
- [82] D. Langlois. “Lectures on inflation and cosmological perturbations”. In: *Lect. Notes Phys.* 800 (2010), pp. 1–57. DOI: [10.1007/978-3-642-10598-2_1](#). arXiv: [1001.5259 \[astro-ph.CO\]](#).
- [83] A. Riotto. “Inflation and the Theory of Cosmological Perturbations”. In: 2018.
- [84] Lev Kofman, Andrei D. Linde, and Alexei A. Starobinsky. “Towards the theory of reheating after inflation”. In: *Phys. Rev. D* 56 (1997), pp. 3258–3295. DOI: [10.1103/PhysRevD.56.3258](#). arXiv: [hep-ph/9704452](#).
- [85] Lev Kofman, Andrei D. Linde, and Alexei A. Starobinsky. “Reheating after inflation”. In: *Phys. Rev. Lett.* 73 (1994), pp. 3195–3198. DOI: [10.1103/PhysRevLett.73.3195](#). arXiv: [hep-th/9405187](#).
- [86] Bruce A. Bassett, Shinji Tsujikawa, and David Wands. “Inflation dynamics and reheating”. In: *Rev. Mod. Phys.* 78 (2006), pp. 537–589. DOI: [10.1103/RevModPhys.78.537](#). arXiv: [astro-ph/0507632](#).
- [87] Y. Shtanov, Jennie H. Traschen, and Robert H. Brandenberger. “Universe reheating after inflation”. In: *Phys. Rev. D* 51 (1995), pp. 5438–5455. DOI: [10.1103/PhysRevD.51.5438](#). arXiv: [hep-ph/9407247](#).
- [88] Andreas Albrecht et al. “Reheating an Inflationary Universe”. In: *Phys. Rev. Lett.* 48 (1982), p. 1437. DOI: [10.1103/PhysRevLett.48.1437](#).
- [89] Rouzbeh Allahverdi et al. “Reheating in Inflationary Cosmology: Theory and Applications”. In: *Ann. Rev. Nucl. Part. Sci.* 60 (2010), pp. 27–51. DOI: [10.1146/annurev.nucl.012809.104511](#). arXiv: [1001.2600 \[hep-th\]](#).
- [90] Daniel J. H. Chung, Edward W. Kolb, and Antonio Riotto. “Production of massive particles during reheating”. In: *Phys. Rev. D* 60 (1999), p. 063504. DOI: [10.1103/PhysRevD.60.063504](#). arXiv: [hep-ph/9809453](#).
- [91] Mustafa A. Amin et al. “Nonperturbative Dynamics Of Reheating After Inflation: A Review”. In: *Int. J. Mod. Phys. D* 24 (2014), p. 1530003. DOI: [10.1142/S0218271815300037](#). arXiv: [1410.3808 \[hep-ph\]](#).
- [92] Jerome Martin and Christophe Ringeval. “First CMB Constraints on the Inflationary Reheating Temperature”. In: *Phys. Rev. D* 82 (2010), p. 023511. DOI: [10.1103/PhysRevD.82.023511](#). arXiv: [1004.5525 \[astro-ph.CO\]](#).
- [93] Rouzbeh Allahverdi et al. “MSSM flat direction inflation: Slow roll, stability, fine tuning and reheating”. In: *JCAP* 06 (2007), p. 019. DOI: [10.1088/1475-7516/2007/06/019](#). arXiv: [hep-ph/0610134](#).
- [94] Daniel Baumann, Hayden Lee, and Guilherme L. Pimentel. “High-Scale Inflation and the Tensor Tilt”. In: *JHEP* 01 (2016), p. 101. DOI: [10.1007/JHEP01\(2016\)101](#). arXiv: [1507.07250 \[hep-th\]](#).
- [95] S. W. Hawking and I. G. Moss. “Fluctuations in the Inflationary Universe”. In: *Nucl. Phys. B* 224 (1983), p. 180. DOI: [10.1016/0550-3213\(83\)90319-X](#).
- [96] David H. Lyth and Antonio Riotto. “Particle physics models of inflation and the cosmological density perturbation”. In: *Phys. Rept.* 314 (1999), pp. 1–146. DOI: [10.1016/S0370-1573\(98\)00128-8](#). arXiv: [hep-ph/9807278](#).

- [97] Pietro Dona and Antonino Marciano. “Non Bunch Davies group coherent states, and their quantum signatures in CMB observables”. In: (). arXiv: [1612.00760 \[gr-qc\]](#).
- [98] Amjad Ashoorioon et al. “Non-Bunch–Davis initial state reconciles chaotic models with BICEP and Planck”. In: *Phys. Lett. B* 737 (2014), pp. 98–102. DOI: [10.1016/j.physletb.2014.08.038](#). arXiv: [1403.6099 \[hep-th\]](#).
- [99] Dionysios Anninos et al. “Late-time Structure of the Bunch-Davies De Sitter Wavefunction”. In: *JCAP* 11 (2015), p. 048. DOI: [10.1088/1475-7516/2015/11/048](#). arXiv: [1406.5490 \[hep-th\]](#).
- [100] E. Yusofi and M. Mohsenzadeh. “Scale-dependent power spectrum from initial excited-de Sitter modes”. In: *JHEP* 09 (2014), p. 020. DOI: [10.1007/JHEP09\(2014\)020](#). arXiv: [1402.6968 \[astro-ph.CO\]](#).
- [101] Rose Baunach et al. “Does Planck actually “see” the Bunch-Davies state?” In: *JCAP* 07 (2021), p. 050. DOI: [10.1088/1475-7516/2021/07/050](#). arXiv: [2104.13410 \[hep-th\]](#).
- [102] Michał Wrochna. “Conformal extension of the Bunch-Davies state across the de Sitter boundary”. In: *J. Math. Phys.* 60.2 (2019), p. 022301. DOI: [10.1063/1.5023646](#).
- [103] Clifford Cheung et al. “The Effective Field Theory of Inflation”. In: *JHEP* 03 (2008), p. 014. DOI: [10.1088/1126-6708/2008/03/014](#). arXiv: [0709.0293 \[hep-th\]](#).
- [104] Leonardo Senatore and Matias Zaldarriaga. “The Effective Field Theory of Multifield Inflation”. In: *JHEP* 04 (2012), p. 024. DOI: [10.1007/JHEP04\(2012\)024](#). arXiv: [1009.2093 \[hep-th\]](#).
- [105] Shinji Tsujikawa. “The effective field theory of inflation/dark energy and the Horndeski theory”. In: *Lect. Notes Phys.* 892 (2015). Ed. by Eleftherios Papantonopoulos, pp. 97–136. DOI: [10.1007/978-3-319-10070-8_4](#). arXiv: [1404.2684 \[gr-qc\]](#).
- [106] Amjad Ashoorioon et al. “Extended Effective Field Theory of Inflation”. In: *JHEP* 02 (2018), p. 172. DOI: [10.1007/JHEP02\(2018\)172](#). arXiv: [1802.03040 \[hep-th\]](#).
- [107] Antony Lewis and Sarah Bridle. “Cosmological parameters from CMB and other data: A Monte Carlo approach”. In: *Phys. Rev. D* 66 (2002), p. 103511. DOI: [10.1103/PhysRevD.66.103511](#). arXiv: [astro-ph/0205436](#).
- [108] Antony Lewis. “Efficient sampling of fast and slow cosmological parameters”. In: *Phys. Rev. D* 87.10 (2013), p. 103529. DOI: [10.1103/PhysRevD.87.103529](#). arXiv: [1304.4473 \[astro-ph.CO\]](#).
- [109] Antony Lewis, Anthony Challinor, and Anthony Lasenby. “Efficient computation of CMB anisotropies in closed FRW models”. In: *Astrophys. J.* 538 (2000), pp. 473–476. DOI: [10.1086/309179](#). arXiv: [astro-ph/9911177](#).
- [110] Cullan Howlett et al. “CMB power spectrum parameter degeneracies in the era of precision cosmology”. In: *JCAP* 04 (2012), p. 027. DOI: [10.1088/1475-7516/2012/04/027](#). arXiv: [1201.3654 \[astro-ph.CO\]](#).
- [111] Radford M. Neal. “Taking Bigger Metropolis Steps by Dragging Fast Variables”. In: *arXiv Mathematics e-prints*, math/0502099 (Feb. 2005), math/0502099. arXiv: [math/0502099 \[math.ST\]](#).
- [112] Andrew Gelman and Donald B. Rubin. “Inference from Iterative Simulation Using Multiple Sequences”. In: *Statist. Sci.* 7 (1992), pp. 457–472. DOI: [10.1214/ss/1177011136](#).
- [113] N. Aghanim et al. “Planck 2018 results. V. CMB power spectra and likelihoods”. In: *Astron. Astrophys.* 641 (2020), A5. DOI: [10.1051/0004-6361/201936386](#). arXiv: [1907.12875 \[astro-ph.CO\]](#).
- [114] N. Aghanim et al. “Planck 2018 results. VI. Cosmological parameters”. In: *Astron. Astrophys.* 641 (2020), A6. DOI: [10.1051/0004-6361/201833910](#). arXiv: [1807.06209 \[astro-ph.CO\]](#).
- [115] N. Aghanim et al. “Planck 2018 results. VIII. Gravitational lensing”. In: *Astron. Astrophys.* 641 (2020), A8. DOI: [10.1051/0004-6361/201833886](#). arXiv: [1807.06210 \[astro-ph.CO\]](#).
- [116] Florian Beutler et al. “The 6dF Galaxy Survey: Baryon Acoustic Oscillations and the Local Hubble Constant”. In: *Mon. Not. Roy. Astron. Soc.* 416 (2011), pp. 3017–3032. DOI: [10.1111/j.1365-2966.2011.19250.x](#). arXiv: [1106.3366 \[astro-ph.CO\]](#).

- [117] Ashley J. Ross et al. “The clustering of the SDSS DR7 main Galaxy sample – I. A 4 per cent distance measure at $z = 0.15$ ”. In: *Mon. Not. Roy. Astron. Soc.* 449.1 (2015), pp. 835–847. DOI: [10.1093/mnras/stv154](https://doi.org/10.1093/mnras/stv154). arXiv: [1409.3242](https://arxiv.org/abs/1409.3242) [astro-ph.CO].
- [118] Shadab Alam et al. “The clustering of galaxies in the completed SDSS-III Baryon Oscillation Spectroscopic Survey: cosmological analysis of the DR12 galaxy sample”. In: *Mon. Not. Roy. Astron. Soc.* 470.3 (2017), pp. 2617–2652. DOI: [10.1093/mnras/stx721](https://doi.org/10.1093/mnras/stx721). arXiv: [1607.03155](https://arxiv.org/abs/1607.03155) [astro-ph.CO].
- [119] D. M. Scolnic et al. “The Complete Light-curve Sample of Spectroscopically Confirmed SNe Ia from Pan-STARRS1 and Cosmological Constraints from the Combined Pantheon Sample”. In: *Astrophys. J.* 859.2 (2018), p. 101. DOI: [10.3847/1538-4357/aab9bb](https://doi.org/10.3847/1538-4357/aab9bb). arXiv: [1710.00845](https://arxiv.org/abs/1710.00845) [astro-ph.CO].
- [120] Florian Beutler et al. “The 6dF Galaxy Survey: Baryon Acoustic Oscillations and the Local Hubble Constant”. In: *Mon. Not. Roy. Astron. Soc.* 416 (2011), pp. 3017–3032. DOI: [10.1111/j.1365-2966.2011.19250.x](https://doi.org/10.1111/j.1365-2966.2011.19250.x). arXiv: [1106.3366](https://arxiv.org/abs/1106.3366) [astro-ph.CO].
- [121] Eleonora Di Valentino et al. “In the Realm of the Hubble tension – a Review of Solutions”. In: (Mar. 2021). DOI: [10.1088/1361-6382/ac086d](https://doi.org/10.1088/1361-6382/ac086d). arXiv: [2103.01183](https://arxiv.org/abs/2103.01183) [astro-ph.CO].
- [122] L. Verde, T. Treu, and A. G. Riess. “Tensions between the Early and the Late Universe”. In: *Nature Astron.* 3 (July 2019), p. 891. DOI: [10.1038/s41550-019-0902-0](https://doi.org/10.1038/s41550-019-0902-0). arXiv: [1907.10625](https://arxiv.org/abs/1907.10625) [astro-ph.CO].
- [123] Jose Luis Bernal, Licia Verde, and Adam G. Riess. “The trouble with H_0 ”. In: *JCAP* 10 (2016), p. 019. DOI: [10.1088/1475-7516/2016/10/019](https://doi.org/10.1088/1475-7516/2016/10/019). arXiv: [1607.05617](https://arxiv.org/abs/1607.05617) [astro-ph.CO].
- [124] Eleonora Di Valentino, Alessandro Melchiorri, and Joseph Silk. “Investigating Cosmic Discordance”. In: *Astrophys. J. Lett.* 908.1 (2021), p. L9. DOI: [10.3847/2041-8213/abe1c4](https://doi.org/10.3847/2041-8213/abe1c4). arXiv: [2003.04935](https://arxiv.org/abs/2003.04935) [astro-ph.CO].
- [125] Eleonora Di Valentino, Alessandro Melchiorri, and Joseph Silk. “Planck evidence for a closed Universe and a possible crisis for cosmology”. In: *Nature Astron.* 4.2 (2019), pp. 196–203. DOI: [10.1038/s41550-019-0906-9](https://doi.org/10.1038/s41550-019-0906-9). arXiv: [1911.02087](https://arxiv.org/abs/1911.02087) [astro-ph.CO].
- [126] Andrei D. Linde. “A New Inflationary Universe Scenario: A Possible Solution of the Horizon, Flatness, Homogeneity, Isotropy and Primordial Monopole Problems”. In: *Phys. Lett. B* 108 (1982). Ed. by Li-Zhi Fang and R. Ruffini, pp. 389–393. DOI: [10.1016/0370-2693\(82\)91219-9](https://doi.org/10.1016/0370-2693(82)91219-9).
- [127] Jerome Martin, Christophe Ringeval, and Vincent Vennin. “Encyclopædia Inflationaris”. In: *Phys. Dark Univ.* 5-6 (2014), pp. 75–235. DOI: [10.1016/j.dark.2014.01.003](https://doi.org/10.1016/j.dark.2014.01.003). arXiv: [1303.3787](https://arxiv.org/abs/1303.3787) [astro-ph.CO].
- [128] Alexander Vilenkin. “The Birth of Inflationary Universes”. In: *Phys. Rev. D* 27 (1983), p. 2848. DOI: [10.1103/PhysRevD.27.2848](https://doi.org/10.1103/PhysRevD.27.2848).
- [129] Alexei A. Starobinsky. “A New Type of Isotropic Cosmological Models Without Singularity”. In: *Phys. Lett. B* 91 (1980). Ed. by I. M. Khalatnikov and V. P. Mineev, pp. 99–102. DOI: [10.1016/0370-2693\(80\)90670-X](https://doi.org/10.1016/0370-2693(80)90670-X).
- [130] Antonio Riotto. “Inflation and the theory of cosmological perturbations”. In: *ICTP Lect. Notes Ser.* 14 (2003). Ed. by G. Dvali et al., pp. 317–413. arXiv: [hep-ph/0210162](https://arxiv.org/abs/hep-ph/0210162).
- [131] Chiara Caprini and Daniel G Figueroa. “Cosmological backgrounds of gravitational waves”. In: *CQG* 35.16 (July 2018), p. 163001. DOI: [10.1088/1361-6382/aac608](https://doi.org/10.1088/1361-6382/aac608). URL: <https://doi.org/10.1088%2F1361-6382%2Faac608>.
- [132] Giovanni Cabass et al. “Updated Constraints and Forecasts on Primordial Tensor Modes”. In: *Phys. Rev. D* 93.6 (2016), p. 063508. DOI: [10.1103/PhysRevD.93.063508](https://doi.org/10.1103/PhysRevD.93.063508). arXiv: [1511.05146](https://arxiv.org/abs/1511.05146) [astro-ph.CO].
- [133] Marc Kamionkowski and Ely D. Kovetz. “The Quest for B Modes from Inflationary Gravitational Waves”. In: *Ann. Rev. Astron. Astrophys.* 54 (2016), pp. 227–269. DOI: [10.1146/annurev-astro-081915-023433](https://doi.org/10.1146/annurev-astro-081915-023433). arXiv: [1510.06042](https://arxiv.org/abs/1510.06042) [astro-ph.CO].
- [134] Daniel Baumann, Daniel Green, and Rafael A. Porto. “B-modes and the Nature of Inflation”. In: *JCAP* 01 (2015), p. 016. DOI: [10.1088/1475-7516/2015/01/016](https://doi.org/10.1088/1475-7516/2015/01/016). arXiv: [1407.2621](https://arxiv.org/abs/1407.2621) [hep-th].

- [135] Robert R. Caldwell, Tristan L. Smith, and Devin G. E. Walker. “Using a Primordial Gravitational Wave Background to Illuminate New Physics”. In: *Phys. Rev. D* 100.4 (2019), p. 043513. DOI: [10.1103/PhysRevD.100.043513](https://doi.org/10.1103/PhysRevD.100.043513). arXiv: [1812.07577](https://arxiv.org/abs/1812.07577) [astro-ph.CO].
- [136] G. Franciolini et al. “Implications of the detection of primordial gravitational waves for the Standard Model”. In: *JCAP* 05 (2019), p. 022. DOI: [10.1088/1475-7516/2019/05/022](https://doi.org/10.1088/1475-7516/2019/05/022). arXiv: [1811.08118](https://arxiv.org/abs/1811.08118) [hep-ph].
- [137] Varun Sahni. “The Energy Density of Relic Gravity Waves From Inflation”. In: *Phys. Rev. D* 42 (1990), pp. 453–463. DOI: [10.1103/PhysRevD.42.453](https://doi.org/10.1103/PhysRevD.42.453).
- [138] Mehrdad Mirbabayi et al. “Gravitational Waves and the Scale of Inflation”. In: *Phys. Rev. D* 91 (2015), p. 063518. DOI: [10.1103/PhysRevD.91.063518](https://doi.org/10.1103/PhysRevD.91.063518). arXiv: [1412.0665](https://arxiv.org/abs/1412.0665) [hep-th].
- [139] Ogan Özsoy, Kuver Sinha, and Scott Watson. “How Well Can We Really Determine the Scale of Inflation?” In: *Phys. Rev. D* 91.10 (2015), p. 103509. DOI: [10.1103/PhysRevD.91.103509](https://doi.org/10.1103/PhysRevD.91.103509). arXiv: [1410.0016](https://arxiv.org/abs/1410.0016) [hep-th].
- [140] William H. Kinney. “Inflation: Flow, fixed points and observables to arbitrary order in slow roll”. In: *Phys. Rev. D* 66 (2002), p. 083508. DOI: [10.1103/PhysRevD.66.083508](https://doi.org/10.1103/PhysRevD.66.083508). arXiv: [astro-ph/0206032](https://arxiv.org/abs/astro-ph/0206032).
- [141] Richard Easther et al. “Imprints of short distance physics on inflationary cosmology”. In: *Phys. Rev. D* 67 (2003), p. 063508. DOI: [10.1103/PhysRevD.67.063508](https://doi.org/10.1103/PhysRevD.67.063508). arXiv: [hep-th/0110226](https://arxiv.org/abs/hep-th/0110226).
- [142] E. Komatsu et al. “Non-Gaussianity as a Probe of the Physics of the Primordial Universe and the Astrophysics of the Low Redshift Universe”. In: (Feb. 2009). arXiv: [0902.4759](https://arxiv.org/abs/0902.4759) [astro-ph.CO].
- [143] Thomas J. Clarke, Edmund J. Copeland, and Adam Moss. “Constraints on primordial gravitational waves from the Cosmic Microwave Background”. In: *JCAP* 10 (2020), p. 002. DOI: [10.1088/1475-7516/2020/10/002](https://doi.org/10.1088/1475-7516/2020/10/002). arXiv: [2004.11396](https://arxiv.org/abs/2004.11396) [astro-ph.CO].
- [144] Alan H. Guth and So-Young Pi. “The Quantum Mechanics of the Scalar Field in the New Inflationary Universe”. In: *Phys. Rev. D* 32 (1985), pp. 1899–1920. DOI: [10.1103/PhysRevD.32.1899](https://doi.org/10.1103/PhysRevD.32.1899).
- [145] Alexei A. Starobinsky. “Spectrum of adiabatic perturbations in the universe when there are singularities in the inflation potential”. In: *JETP Lett.* 55 (1992), pp. 489–494.
- [146] Alexei A. Starobinsky. “Spectrum of relict gravitational radiation and the early state of the universe”. In: *JETP Lett.* 30 (1979). Ed. by I. M. Khalatnikov and V. P. Mineev, pp. 682–685.
- [147] A. A. Starobinsky. “The Perturbation Spectrum Evolving from a Nonsingular Initially De-Sitter Cosmology and the Microwave Background Anisotropy”. In: *Sov. Astron. Lett.* 9 (1983), p. 302.
- [148] Viatcheslav F. Mukhanov and G. V. Chibisov. “Quantum Fluctuations and a Nonsingular Universe”. In: *JETP Lett.* 33 (1981), pp. 532–535.
- [149] Viatcheslav F. Mukhanov, H. A. Feldman, and Robert H. Brandenberger. “Theory of cosmological perturbations. Part 1. Classical perturbations. Part 2. Quantum theory of perturbations. Part 3. Extensions”. In: *Phys. Rept.* 215 (1992), pp. 203–333. DOI: [10.1016/0370-1573\(92\)90044-Z](https://doi.org/10.1016/0370-1573(92)90044-Z).
- [150] Viatcheslav Mukhanov. “Quantum Cosmological Perturbations: Predictions and Observations”. In: *Eur. Phys. J. C* 73 (2013), p. 2486. DOI: [10.1140/epjc/s10052-013-2486-7](https://doi.org/10.1140/epjc/s10052-013-2486-7). arXiv: [1303.3925](https://arxiv.org/abs/1303.3925) [astro-ph.CO].
- [151] Viatcheslav F. Mukhanov and G. V. Chibisov. “The Vacuum energy and large scale structure of the universe”. In: *Sov. Phys. JETP* 56 (1982), pp. 258–265.
- [152] James M. Bardeen. “Gauge Invariant Cosmological Perturbations”. In: *Phys. Rev. D* 22 (1980), pp. 1882–1905. DOI: [10.1103/PhysRevD.22.1882](https://doi.org/10.1103/PhysRevD.22.1882).
- [153] James M. Bardeen, Paul J. Steinhardt, and Michael S. Turner. “Spontaneous Creation of Almost Scale - Free Density Perturbations in an Inflationary Universe”. In: *Phys. Rev. D* 28 (1983), p. 679. DOI: [10.1103/PhysRevD.28.679](https://doi.org/10.1103/PhysRevD.28.679).

- [154] Fred C. Adams et al. “Natural inflation: Particle physics models, power law spectra for large scale structure, and constraints from COBE”. In: *Phys. Rev. D* 47 (1993), pp. 426–455. DOI: [10.1103/PhysRevD.47.426](https://doi.org/10.1103/PhysRevD.47.426). arXiv: [hep-ph/9207245](https://arxiv.org/abs/hep-ph/9207245).
- [155] N. Bartolo, S. Matarrese, and A. Riotto. “Adiabatic and isocurvature perturbations from inflation: Power spectra and consistency relations”. In: *Phys. Rev. D* 64 (2001), p. 123504. DOI: [10.1103/PhysRevD.64.123504](https://doi.org/10.1103/PhysRevD.64.123504). arXiv: [astro-ph/0107502](https://arxiv.org/abs/astro-ph/0107502).
- [156] Jeongyeol Choe, Jinn-Ouk Gong, and Ewan D. Stewart. “Second order general slow-roll power spectrum”. In: *JCAP* 07 (2004), p. 012. DOI: [10.1088/1475-7516/2004/07/012](https://doi.org/10.1088/1475-7516/2004/07/012). arXiv: [hep-ph/0405155](https://arxiv.org/abs/hep-ph/0405155).
- [157] Mark G. Jackson and Gary Shiu. “Study of the consistency relation for single-field inflation with power spectrum oscillations”. In: *Phys. Rev. D* 88.12 (2013), p. 123511. DOI: [10.1103/PhysRevD.88.123511](https://doi.org/10.1103/PhysRevD.88.123511). arXiv: [1303.4973 \[hep-th\]](https://arxiv.org/abs/1303.4973).
- [158] Jerome Martin and Dominik J. Schwarz. “WKB approximation for inflationary cosmological perturbations”. In: *Phys. Rev. D* 67 (2003), p. 083512. DOI: [10.1103/PhysRevD.67.083512](https://doi.org/10.1103/PhysRevD.67.083512). arXiv: [astro-ph/0210090](https://arxiv.org/abs/astro-ph/0210090).
- [159] Jennifer A. Adams, Bevan Cresswell, and Richard Easther. “Inflationary perturbations from a potential with a step”. In: *Phys. Rev. D* 64 (2001), p. 123514. DOI: [10.1103/PhysRevD.64.123514](https://doi.org/10.1103/PhysRevD.64.123514). arXiv: [astro-ph/0102236](https://arxiv.org/abs/astro-ph/0102236).
- [160] Sachiko Kuroyanagi and Tomo Takahashi. “Higher Order Corrections to the Primordial Gravitational Wave Spectrum and its Impact on Parameter Estimates for Inflation”. In: *JCAP* 10 (2011), p. 006. DOI: [10.1088/1475-7516/2011/10/006](https://doi.org/10.1088/1475-7516/2011/10/006). arXiv: [1106.3437 \[astro-ph.CO\]](https://arxiv.org/abs/1106.3437).
- [161] Moslem Zarei. “On the running of the spectral index to all orders: a new model dependent approach to constrain inflationary models”. In: *Class. Quant. Grav.* 33.11 (2016), p. 115008. DOI: [10.1088/0264-9381/33/11/115008](https://doi.org/10.1088/0264-9381/33/11/115008). arXiv: [1408.6467 \[astro-ph.CO\]](https://arxiv.org/abs/1408.6467).
- [162] P. A. R. Ade et al. “BICEP2 / Keck Array x: Constraints on Primordial Gravitational Waves using Planck, WMAP, and New BICEP2/Keck Observations through the 2015 Season”. In: *Phys. Rev. Lett.* 121 (2018), p. 221301. DOI: [10.1103/PhysRevLett.121.221301](https://doi.org/10.1103/PhysRevLett.121.221301). arXiv: [1810.05216 \[astro-ph.CO\]](https://arxiv.org/abs/1810.05216).
- [163] Shinji Mukohyama et al. “Blue Tensor Spectrum from Particle Production during Inflation”. In: *JCAP* 08 (2014), p. 036. DOI: [10.1088/1475-7516/2014/08/036](https://doi.org/10.1088/1475-7516/2014/08/036). arXiv: [1405.0346 \[astro-ph.CO\]](https://arxiv.org/abs/1405.0346).
- [164] Ryo Namba et al. “Scale-dependent gravitational waves from a rolling axion”. In: *JCAP* 01 (2016), p. 041. DOI: [10.1088/1475-7516/2016/01/041](https://doi.org/10.1088/1475-7516/2016/01/041). arXiv: [1509.07521 \[astro-ph.CO\]](https://arxiv.org/abs/1509.07521).
- [165] Marco Peloso, Lorenzo Sorbo, and Caner Unal. “Rolling axions during inflation: perturbativity and signatures”. In: *JCAP* 09 (2016), p. 001. DOI: [10.1088/1475-7516/2016/09/001](https://doi.org/10.1088/1475-7516/2016/09/001). arXiv: [1606.00459 \[astro-ph.CO\]](https://arxiv.org/abs/1606.00459).
- [166] Ogan Özsoy. “Synthetic Gravitational Waves from a Rolling Axion Monodromy”. In: *JCAP* 04 (2021), p. 040. DOI: [10.1088/1475-7516/2021/04/040](https://doi.org/10.1088/1475-7516/2021/04/040). arXiv: [2005.10280 \[astro-ph.CO\]](https://arxiv.org/abs/2005.10280).
- [167] Massimo Giovannini. “The refractive index of relic gravitons”. In: *Class. Quant. Grav.* 33.12 (2016), p. 125002. DOI: [10.1088/0264-9381/33/12/125002](https://doi.org/10.1088/0264-9381/33/12/125002). arXiv: [1507.03456 \[astro-ph.CO\]](https://arxiv.org/abs/1507.03456).
- [168] Massimo Giovannini. “Post-inflationary thermal histories and the refractive index of relic gravitons”. In: *Phys. Rev. D* 98.10 (2018), p. 103509. DOI: [10.1103/PhysRevD.98.103509](https://doi.org/10.1103/PhysRevD.98.103509). arXiv: [1806.01937 \[gr-qc\]](https://arxiv.org/abs/1806.01937).
- [169] Massimo Giovannini. “Blue and violet graviton spectra from a dynamical refractive index”. In: *Phys. Lett. B* 789 (2019), pp. 502–507. DOI: [10.1016/j.physletb.2018.12.068](https://doi.org/10.1016/j.physletb.2018.12.068). arXiv: [1805.08142 \[astro-ph.CO\]](https://arxiv.org/abs/1805.08142).
- [170] Massimo Giovannini. “The propagating speed of relic gravitational waves and their refractive index during inflation”. In: *Eur. Phys. J. C* 78.6 (2018), p. 442. DOI: [10.1140/epjc/s10052-018-5931-9](https://doi.org/10.1140/epjc/s10052-018-5931-9). arXiv: [1803.05203 \[gr-qc\]](https://arxiv.org/abs/1803.05203).

- [171] Michele Cicoli and Eleonora Di Valentino. “Fitting string inflation to real cosmological data: The fiber inflation case”. In: *Phys. Rev. D* 102.4 (2020), p. 043521. DOI: [10.1103/PhysRevD.102.043521](https://doi.org/10.1103/PhysRevD.102.043521). arXiv: [2004.01210](https://arxiv.org/abs/2004.01210) [astro-ph.CO].
- [172] G. Hinshaw et al. “Nine-Year Wilkinson Microwave Anisotropy Probe (WMAP) Observations: Cosmological Parameter Results”. In: *Astrophys. J. Suppl.* 208 (2013), p. 19. DOI: [10.1088/0067-0049/208/2/19](https://doi.org/10.1088/0067-0049/208/2/19). arXiv: [1212.5226](https://arxiv.org/abs/1212.5226) [astro-ph.CO].
- [173] Simone Aiola et al. “The Atacama Cosmology Telescope: DR4 Maps and Cosmological Parameters”. In: *JCAP* 12 (2020), p. 047. DOI: [10.1088/1475-7516/2020/12/047](https://doi.org/10.1088/1475-7516/2020/12/047). arXiv: [2007.07288](https://arxiv.org/abs/2007.07288) [astro-ph.CO].
- [174] D. Dutcher et al. “Measurements of the E-Mode Polarization and Temperature-E-Mode Correlation of the CMB from SPT-3G 2018 Data”. In: (Jan. 2021). arXiv: [2101.01684](https://arxiv.org/abs/2101.01684) [astro-ph.CO].
- [175] Will Handley and Pablo Lemos. “Quantifying the global parameter tensions between ACT, SPT and Planck”. In: *Phys. Rev. D* 103.6 (2021), p. 063529. DOI: [10.1103/PhysRevD.103.063529](https://doi.org/10.1103/PhysRevD.103.063529). arXiv: [2007.08496](https://arxiv.org/abs/2007.08496) [astro-ph.CO].
- [176] Julian B. Munoz and Marc Kamionkowski. “Equation-of-State Parameter for Reheating”. In: *Phys. Rev. D* 91.4 (2015), p. 043521. DOI: [10.1103/PhysRevD.91.043521](https://doi.org/10.1103/PhysRevD.91.043521). arXiv: [1412.0656](https://arxiv.org/abs/1412.0656) [astro-ph.CO].
- [177] Katherine Freese, Joshua A. Frieman, and Angela V. Olinto. “Natural inflation with pseudo - Nambu-Goldstone bosons”. In: *Phys. Rev. Lett.* 65 (1990), pp. 3233–3236. DOI: [10.1103/PhysRevLett.65.3233](https://doi.org/10.1103/PhysRevLett.65.3233).
- [178] G. Hinshaw et al. “Nine-year Wilkinson Microwave Anisotropy Probe (WMAP) Observations: Cosmological Parameter Results”. In: *ApJS* 208.2 (2013), p. 19. DOI: [10.1088/0067-0049/208/2/19](https://doi.org/10.1088/0067-0049/208/2/19). arXiv: [1212.5226](https://arxiv.org/abs/1212.5226) [astro-ph.CO].
- [179] Eva Silverstein and Alexander Westphal. “Monodromy in the CMB: Gravity Waves and String Inflation”. In: *Phys. Rev. D* 78 (2008), p. 106003. DOI: [10.1103/PhysRevD.78.106003](https://doi.org/10.1103/PhysRevD.78.106003). arXiv: [0803.3085](https://arxiv.org/abs/0803.3085) [hep-th].
- [180] Liam McAllister, Eva Silverstein, and Alexander Westphal. “Gravity Waves and Linear Inflation from Axion Monodromy”. In: *Phys. Rev. D* 82 (2010), p. 046003. DOI: [10.1103/PhysRevD.82.046003](https://doi.org/10.1103/PhysRevD.82.046003). arXiv: [0808.0706](https://arxiv.org/abs/0808.0706) [hep-th].
- [181] S. Dimopoulos et al. “N-flation”. In: *JCAP* 08 (2008), p. 003. DOI: [10.1088/1475-7516/2008/08/003](https://doi.org/10.1088/1475-7516/2008/08/003). arXiv: [hep-th/0507205](https://arxiv.org/abs/hep-th/0507205).
- [182] F. Lucchin and S. Matarrese. “Power Law Inflation”. In: *Phys. Rev. D* 32 (1985), p. 1316. DOI: [10.1103/PhysRevD.32.1316](https://doi.org/10.1103/PhysRevD.32.1316).
- [183] Mehdi Shokri, Fabrizio Renzi, and Alessandro Melchiorri. “Cosmic Microwave Background constraints on non-minimal couplings in inflationary models with power law potentials”. In: *Phys. Dark Univ.* 24 (2019), p. 100297. DOI: [10.1016/j.dark.2019.100297](https://doi.org/10.1016/j.dark.2019.100297). arXiv: [1905.00649](https://arxiv.org/abs/1905.00649) [astro-ph.CO].
- [184] Chao-Qiang Geng et al. “Observational constraints on successful model of quintessential Inflation”. In: *JCAP* 06 (2017), p. 011. DOI: [10.1088/1475-7516/2017/06/011](https://doi.org/10.1088/1475-7516/2017/06/011). arXiv: [1705.01329](https://arxiv.org/abs/1705.01329) [gr-qc].
- [185] P. J. E. Peebles and A. Vilenkin. “Quintessential inflation”. In: *Phys. Rev. D* 59 (1999), p. 063505. DOI: [10.1103/PhysRevD.59.063505](https://doi.org/10.1103/PhysRevD.59.063505). arXiv: [astro-ph/9810509](https://arxiv.org/abs/astro-ph/9810509).
- [186] Fedor L. Bezrukov and Mikhail Shaposhnikov. “The Standard Model Higgs boson as the inflaton”. In: *Phys. Lett. B* 659 (2008), pp. 703–706. DOI: [10.1016/j.physletb.2007.11.072](https://doi.org/10.1016/j.physletb.2007.11.072). arXiv: [0710.3755](https://arxiv.org/abs/0710.3755) [hep-th].
- [187] Renata Kallosh, Andrei Linde, and Diederik Roest. “Universal Attractor for Inflation at Strong Coupling”. In: *Phys. Rev. Lett.* 112.1 (2014), p. 011303. DOI: [10.1103/PhysRevLett.112.011303](https://doi.org/10.1103/PhysRevLett.112.011303). arXiv: [1310.3950](https://arxiv.org/abs/1310.3950) [hep-th].

- [188] Renata Kallosh and Andrei Linde. “Superconformal generalizations of the Starobinsky model”. In: *JCAP* 06 (2013), p. 028. DOI: [10.1088/1475-7516/2013/06/028](https://doi.org/10.1088/1475-7516/2013/06/028). arXiv: [1306.3214](https://arxiv.org/abs/1306.3214) [hep-th].
- [189] Alex Kehagias, Azadeh Moradinezhad Dizgah, and Antonio Riotto. “Remarks on the Starobinsky model of inflation and its descendants”. In: *Phys. Rev. D* 89.4 (2014), p. 043527. DOI: [10.1103/PhysRevD.89.043527](https://doi.org/10.1103/PhysRevD.89.043527). arXiv: [1312.1155](https://arxiv.org/abs/1312.1155) [hep-th].
- [190] Hayato Motohashi. “Consistency relation for R^p inflation”. In: *Phys. Rev. D* 91 (2015), p. 064016. DOI: [10.1103/PhysRevD.91.064016](https://doi.org/10.1103/PhysRevD.91.064016). arXiv: [1411.2972](https://arxiv.org/abs/1411.2972) [astro-ph.CO].
- [191] Nan Zhang et al. “Constraints on the generalized natural inflation after Planck 2018”. In: *Chin. Phys. C* 44.9 (2020), p. 095107. DOI: [10.1088/1674-1137/44/9/095107](https://doi.org/10.1088/1674-1137/44/9/095107). arXiv: [1807.03596](https://arxiv.org/abs/1807.03596) [astro-ph.CO].
- [192] Fabrizio Renzi, Mehdi Shokri, and Alessandro Melchiorri. “What is the amplitude of the gravitational waves background expected in the Starobinski model?”. In: *Phys. Dark Univ.* 27 (2020), p. 100450. DOI: [10.1016/j.dark.2019.100450](https://doi.org/10.1016/j.dark.2019.100450). arXiv: [1909.08014](https://arxiv.org/abs/1909.08014) [astro-ph.CO].
- [193] Matthew Civiletti and Brandon Delacruz. “Natural inflation with natural number of e -foldings”. In: *Phys. Rev. D* 101.4 (2020), p. 043534. DOI: [10.1103/PhysRevD.101.043534](https://doi.org/10.1103/PhysRevD.101.043534). arXiv: [2004.05238](https://arxiv.org/abs/2004.05238) [astro-ph.CO].
- [194] Stefano Meza et al. “Numerical analysis of the generalized Starobinsky inflationary model”. In: (Apr. 2021). arXiv: [2104.01139](https://arxiv.org/abs/2104.01139) [gr-qc].
- [195] J. A. Grayson et al. “BICEP3 performance overview and planned Keck Array upgrade”. In: *Proc. SPIE Int. Soc. Opt. Eng.* 9914 (2016), 99140S. DOI: [10.1117/12.2233894](https://doi.org/10.1117/12.2233894). arXiv: [1607.04668](https://arxiv.org/abs/1607.04668) [astro-ph.IM].
- [196] Thomas Essinger-Hileman et al. “CLASS: The Cosmology Large Angular Scale Surveyor”. In: *Proc. SPIE Int. Soc. Opt. Eng.* 9153 (2014), p. 91531I. DOI: [10.1117/12.2056701](https://doi.org/10.1117/12.2056701). arXiv: [1408.4788](https://arxiv.org/abs/1408.4788) [astro-ph.IM].
- [197] B. A. Benson et al. “SPT-3G: A Next-Generation Cosmic Microwave Background Polarization Experiment on the South Pole Telescope”. In: *Proc. SPIE Int. Soc. Opt. Eng.* 9153 (2014), 91531P. DOI: [10.1117/12.2057305](https://doi.org/10.1117/12.2057305). arXiv: [1407.2973](https://arxiv.org/abs/1407.2973) [astro-ph.IM].
- [198] S. W. Henderson et al. “Advanced ACTPol Cryogenic Detector Arrays and Readout”. In: *J. Low. Temp. Phys.* 184.3-4 (2016), pp. 772–779. DOI: [10.1007/s10909-016-1575-z](https://doi.org/10.1007/s10909-016-1575-z). arXiv: [1510.02809](https://arxiv.org/abs/1510.02809) [astro-ph.IM].
- [199] A. Suzuki et al. “The LiteBIRD Satellite Mission: Sub-Kelvin Instrument”. In: *Journal of Low Temperature Physics* 193.5 (Dec. 2018), pp. 1048–1056.
- [200] Kevork N. Abazajian et al. “CMB-S4 Science Book, First Edition”. In: (2016). arXiv: [1610.02743](https://arxiv.org/abs/1610.02743) [astro-ph.CO].
- [201] Giulia Capurri et al. “Let Effective Field Theory of Inflation flow: stochastic generation of models with red/blue tensor tilt”. In: *JCAP* 11 (2020), p. 037. DOI: [10.1088/1475-7516/2020/11/037](https://doi.org/10.1088/1475-7516/2020/11/037). arXiv: [2006.10781](https://arxiv.org/abs/2006.10781) [astro-ph.CO].
- [202] Nicola Bartolo et al. “Characterizing the cosmological gravitational wave background: Anisotropies and non-Gaussianity”. In: *Phys. Rev. D* 102.2 (2020), p. 023527. DOI: [10.1103/PhysRevD.102.023527](https://doi.org/10.1103/PhysRevD.102.023527). arXiv: [1912.09433](https://arxiv.org/abs/1912.09433) [astro-ph.CO].
- [203] M. C. Guzzetti et al. “Gravitational waves from inflation”. In: *Riv. Nuovo Cim.* 39.9 (2016), pp. 399–495. DOI: [10.1393/ncr/i2016-10127-1](https://doi.org/10.1393/ncr/i2016-10127-1). arXiv: [1605.01615](https://arxiv.org/abs/1605.01615) [astro-ph.CO].
- [204] Zaven Arzoumanian et al. “The NANOGrav 12.5 yr Data Set: Search for an Isotropic Stochastic Gravitational-wave Background”. In: *Astrophys. J. Lett.* 905.2 (2020), p. L34. DOI: [10.3847/2041-8213/abd401](https://doi.org/10.3847/2041-8213/abd401). arXiv: [2009.04496](https://arxiv.org/abs/2009.04496) [astro-ph.HE].
- [205] Sunny Vagnozzi. “Implications of the NANOGrav results for inflation”. In: *Mon. Not. Roy. Astron. Soc.* 502.1 (2021), pp. L11–L15. DOI: [10.1093/mnras/1/slaa203](https://doi.org/10.1093/mnras/1/slaa203). arXiv: [2009.13432](https://arxiv.org/abs/2009.13432) [astro-ph.CO].

- [206] Micol Benetti, Leila Lobato Graef, and Sunny Vagnozzi. “Primordial gravitational waves from NANOGrav: a broken power-law approach”. In: (Nov. 2021). arXiv: [2111.04758 \[astro-ph.CO\]](#).
- [207] Sukannya Bhattacharya, Subhendra Mohanty, and Priyank Parashari. “Implications of the NANOGrav result on primordial gravitational waves in nonstandard cosmologies”. In: *Phys. Rev. D* 103.6 (2021), p. 063532. DOI: [10.1103/PhysRevD.103.063532](#). arXiv: [2010.05071 \[astro-ph.CO\]](#).
- [208] Sachiko Kuroyanagi, Tomo Takahashi, and Shuichiro Yokoyama. “Blue-tilted inflationary tensor spectrum and reheating in the light of NANOGrav results”. In: *JCAP* 01 (2021), p. 071. DOI: [10.1088/1475-7516/2021/01/071](#). arXiv: [2011.03323 \[astro-ph.CO\]](#).
- [209] Benjamin P. Abbott et al. “Upper Limits on the Stochastic Gravitational-Wave Background from Advanced LIGO’s First Observing Run”. In: *Phys. Rev. Lett.* 118.12 (2017). [Erratum: *Phys.Rev.Lett.* 119, 029901 (2017)], p. 121101. DOI: [10.1103/PhysRevLett.118.121101](#). arXiv: [1612.02029 \[gr-qc\]](#).
- [210] Nicola Bartolo et al. “Science with the space-based interferometer LISA. IV: Probing inflation with gravitational waves”. In: *JCAP* 12 (2016), p. 026. DOI: [10.1088/1475-7516/2016/12/026](#). arXiv: [1610.06481 \[astro-ph.CO\]](#).
- [211] Andrew Stewart and Robert Brandenberger. “Observational Constraints on Theories with a Blue Spectrum of Tensor Modes”. In: *JCAP* 08 (2008), p. 012. DOI: [10.1088/1475-7516/2008/08/012](#). arXiv: [0711.4602 \[astro-ph\]](#).
- [212] Leila L. Graef, Micol Benetti, and Jailson S. Alcaniz. “Primordial gravitational waves and the H₀-tension problem”. In: *Phys. Rev. D* 99.4 (2019), p. 043519. DOI: [10.1103/PhysRevD.99.043519](#). arXiv: [1809.04501 \[astro-ph.CO\]](#).
- [213] William H. Kinney. “Gravitational Wave Direct Detection does not Constrain the Tensor Spectral Index at CMB Scales”. In: (Feb. 2021). DOI: [10.21105/astro.2103.00281](#). arXiv: [2103.00281 \[astro-ph.CO\]](#).
- [214] B. P. Abbott et al. “Gravitational Waves and Gamma-rays from a Binary Neutron Star Merger: GW170817 and GRB 170817A”. In: *Astrophys. J. Lett.* 848.2 (2017), p. L13. DOI: [10.3847/2041-8213/aa920c](#). arXiv: [1710.05834 \[astro-ph.HE\]](#).
- [215] Neil Cornish, Diego Blas, and Germano Nardini. “Bounding the speed of gravity with gravitational wave observations”. In: *Phys. Rev. Lett.* 119.16 (2017), p. 161102. DOI: [10.1103/PhysRevLett.119.161102](#). arXiv: [1707.06101 \[gr-qc\]](#).
- [216] Xiaoshu Liu et al. “Measuring the speed of gravitational waves from the first and second observing run of Advanced LIGO and Advanced Virgo”. In: *Phys. Rev. D* 102.2 (2020), p. 024028. DOI: [10.1103/PhysRevD.102.024028](#). arXiv: [2005.03121 \[gr-qc\]](#).
- [217] Alexander Bonilla et al. “Forecasts on the speed of gravitational waves at high z ”. In: *JCAP* 03 (2020), p. 015. DOI: [10.1088/1475-7516/2020/03/015](#). arXiv: [1910.05631 \[gr-qc\]](#).
- [218] B. P. Abbott et al. “Multi-messenger Observations of a Binary Neutron Star Merger”. In: *Astrophys. J. Lett.* 848.2 (2017), p. L12. DOI: [10.3847/2041-8213/aa91c9](#). arXiv: [1710.05833 \[astro-ph.HE\]](#).
- [219] Gregory Walter Horndeski. “Second-order scalar-tensor field equations in a four-dimensional space”. In: *Int. J. Theor. Phys.* 10 (1974), pp. 363–384. DOI: [10.1007/BF01807638](#).
- [220] Tsutomu Kobayashi. “Horndeski theory and beyond: a review”. In: *Rept. Prog. Phys.* 82.8 (2019), p. 086901. DOI: [10.1088/1361-6633/ab2429](#). arXiv: [1901.07183 \[gr-qc\]](#).
- [221] C. Deffayet et al. “From k-essence to generalised Galileons”. In: *Phys. Rev. D* 84 (2011), p. 064039. DOI: [10.1103/PhysRevD.84.064039](#). arXiv: [1103.3260 \[hep-th\]](#).
- [222] Tsutomu Kobayashi, Masahide Yamaguchi, and Jun’ichi Yokoyama. “Generalized G-inflation: Inflation with the most general second-order field equations”. In: *Prog. Theor. Phys.* 126 (2011), pp. 511–529. DOI: [10.1143/PTP.126.511](#). arXiv: [1105.5723 \[hep-th\]](#).

- [223] Xian Gao. “Unifying framework for scalar-tensor theories of gravity”. In: *Phys. Rev. D* 90 (2014), p. 081501. DOI: [10.1103/PhysRevD.90.081501](https://doi.org/10.1103/PhysRevD.90.081501). arXiv: [1406.0822](https://arxiv.org/abs/1406.0822) [gr-qc].
- [224] Xian Gao. “Hamiltonian analysis of spatially covariant gravity”. In: *Phys. Rev. D* 90 (2014), p. 104033. DOI: [10.1103/PhysRevD.90.104033](https://doi.org/10.1103/PhysRevD.90.104033). arXiv: [1409.6708](https://arxiv.org/abs/1409.6708) [gr-qc].
- [225] Jérôme Gleyzes et al. “Exploring gravitational theories beyond Horndeski”. In: *JCAP* 02 (2015), p. 018. DOI: [10.1088/1475-7516/2015/02/018](https://doi.org/10.1088/1475-7516/2015/02/018). arXiv: [1408.1952](https://arxiv.org/abs/1408.1952) [astro-ph.CO].
- [226] Frederico Arroja et al. “Large-scale structure in mimetic Horndeski gravity”. In: *JCAP* 05 (2018), p. 050. DOI: [10.1088/1475-7516/2018/05/050](https://doi.org/10.1088/1475-7516/2018/05/050). arXiv: [1708.01850](https://arxiv.org/abs/1708.01850) [astro-ph.CO].
- [227] Frederico Arroja et al. “Cosmological perturbations in mimetic Horndeski gravity”. In: *JCAP* 04 (2016), p. 042. DOI: [10.1088/1475-7516/2016/04/042](https://doi.org/10.1088/1475-7516/2016/04/042). arXiv: [1512.09374](https://arxiv.org/abs/1512.09374) [gr-qc].
- [228] Frederico Arroja et al. “The two faces of mimetic Horndeski gravity: disformal transformations and Lagrange multiplier”. In: *JCAP* 09 (2015), p. 051. DOI: [10.1088/1475-7516/2015/09/051](https://doi.org/10.1088/1475-7516/2015/09/051). arXiv: [1506.08575](https://arxiv.org/abs/1506.08575) [gr-qc].
- [229] Jérôme Gleyzes et al. “Healthy theories beyond Horndeski”. In: *Phys. Rev. Lett.* 114.21 (2015), p. 211101. DOI: [10.1103/PhysRevLett.114.211101](https://doi.org/10.1103/PhysRevLett.114.211101). arXiv: [1404.6495](https://arxiv.org/abs/1404.6495) [hep-th].
- [230] Kazuya Koyama. “Cosmological Tests of Modified Gravity”. In: *Rept. Prog. Phys.* 79.4 (2016), p. 046902. DOI: [10.1088/0034-4885/79/4/046902](https://doi.org/10.1088/0034-4885/79/4/046902). arXiv: [1504.04623](https://arxiv.org/abs/1504.04623) [astro-ph.CO].
- [231] David Langlois and Karim Noui. “Degenerate higher derivative theories beyond Horndeski: evading the Ostrogradski instability”. In: *JCAP* 02 (2016), p. 034. DOI: [10.1088/1475-7516/2016/02/034](https://doi.org/10.1088/1475-7516/2016/02/034). arXiv: [1510.06930](https://arxiv.org/abs/1510.06930) [gr-qc].
- [232] Jibril Ben Achour et al. “Degenerate higher order scalar-tensor theories beyond Horndeski up to cubic order”. In: *JHEP* 12 (2016), p. 100. DOI: [10.1007/JHEP12\(2016\)100](https://doi.org/10.1007/JHEP12(2016)100). arXiv: [1608.08135](https://arxiv.org/abs/1608.08135) [hep-th].
- [233] Marco Crisostomi, Kazuya Koyama, and Gianmassimo Tasinato. “Extended Scalar-Tensor Theories of Gravity”. In: *JCAP* 04 (2016), p. 044. DOI: [10.1088/1475-7516/2016/04/044](https://doi.org/10.1088/1475-7516/2016/04/044). arXiv: [1602.03119](https://arxiv.org/abs/1602.03119) [hep-th].
- [234] Jibril Ben Achour, David Langlois, and Karim Noui. “Degenerate higher order scalar-tensor theories beyond Horndeski and disformal transformations”. In: *Phys. Rev. D* 93.12 (2016), p. 124005. DOI: [10.1103/PhysRevD.93.124005](https://doi.org/10.1103/PhysRevD.93.124005). arXiv: [1602.08398](https://arxiv.org/abs/1602.08398) [gr-qc].
- [235] Simone Peirone et al. “Large-scale structure phenomenology of viable Horndeski theories”. In: *Phys. Rev. D* 97.4 (2018), p. 043519. DOI: [10.1103/PhysRevD.97.043519](https://doi.org/10.1103/PhysRevD.97.043519). arXiv: [1712.00444](https://arxiv.org/abs/1712.00444) [astro-ph.CO].
- [236] Shin’ichi Nojiri and Sergei D. Odintsov. “Modified Gauss-Bonnet theory as gravitational alternative for dark energy”. In: *Phys. Lett. B* 631 (2005), pp. 1–6. DOI: [10.1016/j.physletb.2005.10.010](https://doi.org/10.1016/j.physletb.2005.10.010). arXiv: [hep-th/0508049](https://arxiv.org/abs/hep-th/0508049).
- [237] Andrey N. Makarenko and Alexander N. Myagky. “The asymptotic behavior of bouncing cosmological models in $F(\mathcal{G})$ gravity theory”. In: *Int. J. Geom. Meth. Mod. Phys.* 14.10 (2017), p. 1750148. DOI: [10.1142/S0219887817501481](https://doi.org/10.1142/S0219887817501481). arXiv: [1708.03592](https://arxiv.org/abs/1708.03592) [gr-qc].
- [238] Kazuharu Bamba et al. “Bounce universe from string-inspired Gauss-Bonnet gravity”. In: *JCAP* 04 (2015), p. 001. DOI: [10.1088/1475-7516/2015/04/001](https://doi.org/10.1088/1475-7516/2015/04/001). arXiv: [1411.3852](https://arxiv.org/abs/1411.3852) [hep-th].
- [239] Jia-Xi Feng, Bao-Min Gu, and Fu-Wen Shu. “Theoretical and observational constraints on regularized 4D Einstein-Gauss-Bonnet gravity”. In: *Phys. Rev. D* 103 (2021), p. 064002. DOI: [10.1103/PhysRevD.103.064002](https://doi.org/10.1103/PhysRevD.103.064002). arXiv: [2006.16751](https://arxiv.org/abs/2006.16751) [gr-qc].
- [240] S. D. Odintsov, V. K. Oikonomou, and F. P. Fronimos. “Non-minimally coupled Einstein–Gauss–Bonnet inflation phenomenology in view of GW170817”. In: *Annals Phys.* 420 (2020), p. 168250. DOI: [10.1016/j.aop.2020.168250](https://doi.org/10.1016/j.aop.2020.168250). arXiv: [2007.02309](https://arxiv.org/abs/2007.02309) [gr-qc].

- [241] V. K. Oikonomou and F. P. Fronimos. “Reviving non-minimal Horndeski-like theories after GW170817: kinetic coupling corrected Einstein–Gauss–Bonnet inflation”. In: *Class. Quant. Grav.* 38.3 (2021), p. 035013. DOI: [10.1088/1361-6382/abce47](https://doi.org/10.1088/1361-6382/abce47). arXiv: [2006.05512](https://arxiv.org/abs/2006.05512) [gr-qc].
- [242] S. D. Odintsov and V. K. Oikonomou. “Swampland Implications of GW170817-compatible Einstein-Gauss-Bonnet Gravity”. In: *Phys. Lett. B* 805 (2020), p. 135437. DOI: [10.1016/j.physletb.2020.135437](https://doi.org/10.1016/j.physletb.2020.135437). arXiv: [2004.00479](https://arxiv.org/abs/2004.00479) [gr-qc].
- [243] Christos Charmousis and Jean-Francois Dufaux. “General Gauss-Bonnet brane cosmology”. In: *Class. Quant. Grav.* 19 (2002), pp. 4671–4682. DOI: [10.1088/0264-9381/19/18/304](https://doi.org/10.1088/0264-9381/19/18/304). arXiv: [hep-th/0202107](https://arxiv.org/abs/hep-th/0202107).
- [244] Rong-Gen Cai. “Gauss-Bonnet black holes in AdS spaces”. In: *Phys. Rev. D* 65 (2002), p. 084014. DOI: [10.1103/PhysRevD.65.084014](https://doi.org/10.1103/PhysRevD.65.084014). arXiv: [hep-th/0109133](https://arxiv.org/abs/hep-th/0109133).
- [245] Guido Cognola et al. “Dark energy in modified Gauss-Bonnet gravity: Late-time acceleration and the hierarchy problem”. In: *Phys. Rev. D* 73 (2006), p. 084007. DOI: [10.1103/PhysRevD.73.084007](https://doi.org/10.1103/PhysRevD.73.084007). arXiv: [hep-th/0601008](https://arxiv.org/abs/hep-th/0601008).
- [246] James T. Wheeler. “Symmetric Solutions to the Gauss-Bonnet Extended Einstein Equations”. In: *Nucl. Phys. B* 268 (1986), pp. 737–746. DOI: [10.1016/0550-3213\(86\)90268-3](https://doi.org/10.1016/0550-3213(86)90268-3).
- [247] Baojiu Li, John D. Barrow, and David F. Mota. “The Cosmology of Modified Gauss-Bonnet Gravity”. In: *Phys. Rev. D* 76 (2007), p. 044027. DOI: [10.1103/PhysRevD.76.044027](https://doi.org/10.1103/PhysRevD.76.044027). arXiv: [0705.3795](https://arxiv.org/abs/0705.3795) [gr-qc].
- [248] Tomi Koivisto and David F. Mota. “Cosmology and Astrophysical Constraints of Gauss-Bonnet Dark Energy”. In: *Phys. Lett. B* 644 (2007), pp. 104–108. DOI: [10.1016/j.physletb.2006.11.048](https://doi.org/10.1016/j.physletb.2006.11.048). arXiv: [astro-ph/0606078](https://arxiv.org/abs/astro-ph/0606078).
- [249] Tomi Koivisto and David F. Mota. “Gauss-Bonnet Quintessence: Background Evolution, Large Scale Structure and Cosmological Constraints”. In: *Phys. Rev. D* 75 (2007), p. 023518. DOI: [10.1103/PhysRevD.75.023518](https://doi.org/10.1103/PhysRevD.75.023518). arXiv: [hep-th/0609155](https://arxiv.org/abs/hep-th/0609155).
- [250] Georgios Kofinas and Emmanuel N. Saridakis. “Teleparallel equivalent of Gauss-Bonnet gravity and its modifications”. In: *Phys. Rev. D* 90 (2014), p. 084044. DOI: [10.1103/PhysRevD.90.084044](https://doi.org/10.1103/PhysRevD.90.084044). arXiv: [1404.2249](https://arxiv.org/abs/1404.2249) [gr-qc].
- [251] Sourav Bhattacharya and Sumanta Chakraborty. “Constraining some Horndeski gravity theories”. In: *Phys. Rev. D* 95.4 (2017), p. 044037. DOI: [10.1103/PhysRevD.95.044037](https://doi.org/10.1103/PhysRevD.95.044037). arXiv: [1607.03693](https://arxiv.org/abs/1607.03693) [gr-qc].
- [252] John D. Barrow, Mikjel Thorsrud, and Kei Yamamoto. “Cosmologies in Horndeski’s second-order vector-tensor theory”. In: *JHEP* 02 (2013), p. 146. DOI: [10.1007/JHEP02\(2013\)146](https://doi.org/10.1007/JHEP02(2013)146). arXiv: [1211.5403](https://arxiv.org/abs/1211.5403) [gr-qc].
- [253] Masaki Satoh and Jiro Soda. “Higher Curvature Corrections to Primordial Fluctuations in Slow-roll Inflation”. In: *JCAP* 09 (2008), p. 019. DOI: [10.1088/1475-7516/2008/09/019](https://doi.org/10.1088/1475-7516/2008/09/019). arXiv: [0806.4594](https://arxiv.org/abs/0806.4594) [astro-ph].
- [254] V. K. Oikonomou. “Singular Bouncing Cosmology from Gauss-Bonnet Modified Gravity”. In: *Phys. Rev. D* 92.12 (2015), p. 124027. DOI: [10.1103/PhysRevD.92.124027](https://doi.org/10.1103/PhysRevD.92.124027). arXiv: [1509.05827](https://arxiv.org/abs/1509.05827) [gr-qc].
- [255] J. Haro et al. “Bouncing loop quantum cosmology in Gauss-Bonnet gravity”. In: *Phys. Rev. D* 92.12 (2015), p. 124026. DOI: [10.1103/PhysRevD.92.124026](https://doi.org/10.1103/PhysRevD.92.124026). arXiv: [1506.08273](https://arxiv.org/abs/1506.08273) [gr-qc].
- [256] Guillermo Ballesteros. “The effective theory of fluids at NLO and implications for dark energy”. In: *JCAP* 03 (2015), p. 001. DOI: [10.1088/1475-7516/2015/03/001](https://doi.org/10.1088/1475-7516/2015/03/001). arXiv: [1410.2793](https://arxiv.org/abs/1410.2793) [hep-th].
- [257] Ignatios Antoniadis, J. Rizos, and K. Tamvakis. “Singularity - free cosmological solutions of the superstring effective action”. In: *Nucl. Phys. B* 415 (1994), pp. 497–514. DOI: [10.1016/0550-3213\(94\)90120-1](https://doi.org/10.1016/0550-3213(94)90120-1). arXiv: [hep-th/9305025](https://arxiv.org/abs/hep-th/9305025).

- [258] Shinsuke Kawai, Masa-aki Sakagami, and Jiro Soda. “Instability of one loop superstring cosmology”. In: *Phys. Lett. B* 437 (1998), pp. 284–290. DOI: [10.1016/S0370-2693\(98\)00925-3](https://doi.org/10.1016/S0370-2693(98)00925-3). arXiv: [gr-qc/9802033](https://arxiv.org/abs/gr-qc/9802033).
- [259] Jiro Soda, Masa-aki Sakagami, and Shinsuke Kawai. “Novel instability in superstring cosmology”. In: *International Seminar on Mathematical Cosmology (ISMIC 98)*. Mar. 1998. arXiv: [gr-qc/9807056](https://arxiv.org/abs/gr-qc/9807056).
- [260] Shinsuke Kawai and Jiro Soda. “Evolution of fluctuations during graceful exit in string cosmology”. In: *Phys. Lett. B* 460 (1999), pp. 41–46. DOI: [10.1016/S0370-2693\(99\)00736-4](https://doi.org/10.1016/S0370-2693(99)00736-4). arXiv: [gr-qc/9903017](https://arxiv.org/abs/gr-qc/9903017).
- [261] C. Cartier, Edmund J. Copeland, and R. Madden. “The Graceful exit in string cosmology”. In: *JHEP* 01 (2000), p. 035. DOI: [10.1088/1126-6708/2000/01/035](https://doi.org/10.1088/1126-6708/2000/01/035). arXiv: [hep-th/9910169](https://arxiv.org/abs/hep-th/9910169).
- [262] Cyril Cartier, Jai-chan Hwang, and Edmund J. Copeland. “Evolution of cosmological perturbations in nonsingular string cosmologies”. In: *Phys. Rev. D* 64 (2001), p. 103504. DOI: [10.1103/PhysRevD.64.103504](https://doi.org/10.1103/PhysRevD.64.103504). arXiv: [astro-ph/0106197](https://arxiv.org/abs/astro-ph/0106197).
- [263] Yun-Song Piao, Shinji Tsujikawa, and Xin-min Zhang. “Inflation in string inspired cosmology and suppression of CMB low multipoles”. In: *Class. Quant. Grav.* 21 (2004), pp. 4455–4461. DOI: [10.1088/0264-9381/21/18/011](https://doi.org/10.1088/0264-9381/21/18/011). arXiv: [hep-th/0312139](https://arxiv.org/abs/hep-th/0312139).
- [264] Guido Cognola et al. “String-inspired Gauss-Bonnet gravity reconstructed from the universe expansion history and yielding the transition from matter dominance to dark energy”. In: *Phys. Rev. D* 75 (2007), p. 086002. DOI: [10.1103/PhysRevD.75.086002](https://doi.org/10.1103/PhysRevD.75.086002). arXiv: [hep-th/0611198](https://arxiv.org/abs/hep-th/0611198).
- [265] Mustapha Ishak. “Testing General Relativity in Cosmology”. In: *Living Rev. Rel.* 22.1 (2019), p. 1. DOI: [10.1007/s41114-018-0017-4](https://doi.org/10.1007/s41114-018-0017-4). arXiv: [1806.10122](https://arxiv.org/abs/1806.10122) [[astro-ph](https://arxiv.org/abs/astro-ph).CO].
- [266] Steven Weinberg. “Photons and Gravitons in S-Matrix Theory: Derivation of Charge Conservation and Equality of Gravitational and Inertial Mass”. In: *Phys. Rev.* 135 (1964), B1049–B1056. DOI: [10.1103/PhysRev.135.B1049](https://doi.org/10.1103/PhysRev.135.B1049).
- [267] R. Penrose. “Nonlinear Gravitons and Curved Twistor Theory”. In: *Gen. Rel. Grav.* 7 (1976), pp. 31–52. DOI: [10.1007/BF00762011](https://doi.org/10.1007/BF00762011).
- [268] L. P. Grishchuk and Yu. V. Sidorov. “Squeezed quantum states of relic gravitons and primordial density fluctuations”. In: *Phys. Rev. D* 42 (1990), pp. 3413–3421. DOI: [10.1103/PhysRevD.42.3413](https://doi.org/10.1103/PhysRevD.42.3413).
- [269] Steven Weinberg. “Infrared photons and gravitons”. In: *Phys. Rev.* 140 (1965), B516–B524. DOI: [10.1103/PhysRev.140.B516](https://doi.org/10.1103/PhysRev.140.B516).
- [270] Nima Arkani-Hamed, Howard Georgi, and Matthew D. Schwartz. “Effective field theory for massive gravitons and gravity in theory space”. In: *Annals Phys.* 305 (2003), pp. 96–118. DOI: [10.1016/S0003-4916\(03\)00068-X](https://doi.org/10.1016/S0003-4916(03)00068-X). arXiv: [hep-th/0210184](https://arxiv.org/abs/hep-th/0210184).
- [271] Marco Raveri et al. “Measuring the speed of cosmological gravitational waves”. In: *Phys. Rev. D* 91.6 (2015), p. 061501. DOI: [10.1103/PhysRevD.91.061501](https://doi.org/10.1103/PhysRevD.91.061501). arXiv: [1405.7974](https://arxiv.org/abs/1405.7974) [[astro-ph](https://arxiv.org/abs/astro-ph).CO].
- [272] Paolo Creminelli et al. “Resilience of the standard predictions for primordial tensor modes”. In: *Phys. Rev. Lett.* 113.23 (2014), p. 231301. DOI: [10.1103/PhysRevLett.113.231301](https://doi.org/10.1103/PhysRevLett.113.231301). arXiv: [1407.8439](https://arxiv.org/abs/1407.8439) [[astro-ph](https://arxiv.org/abs/astro-ph).CO].
- [273] Yong Cai, Yu-Tong Wang, and Yun-Song Piao. “Oscillation in power spectrum of primordial gravitational wave as a signature of higher-order stringy corrections”. In: *JHEP* 02 (2016), p. 059. DOI: [10.1007/JHEP02\(2016\)059](https://doi.org/10.1007/JHEP02(2016)059). arXiv: [1508.07114](https://arxiv.org/abs/1508.07114) [[hep-th](https://arxiv.org/abs/hep-th)].
- [274] Yong Cai, Yu-Tong Wang, and Yun-Song Piao. “Is there an effect of a nontrivial c_T during inflation?”. In: *Phys. Rev. D* 93.6 (2016), p. 063005. DOI: [10.1103/PhysRevD.93.063005](https://doi.org/10.1103/PhysRevD.93.063005). arXiv: [1510.08716](https://arxiv.org/abs/1510.08716) [[astro-ph](https://arxiv.org/abs/astro-ph).CO].
- [275] Yong Cai, Yu-Tong Wang, and Yun-Song Piao. “Propagating speed of primordial gravitational waves and inflation”. In: *Phys. Rev. D* 94.4 (2016), p. 043002. DOI: [10.1103/PhysRevD.94.043002](https://doi.org/10.1103/PhysRevD.94.043002). arXiv: [1602.05431](https://arxiv.org/abs/1602.05431) [[astro-ph](https://arxiv.org/abs/astro-ph).CO].

- [276] Jacopo Fumagalli, Sander Mooij, and Marieke Postma. “Disformal transformations as a change of units”. In: (Oct. 2016). arXiv: [1610.08460 \[gr-qc\]](#).
- [277] Xian Gao and Xun-Yang Hong. “Propagation of gravitational waves in a cosmological background”. In: *Phys. Rev. D* 101.6 (2020), p. 064057. DOI: [10.1103/PhysRevD.101.064057](#). arXiv: [1906.07131 \[gr-qc\]](#).
- [278] Toshifumi Noumi and Masahide Yamaguchi. “Non-Gaussianities of primordial perturbations and tensor sound speed”. In: (Mar. 2014). arXiv: [1403.6065 \[hep-th\]](#).
- [279] Lorenzo Bordin et al. “Simplifying the EFT of Inflation: generalized disformal transformations and redundant couplings”. In: *JCAP* 09 (2017), p. 043. DOI: [10.1088/1475-7516/2017/09/043](#). arXiv: [1706.03758 \[astro-ph.CO\]](#).
- [280] John McGreevy, Leonard Susskind, and Nicolaos Toumbas. “Invasion of the giant gravitons from Anti-de Sitter space”. In: *JHEP* 06 (2000), p. 008. DOI: [10.1088/1126-6708/2000/06/008](#). arXiv: [hep-th/0003075](#).
- [281] Freddy Cachazo, Song He, and Ellis Ye Yuan. “Scattering of Massless Particles: Scalars, Gluons and Gravitons”. In: *JHEP* 07 (2014), p. 033. DOI: [10.1007/JHEP07\(2014\)033](#). arXiv: [1309.0885 \[hep-th\]](#).
- [282] G. R. Dvali, G. Gabadadze, and M. Porrati. “Metastable gravitons and infinite volume extra dimensions”. In: *Phys. Lett. B* 484 (2000), pp. 112–118. DOI: [10.1016/S0370-2693\(00\)00631-6](#). arXiv: [hep-th/0002190](#).
- [283] R. Fabbri and M. d. Pollock. “The Effect of Primordially Produced Gravitons upon the Anisotropy of the Cosmological Microwave Background Radiation”. In: *Phys. Lett. B* 125 (1983), pp. 445–448. DOI: [10.1016/0370-2693\(83\)91322-9](#).
- [284] Vijay Balasubramanian et al. “Giant gravitons in conformal field theory”. In: *JHEP* 04 (2002), p. 034. DOI: [10.1088/1126-6708/2002/04/034](#). arXiv: [hep-th/0107119](#).
- [285] V. A. Rubakov and P. G. Tinyakov. “Infrared-modified gravities and massive gravitons”. In: *Phys. Usp.* 51 (2008), pp. 759–792. DOI: [10.1070/PU2008v051n08ABEH006600](#). arXiv: [0802.4379 \[hep-th\]](#).
- [286] Mikhail S. Volkov. “Cosmological solutions with massive gravitons in the bigravity theory”. In: *JHEP* 01 (2012), p. 035. DOI: [10.1007/JHEP01\(2012\)035](#). arXiv: [1110.6153 \[hep-th\]](#).
- [287] Massimo Giovannini. “Production and detection of relic gravitons in quintessential inflationary models”. In: *Phys. Rev. D* 60 (1999), p. 123511. DOI: [10.1103/PhysRevD.60.123511](#). arXiv: [astro-ph/9903004](#).
- [288] Stanley Deser and A. Waldron. “Stability of massive cosmological gravitons”. In: *Phys. Lett. B* 508 (2001), pp. 347–353. DOI: [10.1016/S0370-2693\(01\)00523-8](#). arXiv: [hep-th/0103255](#).
- [289] Steven Carlip et al. “Cosmological Topologically Massive Gravitons and Photons”. In: *Class. Quant. Grav.* 26 (2009), p. 075008. DOI: [10.1088/0264-9381/26/7/075008](#). arXiv: [0803.3998 \[hep-th\]](#).
- [290] Robert de Mello Koch, Jelena Smolic, and Milena Smolic. “Giant Gravitons - with Strings Attached (I)”. In: *JHEP* 06 (2007), p. 074. DOI: [10.1088/1126-6708/2007/06/074](#). arXiv: [hep-th/0701066](#).
- [291] L. P. Grishchuk and M. Solokhin. “Spectra of relic gravitons and the early history of the Hubble parameter”. In: *Phys. Rev. D* 43 (1991), pp. 2566–2571. DOI: [10.1103/PhysRevD.43.2566](#).
- [292] S. P. Miao and R. P. Woodard. “Gravitons Enhance Fermions during Inflation”. In: *Phys. Rev. D* 74 (2006), p. 024021. DOI: [10.1103/PhysRevD.74.024021](#). arXiv: [gr-qc/0603135](#).
- [293] Elias Kiritsis. “Product CFTs, gravitational cloning, massive gravitons and the space of gravitational duals”. In: *JHEP* 11 (2006), p. 049. DOI: [10.1088/1126-6708/2006/11/049](#). arXiv: [hep-th/0608088](#).
- [294] C. P. Burgess. “Intro to Effective Field Theories and Inflation”. In: (Nov. 2017). arXiv: [1711.10592 \[hep-th\]](#).

- [295] Jesus Torrado and Antony Lewis. “Cobaya: Code for Bayesian Analysis of hierarchical physical models”. In: (May 2020). arXiv: [2005.05290](https://arxiv.org/abs/2005.05290) [[astro-ph.IM](#)].
- [296] B. P. Abbott et al. “Upper Limits on the Stochastic Gravitational-Wave Background from Advanced LIGO’s First Observing Run”. In: *Phys. Rev. Lett.* 118 (12 Mar. 2017), p. 121101. DOI: [10.1103/PhysRevLett.118.121101](https://doi.org/10.1103/PhysRevLett.118.121101). URL: <https://link.aps.org/doi/10.1103/PhysRevLett.118.121101>.
- [297] B. P. Abbott et al. “A search for the isotropic stochastic background using data from Advanced LIGO’s second observing run”. In: *arXiv* (Mar. 2019). arXiv: [1903.02886](https://arxiv.org/abs/1903.02886) [[gr-qc](#)].
- [298] Michele Maggiore et al. “Science Case for the Einstein Telescope”. In: *JCAP* 03 (2020), p. 050. DOI: [10.1088/1475-7516/2020/03/050](https://doi.org/10.1088/1475-7516/2020/03/050). arXiv: [1912.02622](https://arxiv.org/abs/1912.02622) [[astro-ph.CO](#)].
- [299] J. Polchinski. *String theory. Vol. 1: An introduction to the bosonic string*. Cambridge Monographs on Mathematical Physics. Cambridge University Press, Dec. 2007. DOI: [10.1017/CB09780511816079](https://doi.org/10.1017/CB09780511816079).
- [300] Michael E. Peskin. “INTRODUCTION TO STRING AND SUPERSTRING THEORY. 2.” In: *Theoretical Advanced Study Institute in Particle Physics - TASI 86*. Mar. 1987.
- [301] Michael E. Peskin and Daniel V. Schroeder. *An Introduction to quantum field theory*. Reading, USA: Addison-Wesley, 1995. ISBN: 978-0-201-50397-5.
- [302] C. P. Burgess. “Lectures on Cosmic Inflation and its Potential Stringy Realizations”. In: *PoS P 2GC* (2006). Ed. by Jean Orloff, Geraldine Servant, and Gerard Smadja, p. 008. DOI: [10.1088/0264-9381/24/21/S04](https://doi.org/10.1088/0264-9381/24/21/S04). arXiv: [0708.2865](https://arxiv.org/abs/0708.2865) [[hep-th](#)].
- [303] Barton Zwiebach. “Curvature Squared Terms and String Theories”. In: *Phys. Lett. B* 156 (1985), pp. 315–317. DOI: [10.1016/0370-2693\(85\)91616-8](https://doi.org/10.1016/0370-2693(85)91616-8).
- [304] M. Gasperini. “Tensor perturbations in high curvature string backgrounds”. In: *Phys. Rev. D* 56 (1997), pp. 4815–4823. DOI: [10.1103/PhysRevD.56.4815](https://doi.org/10.1103/PhysRevD.56.4815). arXiv: [gr-qc/9704045](https://arxiv.org/abs/gr-qc/9704045).
- [305] M. Gasperini and G. Veneziano. “String Theory and Pre-big bang Cosmology”. In: *Nuovo Cim. C* 38.5 (2016), p. 160. DOI: [10.1393/ncc/i2015-15160-8](https://doi.org/10.1393/ncc/i2015-15160-8). arXiv: [hep-th/0703055](https://arxiv.org/abs/hep-th/0703055).
- [306] Enrico Pajer, Guilherme L. Pimentel, and Jaap V. S. Van Wijck. “The Conformal Limit of Inflation in the Era of CMB Polarimetry”. In: *JCAP* 06 (2017), p. 009. DOI: [10.1088/1475-7516/2017/06/009](https://doi.org/10.1088/1475-7516/2017/06/009). arXiv: [1609.06993](https://arxiv.org/abs/1609.06993) [[hep-th](#)].
- [307] Paolo Creminelli. “Conformal invariance of scalar perturbations in inflation”. In: *Phys. Rev. D* 85 (2012), p. 041302. DOI: [10.1103/PhysRevD.85.041302](https://doi.org/10.1103/PhysRevD.85.041302). arXiv: [1108.0874](https://arxiv.org/abs/1108.0874) [[hep-th](#)].
- [308] Yosuke Mishima and Tsutomu Kobayashi. “Revisiting slow-roll dynamics and the tensor tilt in general single-field inflation”. In: *Phys. Rev. D* 101.4 (2020), p. 043536. DOI: [10.1103/PhysRevD.101.043536](https://doi.org/10.1103/PhysRevD.101.043536). arXiv: [1911.02143](https://arxiv.org/abs/1911.02143) [[gr-qc](#)].
- [309] Zhu Yi, Yungui Gong, and Mudassar Sabir. “Inflation with Gauss-Bonnet coupling”. In: *Phys. Rev. D* 98.8 (2018), p. 083521. DOI: [10.1103/PhysRevD.98.083521](https://doi.org/10.1103/PhysRevD.98.083521). arXiv: [1804.09116](https://arxiv.org/abs/1804.09116) [[gr-qc](#)].
- [310] Qiang Wu, Tao Zhu, and Anzhong Wang. “Primordial Spectra of slow-roll inflation at second-order with the Gauss-Bonnet correction”. In: *Phys. Rev. D* 97.10 (2018), p. 103502. DOI: [10.1103/PhysRevD.97.103502](https://doi.org/10.1103/PhysRevD.97.103502). arXiv: [1707.08020](https://arxiv.org/abs/1707.08020) [[gr-qc](#)].
- [311] Seoktae Koh, Bum-Hoon Lee, and Gansukh Tumurtushaa. “Reconstruction of the Scalar Field Potential in Inflationary Models with a Gauss-Bonnet term”. In: *Phys. Rev. D* 95.12 (2017), p. 123509. DOI: [10.1103/PhysRevD.95.123509](https://doi.org/10.1103/PhysRevD.95.123509). arXiv: [1610.04360](https://arxiv.org/abs/1610.04360) [[gr-qc](#)].
- [312] Getbogi Hikmawan et al. “Comment on “Gauss-Bonnet inflation””. In: *Phys. Rev. D* 93.6 (2016), p. 068301. DOI: [10.1103/PhysRevD.93.068301](https://doi.org/10.1103/PhysRevD.93.068301). arXiv: [1512.00222](https://arxiv.org/abs/1512.00222) [[hep-th](#)].
- [313] Peng-Xu Jiang, Jian-Wei Hu, and Zong-Kuan Guo. “Inflation coupled to a Gauss-Bonnet term”. In: *Phys. Rev. D* 88 (2013), p. 123508. DOI: [10.1103/PhysRevD.88.123508](https://doi.org/10.1103/PhysRevD.88.123508). arXiv: [1310.5579](https://arxiv.org/abs/1310.5579) [[hep-th](#)].

- [314] Masa-aki Watanabe, Sugumi Kanno, and Jiro Soda. “The Nature of Primordial Fluctuations from Anisotropic Inflation”. In: *Prog. Theor. Phys.* 123 (2010), pp. 1041–1068. DOI: [10.1143/PTP.123.1041](https://doi.org/10.1143/PTP.123.1041). arXiv: [1003.0056](https://arxiv.org/abs/1003.0056) [astro-ph.CO].
- [315] Zong-Kuan Guo and Dominik J. Schwarz. “Power spectra from an inflaton coupled to the Gauss-Bonnet term”. In: *Phys. Rev. D* 80 (2009), p. 063523. DOI: [10.1103/PhysRevD.80.063523](https://doi.org/10.1103/PhysRevD.80.063523). arXiv: [0907.0427](https://arxiv.org/abs/0907.0427) [hep-th].
- [316] José D. Edelstein et al. “Small free field inflation in higher curvature gravity”. In: *JHEP* 01 (2021), p. 029. DOI: [10.1007/JHEP01\(2021\)029](https://doi.org/10.1007/JHEP01(2021)029). arXiv: [2007.07651](https://arxiv.org/abs/2007.07651) [hep-th].
- [317] Luis Alvarez-Gaume et al. “Aspects of Quadratic Gravity”. In: *Fortsch. Phys.* 64.2-3 (2016), pp. 176–189. DOI: [10.1002/prop.201500100](https://doi.org/10.1002/prop.201500100). arXiv: [1505.07657](https://arxiv.org/abs/1505.07657) [hep-th].
- [318] I. Dalianis et al. “Supersymmetry Breaking and Inflation from Higher Curvature Supergravity”. In: *JHEP* 01 (2015), p. 043. DOI: [10.1007/JHEP01\(2015\)043](https://doi.org/10.1007/JHEP01(2015)043). arXiv: [1409.8299](https://arxiv.org/abs/1409.8299) [hep-th].
- [319] V. K. Oikonomou and F. P. Fronimos. “Non-minimally coupled Einstein–Gauss–Bonnet gravity with massless gravitons: the constant-roll case”. In: *Eur. Phys. J. Plus* 135.11 (2020), p. 917. DOI: [10.1140/epjp/s13360-020-00926-3](https://doi.org/10.1140/epjp/s13360-020-00926-3). arXiv: [2011.03828](https://arxiv.org/abs/2011.03828) [gr-qc].
- [320] S. D. Odintsov et al. “GW170817-compatible constant-roll Einstein–Gauss–Bonnet inflation and non-Gaussianities”. In: *Phys. Dark Univ.* 30 (2020), p. 100718. DOI: [10.1016/j.dark.2020.100718](https://doi.org/10.1016/j.dark.2020.100718). arXiv: [2009.06113](https://arxiv.org/abs/2009.06113) [gr-qc].
- [321] V. K. Oikonomou and F. P. Fronimos. “A Nearly Massless Graviton in Einstein-Gauss-Bonnet Inflation with Linear Coupling Implies Constant-roll for the Scalar Field”. In: *EPL* 131.3 (2020), p. 30001. DOI: [10.1209/0295-5075/131/30001](https://doi.org/10.1209/0295-5075/131/30001). arXiv: [2007.11915](https://arxiv.org/abs/2007.11915) [gr-qc].
- [322] S. D. Odintsov, V. K. Oikonomou, and F. P. Fronimos. “Rectifying Einstein-Gauss-Bonnet Inflation in View of GW170817”. In: *Nucl. Phys. B* 958 (2020), p. 115135. DOI: [10.1016/j.nuclphysb.2020.115135](https://doi.org/10.1016/j.nuclphysb.2020.115135). arXiv: [2003.13724](https://arxiv.org/abs/2003.13724) [gr-qc].
- [323] S. D. Odintsov, V. K. Oikonomou, and F. P. Fronimos. “Canonical scalar field inflation with string and R^2 -corrections”. In: *Annals Phys.* 424 (2021), p. 168359. DOI: [10.1016/j.aop.2020.168359](https://doi.org/10.1016/j.aop.2020.168359). arXiv: [2011.08680](https://arxiv.org/abs/2011.08680) [gr-qc].
- [324] D. Anninos et al. “Cosmological Shapes of Higher-Spin Gravity”. In: *JCAP* 04 (2019), p. 045. DOI: [10.1088/1475-7516/2019/04/045](https://doi.org/10.1088/1475-7516/2019/04/045). arXiv: [1902.01251](https://arxiv.org/abs/1902.01251) [hep-th].
- [325] N. Bartolo et al. “Anisotropies and non-Gaussianity of the Cosmological Gravitational Wave Background”. In: *Phys. Rev. D* 100.12 (2019), p. 121501. DOI: [10.1103/PhysRevD.100.121501](https://doi.org/10.1103/PhysRevD.100.121501). arXiv: [1908.00527](https://arxiv.org/abs/1908.00527) [astro-ph.CO].
- [326] Nicola Bartolo et al. “Cosmic structures and gravitational waves in ghost-free scalar-tensor theories of gravity”. In: *JCAP* 05 (2018), p. 048. DOI: [10.1088/1475-7516/2018/05/048](https://doi.org/10.1088/1475-7516/2018/05/048). arXiv: [1712.04002](https://arxiv.org/abs/1712.04002) [gr-qc].
- [327] S. Ramazanov et al. “Living with ghosts in Hořava-Lifshitz gravity”. In: *JHEP* 06 (2016), p. 020. DOI: [10.1007/JHEP06\(2016\)020](https://doi.org/10.1007/JHEP06(2016)020). arXiv: [1601.05405](https://arxiv.org/abs/1601.05405) [hep-th].
- [328] Sirichai Chongchitnan and George Efstathiou. “Prospects for direct detection of primordial gravitational waves”. In: *Phys. Rev. D* 73 (2006), p. 083511. DOI: [10.1103/PhysRevD.73.083511](https://doi.org/10.1103/PhysRevD.73.083511). arXiv: [astro-ph/0602594](https://arxiv.org/abs/astro-ph/0602594).
- [329] Brett C. Friedman, Asantha Cooray, and Alessandro Melchiorri. “WMAP-normalized Inflationary Model Predictions and the Search for Primordial Gravitational Waves with Direct Detection Experiments”. In: *Phys. Rev. D* 74 (2006), p. 123509. DOI: [10.1103/PhysRevD.74.123509](https://doi.org/10.1103/PhysRevD.74.123509). arXiv: [astro-ph/0610220](https://arxiv.org/abs/astro-ph/0610220).
- [330] Tristan L. Smith, Hiranya V. Peiris, and Asantha Cooray. “Deciphering inflation with gravitational waves: cosmic microwave background polarization vs. direct detection with laser interferometers”. In: *Phys. Rev. D* 73 (2006), p. 123503. DOI: [10.1103/PhysRevD.73.123503](https://doi.org/10.1103/PhysRevD.73.123503). arXiv: [astro-ph/0602137](https://arxiv.org/abs/astro-ph/0602137).

- [331] Hayden Lee. “High-Energy Aspects of Inflationary Cosmology”. PhD thesis. Cambridge U., DAMTP, July 2017. DOI: [10.17863/CAM.20391](https://doi.org/10.17863/CAM.20391).
- [332] Arthur Lue, Li-Min Wang, and Marc Kamionkowski. “Cosmological signature of new parity violating interactions”. In: *Phys. Rev. Lett.* 83 (1999), pp. 1506–1509. DOI: [10.1103/PhysRevLett.83.1506](https://doi.org/10.1103/PhysRevLett.83.1506). arXiv: [astro-ph/9812088](https://arxiv.org/abs/astro-ph/9812088).
- [333] Stephon Alexander and Jerome Martin. “Birefringent gravitational waves and the consistency check of inflation”. In: *Phys. Rev. D* 71 (2005), p. 063526. DOI: [10.1103/PhysRevD.71.063526](https://doi.org/10.1103/PhysRevD.71.063526). arXiv: [hep-th/0410230](https://arxiv.org/abs/hep-th/0410230).
- [334] Carlo R. Contaldi, Joao Magueijo, and Lee Smolin. “Anomalous CMB polarization and gravitational chirality”. In: *Phys. Rev. Lett.* 101 (2008), p. 141101. DOI: [10.1103/PhysRevLett.101.141101](https://doi.org/10.1103/PhysRevLett.101.141101). arXiv: [0806.3082](https://arxiv.org/abs/0806.3082) [[astro-ph](https://arxiv.org/abs/astro-ph)].
- [335] Tomohiro Takahashi and Jiro Soda. “Chiral Primordial Gravitational Waves from a Lifshitz Point”. In: *Phys. Rev. Lett.* 102 (2009), p. 231301. DOI: [10.1103/PhysRevLett.102.231301](https://doi.org/10.1103/PhysRevLett.102.231301). arXiv: [0904.0554](https://arxiv.org/abs/0904.0554) [[hep-th](https://arxiv.org/abs/hep-th)].
- [336] Claudia de Rham and Andrew J. Tolley. “Speed of gravity”. In: *Phys. Rev. D* 101.6 (2020), p. 063518. DOI: [10.1103/PhysRevD.101.063518](https://doi.org/10.1103/PhysRevD.101.063518). arXiv: [1909.00881](https://arxiv.org/abs/1909.00881) [[hep-th](https://arxiv.org/abs/hep-th)].
- [337] Claudia de Rham and Andrew J. Tolley. “Causality in curved spacetimes: The speed of light and gravity”. In: *Phys. Rev. D* 102.8 (2020), p. 084048. DOI: [10.1103/PhysRevD.102.084048](https://doi.org/10.1103/PhysRevD.102.084048). arXiv: [2007.01847](https://arxiv.org/abs/2007.01847) [[hep-th](https://arxiv.org/abs/hep-th)].
- [338] Eugeny Babichev, Viatcheslav Mukhanov, and Alexander Vikman. “k-Essence, superluminal propagation, causality and emergent geometry”. In: *JHEP* 02 (2008), p. 101. DOI: [10.1088/1126-6708/2008/02/101](https://doi.org/10.1088/1126-6708/2008/02/101). arXiv: [0708.0561](https://arxiv.org/abs/0708.0561) [[hep-th](https://arxiv.org/abs/hep-th)].
- [339] Pau Amaro-Seoane et al. “Laser Interferometer Space Antenna”. In: (Feb. 2017). arXiv: [1702.00786](https://arxiv.org/abs/1702.00786) [[astro-ph](https://arxiv.org/abs/astro-ph). [IM](https://arxiv.org/abs/astro-ph)].
- [340] M. Punturo et al. “The Einstein Telescope: A third-generation gravitational wave observatory”. In: *Class. Quant. Grav.* 27 (2010). Ed. by Fulvio Ricci, p. 194002. DOI: [10.1088/0264-9381/27/19/194002](https://doi.org/10.1088/0264-9381/27/19/194002).
- [341] R. D. Peccei and Helen R. Quinn. “CP Conservation in the Presence of Instantons”. In: *Phys. Rev. Lett.* 38 (1977), pp. 1440–1443. DOI: [10.1103/PhysRevLett.38.1440](https://doi.org/10.1103/PhysRevLett.38.1440).
- [342] R. D. Peccei and Helen R. Quinn. “Constraints Imposed by CP Conservation in the Presence of Instantons”. In: *Phys. Rev. D* 16 (1977), pp. 1791–1797. DOI: [10.1103/PhysRevD.16.1791](https://doi.org/10.1103/PhysRevD.16.1791).
- [343] William J. Marciano and Heinz Pagels. “Quantum Chromodynamics: A Review”. In: *Phys. Rept.* 36 (1978), p. 137. DOI: [10.1016/0370-1573\(78\)90208-9](https://doi.org/10.1016/0370-1573(78)90208-9).
- [344] John B. Kogut. “A Review of the Lattice Gauge Theory Approach to Quantum Chromodynamics”. In: *Rev. Mod. Phys.* 55 (1983), p. 775. DOI: [10.1103/RevModPhys.55.775](https://doi.org/10.1103/RevModPhys.55.775).
- [345] R. J. Crewther. “Effects of Topological Charge in Gauge Theories”. In: *Acta Phys. Austriaca Suppl.* 19 (1978), pp. 47–153. DOI: [10.1007/978-3-7091-8538-4_3](https://doi.org/10.1007/978-3-7091-8538-4_3).
- [346] Curtis G. Callan Jr., R. F. Dashen, and David J. Gross. “The Structure of the Gauge Theory Vacuum”. In: *Phys. Lett. B* 63 (1976). Ed. by J. C. Taylor, pp. 334–340. DOI: [10.1016/0370-2693\(76\)90277-X](https://doi.org/10.1016/0370-2693(76)90277-X).
- [347] Varouzhan Baluni. “CP Violating Effects in QCD”. In: *Phys. Rev. D* 19 (1979), pp. 2227–2230. DOI: [10.1103/PhysRevD.19.2227](https://doi.org/10.1103/PhysRevD.19.2227).
- [348] R. J. Crewther et al. “Chiral Estimate of the Electric Dipole Moment of the Neutron in Quantum Chromodynamics”. In: *Phys. Lett. B* 88 (1979). [Erratum: *Phys.Lett.B* 91, 487 (1980)], p. 123. DOI: [10.1016/0370-2693\(79\)90128-X](https://doi.org/10.1016/0370-2693(79)90128-X).
- [349] C. A. Baker et al. “An Improved experimental limit on the electric dipole moment of the neutron”. In: *Phys. Rev. Lett.* 97 (2006), p. 131801. DOI: [10.1103/PhysRevLett.97.131801](https://doi.org/10.1103/PhysRevLett.97.131801). arXiv: [hep-ex/0602020](https://arxiv.org/abs/hep-ex/0602020).

- [350] Steven Weinberg. “The U(1) Problem”. In: *Phys. Rev. D* 11 (1975), pp. 3583–3593. DOI: [10.1103/PhysRevD.11.3583](https://doi.org/10.1103/PhysRevD.11.3583).
- [351] Dimitri V. Nanopoulos. “Towards a renormalizable unified gauge theory of strong, electromagnetic and weak interactions”. In: *Lett. Nuovo Cim.* 8S2 (1973), pp. 873–877. DOI: [10.1007/BF02727401](https://doi.org/10.1007/BF02727401).
- [352] Steven Weinberg. “Nonabelian Gauge Theories of the Strong Interactions”. In: *Phys. Rev. Lett.* 31 (1973), pp. 494–497. DOI: [10.1103/PhysRevLett.31.494](https://doi.org/10.1103/PhysRevLett.31.494).
- [353] A. A. Belavin et al. “Pseudoparticle Solutions of the Yang-Mills Equations”. In: *Phys. Lett. B* 59 (1975). Ed. by J. C. Taylor, pp. 85–87. DOI: [10.1016/0370-2693\(75\)90163-X](https://doi.org/10.1016/0370-2693(75)90163-X).
- [354] R. Jackiw and C. Rebbi. “Vacuum Periodicity in a Yang-Mills Quantum Theory”. In: *Phys. Rev. Lett.* 37 (1976). Ed. by J. C. Taylor, pp. 172–175. DOI: [10.1103/PhysRevLett.37.172](https://doi.org/10.1103/PhysRevLett.37.172).
- [355] Mikhail A. Shifman, A. I. Vainshtein, and Valentin I. Zakharov. “Can Confinement Ensure Natural CP Invariance of Strong Interactions?” In: *Nucl. Phys. B* 166 (1980), pp. 493–506. DOI: [10.1016/0550-3213\(80\)90209-6](https://doi.org/10.1016/0550-3213(80)90209-6).
- [356] Jihn E. Kim. “Weak Interaction Singlet and Strong CP Invariance”. In: *Phys. Rev. Lett.* 43 (1979), p. 103. DOI: [10.1103/PhysRevLett.43.103](https://doi.org/10.1103/PhysRevLett.43.103).
- [357] Michael Dine, Willy Fischler, and Mark Srednicki. “A Simple Solution to the Strong CP Problem with a Harmless Axion”. In: *Phys. Lett. B* 104 (1981), pp. 199–202. DOI: [10.1016/0370-2693\(81\)90590-6](https://doi.org/10.1016/0370-2693(81)90590-6).
- [358] R. D. Peccei. “The Strong CP Problem”. In: *Adv. Ser. Direct. High Energy Phys.* 3 (1989), pp. 503–551. DOI: [10.1142/9789814503280_0013](https://doi.org/10.1142/9789814503280_0013).
- [359] R. D. Peccei. “The Strong CP problem and axions”. In: *Lect. Notes Phys.* 741 (2008). Ed. by Markus Kuster, Georg Raffelt, and Berta Beltran, pp. 3–17. DOI: [10.1007/978-3-540-73518-2_1](https://doi.org/10.1007/978-3-540-73518-2_1). arXiv: [hep-ph/0607268](https://arxiv.org/abs/hep-ph/0607268).
- [360] Frank Wilczek. “Problem of Strong P and T Invariance in the Presence of Instantons”. In: *Phys. Rev. Lett.* 40 (1978), pp. 279–282. DOI: [10.1103/PhysRevLett.40.279](https://doi.org/10.1103/PhysRevLett.40.279).
- [361] Steven Weinberg. “A New Light Boson?” In: *Phys. Rev. Lett.* 40 (1978), pp. 223–226. DOI: [10.1103/PhysRevLett.40.223](https://doi.org/10.1103/PhysRevLett.40.223).
- [362] Markus Kuster, Georg Raffelt, and Berta Beltran, eds. *Axions: Theory, cosmology, and experimental searches. Proceedings, 1st Joint ILIAS-CERN-CAST axion training, Geneva, Switzerland, November 30-December 2, 2005*. Vol. 741. 2008, pp.1–258.
- [363] Curtis G. Callan Jr., Roger F. Dashen, and David J. Gross. “Toward a Theory of the Strong Interactions”. In: *Phys. Rev. D* 17 (1978). Ed. by Mikhail A. Shifman, p. 2717. DOI: [10.1103/PhysRevD.17.2717](https://doi.org/10.1103/PhysRevD.17.2717).
- [364] Jihn E. Kim. “Light Pseudoscalars, Particle Physics and Cosmology”. In: *Phys. Rept.* 150 (1987), pp. 1–177. DOI: [10.1016/0370-1573\(87\)90017-2](https://doi.org/10.1016/0370-1573(87)90017-2).
- [365] Hai-Yang Cheng. “The Strong CP Problem Revisited”. In: *Phys. Rept.* 158 (1988), p. 1. DOI: [10.1016/0370-1573\(88\)90135-4](https://doi.org/10.1016/0370-1573(88)90135-4).
- [366] David J. E. Marsh. “Axion Cosmology”. In: *Phys. Rept.* 643 (2016), pp. 1–79. DOI: [10.1016/j.physrep.2016.06.005](https://doi.org/10.1016/j.physrep.2016.06.005). arXiv: [1510.07633](https://arxiv.org/abs/1510.07633) [[astro-ph.CO](https://arxiv.org/abs/hep-ph)].
- [367] Luca Di Luzio et al. “The landscape of QCD axion models”. In: *Phys. Rept.* 870 (2020), pp. 1–117. DOI: [10.1016/j.physrep.2020.06.002](https://doi.org/10.1016/j.physrep.2020.06.002). arXiv: [2003.01100](https://arxiv.org/abs/2003.01100) [[hep-ph](https://arxiv.org/abs/hep-ph)].
- [368] Pierre Sikivie. “Axion Cosmology”. In: *Lect. Notes Phys.* 741 (2008). Ed. by Markus Kuster, Georg Raffelt, and Berta Beltran, pp. 19–50. DOI: [10.1007/978-3-540-73518-2_2](https://doi.org/10.1007/978-3-540-73518-2_2). arXiv: [astro-ph/0610440](https://arxiv.org/abs/astro-ph/0610440).

- [369] Igor G. Irastorza and Javier Redondo. “New experimental approaches in the search for axion-like particles”. In: *Prog. Part. Nucl. Phys.* 102 (2018), pp. 89–159. DOI: [10.1016/j.pnnp.2018.05.003](https://doi.org/10.1016/j.pnnp.2018.05.003). arXiv: [1801.08127](https://arxiv.org/abs/1801.08127) [hep-ph].
- [370] V. Anastassopoulos et al. “New CAST Limit on the Axion-Photon Interaction”. In: *Nature Phys.* 13 (2017), pp. 584–590. DOI: [10.1038/nphys4109](https://doi.org/10.1038/nphys4109). arXiv: [1705.02290](https://arxiv.org/abs/1705.02290) [hep-ex].
- [371] I. Shilon et al. “Conceptual Design of a New Large Superconducting Toroid for IAXO, the New International AXion Observatory”. In: *IEEE Trans. Appl. Supercond.* 23.3 (2013). Ed. by Steve Gourlay, Gian Luca Sabbi, and Lance Cooley, p. 4500604. DOI: [10.1109/TASC.2013.2251052](https://doi.org/10.1109/TASC.2013.2251052). arXiv: [1212.4633](https://arxiv.org/abs/1212.4633) [physics.ins-det].
- [372] I. Shilon et al. “The Superconducting Toroid for the New International AXion Observatory (IAXO)”. In: *IEEE Trans. Appl. Supercond.* 24.3 (2014). Ed. by Bruce Strauss, p. 4500104. DOI: [10.1109/TASC.2013.2280654](https://doi.org/10.1109/TASC.2013.2280654). arXiv: [1309.2117](https://arxiv.org/abs/1309.2117) [physics.ins-det].
- [373] Ben T. McAllister et al. “The ORGAN Experiment: An axion haloscope above 15 GHz”. In: *Phys. Dark Univ.* 18 (2017), pp. 67–72. DOI: [10.1016/j.dark.2017.09.010](https://doi.org/10.1016/j.dark.2017.09.010). arXiv: [1706.00209](https://arxiv.org/abs/1706.00209) [physics.ins-det].
- [374] S. Beurthey et al. “MADMAX Status Report”. In: (Mar. 2020). arXiv: [2003.10894](https://arxiv.org/abs/2003.10894) [physics.ins-det].
- [375] Matthew Lawson et al. “Tunable axion plasma haloscopes”. In: *Phys. Rev. Lett.* 123.14 (2019), p. 141802. DOI: [10.1103/PhysRevLett.123.141802](https://doi.org/10.1103/PhysRevLett.123.141802). arXiv: [1904.11872](https://arxiv.org/abs/1904.11872) [hep-ph].
- [376] N. Du et al. “A Search for Invisible Axion Dark Matter with the Axion Dark Matter Experiment”. In: *Phys. Rev. Lett.* 120.15 (2018), p. 151301. DOI: [10.1103/PhysRevLett.120.151301](https://doi.org/10.1103/PhysRevLett.120.151301). arXiv: [1804.05750](https://arxiv.org/abs/1804.05750) [hep-ex].
- [377] T. Braine et al. “Extended Search for the Invisible Axion with the Axion Dark Matter Experiment”. In: *Phys. Rev. Lett.* 124.10 (2020), p. 101303. DOI: [10.1103/PhysRevLett.124.101303](https://doi.org/10.1103/PhysRevLett.124.101303). arXiv: [1910.08638](https://arxiv.org/abs/1910.08638) [hep-ex].
- [378] L. F. Abbott and P. Sikivie. “A Cosmological Bound on the Invisible Axion”. In: *Phys. Lett. B* 120 (1983). Ed. by M. A. Srednicki, pp. 133–136. DOI: [10.1016/0370-2693\(83\)90638-X](https://doi.org/10.1016/0370-2693(83)90638-X).
- [379] Michael Dine and Willy Fischler. “The Not So Harmless Axion”. In: *Phys. Lett. B* 120 (1983). Ed. by M. A. Srednicki, pp. 137–141. DOI: [10.1016/0370-2693\(83\)90639-1](https://doi.org/10.1016/0370-2693(83)90639-1).
- [380] John Preskill, Mark B. Wise, and Frank Wilczek. “Cosmology of the Invisible Axion”. In: *Phys. Lett. B* 120 (1983). Ed. by M. A. Srednicki, pp. 127–132. DOI: [10.1016/0370-2693\(83\)90637-8](https://doi.org/10.1016/0370-2693(83)90637-8).
- [381] Andrei D. Linde. “Generation of Isothermal Density Perturbations in the Inflationary Universe”. In: *Phys. Lett. B* 158 (1985), pp. 375–380. DOI: [10.1016/0370-2693\(85\)90436-8](https://doi.org/10.1016/0370-2693(85)90436-8).
- [382] D. Seckel and Michael S. Turner. “Isothermal Density Perturbations in an Axion Dominated Inflationary Universe”. In: *Phys. Rev. D* 32 (1985), p. 3178. DOI: [10.1103/PhysRevD.32.3178](https://doi.org/10.1103/PhysRevD.32.3178).
- [383] David H. Lyth. “A Limit on the Inflationary Energy Density From Axion Isocurvature Fluctuations”. In: *Phys. Lett. B* 236 (1990), pp. 408–410. DOI: [10.1016/0370-2693\(90\)90374-F](https://doi.org/10.1016/0370-2693(90)90374-F).
- [384] Andrei D. Linde and David H. Lyth. “Axionic domain wall production during inflation”. In: *Phys. Lett. B* 246 (1990), pp. 353–358. DOI: [10.1016/0370-2693\(90\)90613-B](https://doi.org/10.1016/0370-2693(90)90613-B).
- [385] A. Vilenkin and E. P. S. Shellard. *Cosmic Strings and Other Topological Defects*. Cambridge University Press, July 2000. ISBN: 978-0-521-65476-0.
- [386] T. W. B. Kibble. “Topology of Cosmic Domains and Strings”. In: *J. Phys. A* 9 (1976), pp. 1387–1398. DOI: [10.1088/0305-4470/9/8/029](https://doi.org/10.1088/0305-4470/9/8/029).
- [387] T. W. B. Kibble, George Lazarides, and Q. Shafi. “Walls Bounded by Strings”. In: *Phys. Rev. D* 26 (1982), p. 435. DOI: [10.1103/PhysRevD.26.435](https://doi.org/10.1103/PhysRevD.26.435).
- [388] A. Vilenkin. “Cosmic Strings”. In: *Phys. Rev. D* 24 (1981), pp. 2082–2089. DOI: [10.1103/PhysRevD.24.2082](https://doi.org/10.1103/PhysRevD.24.2082).

- [389] Richard Lynn Davis. “Cosmic Axions from Cosmic Strings”. In: *Phys. Lett. B* 180 (1986), pp. 225–230. DOI: [10.1016/0370-2693\(86\)90300-X](https://doi.org/10.1016/0370-2693(86)90300-X).
- [390] A. Vilenkin and A. E. Everett. “Cosmic Strings and Domain Walls in Models with Goldstone and PseudoGoldstone Bosons”. In: *Phys. Rev. Lett.* 48 (1982), pp. 1867–1870. DOI: [10.1103/PhysRevLett.48.1867](https://doi.org/10.1103/PhysRevLett.48.1867).
- [391] P. Sikivie. “Of Axions, Domain Walls and the Early Universe”. In: *Phys. Rev. Lett.* 48 (1982), pp. 1156–1159. DOI: [10.1103/PhysRevLett.48.1156](https://doi.org/10.1103/PhysRevLett.48.1156).
- [392] M. C. Huang and P. Sikivie. “The Structure of Axionic Domain Walls”. In: *Phys. Rev. D* 32 (1985), p. 1560. DOI: [10.1103/PhysRevD.32.1560](https://doi.org/10.1103/PhysRevD.32.1560).
- [393] Alessandro Melchiorri, Olga Mena, and Anze Slosar. “An improved cosmological bound on the thermal axion mass”. In: *Phys. Rev. D* 76 (2007), p. 041303. DOI: [10.1103/PhysRevD.76.041303](https://doi.org/10.1103/PhysRevD.76.041303). arXiv: [0705.2695](https://arxiv.org/abs/0705.2695) [astro-ph].
- [394] Steen Hannestad et al. “Cosmological constraints on neutrino plus axion hot dark matter”. In: *JCAP* 08 (2007), p. 015. DOI: [10.1088/1475-7516/2007/08/015](https://doi.org/10.1088/1475-7516/2007/08/015). arXiv: [0706.4198](https://arxiv.org/abs/0706.4198) [astro-ph].
- [395] Steen Hannestad et al. “Cosmological constraints on neutrino plus axion hot dark matter: Update after WMAP-5”. In: *JCAP* 04 (2008), p. 019. DOI: [10.1088/1475-7516/2008/04/019](https://doi.org/10.1088/1475-7516/2008/04/019). arXiv: [0803.1585](https://arxiv.org/abs/0803.1585) [astro-ph].
- [396] Steen Hannestad et al. “Neutrino and axion hot dark matter bounds after WMAP-7”. In: *JCAP* 08 (2010), p. 001. DOI: [10.1088/1475-7516/2010/08/001](https://doi.org/10.1088/1475-7516/2010/08/001). arXiv: [1004.0695](https://arxiv.org/abs/1004.0695) [astro-ph.CO].
- [397] Maria Archidiacono et al. “Axion hot dark matter bounds after Planck”. In: *JCAP* 10 (2013), p. 020. DOI: [10.1088/1475-7516/2013/10/020](https://doi.org/10.1088/1475-7516/2013/10/020). arXiv: [1307.0615](https://arxiv.org/abs/1307.0615) [astro-ph.CO].
- [398] Elena Giusarma et al. “Relic Neutrinos, thermal axions and cosmology in early 2014”. In: *Phys. Rev. D* 90.4 (2014), p. 043507. DOI: [10.1103/PhysRevD.90.043507](https://doi.org/10.1103/PhysRevD.90.043507). arXiv: [1403.4852](https://arxiv.org/abs/1403.4852) [astro-ph.CO].
- [399] Eleonora Di Valentino et al. “Robustness of cosmological axion mass limits”. In: *Phys. Rev. D* 91.12 (2015), p. 123505. DOI: [10.1103/PhysRevD.91.123505](https://doi.org/10.1103/PhysRevD.91.123505). arXiv: [1503.00911](https://arxiv.org/abs/1503.00911) [astro-ph.CO].
- [400] Eleonora Di Valentino et al. “Cosmological Axion and neutrino mass constraints from Planck 2015 temperature and polarization data”. In: *Phys. Lett. B* 752 (2016), pp. 182–185. DOI: [10.1016/j.physletb.2015.11.025](https://doi.org/10.1016/j.physletb.2015.11.025). arXiv: [1507.08665](https://arxiv.org/abs/1507.08665) [astro-ph.CO].
- [401] Maria Archidiacono et al. “Future cosmological sensitivity for hot dark matter axions”. In: *JCAP* 05 (2015), p. 050. DOI: [10.1088/1475-7516/2015/05/050](https://doi.org/10.1088/1475-7516/2015/05/050). arXiv: [1502.03325](https://arxiv.org/abs/1502.03325) [astro-ph.CO].
- [402] Steen Hannestad, Alessandro Mirizzi, and Georg Raffelt. “New cosmological mass limit on thermal relic axions”. In: *JCAP* 07 (2005), p. 002. DOI: [10.1088/1475-7516/2005/07/002](https://doi.org/10.1088/1475-7516/2005/07/002). arXiv: [hep-ph/0504059](https://arxiv.org/abs/hep-ph/0504059).
- [403] Gianpiero Mangano et al. “Relic neutrino decoupling including flavor oscillations”. In: *Nucl. Phys. B* 729 (2005), pp. 221–234. DOI: [10.1016/j.nuclphysb.2005.09.041](https://doi.org/10.1016/j.nuclphysb.2005.09.041). arXiv: [hep-ph/0506164](https://arxiv.org/abs/hep-ph/0506164).
- [404] Pablo F. de Salas and Sergio Pastor. “Relic neutrino decoupling with flavour oscillations revisited”. In: *JCAP* 07 (2016), p. 051. DOI: [10.1088/1475-7516/2016/07/051](https://doi.org/10.1088/1475-7516/2016/07/051). arXiv: [1606.06986](https://arxiv.org/abs/1606.06986) [hep-ph].
- [405] Kensuke Akita and Masahide Yamaguchi. “A precision calculation of relic neutrino decoupling”. In: *JCAP* 08 (2020), p. 012. DOI: [10.1088/1475-7516/2020/08/012](https://doi.org/10.1088/1475-7516/2020/08/012). arXiv: [2005.07047](https://arxiv.org/abs/2005.07047) [hep-ph].
- [406] Julien Froustey, Cyril Pitrou, and Maria Cristina Volpe. “Neutrino decoupling including flavour oscillations and primordial nucleosynthesis”. In: *JCAP* 12 (2020), p. 015. DOI: [10.1088/1475-7516/2020/12/015](https://doi.org/10.1088/1475-7516/2020/12/015). arXiv: [2008.01074](https://arxiv.org/abs/2008.01074) [hep-ph].
- [407] Jack J. Bennett et al. “Towards a precision calculation of N_{eff} in the Standard Model II: Neutrino decoupling in the presence of flavour oscillations and finite-temperature QED”. In: *JCAP* 04 (2021), p. 073. DOI: [10.1088/1475-7516/2021/04/073](https://doi.org/10.1088/1475-7516/2021/04/073). arXiv: [2012.02726](https://arxiv.org/abs/2012.02726) [hep-ph].

- [408] P. A. Zyla et al. “Review of Particle Physics”. In: *PTEP* 2020.8 (2020), p. 083C01. DOI: [10.1093/ptep/ptaa104](https://doi.org/10.1093/ptep/ptaa104).
- [409] Ricardo Z. Ferreira and Alessio Notari. “Observable Windows for the QCD Axion Through the Number of Relativistic Species”. In: *Phys. Rev. Lett.* 120.19 (2018), p. 191301. DOI: [10.1103/PhysRevLett.120.191301](https://doi.org/10.1103/PhysRevLett.120.191301). arXiv: [1801.06090](https://arxiv.org/abs/1801.06090) [hep-ph].
- [410] Fernando Arias-Aragón et al. “Production of Thermal Axions across the ElectroWeak Phase Transition”. In: *JCAP* 03 (2021), p. 090. DOI: [10.1088/1475-7516/2021/03/090](https://doi.org/10.1088/1475-7516/2021/03/090). arXiv: [2012.04736](https://arxiv.org/abs/2012.04736) [hep-ph].
- [411] Francesco D’Eramo, Fazlollah Hajkarim, and Seokhoon Yun. “Thermal axion production at low temperatures: a smooth treatment of the QCD phase transition”. In: (Aug. 2021). arXiv: [2108.04259](https://arxiv.org/abs/2108.04259) [hep-ph].
- [412] Francesco D’Eramo, Fazlollah Hajkarim, and Seokhoon Yun. “Thermal QCD Axions across Thresholds”. In: *JHEP* 10 (2021), p. 224. DOI: [10.1007/JHEP10\(2021\)224](https://doi.org/10.1007/JHEP10(2021)224). arXiv: [2108.05371](https://arxiv.org/abs/2108.05371) [hep-ph].
- [413] Francesco D’Eramo et al. “Hot Axions and the H_0 tension”. In: *JCAP* 11 (2018), p. 014. DOI: [10.1088/1475-7516/2018/11/014](https://doi.org/10.1088/1475-7516/2018/11/014). arXiv: [1808.07430](https://arxiv.org/abs/1808.07430) [hep-ph].
- [414] Ricardo Z. Ferreira, Alessio Notari, and Fabrizio Rompineve. “Dine-Fischler-Srednicki-Zhitnitsky axion in the CMB”. In: *Phys. Rev. D* 103.6 (2021), p. 063524. DOI: [10.1103/PhysRevD.103.063524](https://doi.org/10.1103/PhysRevD.103.063524). arXiv: [2012.06566](https://arxiv.org/abs/2012.06566) [hep-ph].
- [415] Luca Di Luzio, Guido Martinelli, and Gioacchino Piazza. “Breakdown of chiral perturbation theory for the axion hot dark matter bound”. In: (Jan. 2021). arXiv: [2101.10330](https://arxiv.org/abs/2101.10330) [hep-ph].
- [416] A. R. Zhitnitsky. “On Possible Suppression of the Axion Hadron Interactions. (In Russian)”. In: *Sov. J. Nucl. Phys.* 31 (1980), p. 260.
- [417] Jihn E. Kim and Gianpaolo Carosi. “Axions and the Strong CP Problem”. In: *Rev. Mod. Phys.* 82 (2010). [Erratum: *Rev.Mod.Phys.* 91, 049902 (2019)], pp. 557–602. DOI: [10.1103/RevModPhys.82.557](https://doi.org/10.1103/RevModPhys.82.557). arXiv: [0807.3125](https://arxiv.org/abs/0807.3125) [hep-ph].
- [418] P. F. de Salas et al. “2020 global reassessment of the neutrino oscillation picture”. In: *JHEP* 02 (2021), p. 071. DOI: [10.1007/JHEP02\(2021\)071](https://doi.org/10.1007/JHEP02(2021)071). arXiv: [2006.11237](https://arxiv.org/abs/2006.11237) [hep-ph].
- [419] P. F. De Salas et al. “Neutrino Mass Ordering from Oscillations and Beyond: 2018 Status and Future Prospects”. In: *Front. Astron. Space Sci.* 5 (2018), p. 36. DOI: [10.3389/fspas.2018.00036](https://doi.org/10.3389/fspas.2018.00036). arXiv: [1806.11051](https://arxiv.org/abs/1806.11051) [hep-ph].
- [420] Steffen Hagstotz et al. “Bounds on light sterile neutrino mass and mixing from cosmology and laboratory searches”. In: (Mar. 2020). arXiv: [2003.02289](https://arxiv.org/abs/2003.02289) [astro-ph.CO].
- [421] Sunny Vagnozzi. “Cosmological searches for the neutrino mass scale and mass ordering”. In: (July 2019). arXiv: [1907.08010](https://arxiv.org/abs/1907.08010) [astro-ph.CO].
- [422] Sunny Vagnozzi et al. “Bias due to neutrinos must not uncorrect’d go”. In: *JCAP* 09 (2018), p. 001. DOI: [10.1088/1475-7516/2018/09/001](https://doi.org/10.1088/1475-7516/2018/09/001). arXiv: [1807.04672](https://arxiv.org/abs/1807.04672) [astro-ph.CO].
- [423] Sunny Vagnozzi et al. “Constraints on the sum of the neutrino masses in dynamical dark energy models with $w(z) \geq -1$ are tighter than those obtained in Λ CDM”. In: *Phys. Rev. D* 98.8 (2018), p. 083501. DOI: [10.1103/PhysRevD.98.083501](https://doi.org/10.1103/PhysRevD.98.083501). arXiv: [1801.08553](https://arxiv.org/abs/1801.08553) [astro-ph.CO].
- [424] Sunny Vagnozzi et al. “Unveiling ν secrets with cosmological data: neutrino masses and mass hierarchy”. In: *Phys. Rev. D* 96.12 (2017), p. 123503. DOI: [10.1103/PhysRevD.96.123503](https://doi.org/10.1103/PhysRevD.96.123503). arXiv: [1701.08172](https://arxiv.org/abs/1701.08172) [astro-ph.CO].
- [425] Elena Giusarma et al. “Improvement of cosmological neutrino mass bounds”. In: *Phys. Rev. D* 94.8 (2016), p. 083522. DOI: [10.1103/PhysRevD.94.083522](https://doi.org/10.1103/PhysRevD.94.083522). arXiv: [1605.04320](https://arxiv.org/abs/1605.04320) [astro-ph.CO].

- [426] J.R. Bond, G. Efstathiou, and J. Silk. “Massive Neutrinos and the Large Scale Structure of the Universe”. In: *Phys. Rev. Lett.* 45 (1980). Ed. by M.A. Srednicki, pp. 1980–1984. DOI: [10.1103/PhysRevLett.45.1980](https://doi.org/10.1103/PhysRevLett.45.1980).
- [427] M. A. Troxel et al. “Dark Energy Survey Year 1 results: Cosmological constraints from cosmic shear”. In: *Phys. Rev. D* 98.4 (2018), p. 043528. DOI: [10.1103/PhysRevD.98.043528](https://doi.org/10.1103/PhysRevD.98.043528). arXiv: [1708.01538](https://arxiv.org/abs/1708.01538) [[astro-ph.CO](https://arxiv.org/abs/1708.01538)].
- [428] T. M. C. Abbott et al. “Dark Energy Survey year 1 results: Cosmological constraints from galaxy clustering and weak lensing”. In: *Phys. Rev. D* 98.4 (2018), p. 043526. DOI: [10.1103/PhysRevD.98.043526](https://doi.org/10.1103/PhysRevD.98.043526). arXiv: [1708.01530](https://arxiv.org/abs/1708.01530) [[astro-ph.CO](https://arxiv.org/abs/1708.01530)].
- [429] E. Krause et al. “Dark Energy Survey Year 1 Results: Multi-Probe Methodology and Simulated Likelihood Analyses”. In: (June 2017). arXiv: [1706.09359](https://arxiv.org/abs/1706.09359) [[astro-ph.CO](https://arxiv.org/abs/1706.09359)].
- [430] Adam G. Riess et al. “Cosmic Distances Calibrated to 1% Precision with Gaia EDR3 Parallaxes and Hubble Space Telescope Photometry of 75 Milky Way Cepheids Confirm Tension with Λ CDM”. In: *Astrophys. J. Lett.* 908.1 (2021), p. L6. DOI: [10.3847/2041-8213/abdbaf](https://doi.org/10.3847/2041-8213/abdbaf). arXiv: [2012.08534](https://arxiv.org/abs/2012.08534) [[astro-ph.CO](https://arxiv.org/abs/2012.08534)].
- [431] Daniel Grin et al. “A Telescope Search for Decaying Relic Axions”. In: *Phys. Rev. D* 75 (2007), p. 105018. DOI: [10.1103/PhysRevD.75.105018](https://doi.org/10.1103/PhysRevD.75.105018). arXiv: [astro-ph/0611502](https://arxiv.org/abs/astro-ph/0611502).
- [432] Marco Regis et al. “Searching for light in the darkness: Bounds on ALP dark matter with the optical MUSE-faint survey”. In: *Phys. Lett. B* 814 (2021), p. 136075. DOI: [10.1016/j.physletb.2021.136075](https://doi.org/10.1016/j.physletb.2021.136075). arXiv: [2009.01310](https://arxiv.org/abs/2009.01310) [[astro-ph.CO](https://arxiv.org/abs/2009.01310)].
- [433] Adrian Ayala et al. “Revisiting the bound on axion-photon coupling from Globular Clusters”. In: *Phys. Rev. Lett.* 113.19 (2014), p. 191302. DOI: [10.1103/PhysRevLett.113.191302](https://doi.org/10.1103/PhysRevLett.113.191302). arXiv: [1406.6053](https://arxiv.org/abs/1406.6053) [[astro-ph.SR](https://arxiv.org/abs/1406.6053)].
- [434] Eleonora Di Valentino et al. “Snowmass2021 - Letter of interest cosmology intertwined II: The hubble constant tension”. In: *Astropart. Phys.* 131 (2021), p. 102605. DOI: [10.1016/j.astropartphys.2021.102605](https://doi.org/10.1016/j.astropartphys.2021.102605). arXiv: [2008.11284](https://arxiv.org/abs/2008.11284) [[astro-ph.CO](https://arxiv.org/abs/2008.11284)].
- [435] Ciaran O’Hare. *cajohare/AxionLimits: AxionLimits*. Version v1.0. July 2020. DOI: [10.5281/zenodo.3932430](https://doi.org/10.5281/zenodo.3932430). URL: <https://doi.org/10.5281/zenodo.3932430>.
- [436] Ciaran A. J. O’Hare and Edoardo Vitagliano. “Cornering the axion with CP-violating interactions”. In: *Phys. Rev. D* 102.11 (2020), p. 115026. DOI: [10.1103/PhysRevD.102.115026](https://doi.org/10.1103/PhysRevD.102.115026). arXiv: [2010.03889](https://arxiv.org/abs/2010.03889) [[hep-ph](https://arxiv.org/abs/2010.03889)].
- [437] Ciaran A. J. O’Hare et al. “Axion helioscopes as solar magnetometers”. In: *Phys. Rev. D* 102.4 (2020), p. 043019. DOI: [10.1103/PhysRevD.102.043019](https://doi.org/10.1103/PhysRevD.102.043019). arXiv: [2006.10415](https://arxiv.org/abs/2006.10415) [[astro-ph.CO](https://arxiv.org/abs/2006.10415)].
- [438] Theopisti Dafni et al. “Weighing the solar axion”. In: *Phys. Rev. D* 99.3 (2019), p. 035037. DOI: [10.1103/PhysRevD.99.035037](https://doi.org/10.1103/PhysRevD.99.035037). arXiv: [1811.09290](https://arxiv.org/abs/1811.09290) [[hep-ph](https://arxiv.org/abs/1811.09290)].
- [439] Stefan Knirck et al. “Directional axion detection”. In: *JCAP* 11 (2018), p. 051. DOI: [10.1088/1475-7516/2018/11/051](https://doi.org/10.1088/1475-7516/2018/11/051). arXiv: [1806.05927](https://arxiv.org/abs/1806.05927) [[astro-ph.CO](https://arxiv.org/abs/1806.05927)].
- [440] Andreu Font-Ribera et al. “DESI and other dark energy experiments in the era of neutrino mass measurements”. In: *JCAP* 05 (2014), p. 023. DOI: [10.1088/1475-7516/2014/05/023](https://doi.org/10.1088/1475-7516/2014/05/023). arXiv: [1308.4164](https://arxiv.org/abs/1308.4164) [[astro-ph.CO](https://arxiv.org/abs/1308.4164)].
- [441] Michael Levi et al. “The DESI Experiment, a whitepaper for Snowmass 2013”. In: (Aug. 2013). arXiv: [1308.0847](https://arxiv.org/abs/1308.0847) [[astro-ph.CO](https://arxiv.org/abs/1308.0847)].
- [442] K. N. Abazajian et al. “Neutrino Physics from the Cosmic Microwave Background and Large Scale Structure”. In: *Astropart. Phys.* 63 (2015), pp. 66–80. DOI: [10.1016/j.astropartphys.2014.05.014](https://doi.org/10.1016/j.astropartphys.2014.05.014). arXiv: [1309.5383](https://arxiv.org/abs/1309.5383) [[astro-ph.CO](https://arxiv.org/abs/1309.5383)].

- [443] Kevork N. Abazajian and Julian Heeck. “Observing Dirac neutrinos in the cosmic microwave background”. In: *Phys. Rev. D* 100 (2019), p. 075027. DOI: [10.1103/PhysRevD.100.075027](https://doi.org/10.1103/PhysRevD.100.075027). arXiv: [1908.03286](https://arxiv.org/abs/1908.03286) [hep-ph].
- [444] Laurence Perotto et al. “Probing cosmological parameters with the CMB: Forecasts from full Monte Carlo simulations”. In: *JCAP* 10 (2006), p. 013. DOI: [10.1088/1475-7516/2006/10/013](https://doi.org/10.1088/1475-7516/2006/10/013). arXiv: [astro-ph/0606227](https://arxiv.org/abs/astro-ph/0606227).
- [445] Kevork N. Abazajian et al. “CMB-S4 Science Book, First Edition”. In: (Oct. 2016). arXiv: [1610.02743](https://arxiv.org/abs/1610.02743) [astro-ph.CO].
- [446] G. E. Addison et al. “Elucidating Λ CDM: Impact of Baryon Acoustic Oscillation Measurements on the Hubble Constant Discrepancy”. In: *Astrophys. J.* 853.2 (2018), p. 119. DOI: [10.3847/1538-4357/aaa1ed](https://doi.org/10.3847/1538-4357/aaa1ed). arXiv: [1707.06547](https://arxiv.org/abs/1707.06547) [astro-ph.CO].
- [447] R. Allison et al. “Towards a cosmological neutrino mass detection”. In: *Phys. Rev. D* 92.12 (2015), p. 123535. DOI: [10.1103/PhysRevD.92.123535](https://doi.org/10.1103/PhysRevD.92.123535). arXiv: [1509.07471](https://arxiv.org/abs/1509.07471) [astro-ph.CO].
- [448] Eleonora Di Valentino et al. “The cosmological impact of future constraints on H_0 from gravitational-wave standard sirens”. In: *Phys. Rev. D* 98.8 (2018), p. 083523. DOI: [10.1103/PhysRevD.98.083523](https://doi.org/10.1103/PhysRevD.98.083523). arXiv: [1806.07463](https://arxiv.org/abs/1806.07463) [astro-ph.CO].
- [449] Cyril Pitrou et al. “Precision big bang nucleosynthesis with improved Helium-4 predictions”. In: *Submitted to Phys. Rept.* (2018). arXiv: [1801.08023](https://arxiv.org/abs/1801.08023).
- [450] O. Pisanti et al. “PARthENoPE: Public Algorithm Evaluating the Nucleosynthesis of Primordial Elements”. In: *Comput. Phys. Commun.* 178 (2008), pp. 956–971. DOI: [10.1016/j.cpc.2008.02.015](https://doi.org/10.1016/j.cpc.2008.02.015). arXiv: [0705.0290](https://arxiv.org/abs/0705.0290) [astro-ph].
- [451] R. Consiglio et al. “PARthENoPE reloaded”. In: *Comput. Phys. Commun.* 233 (2018), pp. 237–242. DOI: [10.1016/j.cpc.2018.06.022](https://doi.org/10.1016/j.cpc.2018.06.022). arXiv: [1712.04378](https://arxiv.org/abs/1712.04378) [astro-ph.CO].
- [452] S. Gariazzo et al. “PARthENoPE Revolutions”. In: (Mar. 2021). arXiv: [2103.05027](https://arxiv.org/abs/2103.05027) [astro-ph.IM].
- [453] Cyril Pitrou et al. “A new tension in the cosmological model from primordial deuterium?” In: *Mon. Not. Roy. Astron. Soc.* 502.2 (2021), pp. 2474–2481. DOI: [10.1093/mnras/stab135](https://doi.org/10.1093/mnras/stab135). arXiv: [2011.11320](https://arxiv.org/abs/2011.11320) [astro-ph.CO].
- [454] V. Mossa et al. “The baryon density of the Universe from an improved rate of deuterium burning”. In: *Nature* 587.7833 (2020), pp. 210–213. DOI: [10.1038/s41586-020-2878-4](https://doi.org/10.1038/s41586-020-2878-4).
- [455] Ofelia Pisanti et al. “Primordial Deuterium after LUNA: concordances and error budget”. In: *JCAP* 04 (2021), p. 020. DOI: [10.1088/1475-7516/2021/04/020](https://doi.org/10.1088/1475-7516/2021/04/020). arXiv: [2011.11537](https://arxiv.org/abs/2011.11537) [astro-ph.CO].
- [456] Brian D. Fields. “The primordial lithium problem”. In: *Ann. Rev. Nucl. Part. Sci.* 61 (2011), pp. 47–68. DOI: [10.1146/annurev-nucl-102010-130445](https://doi.org/10.1146/annurev-nucl-102010-130445). arXiv: [1203.3551](https://arxiv.org/abs/1203.3551) [astro-ph.CO].
- [457] Richard H. Cyburt, Brian D. Fields, and Keith A. Olive. “An Update on the big bang nucleosynthesis prediction for Li-7: The problem worsens”. In: *JCAP* 11 (2008), p. 012. DOI: [10.1088/1475-7516/2008/11/012](https://doi.org/10.1088/1475-7516/2008/11/012). arXiv: [0808.2818](https://arxiv.org/abs/0808.2818) [astro-ph].
- [458] Laura Salvati et al. “Cosmological constraints on the neutron lifetime”. In: *JCAP* 03 (2016), p. 055. DOI: [10.1088/1475-7516/2016/03/055](https://doi.org/10.1088/1475-7516/2016/03/055). arXiv: [1507.07243](https://arxiv.org/abs/1507.07243) [astro-ph.CO].
- [459] Ludovico Capparelli et al. “Impact of theoretical assumptions in the determination of the neutrino effective number from future CMB measurements”. In: *Phys. Rev. D* 97.6 (2018), p. 063519. DOI: [10.1103/PhysRevD.97.063519](https://doi.org/10.1103/PhysRevD.97.063519). arXiv: [1712.06965](https://arxiv.org/abs/1712.06965) [astro-ph.CO].
- [460] Pauli Virtanen et al. “SciPy 1.0: Fundamental Algorithms for Scientific Computing in Python”. In: *Nature Methods* 17 (2020), pp. 261–272. DOI: <https://doi.org/10.1038/s41592-019-0686-2>.
- [461] Antony Lewis. “GetDist: a Python package for analysing Monte Carlo samples”. In: (Oct. 2019). arXiv: [1910.13970](https://arxiv.org/abs/1910.13970) [astro-ph.IM].

- [462] J. D. Hunter. “Matplotlib: A 2D graphics environment”. In: *Computing in Science & Engineering* 9.3 (2007), pp. 90–95. DOI: [10.1109/MCSE.2007.55](https://doi.org/10.1109/MCSE.2007.55).
- [463] Travis Oliphant. *NumPy: A guide to NumPy*. USA: Trelgol Publishing, 2006. URL: <http://www.numpy.org/>.
- [464] Will Handley. “Curvature tension: evidence for a closed universe”. In: *Phys. Rev. D* 103.4 (2021), p. L041301. DOI: [10.1103/PhysRevD.103.L041301](https://doi.org/10.1103/PhysRevD.103.L041301). arXiv: [1908.09139](https://arxiv.org/abs/1908.09139) [astro-ph.CO].
- [465] Eleonora Di Valentino et al. “Snowmass2021 - Letter of interest cosmology intertwined IV: The age of the universe and its curvature”. In: *Astropart. Phys.* 131 (2021), p. 102607. DOI: [10.1016/j.astropartphys.2021.102607](https://doi.org/10.1016/j.astropartphys.2021.102607). arXiv: [2008.11286](https://arxiv.org/abs/2008.11286) [astro-ph.CO].
- [466] Sunny Vagnozzi et al. “Listening to the BOSS: the galaxy power spectrum take on spatial curvature and cosmic concordance”. In: (Oct. 2020). arXiv: [2010.02230](https://arxiv.org/abs/2010.02230) [astro-ph.CO].
- [467] Sunny Vagnozzi, Abraham Loeb, and Michele Moresco. “Eppur è piatto? The Cosmic Chronometers Take on Spatial Curvature and Cosmic Concordance”. In: *Astrophys. J.* 908.1 (2021), p. 84. DOI: [10.3847/1538-4357/abd4df](https://doi.org/10.3847/1538-4357/abd4df). arXiv: [2011.11645](https://arxiv.org/abs/2011.11645) [astro-ph.CO].
- [468] Suhail Dhawan, Justin Alsing, and Sunny Vagnozzi. “Non-parametric spatial curvature inference using late-universe cosmological probes”. In: (Apr. 2021). DOI: [10.1093/mnrasl/slab058](https://doi.org/10.1093/mnrasl/slab058). arXiv: [2104.02485](https://arxiv.org/abs/2104.02485) [astro-ph.CO].
- [469] George Efstathiou and Steven Gratton. “The evidence for a spatially flat Universe”. In: *Mon. Not. Roy. Astron. Soc.* 496.1 (2020), pp. L91–L95. DOI: [10.1093/mnrasl/slaa093](https://doi.org/10.1093/mnrasl/slaa093). arXiv: [2002.06892](https://arxiv.org/abs/2002.06892) [astro-ph.CO].
- [470] Yingjie Yang and Yungui Gong. “Measurement on the cosmic curvature using the Gaussian process method”. In: *Mon. Not. Roy. Astron. Soc.* 504.2 (2021), pp. 3092–3097. DOI: [10.1093/mnras/stab1085](https://doi.org/10.1093/mnras/stab1085). arXiv: [2007.05714](https://arxiv.org/abs/2007.05714) [astro-ph.CO].
- [471] Andrei D. Linde. “Inflation with variable Omega”. In: *Phys. Lett. B* 351 (1995), pp. 99–104. DOI: [10.1016/0370-2693\(95\)00370-Z](https://doi.org/10.1016/0370-2693(95)00370-Z). arXiv: [hep-th/9503097](https://arxiv.org/abs/hep-th/9503097).
- [472] Andrei D. Linde. “Can we have inflation with $\Omega > 1$?” In: *JCAP* 05 (2003), p. 002. DOI: [10.1088/1475-7516/2003/05/002](https://doi.org/10.1088/1475-7516/2003/05/002). arXiv: [astro-ph/0303245](https://arxiv.org/abs/astro-ph/0303245).
- [473] Bharat Ratra. “Inflation in a closed universe”. In: *Phys. Rev. D* 96.10 (2017), p. 103534. DOI: [10.1103/PhysRevD.96.103534](https://doi.org/10.1103/PhysRevD.96.103534). arXiv: [1707.03439](https://arxiv.org/abs/1707.03439) [astro-ph.CO].
- [474] Béatrice Bonga, Brajesh Gupt, and Nelson Yokomizo. “Inflation in the closed FLRW model and the CMB”. In: *JCAP* 10 (2016), p. 031. DOI: [10.1088/1475-7516/2016/10/031](https://doi.org/10.1088/1475-7516/2016/10/031). arXiv: [1605.07556](https://arxiv.org/abs/1605.07556) [astro-ph.CO].
- [475] Will Handley. “Primordial power spectra for curved inflating universes”. In: *Phys. Rev. D* 100.12 (2019), p. 123517. DOI: [10.1103/PhysRevD.100.123517](https://doi.org/10.1103/PhysRevD.100.123517). arXiv: [1907.08524](https://arxiv.org/abs/1907.08524) [astro-ph.CO].
- [476] Béatrice Bonga, Brajesh Gupt, and Nelson Yokomizo. “Tensor perturbations during inflation in a spatially closed Universe”. In: *JCAP* 05 (2017), p. 021. DOI: [10.1088/1475-7516/2017/05/021](https://doi.org/10.1088/1475-7516/2017/05/021). arXiv: [1612.07281](https://arxiv.org/abs/1612.07281) [astro-ph.CO].
- [477] Junpei Ooba, Bharat Ratra, and Naoshi Sugiyama. “Planck 2015 Constraints on the Non-flat Λ CDM Inflation Model”. In: *Astrophys. J.* 864.1 (2018), p. 80. DOI: [10.3847/1538-4357/aad633](https://doi.org/10.3847/1538-4357/aad633). arXiv: [1707.03452](https://arxiv.org/abs/1707.03452) [astro-ph.CO].
- [478] G. F. R. Ellis et al. “Dynamics of inflationary universes with positive spatial curvature”. In: *Gen. Rel. Grav.* 34 (2002), pp. 1445–1459. DOI: [10.1023/A:1020087004012](https://doi.org/10.1023/A:1020087004012). arXiv: [gr-qc/0109023](https://arxiv.org/abs/gr-qc/0109023).
- [479] Jean-Philippe Uzan, Ulrich Kirchner, and George F. R. Ellis. “WMAP data and the curvature of space”. In: *Mon. Not. Roy. Astron. Soc.* 344 (2003), p. L65. DOI: [10.1046/j.1365-8711.2003.07043.x](https://doi.org/10.1046/j.1365-8711.2003.07043.x). arXiv: [astro-ph/0302597](https://arxiv.org/abs/astro-ph/0302597).

- [480] Gabriel Unger and Nikodem Popławski. “Big bounce and closed universe from spin and torsion”. In: *Astrophys. J.* 870.2 (2019), p. 78. DOI: [10.3847/1538-4357/aaf169](https://doi.org/10.3847/1538-4357/aaf169). arXiv: [1808.08327](https://arxiv.org/abs/1808.08327) [gr-qc].
- [481] Lucia Gordon, Bao-Fei Li, and Parampreet Singh. “Quantum gravitational onset of Starobinsky inflation in a closed universe”. In: *Phys. Rev. D* 103.4 (2021), p. 046016. DOI: [10.1103/PhysRevD.103.046016](https://doi.org/10.1103/PhysRevD.103.046016). arXiv: [2010.04738](https://arxiv.org/abs/2010.04738) [gr-qc].
- [482] David Sloan, Konstantinos Dimopoulos, and Sotirios Karamitsos. “T-Model Inflation and Bouncing Cosmology”. In: *Phys. Rev. D* 101.4 (2020), p. 043521. DOI: [10.1103/PhysRevD.101.043521](https://doi.org/10.1103/PhysRevD.101.043521). arXiv: [1912.00090](https://arxiv.org/abs/1912.00090) [gr-qc].
- [483] Meysam Motaharfar and Parampreet Singh. “On the role of dissipative effects in the quantum gravitational onset of warm Starobinsky inflation in a closed universe”. In: (Feb. 2021). arXiv: [2102.09578](https://arxiv.org/abs/2102.09578) [gr-qc].
- [484] Andrei D. Linde. *Particle physics and inflationary cosmology*. Vol. 5. 1990. arXiv: [hep-th/0503203](https://arxiv.org/abs/hep-th/0503203).
- [485] Andrew R. Liddle and David H. Lyth. “The Cold dark matter density perturbation”. In: *Phys. Rept.* 231 (1993), pp. 1–105. DOI: [10.1016/0370-1573\(93\)90114-S](https://doi.org/10.1016/0370-1573(93)90114-S). arXiv: [astro-ph/9303019](https://arxiv.org/abs/astro-ph/9303019).
- [486] James E. Lidsey et al. “Reconstructing the inflation potential : An overview”. In: *Rev. Mod. Phys.* 69 (1997), pp. 373–410. DOI: [10.1103/RevModPhys.69.373](https://doi.org/10.1103/RevModPhys.69.373). arXiv: [astro-ph/9508078](https://arxiv.org/abs/astro-ph/9508078).
- [487] Mohamed M. Anber and Lorenzo Sorbo. “Naturally inflating on steep potentials through electromagnetic dissipation”. In: *Phys. Rev. D* 81 (2010), p. 043534. DOI: [10.1103/PhysRevD.81.043534](https://doi.org/10.1103/PhysRevD.81.043534). arXiv: [0908.4089](https://arxiv.org/abs/0908.4089) [hep-th].
- [488] Enrico Pajer and Marco Peloso. “A review of Axion Inflation in the era of Planck”. In: *Class. Quant. Grav.* 30 (2013), p. 214002. DOI: [10.1088/0264-9381/30/21/214002](https://doi.org/10.1088/0264-9381/30/21/214002). arXiv: [1305.3557](https://arxiv.org/abs/1305.3557) [hep-th].
- [489] Ricardo Z. Ferreira et al. “On the validity of the perturbative description of axions during inflation”. In: *JCAP* 04 (2016). [Erratum: *JCAP* 10, E01 (2016)], p. 039. DOI: [10.1088/1475-7516/2016/04/039](https://doi.org/10.1088/1475-7516/2016/04/039). arXiv: [1512.06116](https://arxiv.org/abs/1512.06116) [astro-ph.CO].
- [490] Neil Barnaby et al. “Gravity waves and non-Gaussian features from particle production in a sector gravitationally coupled to the inflaton”. In: *Phys. Rev. D* 86 (2012), p. 103508. DOI: [10.1103/PhysRevD.86.103508](https://doi.org/10.1103/PhysRevD.86.103508). arXiv: [1206.6117](https://arxiv.org/abs/1206.6117) [astro-ph.CO].
- [491] Lorenzo Sorbo. “Parity violation in the Cosmic Microwave Background from a pseudoscalar inflaton”. In: *JCAP* 06 (2011), p. 003. DOI: [10.1088/1475-7516/2011/06/003](https://doi.org/10.1088/1475-7516/2011/06/003). arXiv: [1101.1525](https://arxiv.org/abs/1101.1525) [astro-ph.CO].
- [492] Maresuke Shiraishi. “Tensor Non-Gaussianity Search: Current Status and Future Prospects”. In: *Front. Astron. Space Sci.* 6 (2019), p. 49. DOI: [10.3389/fspas.2019.00049](https://doi.org/10.3389/fspas.2019.00049). arXiv: [1905.12485](https://arxiv.org/abs/1905.12485) [astro-ph.CO].
- [493] Jessica L. Cook and Lorenzo Sorbo. “An inflationary model with small scalar and large tensor non-gaussianities”. In: *JCAP* 11 (2013), p. 047. DOI: [10.1088/1475-7516/2013/11/047](https://doi.org/10.1088/1475-7516/2013/11/047). arXiv: [1307.7077](https://arxiv.org/abs/1307.7077) [astro-ph.CO].
- [494] Sanghyeon Chang, C. Hagmann, and P. Sikivie. “Studies of the motion and decay of axion walls bounded by strings”. In: *Phys. Rev. D* 59 (1999), p. 023505. DOI: [10.1103/PhysRevD.59.023505](https://doi.org/10.1103/PhysRevD.59.023505). arXiv: [hep-ph/9807374](https://arxiv.org/abs/hep-ph/9807374).
- [495] Alexander Vilenkin. “Cosmic Strings and Domain Walls”. In: *Phys. Rept.* 121 (1985), pp. 263–315. DOI: [10.1016/0370-1573\(85\)90033-X](https://doi.org/10.1016/0370-1573(85)90033-X).
- [496] Diego Harari and P. Sikivie. “On the Evolution of Global Strings in the Early Universe”. In: *Phys. Lett. B* 195 (1987), pp. 361–365. DOI: [10.1016/0370-2693\(87\)90032-3](https://doi.org/10.1016/0370-2693(87)90032-3).
- [497] Masahide Yamaguchi, M. Kawasaki, and Jun’ichi Yokoyama. “Evolution of axionic strings and spectrum of axions radiated from them”. In: *Phys. Rev. Lett.* 82 (1999), pp. 4578–4581. DOI: [10.1103/PhysRevLett.82.4578](https://doi.org/10.1103/PhysRevLett.82.4578). arXiv: [hep-ph/9811311](https://arxiv.org/abs/hep-ph/9811311).

-
- [498] A. Vilenkin. “Gravitational Field of Vacuum Domain Walls and Strings”. In: *Phys. Rev. D* 23 (1981), pp. 852–857. DOI: [10.1103/PhysRevD.23.852](https://doi.org/10.1103/PhysRevD.23.852).
- [499] J. Ipser and P. Sikivie. “The Gravitationally Repulsive Domain Wall”. In: *Phys. Rev. D* 30 (1984), p. 712. DOI: [10.1103/PhysRevD.30.712](https://doi.org/10.1103/PhysRevD.30.712).
- [500] E. Di Valentino et al. “Axion cold dark matter: status after Planck and BICEP2”. In: *Phys. Rev. D* 90.4 (2014), p. 043534. DOI: [10.1103/PhysRevD.90.043534](https://doi.org/10.1103/PhysRevD.90.043534). arXiv: [1405.1860](https://arxiv.org/abs/1405.1860) [[astro-ph.CO](https://arxiv.org/archive/ph)].